An assessment of tropical dryland forest ecosystem biomass and climate change impacts in the Kavango-Zambezi (KAZA) region of Southern Africa

DAVID, RUUSA-MAGANO

An assessment of tropical dryland forest ecosystem biomass and climate change impacts in the Kavango-Zambezi (KAZA) region of Southern Africa.

Ruusa-Magano David

Thesis submitted for the degree of Doctor of Philosophy

Department of Geography

Durham University

2021

Abstract

The dryland forests of the Kavango-Zambezi (KAZA) region in Southern Africa are highly susceptible to disturbances from an increase in human population, wildlife pressures and the impacts of climate change. In this environment, reliable forest extent and structure estimates are difficult to obtain because of the size and remoteness of KAZA (519,912 km^2). Whilst satellite remote sensing is generally well-suited to monitoring forest characteristics, there remain large uncertainties about its application for assessing changes at a regional scale to quantify forest structure and biomass in dry forest environments. This thesis presents research that combines Synthetic Aperture Radar, multispectral satellite imagery and climatological data with an inventory from a ground survey of woodland in Botswana and Namibia in 2019. The research utilised a multi-method approach including parametric and non-parametric algorithms and change detection models to address the following objectives: (1) To assess the feasibility of using openly accessible remote sensing data to estimate the dryland forest above ground biomass (2) to quantify the detail of vegetation dynamics using extensive archives of time series satellite data; (3) to investigate the relationship between fire, soil moisture, and drought on dryland vegetation as a means of characterising spatiotemporal changes in aridity. The results establish that a combination of radar and multispectral imagery produced the best fit to the ground observations for estimating forest above ground biomass. Modelling of the time-series shows that it is possible to identify abrupt changes, longer-term trends and seasonality in forest dynamics. The time series analysis of fire shows that about 75% of the study area burned at least once within the 17-year monitoring period, with the national parks more frequently affected than other protected areas. The results presented show a significant increase in dryness over the past 2 decades, with arid and semi-arid regions encroaching at the expense of dry sub-humid, particularly in the south of the region, notably between 2011-2019.

Keywords: Above ground biomass, Remote sensing, Synthetic Aperture Radar (SAR), Multispectral data, Climate change, Dryland forest change, Burned area mapping, Biodiversity

DECLARATION

I confirm that no part of the material presented in this thesis has previously been submitted for a degree in this or any other university. In all cases the words of others, where relevant, have been fully acknowledged.

Ruusa-Magano David

Durham University – 2021

ACKNOWLEDGEMENT

I have received a great deal of support during my PhD from many people that I would like to thank. Firstly, I would like to thank my supervisors, Prof. Danny Donoghue and Prof. Nick Rosser for their continued support, assistance and guidance throughout my PhD. Without my supervisor's valuable scientific zeal, intellectual input, encouragement and most importantly their patience, the completion of this research would not have been possible. It has been an amazing privilege to work with you both.

My PhD was funded by the *Commonwealth Scholarship Commission (CSC)*, for which I am most grateful. I would also like to thank the *Royal Geographical Society (with IBG) - Monica Cole Research Grant* and *WWF Namibia Mike Knight* for the fieldwork travel and financial support for my project. I received additional support during my PhD from the *NERC*, which provided me with a loan and training for the Field Spectroscopy equipment (FSF). I would like to thank the *Durham Research Trust* who kindly funded my attendance at 8th European space agency (ESA) advanced training course on land remote sensing, Leicester University, UK, *Geography department Postgraduate Conference Fund at Durham University* for funding my attendance to Google Earth Engine Summit training in Dublin, Ireland and *Funds for Women Graduates (FFWG)* for the support grant to in my writing year.

I am thankful to WWF KAZA Secretariat Dr. Nyambe Nyambe, Chobe National Park Authority Dr. Michael Flyman, and University of Namibia (Katima Branch) Dr. Ekkehard Klingelhoeffer, for their friendliness and the huge amount of logistical advice they have given me during fieldwork, which made the research experience so enjoyable. Additionally, my thanks go to Dr. Jonathan Kamwi, Morgan Kamwi, Nawa Kamwi, for helping me with data collection during the fieldwork. I would like to thank fellow PhD students, and support staff across the Geography Department for their encouragement, friendship and support throughout my time in Durham University. I will never forget your kindness.

My sincere thanks are once again due to my supervisor Prof. Danny for joining me on fieldwork and providing me with financial assistance for my field visits. Finally, I would like to thank my Dad David Joseph, and my family for their encouragement,

support and prayer over the last four years. Above all, I am grateful to the Lord Almighty who is my source of strength.

Dedicate to my parents Mrs Helena Johannes and Mr David Joseph

“Let the b-pressure go up, it will surely come down”

Publications arising from the thesis

This thesis is presented as a collection of papers and chapters. The Supplementary information is presented at the end of each paper/chapter. The reference list and appendices are presented at the end of the thesis. The analytical codes of the thesis have been written in R and Google Earth Engine (Appendix B), and the substantial codes will be uploaded to GitHub. Details and the current status of each paper are shown below:

Remote sensing for monitoring tropical dryland forests: A review of current research, knowledge gaps and future directions for Southern Africa

Chapter 2 is published by *Environment Research Communications, DOI: https://doi.org/10.1088/2515-7620/ac5b84*

Chapter 2 is also published as a policy brief by n*8agrifood for policy makers, https://policyhub.n8agrifood.ac.uk/activity/rapid-evidence-synthesis-training/, DOI: 10.5281/ZENODO.5566492*

The estimation of above ground biomass is improved by combining Sentinel-1 SAR and Sentinel-2 multispectral imagery in the dryland forests of Southern Africa.

Chapter 3 is published in Remote *Sensing of Environment: DOI: https://doi.org/10.1016/j.rse.2022.113232*

Identifying and understanding dryland forest changes and disturbances in Southern Africa using Landsat and MODIS time series and field vegetation data

In progress: Intended for submission to *International Journal of Applied Earth Observation and Geoinformation*.

A spatio-temporal drought and fire analysis for semi-arid dryland ecosystems in southern Africa using moderate resolution satellite imagery.

In progress: Intended for submission to *Remote Sensing in Ecology and Conservation.*

TABLE OF CONTENTS

LIST OF FIGURES

Chapter 1

Chapter 2

Chapter 3

Chapter 4

Chapter 5

Supplementary Figures

LIST OF TABLES

Chapter 2

Chapter 3

Chapter 4

Chapter 5

Supplementary Tables

1 INTRODUCTION AND RESEARCH CONTEXT

1.1 Background and Motivation

Tropical forests play an important role in global carbon storage and are therefore an important natural component of climate change mitigation (Baccini et al., 2017). Tropical dryland forests (TDFs) make up ca. 40% of all tropical forest region, however, they are facing threats both from human-induced and natural factors (Murphy et al., 1986). During the 20th century, substantial change in TDFs through land-cover conversion and modification has been unprecedented throughout Sub-Saharan Africa, resulting in loss of forest biodiversity and land degradation (Eva et al., 2006; Petheram et al., 2006). Brink et al. (2009) noted that the greatest amount of deforestation in Africa is taking place in dryland forests, accounting for about 70% of forest loss between 1975 and 2000 compared to moist tropical forest loss which accounted for 16% of forest loss. Deforestation in Southern Africa is a major concern, with ca. 1.4 million ha of net forest loss annually, contributing to increased land degradation and the ensuant impacts on the balance of ecosystem function (Lesolle, 2012). According to Intergovernmental Panel on Climate Change (IPCC), these changes have impacts on carbon emissions to the atmosphere and forest biodiversity loss, reducing the region’s adaptive capacity and resilience to the impact of high temperatures and varying precipitation (IPCC, 2014).

Tropical countries are beginning to develop policies and initiate projects to reduce greenhouse-gas emissions from deforestation and forest degradation (e.g., REDD+), seeing forests both as environmental resources and carbon sinks (Gibbs et al., 2007; UNCCD, 2015). For these, resource managers, stakeholders, governments, and United Nations (UN) agencies need high-quality reliable information on biomass carbon stocks, forest structure, and the REDD+ -related research in TDFs monitoring (Gizachew et al., 2017; UNCCD, 2009). Recently, the UN called for all to mobilise to deliver 17 Sustainable Development Goals (SDGs) by 2030, including the aim to ensure the conservation, restoration, and sustainable use of forests (SDG 15; UN, 2015). These objectives require the ability to localise, measure, and monitor forest change at both community and regional levels.

The UN argues that to mitigate climate change and biodiversity loss, and to stop degradation and deforestation processes, action must be taken at all levels: people, local, regional, global, and by all countries: poor, middle-income, and rich (UN, 2011). Recently, ecologists have embraced remote sensing to study forest change and biodiversity and have used this to prepare conservation responses to potential threats (Schulte to Bühne & Pettorelli 2018; Dawson et al., 2016). However, remote sensing in tropical forests faces challenges including accessibility to and/or the suitability of different remote sensing data; methods for relating vegetation structural changes to remotely sensed proxies across different ecosystem types; and access to suitable data for validating the estimates of forest changes to detect trends in dryland forests (Lehmann et al., 2015; Privette et al., 2005).

This study was designed and undertaken to further understand the large-spatial and temporal-scale variation of dryland forests dynamics, focussing on the development of an integrated assessment method for use in the context of climate change. In line with the multiple threats forced by climate change and anthropogenic activities, and the challenges of using remote sensing in these landscapes, this research examined these issues in Kavango Zambezi Conservation Area (KAZA) in Southern Africa. This focus constitutes the research gap that this study addresses, by assessing and estimating forest biomass and structural parameters, fire, and climatic impacts at a regional scale using novel application of remote sensing.

This chapter introduces with fundamental aspects of the research problem and aims to demonstrate the appropriateness of remote sensing as the best tool to address fundamental questions about changes in dryland forests.

1.2 Conceptual frameworks

Many of the unique properties of TDFs relate to their rainfall regimes. TDFs are characterised by prolonged dry seasons of six months or more, with rainfall less than 100 mm, which in turn determines the distinctive phenology of the forest

(Murphy et al., 1986). The definition of "dryland forest" remains debatable and controversial, which contributes to be difficulty in accurately assessing and measuring its distribution patterns and status (Blackie et al., 2014). The lack of a clear and comprehensive understanding of general terms including "drylands" and "forests" makes it a challenge to explicitly define dryland forests (Charles-D et al., 2015). Given the fact that dryland forests progressively grade into other vegetation types such as wet forests, woodlands and savannas, also makes clear definitions complex (Putz et al., 2010). Walter et al. (1971) noted that the accuracy of estimates of all tropical forest areas is constrained by uncertainty in the distribution of open woodlands in dryland areas, which are extensive in Africa, Australia, and Latin America.

In the general literature, many different names have been applied to TDFs, including savanna forests, Sudanian woodland and miombo woodland in Africa, monsoon forest in Asia, neotropical dry forests in South America (Chidumayo, 2013; Linares-Palomino et al., 2011; Suresh et al., 2011). The neotropical dry forests in South America have a plethora of names from "caatinga" in northeast Brazil, to "bosque tropical caducifolio" in Mexico, and "cuabal" in Cuba, which in part hinders comparisons (Mayes et al., 2017; Sánchez-Azofeifa et al., 2005). For example, Dexter et al. (2015) identified dry deciduous forest in India (Suresh et al., 2011), miombo woodland in southern Africa (Chidumayo, 2013), and deciduous dipterocarp forest in continental Asia (Bunyavejchewin et al., 2011) as a form of savanna, and not TDFs, despite the formal classification as TDFs by these studies, and the FAO (FAO, 2001).

There are several definitions currently available for TDFs, but there is still a lack of consensus in developing a common understanding. Mooney et al. (1995) defined TDFs as forests occurring in the tropical regions characterised by pronounced seasonality in rainfall, where there are several months of severe, or even absolute drought. A widely accepted definition is that of the FAO, that has identified TDFs as a Global Ecological Zone (GEZ), which includes the drier type of miombo and Sudanian woodlands, savannah (Africa), caatinga and chaco (South America), and dry deciduous dipterocarp forest and woodlands (Asia) (FAO, 2001). Sánchez-Azofeifa et al. (2005) broadly defined TDFs as a vegetation type typically dominated by deciduous trees (at least 50% of trees present are drought deciduous), where the mean annual temperature is ≥ 25 °C, total annual precipitation ranges between 700 and 2000 mm, and there are three or more dry months every year (precipitation < 100 mm per month).

For the scope of this present study, TDFs are defined as forests occurring in tropical regions which include the drier type of miombo and Sudanian woodlands, savanna forests (Africa), caatinga and chaco (South America), and dry deciduous dipterocarp forest and woodlands as defined by FAO (see: Fig. 1.1). The thesis adopted the definition of FAO because it recognises forests occurring in the dry tropical climate globally, then those based entirely on climate definitions. The current climate does not define the biogeography of TDFs, particularly in the context of future unprecedented climate change (IPCC, 2007). If climates become sufficiently warmer and drier in the tropics, dry forests may expand into areas that are currently dominated by rain forests (Putz et al., 2010). The research however acknowledges the diverse definitions and views of different researchers on the topic, such as those pointed out by Dexter et al. (2015) and Murphy et al. (1986).

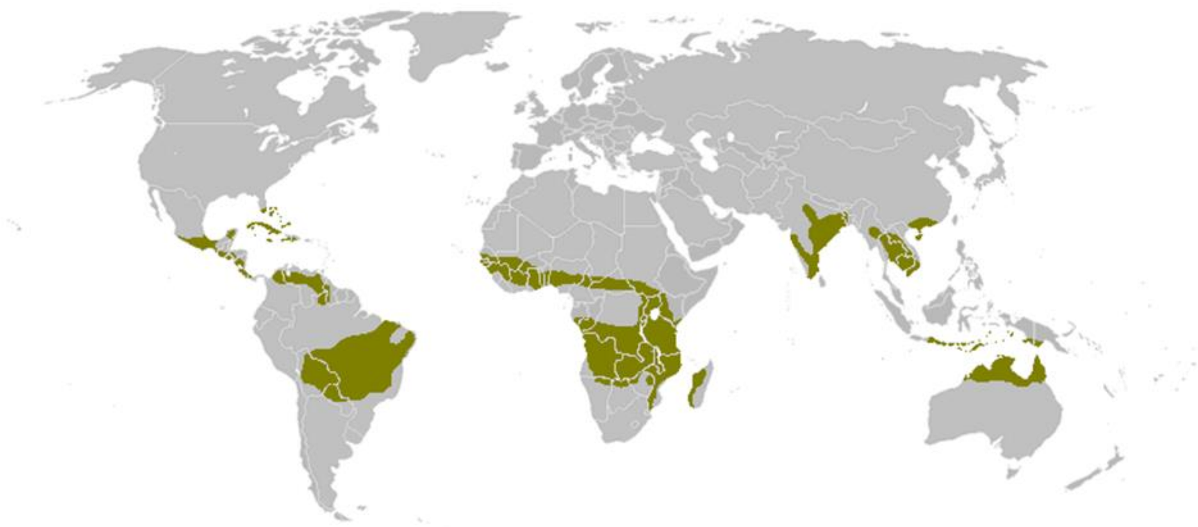

Fig. 1. 1 The graphic illustration shows the relative distribution of tropical dry forests. Source: FAO, (1999). Reproduced with permission.

1.3 Importance of dryland forests

TDFs provide ecosystem services to more than two billion people, including providing habitat for numerous rare and endemic organisms, supporting significant crop production, and forage for wildlife and domestic livestock (Petheram et al., 2006). The dryland ecosystem (including dry forests) harbors considerable biodiversity in terms of species richness, endemism, and functional diversity of plants and animals that sometimes even exceeds that of moist forests (Pennington et al., 2018). Furthermore, TDFs are known to play an important role in supporting the agricultural systems on which millions of rural subsistence farmers depend, and so TDFs are central to achieving broader food security (Chidumayo et al., 2010; Sunderland et al., 2015).

Beyond subsistence farming, TDFs contribute to the direct and indirect provision of various products, including timber and non-timber products to their inhabitants (Petheram et al., 2006). Other ecosystem services provided include flood control, tourism revenue, pollination, local diets with wild fruits, bushmeat, and medicinal plants (Djoudi et al., 2015; Safriel et al., 2006). In dry forested regions, majority of people use firewood and charcoal from TDFs as a source of energy (Sunderland et al., 2015). Drylands have major global climate benefits; their carbon storage (including soil carbon) accounts for more than one-third of global stocks (Durant et al., 2012; Pennington et al., 2018). The capacity to store carbon depends on many factors including climate, past land use, and opportunity for management change (UN, 2011). Growing pressure on dryland forests to meet human and socioeconomic development needs means that TDFs are increasingly being utilised unsustainably, and so the degradation of these resources poses a serious problem (Petheram et al., 2006).

1.4 Threats to tropical dryland forests

1.4.1 Degradation/Deforestation

For more than 20 years, TDFs have been recognised among the world's most threatened ecosystems when compared across all major tropical forest types

(Janzen, 1988). These activities may take place either abruptly (land cover conversion) or gradually (land cover modification) (Hayward et al., 2001; Lambin et al., 2003). Land cover conversion is defined as a shift from one land cover class to another, whilst modification is subtle changes in continuous properties within classes (e.g., plant biomass, canopy cover, leaf area) (Hansen et al., 2012). Human activity causes deforestation through logging of timber and clearing of the forest where extraction exceeds regeneration.

Land degradation, which is sometimes used synonymously with desertification in dryland areas, is a term that refers to the many processes that drive the decline or loss in biodiversity, ecosystem functions or productivity (Scholes et al., 2018). Land degradation includes the degradation of all terrestrial ecosystems (e.g., dry land, semi-arid land, rain-soiled areas in sub-humid areas or grassland, rangeland, forest, and wetland) (Xie et al., 2020). Forest degradation is land degradation that occurs within forest land and is most often loosely defined as a loss of particular forest attributes that negatively affect the structure or function of the stand or site (IPCC, 2003; ITTO, 2003; Scholes et al., 2018; Simula, 2009). Lund, (2009) provides a detailed review of more than 50 definitions of forest degradation. FAO, (2011) defines forest degradation as the change process caused by natural disturbance, and human-induced that leads to the reduction of the capacity of a forest to provide goods and services. Services might include biomass, carbon sequestration, water regulation, soil protection, and biodiversity conservation. According to Simula, (2009) land degradation acts synergistically with forest degradation. Figure 1.2 shows degradation thresholds which shows that degradation can usually be reversible through restoration and management interventions. On the other hand, degradation is sometimes long-term or permanent leading to the irreversible loss of forest (Lund 2009). As shown in Fig. 1.2, it’s considered forest degradation when there is a reduction of the canopy cover or carbon stock within a forest, provided that the canopy cover stays above 10% (FAO, 2000). The status of degraded areas is distinguished in terms of the degree of degradation (e.g., slightly/moderately/severely degraded), as it could help identify priority areas for preventive or corrective action when monitoring changes. The ability to identify a degraded forest is essential to help develop techniques to establish systems for monitoring forest degradation and practical approaches to restore forest cover and structure, species composition and forest regeneration as well as rehabilitation (see: Fig. 1.2 and 1.3) (Chazdon et al., 2016;). In this study, land degradation and vegetation degradation are used to describe degradation taking place in forests and non-forests, while forest degradation was used to refer to degradation largely taking place in forested areas.

Biggs et al. (2008) reported that degradation of dryland landscapes in Southern Africa happen through alteration of intact ecosystems, for example, the fragmentation of habitats, the modifications of forests to pasture, and conversion of extensive land uses to intensive ones, causes a severe loss in biodiversity. Forest degradation has been described using variables such as changes in canopy cover, understory tree density, plant or animal species richness, biomass loss from extensive standing forests, and changes in vegetation attributes as measured against a baseline undisturbed condition (Thompson et al., 2013; Washington-Allen et al., 2008). These changes can be caused by natural disturbance such as wildfire, storms or drought, and also can be human-induced such as via harvesting, road construction, poor agricultural practices, or grazing, which may each vary in extent, severity, and frequency. While deforestation is the rapid transformation from forest to the non-forest area, forest degradation is usually a gradual process though it may be induced by quick, single events such as hurricanes, and it is typically more difficult to discern and quantify than deforestation (Thompson et al., 2013).

These alterations in land-cover/land-use could also impact global and regional climate through alterations in the length of the growing seasons, changes in the climatic regimes, including extreme high temperatures or rainfall, and increases in perturbation regimes such as fires, which in turn impact the structure and function of the dryland forest (Le Houérou, 1996; Naik, 2015). Along with deforestation, forest degradation contributes to global carbon emissions, and reporting on both is required by the United Nations Framework Convention on Climate Change (UNFCCC) through incentives for developing countries through the REDD+ programme (UNFCCC, 2009).

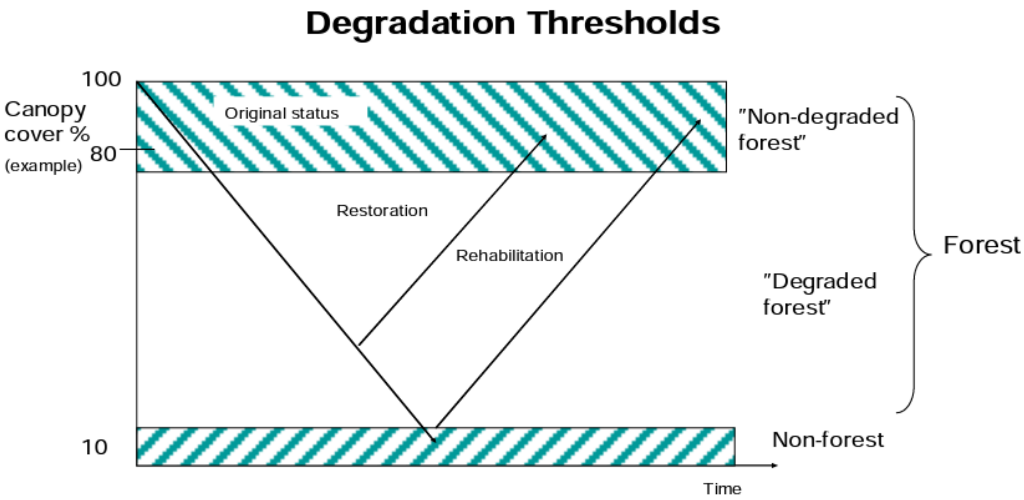

Fig. 1. 2 Illustration of the degradation thresholds within forest and non-forest typically caused by disturbances which vary in terms of the extent, severity, quality, origin, and frequency (Simula, 2009).

1.4.2 Climate and drought

TDFs are known to be extremely vulnerable to predicted changes in climate (Huang et al., 2017), and the effects of these changes are already being experienced in biodiversity showing significant shifts in species ranges in Africa (McClean et al., 2005). There is now abundant evidence from models and observations that suggest rainfall regimes in the seasonal tropics are changing to hotter and drier conditions, with predicted elevated temperatures (Chadwick et al., 2016; Dai, 2013), likely exacerbating the risk of further land degradation (Huang et al., 2016). Dryland CO2 uptake is strongly associated with variations of both precipitation and temperature, and changes in aridity. The effectiveness of each is impacted by deforestation, widespread increases in plant disturbances, and declines in ecosystem function (Williams et al., 2013). Dryland vegetation responses to environmental perturbations depends upon the frequency and magnitude of disturbances (e.g., temperature, precipitation, fire, land use), and the resilience of the ecosystem concerned (see: Fig. 1.2) (Lambin et al., 2010).

African dryland forests are identified as the most threatened and least protected ecosystem on the continent, largely as a result of population growth, climate change, and poor environmental governance and policy frameworks (Brink et al., 2009). The IPCC reported that when climate threats are coupled with a growing population and future changes in land use could lead to severe dry forest biome shifts and biomass degradation, particularly in Southern Africa (King, 2014; Niang et al., 2014). The role of climatic variation, land-use practices, and disturbance regimes, such as herbivory, has been identified by several studies to be among the main drivers of ongoing changes in dryland ecosystems leading to forest degradation and land cover change in Southern Africa (Fig. 1.3) (Anyamba et al., 2002; Prince, 2012; Privette et al., 2005; Shackleton et al., 2010). Biodiversity in the region has responded with significant recorded shifts in species ranges, impacting species composition and productivity (IPCC, 2014; King, 2014). Given that the availability of water is a determinant of forest resources in drylands, these types of change affect forest tree cover, demographic processes, biological diversity, trait composition, habitat quality, and in turn movements of wildlife (Naidoo et al., 2016). Fig. 1.3 provide a schematic representation of factors controlling temporal and spatial heterogeneity of biomass plants. This schematic is not exhaustive but provides a framework of changes in vegetation land cover and main dryland forest attributes, i.e., composition, structure and function, which is addressed in this research. This thesis report on the development of open access codes to map forest structural parameters such as biomass and monitor changes in dryland forests because of climate change and other disturbances such as fire/logging. The changes are mapped using a combination of ground and Earth observation data including multispectral and synthetic aperture radar (SAR) satellite imagery at a regional scale of Kavango Zambezi region.

On a regional level, few studies have evaluated the forest structural parameters and changes in dryland forests of Southern Africa (David et al., 2022a). Majority of these studies are done in Republic of South Africa, for example, Mathieu et al. 2013 and Naidoo et al. (2015) found in dryland forests in Kruger National Park that Woody vegetation cover is accurately mapped with Synthetic Aperture Radar (SAR) data, however these studies observe an overestimation of woody cover below 20% as a results of surface contributions to the signal, such as roughness in radar retrievals (Mathieu et al. 2013; Santoro et al. 2011). There is, however, very limited spatial information on structural parameters such as above ground biomass distribution and forest changes in other part of Southern Africa. To date in most of Southern Africa, most quantitative spatial data on forests are available from products developed globally, such as the pantropical African savanna biomass map (Bouvet et al., 2018), tree density map (Glick et al., 2016), global forest height map (Simard et al., 2011), Global Land Cover Map (Arino et al., 2012), and global tree cover maps (Hansen et al., 2013; Sexton et al. 2013). However, there is unreliability regarding the accuracies of these maps at regional scales, particularly in open forest ecosystems such as savannas and dry forests, because these products were developed primarily to track tropical forest losses (Bastin et al., 2017). Underestimation for the woody cover above 60% has been observed likewise in other studies (Bouvet et al. 2018) because of saturation in dense canopies.

To identify changes to dryland forest, and their drivers, and to separate these from long- and short-term trends, it is essential to select remote sensing data with good temporal coverage (time series data) but also with a sufficiently frequent revisit period and spatial resolution. This is however not an easy task, since the availability of remote sensing data for long-term monitoring purposes is constrained by sensor characteristics (e.g., revisit time) and then the data utility can be significantly influenced by environmental factors (e.g., cloud cover) (Donoghue, 2000; Kuplich et al., 2013).

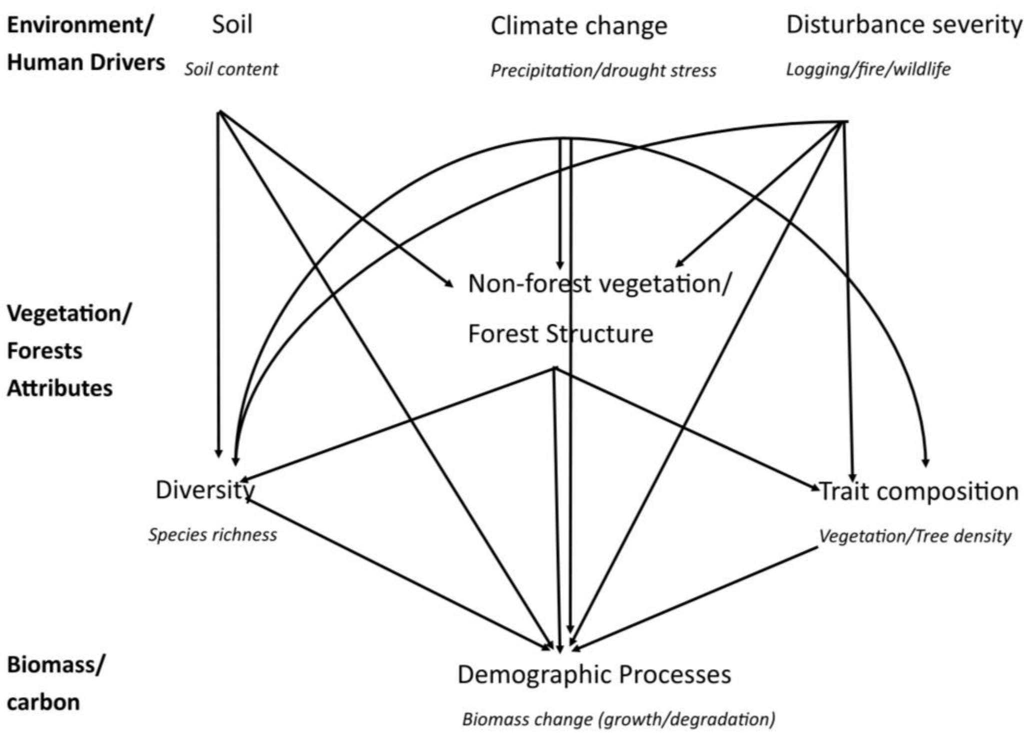

Fig. 1. 3 Conceptual framework depicting the key abiotic factors (disturbance and soil resource availability) and biotic factors (vegetation/forest structure, diversity, and trait composition) controlling temporal and spatial heterogeneity of demographic processes (biomass growth, and degradation). Physical damage by wildfire, mega-herbivores, e.g., elephants, and deforestation e.g., logging/coppicing are one of the main disruptions to the ecosystems. Forest structure (e.g., plot basal area, tree density) is based on all alive trees in the selected plots, while diversity and trait composition are based on the individuals of that demographic group (i.e., vegetation recruits). The dryland forests ecosystem has an option of closed woodland form and open grass form depending on the soil resource availability, climate, disturbances, and anthropogenic disruption e.g., fire. (Reproduced from Van-der-Sande et al., 2017).

1.5 Application of remote sensing

1.5.1 Optical and Synthetic-Aperture Radar (SAR) remote sensing in dryland forests

Remote sensing has contributed greatly to the mapping and understanding of the tropical forest ecosystems in relation to local and global environmental change

(Foody, 2003). Advances in the remote detection of burned areas (Zhang et al., 2011), land-use and land-cover (De Oliveira et al., 2019), forest structure (Hyde et al., 2006), biomass (Cutler et al., 2012) and biodiversity (Rampheri et al., 2020) have also changed the understanding with regards to forest functioning. From the TDF resources perspective, satellite remote sensing has been used to provide three levels of information. The first is information on the spatial extent of forest cover and forest change patterns; the second level comprises information on forest type; and the third provides information on the biophysical and biochemical properties of forests (Boggs, 2010; Higginbottom et al., 2018; Wood et al., 2012). Several studies have established the many advantages of remote sensing over traditional field investigation methods for measuring and monitoring tropical forests (Hyde et al., 2006; Puhr et al., 2000). The most obvious advantages include the potential to survey large areas rapidly or over longer periods at low cost, especially in remote, inaccessible, and sometimes dangerous environments (Rumiano et al., 2020).

In general terms, Earth Observation (EO) platforms have carried two types of sensor: optical and active SAR. The optical systems measure reflected radiation of one or more discrete wavelengths located in the spectral range 400–3000 nm, wherein the wavelengths are notably several orders of magnitude smaller than the leaves, needles, and branches that make up a forest canopy, and so these components absorb and scatter radiation (Boyd et al., 2005). Synthetic-Aperture Radar (SAR) systems measure backscattered microwave radiation at wavelengths between 1 cm and 1000 cm, characterising scattering from leaves, branches, stems trunks and the ground (Mitchard et al., 2009). Optical remote sensing systems may provide information on the amount of foliage and its biochemical properties, while SAR (microwave) systems provide information on woody biomass and forest structure (Armston et al., 2009; Higginbottom et al., 2018). Many SAR sensors can both transmit and receive microwaves with two different polarisations, which enhances the information provided, particularly that which describes surface roughness and geometric regularities in the forest stand (Kasischke et al., 1997). Therefore, satellite remote sensing signals provide additional proxy information that can be linked to forest parameters and health indicators, as well as disturbance factors when using vegetation indices.

1.5.2 Vegetation Indices

In satellite remote sensing for forests, vegetation indices, biophysical variables, and data transformations are often used for data analyses (Morley et al., 2019; Yengoh et al., 2015). The various materials of the earth's surface absorb and reflect different amounts of energy at different wavelengths. The magnitude of energy that an object reflects or emits across a range of wavelengths is called its spectral response pattern (Aggarwal, 2004). The graph below illustrates the spectral response patterns of soils, water, and vegetation (Fig. 1.4). The healthy vegetation has a unique spectral reflectance signature that is dictated by various plant attributes. The visible reflectance of plants is mainly characterised by absorption of the leaf pigments like chlorophyll, carotenoids and xanthophylls (Gibson et al., 2013). Stressed vegetation will give off a different spectral signature corresponding to the effect of the stress on the various leaf pigments. Knowing the typical spectral response characteristics makes it possible to distinguish forests, crops, and soils, and to evaluate their condition (e.g., stressed plants) using remotely sensed images (Ranjan et al., 2012). In the case of vegetation, the measured spectral reflectance values from two or more wavelengths are usually used to estimate vegetation indices. NDVI is one of such indices, commonly used to distinguish live green plant canopies, calculated as a ratio of near-infrared to red vegetation reflectance (Rouse, 1974; Tucker, 1979). NDVI has been used as a proxy of vegetation greenness and has been shown to relate closely to leaf area index (LAI), biomass, and the fraction of photosynthetically active radiation absorbed by vegetation (fAPAR) (Curran, 1980).

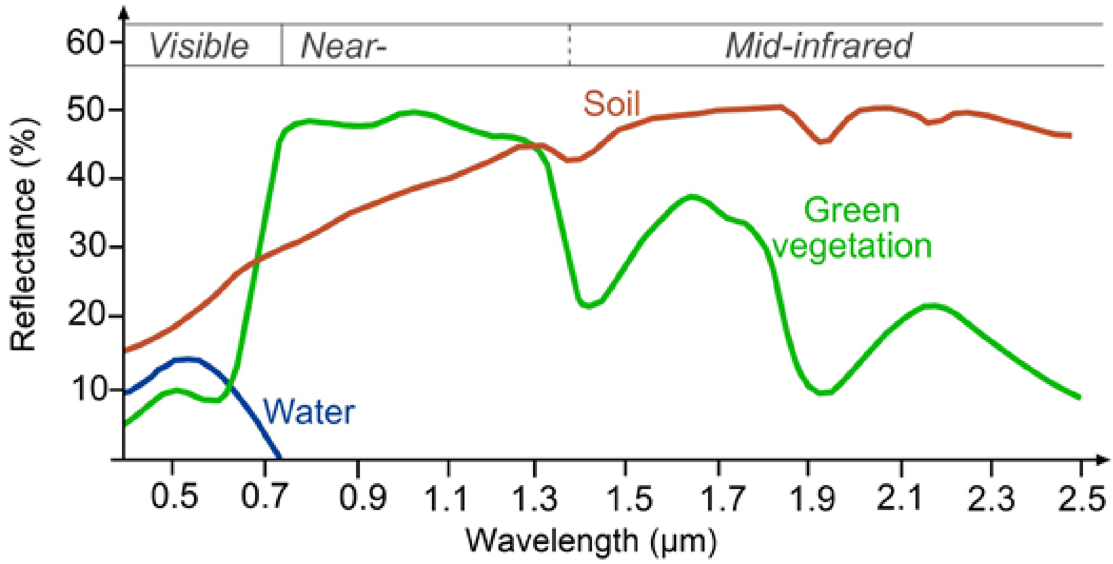

Fig. 1. 4 Spectral signatures as functions of wavelength for vegetation, soil and water. Source: https://seos-project.eu/classification/classification-c01-p05.html/ (accessed 02 May 2021).

Ringrose et al. (1994) and Turner et al. (1999) indicate that the strength of the relationships between forest LAI and vegetation indices, such as the NDVI, is site-, time- and species-specific and that above a LAI of about 5 or 6, NDVI may not be sensitive to LAI variation. Several well-known limitations of NDVI for robust estimation of biomass in drylands exist. NDVI is sensitive to green components and insensitive to woody components where the majority of carbon is stored (Tucker, 1979). Also, Above Ground Biomass (AGB) production is not always uniformly linked to either greenness or plant structure (herbaceous and woody compositions), as moisture content and vegetation species composition have been shown to impact the biomass-NDVI relationship (Asner et al., 2009; Wessels et al., 2006). These observations may help explain reportedly weak relationships between NDVI and tropical forest canopies, particularly for areas with complex and high vegetation amounts as in TDFs (Foody et al., 2001; Sader et al., 1989). For example, Madonsela et al. (2018) investigated the interactions between seasonal NDVI and woody canopy cover in the savanna of the Kruger National Park (NP) to model tree species diversity using a factorial model and found that the interaction between NDVI and woody canopy cover was insignificant. It is also widely reported that the NDVI signal is influenced by woody canopy foliage, underlying canopy background, and soil moisture in sparse vegetative areas (LAI <3), which reduces the apparent NDVI signal and seasonal variations in vegetation phenology (Pettorelli et al., 2005; Wagenseil et al., 2006).

These challenges have led to the development of alternative formulations which include correction factors or constants introduced to account for or minimise, the varying background reflectance (Gitelson et al., 1996; Huete et al., 1999). The Enhanced Vegetation Index (EVI) is a modification of NDVI that provides complementary information about the spatial and temporal variations of vegetation while minimising many of the contamination problems present in the NDVI, such as those associated with canopy background and atmospheric influences (Huete et al., 2002). Other closely related indices include the Simple Ratio (SR), the Green Normalised Difference Vegetation Index (GNDVI), Soil-Adjusted Vegetation Index (SAVI) amongst others. Xue et al. (2017) provides a detailed review of vegetation indices. Critically, an increase in availability of EO data with improved spatial, spectral, and radiometric resolution combined with the machine or deep learning techniques and development in computational resources would enhance the potential dryland forest information to be exploited (Ali et al., 2015). The constraint in spectral, spatial, and radiometric resolutions of remote sensing data may result in different saturation values of AGB depending on vegetation characteristics (Zhao et al., 2016). The spatial resolution of images such as NOAA AVHRR, SPOT Vegetation, and MODIS imagery data particularly at 1-8 km spatial resolution has been reported to result in poor spectral purity and limited identification of broad forest types such as coniferous and lack sufficient spatial details, particularly for less abundant species broad-leafed forests (Immitzer et al., 2018; Xu et al., 2021). Stratoulias et al. (2015) showed that the 10 m spatial resolution of Sentinel 2 allows for detecting fragmented patches in the lakeshore ecosystems but argued that enhanced spectral and spatial capabilities provide further potential in habitat monitoring and classification of environmentally complex areas. Other studies such as Wulder et al. (2004) and Xu et al. (2021) concluded that medium-high resolution Earth observation satellites can be used to produce more accurate results of forest species composition and land cover use classification by providing detailed spectral features of the canopy of tree species (Salajanu and Olson, 2001). Dube et al. (2014) have concluded that fine spatial resolution data with improved spectral bands (e.g., red edge) contains more spectral information critical for accurately predicting forest metrics such as biomass in South Africa. Other remotely sensed studies estimated forest biomass at different scales and concluded that coarse spatial resolution optical sensors are useful for biomass mapping at continental and global scales rather than at local scales because the limited spatial detail of these coarse-resolution images misses the biomass variability in heterogeneous forests (Avitabile et al., 2012; Dube et al., 2014; van der Wer et al., 2006; Zhang and Kondragunta, 2006; Zhu and Liu, 2015). Lu (2006) demonstrated that the use of coarse spatial resolution sensors (i.e., Landsat, MODIS etc.) for AGB estimation resulted in poor prediction accuracy due to the presence of mixed pixels together with a mismatch between the size of field measurements and the pixel (Avitabile et al., 2012). Various statistical methods, vegetation indices and textures have been explored to reduce the impacts of data saturation in Landsat imagery on AGB estimation accuracy (Lu et al., 2016). Studies such as Basuki et al. (2013) and Kajisa et al. (2009) observed that the application of statistical methods, spectral mixture analysis and integrating radar data with Landsat images improves forest AGB estimation accuracy significantly. Time series of Landsat imagery is another alternative explored that can result in more accurate AGB estimation and reduce saturation effects compared to the use of a single NDVI (Gasparri et al., 2010; Zhu and Liu, 2015).

1.5.3 Forest biomass and structural parameters

1.5.3.1 Forest biomass estimation in dryland forests

Biomass, in general, includes the above-ground and below-ground living mass, and is usually expressed as dry weight (Lu, 2006). AGB includes all living biomass above the soil surface that includes the stem, stump, branches, bark, seeds, and foliage. Measuring forest biomass and its change acts as an indicator of climate change and forest health (Pause et al., 2016), however, the majority of studies on biomass have focused on boreal and temperate forests (Dong et al., 2003; Naidoo et al., 2006). Studies on TDFs are limited because they are dynamic with complex species composition and structure, coupled with environmental conditions which are difficult to assess and model (McElhinny et al., 2005). AGB estimation requires field measurements as a prerequisite for developing estimation models, but field measurements are often difficult to implement, especially in remote areas (Lu, 2006; Wingate et al., 2018), and they cannot provide the spatial distribution of biomass across large areas. Thus, remote sensing techniques offer the most practical approach to estimating dryland forest biomass and monitoring changes in forest structure, overcoming the limitations of sample size, timeliness, expense, and access (Lu, 2006; Lucas et al., 2015).

With increasing concern regarding greenhouse gas emissions, there is a need to better quantify the biomass of forests associated with regeneration and clearance (FAO, 2011; UN, 2011). Such information needs to be obtained at scales ranging from entire regions to individual forest stands (e.g., for carbon accounting purposes). However, assessments of biomass are typically obtained by applying species-specific allometric equations to forest inventory data (Chave et al., 2005). Although many studies have investigated the ability to estimate the biomass of forests, including tropical moist forests (Asner et al., 2009), dryland forests (Gizachew et al., 2016), temperate forests, and boreal forests (Dong et al., 2003) from remotely sensed data, a number of problems have been encountered. Of key concern is the generalisation of relationships derived for the accurate prediction of biomass at a specific location or time period (e.g., generalisation between images of one location acquired over a period of time to estimate characteristics at another location) (Woodcock et al., 2001). This problem is common in less well studied ecosystems such as dryland forests and can substantially limit the contribution remote sensing can make to environmental studies. Overall, regional variations in forest biomass arise as a result of differences in tree stem density, growth and disturbances rates, and other species-specific attributes, such as wood density (Asner et al., 2009).

1.5.3.2 Application of optical and SAR sensor in forest biomass

Different remote sensing sensors have been successful in forest biomass studies (Gizachew et al., 2016; Powell et al., 2010). However, in the tropics, where the cloud cover is common, optical data could not be used over large areas. Optical sensors are also less sensitive to variations within dense forests, and can only provide spectral and horizontal distribution and not the vertical distribution (e.g. tree height or difference between single-story and multi-story vertical structural classes) of canopy elements in forests (Joshi et al., 2016). Under these conditions, radar remote sensing provides an alternative (Michelakis et al., 2014; Paradzayi et al., 2013). SAR has the advantage that it includes: the ability to collect data in all weathers, and during day and night; the sensor penetrates cloud, vegetation, dry soil, sand, dry snow; the data is sensitive to surface roughness, dielectric properties and moisture content; and the reflected signal is sensitive to polarisation and frequency (HH, VV, HV, and VH), and can be used for volumetric analysis (Balzter, 2001; Mitchard et al., 2009). However, radar remote sensing also has limitations including uncertainties in estimation, expensive datasets, difficulties in data processing, and data saturation problems (Balzter, 2001; Mitchard et al., 2009). Furthermore, Light Detection and Ranging (LiDAR) has become popular for deriving tree height variables closely related to the AGB (Unger et al., 2014), and a few studies have combined optical and LiDAR for AGB mapping (Lu et al., 2012). However, the applicability of this technique is limited to local regions because of its high economic costs and labour-intensive collection (Gibbs et al., 2007). Alternatively, other authors have explored the combination of optical and SAR (e.g., Cutler et al., 2012; Wingate et al., 2018). Combining frequently available SAR observations with less frequent (due to cloud cover) optical remote-sensing data may provide a sound information source in the tropics, but there remain few studies of this nature in tropical dryland forests.

Accurate delineation of biomass distribution at scales from local (ca. 1 x 10-1 km) to pantropical is significant in reducing the uncertainty of carbon emissions and sequestration, understanding their roles in influencing land degradation, and wider environmental processes (Foody, 2003). However, the lack of spatially explicit maps of biomass and forest structural parameters over dryland forests areas in Southern Africa is one of the largest sources of uncertainty in estimates of carbon emissions (Midgley et al., 2011; Timothy et al., 2016). With regards to tropical forests, forest biomass and structure are often relatively well studied in the tropical rainforests as compared to dryland forests, but rainforests are progressively shifting to TDFs, especially in South America and Africa, often irreversibly because of fire events (Zhao et al., 2021). This phenomenon justifies the importance of studying TDF carbon stocks.

1.5.4 The benefits and challenges of remote sensing in dryland forests

The development of the Earth observation satellites during the past decades has enhanced our ability to assess the status and dynamics of vegetation change as well as impacts of climate change at a large scale (Nicholson, 2011). In forest ecosystems, identifying changes in canopy cover with remote sensing generally requires data at frequent intervals because the spectral signature changes rapidly with regrowth. Optical sensors provide the best alternative for vegetation change mapping and biomass estimation to field sampling due to global coverage and repeatability, given the ability to estimate characteristics such as forest type and leaf area index (LAI) (Lu, 2006; Symeonakis et al., 2018). Such sensors are however limited in the degree to which they can generate structural information and are restricted by cloud occlusion which is particularly problematic in tropical regions (Herold, 2007; Symeonakis et al., 2018). Light Detection Ranging (LIDAR) and Hyperspatial data can observe tree crowns, basal area, tree height and biomass but cannot cover large areas (Falkowski et al., 2008, Blackburn, 2007). The selection of suitable satellite data depends on the ecological characteristics of the ecosystems, spatial and temporal scales of interest (Estes et al., 2018). As the region of interest and temporal extent increases, the volume of data, and the complexity of image-processing becomes significant and an obstacle to many researchers and operational users with limited access to high-performance computing infrastructures (Smith et al., 2019).

Due to the inherent trade-offs between spatial and temporal resolution in EO data, and geographic coverage, the vegetation patterns on both spatial and temporal domains have been revealed by various technological advances resulted in the growing availability of remote sensing data and methods (Toth and Jóźków, 2016; Zhou et al., 2020). The application of non-parametric machine learning regression algorithms, such as decision trees, random forests (RF), support vector machines (SVMs), and k-nearest neighbour have become more predominant and demonstrate the ability to outperform widely used parametric approaches, such as polynomial and multiple linear regression variables used with remotely sensed data in a forest environment (Breiman, 2001; Latifi et al., 2010). Non-parametric machine and deep learning models are sufficiently versatile to uncover complicated nonlinear relationships and able to extract combinations of the input data that are difficult to describe explicitly by humans, particularly, in areas with high structural variability such as dryland forests (Hastie et al., 2009; Shao et al., 2017). Machine and deep learning have been used by many remote sensing studies to provide in-depth forest investigation from the perspectives of hyperspectral image analysis, interpretation of SAR/ LiDAR images, interpretation of high-resolution satellite images and classification, and multimodal data fusion (e.g., the fusion of Hyperspectral, SAR, LiDAR and optical data (Guirado et al., 2020; Shao et al., 2017; Trier et al., 2018). Improved techniques in remote sensing such as Vegetation Indices, VOD, and machine and deep learning have been utilised to estimate dryland forest attributes globally and other dryland ecosystems, however, very few of these focused on the local and regional scale of Southern Africa (e.g., Symeonakis et al., 2020).

The uncertainties reported in many dryland forests studies relating to remote sensing (Bastin et al. 2017), could be decreased following further development, application, and comparison of these improved approaches in future works at local, regional, and continental studies in dryland forest ecosystems. It has been discovered that there is plausible trade-off between spatial resolution, image coverage and frequency in data acquisition, and many studies has shown that coarse spatial resolution optical sensors are useful for biomass mapping at national and global scale rather than at local scale (Wulder et al. 2004; Lu, 2006). For example, Dube et al., (2014) used spaceborne multispectral RapidEye sensor with a fine spatial resolution have the potential to satisfactorily predict intra-and-inter species predicting forest metrics, such as biomass in areas of closed and dense vegetation. The RapiEye have the capability to provide a better prediction for biomass because they contain more spectral information critical for vegetation mapping in comparison to the existing broadband multispectral images (Dube et al., 2014). The rise of innovative and high-performance computing facilities and web-based software tools such as Google Earth Engine (GEE) platform and growing use of machine learning algorithms helps to overcome many barriers, enabling large volumes of data to be integrated, processed, and analysed for large areas and over long time periods (Warren et al., 2015). For a detailed review of machine learning and deep learning for remote sensing and Sustainable Development Goals, see Zhu et al. (2017) and Holloway and Mengersen (2018). Also, more information on research trends, benefits, and challenges of remote sensing in dryland forests are provided in David et al., 2002a, (Chapter 2). Using the new advances in data management and cloud computing capabilities of Google Earth Engine led to a recent discovery that forests in drylands exceeds previous estimates by over 40% (Bastin et al., 2017).

1.5.5 Google Earth Engine platform

The Google Earth Engine (GEE) platform provides pre-processed satellite imagery, enabling large volumes of data to be integrated, processed, and analysed for large areas and over long time periods (Warren et al., 2015). The platform provides online access to extensive imagery including the entire Landsat archive, complete archives of data from MODIS, Sentinel-1 and Sentinel-2. GEE also co-locates climate forecast data, land cover data, and many other environmental and socioeconomic data covering much of the planet. All processing and computations are done on-the-fly in the cloud which allows the user to process data in close to real-time (Hansen et al., 2013). The catalogue is continuously updated, and users can request the addition of new datasets to the public catalogue, or they can upload their private data via a REST (representational state transfer) interface using either browser-based or command-line tools (Gorelick et al., 2017).

GEE's functionality affords a unique opportunity to overcome the limitations imposed by the volume of data and the scale of analysis that would otherwise prevent analysis in many organisations in tropical dryland regions (Hansen et al., 2013; Shelestov et al., 2017). Although GEE has removed many computational and analysis barriers, the technology is not yet comprehensive. The approach is still evolving and there are shortcomings around the challenges of completing analysis that would normally be better suited to a GIS environment, such as the intersection of raster- and vector-based datasets. This thesis has, therefore, utilised other analytical software such as R and ArcGIS since GEE allows files and data to be imported and exported for use elsewhere.

1.6 The world's largest conservation park

The Kavango-Zambezi Transfrontier Conservation Area (KAZA TFCA) was established in 2011 by its member states of Angola, Botswana, Namibia, Zambia, and Zimbabwe, with support from World Wide Fund for Nature (WWF) and the Peace Parks Foundation (WWF, 2016). KAZA TFCA is the World's largest transfrontier conservation area covering a land area of 519,912 km^2 (200,739 sq. mi, equivalent to the area of Spain or Thailand) (Murphy, 2008). About 71% of KAZA is protected to create economic development and conserve the unique biodiversity within the region, and only 29% of the land is not protected.

One key aim of KAZA is to connect and coordinate efforts across protected areas and create free movement for wildlife within its borders, without political boundaries hampering the ability to meet conservation objectives (Cumming, 2008). KAZA links several conservation areas including 20 protected national parks, 103 wildlife management areas, 85 forest reserves, 11 game management areas, 11 sanctuaries, and communal lands (Fig. 1.5) (Karidozo et al., 2016). The area hosts the largest population (ca. 250,000) of the African elephant, one quarter (25%) of the African wild dog population, amongst other wildlife, and a human population of 2,677,086 (Karidozo et al., 2016). The growing human population and increasing wildlife population in KAZA have given rise to human encroachment and increased human-wildlife conflict (Stoldt et al., 2020).

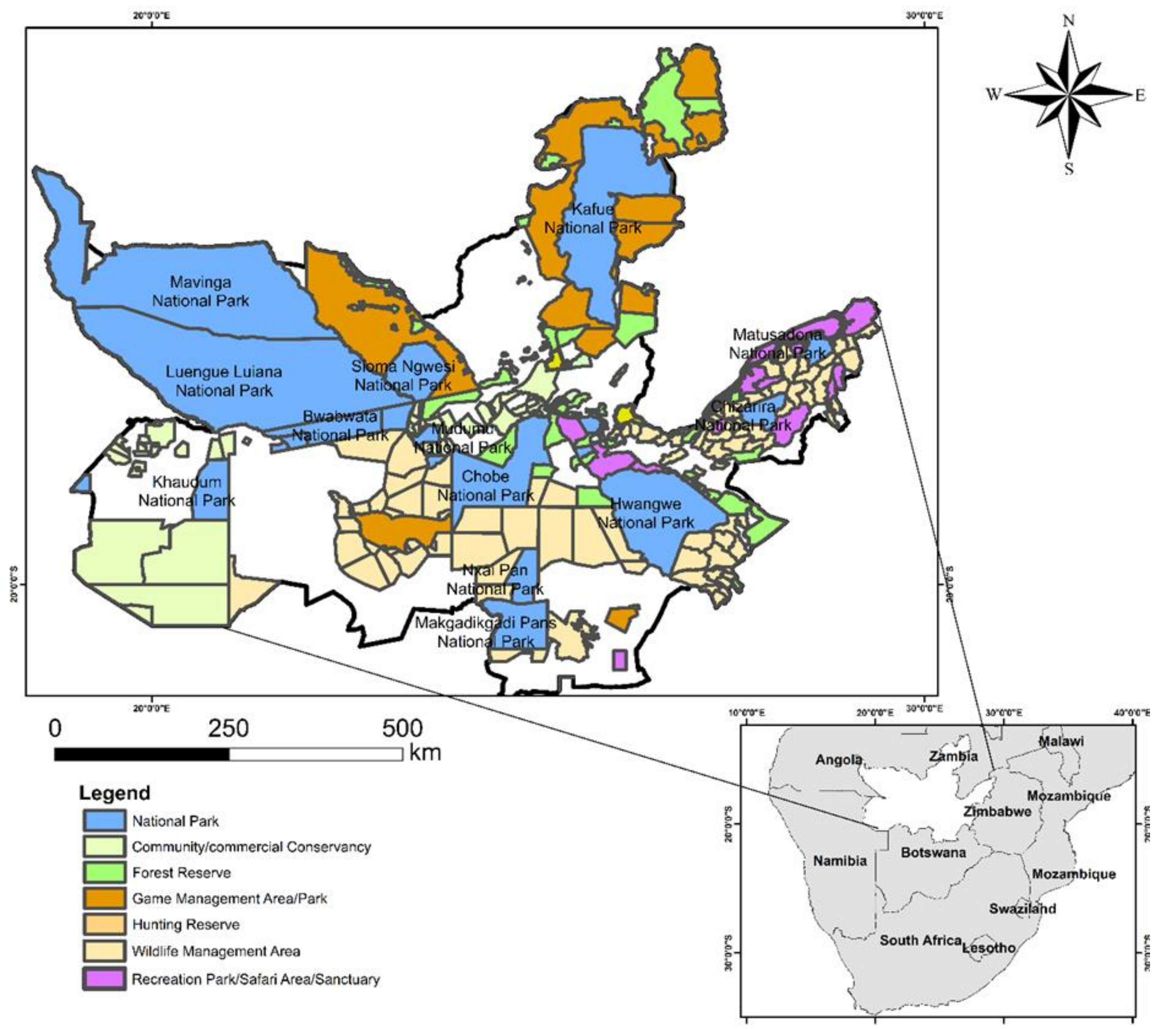

Fig. 1. 5 Map of the study area showing KAZA region in Southern Africa and the and land management classes as designated by the World Database on Protected Areas (WDPA).

1.6.1 Rationale of the study

It is important to acknowledge the inherent pressure on dryland resources from the perspective of the local population that depends on these ecosystems for livelihoods, even in the remote and protected areas of the KAZA region. The vegetation structure of KAZA consists of desert shrubs in the southwest, and dryland forest in the northeast, with Baikiaea, miombo, mopane, and acacia woodland species occupying by far the greatest portion of the area (Cumming, 2008). Within this region, forest loss and degradation are a major concern because TDFs are already severely degraded as a result of competing land use, and from overuse (Kamwi et al., 2020; Shackleton et al., 2010), as shown by field photos collected in 2019, from Namibia and Botswana (Fig. 1.6).

These changes do not only directly impact wildlife species distribution, but can also undermine efforts to maintain, expand and link wildlife populations and economic sustainability (Naidoo et al., 2016). Dryland vegetation in arid, semi-arid, and dry sub-humid areas of Southern Africa are highly sensitive because precipitation is scarce and typically more or less unpredictable, temperatures are high, humidity is low and soils generally contain small amounts of organic material (King, 2014; Meadows, 2006; Niang et al., 2014).

For KAZA, no large-scale study exists that provides spatially explicit and up-to-date information on both the protected areas and forests throughout the region, that also includes detailed information on forest biomass, vegetation density, fire and drought impact, and land degradation (Cumming, 2008). This hampers efforts to mitigate the threats against KAZA. For example, many species (flora and fauna) are identified as endangered or threatened and would almost certainly merit Alliance for Zero Extinction (ACE) ranking (IUCN, 2020). For example, the Baikiaea plurijuga (Zambezi Teak) is on the International Union for Conservation of Nature (IUCN) red list due to overexploitation through logging and fire damage in Zambia and Namibia. The Zambezi and Kavango East regions within KAZA have low levels of income and high levels of poverty and are the most heavily forested regions in Namibia (USAID, 2010). A large part of the Zambezi region's land surface is state-run protected areas, where there is an ongoing land-use pressure, agricultural expansion, and conversion of closed woodland into secondary woods and shrubs (Kamwi et al., 2015). Due to the remoteness of the area, wildlife dangers, and the fact that KAZA extends across international borders, continuous and in-situ field sampling to measure and assess vegetation characteristics is an effectively impossible and expensive task. With a view on time and expense, satellite remote sensing is therefore here considered as an appropriate methodology for measuring changes in the dryland of KAZA, building on a limited number of localised previous studies (e.g., Schultz et al., 2018). This study provides an initiative for a significant advancement in mapping the dryland forests using remote sensing technology.

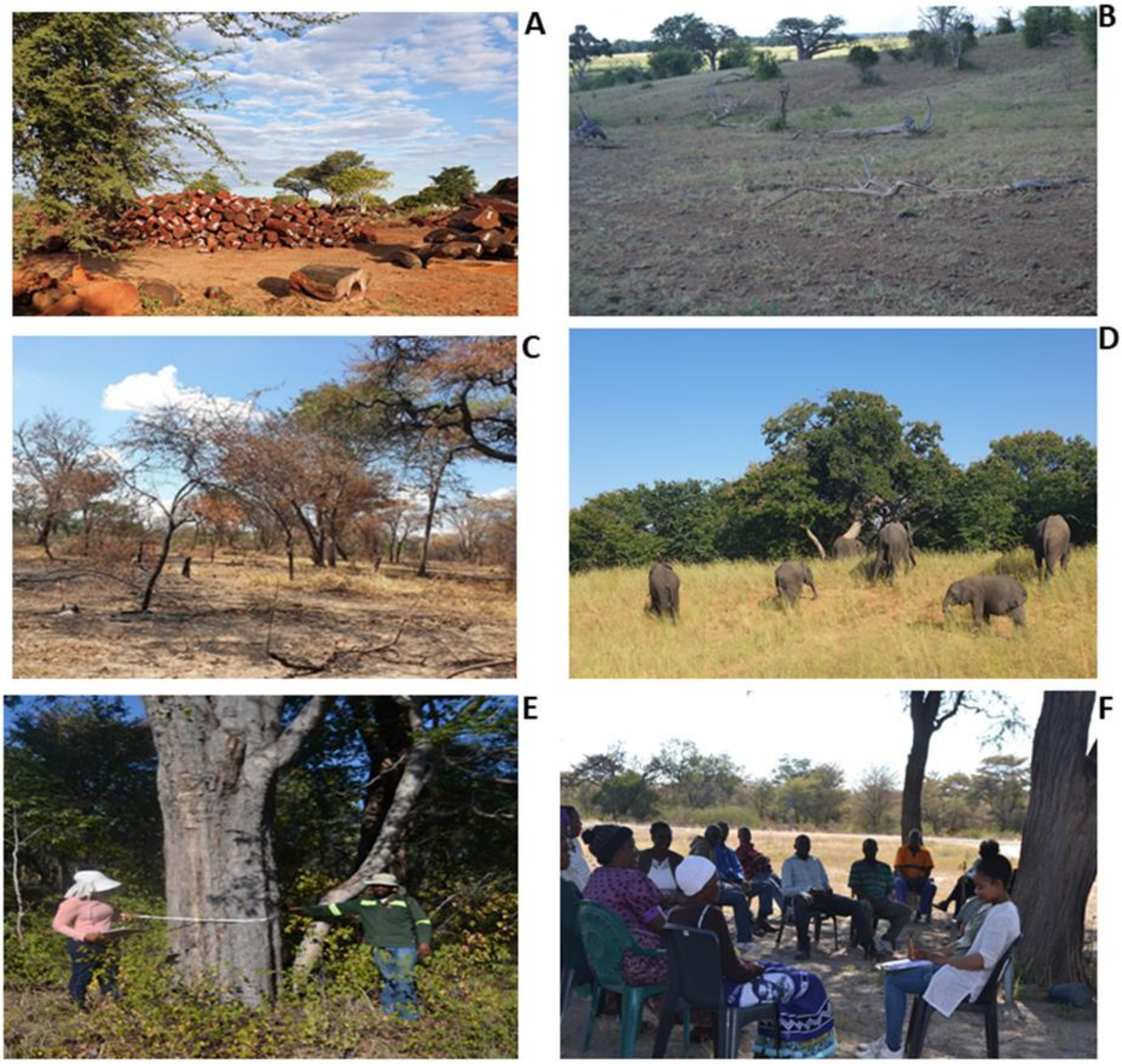

Fig. 1. 6 Example of ground data captured during a field campaign in February to May 2019; (A) deforestation in Zambezi state forest in Namibia; (B) forest degradation in Chobe National Park in Botswana; (C) Burned forest for cultivation near the protected area of Mudumu NP, Namibia; (D) elephant browsing; (E) Sampling diameter at breast height of all tree per plot; (F) Meeting and interviews with community members concerning dryland forests.

1.7 Aims and Objectives

Aims

The fundamental aim of this thesis is to estimate and characterise forest parameters, disturbance, and land cover change in the context of climate change in the KAZA region of Southern Africa. Throughout the thesis, the goal is to explore the use of novel application of remote sensing approaches and the fusion of multiple remote sensing data from optical and SAR sensors. The research seeks to consider their combination to ascertain the potential insights into the spatial and temporal change of dryland forests that remote sensing is able to provide. To address the aim, the thesis will tackle the following objectives:

Objectives

Objective 1: Provide a systematic review of the scientific literature related to the use of remotely sensed data within the context of dryland forests, with a focus on Southern Africa.

- Provide a detailed overview of the current approaches and limitations for monitoring dryland forests using optical and radar remote sensing data.
- Quantify general trends in remote sensing data studies focusing on monitoring dryland forests in Southern Africa.
- Identify research gaps and make recommendations for monitoring dryland forests using remote sensing data.

Objective 2: To assess the feasibility of using remote sensing data derived from SAR, multispectral, and ground measurements to estimate dryland forest above ground biomass.

- Develop empirical models to determine the relationship between field-measured AGB and Sentinel-1 SAR backscatter coefficients, S Sentinel-2, and Landsat-8 multispectral reflectance in the dryland forest environment.

The focus will be on the contribution and prediction potential of SAR data, multispectral bands, and their spectral indices, both individually and in combination.

- Develop parametric and non-parametric models for estimating and testing the accuracy of AGB estimation and mapping.
- To compare these models to different published biomass estimates in the dryland forest environment.
- To discuss the suitability of different models for land and wildlife management at different spatial scales (regional to global).

Objective 3: Investigate the evidence for water stress conditions across KAZA and to test the utility of structural breaks for detecting dryland forest changes using two methods: (1) BFAST and (2) BEAST change detection in the dryland forests of KAZA.

- Spatial characterisation of climatic data with vegetation indices as a proxy indicator of climate variability to improve understanding of vegetation response to drought.
- Compare the common vegetation index NDVI with GNDVI to evaluate their respective sensitivities and performance in detecting changes.
- To characterise changes in trends and phenological patterns using Breaks for Additive Seasonal and Trend (BFAST), and Bayesian Estimator of Abrupt change, Seasonality, and Trend (BEAST).

Objective 4: Investigate the relationship between fire and different climate effects on vegetation spectral characteristics at the regional scale of KAZA.

- To characterise drought conditions using climatic data (SPEI, root soil moisture, temperature, and precipitation) and explore the variability of drought using monitoring indicators (i.e., the drought duration, severity, and magnitude)

- To characterise the frequency, seasonality, and extent of fires through time on different land use management in the KAZA region
- To investigate the spatiotemporal changes in aridity in the KAZA region from 2002 to 2010 and 2011 to 2019

1.8 Thesis Structure

The thesis comprises six chapters structured as follows.

Chapter 1 has introduced the general background, motivation and critically examines concepts and remote sensing of TDFs.

Chapter 2 presents a detailed review of the scientific literature related to the use of remotely sensed data including synthetic aperture radar (SAR) and optical sensors within the context of dryland forests, with a focus on Southern Africa. The research presents examples of the literature from 1997 to 2020 that summarises past achievements, current efforts, and geoinformation knowledge gaps.

Chapter 3 assesses the combination of synthetic-aperture radar (SAR) and multispectral data to estimate in dryland forests. Different parametric and non-parametric models for estimating parameters are developed and resulting maps accuracy is tested with ground measurements and different published biomass models in the dryland forest environment.

Chapter 4 examines water stress conditions on vegetation and changes in dryland forests using multiple data streams for time series assessment over National parks and surrounding communal areas within KAZA. BFAST and BEAST algorithms were applied to evaluate their sensitivity to detect changes in trend and seasonality in tropical dryland forests. Different vegetation indices suitability in drylands were tested.

Chapter 5 seeks to investigate the relationship between fire and different climate effects on vegetation spectral characteristics at the regional scale of KAZA. The chapter investigating the impacts, severity, and characteristics of drought a conditions in drylands. The fire dynamics are also investigated at the regional scale of KAZA. The purpose is to expand the understanding from Chapter 4, linking it to climate and fire.

Chapter 6 draws together the key findings presented in Chapters 2-5, addressing the research aim, bringing the findings into the wider research context, and contains the primary recommendations and conclusions of the research presented in the thesis.

2 Remote sensing for monitoring tropical dryland forests: A review of current research, knowledge gaps and future directions for Southern Africa

Chapter 2 is published by *Environment Research Communications*, DOI: https://doi.org/10.1088/2515-7620/ac5b84

Chapter 2 is also published as a policy brief by n8agrifood for policy makers, https://policyhub.n8agrifood.ac.uk/activity/rapid-evidence-synthesis-training/, DOI: 10.5281/ZENODO.5566492

Title: Remote sensing for monitoring tropical dryland forests: A review of current research, knowledge gaps and future directions for Southern Africa

Authors: Ruusa M. David, Nick J. Rosser, Daniel N.M. Donoghue

Department of Geography, Durham University, Science Laboratories, DH1 3LE Durham, UK

Author Contribution

David Ruusa- Design the research, perform the data analysis, interpret the results, wrote the manuscript, and revised the manuscript. Nick Rosser- Contributed to the research design, manuscript editing and supervision. Daniel Donoghue- Contributed to the research design, manuscript editing and supervision.

Abstract

Climate change, manifest via rising temperatures, extreme drought, and associated anthropogenic activities, has a negative impact on the health and development of tropical dryland forests. Southern Africa encompasses significant areas of dryland forests that are important to local communities but are facing rapid deforestation and are highly vulnerable to biome degradation from land uses and extreme climate events. Appropriate integration of remote sensing technologies helps to assess and monitor forest ecosystems and provide spatially explicit, operational, and long-term data to assist the sustainable use of tropical environment landscapes. The period from 2010 onwards has seen the rapid development of remote sensing research on tropical forests, which has led to a significant increase in the number of scientific publications. This review aims to analyse and synthesise the evidence published in peer review studies with a focus on optical and radar remote sensing of dryland forests in Southern Africa from 1997-2020. For this study, 137 citation indexed research publications have been analysed with respect to publication timing, study location, spatial and temporal scale of applied remote sensing data, satellite sensors or platforms employed, research topics considered, and overall outcomes of the studies. This enabled us to provide a comprehensive overview of past achievements, current efforts, major research topics studies, EO product gaps/challenges, and to propose ways in which challenges may be overcome. It is hoped that this review will motivate discussion and encourage uptake of new remote sensing tools (e.g., Google Earth Engine (GEE)), data (e.g., the Sentinel satellites), improved vegetation parameters (e.g., red-edge related indices, vegetation optical depth (VOD)) and methodologies (e.g., data fusion or deep learning, etc.), where these have potential applications in monitoring dryland forests.

Keywords: Remote sensing, Dryland forests, Southern Africa, Forest monitoring, SAR, Optical, Systematic review

2.1 Introduction

2.1.1 Tropical dryland forest

Approximately 40% of the Earth's tropical and subtropical land surface is covered by open or closed forests. Of this, tropical dryland forests account for the largest share at 42%; the remaining 33% is moist forest, and only 25% is rain forest (Murphy et al., 1986; Janzen, 1988). The largest proportion of dryland forests ecosystems are found in Africa, accounting for 60 - 80% of the total biome area (three times the area covered by African rain forest) (Bodart et al., 2013; Bullock et al., 1995). Dryland forests hold a significant amount of terrestrial organic carbon that may contribute more to climate mitigation and adaptation than previously appreciated (Valentini et al., 2014). Dryland forests also provide diverse ecosystem services, including water regulation and erosion control, the provision of food, fuel, and tourism opportunities (Djoudi et al., 2015; Schröder et al., 2021). On the other hand, dryland forests are subject to prolonged dry seasons and their rate of conversion to secondary forests has historically been higher than other tropical forest types (Pennington et al., 2018). According to the Intergovernmental Panel on Climate Change (IPCC), these changes have impacts on carbon emissions to the atmosphere and forest biodiversity loss that reduce adaptive capacity and resilience to the impact of high temperatures and varying precipitation (IPCC, 2014).

The definition of “dryland forest” remains debatable and controversial, which contributes to the difficulty in accurately assessing and measuring its distribution patterns and status (Blackie et al., 2014). The lack of a clear and comprehensive understanding of general terms including “drylands” and “forests” makes it a challenge to explicitly define dryland forests (Charles-D et al., 2015). Given the fact that dryland forests progressively grade into other vegetation types such as moist tropical forests, woodlands, and savannas, also makes clear definitions complex (Putz et al., 2010). Walter et al. (1971) noted that the accuracy of estimates of all tropical forest areas is constrained by uncertainty in the distribution of open woodlands in dryland areas, which are extensive in Africa, Australia, and Latin America.

In the scientific literature, many different names have been applied to tropical dryland forests, including savanna forests, Sudanian woodland and miombo woodland in Africa, monsoon forest in Asia, neotropical dry forests in South America (Chidumayo, 2013; Linares-Palomino et al., 2011; Suresh et al., 2011). The neotropical dry forests in South America have a plethora of names from “caatinga” in northeast Brazil, to “bosque tropical caducifolio” in Mexico, and “cuabal” in Cuba, which in part hinders comparisons (Mayes et al., 2017; Sánchez-Azofeifa et al., 2005). For example, Dexter et al. (2015) identified dry deciduous forest in India (Suresh et al., 2011), miombo woodland in southern Africa (Chidumayo, 2013), and deciduous dipterocarp forest in continental Asia (Bunyavejchewin et al., 2011) as a form of savanna, and not TDFs, despite the formal classification as TDFs by these studies, and the FAO (FAO, 2001). The Caatinga and Chaco vegetation in Latin America is also considered by some authors as part of the dry forests (Gasparri and Grau, 2009; Pennington and Ratter, 2006), although Olson et al., (2001) classifies these regions as a shrubland ecosystem.

There are several definitions currently available for TDFs, but there is still a lack of consensus in developing a common understanding. Mooney et al. (1995) defined TDFs as forests occurring in the tropical regions characterised by pronounced seasonality in rainfall, where there are several months of severe, or even absolute drought. Sánchez-Azofeifa et al. (2005) broadly defined TDFs as a vegetation type typically dominated by deciduous trees (at least 50% of trees present are drought deciduous), where the mean annual temperature is ≥ 25 °C, total annual precipitation ranges between 700 and 2000 mm, and there are three or more dry months every year (precipitation < 100 mm per month). A widely accepted definition is that of the FAO, which has identified TDFs as a Global Ecological Zone (GEZ), experiencing a tropical climate, with a dry period of 5 to 8 months and annual rainfall ranges from 500 to 1500 mm; GEZ includes the drier type mbo and Sudanian woodlands, savannah (Africa), caatinga and chaco (South America), and dry deciduous dipterocarp forest and woodlands (Asia) (FAO, 2001). For the scope of this review, the FAO. (2001) definition of TDFs was followed because it recognises forests occurring in the dry tropical climate globally including areas with relatively open canopies such as woodlands, and woody stands, then those based entirely on climate definitions. The growing body of evidence suggests that the current climate does not define the biogeography of TDFs or determine biome distributions (Staver et al., 2011; Sunderland et al., 2015), particularly in the context of future unprecedented climate change (IPCC, 2007). If climates become sufficiently warmer and drier in the tropics, dry forests may expand into areas that are currently dominated by moist tropical forests (Putz et al., 2010).

2.1.2 Recent research trends on tropical dry forests

2.1.2.1 Geographical research trends on tropical dry forests

Studies have pointed out that dryland forests generally receive a lower number of scientific publications and are under-represented in research in comparison with tropical moist forests (Miles et al., 2006; Quesada et al., 2009). Global reviews on dryland forests addressed the imbalance in the geographical coverage of dryland forest publications using remote sensing with certain tropical countries such as Latin America receiving the highest publications on dryland forests in comparison to most places in Africa (Blackie et al., 2014; Schröder et al., 2021). To investigate the geographical distribution of tropical dry forest studies, the study initially searched for publications in ISI web of knowledge and Scopus on tropical dryland forests from Asia, Africa, America, and Australia. This search was conducted by using the keywords 'Dry Forest', 'Dryland Forest' 'Savan* Woodland', 'Savan* Tree', 'Dryland Vegetation', 'Dry Vegetation' 'Satellite', 'Remote Sensing', 'Optical', 'Radar', 'Image', 'SAR', 'Earth Observation', 'country/continent e.g., Africa'. In the search period from 1997 to 2020, the study identified 1662 papers for Africa, 1639 for Australia, 1338 for America, and 1134 for Asia. In Africa, when the search was narrowed to individual countries, the results showed that about 743 publications are from the Republic of South Africa (RSA) while 355 publications were from the Sahel region of Nigeria. The study also investigated scientific publications from other Southern African countries with dryland forest and 369 publications were identified, including from Botswana (87), Zimbabwe (69), Mozambique (60), Namibia (68), Zambia (49), Angola (24), Lesotho (6), Swaziland (5). When the review combined the scientific publications from the above 8 Southern African countries, the results were 369 publications, indicating that publications on dryland forests for the Republic of South Africa were 2.01 times higher than all 8 Southern African countries combined. These results confirm that much less progress has been made in developing objective methods for assessing the rates of deforestation/conservation and threats to dryland forests ecosystems in most Southern African countries except for the Republic of South Africa.

The dryland forests in other parts of the world like Latin America are increasingly well studied at local, regional, national and continental scale, particularly with regards to carbon/biomass (Chazdon et al., 2016; Marín-Spiotta et al., 2008), fire (Campos-Vargas et al., 2021; White, 2019; Pereira et al., 2014), climate change (Mendivelso et al., 2014; Castro et al., 2018; González-M et al., 2021), floristic and diversity composition (Alvarez-Añorve et al., 2012; Gillespie et al., 2000), ecosystem services (Castillo et al., 2005; Paruelo et al., 2016), Payment for Environmental Services (PES) (Alcañiz and Gutierrez, 2020; Corbera et al., 2009), novel conservation approaches (e.g., sustainable intensification for protected/conservation areas) (Méndez et al., 2007; Reynolds et al., 2016) and has the most comprehensive forest change/deforestation and biophysical aspects including species population changes, with extensive use of remote sensing (do Espírito-Santo et al., 2020; Gasparri and Grau, 2009; Stan and Sanchez-Azofeifa, 2019; Trejo and Dirzo, 2000; Portillo-Quintero et al., 2012). In terms of reviews, many remote sensing reviews are providing valuable information on TDF's biophysical, ecological and socioeconomic at a regional level of Latin America (Castro et al., 2003; Metternicht et al., 2010; Portillo, 2010; Sanchez-Azofeifa et al.,2003; Sánchez-Azofeifa et al., 2005; Sánchez-Azofeifa et al., 2013; Stan and Sanchez-Azofeifa, 2019; Quijas et al. 2019), and Australia (Lawley et al., 2016; Moore et al., 2016; Fensham et al., 2002). Also, reviews of current progress on dryland forests in individual countries can be found in many neotropics countries such as Mexico (Castillo et al., 2005; Curry, 2020), Venezuela (Fajardo et al., 2005; Rodríguez et al., 2008), and Costa Rica (Frankie et al., 2004; Stoner et al., 2004) enabling the identification of knowledge gaps and aiding in the development of a policy-relevant approach to conservation of these forests (Miles et al., 2006).

Latin America is one of the best-represented areas for remote sensing research in dryland forests, for example, Portillo-Quintero and Sánchez-Azofeifa. (2010)

utilised remote sensing data at continental America, dryland forests ecoregion, and neotropics countries to show that 66% of tropical dry forest in the region has already been converted and that in some countries the conversion rate is as high as 86% and 95%, respectively. Aide et al. (2012) using Moderate Resolution Imaging Spectroradiometer (MODIS) satellite data estimated that 200,000 km^2 of woody vegetation of Latin American and the Caribbean region were lost due to deforestation between 2001 and 2010. Nanni et al. (2019) utilised MODIS satellite data at 250 m spatial resolution to assess reforestation at the regional level and reported that the reforestation hotspots cover 167,667.7 km^2 (7.6 %) of Latin America between 2001 and 2014. While there are continental studies in Africa utilising remote sensing on biophysical parameters such as biomass/deforestation (Bouvet et al., 2018; Bodart et al., 2013), as compared to Latin America, these studies may not consider the empirical observations of dryland forests extent/change per region or country level. In addition, most continental studies in Africa rather focus the attention on tropical rainforest in Central Africa (e.g., core Congolese forest) which may under-represent dryland forest (e.g., Aleman et al., 2018). Global applications often report general land use/cover change which results in inaccurate or poor estimates of dryland forest (Smith et al., 2019; Aleman et al., 2018).

Several studies using optical and passive microwave instruments in the African Sahel (Horion et al., 2014; Brandt et al., 2016; Olsson et al., 2005; Tian et al., 2017) has reported that the density/size of woody vegetation stands have increased, with few areas in northern Nigeria reported to experience logging and agricultural expansion into forest reserves. Deforestation in Southern Africa is a major concern, with ca. 1.4 million ha of net forest loss annually, contributing to increased land degradation and the ensuant impacts on the balance of ecosystem function (Lesolle, 2012). A global study by Tian et al. (2017) utilising the optical Normalised Difference Vegetation (NDVI) index and passive microwave VOD across tropical drylands has reported a decreasing trend in woody vegetation in Southern African countries such as Botswana and Zimbabwe. Mitchard and Flintrop. (2013) conducted a coarse-scale analysis of changes in woody vegetation from 1982 to 2006 using NDVI time series from the Global Inventory Modeling and Mapping Studies (GIMMS) dataset and found that significant woody encroachment is occurring in most west African countries, but, in contrast, in Southern Africa, a rapid reduction in woody vegetation (deforestation) is occurring. Bodart et al. (2013) used Landsat satellite imagery between 1990 and 2000 to estimate forest cover and forest cover changes in the African continent and found that 84% of the total deforested area occurred in the dry ecosystems of the Southern African region, with large spatially concentrated areas of forest loss found in Angola, Mozambique, Tanzania, Zambia and Zimbabwe, and isolated hotspots found in Nigeria and the border of the humid forest in Ghana. While such global and continental level studies are useful to highlight and reinforce the need to direct more attention and resources to these threatened/poorly studied ecosystems, research efforts on forest change/deforestation and climate change impacts of dryland forests at the regional level of Southern Africa are much harder to come by (Blackie et al., 2014).

2.1.2.2 Remote Sensing approaches research trends in tropical dry forests

In recent decades, satellite remote sensing or Earth observation (EO) has proved a valuable tool in forest ecology, owing to its capability to perform systematic, frequent, and synoptic observation of the Earth, resulting in large data volumes and multiple datasets at varying spatial and temporal scales (Donoghue, 2002; Zhu, 2017). There are several sensors including multi-spectral scanners, laser scanners (LiDAR), hyper-spectral scanners as well as satellite-borne Synthetic Aperture Radar (SAR), that provide information on the colour and structure of forest environments (Donoghue, 2002). EO has been applied to mapping the distribution, changes in cover and condition including deforestation, desertification, fire damage, and climate impact (Dogru et al., 2020; Smith et al., 2019). Additionally, these data have been used to estimate biophysical characteristics such as total above ground biomass (AGB), leaf area index (LAI), woody area index, tree diameter, and canopy height which are key inputs into a variety of ecological models, as well as calculations of carbon balance and primary production (Barbosa et al., 2014; Donoghue, 2000). The continuous forest metrics obtained using EO data can be extracted at leaf and crown level to evaluate spectral elements of leaf or species properties and at stand-level and plot-level, or beyond to understand the variation between and among species, and through time (Muraoka et al., 2009). Monitoring of dryland forest cover and forest metrics using EO data also helps to improve the understanding of the ecological drivers behind land cover change dynamics (Chambers et al., 2007; Veldkamp et al., 2001).

Biomass has extensively been estimated based on the spectral reflectance values from two or more wavelengths, and the sensitivity of optical and near-infrared wavelengths to photosynthetic canopy cover has long been used for vegetation analyses (Rouse, 1974; Tucker, 1979). Spectral vegetation indices (VIs), including the NDVI index, are commonly used as a proxy of vegetation cover and have been shown to relate closely to LAI, biomass, and the fraction of photosynthetically active radiation absorbed by vegetation (fAPAR) (Curran, 1980). Several well-known limitations of NDVI for robust estimation of biomass in drylands exist. NDVI is sensitive to green components and insensitive to woody components where the majority of carbon is stored (Tucker, 1979). Also, AGB production is not always uniformly linked to either greenness or plant structure (herbaceous and woody compositions), as moisture content and vegetation species composition have been shown to impact the biomass-NDVI relationship (Asner et al., 2009; Wessels et al., 2006). These observations may help explain reportedly weak relationships between NDVI and tropical forest canopies, particularly for areas with complex and high vegetation amounts as in TDFs (Foody et al., 2001; Sader et al., 1989). For example, Madonsela et al. (2018) investigated the interactions between seasonal NDVI and woody canopy cover in the savanna of the Kruger National Park (NP) to model tree species diversity using a factorial model and found that the interaction between NDVI and woody canopy cover was insignificant. These challenges have led to the development of alternative formulations which include correction factors or constants introduced to account for or minimise, the varying background reflectance (Gitelson et al., 1996; Huete et al., 1999). The Enhanced Vegetation Index (EVI) is a modification of NDVI that provides complementary information about the spatial and temporal variations of vegetation while minimising many of the contamination problems present in the NDVI, such as those associated with canopy background and atmospheric influences (Huete et al., 2002). Other closely related indices include the Simple Ratio (SR), the Green Normalised Difference Vegetation Index (GNDVI), Soil-Adjusted Vegetation Index

(SAVI) amongst others. Xue et al. (2017) provides a detailed review of vegetation indices.

Although vegetation monitoring has been largely based on the multispectral “greenness” indices, which have proven invaluable for monitoring biophysical and biogeochemical parameters, it has been widely reported in the literature that they suffer from several weaknesses in dryland ecosystems (Tian et al., 2016; Shi et al., 2008). Other remote sensing systems such as the passive microwave-based satellite systems capture the biomass signal in the parameter termed vegetation optical depth (VOD) which has been used to monitor changes in vegetation dynamics (Andela et al., 2013; Brandt et al., 2018a; Brandt et al., 2018b). Unlike the optical remote sensing-based vegetation indices that are sensitive to chlorophyll abundance and photosynthetically active biomass of the leaves, the vegetation information (e.g., VOD) deriving from passive microwave instruments is sensitive to the water content in the total aboveground vegetation, including both the canopy (e.g. woody plant foliage) and non-green woody (e.g. plant stems and branches) components due to greater penetration and sensitivity (Liu et al., 2011; Shi et al., 2008). The passive microwave observations VOD is relatively insensitive to signal degradation from solar illumination and atmospheric effects and provide a valuable alternative tool for rapid monitoring of carbon stocks and their changes (Jones et al., 2011). One of the advantages of passive microwave-derived VOD is that it continues to distinguish biomass variations at a relatively high biomass density, as compared to optical-based vegetation indices which are likely to become saturated over dense canopies (Jones et al., 2011; Liu et al., 2015). The main disadvantage of passive microwave observations is the relatively coarse spatial resolution (>10km), as compared to satellite data in the visible and near-infrared parts of the spectrum; however, these data still have highly useful applications at regional and global scales (Liu et al., 2015; Rahmoune et al., 2013; Owe et al., 2001). Some recent global and local studies from Latin America and Africa in the dryland ecosystems found VOD to be more robust against the NDVI drawbacks of saturation effect and continues to distinguish structural differences for vegetation with a near-closed canopy when used as a proxy for vegetation productivity (van Marle et al., 2015; Cui et al., 2015; Liu et al., 2011; Tian et al., 2016). Apart from the VOD and NDVI, an intercomparison between several vegetation indices including other passive microwave-based vegetation indices, such as the Microwave Polarisation Difference Index (MPDI) (Becker & Choudhury, 1988), and the Microwave Vegetation Indices (MVIs) (Shi et al., 2008) would be of benefit in monitoring dryland biomes.

2.1.3 Review focus justification

The majority of the residents of Southern Africa are poor and about 75% of them live in rural areas with high reliance on dryland forests (Bond 2010). Additionally, these dryland areas display a high susceptibility to bush encroachment (O'Connor et al., 2014) and economic reliance on tourism (Ferreira 2004) and forest products (Kamwi et al., 2020), which means that both agriculture and tourism development encroach on the dryland forests, resulting in loss of forest biodiversity and land degradation (Eva et al., 2006; Petheram et al., 2006). Across Southern Africa, sustainable management of dryland ecosystems is hindered by complex land tenure due to historical legacy, weak links between policy and woodland use and management, and cultural drivers (Balint and Mashinya, 2006; Dewees, 1994). Also, the dryland ecosystems of Southern Africa are dominated by private land ownership, a high concentration of wildlife and human populations, and agriculture where TDFs occur (Child et al. 2012). This review focuses on Southern Africa because there is a gap in knowledge on carbon storage, biomass, and the long-term trend of forest distribution and degradation in dryland forests. Much of the research on dryland forests in Southern African has concentrated on livelihoods, community forest management, and conservation/development trade-offs (Chidumayo et al., 2010; Chidumayo and Gumbo, 2010; Chidumayo, 2019; Djoudi et al., 2015, Dewees 1994; Du Preez, 2014; Ryan et al., 2016), leaving forests highly vulnerable to deforestation and degradation (Keenan et al., 2015). The social and economic aspects are important given the large numbers of African people that rely on dry forests for their livelihoods and a range of goods and services. However, the gap in biophysical aspects, threats status, and adaptation to climate change identified for Southern African TDFs at the regional and national level (Blackie et al., 2014; Sunderland et al., 2015), presents an urgent need for an assessment of the effectiveness of the EO scientific foundation on current understanding of TDFs in Southern Africa; this can aid in the development of policy-relevant approaches and long-term, regional perspective for planning and conservation of the TDFs.

With the prospects of multiple free datasets from optical and SAR sensors being available; combining information from optical sensors on photosynthetic activity (e.g., through various vegetation indices) with SAR-derived information on forest structure and volume brings the benefits of higher spectral resolution and compensating for the shortcomings of using single data products alone. Based on this hypothesis, this review focuses on examining the studies using optical and SAR sensors, both individually and the combination of the two types of EO data in monitoring tropical forests. While forest distribution, carbon storage, and reducing emissions from deforestation and forest degradation (REDD+) related research exists in African dryland forests, the geographical focus has tended to be confined to several West/Central African countries, whereas Southern Africa is relatively poorly analysed (Lewis et al., 2013; Sunderland et al., 2015). Although numerous reviews have been conducted discussing the application of optical and radar remote sensing, they are either concentrated on mangroves forests (Kuenzer et al., 2011; Wang et al., 2019), rain forests (Dupuis et al., 2020), or ecosystem services (Barbosa et al., 2015). To date, reviews on remote sensing and EO in Southern Africa have focused on research conducted in the Republic of South Africa (RSA) (Hoffman et al., 2000; Mutanga et al., 2016; Mutanga et al., 2009).

As shown in Fig. 2.1, the climate threats coupled with a growing human population and future anticipated changes in land use are predicted to lead to severe dry forest biome shifts and degradation across the whole of Southern Africa, hence the need to expand the geographical scope of this review from previous work (IPCC, 2014; King, 2014). This paper provides a systematic review of the scientific literatures related to the use of Earth observation data including SAR and optical sensors used to study dryland forests, with a focus on Southern Africa. To achieve this, examples from the literature that summarise past achievements, current efforts, and knowledge gaps are presented. The objectives of this review are to (i) to provide a detailed overview of the current approaches and limitations for monitoring dryland forests using optical and radar remote sensing data. (ii) to provide a critical evaluation and synthesis of the literature monitoring dryland forests using remote sensing data and discuss how EO data can contribute to dryland forest monitoring and forest conservation in Southern Africa. (iii) to identify knowledge gaps and make recommendations for research that will enhance monitoring of dryland forests using remote sensing data.

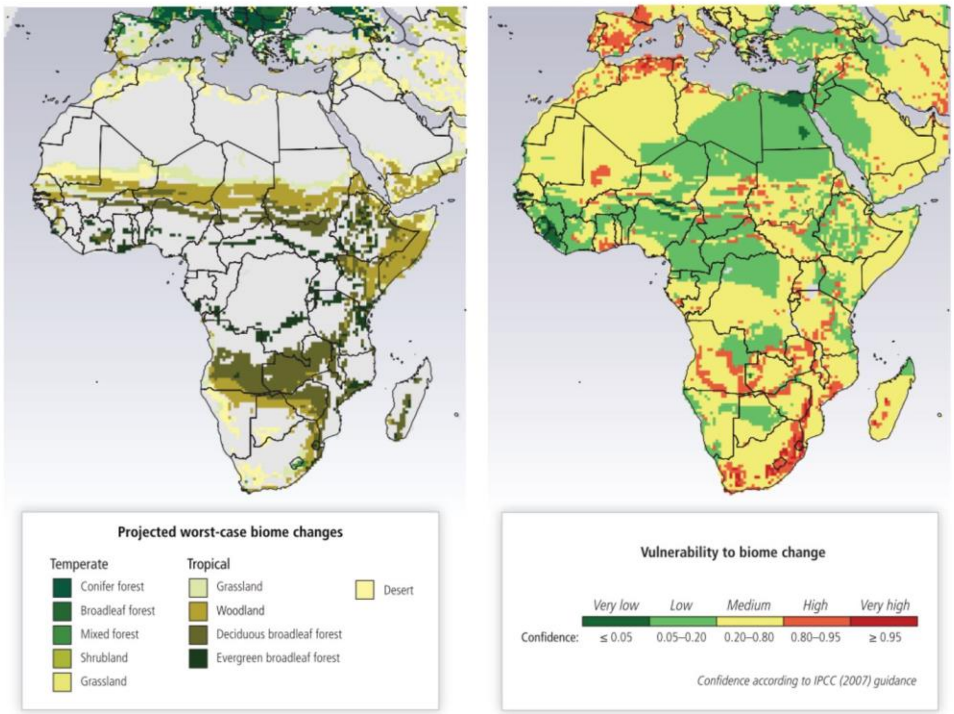

Fig. 2. 1 (a) Projected biome change from the periods 1961–1990 to 2071–2100 using the MC1 Dynamic Vegetation Model. (b) Vulnerability of ecosystems to biome shifts based on historical climate (1901–2002) and projected vegetation (2071–2100) (source: IPCC, 2014).

2.2 Remote sensing applications in dryland forest

2.2.1 Optical data

In broad terms, the satellite platforms developed over the past 40 years (since 1972) have carried two broad types of sensor systems; passive optical and active synthetic aperture radar (SAR). Successful change detection and parameter estimation over tropical dryland forests require: (a) correct selection and application of sensor type; (b) coupling with field observation data for calibration and validation, and (c) data integration and appropriate techniques for modelling (Fig. 2.2). Optical sensors have been widely used for land cover and forest resource mapping, providing access to long-term data dating back to the launch of Landsat ERTS (Earth Resources Technology Satellite) satellites in 1972. Landsat and several other coarse/medium spatial resolution optical sensor missions (National Oceanic and Atmospheric Administration (NOAA) - Advanced Very High-Resolution Radiometer (AVHRR); the National Aeronautics and Space Administration (NASA) -Aqua/Terra- Moderate Resolution Imaging Spectroradiometer (MODIS); Indian Remote Sensing Satellites-1C/1D (ISRO-IRS-1C/D), Sentinel-2) provide well-calibrated, nadir-viewing, near-global systematic coverage which have built up a valuable archive of image data that can be used to analyse ecosystem dynamics (Congalton, 2018; Donoghue, 2000). In 2014, ESA launched the Multispectral Instrument (MSI) onboard Sentinel-2 as part of its Copernicus EO mission. Sentinel-2 MSI uses two identical satellite sensors to measure the Earth's reflected radiance with a revisit time of 5 days and a fine spatial resolution of 10 - 20 m pixel size. The length of the Sentinel-2 archive is short (from 2015), compared to the Landsat mission from 1972-present, NOAA-AVHRR 1979-present; Satellite Pour l'Observation de la Terre VEGETATION (SPOT/VGT) (1998-present), IRS-1C/1D (ISRO-IRS-1C/D) (1995-2010), ENVISAT - Medium Resolution Imaging Spectrometer (MERIS) (2002-2010) and the NASA - MODIS (2000-present) and the French Space Agency (CNES-Centre national d'études spatiales) high-resolution SPOT satellite constellation (6 m - 20 m pixel size) - SPOT-1 in 1986-1990, SPOT-2 in 1990-2009, SPOT-3 in 1993-2009; SPOT-4 in 1990-2013; SPOT-5 in 2002-present; SPOT-6 in 2012-present; SPOT-7 in 2014-present. The VEGETATION 1 (VGT 1) (1998-2012) and VEGETATION 2 (VGT 2) (2002-2014) instrument on the SPOT 4 and SPOT 5 (SPOT/VGT) satellites provided global daily monitoring of vegetation cover, and it is successor the European PROBA-V satellite (2013-present), with a pixel size of 1 km, 300 m and 100 m are supplied by the VEGETATION image Processing Centre (CTIV) of VITO (Belgium), which can be accessed through the internet site http://free.vgt.vito.be. Although a large number of satellite sensors have been launched that are capable of observing land dynamics, and their pixel size has decreased from 80 m of the Landsat-1 to 0.41-1.65 m of the GeoEye-1 satellites (Aguilar et al., 2013), very few sensors provide well-calibrated multispectral, nadir-viewing observations and even fewer systematically capture all global data and provide a long-term archive of data free of charge to the public. Except for AVHRR and Landsat, no other sensor or sensor line offers the chance of long-term monitoring of an area to be monitored back in time to the 1970s, covering about four decades.

There are several non-systematic commercial high-resolution satellites that allow the detection of individual trees or populations. Maxar Technologies Inc. launched 4 very fine resolution satellites - WorldView-1 in 2007, WorldView-2 in 2009, WorldView-3 in 2010, and WorldView-4 in 2019 that acquire images with spatial resolution of 0.5, 0.41, and 0.31 m, respectively. From 2009 onward, Planet labs launched a swarm of micro-satellites including PlanetScope (PS), RapidEye (RE), and SkySat (SS) Earth-imaging constellations with multispectral imaging capability with the aim of acquiring daily image capture for any part of the world at a spatial resolution of 3.125 m to 6.5 m (Marta, 2018). In 2011 and 2012, the Space Agency of France (CNES) launched the Pléiades – fine resolution optical imaging satellite constellation (Pléiades-1A and Pléiades-1B), with a fine spatial resolution of 0.7 – 2.8 m. Other very fine-resolution commercial space imaging satellites include Earlybird (1997), GeoEye (2008), EROS-A (1998), IKONOS (1999), QuickBird (2001), OrbView (2001) (Maglione, 2016). In Africa, South Africa started satellite developments in the 1990s, with the successful launch of SunSat-1 with a spatial resolution of 15 m in 1999 and SumbandilaSat low orbit satellite with a high fine resolution of 6.25 m in 2009 (Cho et al., 2012; Mutanga et al., 2016). While the first Nigerian satellite, a microsatellite called NigeriaSat-1, was successfully launched into low earth orbit in 2003, followed by Nigeriasat-2 with a higher spatial resolution of 2.5 – 5 m, built by Surrey Satellite Technology Limited (SSTL) of UK (Agbaje, 2010).

Nevertheless, the use of data acquired by higher spatial resolution optical sensors, particularly at regional and global scales, can be limited by their relatively high cost, huge data volumes, and low frequency of data acquisition compounded further in tropical regions where cloud cover is prevalent (Lehmann et al., 2015; Zhu et al., 2012). The temporal resolution of sensors has also increased from, for example, 16 days for Landsat to nearly 1 day for the NOAA-AVHRR, NASA-

Aqua/Terra-MODIS, NOAA-AVHRR, SPOT, SPOT/VGT (PROBA-V), and/or ENVISAT-MERIS data, but with a coarse spatial resolution of 250 m to 1 km (Arino et al., 2007; Herold et al., 2008). Although lacking fine spatial detail, the daily temporal resolution of such sensors enables frequent estimation of deforestation, detection of disturbances using dense time series data, and enables gaps due to cloud cover to be overcome (Mbow et al., 2015). It is important to mention that the acquisitions of some satellites such as NOAA-AVHRR, IRS-1C/1D, and MERIS ceased operations, however, the Sentinel, MODIS, SPOT-VGT, and Landsat series continue to operate, with ongoing continuity of data collection ensured with the recent launch of Landsat-9 in September 2021.

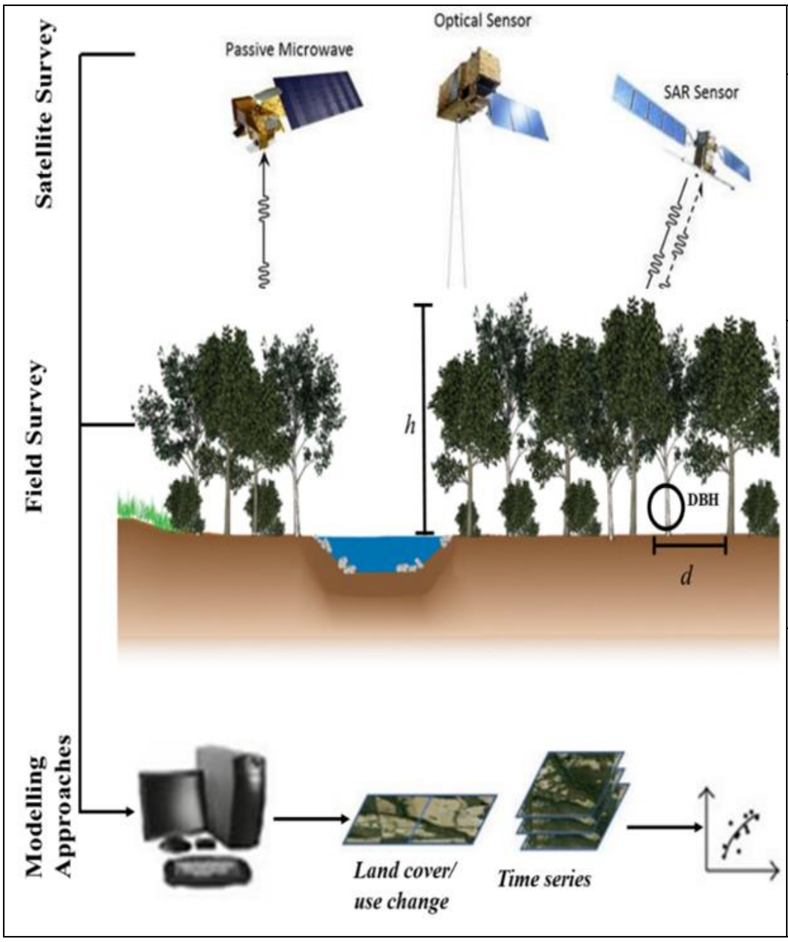

Sources of variability	Challenges
Resolution -Spectral -Radiometric -Spatial -Temporal	-Temporal and spatial availability -Imagery quality(clouds) -Financial constraints -Know-how
Ground truthing -Temporal and spatial heterogeneity -Physiognomies	-Accessibility (wildlife, complex forest structures) -Logistics -Time -Financial constraints
Modelling -Allometric Equation -Uncertainty -Model inversion -Classification schemes -Vegetation Indices	-Availability of allometric equation from the destructive survey -Sufficient sampling -generalisation -Know-how

Fig. 2. 2 Interaction mechanisms for dryland forest canopies and source of variability and challenges related to each stage of remote sensing monitoring tropical dryland forest extents. Adapted from Barbosa et al., 2014.

2.2.2 Synthetic Aperture Radar (SAR)

SAR sensors for civilian applications first appeared in 1978 with NASA's SeaSat but have grown in importance as a tool for forest studies. SAR sensors can operate at different frequencies and polarisations; these system parameters provide information on the roughness and scattering properties of forest canopies and data can be captured day and night independent of weather conditions (Durden et al., 1989). Since SAR can penetrate cloud, rain, smoke, and haze, and it is a valuable source of data when atmospheric conditions hamper optical data capture, particularly in the tropical dryland forest such as Southern Africa where the cloud and smoke from forest fires are prominent features (Le Canut et al., 1996). Radar signals are sensitive to moisture, variations, surface roughness, and vegetation structure properties, whereas data from optical systems use characteristics related to reflected solar illumination or surface temperature (for thermal infrared sensors) as a basis for discrimination of the land cover (Kasischke et al., 1997; Mitchard et al., 2009). Cloud cover-free SAR images have great potential in the dryland tropical areas but have been used less often for forest monitoring applications compared to optical imagery, partly because of the scarcity of data (Castro et al., 2003). Since the launch of the Sentinel-1A and B, dense SAR time-series data are now available over tropical forest areas freely and openly, with systematic acquisitions at a 10 m spatial resolution and a 6 - 12 day revisit time (dependent on the location) in all weather conditions.

Over the last 30 years, several satellite-borne SAR has been launched, including the United State Spaceborne Imaging Radar-Synthetic Aperture Radar (SIR-C/X-SAR), European Remote Sensing (ERS-1/-2), Advanced Synthetic Aperture Radar (ASAR), Japanese Earth Resources Satellite (JERS-1), Advanced Land Observation Satellite (ALOS/PALSAR-1/-2), German TerraSAR-X, and the Canadian RADARSAT-1/-2 (Shimada, 2018). Depending on the sensor configuration, a single channel (wavelength/frequency) or multiple channels may be recorded in either single or multiple polarisations. Generally, studies have reported that the longer the wavelength (e.g. P (30–100 cm) and L (15–30 cm)), the further is its penetration into the forest and the greater the importance of scattering beyond the upper canopy (Huang et al., 2015). Besides the greater sensitivity of longer radar wavelengths to forest structure, different studies indicate that cross-polarised backscatter (HV-horizontally transmitted, and vertically received, VH-vertically transmitted and horizontally received) often exhibits greater sensitivity to forest biomass than like-polarised backscatter (co-polarised bands: HH-horizontally transmitted and horizontally received, VV-vertically transmitted and vertically received) (Kasischke et al., 1997).

2.2.3 Limitations of optical and radar, and benefits of combining sensors

Despite the different generations and types of satellite sensors, no one sensor currently meets fully the requirements of a comprehensive forest resource assessment EO system. The selection of an appropriate source of data requires first the identification of the ecological question being asked, identification of the limitations and advantages of each sensor. The varying temporal, spatial, spectral, and radiometric resolutions unique to the individual sensor system, result in different advantages and disadvantages to the monitoring of dryland ecosystems (Lu, 2006). Optical data are limited in the monitoring of this forest type. For example (1) cloud and smoke severely limit the use of optical products (Le Canut et al., 1996); (2) Dramatic seasonal changes in the dryland forests conditions including droughts and leaf shedding make it unsuitable for systematic all-season monitoring of this forest type (Boggs, 2010). One of the reasons for this is associated with the seasonality of the tropical vegetation: during the wet season, cloud-free satellite imagery is difficult to acquire, while during the dry season when the imagery is more available, the leaf-off configuration of the forest causes misclassification with savanna shrubland or grassland; (3 Optical data is sensitive at the early stages of growth but as forest canopies close, reflected radiation is no longer sensitive to biomass as the reflectance signal saturates at higher biomass values (Lu, 2006); (4) Passive optical sensors only detect the surface top layer, meaning that forest canopy obscures the understory, and similarly grasses/crops obscure soil; (5) Changes in the spectral properties of the soil and atmosphere can also hinder the inference of forest cover properties (Santos et al., 2002; Wang et al., 1998).

Similarly, there are a number of challenges to analysing and interpreting radar images for tropical forest applications, which include: (1) Difficulty in interpreting radar backscatter, including, for example, speckle, which is unwanted random noise inherent in all SAR images, which may increase measurement uncertainty and make interpretation difficult (Klogo et al., 2013); (2) Topography is a major limitation in mountainous regions due to geometric and radiometric effects such as radar shadowing caused by foreshortening and layover when the satellite is not able to illuminate the whole ground surface (Mitchard et al., 2009); (3) SAR observations often lack a long-term and dense time series because they demand a relatively high energy provision on satellite platforms. Until recently, satellite-based SAR data for multi-temporal assessments over large areas were constrained by coarse spatial and temporal coverage at medium resolution, although this now may be overcome with acquisitions from the recently launched C-band Sentinel-1 and L-band ALOS-2 satellite missions (Reiche et al., 2016).

Rather than using EO data from a single satellite sensor, the synergy of remotely sensed data from multiple sensors, particularly SAR systems with those acquired by optical sensors, has been shown to be beneficial for forest resource assessment (Lehmann et al., 2015). Because optical data is capable of measuring the reflectance of the topmost layer of the forest canopy and SAR data deliver useful within-canopy biophysical parameters without being affected by cloud cover and weather conditions, one dataset may compensate for the shortcomings of the other (Reiche et al., 2016). Previous research indicated that integration of optical and radar can improve land and forest cover characterisation (Symeonakis et al., 2018). For example, the fusion of optical and radar sensor data has the potential to improve AGB estimation because it may compensate for the mixed pixels in a tropical forest area. In addition to the spectral synergy afforded, the cloud penetrating capability of microwave radar sensors allows areas that have missing optical data to be included in analyses, particularly if multi-temporal methods are being employed (Reiche et al., 2016).

2.3 Methodology

This review focused on scientific papers studying tropical dryland forests and made use of remote sensing data to monitor and estimate changes in dryland forests. Airborne remote sensing studies were excluded from this review process, since the review’s major focus lies on satellite Earth observation of dryland forests and because the acquisition of airborne sensors have low area coverage and high cost per unit area of ground coverage (e.g., the airborne hyperspectral images), making them spatially and temporally limited in most African countries. The systematic search approach taken to querying the literature was carried out by making use of selective keyword searches in the form of structured queries using field tags and Boolean operators through the Web of Science (http://apps.webofknowledge.com) and Scopus (http://www.scopus.com) databases. At each query, terms and keywords such as ‘*Dryland forests*’, ‘*Savan**’, ‘*Woodland*’, ‘*Tree*’, ‘*Vegetation*’, ‘*Satellite*’, ‘*Remote Sensing*’, ‘*Optical*’, ‘*Radar*’, ‘Image’, ‘*SAR*’, and ‘*Earth Observation*’ were used to produce an extensive list of articles, where * is a wildcard search. The results were further refined with keywords such as ‘*Forest change*’, ‘*Degradation*’, ‘*Deforestation*’, ‘*Trend*’, ‘*Biodiversity*’, ‘P*henology*’, ‘*Biomass*’, ‘*Structural parameter*’, and also keywords representing the countries in Southern Africa, such as ‘*Botswana*’, ‘*Namibia*’, ‘*Mozambique*’, ‘*South Africa*’, to provide a comparison in terms of the numbers of studies undertaken across the region. Within the context of this review, all research articles were categorised into eight categories, including: ‘Land-use/land-cover’, ‘Forest cover/types’, ‘Biomass’, ‘Forest structure’, ‘Biodiversity/habitats’, ‘Phenology’, ‘Plant traits’, and ‘Disturbances’. Articles with a publication date between 1997 and 2020 were considered, capturing a period of two decades within the review, based on a broad set of inclusion criteria:

1. The paper should address dryland forests and remote sensing as either main or secondary subjects.

2. The selection terms and keywords should exist as a whole in at least one of the fields: title, keywords, and abstract.

3. The paper should be published in a peer-reviewed scientific journal.

4. The paper should be written in the English language.

During the data extraction process and literature search, the research aimed to find studies meeting the criteria for peer-reviewed publications, available through the chosen indexed bibliographic databases. For this reason, the literature search did not include general non-scientific reports, books, grey literature, thesis documents or dissertations, extended abstracts, or presentations. The initial steps of the search process returned 1,478 published articles. Additional publications were added to the total set of studies by identifying relevant literature found in the reference lists of these selected papers that conform to the inclusion criteria. The review methodology was guided by the Guidelines for Systematic Review and Evidence Synthesis in Environmental Management (Collaboration for Environmental Evidence, 2013). A systematic review and meta-analysis were undertaken and framed based on the PICO (population, intervention, comparison, outcomes) model (McKenzie et al., 2019) and reported using PRISMA (Preferred Reporting Items for Systematic reviews and Meta-Analyses) flow diagram (Moher et al., 2009). The 1,478 articles were reduced to 870 articles as only the studies that had a full text available in English, papers published in peer-reviewed journals were selected for inclusion in the review, and all repetitions across databases were removed. Initially, the titles and abstracts were screened to assess eligibility, by searching for predefined keywords and terms of the abstract or summary, identifying terms ‘dry or dryland forests and the country or countries where the research took place. In this way, studies not conducted in Southern Africa or dryland forests were filtered out, which reduced papers from 870 to 599 papers. The screening was followed by a full-text assessment that reduced the papers to 270 by excluding studies that, for example, mentioned the term ‘dryland forest’ once in the abstract but did not investigate dryland forests, as outlined in the PRISMA flow diagram in Fig. 3.3. The search was subsequently refined by assigning the papers to each of the study aims they addressed and to each category for the variables identified in the search protocol, reviewing the methodologies of each publication, excluding them from further analysis if they did not meet the inclusion criteria on review. These steps reduced the total number of entries to 137 scientific publications. The selected literature was reviewed systematically, searching for specific information regarding the publication temporal development, study location, remote sensing sensor/platform used, spatial and temporal coverage, remote sensing product (e.g., biophysical indices) used, and application areas of the study (e.g., land cover, forest biomass). The parameters used to extract relevant information from the remaining 137 identified scientific publications are in Table 2.1. Fig. 3.3 is a PRISMA schematic representation of the methodology used and the derivation of the final number of articles selected.

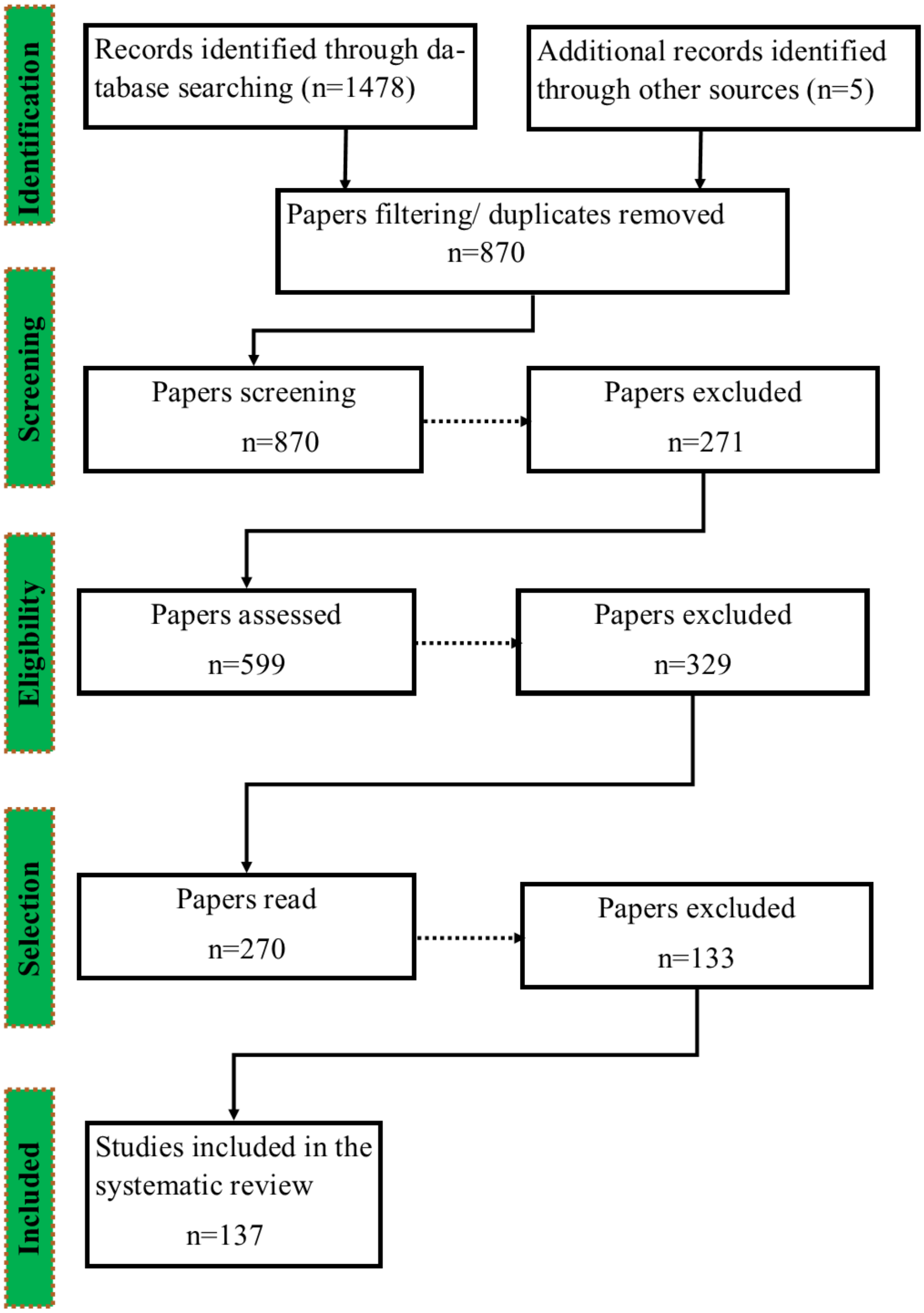

Fig. 2. 3 PRISMA follow diagram (Moher et al., 2009) showing the flow of information through the different phases of the systematic review

Table 2. 1 Parameters used to extract relevant information for this review

General information
Paper Id
1st author’s institution
Research institute city
Publication year
Publishing Journal
Journal category
No of Citation
Study type
Site specific information
Location of the study area
Study country
Forest management area
Predominant forest type
Information on remote sensing data
Sensor Type
Instrument name
Image resolution
Time period observed
Temporal resolution of EO data
Database used
Information on research
Research topic considered: Forest cover/type, disturbance, phenology, biodiversity/habitats, plant traits, land cover/land use
Parameters examined in the study
Examined object scale
Applied methodology
Information on validation and accuracy of results
Database used

2.4 Results

2.4.1 Temporal development of publications and author affiliations

From the literature search, the cumulative number of published research papers integrating remote sensing data in dryland forests of Southern Africa grew exponentially from 2 in 1997 to 155 in 2020. The temporal development of the 137 investigated research articles is illustrated in Fig. 2.4. The graphic shows that the number of studies has increased significantly over the last 23 years, with the majority of the studies published from 2013. More than 105 (80%) of articles were published from 2009 to 2020 and only 4 (3%) of articles were published before 2000. The growth in number is also related to the increased availability of remote sensing platforms, sensors, data, for example, Landsat 8 in 2013 and Sentinel satellite in 2014, respectively.

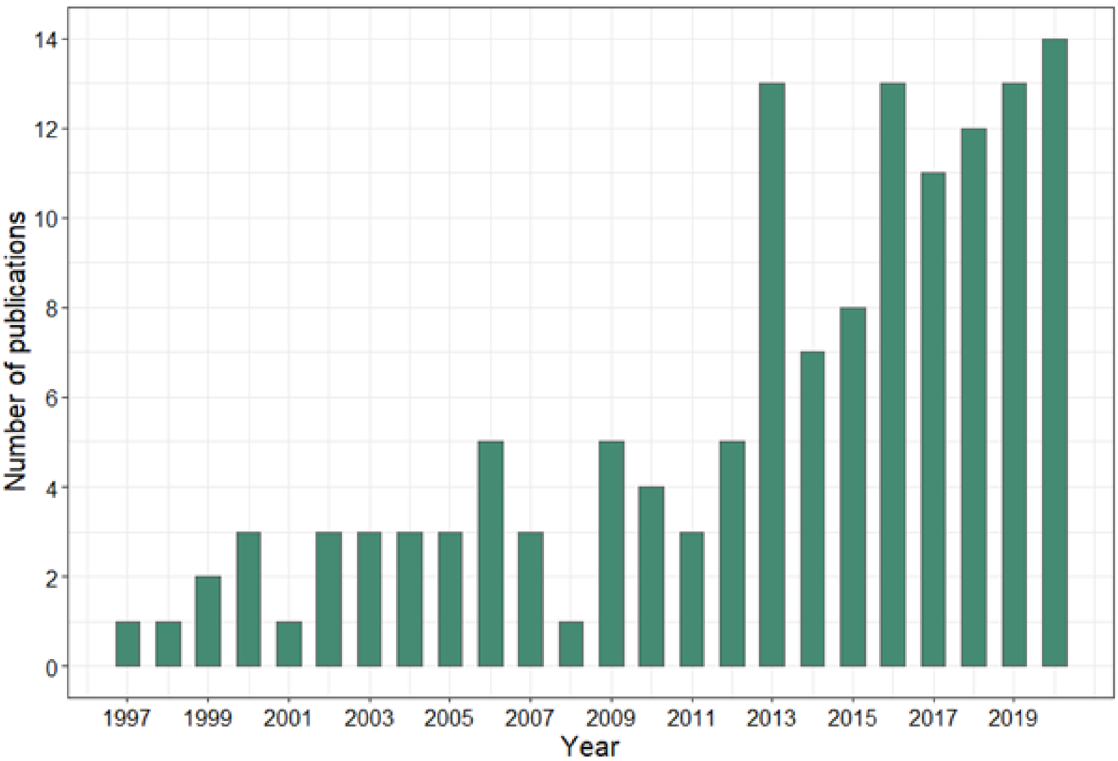

Fig. 2. 4. Number of papers included in the review integrating remote sensing and dryland forests in Southern Africa published annually between 1997 and 2020.

In the review, only studies within Southern Africa were considered; however, the majority of first authors, 83 (61%) of 137 investigated papers, are mainly scientists from international research institutions outside of the focus region, mainly the USA, UK, Portugal, Germany, and The Netherlands (Fig. 2.5). Conversely, the majority of first author institutions from Africa, 37 (27%) of published papers, were from RSA research institutions. The state funded research institutions in Southern Africa shown in Fig. 2.5 include South African Council for Scientific and Industrial Research (CSIR), South African National Space Agency (SANSA), Water Resource Commission of South Africa, South Africa Agricultural Research Council, Range and Forage Institute, Botswanan Harry Oppenheimer Okavango Research Centre, Desert Research Foundation of Namibia, and Namibia Ministry of Environment and Tourism. Considering the 137 studies conducted, about 120 (90%) of the first authors are affiliated with either International and RSA institutions, but no first authors were from Zambia, Lesotho, or Angola.

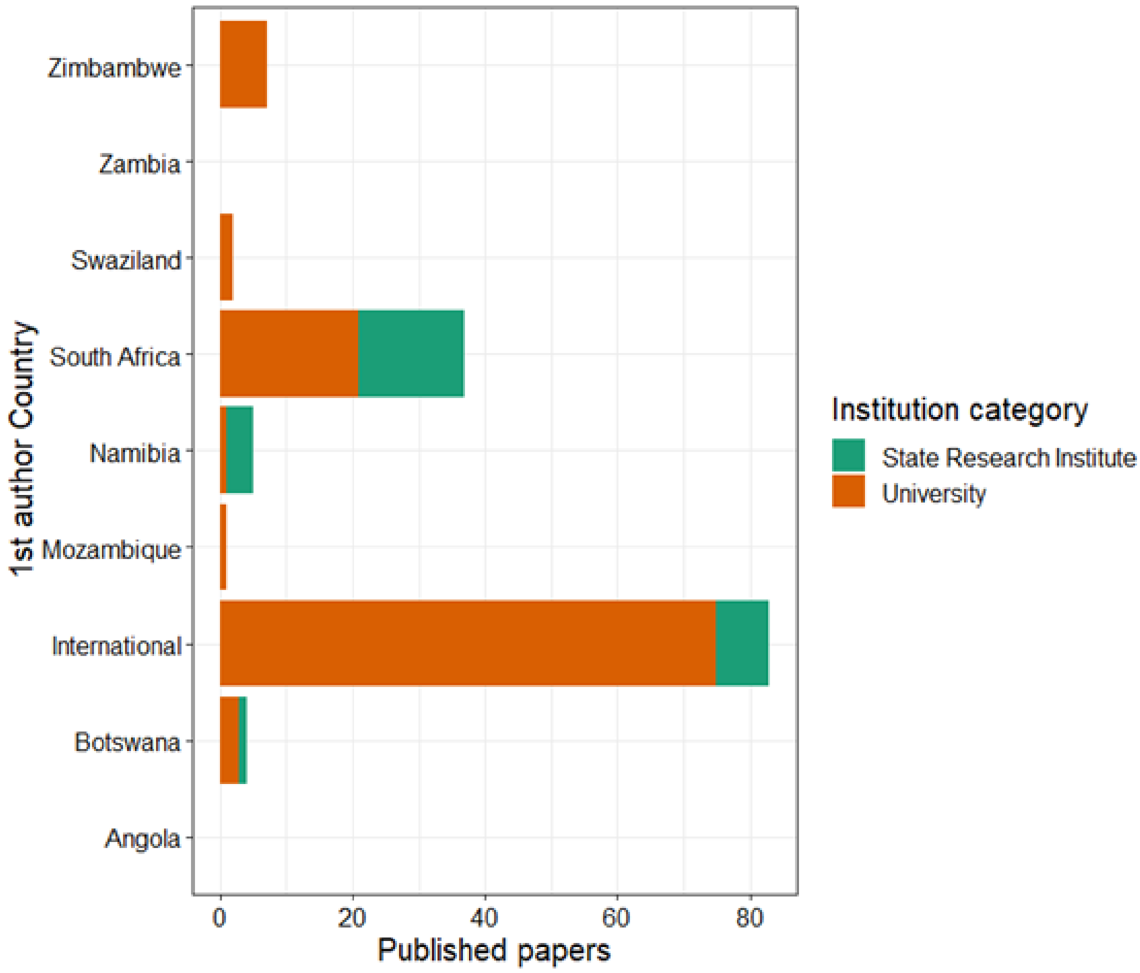

Fig. 2. 5. Number of papers by research institutions.

2.4.2 Spatial coverage, spatial extent, and investigated protected areas

Looking at the spatial scale of the study areas, the research distinguished between studies done at a local community level in a single country, termed local scale, and studies done at more than one local community or province termed regional scale. Also studies done at the national level and the whole of Southern Africa were considered. If a study covered more than three countries, it was counted as an analysis of Southern Africa. The spatial extent of the studies in the review is shown in Fig. 2.6. The majority 88 (64%) of the investigated studies focused on a local scale, despite the need for regional scale information on dryland forest distribution. From Fig. 2.6, out of 137 investigated research papers, 20 (15%) and

13 (9%) research papers covered regional and national scales, respectively. Only 10 (7%) out of 137 research papers dealt with transboundary protected areas, while 6 (4%) of research papers were covering Southern African, considering the region as a whole, using mainly multispectral data of large spatial resolution of 1km to 8km (MODIS, SPOT, and AVHRR) to generate information on phenology, and vegetation condition (fire or drought), as shown in Fig. 2.8.

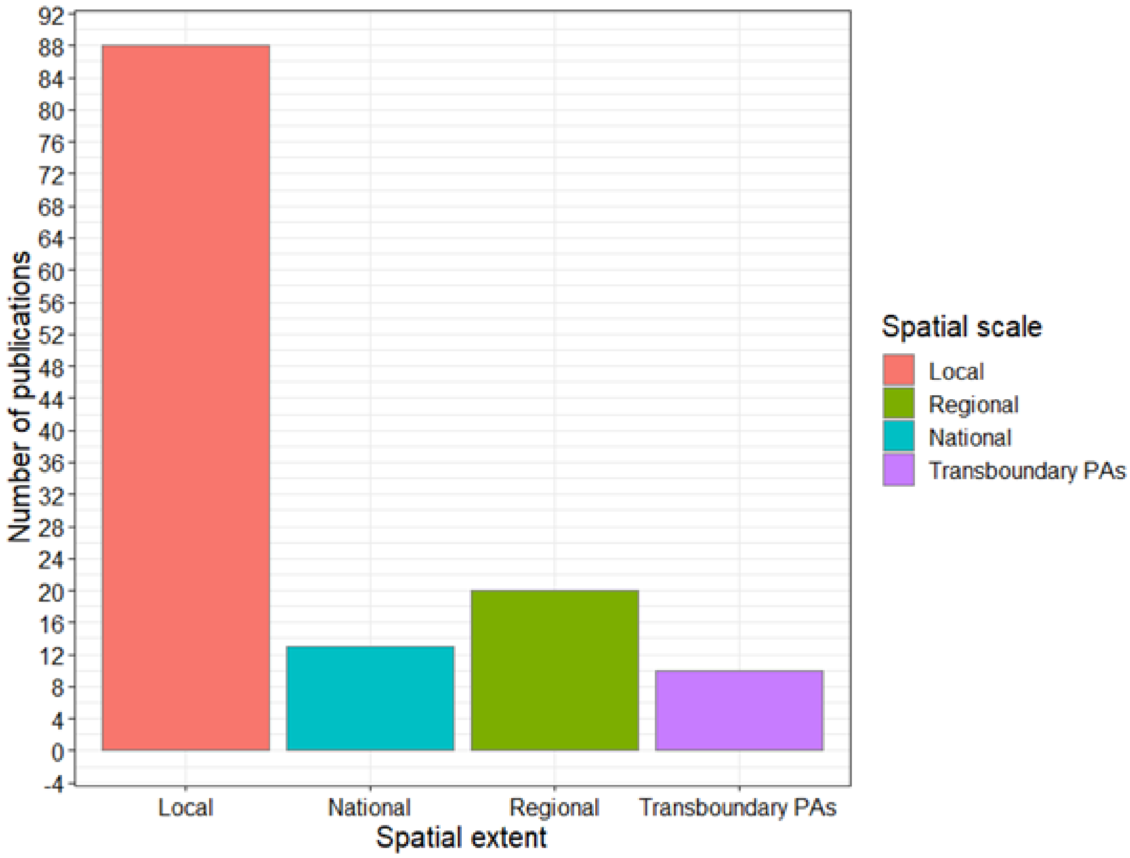

Fig. 2. 6. Spatial extent of investigated studies.

From Fig. 2.7, it is evident that considerable gaps in geographical focus of research on tropical dryland forests mapping still exist in Southern Africa. With respect to spatial coverage of the research, most studies, 50 (36%) of research papers were carried out in RSA, followed by Namibia and Botswana, with 22 (16%) and 18 (13%) of research papers, respectively. Swaziland, Angola, and Lesotho were the least frequently investigated, each with < 10 papers. Angolan dryland forests are even less well studied with 4 (6%) of research papers, despite being found extensively in that country. Fig. 2.7 also shows the location of the most frequently studied protected areas. By far, the most studied was the Kruger National Park (NP) in RSA, involving research by local and foreign researchers from as far afield as the USA, the UK, and beyond. With this interest in the Kruger NP, there is, unfortunately, a lack of attention on other conservation areas and parks in Southern Africa. Kruger NP was the only subject of more than one-third, 23 (37%) of the 61 of all reviewed papers on protected areas. The second most frequently studied protected areas are the Etosha NP in Namibia with 6 (8%) of papers, Chobe NP with 4 (7%) of papers, and Kwando, Kavango and Zambezi transboundary NP with 8 (13%) of papers). Malipati Safari Area, South Luangwa NP, Gorongosa NP, and Central Kalahari Game Reserve were each studied 3 (5%) and 2 (3%) times.

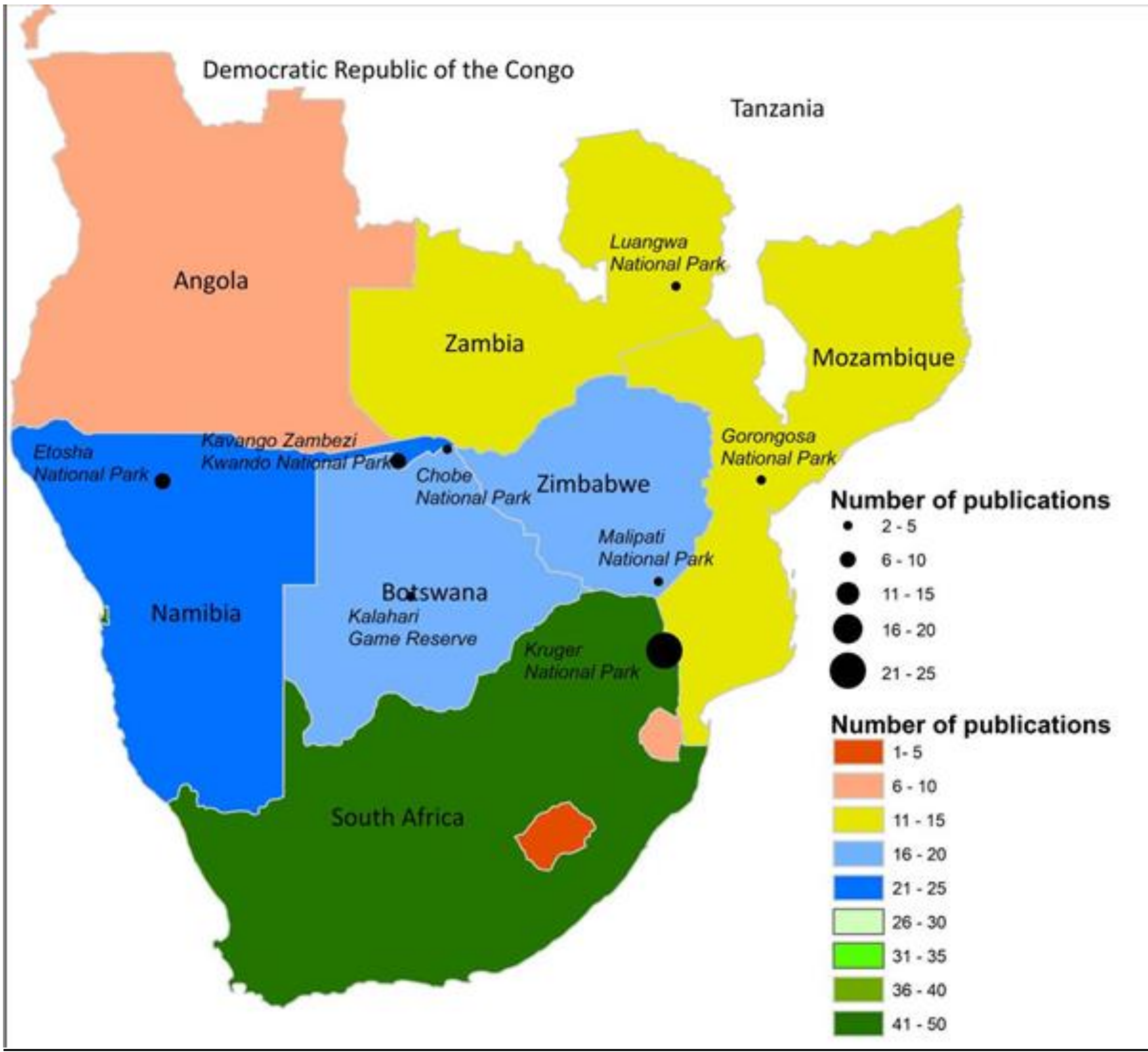

Fig. 2. 7. Number of studies per country and National Park in Southern Africa. (Note: The data are not scaled to the proportion of dryland forest area of countries, and National Parks with fewer or no publications are not shown. Source: FAO, (1999). Reproduced with permission).

To identify land surface changes and the drivers behind these, as well as short- and long-term trends, it is essential that EO temporal coverage has sufficiently frequent revisit periods and resolutions. Nonetheless, this is not an easy task since the availability of remote sensing data for long-term monitoring is constrained by sensor characteristics (e.g., revisit time) and environmental factors (e.g., cloud cover). Looking at the temporal resolution of the EO datasets used, the research distinguished between data acquired at a single point in time on a monthly basis, termed mono-temporal analyses, and on a single annual basis, termed mono-annual analyses. In addition, multi-temporal and multi-annual to separate monthly and yearly analyses studies were considered. From Fig. 2.8 it is seen that the majority of published material has focused on a single temporal period. The majority of studies involved mapping over two or more years (multi-temporal/multi-annual) comparing images at two or more different times, with a bi-temporal approach based on discrete classification (e.g., Chiteculo et al., 2018; Coetzer-Hanack et al., 2016; Matavire et al., 2015). Although the bi-temporal approach is mathematically simple and does not require large data storage, it is less useful compared to the time series approach that can provide a more comprehensive understanding of the complexity of the Earth's land surface dynamics. Very few studies feature time series analysis, which is required to perform continuous long-term monitoring of changes in a tropical forest ecosystem. The majority of articles on time series analysed multi-annual data, which masks within-year variations, as compared to the detail provided at a monthly temporal scale (e.g., Akinyemi et al., 2019; Venter et al., 2020; Verlinden et al., 2006a; Wessels et al., 2006). Only 22 (16%) out of the 137 studies analysed more than 15 years and only 11 (8%) studies covered more than 20 years using monthly time series (e.g., Bunting et al., 2018; Schultz et al., 2018).

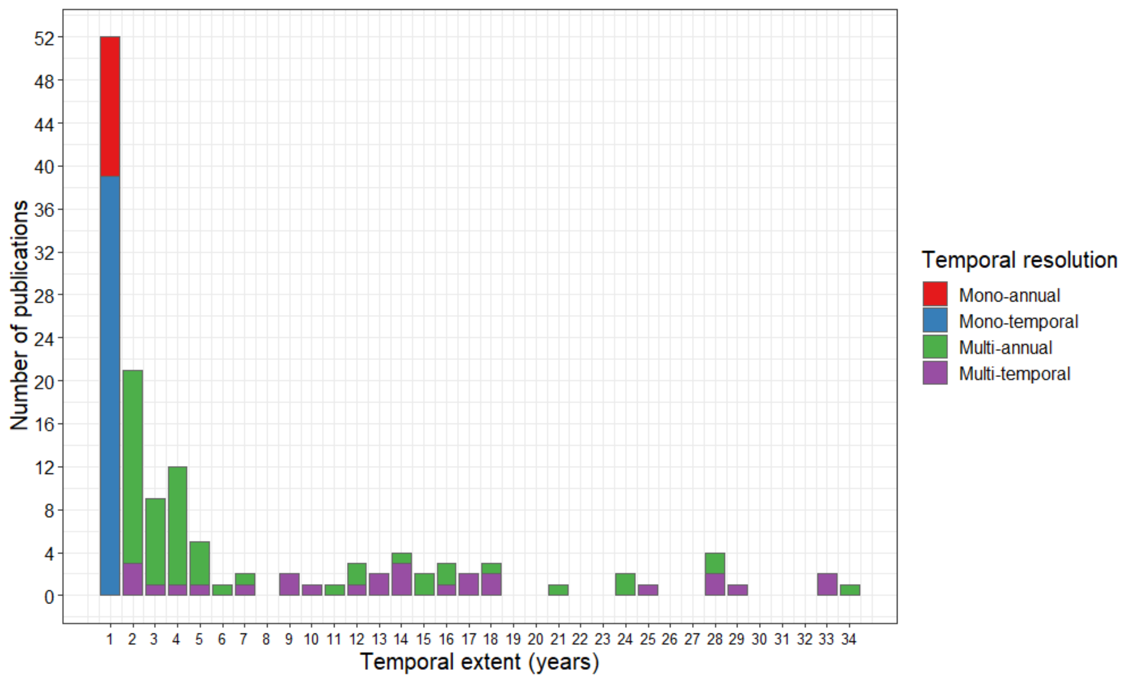

Fig. 2. 8. Temporal duration of studies included in the review integrating remote sensing and dryland forests in Southern Africa between 1997 and 2020.

2.4.3 Research topics

The study classified the large number of research topics into eight broad categories that cover the diversity of research into dryland forests. The eight categories, and the number of studies belonging to each of them, are shown in Fig. 2.9.

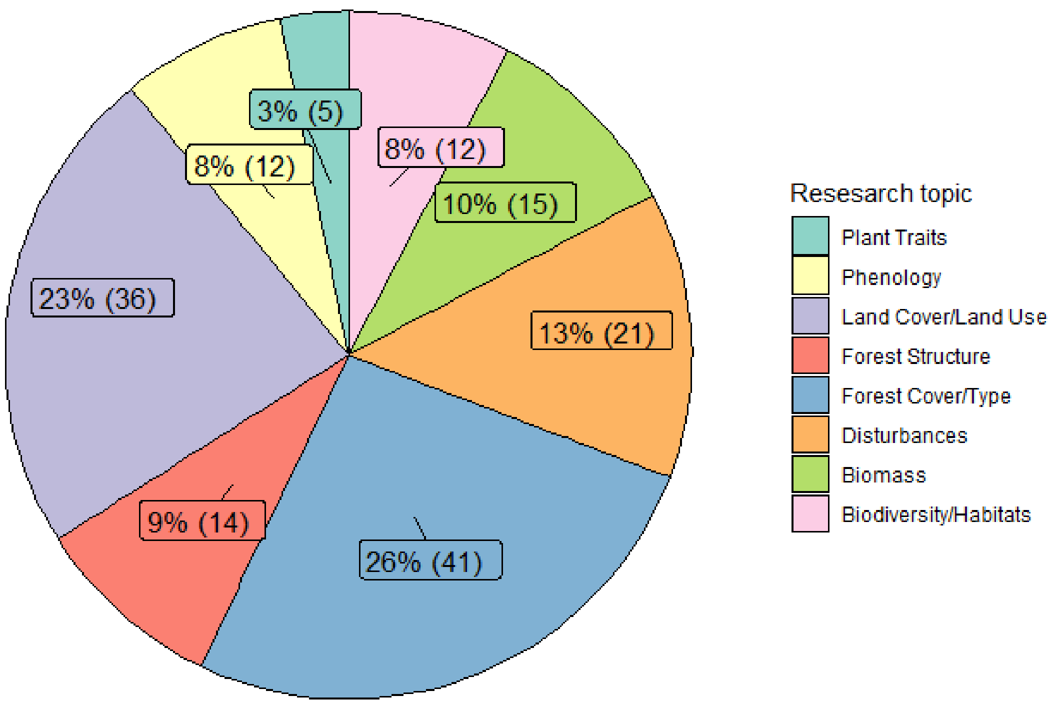

Fig. 2. 9. Research topic categories of reviewed articles between 1997 and 2020. Note that some studies cover different topics, which may result in multiple entries.

2.4.3.1 Land cover/land use

Land-cover change is one of the most researched areas using EO in Southern Africa, with 36 (23%) publications making it the second most common topic. Land-use/cover describing land surface classification, typically represented in thematic maps of different dryland vegetation were considered. Land-use/cover changes with a specific focus on other dryland vegetation such as rangelands, grassland, coastal vegetation, or plantation forests without covering dryland forests were excluded. The majority of publications on land-use/land-cover used optical data. For example, Landsat data have been used by more than 90% of publications, except Daskin et al. (2016) and Hüttich et al. (2011) which used RapidEye and MODIS data. Only one publication used a combination of Radar and optical data (Symeonakis et al., 2018). Sentinel data have not been utilised for land cover and land use study in the reviewed papers, probably due to the relatively recent availability of these data. Looking at scale, the majority of papers on land-cover change focused on the local scale in Southern Africa, but there is still a general lack of synthesis of land-use /cover change assessment at the regional, national or subcontinental scale (Fig. 2.6).

2.4.3.2 Forest cover/type

The majority of publications, 46 (31%) of studies cover the topic “Forest cover/type”. The forest cover/type comprises the generation of a forest/non-forest mask (Dlamini, 2017; Heckel et al., 2020), forest cover change estimation (Erkkilä et al., 1999; Ringrose et al., 2002), forest type discrimination between dryland forests (McCarthy et al., 2005), forest health assessment (Herrero et al., 2020), woody cover (Boggs, 2010; Ibrahim et al., 2018), and tree species classification (Adelabu et al., 2013; Hüttich et al., 2009). The majority of forest type/cover mapping was undertaken with optical multi-spectral data including Landsat, MODIS, and AVHRR and a few studies used high-resolution data such as RapidEye, GeoEye, and WorldView. On the other hand, a few studies on forest cover/type mapping used a combination of multispectral and spaceborne SAR data (X-band, C-band, and L-band) such as Landsat and JERS-1 (Bucini et al., 2009), Landsat and ALOS PALSAR (Higginbottom et al., 2018; Naidoo et al., 2016) and Sentinel-1 and -2 (Heckel et al., 2020) (Fig. 2.10).

A few studies on forest cover/type mapping relied on field data (Bucini et al., 2009; Ibrahim et al., 2018; Schultz et al., 2018) or forest inventory plots (Heckel et al., 2020). Most studies did not include detailed field measurements (species composition, density, frequency, dominance, and basal area, percentage soil cover, total height) and had very few field samples (Gessner et al., 2013). Other studies relied on fine resolution EO data (Dlamini, 2017; Higginbottom et al., 2018), and published maps (Westinga et al., 2020) as reference data to validate their results. The majority of studies did not perform any form of accuracy assessment or validation of quantitative estimates (e.g., Campo-Bescós et al., 2013; Harris et al., 2014). Forest cover and species mapping is essential for many forestry-related tasks and play a key role in sustainable forest management; the importance of these topics can be seen in the fact that they are addressed across all countries in Southern Africa, with the majority of studies conducted in RSA, followed by Namibia and Botswana (Fig. 2.11).

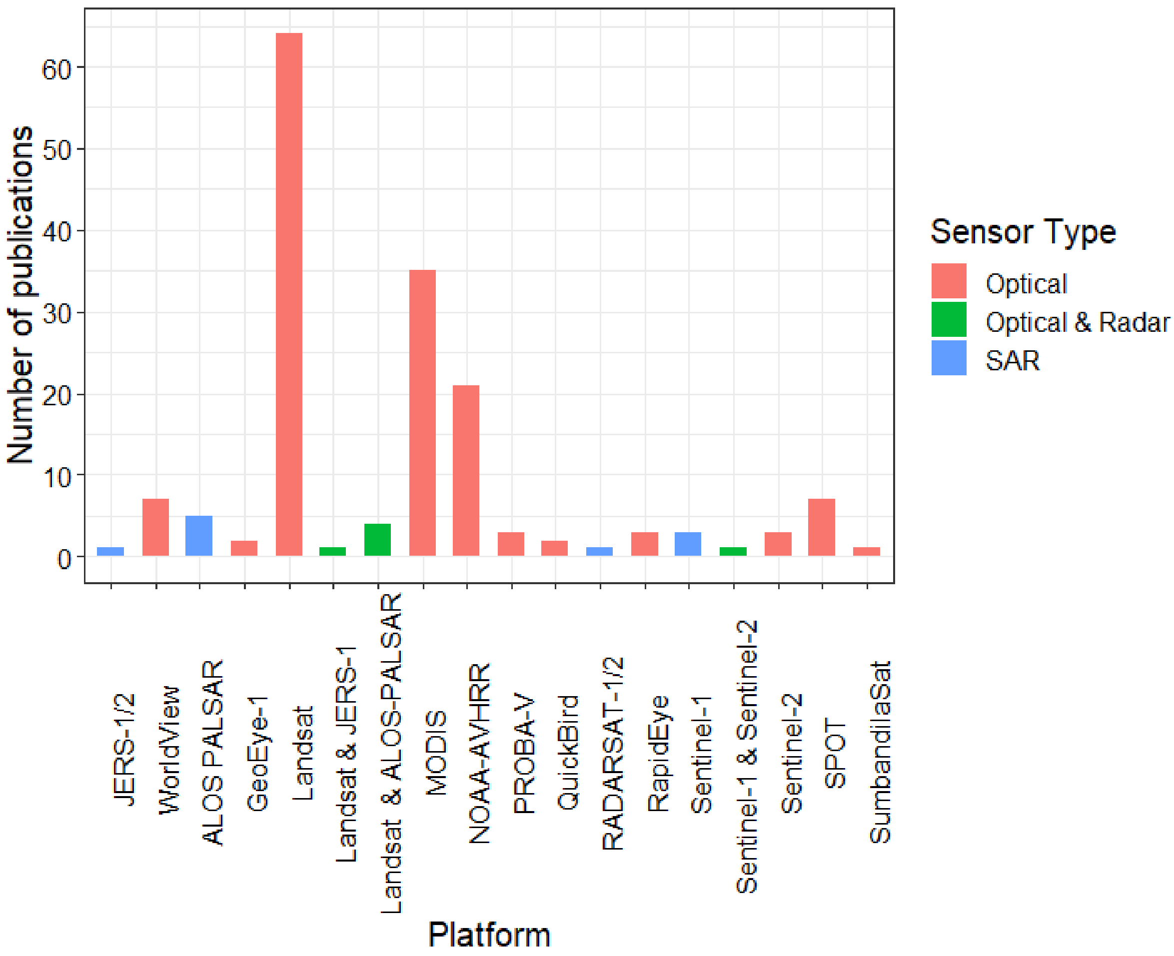

Fig. 2. 10. Number of studies based upon platform and sensor type. Note that studies investigating forest change with multiple platforms were counted multiple times.

2.4.3.3 Forest biomass and structures

Fifteen research papers (10%) studied forest biomass, and fourteen publications (10%) assessed "forest structure". Studies on biomass included the estimation of AGB (Dube et al., 2018; Mutanga et al., 2006), and changes in carbon stock (Gara et al., 2017). Some of the publications used National Forest Inventory (NFI) data (Halperin et al., 2016; Verbesselt et al., 2007), and field-based samples (Mareya et al., 2018; Tsalyuk et al., 2017) to estimate biomass in Southern Africa.

Forest structure in the review includes research on stand structure (Mathieu et al., 2013), canopy cover (Erkkilä et al., 1999; Huemmrich et al., 2005), canopy gaps (Cho et al., 2015), and stand density (Adjorlolo et al., 2013). The majority of studies on "forest structure" in Southern Africa dealt with canopy cover (e.g., Adjorlolo et al., 2014; Yang et al., 2000). Very few studies considered vertical forest structure including tree height and tree crown diameter (e.g., Verlinden et al., 2006b). Mareya et al. (2018) utilised freely available fine resolution Google satellite imagery in combination with object-based image analysis (OBIA) to estimate tree crown areas in miombo forests and found the overall accuracy to be low and unsuitable when high accuracy is required. Some of the "forest structure" publications are also assigned to the research topic "biomass", which discusses the relevance of forest structure for biomass (Meyer et al., 2014). Forest structure is also a very important parameter when it comes to habitat suitability, species diversity, biodiversity estimation, and conversation studies and thus some publications cover both topics (e.g., Akinyemi et al., 2019).

The methods applied in the biomass and forest structure publications are diverse. Most studies employed some sort of regression analysis between in-situ field data and EO data, with the most popular methods being random forests, support vector machines, kriging, linear and generalised linear models (Berger et al., 2019; Carreiras et al., 2013; Halperin et al., 2016; Mutanga et al., 2006; Wingate et al., 2018). Williams et al. (2013) utilised the simple ensemble model to analyse biomass dynamics and found that biomass distributions can diagnose disturbance processes in miombo woodlands. Most studies utilised the normalised difference vegetation index (NDVI) in dryland forest mapping to correlate with biomass (Gizachew et al., 2016; Wessels et al., 2006), but very few studies considered other vegetation indices such as red-edge (RE)-computed indices (e.g., Dube et al., 2018; Gara et al., 2016). For the most part, optical sensors were used to derive forest biomass and structures, only four papers utilised radar data, and one paper used a combination of radar and optical data to estimate biomass (Wingate et al., 2018). More research is needed to explore the improvement of forest AGB and forest structure estimation through multi-sensor (optical and radar) data fusion.

2.4.3.4 Climate change and disturbances

Here the study refer to dryland forests stress monitoring e.g., damage due to fire, climate/weather-related hazards including drought events, floods, extreme temperatures as part of climate change and disturbances. Twenty-one papers (13%) investigated disturbances to forest cover. Among the different forms of disturbance, fire damage was the most commonly studied (Mayr et al., 2018; Pricope et al., 2012; Roy et al., 2019; Silva et al., 2003). In the context of threats of climate change, other disturbances included drought (Lawal et al., 2019; Marumbwa et al., 2021; Urban et al., 2018) and floods (Pricope et al., 2015). A regional studies Lawal et al. (2019) used gridded climate data from the Climate Research Unit and GMMS NDVI to characterise the impact of drought to vegetation in southern Africa from 1981 to 2005; They found that the responses of vegetation varied according to season and biome, and showed that droughts had extensive impacts over the central parts of South Africa and Namibia, and the southern border of Botswana and the western parts of Zambia. In this review, only studies that investigated climate change in terms of temperature/drought in dryland forests where satellite data are a primary or secondary source of data were considered. Although there are a number of studies on climate change modelling in Southern Africa, the results show that there is a striking lack of studies investigating climate change into dryland forest change and stress monitoring.

The sensors used to detect disturbances differs, with most studies using MODIS (Alleaume et al., 2005; Archibald et al., 2009; Chongo et al., 2007; Giglio et al., 2009), two publications used SPOT-VGT (Silva et al., 2003; Verbesselt et al., 2006), and one Landsat and Sentinel-2 (Roy et al., 2019). Only two publications utilised SAR data. Mathieu et al. (2019) investigated SAR Sentinel-1A C-band images for detecting surface fires in the Kruger NP, while Williams et al. (2013) used ALOS PALSAR to analyse known disturbance agents in tropical woodlands in Mozambique. The research by Urban et al. (2018) used Sentinel-1 SAR time series NDVI from Sentinel-2 and Landsat-8 to derive surface moisture for drought monitoring in the Kruger NP between 2015 and 2017. A combination/fusion of SAR and Optical data for detecting disturbances is not tested by any study. Only one study used field data as input data for validation (Alleaume et al., 2005), while two studies used forest inventory data (Verbesselt et al., 2006; Verlinden et al., 2006a).

2.4.3.5 Biodiversity, plant traits, and phenology

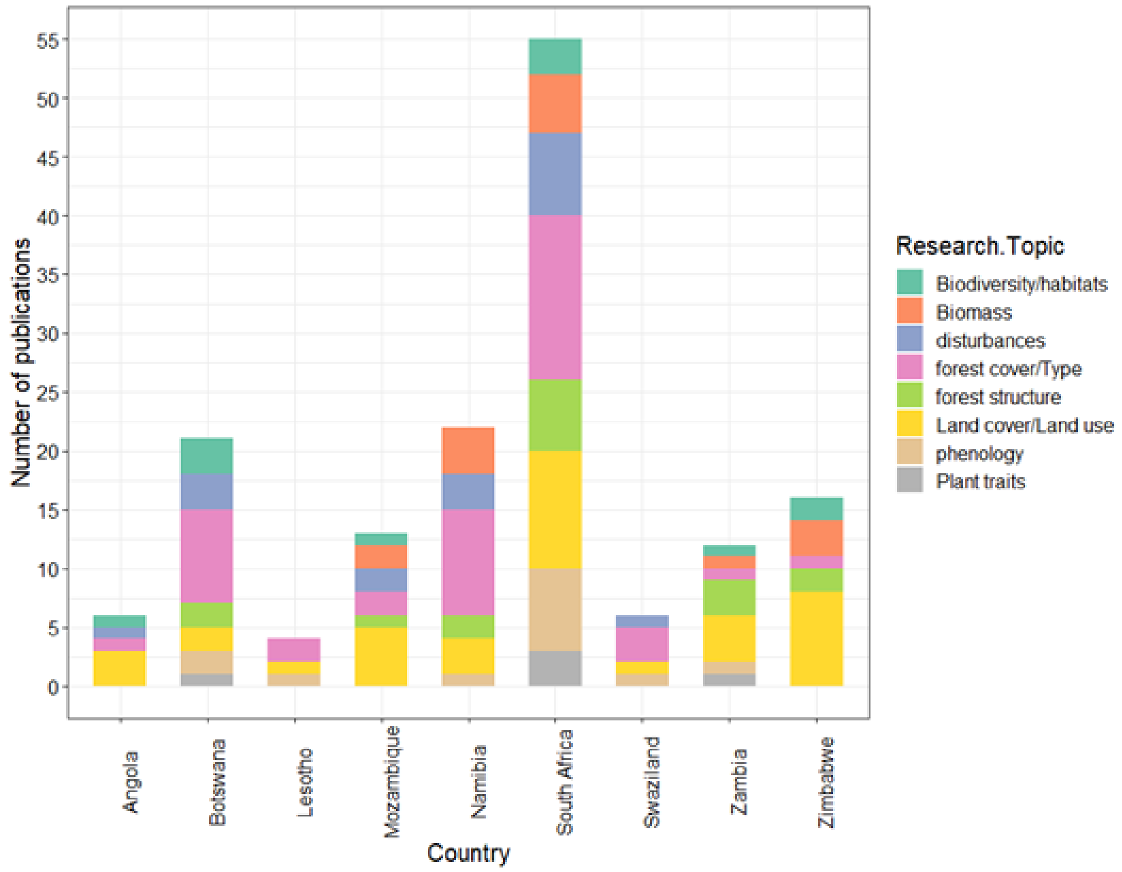

Fig. 2. 11. Research topic by country. Note that the order of the mentioned topics has changed when compared to Fig. 2.9 as some studies were conducted in several countries.

Twelve (8%) of the reviewed publications dealt with research questions in the context of forest biodiversity. Almost half of the papers on forest biodiversity examined plant species diversity (Adjorlolo et al., 2014; Chapungu et al., 2020; Mapfumo et al., 2016). Others looked at animal species and habitat suitability (e.g., Cáceres et al. (2015) for birds, Ducheyne et al. (2009) for tsetse flies, impala (Van Bommel et al., 2006), and elephants (Marston et al., 2020). Forest biodiversity is often related to structural canopy parameters. Most studies, nine (75%) of twelve used Landsat to derive parameters such as plant canopy height, species occurrence, richness, and diversity. Three (25%) of the studies used MODIS data (e.g., Fullman et al. (2014) used MODIS at 250 m pixel resolution and a Moving Standard Deviation Index (MSDI) to detect elephant-modified vegetation along the Chobe riverfront in Botswana; Akinyemi et al. (2019) utilised 1 km spatial resolution of SPOT - VGT and PROBA-V annual time series of 18 years to understand species diversity and richness assessment based on the Vegetation Degradation Index in Palapye Botswana.; Adjorlolo et al. (2014) investigated the utility of SPOT-5 multispectral data to assess tree equivalents and total leaf mass to model grazing and browsing capacity in KwaZul-Natal province in RSA.

Five papers (3%) dealt with different plant characteristics, known as plant functional traits. These include canopy chlorophyll content (Cho et al., 2012), leaf nitrogen concentration (Cho et al., 2013), and vegetation water content (Verbesselt et al., 2006), and Leaf Area Index (LAI) (Scholes et al., 2004). Plant functional traits including vegetation biophysical and biochemical properties (e.g., pigment levels, nitrogen content) are often related to patterns of biodiversity. Huemmrich et al. (2005) explored monthly MODIS data at 1 km spatial resolution over two years to estimate LAI and the fraction of absorbed photosynthetically active radiation (FAPAR) and found that ground-measured LAI values correspond well with MODIS LAI, and showed a discrepancy with FAPAR. Cho et al. (2012) utilised variogram analysis and the red edge shift from SumbandilaSat and SPOT 5 to estimate canopy chlorophyll content in Dukuduku forest in Southern Africa and found that SumbandilaSat provides additional information for quantifying stress in vegetation as compared to SPOT image data. All studies on plant traits were undertaken at the local scale.

Looking at research categories per country, biodiversity/habitat publications were mainly undertaken in Botswana and RSA (Fig. 2.11). All studies in the context of forest biodiversity and plant traits covered only mono-temporal and multi-annual classifications. Only two studies utilised multi-annual time series (Akinyemi et al., 2019; Verbesselt et al., 2006), and one study used MODIS multi-temporal time series over two years (Huemmrich et al., 2005). All of these studies focused on a coarse resolution of 1 km.

Phenology is also strongly linked to plant traits, but analysis puts more emphasis on the seasonal variations including growing season (green-up date) (Archibald et al., 2007; Whitecross et al., 2017), end of the season, and length of the season (Davis et al., 2017). To date, phenological research in Southern African dryland forests is limited, and more than half of the published papers on phenology focused only on examples from RSA. In the few studies that have analysed phenology, most studies dealt with estimating leaf flush and early-greening dates (Chidumayo, 2001; Higgins et al., 2011). For example, Archibald et al. (2007) developed an intricate algorithm that used MODIS NDVI products and field-based parameter estimates to predict green-up dates for grass and tree components at a site in the Kruger NP in RSA. Jolly et al. (2004) compared a water balance model to a 3-year NDVI time series and found the deviation between the onset of leaf flush predicted by the model and empirical data was between 10 and 40 days.

2.5 Discussion

2.5.1 Temporal extent

In this article, the current research with EO on dryland forests, with a particular focus on Southern Africa were synthesised. Although the volume of scientific literature has demonstrated a sharp increase, the use of remote sensing is still limited, and up until 2013, the number of publications on this topic was relatively small. Substantial research on the dryland forests of Southern African is mainly based on single-date observations, and comparing classified images at two or more different times. Maps that relate successive land cover change between two dates typically lack information regarding underlying processes and do not enable insights on the nature of the transformations present, such as the rate or persistence of change (Lambin et al., 2003). Time series analysis on dryland forests, which enables tracking changes is scarce, only 22 (16%) out of 137 studies feature time series lengths that exceed 15 years and only 11 (8%) studies that cover more than 20 years. Longer time series of remote sensing data afford the ability to assess the dynamics of forest structures, biodiversity, degradation, disturbance from climatic extremes, and change in phenology, in which a gap still exists.

2.5.2 Spatial scale

Another finding that stands out from the analyses is that there are very few studies at the national and regional levels. Despite new sensor and EO data availability, it is clear that a systematic and consistent regional monitoring of dryland forests is not yet fully exploited and is still in its infancy in Southern Africa. In fact, the majority of publications 88 (64%) concentrated their research efforts on local scale investigations (Fig. 2.6). Desanker et al. (2001) and Geist (2002) also emphasised that Southern Africa is limited to local-scale studies, thereby lacking a simultaneous analysis of the impacts of these changes at a larger scale. To fully assess regional and long-term implications for tropical dryland forest change studies, analyses on large(r) scales are needed, ideally with higher spatial resolutions and longer temporal duration.

2.5.3 Accuracy assessment

Through evaluation of the literature, the review identified that the assessment of accuracy for thematic/classified maps and statistical data to be another important issue, with only 54 (39%) of the studies appearing to have performed some form of accuracy assessment. The results show there is limited information on sources of error and uncertainty levels of the estimates provided by most studies. The review found that most forest and vegetation-related scientific outputs in Southern Africa are not yet strongly linked to field measurements and forest inventory data. Among the reviewed studies, very few studies utilised field test sites/ ground-based independent datasets for accuracy assessment, while other studies estimated uncertainties using other procedures e.g., using a sample of finer spatial resolution remote sensing data, or did not report the map uncertainty. Some studies employed root-mean-square error to assess model accuracy (RMSE) (e.g., Adjorlolo and Mutanga, 2013; Higginbottom et al., 2018), while many studies used an error matrix to assess map uncertainties, which was employed for instance (e.g., Adelabu et al., 2013; Hüttich et al., 2011). However, some studies used sample points below the desirable target number of validation points per class (e.g., Cabral et al., 2011), while studies briefly mentioned that a confusion matrix was calculated but did not report how many sample points were used for validation (e.g., Chagumaira et al., 2016). Congalton. (1988) suggests planning to collect a minimum of 50 samples for each map class for maps of less than 1 million acres in size with less than 12 classes. It has been empirically confirmed that a good balance between statistical validity and practicality for larger area maps or more complex maps can be achieved with about 75 to 100 sample sites per class (Congalton & Green, 2009).

Globally, owing to TDFs low commercial importance in comparison to other tropical forests such as moist forest, they are often not assessed by field surveys, or surveyed regularly by governments (Keenan et al., 2015). Independent validation data for dryland forest estimations are rarely available because acquiring appropriate field survey data is a time-consuming and expensive task. In Southern Africa, these areas are often remote and dangerous to visit in the field, due to the hazard posed by wildlife and if present, unexploded landmines, almost impracticable to obtain independent validation data for large(r) area studies, especially for many protected areas. Despite challenges to obtain ground-based observation, effective integration of these data and remote sensing methods will be key to accurately mapping and monitoring dryland forest across a range of spatial scales and in reporting the accuracy of models. However, the applicability of remotely measured geospatial data is reliant on quality and translating remote sensing data into accurate and meaningful information is often a challenge prone to errors (Congalton et al., 2009; Donoghue, 2002). In this context, it is critical to ensure the validity of these data and their suitability for each particular application, particularly where coarse spatial maps can be misleading. In addition, characterising dryland forest for large areas of Africa cannot entirely rely on global and pantropical monitoring studies for dry forest estimation because global forest monitoring generally underestimates, and in some instances overestimates, dryland biomes (Bastin et al., 2017).

2.5.4 Research topics and geographical focus

The classification of studies into eight broad subject categories revealed forest cover/types 41 (26%) and land cover/land use 36 (23%) to be the most commonly researched topics. Topics receiving less attention included phenology, plant traits, and biodiversity/habitats, and disturbances with regards to climate change (Fig. 2.9). With regards to disturbances, fire damage was the most commonly studied but there is a missing body of literature on the climate change impact on the composition, biodiversity, and ecological health of dry forest ecosystems in most countries of Southern Africa. The thesis also found an interesting, non-uniform spatial distribution of dryland vegetation and forest studies using spaceborne remote sensing, particularly when considering disparities among countries and across protected areas. The distribution of research categories by country reveals that RSA is, by far the most studied nation across all categories in Southern Africa (Fig. 2.7). It should be noted that care should be taken here not to assume that the number of studies equates to research quality, which remains difficult to articulate from a review of this nature. However, the dryland forests of Mozambique, Lesotho, Swaziland, and Zambia are noticeably very poorly studied. Studies on the dryland forests of Angola are even less frequent, receiving relatively little global attention, and the few studies conducted on its forests were mostly conducted by researchers from Portuguese Universities (Catarino et al., 2020; Leite et al., 2018). The focus of publications tended to be biased towards conservation and national parks, particularly as a large proportion of studies were undertaken in the Kruger NP, leaving many other private and international protected areas relatively understudied. Transboundary conservation areas, such as Kavango-Zambezi (KAZA), have received relatively little attention but merit further research in terms of the vast dryland forests extent, biodiversity, species abundance and diversity, and the potential for this area to form important corridor areas for wildlife animals. There is a further concern as a result of such gaps because some of the dryland forests, and species to which they are home, notably in countries like Angola and Zambia, are listed on the IUCN red list and would almost certainly merit Alliance for Zero Extinction (ACE) ranking (Cumming, 2008). Furthermore, future efforts to estimate important variables such as forest cover and biomass need not be restricted by country boundaries. Future studies, based on medium-fine resolution EO and validated with field data, will provide information to improve the understanding of African dryland vegetation and its management.

2.5.5 Vegetation indices, optical, SAR, and fusion of optical and SAR sensors

The most commonly used vegetation index was the NDVI, with more than half of the studies, 84 (54%) of papers utilising this index, but only 13 (8%) of papers used Enhanced Vegetation Index (EVI) and soil-adjusted vegetation index (SAVI).

Other vegetation indices such as the Green Normalised Difference Vegetation Index (GNDVI) and Sentinel red-edge related indices and passive microwave observations such as Vegetation Optical Depth were not utilised in studies considered in this review. One major problem commonly encountered in the less studied ecosystems, such as dryland forests, is that of generalising or transferring knowledge and methods derived from remotely sensed imagery over both space and time (Foody et al., 2003). For example, commonly used vegetation indices and classification schemes are in general mainly been calibrated on other, better-studied ecosystems, such as temperate or rain forests, and this has led to poor accuracy results when extrapolated, to for example, tropical dryland forests. This phenomenon justifies the importance of utilising a range of vegetation indices when studying dryland forests using EO data. Imagery from optical sensors is most commonly used, out of all sensor types, providing the data used in 90% of papers reviewed, followed by SAR data with 6%. The fusion of optical and radar data was rarely used, with only 4% of publications exploring this. The most frequently used platforms are Landsat, followed by MODIS and AVHRR. Imagery taken by the Sentinel-1/2 satellites only makes up a small portion of the remote sensing data on dryland forests. For example, Sentinel-2 was only used by 2% of investigated studies, but this may reflect the relatively short period (since 2015) when these data have been available.

2.5.6 Remote sensing platforms and cloud-based computing

Most of the EO data used in the publications reviewed were downloaded, and are available at no cost from a number of online portals, including the Oak Ridge National Laboratory (ORNL), the United States Geological Survey (USGS) Distributed Active Archive System (DAAC) and Earth Explorer (EE) tool. The lack of remote sensing research centres in most Southern African research institutions may contribute to limit the number of African Scientists engaged in monitoring forests resources. For example, most studies in RSA made use of remote sensing data through the University of the Witwatersrand, Satellite Application Centre (SAC), the South African National Space Agency (SANSA), and the Council of Science and Industrial Research (CSIR). The development of remote sensing capacity at local universities has inevitably contributed to RSA universities and research institutions conducting the majority of studies in Southern Africa (Fig. 2.5). To improve EO data access, and the skills to handle and interpret this across Southern Africa, there is a need to increase the number of local institutions that distribute the remote sensing data, and who have the capacity to access and use innovative web-based platforms such as the Google Earth Engine (GEE) and Amazon Web Services to overcome some of the logistical and financial constraints of this type of research.

Southern African countries face considerable technical challenges with remote sensing, particularly in respect to REDD+-related research on dryland forests monitoring. Freely available tools, for example, the cloud-based geospatial analysis platform Google Earth Engine (GEE), make it easier to access powerful computing resources for processing and analysing pre-processed large-scale datasets (Shelestov et al., 2017). However, only nine papers (6%) out of 137 used GEE to access or analyse remote sensing data. The "near real-time" remote sensing data offered by GEE is of particular interest for monitoring changes and automating the analysis of time-series, when detecting and tracking trends in surface reflectance properties. With increasing spatio-temporal coverage of satellite data and computational platforms that reduce the need for costly local infrastructure (e.g., GEE), there is an opportunity to overcome the limitations previously enforced by large volumes of data and the scale of analysis, whereby the knowledge of dryland forest dynamics can be improved in the upcoming years.

2.6 Conclusion

This review summarises research progress towards the use and integration of remote sensing data within the context of monitoring dryland forests in Southern Africa, using a systematic review methodology that focused on 137 most relevant research articles. The study has systematically reviewed the temporal and spatial coverage of these studies, their application area, and the remote sensing platforms and sensors used. Based on the results, the following conclusions can be drawn. There is a broad range of topics covered by research on dryland forests, from which land-use/land-cover and forest cover and disturbances from the fire were the most frequently studied. However, there is still a relative lack of studies assessing dryland forest structure, phenology, biodiversity/habitats, plant traits, and disturbance from climatic extremes, suggesting additional research is required. The majority of studies relied on single-date or annual data and bi-temporal discrete classification; only a very few studies employed time series analysis.

The thesis considers some of the limitations of the research reviewed, which indicates a need for more frequent use of field and inventory data, a greater use of validation/accuracy assessments, and testing other vegetation indices beyond NDVI and EVI such as the Vegetation Optical Depth and Sentinel-2 red-edge related indices. In addition, further improvements should focus on for extensive combination and fusion of SAR and optical data in order to have a temporally and spatially consistent data set necessary for several applications in dryland forests. Given the state of decline of woody vegetation condition in Southern Africa, long-term monitoring of monthly time series of EO data at regional and transboundary scale clearly hold potential to capture dryland forests dynamics and to understand their current status and future trends. A significant move from EO predictions that are extremely site-dependent to large(r) ecoregional level monitoring approach that integrates a range of remotely-sensed data of sufficiently fine spatial and temporal resolution with field measurements and using machine/deep learning models could provide a sound basis for assessing dryland forest-related changes and dynamics. Information inferred from these kinds of models would be extremely useful for the current knowledge, management and conservation of the dryland forests as well as for understanding their responses to disturbance (natural or anthropogenic) and climatic change at regional to sub-continental level. Finally, there is significant geographical heterogeneity in study coverage; whilst there is substantial research on the forests in the Kruger NP and across RSA, the same cannot be said for other areas of Southern Africa. The EO interventions not only assess deforestation rate, but also support other forest related REDD+ activities such as sustainable forest management which reduce forest degradation and enhance forest carbon stocks at a range of scales, transcending both provincial and national boundaries e.g., Kavango-Zambezi Transfrontier Conservation Area (KAZA TFCA). Nevertheless, REDD+-related research on dryland forests in most Southern African countries and protected areas has been limited, with clear gaps across Angola, Mozambique, Zambia, and Zimbabwe. Finally, Africa has the potential to emulate other continents, such as Latin America, that have made notable progress in employing freely available remote sensing data to monitor tropical dryland forest area change and biomass on a large scale.

2.7 Acknowledgments

This work was supported by the Commonwealth Scholarship Commission Ph.D grant number: NACS-2017-409 from 2017–2020, Geography doctoral program at Durham University. The authors would like to acknowledge the support provided through the Rapid Evidence Synthesis Training (REST) programme. REST was organised and delivered through a collaboration between the University of Leeds, The University of Newcastle, and the N8 AgriFood Programme and supported by Research England QR-SPF funds from The University of Leeds and University of York.

3 IMPROVING ABOVE GROUND BIOMASS ESTIMATES OF SOUTHERN AFRICA DRYLAND FORESTS BY COMBINING SENTINEL-1 SAR AND SENTINEL-2 MULTISPECTRAL IMAGERY.

Chapter 3 is published in *Remote Sensing of Environment*: DOI:
https://doi.org/10.1016/j.rse.2022.113232

Title: Improving above ground biomass estimates of Southern Africa dryland forests by combining Sentinel-1 SAR and Sentinel-2 multispectral imagery.

Authors: Ruusa M. David, Daniel N.M. Donoghue, Nick J. Rosser

Department of Geography, Durham University, Science Laboratories, DH1 3LE Durham, UK

Author Contribution

David Ruusa- Design the research, perform the data analysis, interpret the results, wrote the manuscript, and revised the manuscript. Nick Rosser- Contributed to the research design, manuscript editing and supervision. Daniel Donoghue- Contributed to the research design, conducting fieldwork, manuscript editing and supervision.

Abstract

Having the ability to make accurate assessments of above ground biomass (AGB) at fine spatial resolution is invaluable for the management of dryland forest resources in areas at risk from deforestation, forest degradation pressure and climate change impacts. This study reports on the use of satellite-based synthetic-aperture radar (SAR) and multispectral imagery for estimating AGB by correlating satellite observations with ground truth data collected on forest stands from dryland forests in the Chobe National Park, Botswana. The study undertooks nineteen quantitative experiments with Sentinel-1 (S1), Sentinel-2 (S2) and Landsat 8 OLI (LC8) and tested simple and multivariate regression including parametric (linear) and non-parametric (random forests) algorithms, to explore the optimal approaches for AGB estimation. The largest AGB value of 145 Mg/ha was found in northern Chobe while a large part of the study area (85%) is characterised by low AGB values (< 80 Mg/ha), with an average estimated at 51 Mg/ha. The results show that the AGB estimated using SAR backscatter values from vertical transmit receive (VV) polarisation is more accurate than that based on horizontal receive (VH) polarisation, accounting for 58% of the variance compared to 32%. Nevertheless, the combination of S1 SAR and S2 multispectral image data produced the best fit to the ground observations for dryland forests explaining 83% of the variance with an accuracy of 89%. Furthermore, the optimal AGB model performance was achieved with a multivariate random forest (MRF) regression trees algorithm using S1 (SAR) and S2 (multispectral) image data (R^2 = 0.95; RMSE = 0.25 Mg/ha). From the 11 vegetation indices tested, GNDVI, Normalised Difference Red Edge (NDRE1), and NDVI obtained the highest linear relationship with AGB (R^2 = 0.71 and R^2 = 0.56, $p < 0.001$), however, GNDVI and NDRE1 improved the AGB estimation at medium to high-density forests compared to NDVI. The GRVI and EVI were the least correlated with AGB (R^2 = 0.09 and R2 = 0.31) at a significance level of $p < 0.001$, respectively. The thesis shows that NDVI saturates in areas with >80 Mg/ha AGB, whereas the inclusion of SAR backscatter and optical red edge bands (B5) significantly reduces saturation effects in areas of high biomass. GNDVI and red edge (B5) derived vegetation indices have more potential for estimating AGB in dryland forests than NDVI. This study results demonstrate that dryland AGB can be estimated with a reasonable level of

precision from open access Earth observation data using multivariate random forest regression.

Keywords: Dryland forests, Above ground biomass, Random forest, Linear regression, Sentinel, SAR, Southern Africa, Chobe, Conservation

3.1 Introduction

Dryland forests in Southern Africa are currently experiencing high rates of forest loss as a result of overexploitation, wildfire, and herbivory, and are projected to experience the impacts of climate change (Miles et al., 2006). Although large uncertainties surround the contribution of tropical savanna forests and open woodland (hereafter referred to as dryland forests) to the global carbon budget, recent studies have shown that dryland above ground biomass (AGB) is a more dominant driver of variations in the global carbon cycles when compared with moist tropical forests (Ahlström et al., 2015; Poulter et al., 2014). However, wildfires and a high density of mega-herbivores in most protected/conservation areas (particularly elephants, *Loxodonta africana*) can have a significant impact on tree cover and structural diversity by modifying vegetation structure through grazing and physical damage thereby making trees less tolerant to fire (Ben-Shahar, 1996; Shannon et al., 2011). With these pressures degrading the dryland forests, techniques are urgently needed to measure, map, and monitor the forest stand parameters reliably and to produce this information at appropriate scales to support conservation and management actions. AGB estimates from sub-tropical dryland forests have received less attention than many other biomes and so estimates of AGB remain highly uncertain, despite the importance of these areas as carbon stores and for ecosystem services (Pennington et al., 2018; Olson and Dinerstein, 2002). For instance, studies of tropical moist forests are well represented in the scientific literature (Salis et al., 2006; Williams et al., 2008), primarily because they have the highest carbon (C) uptake of the World's forests (Olson and Dinerstein, 2002). The largest proportion of dryland forests ecosystems are found in Africa, accounting for 60 - 80% of the total biome area (three times the area covered by African rain forest) (Bodart et al., 2013; Bullock et al., 1995), which provides a significant carbon stock for the African continent.

AGB is recognised as an essential terrestrial climate variable (ECV) by the Global Climate Observing System (GCOS) led by the UN Framework Convention on Climate Change (UNFCCC) (Bojinski et al., 2014). In addition, having information on AGB, and other biophysical structural parameters such as canopy height and habitat density in dryland forests can feed into a wide range of activities related to carbon accounting and conservation purposes (Wulder et al., 2012). Information about the distribution of biomass at local, regional, and global scales can also detect land changes due to factors such as deforestation (a reduction in a woodland area) and forest degradation (Harris et al., 2012; Saatchi et al., 2011). However, at the same time, dryland forests experience an increase in woody carbon stock, including widespread regrowth following shifting cultivation, bush encroachment, and a reduction in browsing megaherbivores (McNicol et al., 2018). Southern Africa, particularly the KAZA region, is experiencing large-scale shifts in vegetation cover, biomass degradation, and increased vulnerability to climate change which hold significant implications for forest ecosystem function (Cumming, 2008; King, 2014; Niang et al., 2014). Yet, the location and rates of the AGB and biomass loss and regrowth, and the above ground woody carbon stocks are largely unknown (David et al., 2022a).

Estimates of biomass using conventional techniques based on field measurements are the most accurate ways of collecting biomass data. However, extensive fieldwork is not feasible due to the inaccessibility, and logistical challenges of such field surveys which limit the number of plots that can reasonably be surveyed which impact AGB characterisation over large areas (Næsset et al. 2016). Biomass measurements based on Earth observation measurements are obtained through statistically-based integration of tree-level allometric equations with biophysical or structural information derived from satellite data (Boisvenue & White, 2019). The shortcoming of utilising satellite imagery for AGB estimation is related to selecting suitable models and data availability (Houghton et al., 2009; Lu, 2006). In terms of optical sensors, Landsat is one of the most utilised datasets because it provides freely accessible imagery, at a high temporal coverage with a medium spatial resolution (Dogru et al., 2020). In their study within miombo forests, Gizachew et al. (2016) identified a linear relationship between AGB and Landsat 8 derived spectral variables, concluding that the approach was suitable for monitoring and reporting of biomass baselines in low-biomass, open-canopy woodlands for REDD+ projects. The launch of the Sentinel-2 series satellites through the EU Copernicus program provides new opportunities to enhance forest monitoring in tropical countries on a large scale (ESA, 2020). Compared to Landsat, the Sentinel-2 data provides four additional spectral bands strategically positioned in the red-edge region that are expected to contribute to improved AGB estimation and mapping (Li et al., 2021; Mutanga et al., 2012). Previous studies that compared Sentinel 2 to Landsat 8 found Sentinel 2 to have spatial and spectral capabilities that improved the estimation of AGB in different vegetations (Sibanda et al., 2016; Forkuor et al., 2018). Such optical sensors are however limited in the degree to which they can generate structural information because they have difficulty penetrating beyond upper canopy layers and optical data can be obscured by frequent cloud cover (Hyde et al., 2006). Certain limitations related to data saturation also exist, particularly at sites with high woody cover, or those areas with complex vegetation structures such as dryland vegetation, as so many satellite sensors can be insensitive to large AGB variations (Lu et al., 2012; Powell et al., 2010). Optical sensors are also limited in their ability to estimate higher biomass levels as they are more sensitive to canopy density/cover rather than canopy height (Joshi et al., 2016). Biomass saturation for low and medium spatial resolution passive optical sensors such as the Moderate Resolution Imaging Spectroradiometer (MODIS) or Landsat is a well-recognised problem (Steininger, 2000; Zhao et al., 2016).

Space-borne Synthetic Aperture Radar (SAR) sensors such as Sentinel 1, TerraSAR-X, ALOS PALSAR can be used to estimate AGB through cloud, as well as provide detailed vegetation structural information from backscatter (Berninger et al., 2019; Lucas et al., 2008). SAR data has the advantage that it includes the ability to collect data in all weathers, during both day and night; the sensor has the capability to penetrate through cloud and forest canopy; data are sensitive to surface roughness, dielectric properties, and moisture content (Balzter, 2001; Santos et al., 2002). The radar backscatter and the reflected signal is sensitive to polarisation and frequency (HH, VV, HV, and VH), and can be used for volumetric analysis rather than just the colour and density of leaves and so has the potential to be more sensitive to AGB in the woodlands of savanna (Balzter, 2001; Mitchard et al., 2011). Recent research has shown that SAR data are suitable for classifying vegetation types and assessing biomass at regional scales (Omar et al., 2017). Minh et al. (2016) used SAR tomography to model tropical forest biomass and height in central French Guiana and found a high correlation between the backscatter signal and AGB in the high-biomass forest areas. In Africa, Bouvet et al. (2018) created an ALOS PALSAR map at 25-m spatial resolution using an L-band PALSAR mosaic produced by JAXA and in situ data, to estimate AGB over the whole of Africa. Conversely, the saturation problem is also common in radar data at the middle to high biomass levels, depending on wavelength and forest type, as documented by Balzter (2001) and Lucas et al. (2008). The saturation level has been found to vary as a function of the wavelength and polarisation of the incident radiation and studies have reported saturation at approximately 30 - 50 Mg/ha, 60–100 Mg ha and 100–150 Mg ha for C-, L- and P-band respectively (Lucas et al., 2006; Lucas et al., 2015). Water content, forest spatial structure, and surface geometry (terrain slope) derive errors and can cause saturation (Balzter, 2001). Studies have successfully demonstrated the capabilities of Light Detection And Ranging (LiDAR) for measuring vegetation distribution and estimating associated biophysical parameters (Popescu, 2007). LiDAR can be used to directly estimate a spatially explicit 3D canopy structure as a laser pulse emitted from the LiDAR sensor can penetrate the multi-layered tree canopies reaching the ground, which has great potential for improving the estimates of vegetation parameters (Pearse et al., 2019). This leads to more accurate estimations of basal area, tree height and stem volumes (Pirotti, 2011), but such approaches remain intensive and unsuited to regional or global coverage (Gibbs et al., 2007). For the direct derivation of biomass from optical, radar and LiDAR data, no single data type can fulfil all requirements with each limited by either weather, saturation, and other bio-physical conditions (Kellndorfer et al., 2010). Given these limitations, research exploring the fusion of different data types is crucial to develop accurate AGB maps (Koch, 2010).

To assess and monitor forest structural parameters, various approaches to reduce the impacts of data saturation in optical imagery in AGB estimation have also been explored. Vegetation indices and textures generated from optical and airborne

LiDAR data are often used as an alternative (Zhao et al., 2016). Many factors influence data saturation, ranging from spectral, spatial, and radiometric resolutions, vegetation type, or topographic features, which may lead to different saturation values of AGB (Lu et al., 2016). For example, Lu et al. (2004) compared different vegetation indices in the moist tropical region of the Brazilian Amazon and found that vegetation indices including near-infrared (NIR) improved correlations with AGB in relatively simple forest stand structures. Gizachew et al. (2016) used Landsat 8 derived NDVI to estimate total living biomass (TLB) in the miombo woodlands of Liwale district, south-eastern Tanzania. Despite its wide application, NDVI has major limitations for modelling the spatial variability of biomass including its instability. The NDVI signal is influenced by the underlying canopy background, varying with soil colour, canopy structure, leaf optical properties, and atmospheric conditions (Tucker, 1979; Pettorelli et al., 2005). Madonsela et al. (2018) investigated the interactions between seasonal NDVI and woody canopy cover in the savanna of the Kruger National Park (KNP) to model tree species diversity using a factorial model and found that the interaction between NDVI and woody canopy cover was insignificant. NDVI is known to give poor estimates in the growing seasons and in estimates of areas with high-density wood cover. These challenges have led to the development of alternative formulations which include correction factors or constants introduced to account for or to minimise the varying background reflectance, such as the Enhanced Vegetation Index (EVI) (Huete et al., 1999). Xue et al. (2017) reviews other closely related indices that include the Normalised Burn Ratio (NBR), the Green Normalised Difference Vegetation Index (GNDVI), Soil-Adjusted Vegetation Index (SAVI), the Transformed Soil Adjusted Vegetation Index (TSAVI) and the Green Red Vegetation Index (GRVI) amongst others. Some studies have demonstrated that the use of vegetation indices derived from the NIR narrow and red-edge bands situated between red and near-infrared at wavelengths 680–780 nm can yield a higher accuracy of AGB estimation as compared to conventional NDVI (Cho et al., 2007; Laurin et al., 2016). Ramoelo et al. (2015) and Li et al. (2021) found a strong correlation between biomass and the red edge position for a rangeland and grassland ecosystem in South Africa and China, respectively. Comparable research in dryland forested regions remains extremely limited (Michelakis et al., 2014; Forkuor et al., 2020), thus this study has tested vegetation indices derived from the NIR narrow and red-edge bands, GNDVI, EVI, NDVI, NBR, NBR2, SAVI, MSAVI in dryland forest of Southern Africa. In this study vegetation indices such as NDVI, GNDVI, NBR, and NDRE (Table 3.2) were selected because they all use a NIR band but differ in terms of the second band, e.g., NDVI utilised the red band, GNDVI the green band, NBR the SWIR2 and NDRE the red-edge band. Furthermore, it is important to choose a suitable method to estimate forest AGB. The linear and multiple regression (LR and MLR) method has been the most commonly utilised statistical algorithm for AGB estimation in past research (Propastin, 2012). However, it is documented that the linear regression method does not effectively explain the complex nonlinear relationship between biomass and Earth observation data and has been known to be unreliable at values beyond a saturation point of the canopy reflectance (Lu, 2006; Puhr and Donoghue, 2000). Also, identifying suitable variables for developing a multiple regression model is critical because some variables are weakly correlated with AGB or are likely to suffer from multicollinearity (Jong et al., 2003). Thus, understanding the performance and contribution of multiple sources of data and methods for forest biomass estimation has the potential to exploit the strengths of each and can help minimise the limitations of single sensors.

Several assessments have indicated that global forest cover datasets based on satellite data have clear limitations for characterising forest structural parameters in areas where the tree canopy is open, such as in savannas (McElhinny et al., 2005). Approaches that integrate forest structural parameters and remote sensing need to be replicated and tested across different regions, and geographic scales (Lehmann et al., 2015; Mitchard et al., 2013). Furthermore, Foody et al. (2003) and Woodcock et al. (2001) have pointed out concerns of generalising or transferring methods and results derived from remotely sensed imagery over both space and time. Many studies lack field data to build and validate AGB models, particularly in tropical dryland forests where national forest inventory data is not available (Grainger, 1999; Schimel et al. 2015). To the best of the author’s knowledge, there are very few studies that have tested the combination of synthetic-aperture radar (SAR) and multispectral data to map AGB in Southern African dryland forests. Such structural diversity maps are an invaluable data source for monitoring and managing biodiversity of forests and conservations of wildlife habitats and corridors reducing the isolation of wildlife populations. Such maps also contribute to the ecological functioning and health of savanna ecosystems. This study aims to assess the feasibility of using remote sensing data derived from SAR, multispectral, and ground measurements to estimate AGB in an area of typical African dryland forests. The study developed parametric and non-parametric models for estimating and testing the accuracy of AGB estimation and mapping. The models developed by this thesis are compared to different published biomass models in the dryland forest environment (Avitabile et al., 2016; Baccini et al., 2017; Bouvet et al., 2018. The study presents a novel remote-sensing approach of dataset combination and methodology, that can, in principle, be applied to the estimation and mapping of AGB in dryland forest sites worldwide.

3.2 Materials and methods

3.2.1 Study area

This study area is situated in Chobe National Park, in the north-east of Botswana covering an area of around 10,589 km^2 (18.7″S and 24.5″E) (see: Fig. 3.1) within the Kavango Zambezi Transfrontier Conservation Area (KAZA) of Southern Africa. KAZA is the World's largest conservation area with an enclosed area of 519,912 km^2. KAZA is shared by Angola, Botswana, Namibia, Zambia, and Zimbabwe and links together over 36 proclaimed protected areas including national parks, forest reserves, and wildlife management areas. Chobe National Park was chosen as the field site because it is one of the largest protected areas in Botswana featuring an impressive population of large mammals and several endemic plant species, including large areas of the dryland forests and globally significant wetlands. Within these habitats, there is a broad range of vegetation types ranging from low herbaceous to high-density woody cover (McIntyre, 2010). The largest population of African elephants (>150,000) is in northern Botswana drawn by the Chobe River basin which serves as a source of surface water in the dry season when animals converge on this stretch of water (Fullman, 2009).

Chobe NP is a relatively flat area with an average elevation of 980 m. The climate is semiarid with a highly variable mean annual rainfall of about 600 - 700 mm, mainly falling between November and March and a mean annual temperature of 21.8 °C (Fullman and Child, 2013). There is a general absence of rainfall in the dry season (April–October). The nearest permanent water source is the Chobe River forming the northern boundary of the park and the political border between Botswana and Namibia. A high concentrations of large mammalian herbivores including elephant, giraffe (Giraffa camelopardalis (L.)), impala (Aepyceros melampus), and buffalo (Syncerus caffer) are found along the Chobe River front during the dry season when seasonal pans are dry (Melton, 1985). Vegetation in Chobe National Park is dominated by savanna grassland and low-density woodland. Within these habitats, there is a broad array of vegetation types from low herbaceous to high-density woody cover (McIntyre, 2010). The vegetation found on the banks of the river is riparian woodland including *Capparis tomentosa, Trichilia emetica, Acacia nigrescens, and Croton megalobotrys*. Because of the intense pressure from elephants, vegetation along the Chobe riverfront has been heavily impacted and is now dominated by low shrubs and very few large trees (Fullman and Child, 2013). Often, the remains of dead trees suggest they have been ring-barked, heavily browsed and toppled by elephants causing mortality. In the south of the Chobe River, the most dominant woodland species are *Baikiaea plurijuga, Burkea africana, Ochna pulchra* (Mosugelo et al., 2002).

The high population of elephants has a wider destructive influence on vegetation, especially within the Chobe River basin as they migrate to neighbouring countries including Angola, Zambia, and Namibia. According to the United Nations Framework Convention on Climate Change (UNFCCC) many of the countries of southern Africa, including Botswana, Zambia, and Namibia, has been classified as highly vulnerable to climate change and its effects (McGann, 2004). The visible forest loss, especially that along the Chobe River frontage, has caused concerns among stakeholders regarding dryland forest degradation pressure and accompanying loss of biodiversity (see: Fig. 3.2A-F) (Nichols et al., 2017). In addition to climate change and wildlife damage, it is estimated that 55% of year-old saplings across all woodland species are killed by fire in Chobe National Park (Fidzani, 2014). The KAZA region has been identified as biodiversity hot spot and estimates of dryland forest cover and distribution not only are important tools to help conservation and sustainable management of forests but also because of the risk to dryland forest areas from several potential threats: climate change, forest fragmentation, fire, conversion to agriculture, and increasing wildlife population density (Cumming, 2008).

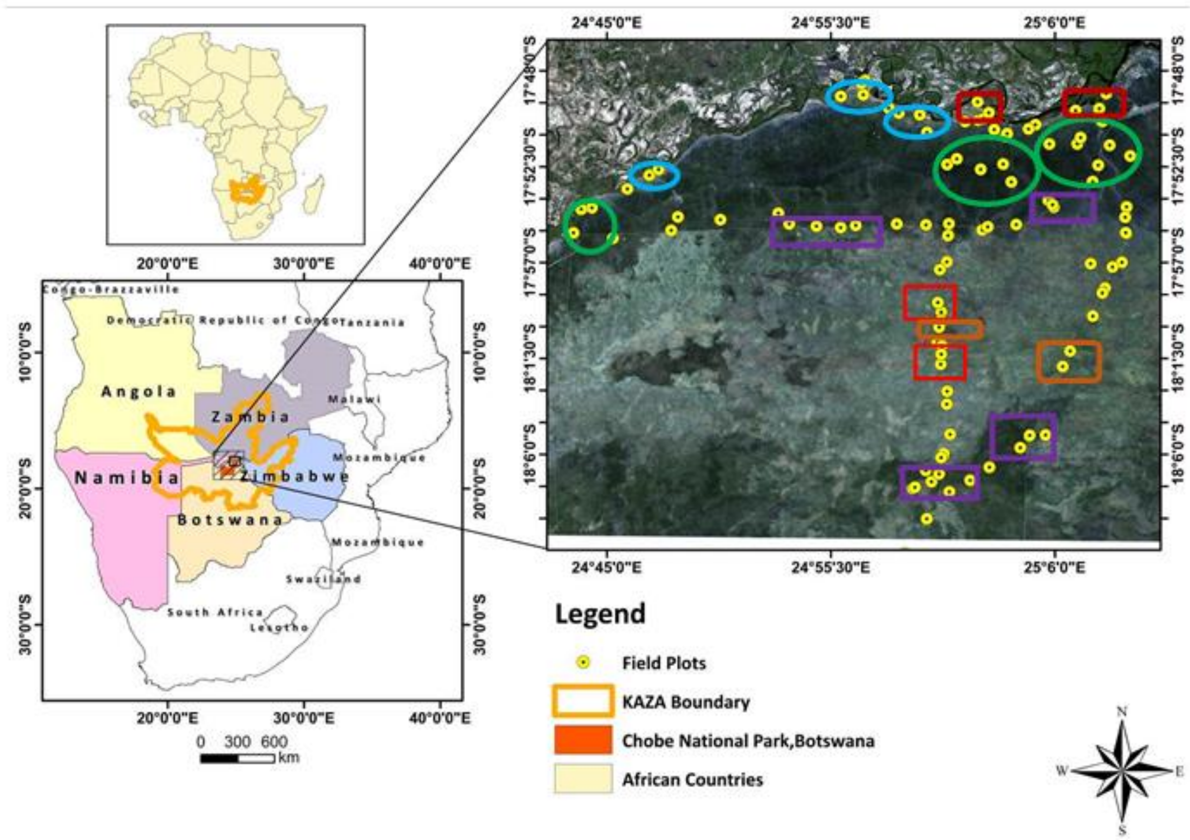

Fig. 3. 1. Location of the study area highlighting the countries (Botswana, Namibia, Angola, Zambia and Angola) and Chobe National Park where the field work was conducted. The coloured polygons around the sampled points indicate the type of vegetation structural formation and a range of land cover types that field sites represent (e.g., green-coloured circle: closed forests, purple-coloured square: open forests, orange-coloured square: shrubs, red-coloured square: grassland).

3.2.2 Fieldwork and sampling design

Fieldwork was carried out during March 2019, which is the growing season, when the vegetation photosynthetic activity is still high. Sentinel-2 (S2) and Landsat 8 OLI (LC8) wet season images (February - April) were acquired then classified into four classes (forests, open woodland, shrubs, and grassland) as these classes represent the main land cover types in the study area of Chobe NP. The allocation of field plots followed a stratified random sampling approach based on the four strata (forest, open woodland, scattered trees with low herbaceous cover, and non-forest) that represent broad vegetation types, and capture change between key land cover types well. Measurements were collected from a total of 101 individual sample plots throughout the savanna landscape of Chobe National Park. The sample plots were widely distributed across Chobe NP (Fig. 3.1) and encompassed relatively homogeneous tracts across a range of typical ecosystems (e.g., savanna grasslands, shrubs) and structural formations (open woodland to closed forest). Data from 61 of the 101 plots surveyed represented forest, and 40 samples described represented non-forest land cover types. Examples of the collected ground truth of typical forest cover types and recent vegetation degradation activities through herbivory, drought, and burning captured during the field campaign in 2019 are shown in Fig. 3.2. Within the 61 sample plots, a total of 4337 individual trees were measured. Table 3.1 presents stand parameters statistics based upon this survey for dryland forests. Fig. A. 1 shows the density and histogram plots of Aboveground biomass (AGB) and Carbon stock (Mg/ha) of each field plot within savanna forest.

Prior to fieldwork, the size of field sampling plots was defined based on S2 with 10, 20 m and LC8 multi-temporal data with 30 m pixel resolution, respectively. Hence, plot sizes of (20 m × 20 m, 0.04 ha) and (10 m × 10 m, 0.01 ha) were considered adequate in this study to ensure correspondence between field-measurement and pixel size in the image. This area was large enough to contain almost the complete diversity of the known plant community. 0.04 ha plots have been widely applied in the National Forest Monitoring Plan in Botswana (Manatsha and Malebang, 2016) and in different forests elsewhere (Baker et al., 2004; Carreiras et al., 2013) as it normally encompasses a representative sample of trees within a single stand and allows detection of changes in vegetation structure.

The field measurements of stand characteristics included: mean height, diameter at breast height (DHB), tree density, canopy closure, and tree species. Sample plots were circular and the UTM coordinates at the centre of each plot were recorded in the field with a hand-held Garmin GPS 64S. Tree height of each individual tree was measured using an ultrasonic Vertex III hypsometer which requires finding a suitable position to observe each tree tip (Božić et al., 2005), while stem diameter was measured using a Diameter above Breast Height (DBH) tape. All trees with a stem diameter of >3 m and >1.5 m height were recorded. Fractional vegetation cover (FVC) of shrubs between 1 and 6 m in height was estimated visually within all plots in the field. In the case of multi-stemmed species, such as *Burkea Africana*, *Compretum collinum* and *Baikiaea plurijuga*, individual stems are recorded as an individual.

Table 3. 1. Summary statistics for field sample data in Chobe National Park.

Variables	AGB (Mg/ha)	Carbon Stock (Mg/ha)	BA (m2/ha)	MDBH (cm)	MH (m)	TD (no. trees/ha)
Minimum	2.07	1.03	0.62	4.73	3.14	103.50
Maximum	166.98	83.49	35.42	30.07	15.23	4297.20
Mean	54.99	26.93	11.18	8.78	5.58	1183.40
S.D.	44.27	22.34	8.80	4.69	1.87	1019.68

*AGB= above ground biomass, MDBH=mean diameter at breast height, BA=basal area, MH= mean height, TD= tree density, S.D. =standard deviation.

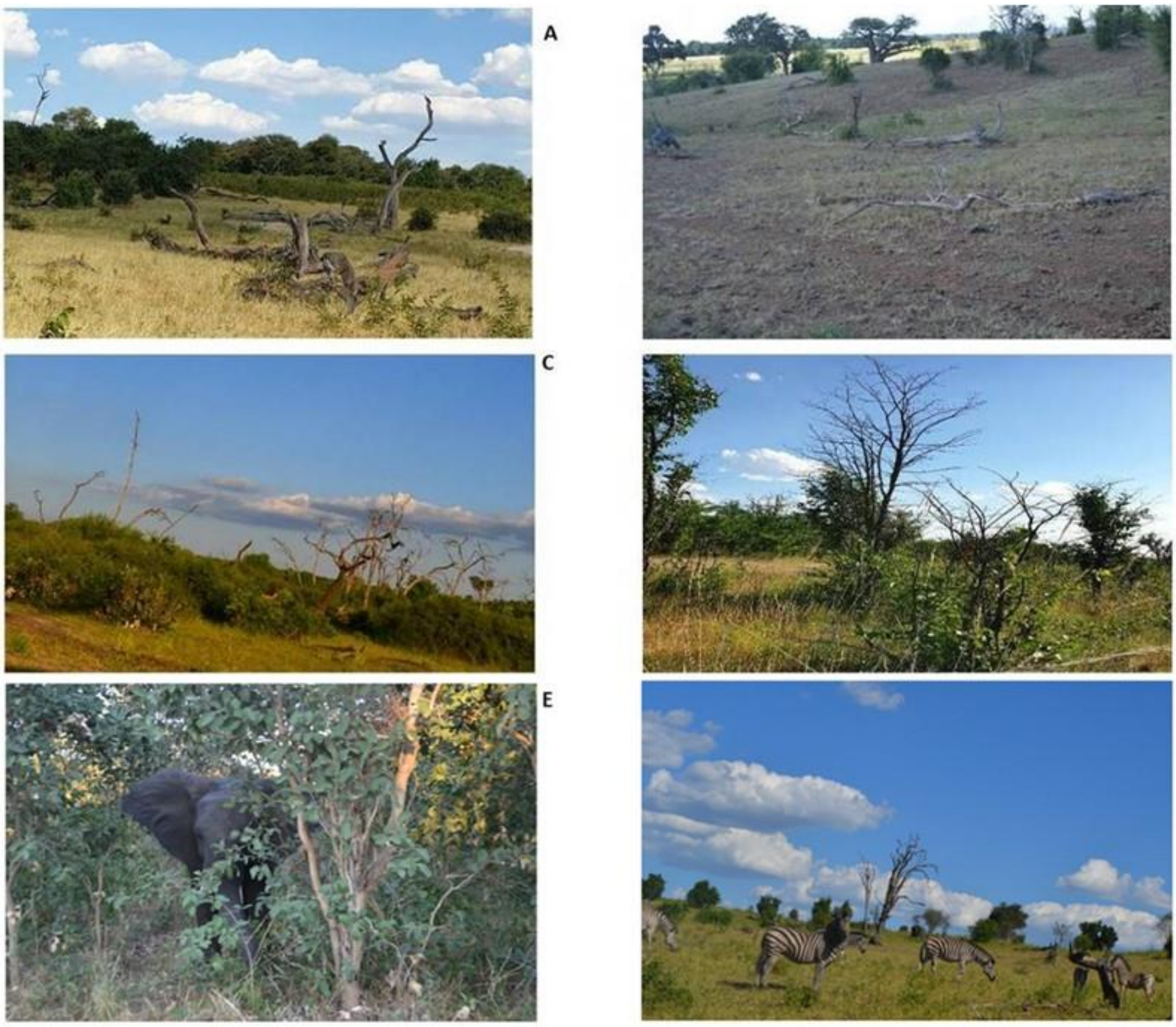

Fig. 3. 2. Examples of collected ground truth captured during a field campaign in Chobe National Park in 2019. The photos represent typical forest cover types and recent degradation activities resulting from A: drought impacts, B: Trees toppled by elephants causing mortality, C and D: Trees destroyed by wildfire, and E and F: elephant and herbivory browsing.

3.2.3 Satellite image data collection

The imagery included Sentinel-1 Synthetic Aperture RADAR (S1-SAR), Sentinel-2 Multispectral Instrument (MSI) data, and Landsat 8 - Operational Land Imager (OLI) were all accessed via Goggle Earth Engine (GEE) (Table 3.2). The GEE platform provides pre-processed top and bottom-of-atmosphere reflectance data, enabling large volumes to be integrated, processed, and analysed for extensive areas over long time periods (Warren et al., 2015). The Sentinel 1 and 2 data were acquired as close in time to the fieldwork as shown in Table A 1.

3.2.3.1 Sentinel-1 image pre-processing

S1 is a C-band SAR remote sensing satellite launched into orbit on 03.04.2014. There are four imaging modes (Stripmap [SM], Interferometric Wide swath [IW], Extra Wide swath [EW], and Wave [WV]), but the level-1 Interferometric Wide (IW) Ground Range Detection (GRD) were also used in the study. Radar data were analysed using the single co-polarisation with vertical transmit/receive and dual-band co-polarisation, with vertical transmit and horizontal receive (VV + VH) from Sentinel-1A and 1B C-band SAR. Within GEE, S1 images are pre-processed using the S1 Toolbox (ESA, 2020) to an analysis-ready format using border and thermal noise removal, radiometric calibration, and orthorectification (Google, 2020). Radar data is not significantly affected by cloud cover, so a considerable number of complete images can be obtained each month. However, radar data can be affected by recent rainfall or wind and so an image from a period of good weather (14.3.19), close to the field data collection date, was selected for analysis. The date closest to the date of field collection (February-March 2019) was selected because 2019 was an extreme drought year in Southern Africa including Chobe NP, and there was minimal recorded rainfall or soil moisture in the area during the time period, hence soil moisture will have a minimal influence on the backscatter (Chikoore and Jury, 2021; Lucas et al., 2006; Liu and Zhou, 2021).

3.2.3.2 Sentinel-2 image pre-processing

S2 MSI data, processed to level-2A were used. These data have been orthorectified and radiometrically corrected providing Bottom-Of-Atmosphere (BOA) corrected reflectance values (ESA, 2013). S2 images were further pre-processed with an automatic cloud masking procedure using QA bands provided for the S2 2A product, masking both opaque and cirrus cloud cover. Ten of the thirteen bands from S2 (4 visible, 4 red edge, 2 short-wavelength infrared (SWIR)), were extracted for pre-processing and analysis. The 20 m bands of S2 (SWIR and red edge bands) were resampled to 10 m using the cubic convolution algorithm. S2 spectral indices, (see: Table 3.2 for all indices and their derivation) were used to create the “indices” datasets. Previous studies suggested that numerous spectral vegetation indices provided more information than the individual spectral bands for retrieval of forest structure (Lu et al., 2012). Eleven spectral vegetation indices from S2 previously shown useful for biomass modelling and estimation were computed (Hawryło et al., 2018).

3.2.3.3 Landsat 8 image pre-processing

LC8 was launched on 11.03.13 and provides multispectral images at 30 m resolution with a 16-day return cycle. The study used LC8 Level 2 Tier 1 ortho-rectified collections from 15.03.19. These data are derived from L8's OLI/TIRS sensors and have been orthorectified and atmospherically corrected to obtain surface reflectance. The LC8 reflectance orthorectified product was used because GEE has already converted digital number (DN) values into surface reflectance data as a result of standardising across image products to a common radiometric scale (Chander et al., 2009). A cloud masking procedure was applied using the Function of Mask (FMask) band included with the Landsat data (Zhu and Woodcock, 2012). Eight spectral indices from LC8 were computed as "indices" datasets. As shown in Table 3.2, a total of 39 initial variables were used for the statistical analysis of the forest parameter estimation in this study.

3.2.3.4 Land Cover Classification

In order to allocate field plots throughout landscape using a stratified random sampling approach, the sentinel 2 images in 2019 were independently classified into four main land cover classes in GEE using a RF classifier because of its robustness (Belgiu et al., 2016; Breiman, 2001). Based on the prior knowledge of the study area, spectral clusters from the classification were assigned to four general land cover classes: Forests, open forests, grassland, and shrubs. A total of 367 ground points were randomly distributed on the study area, and they were split equally into 50% of points as reference points for image classification and the remaining 50% of points used for accuracy assessment.

Table 3. 2. Description of predictor variables for the AGB estimation.

Satellite	*Band*	*Description, wavelength, spatial resolution)*
S1 GRD (14.03.2019)	*VV - Vertical transmit-vertical channel*	*5.6 cm (10 m)*
	VH - Vertical transmit-horizontal	*5.6 cm (10 m)*

	channel	
	Band 1 – Coastal aerosol	*0.443nm - (60 m)*
	Band 2 – Blue	*0.490nm -(10 m)*
	Band 3 – Green	*0.560nm - (10 m)*
	Band 4 – Red	*0.665nm -(10 m)*
S2 SR (14.03.2019)	*Band 5 – Vegetation red edge*	*0.705 nm -(20 m)*
	Band 6 – Vegetation red edge	*0.740 nm - (20 m)*
	Band 7 – Vegetation red edge	*0.783 nm - (20 m)*
	Band 8 – NIR	*0.842 nm - (20 m)*
	Band 8A – Narrow NIR	*0.865 nm - (20 m)*
	Band 11 – SWIR	*1.61 nm - (20 m)*
	Band 12 – SWIR	*2.19 nm - (20 m)*
LC8 OLI TOA (15.03.2019)	*Band 1 Coastal*	*0.43 - 0.45 nm (30 m)*
	Band 2 Blue	*0.45 - 0.51 nm (30 m)*
	Band 3 Green	*0.53 - 0.59 nm (30 m)*
	Band 4 Red	*0.63 - 0.67 nm (30 m)*
	Band 5 NIR	*0.85 - 0.88 nm (30 m)*
	Band 6 SWIR 1	*1.57 - 1.65 nm (30 m)*
	Band 7 SWIR 2	*2.11 - 2.29 nm (30 m)*
Vegetation Indices	*Normalised vegetation index (NDVI)*	*(NIR –R/NIR + R)*
	Green red vegetation Index (GRVI)	*(G-R)/(G + R)*
	Enhanced Vegetation Index (EVI)	*2.5NIR−RED(NIR+6RED−7.5 BLUE)+1*
	Green NDVI (GNDVI)	*(NIR – G)/(NIR + G)*
	Normalised Difference NIR/SWIR2 NBR)	*NIR−SWIR/NIR+SWIR*
	Normalised Difference SWIR1/SWIR2 (NBR2)	*(SWIR1 – SWIR2) / (SWIR1 + SWIR2)*
	Soil-adjusted vegetation index (SAVI)	*(NIR –R)/(NIR + R + L)*1.5*
	Modified Soil-adjusted vegetation index (MSAVI2)	*(2 * NIR + 1 – sqrt ((2 * NIR + 1)^2 – 8 * (NIR – R))) / 2.*
	Normalised Difference Index 45 (NDI45)	*B5-B4/B5+B4*
	Inverted red-edge chlorophyll index (IRECI)	*RE3 –R/(RE1/RE2)*
	Normalised difference red edge index (NDRE1)	*(NIR –RE1)/(NIR + RE1)*

*RE: Red-edge; NIR: Near infra-red; SWIR1: Short-wave infra-red 1; SWIR2: Short-wave infra-red 2.

3.2.4 Methods and modelling

A full overview of the methodological approach for AGB is shown in Fig. 3.3. For all forest parameters, analysis was undertaken using S1 backscatter values (VV and VH polarisations) the reflectance values from individual spectral bands (B2-12), and spectral vegetation indices from S2 and LC8 OLI (NDVI, GRVI, EVI, GNDVI, NBR, NBR2, SAVI, MSAVI2, NDI45, IRECI, and NDRE1) as shown in Table 3.2. All models and their combinations are shown in Table 3.3 and 3.4.

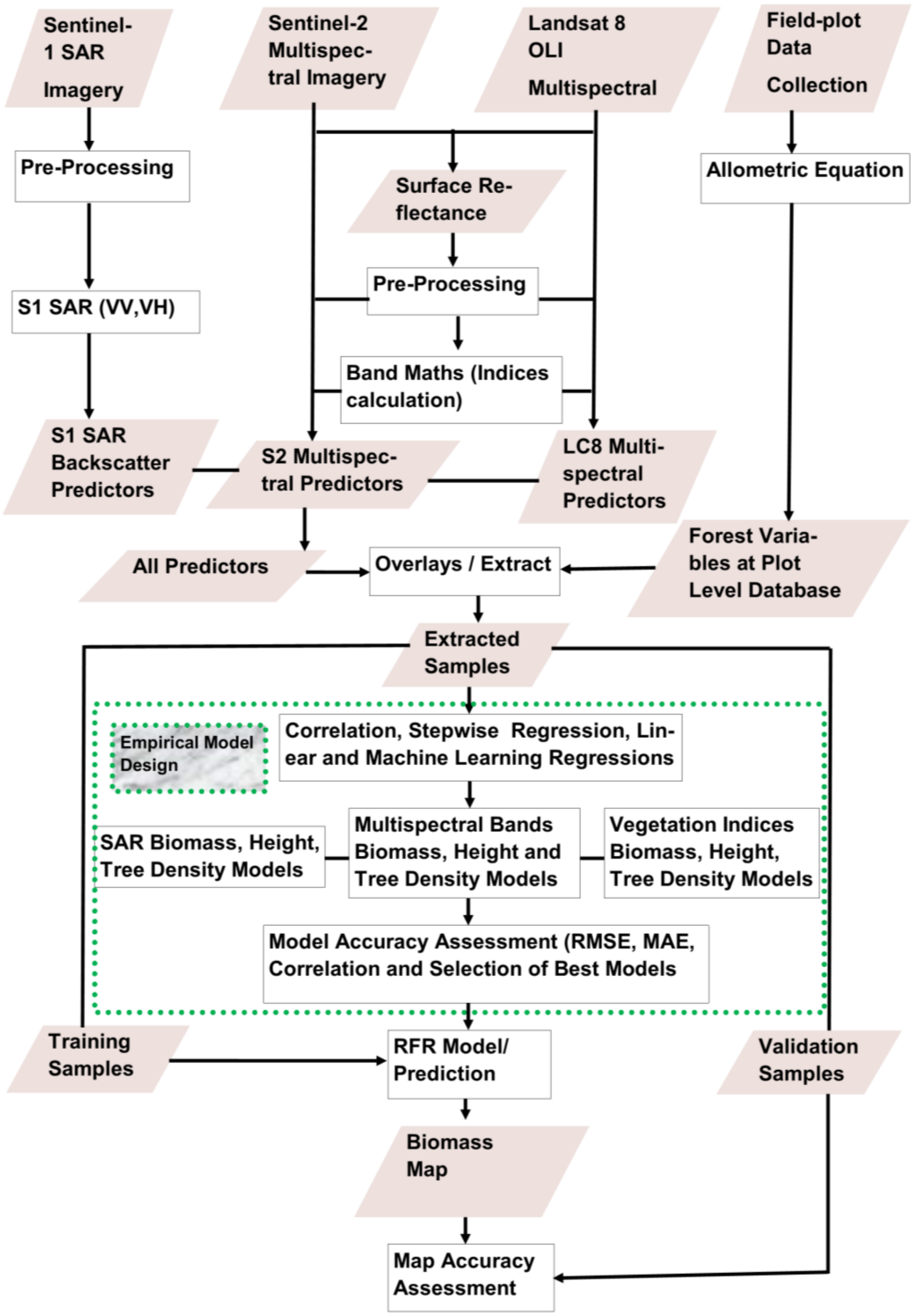

Fig. 3. 3. Overview of methodological approach

3.2.4.1 Calculation of AGB at the tree level

Locally defined allometric equations are not available for most of the species in the study area; AGB in kilograms per tree was estimated using the following generalised biomass estimation model (Eq. 3.1) developed for tropical dry forests (Chave et al., 2005).

$$AGB_{est} = exp(-2.187 + 0.916 \times ln(\rho D^2 H\ )) \equiv 0.112 \times (\rho D^2 H)^{0.916}) \quad \text{(Eq.3.1)}$$

Where AGB is the above ground biomass in kg per tree; H = height (m); D = diameter at breast height; ρ = wood density (g cm^{-3}).

The AGB of each individual tree was first calculated based on wood density, and then the total AGB per plot was summed based on the number of trees and the proportion between species. The wood density for species was obtained from the World Agroforestry Database (worldagroforestry, 2019). The biomass values were produced using the allometric equation developed by Chave et al. (2005) using Statistical Package R software (version 4.1.1) (R Core Team, 2013). Three tree-specific variables (tree wood density, DBH, height) were then generated and normalised by the area of the plots to estimates AGB in Mg/ha. The allometric model accounts for uncertainty and error in the estimation due to both data measurement and model uncertainty by averaging out the tree-level uncertainties at the stand scale, which is typically less than 10% of the mean as detailed in Chave et al., 2014. According to Baker et al. (2004) and Chave et al. (2005) excluding wood density and height would result in a poor overall AGB prediction and overestimation of the forest AGB. Rahman et al., 2021 showed that the generic allometric models overestimated AGB between 22% and 167% compared to the species-specific models and AGB was overestimated by up to 20% when using plot top height and underestimated by 8% using plot average height data from databases rather than individual tree heights in the mangroves (Rahman et al., 2021).

The allometric equation used in the study was specifically developed for tropical dryland forests and already includes the uncertainty and correction factor. The dryland forest model typically achieves 90% accuracy in AGB stock estimation and the standard error in estimating stand biomass was 12.5% if height is available, and 19.5% if height is not available for dryland forests (Chave et al., 2005). Therefore, this research used species-specific models and individual tree measurements including DBH, tree height and wood density as independent variables in the allometric equation to reduce uncertainty and improved the quality of the AGB prediction. This study didn't calculate the allometric equation uncertainty since the error due to the DBH, height, and wood density measurements are already calculated and factored in one error term of the allometric equation (Chave et al., 2004). The average and total AGB and carbon stocks per land cover class (i.e., closed forest, open forest) were estimated, as well as the total AGB and carbon stock in the forests of Chobe NP. The amount of carbon in biomass was determined by multiplying by a factor of 0.5 to obtain the amount of carbon existing in dry wood biomass, assuming biomass is approximately 50% of dry weight (Brown and Lugo, 1982; Chave et al., 2005). Table 3.1 presents plot summary statistics (minimum, maximum, mean, and standard deviation) for the variables of interest. The density and histogram plots of AGB and carbon stock (Mg/ha) of each field plot with woodland trees are presented in the supplementary materials as Fig. A3.

3.2.4.2 Extraction of remote sensing data at field plot location

Each circular field plot had a radius of 10 and 20 m, and for each plot location, the coordinates of each plot centre were established with GPS. Field plot location data were then overlaid on the SAR and S2 images to create a vegetation plot region-of-interest (ROI) map, based upon plot centre GPS position. Although the coordinates of each plot centre were collected with a high-quality device with GPS and GLONASS sensors, there may be small positional errors, especially when differential corrections are unavailable (errors up to 8–10 m are common). To compensate for possible positional errors, a 20 m radius buffer was created around the plot centre. This buffer was used to collect biomass image spectra. All pixels inside each 20 m buffer were extracted, with several metrics computed (mean, minimum, maximum, and standard deviation) (see Table 3.1), and these data were used to establish relationships with the AGB at plot level. As the original Sentinel data mosaic had a 10 m resolution and the buffer around each plot centre was set to 20 m, the extracted values per plot were those located approximately on a 4 × 4-pixel window size, thus extracting from a 40 × 40 m area.

3.2.4.3 Selection of relevant predictors

The selection of suitable variables is critical for developing biomass estimation models, as some variables are weakly correlated with AGB, or the variables can be co-dependent. Selected variables should be significantly correlated with AGB, but independent (Lu, 2006). In order to obtain valid predictor variables, correlation analysis was first used for candidate variable selection. Pearson correlation coefficients (p) and scatterplots were used to examine the nature of the AGB correlation, then variables were accepted for further analysis based on their significance ($P < 0.05$). In addition to the p-value, the variation inflation factor (VIF) generated for each predictor variable was used to minimise multicollinearity in the model. The VIF measures the increase in the variance of an estimated regression coefficient due to collinearity, indicating how much larger the variance is compared to when the independent variables are not linearly related in the model (Fox, 2015). A VIF of 1, indicates no collinearity and several studies have used a VIF < 10 to avoid serious multicollinearity between the chosen predictor variables. Generally, a VIF greater than 10 indicates high collinearity with other predictor variables in the model and interpreting the regression estimates associated with a high VIF predictor variable can lead to unstable estimates (James et al., 2013; O'Brien, 2007). VIF has been used in the field of remote sensing to check multicollinearity in a model with independent predictors (Tu et al., 2018; Yang et a l., 2012). To test for collinearity between the selected variables, a variance inflation factor (VIF) threshold of 10 was applied.

3.2.4.4 Model development and selection

Different statistical models were developed including parametric linear regression and non-parametric machine learning using random forest regression in the R programming platform. The dataset was first subjected to linear regression (Simple linear (SL) regression, Multivariate linear (ML) regression, and STEPWISE-AIC regression) to determine the optimum model (Bozdogan, 1987). Since biomass is usually nonlinearly related to remotely sensed variables, to improve the nonlinear estimation of the biomass model, non-parametric random forest (RF) models are widely used in satellite-based estimation of the forest AGB (Nandy et al., 2017; Wu et al., 2014). RF does not make a priori assumptions regarding the probability distribution of variables, and thus offers a significant advantage over parametric statistical models which assume a Gaussian distribution. Ensemble learning methods like RF (Breiman, 2001) play a significant role in remote sensing and forest mapping because of their robustness, processing ability for high-dimensional features, and ability to handle complex relationships between independent variables in biomass estimation modelling (Belgiu et al., 2016; Adam et al., 2014).

A challenge is to select the fewest number of predictors that offer the best predictive power and help in the interpretation of the final model. 12 experiments were conducted to explore the suitability of different datasets (SAR, optical spectral bands, and indices) and their combinations, in estimating AGB. To overcome the challenge of selecting the fewest number of predictors that offer the best predictive power and to help in the interpretation of the final model, the RF was used to rank the predictor variables. This was followed by a backward feature elimination method (BFE) as part of the evaluation process for the final model selection (Guyon and Elisseeff, 2003). The BFE starts with all the possible predictors and progressively drops the least promising variable, in this case, the SAR, optical spectral bands, and indices. The model optimisation and comparison was based on absolute and relative measures of fit: by calculating the accuracy assessment (Acc%) and error statistics for the models including Root Mean Squared Error (RMSE), Mean Absolute Error (MAE), Mean Absolute Percentage Error (MAPE), coefficient of determination (R^2), adjusted R^2 (R^2_{adj}), and Akaike information criterion (AIC) and VIF. The concordance index was adopted to rank the effectiveness of the ML and RF models (Gerds et al., 2012). The smallest subset of variables with the highest coefficient of determination (R^2), accuracy, adjusted R^2 (R^2adj), and lowest RMSE, VIF, and AIC were then selected to predict the AGB. Table 3.4 details the 19 multivariate models and the datasets used for estimating AGB.

The RF regression tree algorithm was selected to model forest parameters after analyses showed that it performed better than ML regression algorithms. The decision tree-based models such as random forests, make no assumptions regarding the distribution of the input data and can capture non-linear relationships between the response and predictor variables (Breiman, 2001; Liaw and Wiener, 2002). It is essential to optimise the model with the best combination of parameters. For RF, only two parameters need to be tuned: *ntree* (with a default value of 500 trees) that controls the number of trees to grow (k), and *mtry* (with a default value is 1/3 of the total number of the predictors) that controls the number of variables randomly sampled at each split (m). The study dentified the number of trees ($k = 1000$) and *mtry* (the default was accepted) because it minimised the error rate and produced the best results for AGB estimation in this study.

3.2.4.5 Model Validation

The field dataset (n = 101) was randomly split 70/30 for training and validation, respectively (Ismail et al., 2006). The training dataset was used to optimise the random forest regression and train the prediction model, and to assess the goodness of fit of each model, the accuracy and the reliability of the prediction model were assessed using the 30% validation sample. A regression equation developed from the training data set (n = 71) was then used to predict AGB on the independent test data set (n = 30). Validation techniques such as leave one out for cross-validation and k-fold cross-validation are widely used in previous studies to assess the model performance using reference data (Fassnacht et al., 2014). Cross-validation is very similar to the out-of-bag (OOB) estimate, which is a formal approach to quantify the predictive performance of a model, automatically accounting for model complexity (Hastie et al., 2009). The sensitivity of the model to the selection of the training and validation datasets was evaluated using a repeated k-fold cross-validation and bootstrapping where the data are randomly divided and spatially independent. The k-fold cross-validation procedure was used to test for overfitting by partitioning the data K times (K=5), using the shuffle option of three repetitions (S=3) when splitting the samples into 5 folds. In addition, to assess the model uncertainty, a 1000 runs of bootstrapping was used. The random forest regression performance in estimating AGB was compared with the commonly utilised multiple linear regression. The correlation between measured and predicted AGB from the independent validation plots was examined.

3.3 Results

3.3.1 Land cover classification

The results of the land cover classification are presented in Fig. A. 5. Open forests were the dominant form of land-cover occupying 43%, followed by grassland with 25%, forests with 23% and shrubs with a total of 9% of the land total area (see Table A 2). The difficulty was experienced in the separation of forests and open woodland due to difficulty in interpreting them. As shown in Table A 3, the overall classification accuracy was 97% and the Kappa statistic of 60% which denotes a good agreement between classes indicating generally low misclassification error, with the highest confusion arising between forests and open woodland. The validation overall accuracy was 67% which is reasonable for the random stratification purpose. A total of 101 ground plots were surveyed in Chobe NP. A total of 61 of the 101 plots surveyed represented forest, and 40 samples represented non-forest land cover types as shown in Fig. 3.2.

3.3.2 Simple linear regression (SLR)

Table 3.3 summarises the strength of the linear relationship between all variables derived from S1, S2, and LC8 data. S1 VV polarisation is substantially more sensitive to AGB (R^2 = 0.58 and RMSE =0.70 Mg/ha) as compared to VH polarisation (R^2 = 0.32 with RMSE = 0.89 Mg/ha) at 99% confidence level. Among the S2 spectral bands, the highest coefficient of determination for AGB was obtained using spectral bands blue (B2), green (B3), red edge 1 (B5) (R^2=0.73, R^2=0.73, and R^2=65 at p-value 0.001, respectively). The relationships of S1 polarisations and selected S2 spectral bands (B3 and B5) with AGB are shown in Fig. A. 4A-D. S2 spectral indices Green Normalised Difference Vegetation Index (GNDVI) and Normalised Difference Red Edge (NDRE1) and Normalised Difference Vegetation Index (NDVI) obtained the highest linear relationship with AGB (R^2 = 0.71 and R^2 = 0.56) at 99% confidence level, respectively.

Table 3.3. Simple linear relationship of satellite-based predictors with AGB. The backscatter polarisation, spectral bands, and indices with a strong linear relationship with

AGB are highlighted in bold. The R^2 >0.5 is considered to indicate relatively a strong relationship between the variable (Silvy et al., 2020).

Modelling Group	Response	Bands/Predictors	Intercept	Slope	R^2	RMSE error Mg/ha	AIC
S1	AGB	**VV**	**9.35**	**0.51**	**0.58*** **	**0.70**	**104.06**
		VH	39.04	-0.04	0.32***	0.89	125.95
S2		**B2**	**6.69**	**-72.99**	**0.73*** **	**0.56**	**83.15**
		B3	**6.98**	**-47.73**	**0.73*** **	**0.56**	**83.23**
		B4	6.15	-36.09	0.63***	0.66	98.48
		B5	**7.37**	**-31.21**	**0.65*** **	**0.64**	**95.61**
		B6	10.84	-30.22	0.41***	0.83	119.68
		B7	8.76	-18.05	0.15*	1.0	136.30
		B8	7.65	-13.86	0.09*	1.03	139.47
		B8A	8.12	-14.32	0.09*	1.03	139.50
		B11	**9.97**	**-24.19**	**0.57*** **	**0.71**	**104.50**
		B12	**7.079**	**-20.75**	**0.57*** **	**0.71**	**104.89**
		NDVI	**-1.70**	**8.52**	**0.56*** **	**0.72**	**106.40**
		GRVI	3.48	5.93	0.09*	1.03	139.29
		EVI	-0.73	10.44	0.31***	0.90	126.56
		GNDVI	**-4.09**	**12.43**	**0.71*** **	**0.59**	**87.38**
		SAVI	-1.72	13.53	0.39***	0.84	121.01
		MSAVI	-0.82	11.82	0.36***	0.87	123.34
		NBR	1.52	7.29	0.46***	0.80	115.79
		NBR2	-0.05	15.86	0.52***	0.75	109.86
		NDI45	0.80	10.04	0.33***	0.89	125.54
		IRECI	1.18	5.24	0.35***	0.87	123.96
		NDRE1	**-0.52**	**9.67**	**0.56*** **	**0.72**	**105.92**
		NDRE2	0.59	28.63	0.46***	0.80	115.71
LC8		**B2**	**10.62**	**-78.30**	**0.52*** **	**0.75**	**109.72**
		B3	**7.77**	**-49.61**	**0.54*** **	**0.73**	**108.16**
		B4	6.27	-34.78	0.48***	0.78	113.80
		B5	7.25	-12.48	0.07.	1.05	140.65
		B6	8.27	-21.99	0.41***	0.83	119.50
		B7	6.29	-22.15	0.43***	0.81	117.58
		NDVI	**-2.59**	**10.42**	**0.52*** **	**0.75**	**110.38**
		GRVI	2.98	11.42	0.26***	0.93	130.16
		EVI	-2.40	11.77	0.43***	0.82	118.29
		GNDVI	**-5.89**	**16.90**	**0.62*** **	**0.67**	**99.53**
		NBR	-0.27	13.80	0.44***	0.81	117.44
		NBR2	0.24	7.89	0.44***	0.81	116.71
		SAVI	-3.95	19.95	0.45***	0.80	116.47
		MSAVI	-2.98	18.43	0.42***	0.82	118.37

Significance codes: '***' 0.001 '**' 0.01 '*' 0.05 '.' 0.1 ' ' 1

3.3.3 Multivariate linear (ML) regression models

Table 3.4 presents the multivariate relationships and validation results of the 19 experiments conducted with S1 SAR signals, S2, and LC8 spectral bands, and indices for AGB. The results show that the relationship strength with AGB, and associated errors, are improved when the polarisation variables are combined. Further improvements were attained when predictors are combined, from either a single sensor or by integrating both sensors. Taking the linear relationship from S1 VV and VH polarisation, with R^2 of 0.58 and 0.32 respectively, the R^2 increased to 0.61 when combined. On the other hand, a combination of both S1 and S2 bands generated a higher R^2 of 0.85 and reduced the RMSE to 0.42 Mg/ha with an increased estimation accuracy of 90%. A step-wise regression obtained the highest R^2 of 0.95, a very low RMSE of 0.25 Mg/ha, and the highest accuracy of 94% for S1 backscatter and S2 spectral variables.

However, although the models with all S2 and LC8 spectral variables and stepwise-regression models have high R^2 values and low errors, they were excluded from estimation because of high co-dependence between spectral bands and indices, resulting in a high VIF (Table 3.4). A backward stepwise approach is useful to reduce the number of parameters within the model in a systematic way. Based on R^2, MAE, and RMSE, the most suitable predictive model was obtained with S1 SAR VV polarisation, the green (B-3) and red edge spectral band (B-5) of S2, explaining 82% of the variance but with a VIF of less than 10 for AGB (Table 3.4). The inclusion of SAR data with optical data strengthens the relationship between biomass and remote sensing variables, and consequently improves the model performance as shown in Table 3.4. The results of the repeated k-fold cross-validation shown in Supplementary materials in Fig A 3, show that the model fit is not sensitive to the selection of training and validation sampling. The results of the bootstrap validation in Fig A. 4 indicate that the model performance was stable across bootstrap replicates. The bootstrap distribution, errors, and intercepts correspond very closely to the linear model estimates, see Table 3.5 and 3.6 for parameter values. If the predicted bootstrapping R^2 was found to be significantly smaller than the original multiple linear model R^2, that would indicate that the model was over-fitted which is not the case with the linear model. The lower = .025 and upper = .975 of the 95-percent confidence interval for the coefficients of the multiple linear and the bootstrap regression are shown in Table 3.6. The bootstrap approach yields a similar estimation for AGB without relying on assumptions, and this helps to confirm the stability of the model coefficients for the multiple linear regression used in this study.

Table 3.4. Multivariate linear relationship and validation results of 19 experiments/models conducted for AGB modelling (label a-k represents S1 and S2) and (label l-p represents LC8). The best model is highlighted in grey.

AGB Model Label	*Variables*	*R^2*	*RMSE (Mg/ha)*	*MAE*	*MAPE*	*ACC %*	*AIC*	*VIF*
a	**S1 bands all**	0.61	0.68	0.55	0.21	0.84	102.8	1.46
b	**S2 bands all**	0.79	0.50	0.41	0.14	0.88	88.48	67.70
c	**S2 bands & S1 bands all**	0.85	0.42	0.35	0.12	0.90	77.25	77.17
d	**S2 indices all**	0.85	0.42	0.35	0.12	0.89	83.39	19063.24
e	**Step regression S1 bands, S2 bands & indices all**	0.95	0.25	0.19	0.06	0.94	47.79	11600.7
f	**Step backward selection with selected** S1 & S2 B3, B5, S1 VH, S1 VV, GRVI, GNDVI, NDRE1, NDI45	0.88	0.38	0.31	0.10	0.90	61.92	2927.90
g	**Step backward selection with selected S2 Bands & indices** B3, B5, GRVI, GNDVI, NDRE1, NDI45	0.82	0.46	0.36	0.13	0.89	74.34	2493.00
h	**Step Backward Selection with selected** S1 & S2 B3, B5, S1 VV, S1 VH, GNDVI, NDRE1	0.84	0.43	0.37	0.13	0.89	69.13	1143.50
i	**Step Backward Selection with selected S1 Bands & S2 indices** GNDVI, NDRE1, S1 VV, S1 VH	0.82	0.45	0.38	0.14	0.88	69.98	9.8
j	**Step Backward Selection with selected S1 & S2 Bands** B3, B5, S1 VV, S1 VH	0.83	0.45	0.37	0.13	0.89	69.15	10.1
k	**Selected AGB model B3, B5, S1 VV**	**0.82**	**0.45**	**0.36**	**0.13**	**0.90**	**67.92**	**9.9**
l	**LC8 bands all**	0.68	0.62	0.47	0.18	0.87	102.00	75.28
m	**LC8 Indices all**	0.69	0.60	0.45	0.18	0.87	104.28	9408.0
N	**Step regression LC8 bands and indices**	0.72	0.57	0.42	0.17	0.88	99.23	11926.0
o	**Step backward selection with selected LC8 bands & indices** B3, B4, B7, GNDVI, NBR2	0.68	0.61	0.45	0.18	0.87	98.97	282.24
p	**Step backward with selected LC8 indices** GNDVI, NBR2	0.67	0.62	0.47	0.19	0.86	94.94	9.1

Table 3. 5. Summary statistics and coefficients of linear and bootstrap regression for AGB

	Linear Regression	**Bootstrap**

R^2	0.82	0.80
RMSE	0.45	0.42
MSE	0.36	0.32
Intercept	8.65	8.54
B3	-52.46	-56.11
B5	13.15	13.66
S1-VV	0.26	0.23

Table 3. 6. Confidence intervals (95 %) of linear and bootstrap regression for AGB

	2.5%	**97.5%**	**2.5%**	**97.5%**
	Linear Regression	**Linear Regression**	**Bootstrap**	**Bootstrap**
Intercept	7.58	9.72	7.47	9.65
B3	-78.68	-26.23	-74.88	-37.35
B5	-5.12	31.42	0.13	26.83
S1-VV	0.15	0.38	0.11	0.36

3.3.4 Comparing parametric and non-parametric machine learning for estimating stand parameters

Table 3.7 shows the summary statistics for the ML and RF regression models for AGB using the three optimum predictor variables (S1 VV polarisation, S2 green (B3), and red edge (B5)) hereafter referred to as S1S2), from the final models. It can be seen that features derived from the MRF regression model offer the most accurate estimates for all forest parameters compared to the ML regression model. Graphical illustrations for the performance of the AGB models are presented in Fig. 3.4 that show the ML and RF fitted regression models for AGB and the associated residuals. The plots of observed vs predicted AGB and residuals, indicate that the RF residuals were rather stable across medium and high AGB values and had an average around zero compared to ML that under predicted AGB across the same data range. It can also be seen that low AGB values are not estimated well by any of the regression methods, although RF still had a more accurate estimation than the ML regression model. For AGB, the RF regression has the highest R^2 of 0.95 and an RMSE of 0.25 Mg/ha compared to ML regression model with an R^2 of 0.82 and RMSE of 0.45 Mg/ha. Based on R^2, RMSE, MSE, and concordance between predicted and observed value, the MRF regression performed better than the ML and so the MRF regression model was used for estimating forest stand parameters. Graphical illustrations for the performance of the AGB models are presented in Fig. 3.4.

Table 3. 7. Summary diagnostics for the AGB models developed by ML and RFR regression methods using the S1S2 model. In this study, the best model throughout the study was the RF regression model, highlighted in grey.

Model Type	*R^2*	*RMSE*	*MSE*	*Concordance*
ML Regression AGB	*0.82*	*0.45*	*0.21*	*0.88*
RF Regression AGB	*0.95*	*0.25*	*0.06*	*0.95*

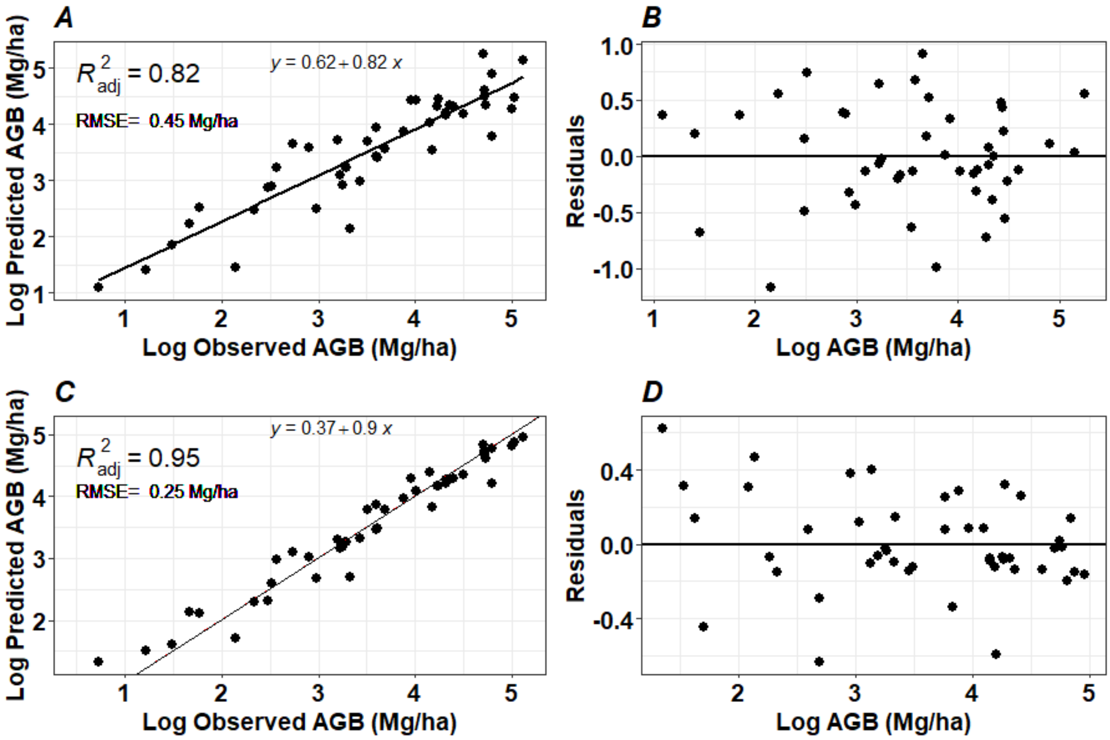

Fig. 3. 4. Optimal AGB model. A: Observed and predicted AGB using ML regression. B: ML regression standardised residuals. C: Observed and predicted AGB using MRF regression. D: MRF regression standardised residuals.

3.3.5 Spatial distribution of AGB

Fig. 3.5 maps the spatial distribution of the AGB estimations across the study area using the RF regression-based model and S1 SAR and S2 spectral bands (S1S2). The distribution of AGB ranges from 4.0 Mg/ha to 145 Mg/ha, which closely corresponds to the range of values measured in the field where the highest AGB values were 167 Mg/ha. The estimated AGB map revealed that the highest AGB values range from 80 to 145 Mg/ha in northern Chobe, while a large part of the study area (80%) is characterised by low AGB values < 80 Mg/ha, with an average AGB estimated at 51 Mg/ha. In the southern part of the study area, there is a mixture of high and low-density forests, as shown in both the modelled maps and S2 imagery. Similarly, the lowest AGB estimates were found in the central part of the study area, which is consistent with field conditions where grassland, shrubs, and scattered trees are found, as a result of degradation associated with overgrazing and wildfire. The field photos corresponding to the mapped land cover types are shown in Fig. 3.6A, which shows an example of a typical forest plot where AGB ranges from 80 Mg/ha to 145 Mg/ha, as shown in dark green colour in Fig. 3.5A. Fig. 3.6B represents an open woodland with AGB ranging from 41 Mg/ha to 80 Mg/ha, shown in light green colour in Fig. 3.5. The field photo in Fig. 3.6C shows an example of scattered trees with herbaceous cover, corresponding to AGB ranges between 11 Mg/ha and 40 Mg/ha, as shown in yellow colour in Fig. 3.5. Fig. 3.6D represents non-forest land cover with occasional scattered trees and/or shrubs which matches AGB values of <10 Mg/ha.

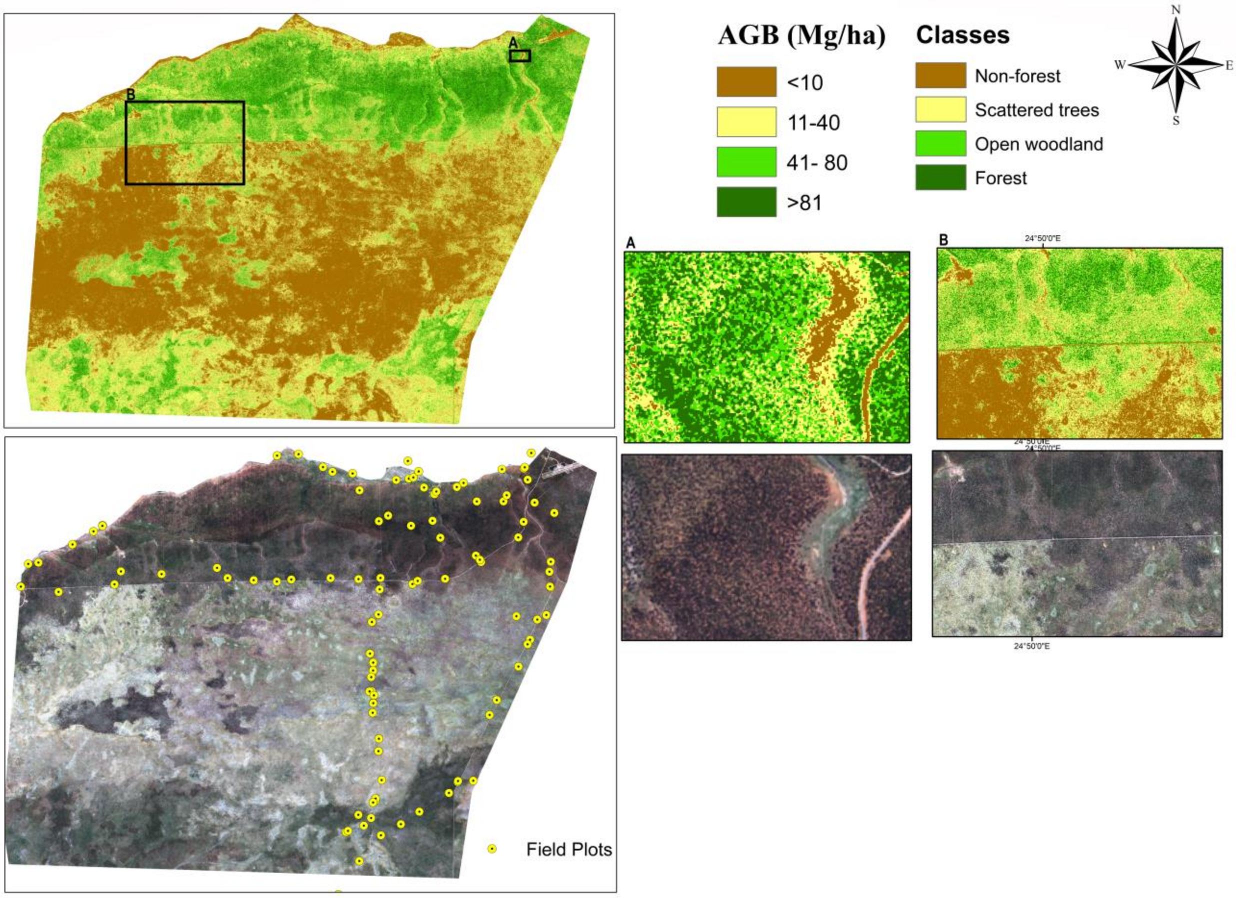

Fig. 3. 5. Modelled AGB maps of a dryland forest landscape of the study area and the RGB 432 S2 image (10 m).

Fig. 3. 6. Examples of dryland forest types and their respective ground pictures across

Chobe National Park. A: closed canopy forest. B: open canopy woodland. C: scattered trees with low herbaceous cover. D: non-forest land cover.

This study selected and compared the combination of S1 C-band SAR, LC8 and S2 optical data (S1S2), S1 polarisations and vegetation indices (NDRE1 and NDVI) that were suitable for forest structural parameter estimation. The results in Fig. 3.7 show that the combination of S1 C-band SAR and S2 optical data estimated medium to high biomass density with a higher level of accuracy as compared to either sensor alone. A saturation effect for the S2 NDVI (S2NDVI) model was observed, wherein the sensitivity to biomass variability declines when biomass density exceeds 80 Mg/ha (see Fig. 3.7A). The saturation points for S1 polarisation (Fig. 3.7B) and NDRE1 (Fig. 3.7C) models were higher in comparison to NDVI. The combination of S1 backscatter values and S2 red edge position bands (S1S2) are capable of estimating biomass > 80 Mg/ha (black colours) and did reduce the saturation effect in high-density forest areas as shown in Fig. 3.7B. The maps in Fig. 3.7 confirm that the S1S2 model produced the best fit with the ground observations for dryland forests, while reducing the under-estimation of large AGB values estimated by the S2NDVI model. The study observed a small but noticeable over-estimation for low values of biomass areas in the S2-NDVI model, although this was more prevalent in the degraded and fragmented vegetation areas e.g., along the Chobe River frontage (see: Fig 3.7).

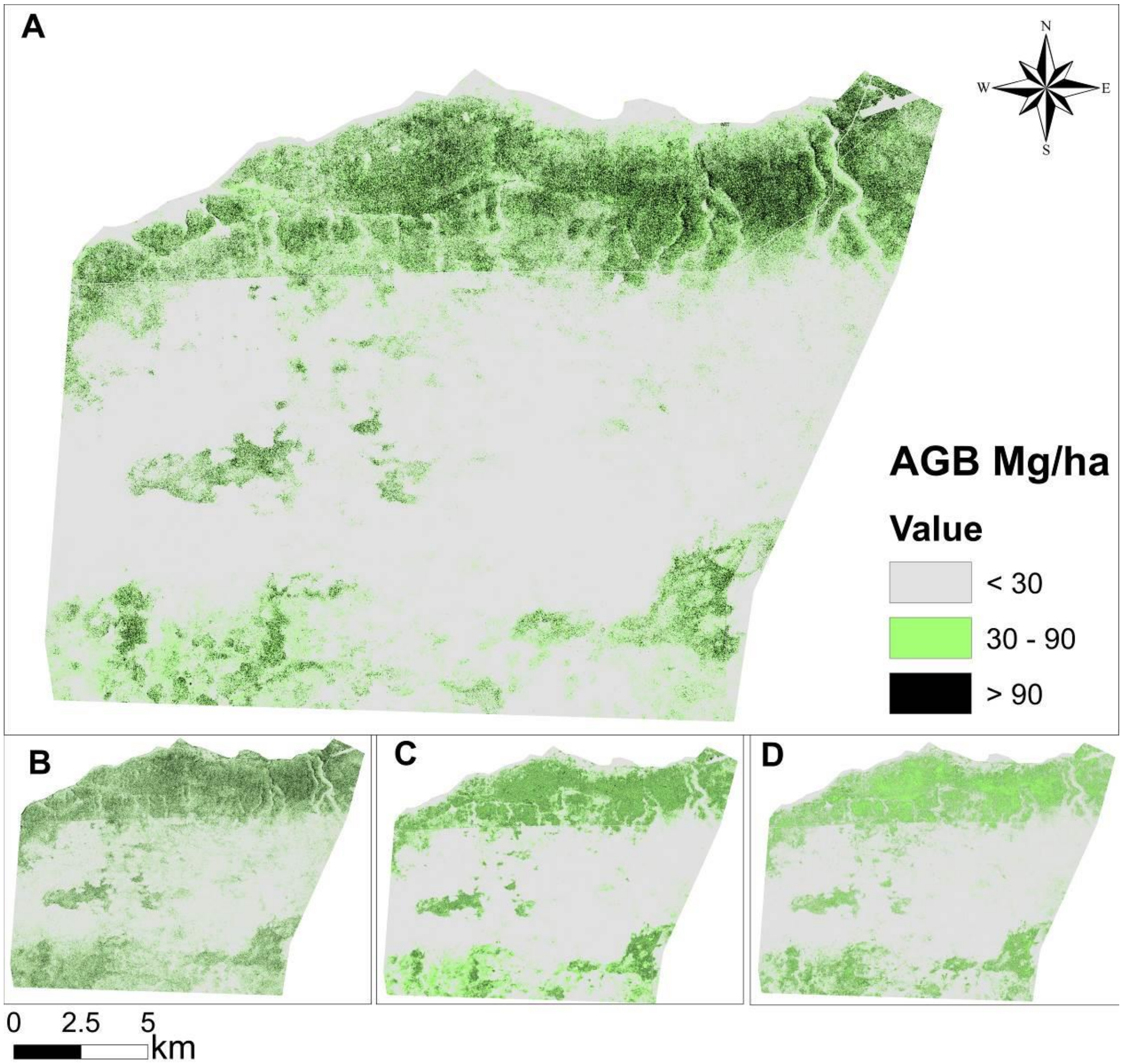
A
N
W
E
S
AGB Mg/ha
Value
< 30
30 - 90
> 90
B
C
D
0 2.5 5
km

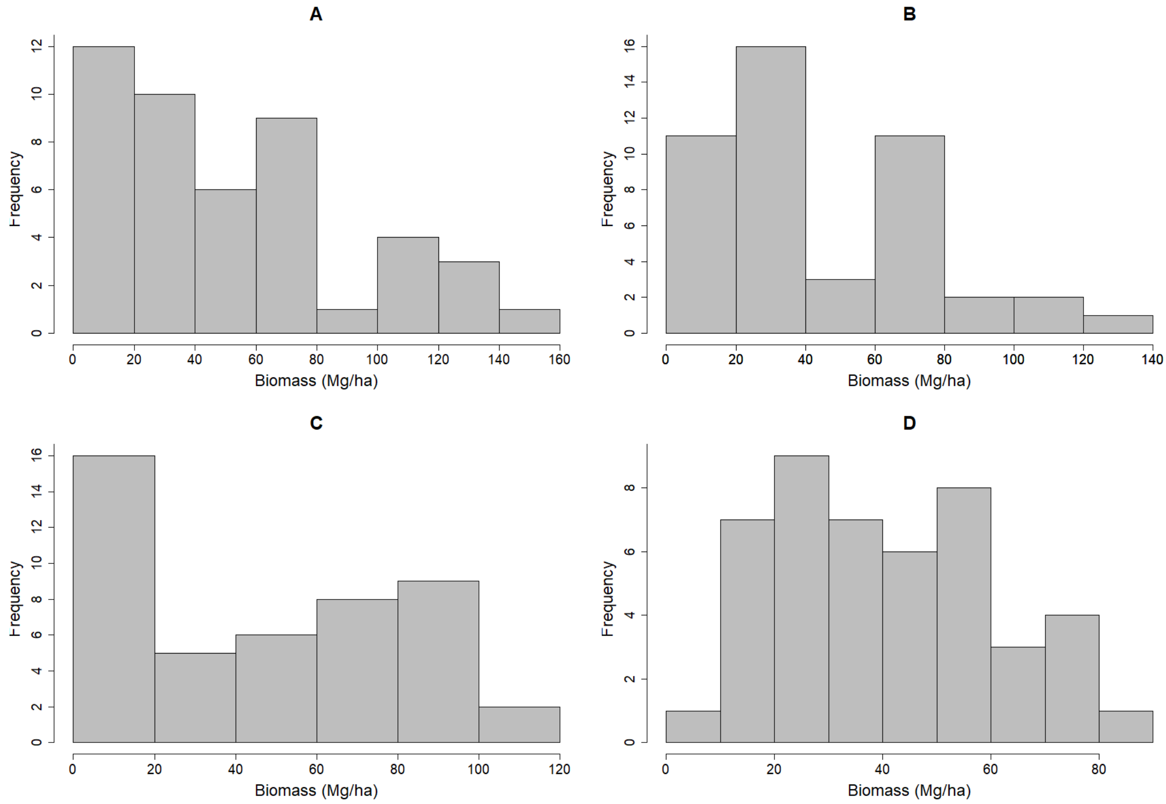

Fig. 3. 7. A: AGB maps and histograms with the A: S1S2 model. B: S1 VV model. C: Modelled AGB map with NDRE1 model. D: Modelled AGB map with the NDVI model (the NDVI model saturates at values >80 Mg/ha).

In addition to cross-validation, the AGB map was evaluated by comparison with the most recent published pan-tropical AGB datasets (Avitabile et al., 2016; Baccini et al., 2017; Bouvet et al., 2018). The differences between models were analysed as displayed in Fig. 3.8, 9, and 10. Avitabile et al. (2016) integrated two existing global datasets of AGB from Saatchi et al., (2011) and Baccini et al. (2012) to create an improved pan-tropical AGB map at 1 km resolution, using an independent reference dataset of field observations to reduce bias and improve the accuracy. Baccini et al. (2017) used Landsat data to produce an AGB map at 30 m resolution, while Bouvet et al. (2018) used an ALOS PALSAR mosaic produced by JAXA in 2010 to produce an AGB map at 25 m resolution for continental Africa.

Fig. 3.8 shows a comparison between this study AGB estimates with these three published pan-tropical AGB datasets. A comparison with Avitabile et al. (2016) predicts low AGB values in the 0 to 30 Mg/ha range with a very low R^2 of 0.20 and a precision of 36.21 Mg/ha. The result from Bouvet et al. (2018) using ALOS PALSAR shows the highest agreement with this study with a coefficient of determination R^2 of 0.50, compared to Baccini et al. (2017) which reported precision for the AGB estimates of 31.31 Mg/ha and an R^2 of 0.41. The pan-tropical maps all exhibited a high RMSE and a low R^2 when compared with this study, which has AGB estimates with R^2 of 0.95 and RMSE of 0.25.

Fig. 3.9 shows the spread, and distribution of the AGB from this study and three published pan-tropical AGB datasets. The mean AGB varied from 5.92 Mg/ha with the Avitabile et al. (2016), 18.5 Mg ha^{-1} for Baccini et al., (2015), 26.7 Mg/ha for Bouvet et al., (2018) to the highest 51 Mg/ha for this study (Fig. 3.9). The lowest median is observed in Avitabile et al. (2016) and a relatively high variance is observed in this study. Some bimodality is suggested by Avitabile et al. (2016) and Baccini et al., (2015). This study and Bouvet et al., (2018) have a similar AGB spread and the highest mean AGB estimation, with this study estimating a AGB of 145 Mg ha compared to 66 Mg/ha from Bouvet et al., (2018), 49 Mg/ha from Baccini et al., (2015) and 28.8 Mg/ha from Avitabile et al. (2016). Bouvet et al. (2018) was derived by limiting the model-based inversion method in predicting AGB of forest plots to not exceed 85 Mg/ha for dryland ecosystem, and this could explain the low AGB estimation in the high-density forest of the study area.

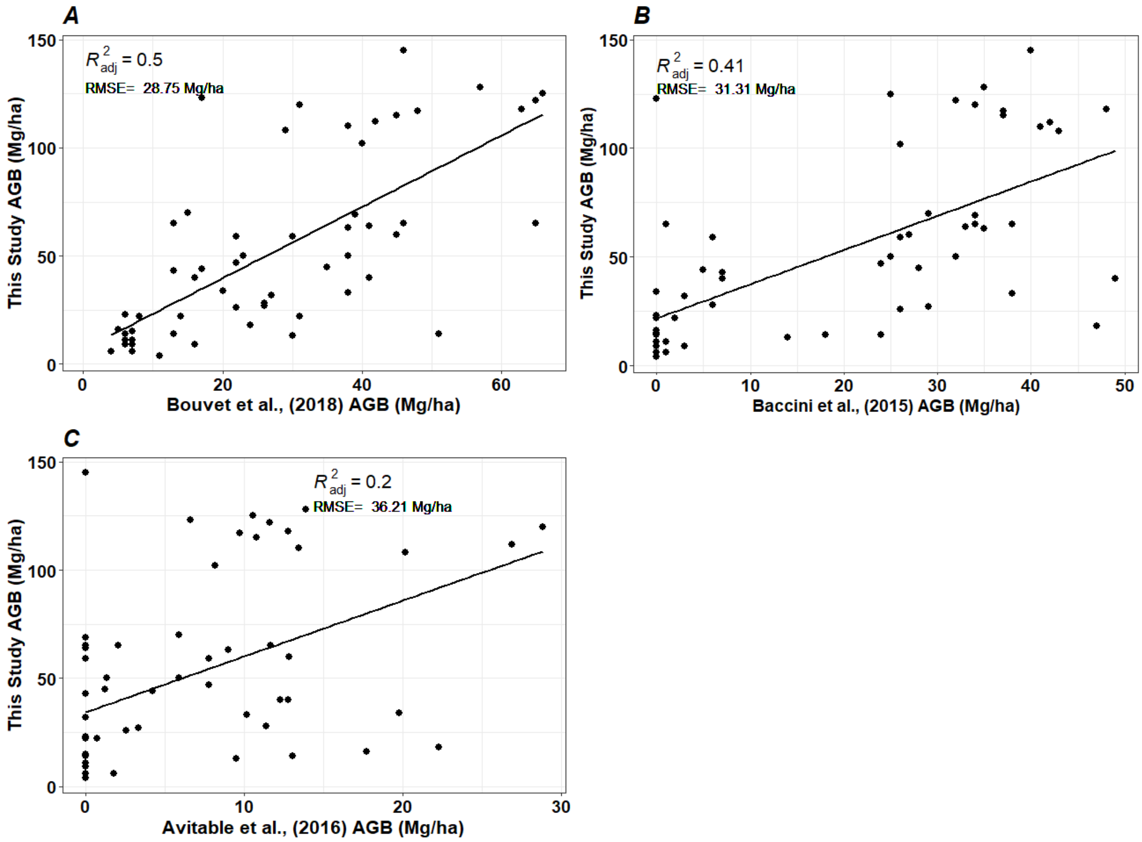

Fig. 3. 8. Comparison between A: This Study AGB estimates and the AGB estimates from Bouvet et al. (2018). B: This Study AGB estimates and the AGB estimates from Baccini et al. (2017). C: This Study AGB estimates and the AGB estimates from Avitabile et al. (2016).

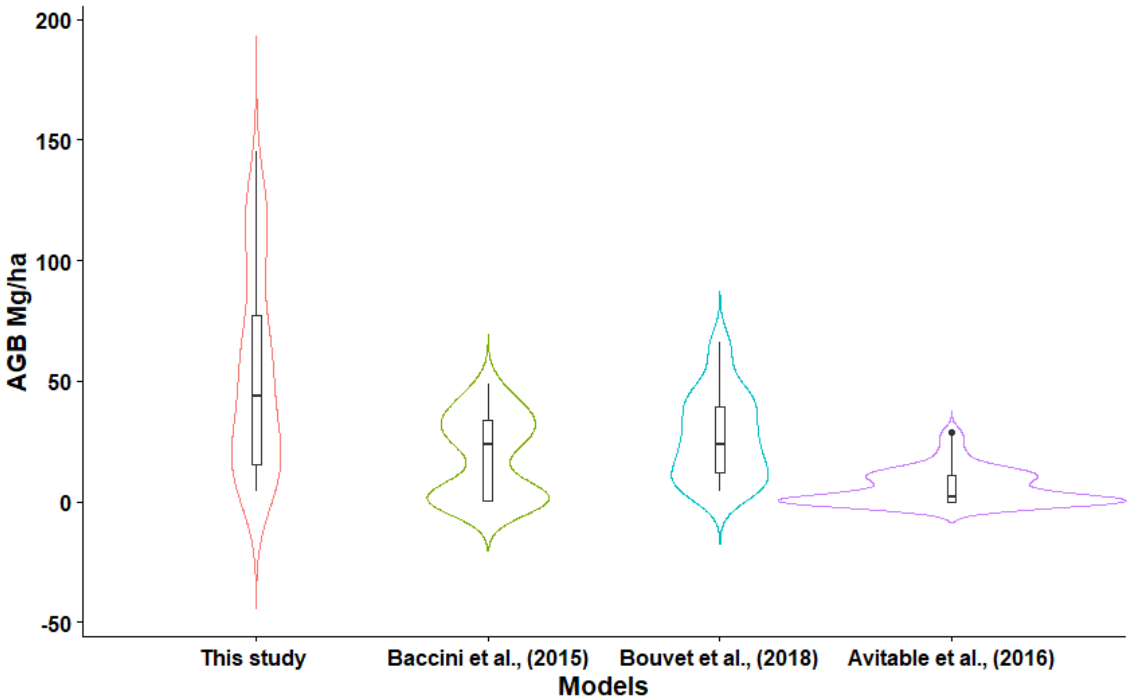

Fig. 3. 9. Comparison of AGB distribution (Mg/ha) among the different AGB estimates from this study, Avitabile et al. (2016), Baccini et al. (2017), and Bouvet et al. (2018). The models are arranged from the highest median AGB to the lowest. The horizontal line of the box plot for each model represents the median and the width of violin plot represents the proportion of the data using a kernel probability density.

3.4 Discussion

3.4.1 Relationship between S1 SAR, S2, and LC8 with AGB

In this study, simple linear regression models from S1 backscatter, S2, and LC8 spectral coefficients were statistically significant ($p < 0.001$). However, the simple models estimating the AGB from all sensors provided low R^2 values and high RMSE that are considered unreliable for estimating forest structure parameters for practical forest management and habitat mapping. The RMSE observed in this study is lower than other AGB studies reported in the region, but it is similar to Mutanga et al. (2012) who predicted biomass using a similar sized plot from homogeneous areas (20 m × 20 m) to compute 3 NDVIs from the WorldView-2 red edge and NIR bands and yielded an RMSE of 0.441 kg/m^2. The highest R^2 was generated using multivariate models that employed both SAR and optical data (S1S2) highlighted in grey in Table 3.4, indicating the responsiveness of SAR to forest parameters particularly when sensors are used in combination for monitoring structural parameters in dryland forests, as reported by Townsend (2002).

In terms of the radar polarimetric parameters, VV polarisation showed a better correlation and relationship with AGB and is shown to be more useful for the AGB estimations as compared to VH. However, the combination of VV and VH polarisation improves the R^2 and lowers the RMSE. This result is not consistent with the results obtained by Liu et al. (2019) but it is similar to the results of Omar et al. (2017) and (Pham et al. (2020) who found VV polarisation to perform better in estimating AGB and sensitive to the increase in AGB as compared to VH. Nizalapur and Madugundu, (2010) used backscatter intensities obtained in X, C, L and P- bands from DLR-¬ESAR data in Indian tropical forests, in which VV was found to correlate with biomass when compared to HH, HV and VH polarisations. The selection of VV polarisation and their strong correlation with AGB and forest parameters estimation also aligns with the studies by Ouaadi et al. (2020) and Wijaya et al. (2015).

Further, it could be observed that the SAR data was better at detecting aggregations of individual trees in the savanna landscape than its optical counterpart, while overestimating AGB and tree density cover in this area. This effect was also shown in a study that was conducted in the Sahel dryland ecosystems using S1/2 data (Zhang et al., 2019). The overestimation of AGB was reduced from the combined use of S1 and S2 as compared to the single use of any of the sensors.

For optical data, although NDVI and EVI remain two of the most widely used vegetation indices, they were outperformed by the NDRE1 and GNDVI in estimating AGB, for dryland forests. The results are in agreement with the study by Wang et al. (2007) that tested the capabilities of GNDVI for estimating the Leaf Area Index (LAI), which were tested under different circumstances, and found that GNDVI performed better than the conventional NDVI in both circumstances. The results also align with the study by Otsu et al. (2019) who found that GNDVI performed best in distinguishing broad leaf from needle leaf forests as compared to NDVI. Another study by Yoder et al. (1994) used the green channel in a vegetation index and found that it had a better correlation with the photosynthetic activity of the tree canopy in miniature Douglas-firs as compared to the red channel. The main reason for the difference in the performance of NDVI and GNDVI is likely because the former is more sensitive to low chlorophyll concentrations, while GNDVI is more sensitive to high chlorophyll concentrations and so is more accurate for assessing chlorophyll content at the tree crown level (Gitelson et al., 1996). Besides the use of the green channel in a vegetation index, the red edge band is found to be more effective in estimating AGB at high canopy density as compared to conventional vegetation indices because it covers chlorophyll absorption and leaf cell structure reflection (Mutanga and Cho., 2012, Eitel et al., 2011).

The study found that a combination of S1 polarisation, S2 green, and red edge bands, have led to the mitigation of data saturation in high-density biomass, when compared to S2 NDVI models that saturate at biomass levels above 80 Mg/ha. The saturation of the relationship between biomass and the NDVI due to strong absorption in the red wavelength is a well-recognised problem (Zhao et al., 2016). SAR acquired across the range of frequencies (namely C-, L- and P-band) has a demonstrated capacity to quantify biomass up to a saturation level after which sensitivity is lost, depending on the frequency used. For example, it is reported that the C-band radar backscatter response saturates at biomass values of 30 Mg/ha to 50 Mg/ha, and the L-band backscatter is generally reported to occur between 70 Mg/ha and 150 Mg/ha and P-band backscatter can measure from 100 Mg/ha up to 200 Mg/ha (Lucas et al., 2015). For this study, the synergy between the two data sources, particularly the inclusion of SAR backscatter values from VV polarisation and the red-edge (B5) spectral bands have reduced saturation effects typical in optical and radar backscatter remote sensing data for the dense or mature forest with complex stand structures in dryland forest (Liu et al., 2019).

3.4.2 Selection of suitable algorithms and methods

The estimations derived from the machine learning algorithm showed the ability for improved the estimation of all forest parameters including AGB. Although the results from ML regression models exhibited a strong linear relationship, this study found that the RF regression algorithm performed better than ML regression, reducing the RMSE for the estimation models by almost 50% in all instances. In this study, ML regression derived relationships between observed and estimated AGB and residuals show some linearity, that is, overestimations and underestimations for the low and high biomass observations, respectively. This demonstrates the problem of using linear regression models, as identified by Zhao et al. (2016) who used Landsat and linear regression to estimate biomass saturation values in the Zhejiang Province of Eastern China.

Even though MRF regression models reduce the overestimation and underestimation of biomass compared to ML regression models in this study, there remains room for improvement. Specifically, the RF regression model estimated medium and high-density forests with good accuracy but showed variation in low-density forests <30 Mg/ha. Most of these low-density forest plots include understoreys and low herbaceous cover such as grassland, open forest, and burned woodlands, often with relatively low canopy density. Therefore, soil and moisture conditions under the canopy would have a significant impact on surface reflectance and considerably influence AGB estimation. These results are similar to numerous studies that assessed dryland forests using radar backscatter signals and decision tree models (Baccini et al., 2004; Santos et al., 2002; Wang et al., 1998) which all found that variations in understorey and ground conditions had an impact on the interaction of microwave radiation with vegetation cover. Using Radar C- and L-band, Wang et al. (1998) noted that the sensitivity of SAR to surface parameters is most pronounced for co-polarisation signals C-VV and C-HH angles at low biomass levels, with a sensitivity decrease for high biomass stands. This was also an issue in this study because data were acquired during the wet season where errors associated with moisture are likely (Mitchard et al., 2013).

3.4.3 Comparing regional AGB estimates with pan-tropical maps

The spatial distribution of high values of AGB (>145 Mg/ha) closely corresponds to field measurements, with the forests in the northern part of Chobe National Park found to have the highest AGB values. This can be attributed to the predominance of species with large DBH such as Zambezi teak (*Baikaea Pluijuga*). Also, the impacts of fire on the northern part of Chobe Park are better controlled than the southern areas, as they commonly experience a higher burning frequency (Dube, 2013).

Fig. 3.10 (I) shows a detailed view of a subset of forests in the northern part of the study area, dominated by high density forests. The inability to estimate AGB heterogeneity and a large under-estimation of biomass in dryland forests can be clearly seen in the AGB map of Avitabile et al. (2016) when compared to all the other AGB datasets. In contrast, Baccini et al. (2017) using Landsat imagery underestimate AGB in the area of high-density forest around the airport situated to the northeast of the study area (0-10 Mg/ha). Bouvet et al. (2018), using ALOS

PALSAR, predict higher levels of biomass than Baccini et al. (2017) around the airport area (10-30 Mg/ha), but these estimates are lower than this study estimates of >80 Mg/ha. This study estimates higher biomass stocks in large areas of northern Chobe > 80 Mg/ha particularly when compared to Bouvet et al. (2018) and Baccini et al. (2017).

The area shown in Fig. 3.10(II) is along the Shimwanza Valley, characterised by bare ground, gullies, tall shrub savanna, and open woodland with a mixture of medium and large trees. Results showed very large discrepancies from the pan-tropical map in this area. For example, it can be seen that Bouvet et al. (2018) underestimated a large portion of large and mature individual trees and were not able to characterise the variability in dryland forests or the patterns of open woodland. In addition, Bouvet et al., (2018) estimated high biomass of 50 Mg/ha to 70 Mg/ha in the degrading forest along the Chobe River frontage (see: Fig. 3.9B). The S2 image reveals that there are actually fewer trees in this area with more bare ground in between. The S1S2 model from this study was able to clearly show the fine details of trees in different AGB ranges, with a mix of very low biomass (due to different degrees of degradation) to intermediate biomass for certain areas with very large but scattered trees, as shown in S2 imagery (see: Fig. 3.10E). Baccini et al. (2017) shows a broad range of AGB (low to intermediate) similar to this study AGB estimates in the Chobe River frontage; although their study estimated lower biomass in high-density forest areas (see: Fig. 3.10C).

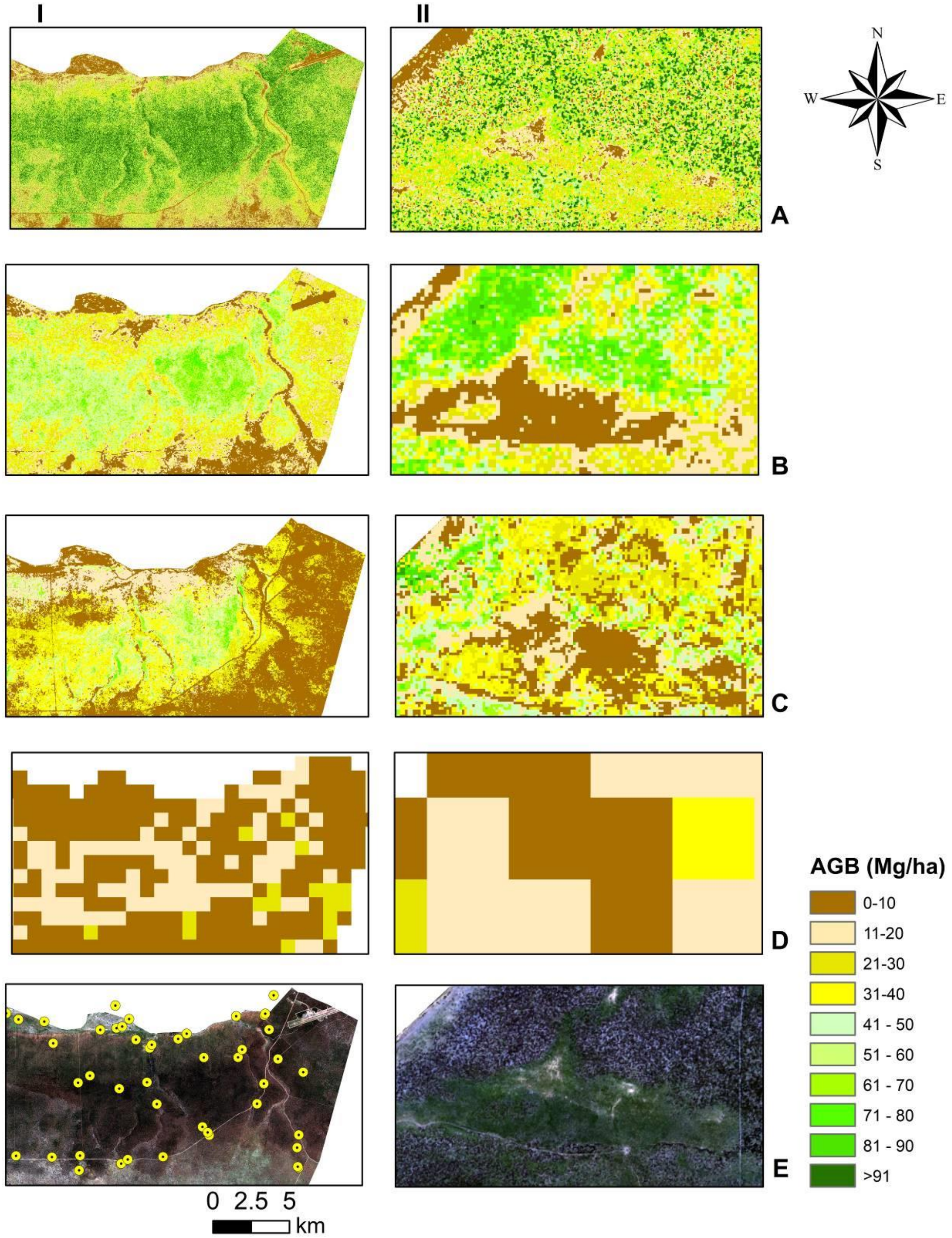

Fig. 3. 10. Biomass map in a subset of forests in the (I) northern part of the study area and (II) Shimwanza valley. A: estimated AGB map by this study. B: estimated AGB map by Bouvet et al. (2018). C: estimated AGB map by Baccini et al. (2017). D: estimated AGB map by Avitabile et al. (2016). E: RGB 432 S2 image.

3.4.4 Suitability of different models for land and wildlife management

Optical Landsat imagery utilised by Baccini et al. (2017) was able to capture broad-scale information on forest biomass but was less able to describe fine-scale disturbance. Where it captured the patterns of biomass fragmentation, it mostly overly overestimated AGB (Baccini et al., 2017). While Bouvet et al. (2018), using ALOS PALSAR L-band, was effective in mapping biomass structural density, but it was less capable at distinguishing biomass from degraded habitat areas, and largely failed to capture biomass variability and relatively small-scale changes associated with features such as roads, which were captured by this study and to a larger extend by Baccini et al. (2017) (see: Fig. 3.11). The large discrepancies in biomass distribution from Pan-tropical datasets can also be attributed to forest masks derived from different land cover maps which excluded certain woodland/vegetation types from their estimation. For example, Avitabile et al. (2016) used the GLC2000 map from Bartholomé & Belward. (2005) as a forest mask, while Bouvet et al. (2018) masked out forest classes (broadleaf evergreen closed to open forest) using the ESA CCI Land Cover 2010 map from ESA (2014), which can have a large impact on the estimation of biomass and carbon stocks in dryland forests. The AGB map generated by this study is the most accurate and detailed published for the study area and complements the global products, therefore facilitating regional to international reporting of biomass and carbon dynamics. This is in agreement with (Lucas et al., 2008) who utilised ALOS PALSAR data and the Landsat-derived Foliage Projected Cover (FPC) in Queensland, Australia, and reported that the combination of radar and optical data has the ability to allow better assessment of deforestation patterns, regeneration and woody thickening, tree death from climate change, and biomass change. In addition, the AGB model from this study showed that biomass for dryland forests exceeds estimates derived from pan-tropical products which underestimate biomass and forests in dryland ecosystems of less-studied areas such as the KAZA region, which are often neglected in this type of analysis (David et al., 2022a). The sensor fusion explored here complements this study and encouragingly suggests a high potential for separating biomass in dryland cover types that are structurally distinct but spectrally similar, which are notably those areas that are challenging to distinguish through optical remote sensing alone (Buhne and Pettorelli, 2018; Treuhaft et al., 2004).

In addition to sensor integration, issues of scale are critical for biomass and habitat mapping, where the adequacy of spatial resolution is key (Buhne and Pettorelli, 2018). For example, biomass mapping at a regional scale utilising the fusion of optical and radar data in this study reduced the saturation effect at high AGB values above 80 Mg/ha, allowing the identification of habitat fragmantation, and small-scale degradation patterns of biomass compared to broader scale maps. Maps of AGB, if sufficiently detailed, can assist conservation managers, practitioners, and policymakers to formulate specific practices (e.g., corridor planning, tree thinning, fire control, biodiversity surveys, etc.) that are appropriate to support the conservation of forest habitats and their management. Many countries presently lack the capacity to produce their own local maps of forest biomass and so must rely on existing biomass maps founded upon broader pan-tropical and global datasets. Whilst the AGB maps produced by Baccini et al. (2017) and Bouvet et al. (2018) may be used to meet national-scale emissions reporting requirements when no finer scale information is available, these maps need to be validated against local forest stock surveys or local/regional AGB maps from higher resolution satellite imagery. Given the decision-making on sustainability at national and subnational levels, this study contends that the pan-tropical and global data sets are unable to provide finer scale mapping of aspects that are relevant to wildlife habitat and biodiversity in dryland forests. These results support the assertion that countries should not rely on pan-tropical datasets but should rather estimate biomass and carbon stocks at the regional and local level, which in turn feeds into meeting the United Nations' Sustainable Development Goals (SDGs), as suggested by Mitchard et al. (2013). This is essential for land and forest management in these areas, particularly in protected zones, given the vulnerability to anthropogenic pressure, disturbance from wildlife, and climatic fluctuations.

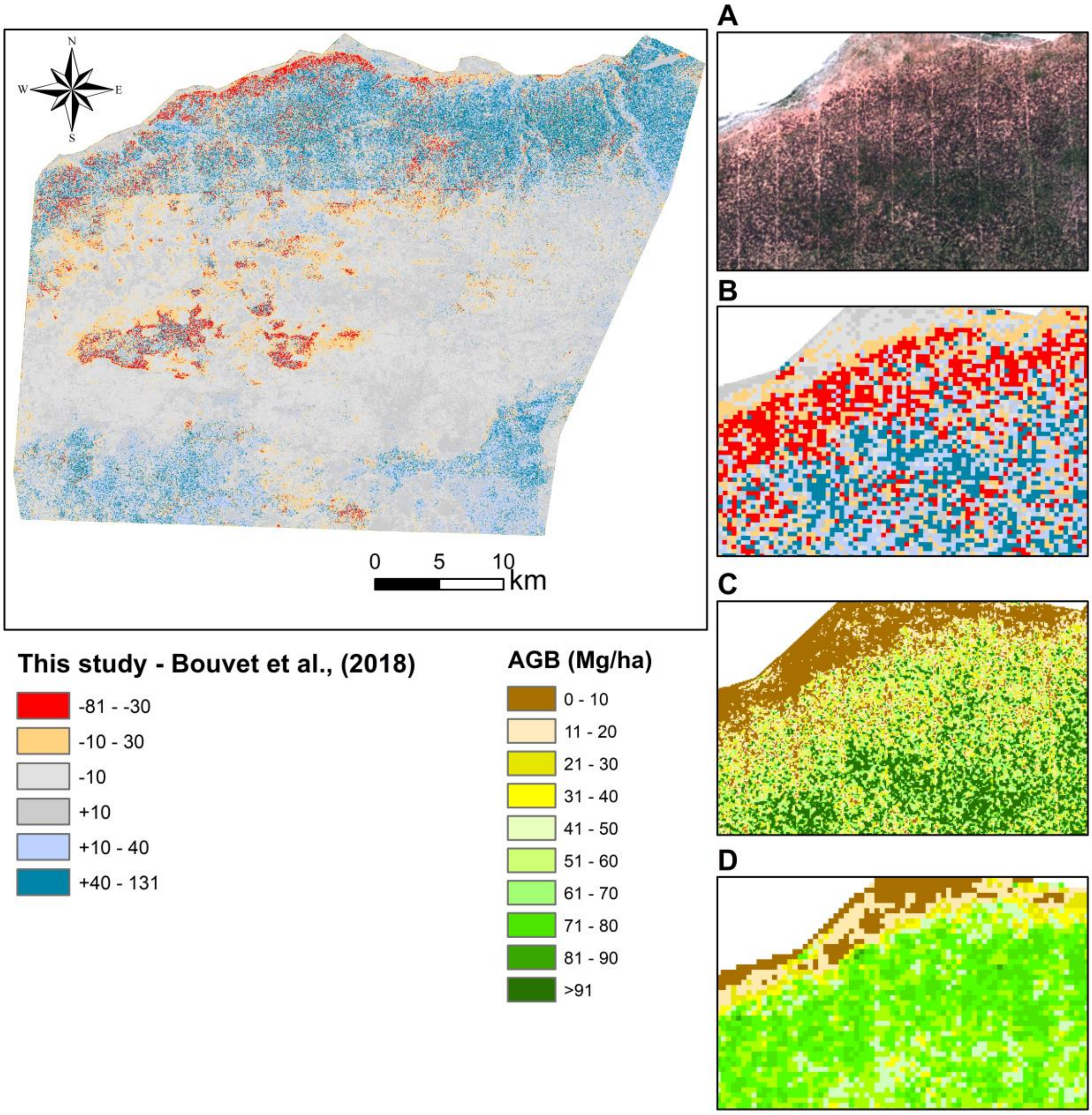

Fig. 3. 11. A: RGB 432 S2 image. B: S2 a difference map between this study and Bouvet et al., 2018 (This study –Bouvet et al., (2018), C: This study AGB map. D: Bouvet et al., 2018 AGB map.

3.5 Conclusion

This study combined satellite-based synthetic-aperture radar (SAR) and multispectral imagery with ground truth data to map above ground biomass throughout the dryland forests in the Chobe region of Botswana. The main finding from the results is that using a combination of data types (SAR and multispectral sensors) it is possible to estimate above ground biomass in dryland forests with a good level of precision. The estimations of AGB reveal that the highest biomass values of 80-145 Mg/ha were found in northern Chobe where the dominant tree species are *Baikiaea plurijuga, Burkea africana,* and *Pterocarpus angolensis*. A large part of the study area (85%) is characterised by low AGB values (< 80 Mg/ha). In Southern Chobe and along the Chobe River frontage area, a high burning frequency and degradation associated with overgrazing and elephant damage may have contributed to the generally low AGB values observed. Three main conclusions can be drawn from this study:

First, combining freely available SAR and multispectral imagery (S1 and S2) has the potential to estimate biomass at local and regional levels with a good level of precision compared to using single sensors alone. The research observed that the relatively fine resolution of Sentinel (10 m pixels) reduced the mixed pixel problem observed in medium spatial resolution data (30 m pixels; e.g. Landsat 8), which led to an increase in the precision of biomass estimation. The results demonstrated that SAR backscatter in conjunction with the strategically positioned optical bands (red edge wavebands) significantly improved forest stand parameter estimations and the reduced saturation effect in areas of high biomass in dryland forests. The NDRE1 and GNDVI yielded a higher linear relationship than NDVI, while GRVI and EVI yielded the lowest correlation with AGB.

Secondly, dryland forest ecosystems and conservation organisations can use global and continental datasets as sources of information that could provide early warnings of regional-scale ecological change. However, regional and local studies are critical and serve to provide useful information in evidence-based decision making for improved estimation of carbon stocks, monitoring the impacts of climate change, and the conservation of dryland forest habitats under pressure.

Finally, after comparing and analysing the effects of the various empirical models using ML and RF regression approaches, this study found that the decision tree model (RF regression algorithm) is the most robust for estimating AGB in dryland forests, as compared to linear analysis. The precise and timely quantification of AGB can help improve the understanding of dryland forest habitats and to plan and monitor land and forest resources in conservation areas, which are critical for wildlife function and sustainable land management at present and into the future.

3.6 Acknowledgments

This work was supported by Commonwealth Scholarship Commission PhD grant number: NACS-2017-409 from the 2017–2020, Geography doctoral program at Durham University. The authors acknowledge financial support from the Royal Geographical Society (with IBG) - Monica Cole Research Grant (grant number: MC 08/19) and WWF Namibia Mike Knight for travel support grant number: T225. I thank WWF KAZA TFCA Secretariat Dr Nyambe Nyambe, Chobe National Park Authority Michael Flyman, and University of Namibia (Katima Branch) Dr. Ekkehard Klingelhoeffer for the support during the field. I also thank Morgan Kamwi who helped with data collection.

3.7 Supplementary Information 1

Table A. 1. Image acquisition date and scene ID.

Satellite	***Cloud cover***	***Acquisition Date***	***Satellite Name***
S1	0	15/03/2019	COPERNICUS/S1_GRD
S2	0	14/03/2019	COPERNICUS/S2_SR/20190314T080709_20190314T083245_T35KKA
LC08	0	15/03/2019	LANDSAT/LC08/C01/T1_SR/LC08_174072_20190315

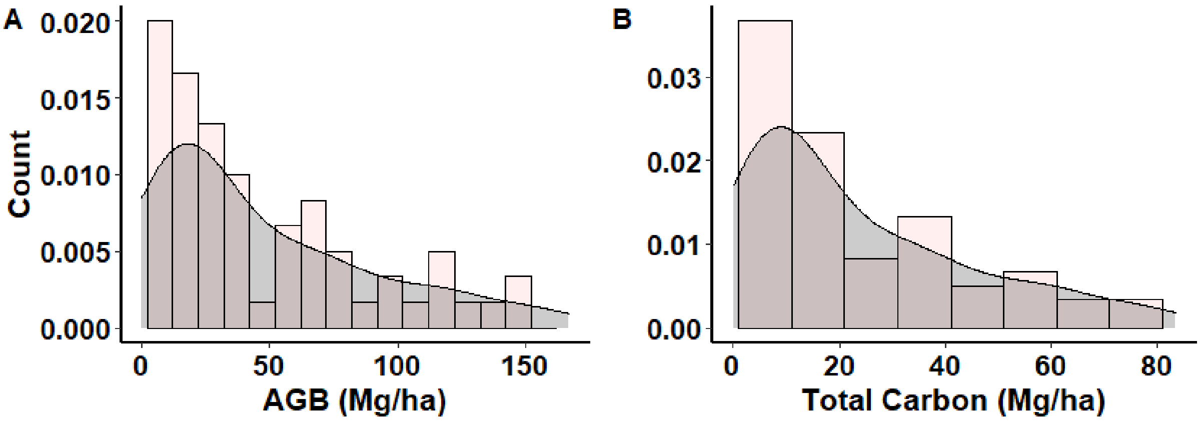

Fig A. 1. Density and histogram plots A: Aboveground biomass (AGB); B: Carbon stock (Mg/ha) of each field plot with woodland trees.

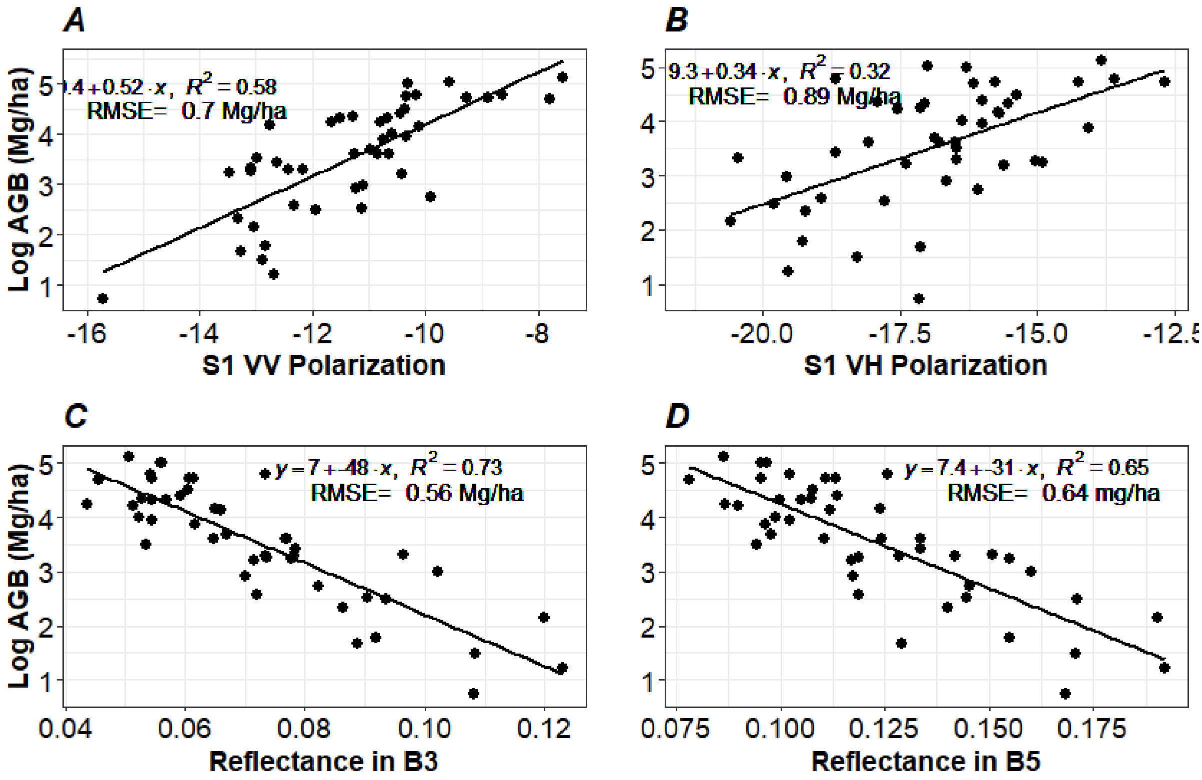

Fig A. 2. Relationships of S1 polarisations and S2 spectral bands with stand forest parameters in the study area. A: S1 VV polarisation vs AGB. B: S1 VH polarisation vs AGB. C: S2 B3 vs AGB. D: S2 B5 vs AGB.

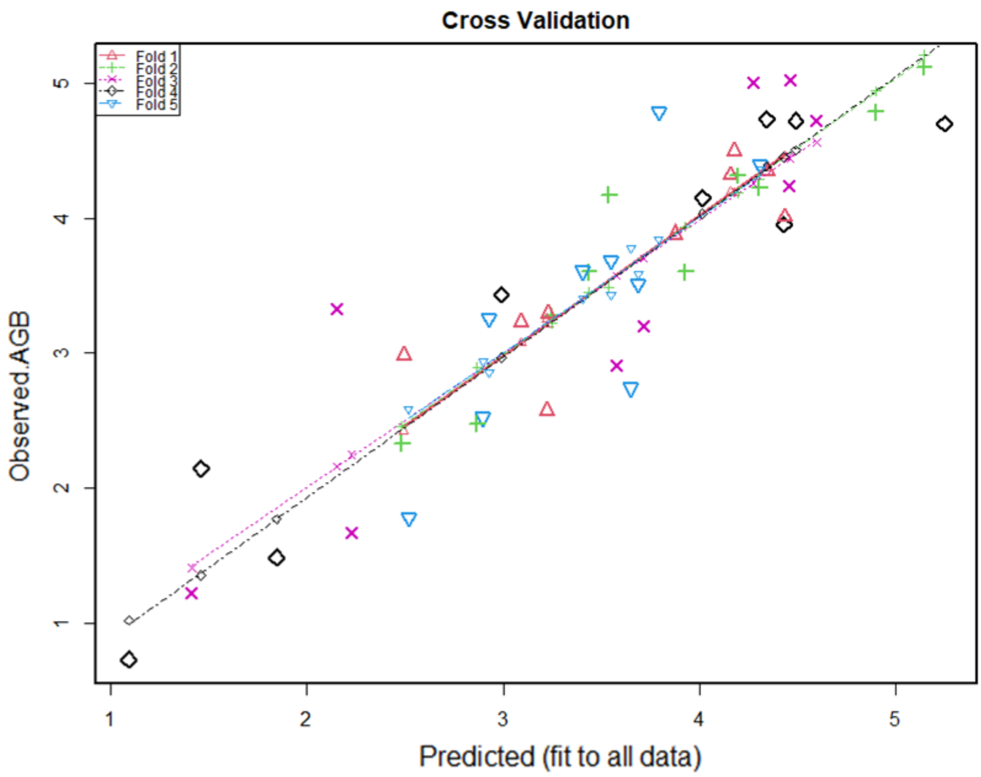

Fig A. 3. Dispersion diagram of the observed versus predicted biomass at each fold on a log scale using 70% of the training data.

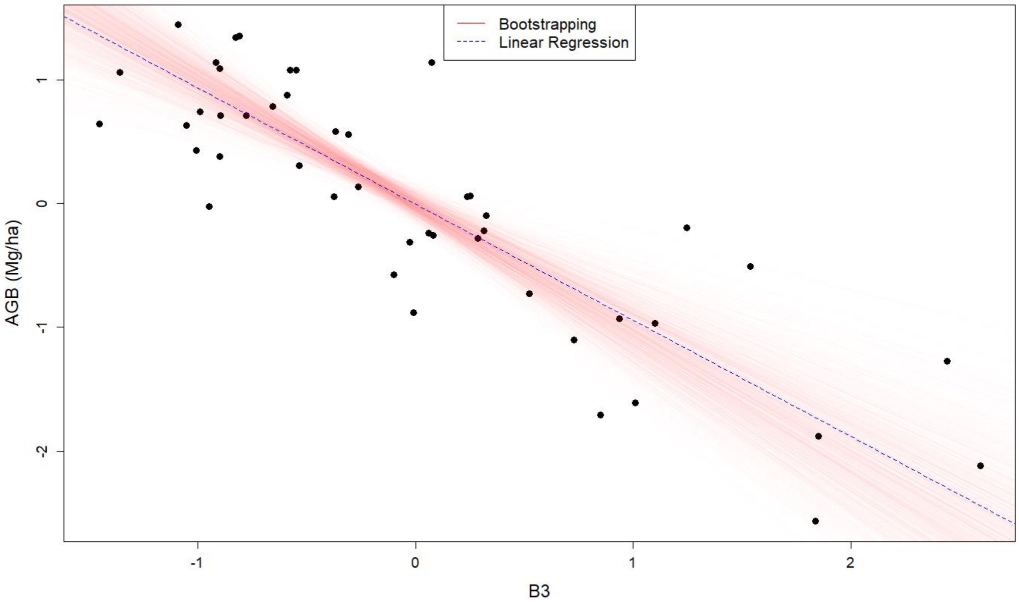

Fig A. 4. Linear and Bootstrap regression of Sentinel 2 Band 3 on a standardised scale.

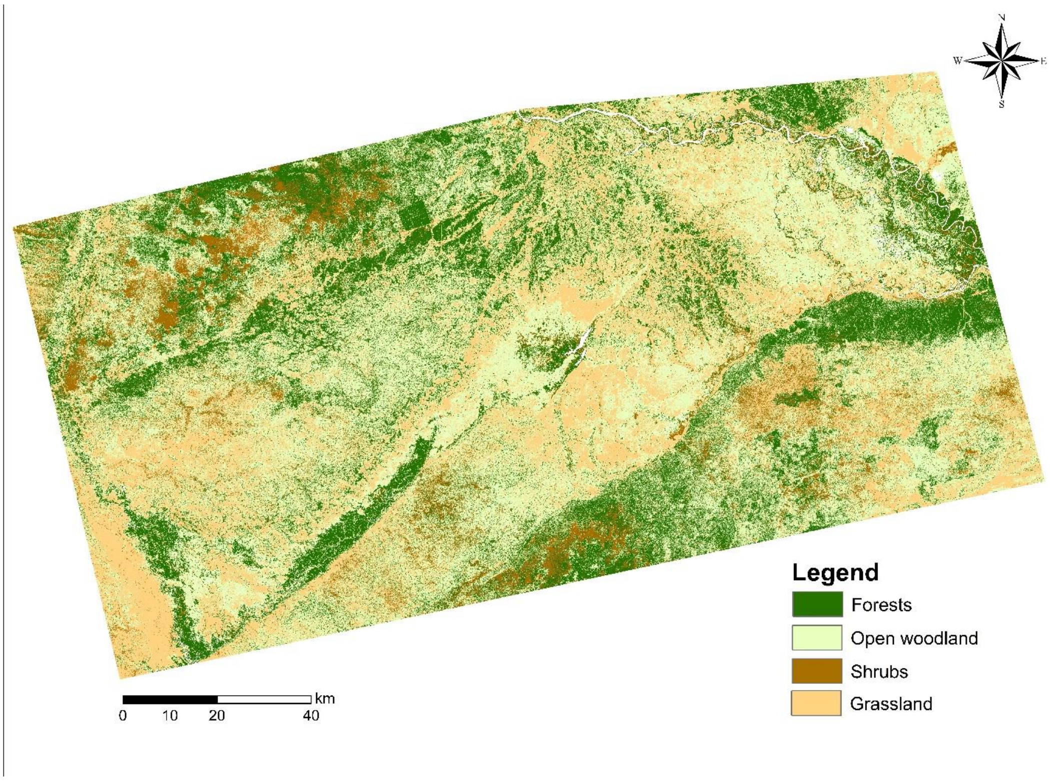

Fig A. 5. Land cover classification map of Zambezi region in Namibia and Chobe District in Botswana for 2019

Table A. 2. Area statistics of the land cover classes.

Land cover classes	**Total Area (km^2)**	**Percentage (%)**
Forests	4,475	23
Open woodland	8,216	43
Grassland	4,910	25
Shrubs	1,719	9
Sum	19,321	100%

Table A. 3. Accuracy assessment of the land cover classification

Accuracy	**Percentage (%)**
Overall Accuracy	97%
Validation Overall Accuracy	67%
Kappa coefficient	60%

4 IDENTIFYING AND UNDERSTANDING DRYLAND FOREST CHANGES AND DISTURBANCES IN SOUTHERN AFRICA USING LANDSAT AND MODIS TIME SERIES AND FIELD VEGETATION DATA

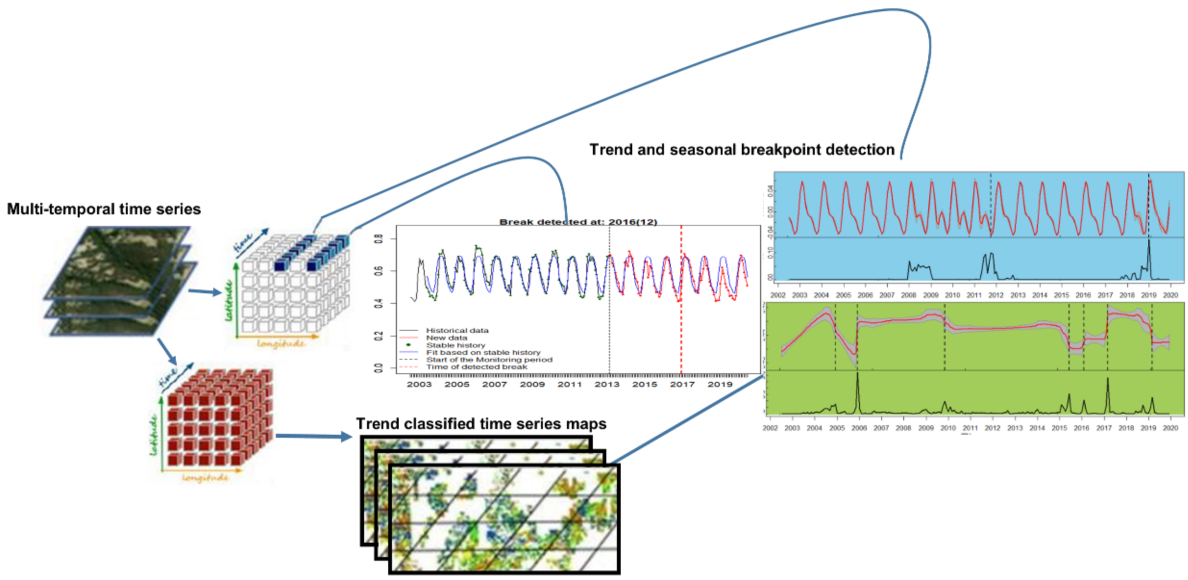

Chapter 4 Manuscript in progress: Intended for submission to *International Journal of Applied Earth Observation and Geoinformation*.

Title: Identifying and understanding dryland forest changes and disturbances in Southern Africa using Landsat and MODIS time series and field vegetation data.

Author contributions

David Ruusa- Design the research, perform the data analysis, interpret the results, wrote the manuscript, and revised the manuscript. Nick Rosser- Contributed to the research design, manuscript editing and supervision. Daniel Donoghue- Contributed to the research design, conducting fieldwork, manuscript editing and supervision.

Abstract

The Kavango Zambezi (KAZA) Transfrontier Conservation Area is sensitive to water availability, and drought, in addition to anthropogenic disturbances, impacts vegetation cover in the region. An effective method for change detection to examine vegetation response across KAZA needs to account for seasonal as well as abrupt changes over at fine temporal resolutions (e.g., monthly) rather than yearly basis. In this study, an approach that quantifies dryland forest change by combining Landsat and MODIS imagery with climate data, validated against ground-based measurements collected from Namibia and Botswana was presented. The Breaks for Additive Seasonal and Trend (BFAST), and Bayesian Estimator of Abrupt change, Seasonality and Trend (BEAST) algorithms were applied to evaluate their ability to detect changes in both long-term trend and seasonality based upon the MODIS normalised difference vegetation (NDVI) and Green normalised difference vegetation (GNDVI) time series. The results demonstrate that there is a close relationship between the ground survey data and the estimated changepoints. The Bayesian analysis (BEAST) was found to give the best performance in identifying abrupt changes associated with fire, drought, and seasonal changes driven by climate and clear-cutting events as compared to BFAST. BFAST failed to detect seasonal shifts in the entire study period. GNDVI was an effective dataset for detecting both small and large magnitude changes (e.g., deforestation, fire, and drought), while the NDVI was most effective in detecting large magnitude changes, particularly those that resulted in complete land-cover class changes (e.g., deforestation). The study found that the NDVI was more influenced by canopy background variations and herbaceous layers when detecting changes with regrowth of herbaceous layers than the GNDVI. Tropical dryland forests in KAZA are highly dynamic and water-sensitive with high rates of deforestation and widespread degradation, which mainly result in abrupt vegetation changes, continuous vegetation recovery and regrowth. The approach presented can accurately identify the vegetation changes, phenological variations and time of disturbance in both the spatial and temporal domains. Therefore, it can contribute to the understanding of forest decline and habitat changes and their

vulnerability in the context of land cover change, climate change and sustainable development policies in tropical dryland forests.

Keywords: Change detection, Time-series decomposition algorithm, Forest disturbance, Bayesian estimators, BFAST, Abrupt change, Southern Africa

4.1 Introduction

Tropical dryland forests experience a high degree of pressure from human activity but monitoring forest degradation in these systems is challenging due to high canopy complexity, phenology, climatic variability, and diverse degradation drivers (Grainger, 1999, McElhinny et al., 2005, McNicol et al., 2018). Protected Areas (PAs) underpin global efforts to preserve the Earth's biodiversity and maintain functional terrestrial and aquatic ecosystems (Wiens et al., 2009). The Kavango Zambezi Transfrontier Conservation Area (KAZA TFCA) is the largest "hyper" hotspot for endemism and conservation support. However, the tropical savanna forests and woodlands (hereafter referred to as "dryland forest") face an increasing number of threats, ranging from those originating from climate, disturbance by large mammalian herbivores, to those associated with the increasingly invasive competition for diminishing resources. These multiple threats have led to deforestation and degradation of protected landscapes, which directly impacts wildlife species distributions (Cumming, 2008). Changes in climate regimes and competition for the available natural habitats have contributed to the escalation of human-wildlife conflict (HWC) in the KAZA region, especially in Namibia and Botswana (FAO, 2009). Furthermore, climate modelling of Africa has shown that dryland forest in and around KAZA TFCA is among the world's most vulnerable at warming levels of 1.5–2.0° (IPCC, 2014).

Monitoring long-term ecological processes in these PAs is therefore crucial to ecological conservation and biodiversity (FAO, 2009). The possibility that arises when changes are not monitored routinely is that the adverse impacts may have already occurred and it may be too late to reverse the change or even adapt to it (Sheffield et al., 2008). This will lead to large-scale destruction of important habitats for many species and a dramatic decrease in wildlife habitats. Thus, for conservation goals to be met, it is essential to detect whether vegetation changes and degradation are occurring within the forests of PAs and their causes. Assessment of the regional impacts of land use and land cover (LULC) change are fundamental for determining the appropriate policy responses to forest decline, increased human-wildlife conflicts, and managing of animal movement patterns and wildlife corridors in KAZA TFCA (Stoldt et al., 2020). Such efforts are equally important for enhancing forest carbon sequestration and avoiding deforestation for developing nations, as encouraged by Reducing Emissions from Deforestation and forest Degradation (REDD+) schemes.

In Africa, almost all remaining dryland forests in PAs are threatened by deforestation and degradation and so should be given high conservation priority (Clark et al., 2008). Although the focus in detecting forest cover loss using different indices soon after they occur overwhelmingly remains in humid forests (Janzen, 1988; Masiello et al., 2020), dryland forests are beginning to receive more attention. However, published studies on dryland forests in Africa are generally concentrated on the Sahel in West Africa (Liu et al., 2017), while most studies in Southern Africa have been confined to Kruger NP (Bucini et al., 2010). Unfortunately, the forests in PAs of other parts of Southern Africa such as KAZA TFCA have received far less attention. An additional challenge is understanding the sensitivity and therefore suitability of conventional satellite-based NDVI measurements in detecting large and small-scale forest disturbances and seasonal change in highly heterogeneous forest environments such as drylands (Blackie et al., 2014). The lack of historical disturbance events in KAZA TFCA constitutes a challenge for in-depth temporal and spatial analysis which is crucial to ecological conservation and biodiversity. This is raising concerns that disturbances within the dryland, natural resources and wildlife habitat management areas might increasingly interfere with continuous and sustainable provisioning of ecosystem services to society and wildlife.

The availability of MODIS satellite data and new automated data processing techniques that provide high-quality continuous time-series data represent a major advancement for the automated monitoring at monthly rather than annual intervals which potentially masks considerable within-year variations. The daily temporal resolution of the MODIS NDVI has a significant advantage over Landsat data for monitoring the disturbance and recovery state. The limitation of MODIS based Vegetation Indices (VIs) for change detection is associated with the moderate spatial resolution. With the advancement of cloud computing, particularly the Google Earth Engine (GEE) platform, which provides an archive of data including MODIS and Landsat with associated data processing capacity at no cost (Gorelick et al., 2017), has become a valuable tool for change monitoring in tropical environments. Access to such temporally rich time series has also led to an increase in methods that aim to track the occurrence of disturbance events at regional scale. It is reported that disturbance rates in dryland forests have increased in recent decades, and there is evidence that climate change and past land use both have contributed to the disturbance increasing rate (Wilcox, et al., 2011). Continuous disturbances in an area consisting of natural habitats result in habitat fragmentation and reduce its ability to support the ecosystems and surroundings that are essential for their sustainability (Visscher, 2006). The accurate reconstruction of past forest disturbance dynamics at spatial, temporal, and thematic scales offered by time series will allow ecological analyses to help provide a better understanding of disturbance regimes (Senf et al., 2017). The dense time series information enables the quantification and characterisation of disturbances in terms of disturbance magnitude, duration, and attribution of recent disturbance activities (Kennedy et al., 2012). Before the availability of time series analysis, forest change detection mapping was done using bi-temporal differences or supervised image classifications (David et al., 2022a). Bi-temporal image classifications were able to detect large-scale deforestation, but they are less useful for assessing small-scale deforestation, degradation, and regrowth because they fail to capture the dynamic behaviour of vegetation during the year and over longer time periods (Hamunyela et al., 2020; Zhu and Woodcock, 2014). Moving from a relatively static, bi-temporal view of change toward a more continuous view of ecosystem dynamics can improve understanding regarding the disturbance's spatiotemporal patterns, their causes, and consequences (Kennedy et al. 2014). Effective change detection ideally identifies variations at the seasonal scale while simultaneously detecting abrupt, and subtle changes in any long-term trends. Breaks For Additive Seasonal and Trend (BFAST), BFAST Seasonal and Bayesian Estimator of Abrupt change, Seasonality and Trend (BEAST) algorithms have been developed to do this (Verbesselt et al., 2012; Zhao et al., 2019). However, their effectiveness in tropical dryland forests, where vegetation response is typically aseasonal, has yet to be assessed.

This paper aims to provide a systematic assessment of vegetation dynamics and spatially detailed patterns of change in the dryland forests. To do this, the research employs multiple data streams for the time series assessment of forest change over parks and surrounding areas within KAZA TFCA from 2002–2019. The premice is that by taking advantage of the different characteristics of vegetation indices and different change detection model, change detection results could be improved in dryland forests. The general objective was to investigate the evidence of water stress conditions and assess the suitability of the change detection model on MODIS time series data for mapping forest disturbances (e.g., clear-cutting, drought) in dynamic and diverse tropical dryland forests. Specifically, this paper reports three steps: (1) spatial characterisation of climatic data with vegetation indices as a proxy indicator of climate variability to improve understanding of vegetation response to drought; (2) Compare the commonly used NDVI vegetation index with GNDVI and evaluate their sensitivities and performances in detecting changes; and (3) Characterise changes in trends and phenological patterns using BFAST and BEAST algorithms. (4) Quantify and identify the LULC change, locations, types, and trends of the land cover during the 19-year period in communal and protected areas of Zambezi region. Ideally, such an analysis will provide conservation efforts with frequently updated information for monitoring disturbances and potentially deforested areas, allowing targeted mitigation actions to be taken.

4.2 Materials and methods

4.2.1 Study area

The KAZA TFCA (18.00°S, 23.00°E) in Southern Africa, is an iconic PA that inhabits a rich ecology and enormous wildlife. KAZA TFCA is established in March 2013 with an enclosed area equivalent to the size of France at 519,912 km^2 (Cumming, 2008), and is situated in the Kavango and Zambezi River basins- and is shared by

Angola, Botswana, Namibia, Zambia, and Zimbabwe. Within this area, 371,394 km^2 are under conservation and the remaining 148,520 km^2 are mainly used for agricultural activities including rangeland.

This conservation area is considered to be an important means to create economic development and conserve the unique biodiversity by establishing links between fragmented habitats with a particular focus on large-scale migrations of wildlife (WWF, 2016). KAZA links together over 36 proclaimed PAs including national parks (NPs), forest reserves, community conservancies, and wildlife management areas. PAs carry substantial populations of large mammals and several plant endemic plant species, including large areas of the dryland forests, and globally significant wetlands. The dryland vegetation domain in KAZA ranges from forest formations with a dense canopy cover to shrubs and grasslands ranges, which are also considered a biodiversity hotspot. However, these areas are under severe pressure from agricultural expansion and settlement, wildlife, large-scale burning, and timber harvesting (NACSO, 2014) (see: Fig. 4.1). This study focuses on the Namibian and Botswanan components of the KAZA TFCA. In particular, the study was conducted in three protected areas situated in the Okavango Zambezi region: (a) Chobe NP in Botswana, (b) Zambezi state forest (ST) in Namibia, and (c) Mudumu NP in Namibia. The selection of study sites depended on the ecological importance and the land conservation practices implemented within the region. The selection of sites in Namibia included state-run protected areas such as Zambezi state forest (red-coloured polygon), a conserved forest area which was traditionally protected by the government and residents in the area (see: Fig. 4.1). Zambezi state forest is designed to be only used sustainably used for timber and other forest products but has now been pushed back by human settlement (Bollig and Vehrs, 2021). The Mudumu National Park (Aqua-coloured polygon) is one of the largest protected areas in the Zambezi region established as a core wildlife area with animals migrating from the park to surrounding communal conservancies, where they can be used for quota hunting or through tourism (O'Connell et al., 2000). The unprotected surrounding communal area including the communal conservancies that depend on agriculture and tourism development and both encroach on the dryland forests (Hank, 2003).

The Chobe NP, in the north-east of Botswana (18.7°S, 24.5°E), features the largest number of elephants in KAZA; the number of elephants in northern Botswana alone is estimated at more than 156,000 (Junker, 2009). The Chobe River basin serves as a source of surface water for the Chobe District and in the dry season, animals converge on this stretch of water from Northern Botswana (Hanks, 2003). Chobe NP contrasts with the Namibian component of KAZA TFCA. The Zambezi Region (17.8° S, 23.9° E), in the heart of KAZA, is a long strip of land with multiple land uses, containing several national parks much smaller by comparison to Chobe NP. The Mudumu NP, in north-eastern Namibia, and is bordered by the Kwando River. The park is in the centre of KAZA TFCA and as there is no boundary fence, it acts as a corridor for large game species such as African elephants, as migrating between Botswana, Zambia, Angola, and Zimbabwe. The Zambezi ST area is surrounded by conservancies and communally governed areas. The Zambezi ST generally features very high population densities with consequent overgrazing and widespread unsustainable wood harvesting with many areas considered now degraded.

Topography in both parks is relatively flat characterised by low elevations ranging from 910 to 1100 m above sea level (Omphile et al., 2002). Climatically, the sites have similar rainfall patterns throughout the year, and so the KAZA region has a subtropical dry climate characterised by highly variable rainfall. The annual average rainfall is approximately 650 mm, with almost all falling between November to March, followed by a dry season from April to October. Daytime temperatures increase towards the end of the dry season, when the heat soars and the expectation of rain is high. Average temperatures range between 15.2°C - 30.2°C.

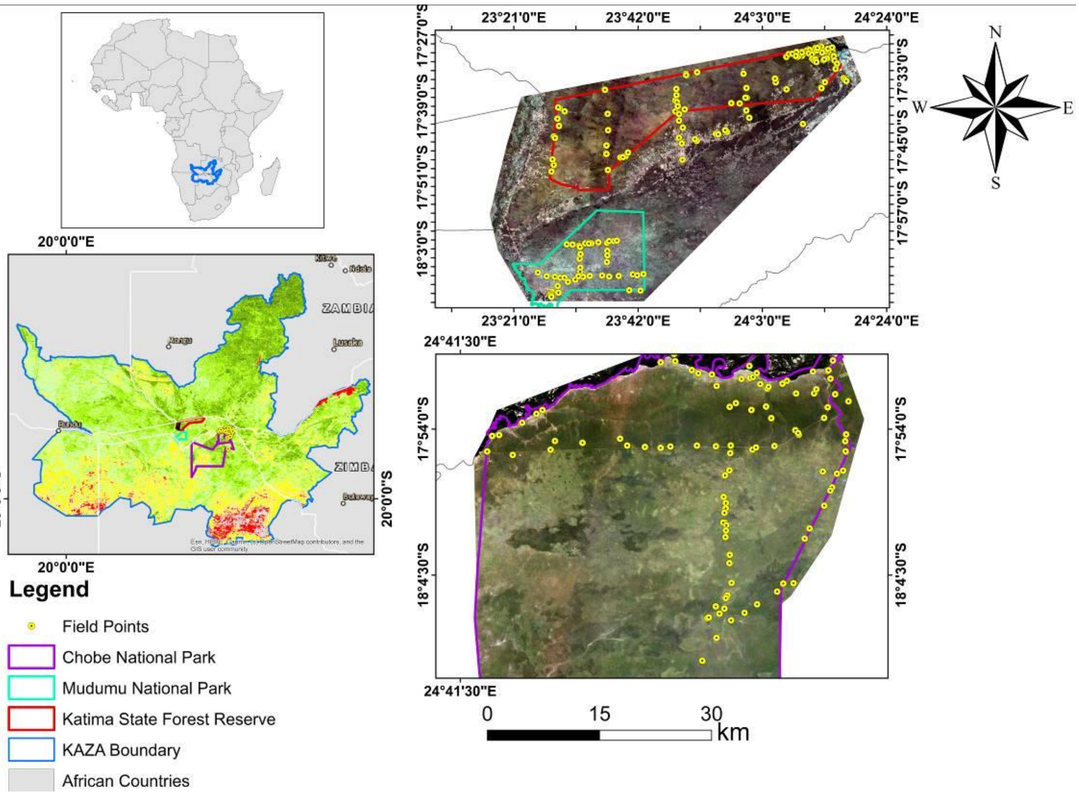

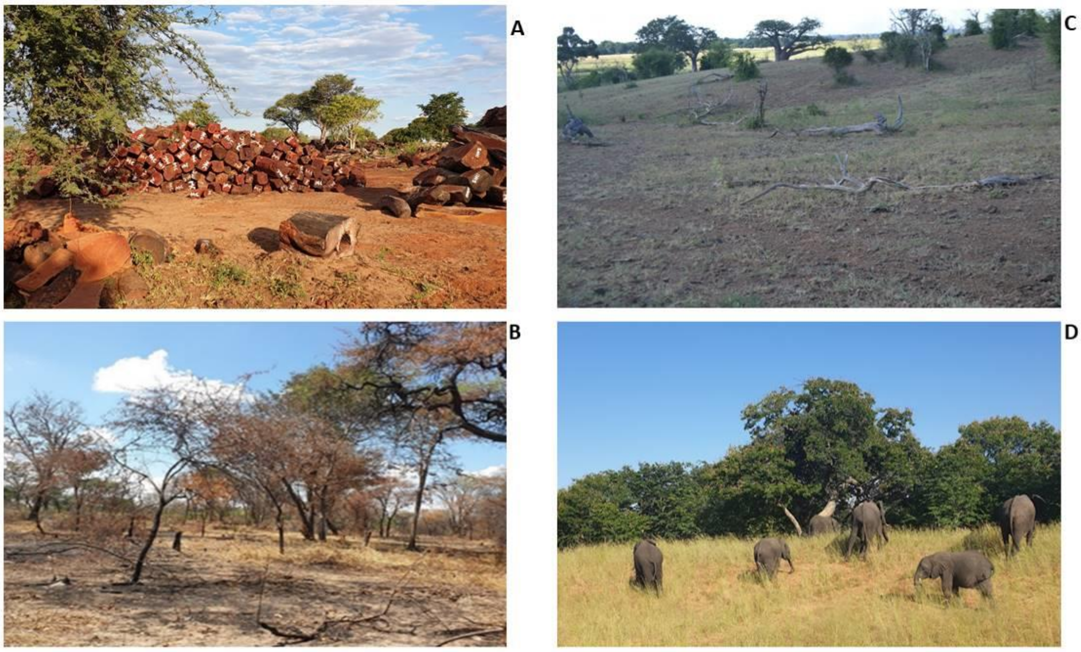

Fig. 4. 1. Location of the study area in KAZA TFCA. The yellow circles show sampling sites in Zambezi ST, and Mudumu NP Namibia (top), and Chobe NP (bottom). Examples of sample plots representing disturbance types and recent degradation activities captured during a field campaign in 2019 are shown, A) clear-cut deforestation of forest area in Zambezi ST Namibia, B) Burned forest for cultivation near protected area of Mudumu NP, Namibia, C) the visible forest loss, especially the woodland along the Chobe riverfront, D) high population of elephants destructive influence on vegetation.

4.2.2 Fieldwork and sampling design

Survey fieldwork was undertaken to record forest tree stands and observe the different land cover types present in the study area during the growing season (1st February - 30th April 2019). The field samples of the five main land cover classes (forests, open woodland, shrubs, grassland, and bare land) were collected at three sites in the KAZA TFCA region; one park was located in Botswana, the Chobe NP. The other two sites are located in Namibia - the Mudumu NP, and Zambezi ST (see: Fig. 4.1). These sites were chosen because dryland forests within and around the PAs are particularly susceptible to disturbance and drought, warranting particular attention (Feng et al., 2013). However, these areas are often remote and dangerous to visit in the field, due to the hazard posed by wildlife and if present, unexploded landmines (see: Fig. 4.1). Another challenge is there are very little plot data in the dryland forests, which are more sensitive to inter-annual variations in climate than humid forests (Grainger, 1999). This is particularly true for the forest in the KAZA region that experienced several extreme droughts in recent.

The allocation of plots followed a stratified random sampling approach based on the four strata (forest, open woodland, scattered trees with low herbaceous cover, and non-forests). The plot sizes of (20 m × 20 m) and (10 m × 10 m) were considered adequate to enable sampling a good number of trees in each plot. Smaller plot sizes of (10 m × 10 m) were adopted only in areas of very high tree density that were dangerous to visit due to the hazard posed by wildlife. In total, measurements were collected from 271 individual sample plots randomly distributed throughout the dryland landscape. A total of 101 plots in Chobe NP, 115 plots in Zambezi ST, and 50 plots in Mudumu NP were visited. In Botswana, 61 sample plots represent woody vegetation, 40 sample plots represented non-woodland cover, while in Namibia 95 sample plots represent woody vegetation, and 75 represented non-woodland cover. The total number of individual trees measured was 4337 in Botswana, 2400 trees in Zambezi ST, and 1600 trees in Mudumu NP. For each tree inside the plot, mean height, diameter at breast height (DHB), tree density, canopy closure, and tree species were recorded. The UTM coordinates at the centre of each plot were taken with the hand-held GPS. Although the coordinates of each plot centre were collected with a high-quality device with

GPS and GLONASS sensors, there may be small positional errors, especially when differential corrections are unavailable (errors up to 8–10 m are common). The images used in this chapter have a spatial resolution of 30 m for Landsat and 500m for MODIS data which have a coarser pixel size which compensated for the possible positional error of the GPS used. Heights of individual trees were measured using an ultrasonic Vertex III hypsometer which requires finding a suitable position to observe each tree tip (Božić et al., 2005), while stem diameter was measured using a Diameter above Breast Height (DBH) tape. The diameters of all the trees in each plot were measured at breast height, which is at 1.37 m above the ground surface. All trees with a stem diameter >3 cm and 1.5 m height were recorded. Field surveys of woody plants were conducted on sites where damage to plants was specifically observed to identify where drought had an obvious impact.

4.2.3 CHIRPS precipitation data

Climate data were selected under the assumption that plant growth in the region is limited by water availability, temperature, and/or incident radiation (Field et al., 1995). Changes in either of these parameters might induce changes in vegetation productivity and the proxy NDVI signal. For this region, water availability is determined by the amount of precipitation, and so the study confined this parameter to precipitation as productivity here is water rather than temperature limited (Nemani et al., 2003). However, for most parts of Africa, and especially the semi-arid lands, the network of climatological stations is not dense enough to provide a coherent spatial picture of climate variability. As a result, the spatial characterisation of the effects of drought events on the land surface is not well defined. The study used satellite-based monthly precipitation estimates from the Climate Hazards Group InfraRed Precipitation with Station data (CHIRPS) product (0.05° × 0.05°). CHIRPS data span from 1981 to the present. CHIRPS incorporates in-situ station data and CHPclim, 0.05° resolution satellite imagery to represent sparsely gauged locations such as Southern Africa (Funk et al., 2015a). To be consistent with MODIS VIs, the CHIRPS rainfall data from 2002 to 2019 was used.

4.2.4 Vegetation indices from remote sensing imagery

The vegetation datasets used in this study include NDVI and GNDVI greenness vegetation indices derived from the MODIS sensors. The vegetation indices use the wavelength and intensity of the reflected light within the visible and near-infrared wavelengths to measure the density of green leaf vegetation, acting as proxies for leaf area index (LAI), fractional vegetation cover, and photosynthetic capacity (Broge et al., 2001). Generally, the plant is under stress when there is a change in the health condition of the plant foliage, reflected by a corresponding decrease of LAI. Under stress conditions, plants increase their reflectance in the green and red portions as leaves become yellowish or chlorotic. This has led to the suggestion that the VIS portion is the most consistent leaf reflectance indicator of plant stress (Carter, 1993).

The Normalised Difference Vegetation Index (NDVI) is a commonly used vegetation index that measures green healthy vegetation as it utilises the regions of the electromagnetic spectrum most associated with high absorption of chlorophyll in the red band, and high reflectance of NIR by mesophyll layers in green leaf biomass (Rouse, 1974). It is calculated as a normalised ratio between Red and NIR reflectance values (Eq. 4.1). Higher NDVI values suggest higher amounts of photosynthetic active biomass. The NDVI was used in this study because it is a biophysical parameter that correlates with the photosynthetic activity of vegetation and is an indicator of the greenness of the biomes (Robinson et al., 2017; Tucker, 1979). NDVI is also able to offer valuable information to monitor vegetation health, drought effects, changes in plant growth, land degradation, deforestation, change detection/monitoring, and in relating large-scale inter-annual variations in vegetation to climate (Smith et al., 2019). Restrictions, however, have existed due to the effects of external factors, for example, soil and dead material, solar and viewing geometry as well as meteorological events, all of which pose a challenge in carrying out a proper assessment (Zhu et al., 2012). Particularly, in drylands with generally low vegetation canopy cover, the soil background tends to significantly influence NDVI, leading to a need for further development of vegetation indices. The study includes another greenness index, which is a variation of the NDVI and designed to reduce saturation issues identified with this index. The GNDVI is computed similarly to the NDVI, but the Green band is used instead of the Red band (Eq. 4.2) (Gitelson et al., 1996). Thus, GNDVI is more sensitive to chlorophyll concentration than NDVI and ranges from 0 to 1.0. It is related to the proportion of photosynthetically absorbed radiation and is linearly correlated with Leaf Area Index (LAI) and biomass (Hunt et al., 2008). By exploring various combinations of available spectral bands, the study additionally examined the sensitivity of other indices such as MSAVI, EVI to find the most sensitive VI to detect changes in the dryland forest. MSAVI and EVI were outperformed by GNDVI and thus GNDVI is presented in comparison to NDVI.

$$\mathrm{NDVI} = \frac{NIR - Red}{NIR + Red} \quad \text{(Eq. 4. 1)}$$

$$\mathrm{GNDVI} = \frac{NIR - Green}{NIR + Green} \quad \text{(Eq. 4. 2)}$$

Table 4. 1. Characteristics of the main datasets used in this study

Climate Data			
Dataset	***Timespan***	***Resolution***	***Source***
MODIS 8-day Terra Surface Reflectance (MOD09A1.006)	2002-2019	500m	GEE
Climate Hazards Group InfraRed Precipitation with Station Data (CHIRPS)	2002-2019	0.05 degrees	GEE
MODIS vegetation Data			
Terra Surface Reflectance 8-Day Global 500m	2002-2019	500m	GEE

(MOD09A1.006)			
LANDSAT Data			
Landsat 5 ETM sensor-Surface Reflectance	2002-2012	30m	GEE
Landsat 8 OLI sensor-Surface Reflectance	2013-2019	30m	GEE

4.2.5 Landsat Imagery

In the Google Earth Engine platform, 2004 Landsat-5 TM (Thematic Mapper and 2019 Landsat-8 OLI (Operational Land Image) surface reflectance 30 m spatial resolution satellite images were utilised for landcover cover classification over the study region (Gorelick et al., 2017). For both Landsat 5 and Landsat 8 data, only optical 30 m spatial resolution spectral bands (visible and infrared) were selected for classification. Bands 1 and 9 were not used due to strong atmospheric absorption. The study aims to use Landsat images from 2002 for the classification, however, the year 2002 had 0 images available for the study site, while 2003 had 5 images available for the study area, and they only cover 1/5 of the study area. Therefore, the Landsat images for 2004 were used because it was the closest date to 2002 with a total of 35 available images which cover the whole study area. In 2019, a total of 84 images were available and selected for classification.

4.2.6 Validating data

The ground field sample points were used to validate the change detected by the algorithms. The verification was carried out quantitatively using field data collected from the field and the classified/change maps by generating a confusion matrix to assess the effectiveness of the land cover classification generated by the Random Forest classification in section 4.3.5. The BFAST change detection was validated using an area change using sample-based estimates in section 4.3.6. Additional verification was also conducted through visual interpretation of the Landsat surface reflectance 30 m spatial resolution satellite images (LANDSAT/LT05/C01/T1_SR) and (LANDSAT/LC08/C01/T1_SR) that are atmospherically corrected using LEDAPS and using LaSRC to ensure the data consistency and comparability (see: Table 4.1) (Claverie et al., 2015). The acquisition date of the Landsat image in which the disturbance event was first visible was used as a surrogate time for when the disturbance has occurred, and such data was used to verify the detected changes of BFAST and BEAST and note the timing of the change. This interpretation is commonly used by other comparable studies on change detection using BFAST (Cohen et al., 2010; Dutrieux et al., 2015). Using high resolution data, Cohen et al. (2010) used visual detection of a large proportion of historic change processes in the forest. Their study highlighted the importance of visual interpretation technique of change points using high resolution images and photo interpretation because historic events can be very difficult to ascertain. For example, DeVries et al. (2015) and Hamunyela et al. (2016) visually examined the Landsat image time series data to validate forest change occurred for a specific pixel detected using BFAST algorithm. Zhao et al. (2019) developed the BEAST algorithm (also tested in this study) and visually validated the ground-reference data on disturbances and changepoints by interpretation of multisource imagery.

4.3 Methods

An overview of the methods for this research is shown in Fig. 4.2. The four main steps were as follows: (1) high-quality NDVI time series data preparation. A time series was first pre-processed to remove noise and obtain an uninterrupted data stream. (2) Temporal and spatial analysis of climate and vegetation time series to detect anomalies and drought impacts. (3) Trend and seasonal breakpoint detection using BFAST and BEAST algorithms. (4) Validation of the change detection algorithms and discussion of the potential factors driving vegetation change.

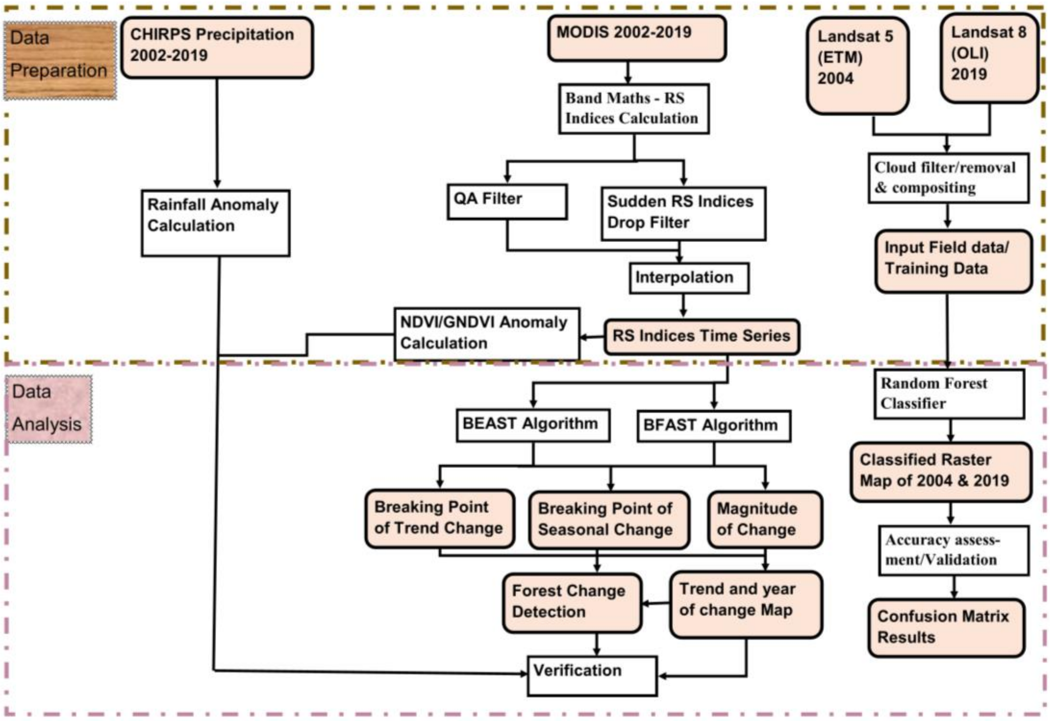

Fig. 4. 2. Flow chart of data and methods.

4.3.1 Preparation of high-quality MODIS datasets

Satellite image time series are rarely complete. Noise in a time series is brought about by cloud contamination and other factors such as snow or device malfunction (Vermote et al., 2002). Tropical environments such as Southern Africa present a unique challenge for optical time series analysis, primarily owing to fragmented data availability, persistent cloud cover, and atmospheric aerosols. Pre-processing is necessary to reduce this noise because it may conceal actual trends in a time series. In this study, although the monthly maximum value composite (MVC) method has been used to decrease cloud and other atmospheric effects in the original VIs data (Holben, 1986), residual noise resulting from poor atmospheric conditions, cloud cover, aerosol loading and unfavourable sun sensor surface viewing geometries remain (Huete et al., 2002). Therefore, the corresponding MODIS quality assurance (QA) data layer was used to help identify and remove low-quality observations, and only the time points in a time series that are higher quality, cloud-free, and have nadir-view pixels with minimal residual atmospheric aerosols are retained. The cloud-contaminated pixels and extreme off-nadir sensor view angles are considered lower quality were excluded from the composite.

In addition to the QA data, to retain good quality values throughout the time series, an assessment for data transmission errors, such as line drop out or moving from cloudy to clear sky conditions, which can cause localised Vegetation Indices (VIs) to increase or suddenly drop, were conducted. These fluctuations in VIs are not compatible with the gradual process of plant regrowth. The algorithm uses a threshold of 20% as an acceptable percentage increase in VIs for regrowth from fire or drought for arid/semi-arid dryland grassland though to dryland forests (Viovy et al., 1992). A low filtering threshold means that most MODIS VIs pixels with high-frequency noise related change are included, while a high filtering threshold produces a smoother temporal profile and can smooth out important changes. This study used a 20% threshold to reject fluctuations attributed to data errors. By utilising the MVC, QA data, and implementing the test for sudden drops, the observation points contaminated by noise were detected and discarded from the time series. The presence of contaminants such as clouds and cloud shadows, caused anomalous values which can be detected and removed to some degree, leaving gaps in the time series (see: Fig. B. 1). As with noise, robustness to missing data is therefore a crucial component to evaluate when considering change detection methods, especially when applying change detection to parts of the world with persistent cloud such as Southern Africa. The missing values at those points were then filled by implementing a linear average interpolation method (see: Fig. B. 1). However, this method still requires a time series of images with low cloud cover. The linear interpolation method has been proven to be efficient, and most of the time it is better than non-linear interpolations for predicting missing values in ecological phenomena time series (Gnauck, 2004). Fig. 4.3 shows the time series of the main land cover present in the study area, including forest, grassland, altered forest, and agricultural land.

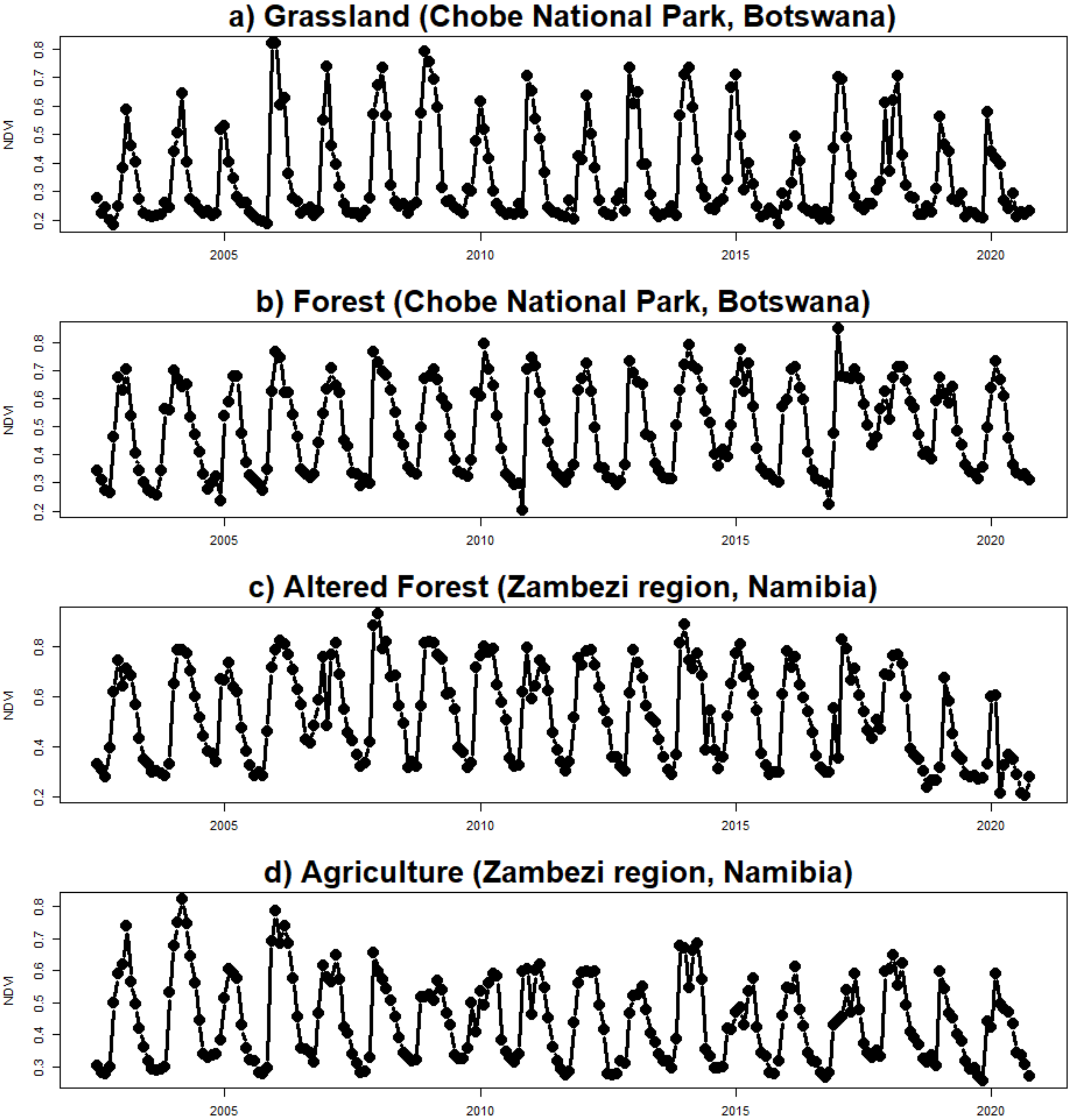

Fig. 4. 3. Time series representing forest, grassland, altered forest, and agricultural land.

4.3.2 Vegetation and precipitation time series anomaly

Here, satellite data was used to first quantify the extent and severity of rainfall anomalies and droughts with respect to long-term patterns, with a baseline of 17 years, and then to investigate the impacts of droughts and water stress on the dryland forest vegetation. The study focused on summer vegetation activity during the growth period. Hence the main season of interest here is January–March (JFM) since it is a period that contributes significantly to the summer rainy season across

Southern Africa and approximately coincides with the mature phase of El Niño (Lyon et al., 2007).

For this study, to identify and map the spatial extent of drought response in vegetation, the NDVI and GNDVI anomalies for a different season (the growing season is presented) for the KAZA region are calculated relative to a base period of 2002–2019. The anomalies are constructed by subtracting the growing season VIs (calculated over 2002–2019) from the long-term mean patterns for that period (e.g., month or seasons). The departures from a base mean period are used to detect periodic temporal patterns in VIs. This isolates the variability in the vegetation signal and establishes a meaningful historical context to determine relative drought severity. The NDVI and GNDVI anomaly was calculated using MODIS data. The 2010 to 2019 period is presented because it is representative of the record of the 21st century where drought events are extreme.

4.3.3 Change detection algorithms

Remote multispectral and hyperspectral measurements, especially in recent years, have been an imperative source of data for drought and vegetation dynamics assessment. Satellite remote sensing complements traditional ground-based data collection through synoptic spatial coverage and reduced costs (Galiatsatos et al., 2020). Numerous time-series methods have been introduced to study the temporal trends in pixel values across remote sensing images addressing the detection of temporal-scale changes including *seasonal, abrupt, and gradual* changes. These methods include BFAST (Verbesselt et al., 2010a), LandTrendr (Kennedy et al., 2010), Estimating Segments in Trend (DBEST) (Jamali et al., 2015), and BEAST (Zhao et al., 2019). These change detection methods detect when a pixel value drastically changes, indicating a change in surface reflectance, and thus, in land cover or land use (Zhu, 2017).

Producing forest cover change information requires approaches that also account for intra-annual seasonal or cyclic signals to identify changes in the phenological patterns, which indicates species' responses to environmental conditions (Menzel et al., 1999). The study utilised BFAST and BEAST algorithms because the two approaches use a season-trend decomposition model to take account of both inter-and intra-year variation in a time series, unlike other methods. These algorithms consider seasonal changepoints in plant phenology caused by changes in temperature and rainfall regimes as opposed to other trend detection methods such as Detecting Breakpoints and Estimating Segments in Trend (DBEST) which do not consider seasonality if any.

4.3.3.1 BFAST

BFAST is a widely used method for detecting trends and seasonal breaks in time series. The BFAST approach iteratively decomposes a time series to find both trend and seasonal changes in vegetation dynamics over a univariate time-series object (Verbesselt et al., 2010b). The function fits a model to the data by Ordinary Least Square (OLS) fitting on a stable history period, and to check for stability of that same model during the monitoring period. The nonlinearity in the trend component is also simplified into a number of individual trend segments, in order to identify sudden structural shifts. The trend is composed of segments with gradual changes, separated from each other by relatively brief, abrupt changes (Verbesselt et al., 2010a). The discrepancy between the model predictions and the data during the monitoring period is estimated using a moving sum of residuals (MOSUM) window to test whether one or more breakpoints occur. When observed data significantly deviate from the model, a break is detected (DeVries et al., 2015). The hypothesis of structural stability is rejected when the MOSUM window significantly deviates from 0 and crosses a boundary defined by the functional central limit theorem (Zeileis et al., 2005). The difference between the intercept and slope terms of consecutive models is used to calculate change magnitude between breakpoints (Verbesselt et al., 2010a). Having a sufficiently long stable history period for model fitting is critical for accurate detection of change. The history period needs to be free of disturbances and is referred to as a 'stable history'. Verbesselt et al. (2012) provide a guideline of a stable history equal to or longer than two years for change monitoring with BFAST. Detailed descriptions of BFAST can be found in Verbesselt et al. (2010a).

4.3.3.2 BEAST

The Bayesian estimator of abrupt change, seasonal change, and trend (BEAST) is a recent algorithm that fits both linear and nonlinear trends and disentangles trends from seasonality; it further pinpoints abrupt shifts in the two isolated signals (Zhao et al., 2019). The model structure of BEAST applies a Bayesian ensemble modeling technique to aggregate numerous competing models to reduce uncertainty, overfitting, and model misspecification. From the numerous competing candidate models, BEAST evaluates how probable each of them is to be a true model and synthesises these into an average to capture multiple and subtle phenological changes (Zhao et al., 2019). BEAST algorithm uncovers complex nonlinear dynamics from time-series of any variables, such as LAI, climatic data, or soil moisture. To detect the rate of change in trends, BEAST infers the sign of the change (e.g., greening, or browning) as well as the associated error and probability of having a phenological shift, greening or browning at any time. Time series decomposition was performed using BFAST R package and RBEAST R package in R version 4.0.3 (R Development Core Team, 2013). Detailed descriptions of BEAST can be found in Zhao et al. (2019).

4.3.4 Land cover classification

Figure 4.2 presents a flow chart to classify land cover from Landsat data using Random Forest (RF) classifier. The less-cloudy, multiple-temporal Landsat images for the selected years (2004 and 2019), were collected and merged over the study area. This study used Quality Assurance bands and Function of Mask (Fmask) algorithm (Zhu and Woodcock, 2012) to mask out cloud and cloud shadows. The Quality Assurance (QA) band sets a cloud score threshold, and any pixel scoring higher than the threshold will be masked and merged with another image from the same area that doesn't have any clouds. Essentially, a cloud score greater than 0.2 for a pixel shows that the pixel is a cloud (Housman et al., 2018). The composite algorithm in Earth Engine library was also used to reduce the effect of the cloud (Lück and van Niekerk, 2016). In the end, all imagery used for land cover detection used in this study are free of clouds. Before land cover classification, a spatial clipping operation was performed on images to extract the exactly defined area of study sites within GEE.

Ground surveys to collect data on forests, open forests, agriculture, shrubs/grassland and other land cover classes were conducted in fieldwork in Namibia in 2019, see section 4.2.2 for details on fieldwork and sampling design. A total of 165 points were visited and collected from the field, and additional points of 498 points were randomly added. A total of 674 points were available for the land cover mapping. Half of the 674 points collected for training the classifiers (i.e., 'train' points on GEE), and the other half (341 points) were used for accuracy assessment. Additional ground truth data for land cover classification training and verification for 2004 was also collected through Landsat, Sentinel 2, high-resolution Google Earth, and Open Street Map using a visual interpretation. These sources were selected because they are freely accessible, consist of high-quality images, and this technique was also used by previous studies (Rwanga and Ndambuki, 2017). Based on local knowledge, this study categorised land cover into five groups, including forest, open forests/shrubs, agriculture/barren, water, and urban areas.

The classification of multi-temporal satellite imagery was performed on a per-pixel basis using RF classification (Li et al., 2017). The classifiers are trained with the spectral characteristics of these known areas, by assigning each pixel to the five target classes including forest, open forests/shrubs, agriculture/barren, water, and urban areas. RF is a popular method of classification and clustering based on an ensemble of decision trees (DT). RF was used because it overcomes problems of overfitting experience by other decision trees (DT) classifiers such as Classification and Regression Tree (CART) (Cánovas-García et al., 2017). RF is a development of the CART method by applying bagging and random feature selection to DT, which is to randomly select several trees that have many iterations so that they resemble forests (Breiman, 2001).

4.3.5 Accuracy assessment

Once the Land cover classification is completed, the final step is to conduct an accuracy assessment to quantitively assess the effectiveness of the method in correctly assigning the pixels to the proper land cover classes. Accuracy assessments are one of the most important steps of classification because it validates the output classification product as well as the quality of the data itself, by comparing the pixels of the classified image with ground truth data (Congalton et al., 1983). In this study, the full set of 165 training data visited and collected in the field and 498 added training data were divided into two subsamples, one used for algorithm training and the other used for error testing so that the same sample is never used for both training and testing (Geiß et al., 2017). For each classification accuracy assessment, this study used the popular measures extracted from confusion matrix reports, such as overall accuracy (OA), producer accuracy (PA) and user accuracy (UA) (Janssen and Vanderwel, 1994; Story and Congalton, 1986). An error matrix is generated by comparing the Land cover types calculated by the algorithm for a given pixel with the true Land cover class identified by the ground truth sample. The error matrix is a simple grid that lists the target classes and their respective number of correct and incorrect pixel classifications (Congalton et al., 1983). The uncertainty in estimated classification accuracy depends on the uncertainty in the true accuracy of the classifier, the number of samples and the accuracy of the observed ground truth (Carlotto, 2009). An overall classification error including kappa coefficient, commission and omission statistics were also calculated (Fung and LeDrew, 1988).

4.3.6 Validation of estimated forest changes and disturbance

The BFAST change detection was conducted to provide precise estimates of changed and unchanged forest areas. To evaluate the accuracy of the change map and validate the estimates of the predicted change for the whole study area, the study used 341 points in total, 165 points were visited and collected in the field and 176 points were randomly added as detailed in the above section. A change analysis using a stratified random sampling design was conducted to provide precise estimates of disturbances in the study area. Stratification was on patterns of past disturbances selected according to "the risk of disturbances". The communal areas that are unprotected were assigned “High risk”, the Zambezi State Forest that is semi-protected (red-coloured polygon) was assigned “Medium risk” and the Mudumu National Park (Aqua-coloured polygon) that is protected was assigned “Low risk” (see: Fig. 4.1). The accuracy of detected changes and unchanged estimates from BFAST was independently identified using various information sources including ground observation data collected from the field in 2019, land cover classification and image interpretation of high spatial resolution satellite imagery including Landsat, Google Earth images, and Sentinel 2. The study used the method of accuracy assessment as recommended by the GOFC-GOLD, 2014 guidelines to help identify and quantify uncertainty in the level and rate of disturbances in dryland forest areas (GOFC-GOLD, 2014). Watt et al. (2020) and Galiatsatos et al. (2020) utilised this method to develop monitoring, reporting and verification (MRV) systems to quantify and validate the accuracy of the change in forest cover carbon and carbon emissions in Guyana. This study adopted this method to validate the estimated changes because it allows the generation of detailed, consistent, transparent, and verifiable assessment of forest area change (GFOI, 2016).

4.4 Results

4.4.1 Spatial pattern of vegetation and drought stress in KAZA TFCA

To provide insights into the relationship between precipitation and disturbances, and the general vegetation dynamics response to drought, the spatial and temporal variations of the VIs (NDVI and GNDVI) anomaly for the growing seasons of 2002 to 2019 were plotted as shown in Fig. 4.4. The spatial pattern of both NDVI and GNDVI anomaly shows vegetation productivity increased (green to dark green colours; > 0.05) in 2006, 2008, and 2017 which correspond to higher than average rainfall in these years. Regionally, negative seasonal vegetation anomalies (NDVI and GNDVI) were mainly caused by large-scale droughts. The anomalies of precipitation in the JFM season (see: Fig. 4.4) remained negative over the entire KAZA region in 2002-2003, 2015-2016, and 2019 (red to dark red colours). The centre of the maximum rainfall deficit was mostly concentrated eastward of KAZA in 2016 and 2018. For vegetated land areas in KAZA, precipitation is a dominant factor controlling the growing season in the region, as indicated by the anomaly in vegetation and rainfall (see: Fig. 4.4). A close comparison indicates that the extreme droughts in 2015 and 2019 (red to dark red colours) greatly reduced vegetation productivity (brown colours in NDVI and GNDVI) which is coincident with severe water stress in these years. The lag in vegetation greenness between drought stress and browning rates extending to 2016, stands out based on the extent of severe decrease of greenness regardless of rainfall returning to normal.

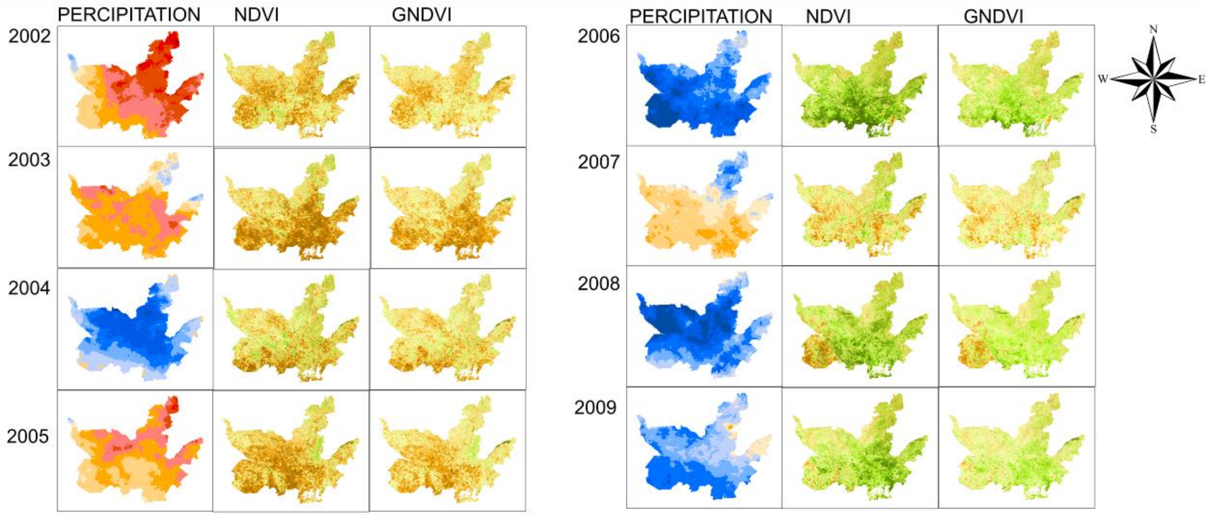

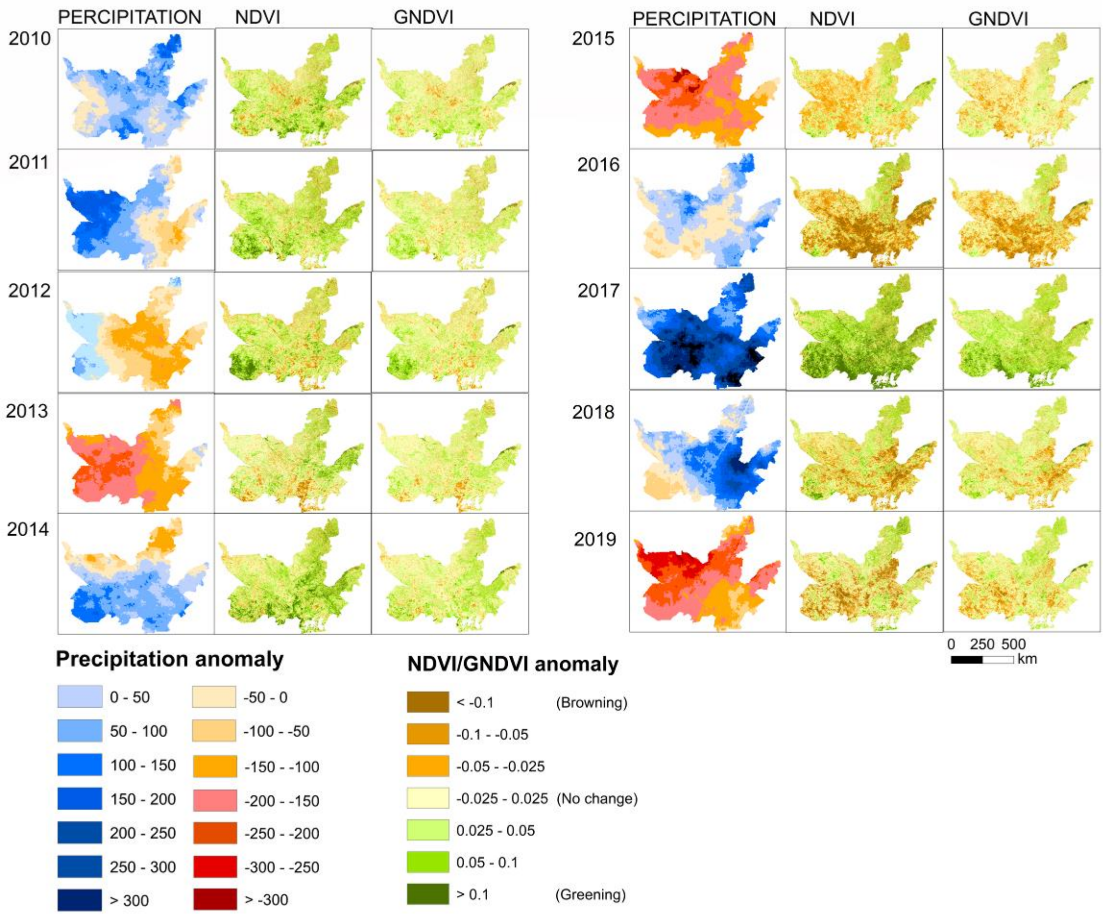

Fig. 4. 4. Spatial pattern of ndvi and gndvi and precipitation anomalies for the 21st century from 2010 through 2019.

4.4.2 Comparison of the sensitivity of BFAST and BEAST algorithms

The study examined and compared the effectiveness of two time-series decomposition algorithms (BFAST and BEAST) on three events to illustrate the proposed methodology, which included: 1. Clear-cut and burnt forest, 2. Drought impact and degradation forest, and 3. A stable, recovering forest. Table 4.2 shows the dates of detected trend and seasonal breakpoints identified using BFAST and BEAST algorithms for both NDVI and GNDVI time series.

Table 4. 2. Dates of trend and seasonal breakpoint detection relative to BFAST and BEAST algorithms. The Bold date represents the seasonal shift with the highest probability with a vertical dotted line.

Clear-cut and burnt forest			
		Trend change Date	*Seasonal change Date*
BFAST	*NDVI*	*2003, 2005, 2018*	*0*
	GNDVI	*2003, 2005, 2009, 2018*	*0*
BEAST	*NDVI*	*2003, 2005, 2007, 2017, 2018*	***2015-2017***
	GNDVI	*2003, 2005, 2006, 2007, 2009, 2017, 2018*	*2015-2017,* ***2019***
Degrading Forest			
BFAST	*NDVI*	*0*	*0*
	GNDVI	*2004, 2005, 2017*	*0*
BEAST	*NDVI*	*2004, 2005, 2015, 2017, 2019*	***2008-2009,*** *2012-2013*

	GNDVI	*2004, 2005, 2010, 2015, 2016, 2017, 2019*	*2008-2009,* ***2011-2013, 2018-2019***
A stable, recovering forest			
BFAST	*NDVI*	*0*	*0*
	GNDVI	*0*	*0*
BEAST	*NDVI*	*2017*	***2008,*** *2010-2011, 2015-2016*
	GNDVI	*2017*	***2006,*** *2008,* ***2015-2016***

4.4.2.1 Clearing of forest to non-forest

Fig. 4.5 and 6 show a forest stand plot that was forest initially, however the forest experienced a series of disturbances including a fire event around 2017 causing a sudden loss in forest cover, and a clear-cut activity that resulted in complete forest loss between 2018 and 2019. There were also major drought events that took place in 2002-2003, 2005, 2015 and 2019 (see: Fig. 4.4). Photos taken in February-May 2019 of each corresponding stand forest plot and Landsat time series images illustrating changes are shown in the supplementary information (see: Fig. B. 1 and B. 2).

4.4.2.1.1 BFAST algorithm application on a Clear-cut and burnt forest:

As shown in Fig 4.5, BFAST algorithm decomposed the NDVI time series and fitted seasonal, trend, and remainder components. BFAST algorithm applied on the NDVI time series detected three breakpoints in the trend component. BFAST predicted a disturbance around 2003 and 2005 because of severe drought in the region, which caused the forest to be stressed and the NDVI to decrease significantly. BFAST algorithm run on the NDVI time series also identified the occurrence of a breakpoint from clear-cut forest conversion to non-forest at the end of 2018. Around 2017 this location undergoes burning which triggered disturbance around the plot, however, BFAST failed to identify this trend in the NDVI trajectory. Furthermore, BFAST algorithm applied to the NDVI time series also failed to identify the disturbance in forest caused by a moderate drought event in 2007 and its recovery in 2009.

On the other hand, BFAST algorithm run on the GNDVI time series produced four breakpoints in the trend component: three breakpoints in 2003, 2005 as a result of severe drought and deforestation towards the end of 2018. Further, using the GNDVI time series, BFAST identified the abrupt changes caused by vegetation recovery in 2009 that are not identified by the NDVI time series trajectory as shown in Fig 4.5. Even though using GNDVI time series, BFAST identified the vegetation recovery in 2009, it also failed to identify the breakpoint caused by a moderate drought event in 2007. BFAST algorithm did not detect abrupt changes in the seasonal component of NDVI and GNDVI time series (Fig. 4.5).

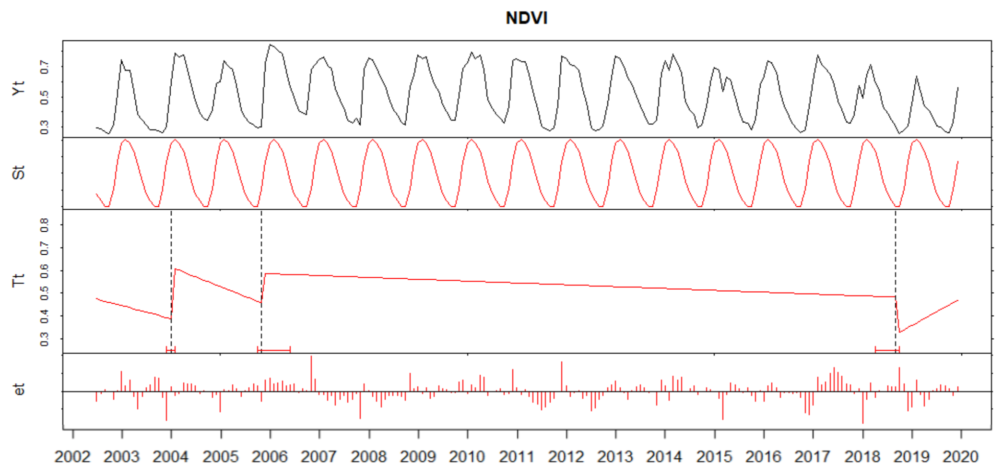

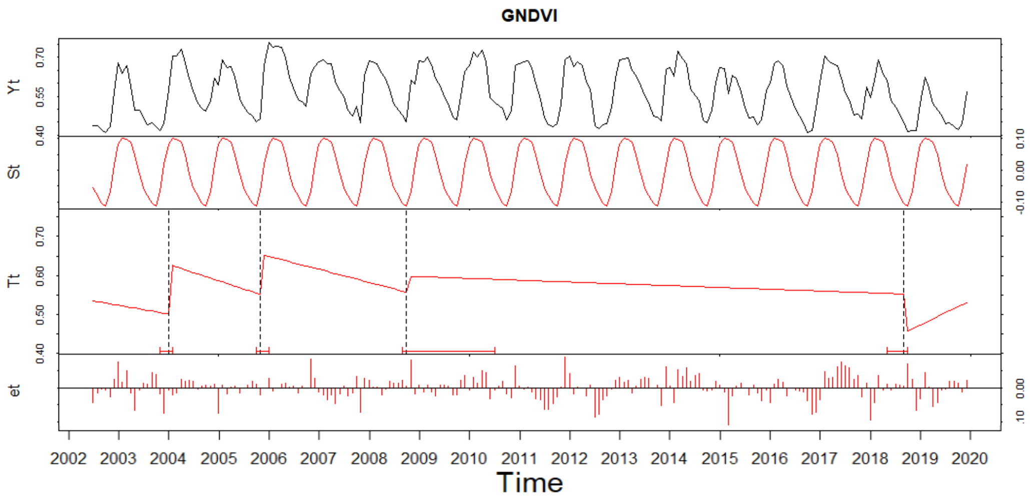

Fig. 4. 5. Example of the corresponding BFAST algorithm output for NDVI and GNDVI extracted from a forest stand that underwent conversion from clear-cut to non-forest vegetation. The vertical dotted lines represent the dates of detected breakpoints, while the red horizontal bars represent the associated confidential intervals. The raw time series (Yt), the seasonal component (St), the trend component (Tt), and the noise (et) component, are also shown. The location of the corresponding pixels, field photo taken in Namibia in 2019 and Landsat time series images illustrating changes are shown in the supplementary information (see: Fig. B. 1 and B. 2).

4.4.2.1.2 BEAST algorithm application on a Clear-cut and burnt forest:

Fig. 4.6 shows BEAST algorithm applied to the NDVI and GNDVI time series to detected phenological and trend changes. BEAST algorithm applied on the NDVI time series detected five breakpoints in the trend component. The four breakpoints including two breakpoints in 2003 and 2005 as a result of severe drought, one breakpoint in 2018 from deforestation and one abrupt change caused by 2009 moderate drought, similar to the changes identified by BFAST on the GNDVI time series in Fig. 4.5. However, the application of BEAST algorithm on the NDVI time series also detected one breakpoint in the trend component in 2017 as a result of vegetation increase (due to increase in rainfall in 2017) following the fire event in 2017 that neither application of BFAST was able to detect.

The application of BEAST algorithm to the GNDVI time series detected the occurrence of five breakpoints, two from drought in 2003 and 2005, the fire event of 2017, the forest clear-cut in 2018, and vegetation increase in 2017, similar to exploring the NDVI signal with BEAST algorithm. However, BEAST algorithm applied to the GNDVI time series was also able to uncover the beginning of vegetation disturbance and the vegetation recovery, for example it captures the correct year of the subtle decrease in forest cover in 2007 due to 2007 drought and its recovery in 2009. Similarly, it detects another decrease in forest cover due to drought in 2015 and its recovery in 2017 that was not detected using BEAST on NDVI time series. For both indices, BEAST algorithm detected phenological changes resulting from the 2015-2016 drought. BEAST applied to the GNDVI time series further detected a seasonal shift associated with 2019 logging and drought (see: Fig. 4.6). In contrast, BFAST algorithm uncovered a stable seasonal trajectory (see: Fig. 4.5), suggesting no phenological change during this period (2002-2019).

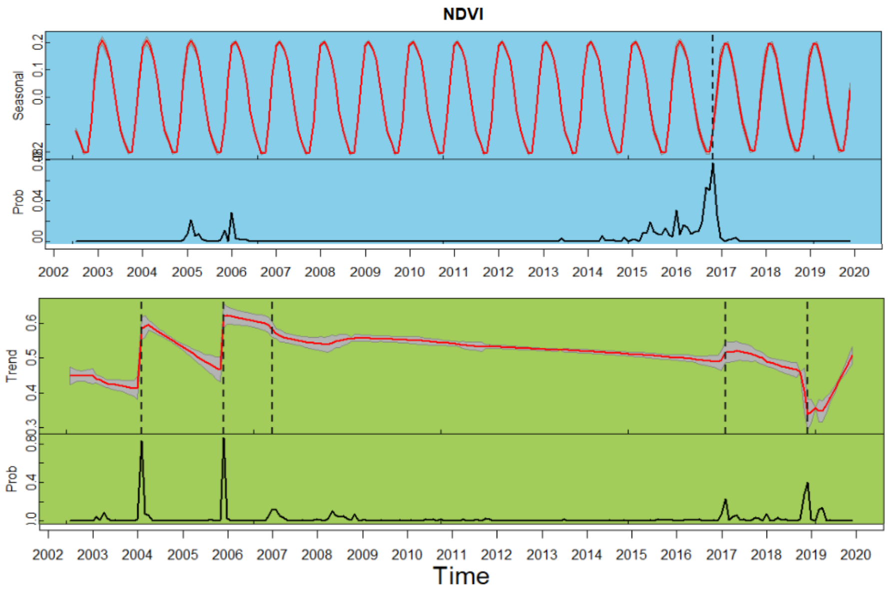

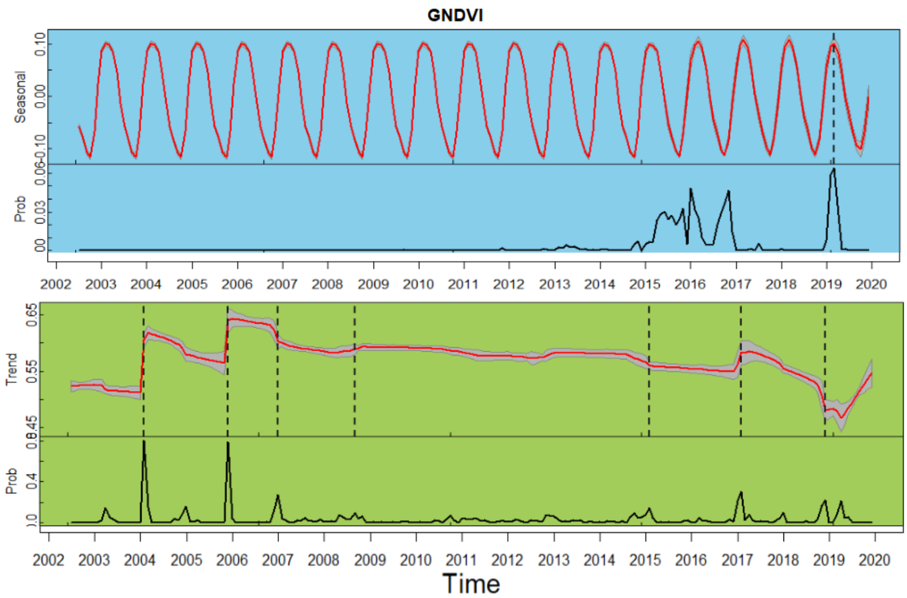

Fig. 4. 6. Example of the decomposition generated by the application of BEAST algorithm for the NDVI and GNDVI time series extracted from a forest stand that underwent conversion from clear-cut to non-forest vegetation. Seasonal and Trend represent the best fitted seasonal and trend signals (red line), respectively. The vertical dotted lines represent the dates of detected breakpoints in the trend/seasonal components, while the black lines at the bottom panels represent the probabilities of the changepoint in the seasonal/trend components. The location of the corresponding pixels, field photo taken in Namibia in 2019 and Landsat time series images illustrating changes are shown in the supplementary information (see: Fig. B. 1 and B. 2).

4.4.2.2 Drought impact and degraded forest

Fig. 4.7 and 8 show the results from modelling a forest stand plot that has undergone multiple disturbances from drought coupled with wildlife grazing and mega-herbivore pushovers, as a result of its location near to the Chobe river frontage. Photos taken in February-May 2019 of each corresponding stand forest plot and Landsat time series images, both illustrating changes are shown in the supplementary (see: Fig. B. 3 and B. 4).

4.4.2.2.1 BFAST algorithm application on a degraded forest:

Fig. 4.7 presents BFAST algorithm decomposition of the NDVI and GNDVI time series. BFAST was not able to capture any meaningful information relating to disturbances to the forest from the trend and seasonal components throughout the period of 2002 to 2019. None of the severe climatic events or moderate drought years were identified, and the NDVI trend appeared stable when using BFAST algorithm. This is despite the original time series showing some instances of an NDVI drop during this period.

However, using BFAST algorithm on the GNDVI time series, three breakpoints were detected in 2004, 2005 and 2017. The two abrupt changes in 2004 and 2006, correspond to the drought event in 2003 and 2005 (or to an increase in rainfall in 2004 and 2006 after the drought), were detected (see: Fig. 4.4 and 7). The breakpoint in 2017 represent a vegetation increase as a result of rainfall increase in 2017. BFAST did not detect abrupt changes in the seasonal component of NDVI and GNDVI time series as shown in Fig. 4.7.

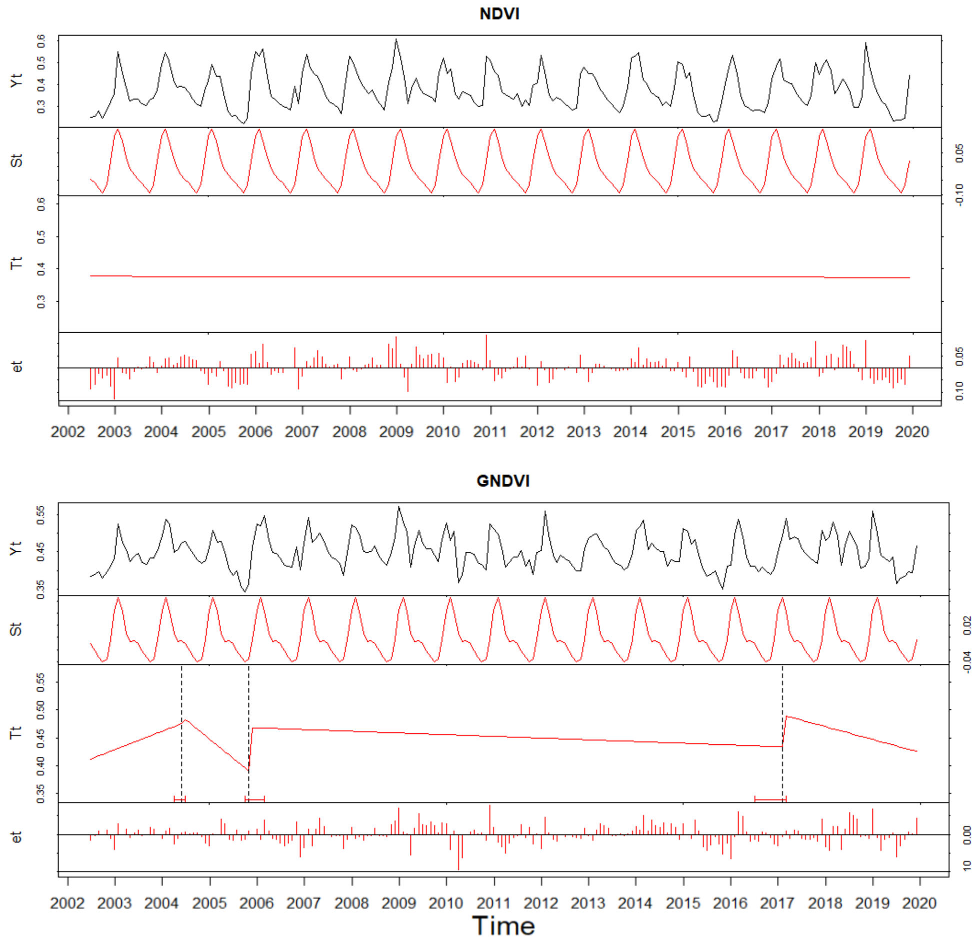

Fig. 4. 7. Example of the corresponding BFAST for NDVI and GNDVI extracted from a forest stand of a degraded forest. The vertical dotted lines represent the dates of detected breakpoints, while the red horizontal bars represent the associated confidential intervals. The raw time series (Yt), the seasonal component (St), the trend component (Tt), and the noise (et) component, are also shown. The location of the corresponding pixels, field photo taken in Botswana in 2019 and Landsat time series images illustrating changes are shown in the supplementary information (see: Fig. B. 3 and B. 4).

4.4.2.2.2 BEAST algorithm application on a degraded forest:

BEAST algorithm applied to the NDVI time series (Fig. 4.8) detected five breakpoints as a result of extreme effects of the 2005, 2015, 2019 droughts and the increase in rainfall in 2004, 2006, and 2017, which BFAST algorithm applied to the same time series did not detect, as shown in Fig. 4.7. The application of BEAST algorithm to the GNDVI time series was able to detect seven breakpoints, including the similar extreme droughts as shown with the NDVI, which were timed to similar dates. The increase in rainfall in 2008, and the drought stresses of 2010-2012, which both have a smaller magnitude of abrupt change, were also identifiable in the trend within the GNDVI, but not in the NDVI. BEAST algorithm was also able to describe the magnitude of drought impacts and recovery more clearly than when using BFAST. The drought impact detected by applying BEAST algorithm to the GNDVI time series in 2010, which is smaller in terms of the magnitude of the abrupt change, was not detected when using NDVI by either algorithm, as shown in Fig. 4.8. The Bayesian approach (BEAST) detected a phenological shift in 2008 when applied to the NDVI time series. Three seasonal shifts resulting from changes in precipitation in 2008, 2010, and the 2019 drought, were noticeable in BEAST-derived seasonal trend of the GNDVI time series as shown in Fig. 4.8.

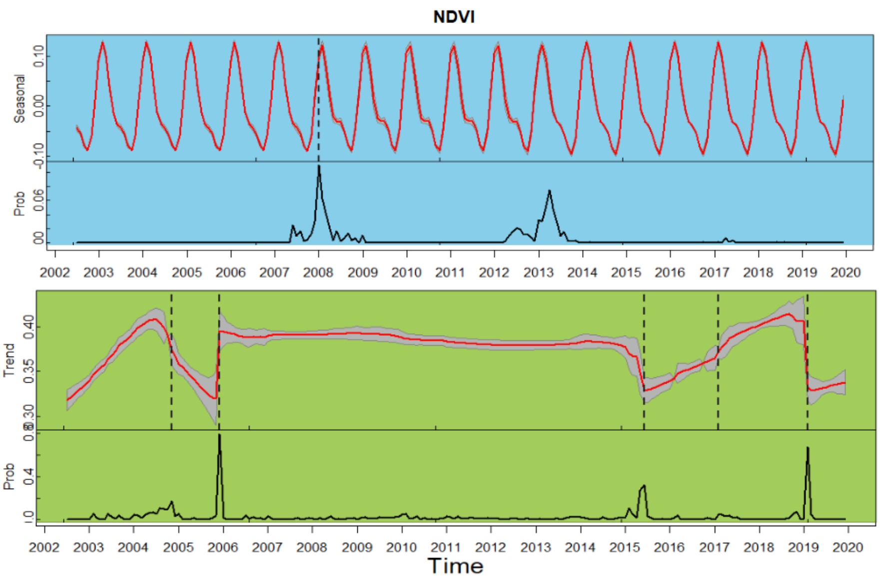

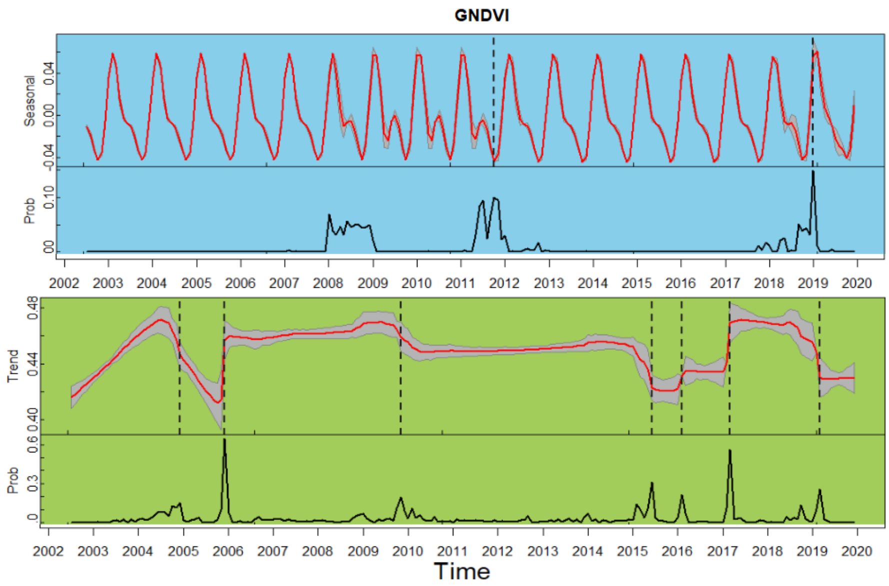

Fig. 4. 8. Example of the decomposition generated by the application of BEAST algorithm for the NDVI and GNDVI time series extracted from a forest stand of a degraded forest. Seasonal and Trend represent the best fitted seasonal and trend signals (red line), respectively. The vertical dotted lines represent the dates of detected breakpoints in the trend/seasonal components, while the black lines at the bottom panels represent the probabilities of the changepoint in the seasonal/trend components. The location of the corresponding pixels, field photo taken in Botswana in 2019 and Landsat time series images illustrating changes are shown in the supplementary information (see: Fig. B. 3 and B. 4).

4.4.2.3 Stable forest

Fig. 4.9 and 10 show the results from modelling a forest stand plot that has experienced limited human and wildlife disturbance and is considered to be stable. Photos taken in February-May 2019 of each corresponding stand forest plot and Landsat time series images, both illustrating changes are shown in the supplementary (see: Fig. B. 5 and B. 6).

4.4.2.3.1 BFAST algorithm application on a stable forest:

BFAST algorithm detected no breakpoints in trend and seasonality using both the NDVI and GNDVI time series. Both indices show a gradual increase in the forest cover. In both indices, the application of BFAST failed to detect any seasonal change.

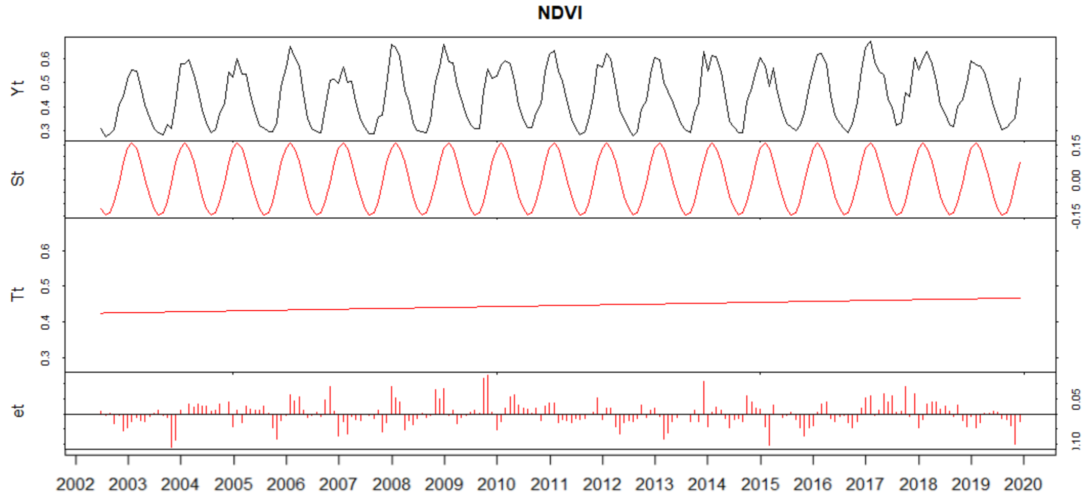

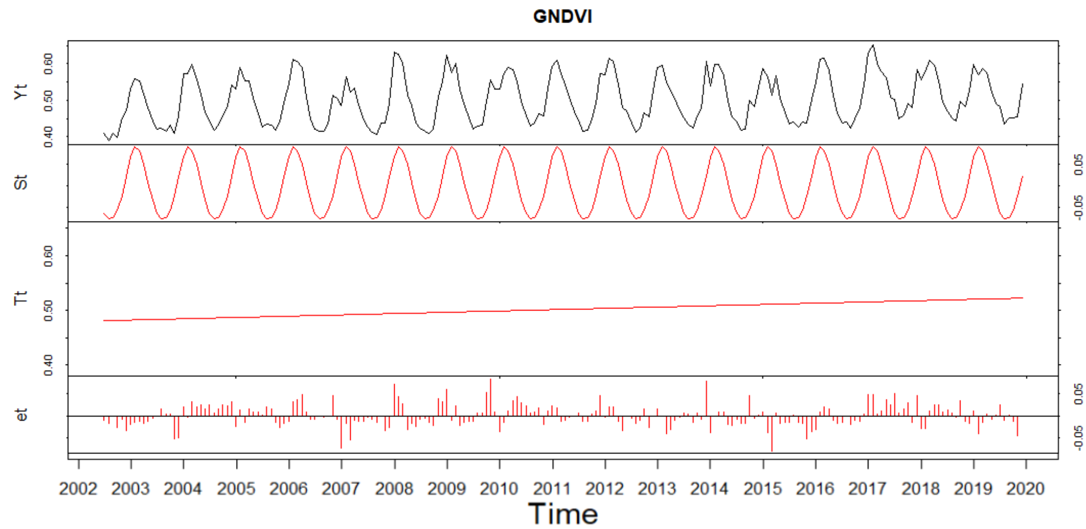

Fig. 4. 9. Example of the corresponding BFAST algorithm output for NDVI and GNDVI extracted from a forest stand that considered stable. The vertical dotted lines represent the dates of detected breakpoints, while the red horizontal bars represent the associated confidential intervals. The raw time series (Yt), the seasonal component (St), the trend component (Tt), and the noise (et) component, are also shown. The location of the corresponding pixels, field photo taken in Namibia in 2019 and Landsat time series images illustrating changes are shown in the supplementary information (see: Fig. B. 5 and 4. 6).

4.4.2.3.2 BEAST algorithm application on a stable forest:

BEAST algorithm showed a gradual increase in forest, and no abrupt trend as a result of a disturbance was identified in in either the NDVI or the GNDVI time series as shown in Fig. 4.10. One exception was an abrupt change as a result of forest cover increases was evident in 2017, as indicated by a high probability of this change in both indices, which was associated with plentiful rainfall in 2017. In terms of a seasonal signal, both indices show the phenological shifts around the 2008 and 2015-2016 drought events, although the GNDVI time series was able to detect a larger number of seasonal shifts. These seasonal changes are detected in severe drought years that were followed by an increase in rainfall. For example, the seasonal shift in the 2005 drought was followed by an increase in rainfall in 2006, and the seasonal shift in the 2015-2016 drought was followed by relatively high levels of precipitation in 2017, as shown in Fig. 4.4 and 4.10.

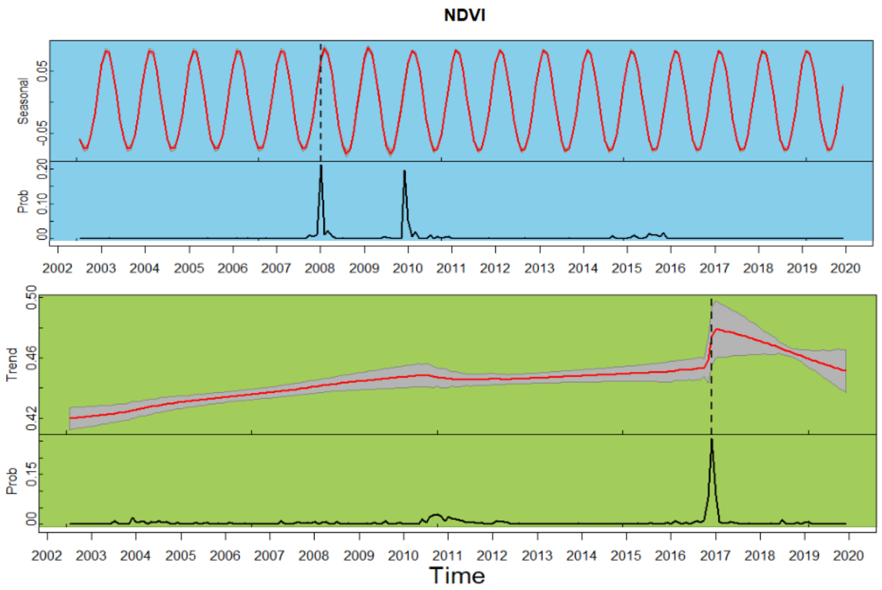

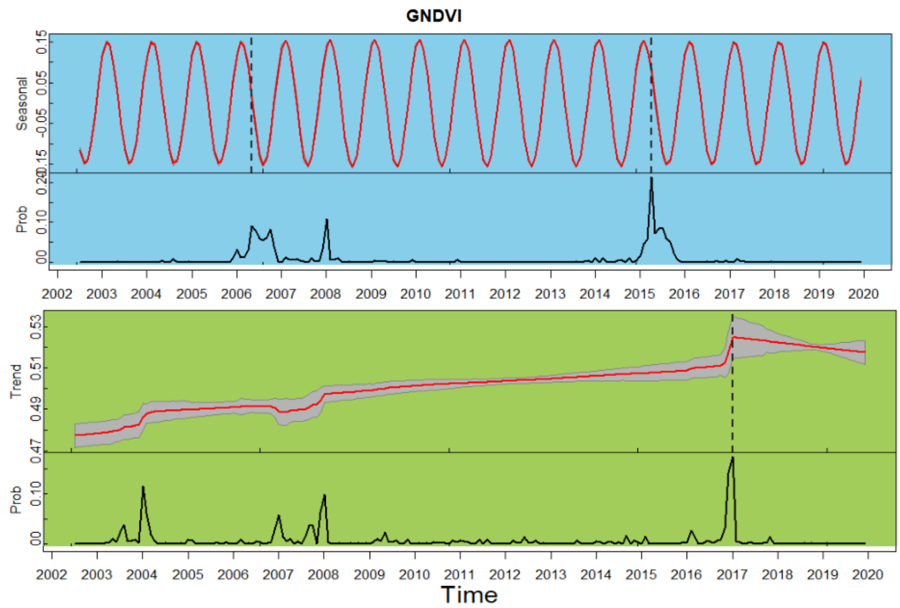

Fig. 4. 10. Example of the decomposition generated by the application of BEAST algorithm for the NDVI and GNDVI time series extracted from a forest stand that considered stable. Seasonal and Trend represent the best fitted seasonal and trend signals (red line), respectively. The vertical dotted lines represent the dates of detected breakpoints in the trend/seasonal components, while the black lines at the bottom panels represent the probabilities of the changepoint in the seasonal/trend components. The location of the corresponding pixels, field photo taken in Namibia in 2019 and Landsat time series images illustrating changes are shown in the supplementary information (see: Fig. B. 5 and B. 6).

4.4.3 Robustness of predicting forest dynamics using breakpoints and change magnitude

The examples shown in Fig. 4.11 demonstrate the differences in magnitude of GNDVI that were commonly observed to be associated with varying degrees of forest cover change. The cumulative probability of each of the change classes (deforestation, degradation, vegetation regrowth, or no-change) detected from the application of BFAST algorithm using the MODIS time series from 01/01/2010 to 31/12/2019 is shown in Fig. 4.11 and 12. The study only shows the breakpoints from 2010 to 2019 as these years help to highlight the impact of exceptional drought events (Fig. 4.4), fire, and large-scale forest clear-cutting events in the Mudumu NP and Zambezi ST, resulting in a negative breakpoint magnitude. Fig. 4.11A presents 2002 Landsat 5 (LC5) ETM, 2019 Landsat 8 (LC8) OLI images, and the cumulative change map overlaid with field points collected with land cover and vegetation measurement (black-coloured circles) mapped in Zambezi ST. The results of the survey plot (black circle coloured blue) shown with an arrow are represented in Figure 4. 11 A-C. Figure 4. 11A shows the Landsat image in 2002 and 2019 with the survey plot undisturbed (forest) in 2002, and when it is turned into a non-forest in 2019. A cumulative change map of MODIS produced with BFAST in Figure 4. 11 A shows the negative break of the same survey plot. Similarly, figure 4. 11 B shows the time series of the forest pixel with a negative break detected in April 2015, while Figure 4. 11 C represents the actual photograph of the survey plot with cut-down trees on the ground. This approach used prior knowledge of disturbances such as clearing, and BFAST allowed the most significant change event in the time series to be detected. Prior knowledge of disturbances such as clearing was used in this approach and BFAST allowed the most significant change event in the time-series to be detected. For mapping cumulative change, the probability of the deforestation class increased with decreasing change magnitude, showing a strong negative relationship with change magnitude, whilst the probability of the degradation class showed a weak negative relationship with change magnitude. The probability of vegetation growth class increased with increasing change magnitude, showing a positive relationship with change magnitude.

Maps showing the time of the changepoint event and the magnitude of the GNDVI change are displayed in Fig. 4.11 and 12. Fig. 4.11A shows the negative breakpoint with high mean negative magnitude of change due to forest logging and clear-cutting to almost no vegetation between 2018 and 2019 as shown by the top circle. Other breakpoints with high mean negative magnitude due to forest clearing for agriculture and urban areas are also observed and shown with the two bottom circles. The breakpoint with positive mean magnitude is observed in a square showing an agricultural area (farmland) that was abandoned and vegetation regrowth gradually increased by 2019 (Fig. 4.11A). As shown by the plot shown by the black arrow (see: Fig. 4.11A), the negative break in the forest pixel is detected in April 2015 and is associated with extreme drought, as shown by the red vertical line in the GNDVI time series in Fig. 4.11B. Another disturbance in the forest stand plot caused a large reduction in GNDVI in 2019 as a result of forest clear-cutting for timber, as also illustrated in the change map (Fig. 4.11A), the time series (Fig. 4.11B), and the field photo taken in 2019 (Fig. 4.11C).

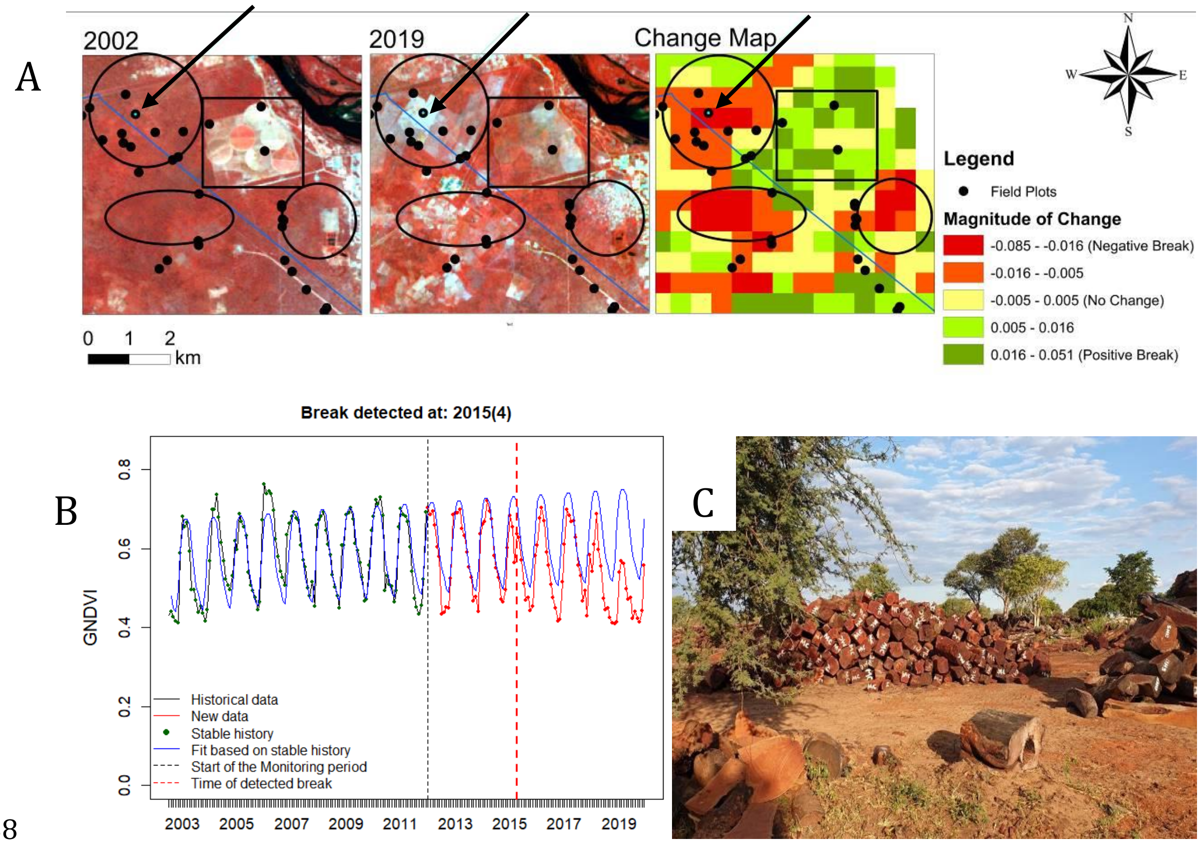

Fig. 4. 11. A: 2002 LC5 ETM, 2019 LC8 OLI image and a map of the magnitude of change in the trend component from 01/01/2010 to 01/12/2019 generated by BFAST algorithm in and around the Zambezi ST and Mudumu NP; the colour scale represents the magnitude and direction of change. The circles here represent abrupt changes with a negative magnitude; a square represents a vegetation regrowth with a positive magnitude, and the arrow shows a forest stand plot for a forest disturbed by drought and subsequent forest canopy clearing. Fig.4.11. B: MODIS time series from 01/01/2002 to 31/12/2019 for a plot shown by an arrow in Fig. 4.11. A. Fig. 4.11. C: Shows the photograph of the selected plot (location coordinate is 17.49°S, 24.21°E) in Fig. 4.11. A, with logged for timbers photographed during a field campaign in Zambezi ST near the border of Namibia and Zambia in 2019.

4.4.4 Spatial pattern of predicted forest changes using breakpoints and magnitude

Fig. 4.12 presents the spatial pattern of the extracted trend classification, showing the predicted magnitude of change in the trend component and the estimated date of change generated from BFAST algorithm applied to the GNDVI time series on the

Zambezi region, Namibia. The final disturbance map showing disturbed versus undisturbed areas highlights distinct spatial patterns across the study area. Fig. 4.12A shows the predicted abrupt change in the trend component. It can be seen that the Mudumu NP remains undisturbed, although there are distinct spatial patterns of forest degradation indicated by low magnitude negative breakpoints at the edge of the park, around the communal villages in Sobbe conservancy. Examining the disturbance map, forest decline from clear-cutting and forest conversion to agricultural land were observed in Zambezi ST and in the community conservancy and communal area surrounding the Zambezi SF and Mudumu NP. The disturbance trends and extreme vegetation loss from deforestation and clear-cuts are shown by extreme magnitude negative breaks and vegetation degradation (Fig. 4.12A). Although most of the clear-cuts are associated with an extreme magnitude negative breakpoint, some cases are associated with a low magnitude negative/positive breakpoint. This is shown, for example, in areas with forest clear-cuts replaced by matured shrubs in the northernmost section of the study area (Zambezi ST) near the border between Namibia and Zambia.

The map also shows continuous patches of forest showing a positive magnitude breakpoint, which denotes a forest recovery, vegetation regrowth that follows an earlier event, and vegetation less affected by disturbance as shown by positive magnitude of change in Fig. 12 A. More than 50% of the breakpoint dates are in the period between 2016 and 2019, with 2018 having the highest number of breakpoints. The high percentage of breakpoints detected in this period, and a negative magnitude, reflect both the impact of the 2015/2016 and 2018/2019 droughts, coupled with clear-cutting of the forest stands.

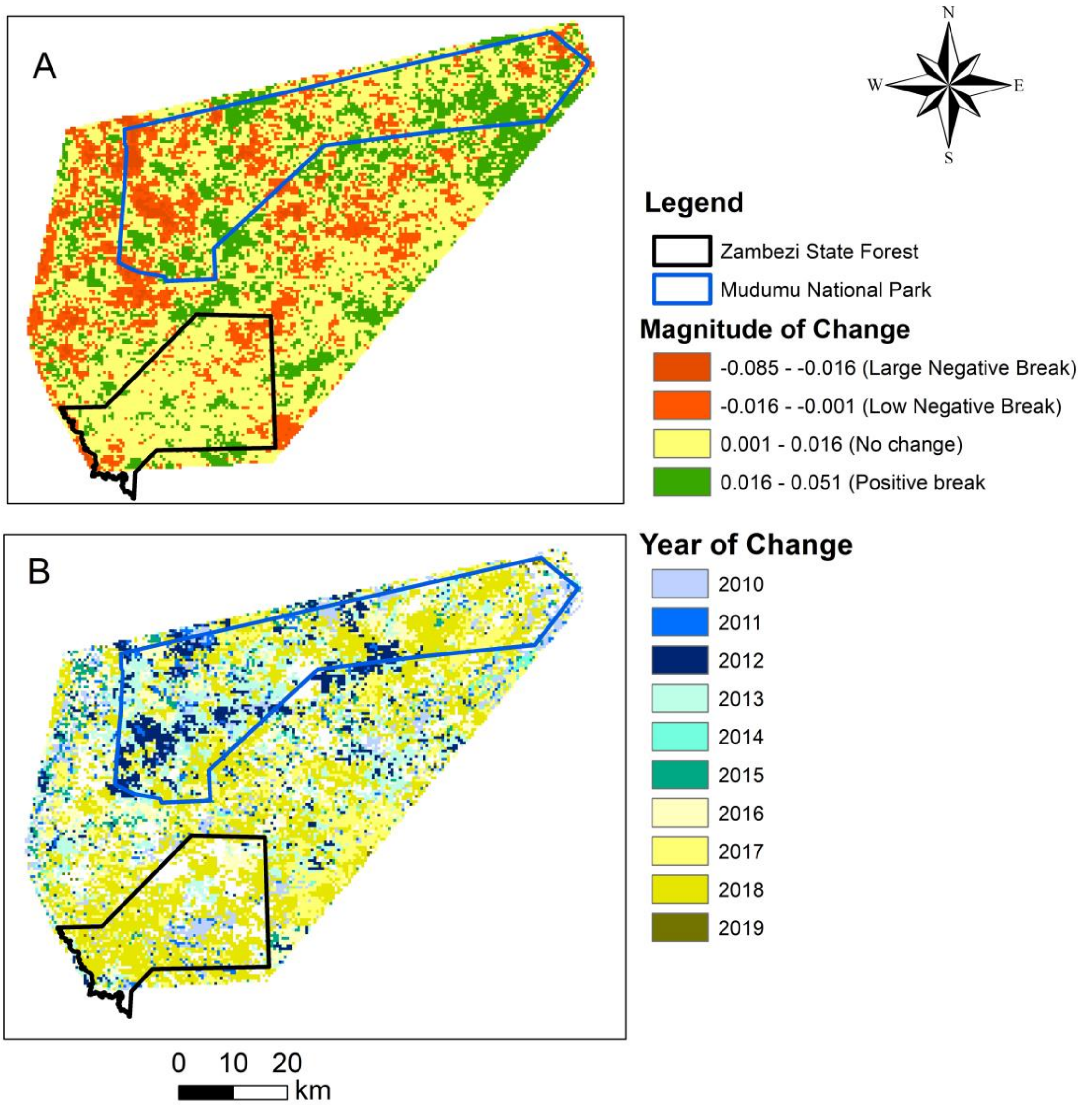

Fig. 4. 12. A. shows the magnitude of change in the trend component and the predicted time of change generated by BFAST; red colour represents negative breakpoint typically associated with vegetation loss. Green colour represents positive breakpoint associated with vegetation gain. The turquoise polygon shows Zambezi ST, and the black polygon shows Mudumu NP. B: shows the estimated year of change from 2010 to 2019.

4.4.5 Validation of spatial pattern of predicted forest changes and disturbances

The BFAST model was used to estimate forest disturbance for the complete study area (Fig. 4.12). The validation assessment used a weighted average of the within-stratum estimates to ensure the weights are proportional to size of high, medium and low 'risk of change' strata. The results of the comparable land cover classes for the BFAST time series analysis and the interval-based per-pixel Random Forest classification are shown in Tables 4.3 and 4.4. The complete tables with all the area change classes for the two approaches are in the supplementary material (Tables B.2, B.3 and B.4). The land cover classes for the interval-based per pixel classification in Table B.3 were calculated based on post-classification reorganisation of land cover area transition table (Table B. 4), where the similarly classified class areas were summed together.

The results are presented in Table 4.4 and both methods show a land transition from forest to non-forest (deforestation) in the region. The interval-based per-pixel classification estimated that the conversion of forest to non-forest land was 87,251 ha. The BFAST time series estimates of deforestation are corresponding to the two-interval pixel-based classification showing an area change of 99,911 ha (SE 9,753 ha) throughout the entire 2002–2019 period. The two-interval classification estimated that the total unchanged forest area was 147,875 ha. These values are higher as compared to 106,390 ha of unchanged forest land estimated by BFAST time series analysis. The interval-based pixel-based classification which bases the change estimates on differencing between images at only two points in time has little capability to distinguish forest degradation, which is the progressive reduction/losses in forest cover that do not qualify as deforestation. As a result, it is likely that the interval-based classification does not detect forest degradation as well as BFAST (time series) approach. The BFAST time series analysis captures the subtle change of forest conversion to the degraded forest with an estimate of 33,131 ha (SE 6,859 ha). In addition, BFAST time series analysis found that approximately 23,409 ha (SE 556,8 ha) of degraded forest was converted to forest land. However, the degraded forest estimates from the BFAST time series are not comparable with the two-based interval per pixel classification because it does not detect degradation (see: Table 4.4). The BFAST algorithm can iteratively estimate and characterize temporal changes (time) and characterizes the spatial change by its magnitude and direction ("deforestation", "degradation" and "no change"). The sample-based estimates and validation of BFAST used in this study also provide the standard error for the continuous changes. For this study, the standard error for the non-disturbed forest class was lower as compared to the disturbed classes (see: Table 4. 3). It is also important to note that the region has no Landsat images available in 2002, and few images for the year 2003, therefore the two-interval classification used the starting year of 2004, which can account for some difference in land cover class areas. In summary, BFAST (time series) approach at one level agrees with a two-interval traditional classification when identifying discrete change but it also identifies areas of more subtle change and so adds value to the analysis and interpretation. In broad terms, the two approaches agree where direct comparison is possible, but the differences also help to stimulate important questions about the differences.

Table 4. 3. Area changes of BFAST using sample-based estimates and the observed disturbance change rates.

Change identified by BFAST	**Area Hectares (ha)**	**Standard Error (ha)**	**2.5 % (ha)**	**97.5 % (ha)**
Non-disturbance (no change) *(Stable Forest)*	106,390	9,817	87,148	125,631
Non-disturbance -low negative change *(Stable forest to Degradation)*	33,132	6,859	19,688	46,576
Non-disturbance -large negative change *(Stable Forest to Deforestation)*	99,911	9,753	80,795	119,027
Low negative break -large negative change *(Degradation to Deforestation)*	59,515	8,154	43,533	75,497
Low negative changes -non-disturbance	23,409	556,8	12,497	34,322

(Degradation to Stable Forest)				

Table 4. 4. Types of changes identified by BFAST and Random Forest classification for the period 2004 and 2019.

Type of Changes	**Two interval Classification 2004 and 2019 Area(ha)**	**BFAST Time Series analysis 2002 to 2019 Area (ha)**
Forest	147,875	106,390
Forest to Non-forest	87,251	99,911
Forest to Degraded Forest	-	59,515
Degraded Forest to Forest	-	33,131
Degraded Forest to Non-forest	-	23,409
Non-forest-Forest	41,447	54,517

4.4.6 Land cover classification

The land cover classifications using the RF algorithm, in 2004 and 2019, are illustrated in Fig. 4.13. To quantify the land use changes over the years, the study analysed the error matrix which showed any classification errors that may have occurred such as a pixel being misclassified. Table 4.6 presents the confusion matrix and accuracy assessment for land cover classification in the years 2004 and 2019. For classification accuracy, Landis and Koch et al (1977) suggested the Kappa result with values ≤ 0 indicate no agreement and 0.01–0.20 denote none to slight, 0.21–0.40 fair, 0.41– 0.60 moderate, 0.61–0.80 indicate substantial, and 0.81–1.00 as almost perfect agreement (Sim and Wrigh, 2005). The accuracy assessment on the 2004 and 2019 classified images showed an overall classification accuracy of 82% and 88%, and an overall Kappa Statistic of 0.74 and 0.83, respectively. The classification results and Kappa statistics obtained in this study show a very good agreement between classes which is considered sufficient for the land cover map in the Zambezi region. The five classes that were used (forest, open forests/shrubs, agriculture/barren, water, and urban areas) resulted in 100% accuracy for the water and urban areas, and 90% for agriculture. However, accuracy was somewhat lower in the other two classes of forest and open forest/shrubs areas, with 82% and 76% accuracy, respectively (Table 4.6). The reason for the high accuracy of water was due to the small area comprised of water and urban areas. The two classes had a low number of training sample pixels because the training points were distributed proportionally to the study area. The classification for forests, open forest/shrubs and agriculture/barren exhibited low scores in both user accuracy and producer accuracy. The reason for the low accuracy of open forests/Shrubs was due to this class being often mixed with forests and agriculture/barren in this study, reducing a large percentage of accuracy (more than 20% reduction).

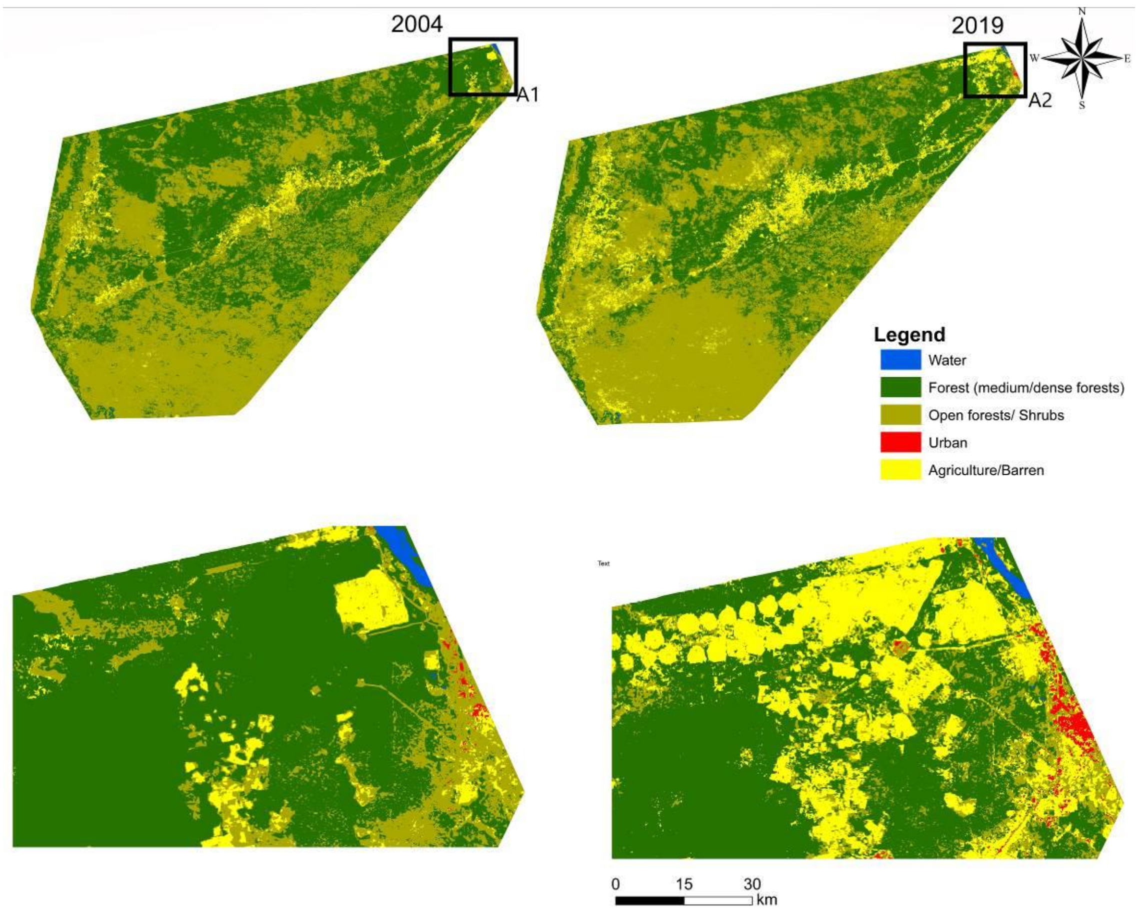

Fig. 4. 13. Land cover classification in 2004 and 2019; panel A1 and A2 are zoom in of land cover in 2004 and 2019.

Table 4. 5. Confusion matrix of land cover classification in 2004 and 2019 using Random Forest.

Specification	**Ground Truth**								
	Class Name	**Water**	**Forest**	**Open Forests/ Shrubs**	**Urban**	**Agriculture**	**Total**	**User's Accuracy**	**Error of commission (%)**
Classified Map	**2004**								
	Water	21	0	0	0	0	21	1	0
	Forest	3	111	20	0	2	154	0.82	0.16
	Open Forests/ Shrubs	1	23	101	2	6	133	0.76	0.24
	Urban	0	0	0	22	0	22	1	0
	Agriculture	0	0	1	2	26	29	0.90	0.1
	Total	25	134	122	26	34	341		
	Producer's Accuracy	0.84	0.83	0.83	0.85	0.76	**Overall Accuracy**	0.82	
	Error of omission (%)	0.16	0.17	0.17	0.15	0.24	**Kappa coefficient**	0.74	
2019									
Classified Map	**Water**	27	0	0	0	0	27	1	0
	Forest	0	40	10	0	1	51	0.78	0.21
	Open Forests/ Shrubs	0	8	109	0	9	126	0.87	0.13
	Urban	0	0	2	24	0	26	0.92	0.07

	Agriculture	0	1	9	0	101	111	0.91	0.09
	Total	27	49	130	24	111	341		
	Producer's Accuracy	1	0.82	0.84	1	0.91	**Overall Accuracy**	0.88	
	Error of omission (%)	0	0.18	0.16	0	0.09	**Kappa coefficient**	0.83	

4.4.7 Land cover change detection

The land cover change map conversion from 2004 to 2019, is illustrated in Fig. 4.14. In general, open forest/shrubs were the dominant land cover type followed by forests in both years. In the northeast of the Zambezi State Forests, there was a significant change as forested areas were replaced by barren/agricultural land as a result of forest logging. A closer inspection of the classified maps revealed that most of the agricultural expansion occurs primarily around the communal areas in the northern part of the study area, in comparison to the southern part where protected areas such as Mudumu National Park are found. The conversion from forests to open forest/shrubs was significant with 76345.98 ha (15%) and occurred mainly in the Mudumu National Park in the Southern part and Zambezi State Forest in the northern part of the region. Table B 1 presents the land cover change matrix between 2004 and 2019. Three major changes were an increase in open forests/shrubs and agricultural/barren land and a reduction in forest land. In 2004, agricultural/barren land accounted for only 2.8% (143,77.87 ha) of total land. In 2019, this figure increased to 8.47% (429,36.31 ha) (see: Table B 1). On the contrary, forest land experienced a significant decline of 9.04%, from 46.41% (235,140.91 ha) to 37.37% (189,334.60 ha) of the total area in 2004 and 2019, respectively (see: Table B 1). The forest loss mainly was due to conversion to open forest/shrub (76,345.9), followed by agricultural/barren land (10,634.1 ha) (see Fig. 4.14). At the same time, other land uses are also converted to forest. For example, 40,172.9 ha of open forests/shrubs was converted to forest, followed by agricultural/barren land (236,77.1 ha) (see Fig. 4.14).

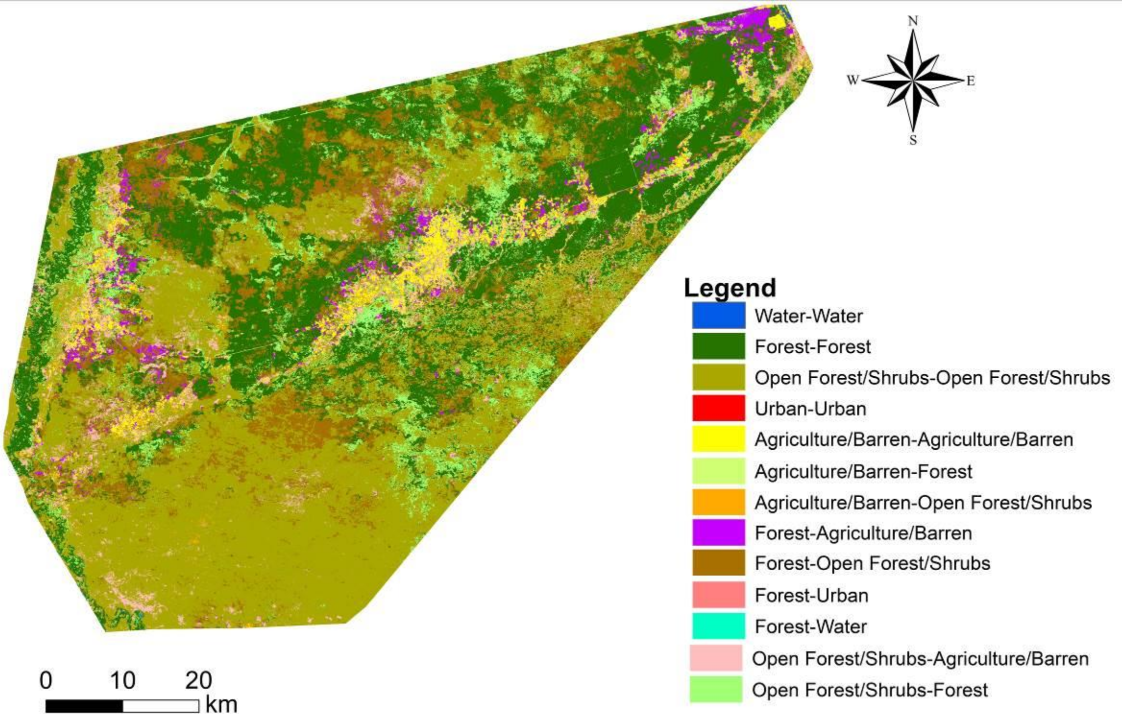

Fig. 4. 14. Changed areas for the epoch (2004–2019) in the study area

4.5 Discussion

4.5.1 Effectiveness of BFAST and BEAST algorithms for characterising change in dryland forests

4.5.1.1 Trend

Despite BFAST and BEAST algorithms being able to handle unfiltered data, the study found in the preliminary testing phase of the analysis that the use of filtered MODIS time series yields accurate results and improved forest change detection, as compared to the unfiltered data (see supplementary: A1). Identified changes that occur in the trend component indicate both gradual and abrupt changes in land cover, while changes occurring in the seasonal component indicate phenological variation. In terms of deforestation, BFAST and BEAST algorithms identify a consensus in time of breakpoints of larger magnitude, such as those associated with clear-cutting of the forest to non-forest. This agreement shows that both algorithms can be used to detect large-scale disturbances in the dryland forest. In terms of drought, BEAST algorithm was found to be the most successful in identifying abrupt changes from vegetation disturbance caused by drought. BFAST algorithm performed well in detecting abrupt changes of some known large magnitude drought events, however, BFAST did not identify abrupt changes in forest response for most drought and fire events, especially the lower magnitude of change. A study by Watts et al. (2014) reported that BFAST did not detect abrupt changes in vegetation as a result of well-known flood events. In this study, the advantage of BEAST was the capability to detect the impact of exceptional climatic conditions in both high and low magnitude drought years of 2002/03, 2005, 2010/11, 2015/16, and 2019 on forest stand development. Conversely, BFAST algorithm was not able to detect such abrupt changes, as was seen in an example of a fire event in 2017 that resulted in a known disturbance within the forest plot. In this study, when using BFAST, sometimes 'minor changes', such as beginning or end of periods of disturbance and recovery are not included in the identified trend, and these breakpoints are often (incorrectly) counted as false positives. With such limitations in the performance of BFAST algorithm, disturbance or drought events can therefore be easily missed. A similar problem was found in a study by Wu et al. (2020), where BFAST algorithm was applied to an NDVI time series to detect changes within forest areas in China. They found that BFAST algorithm failed to detect slow urban expansion which resulted in a partial forest cut within the pixel, until the whole area of the pixel was changed.

By comparing MODIS vegetation indices in detecting disturbance and trends in dryland forests, GNDVI outperformed NDVI in both algorithms. Particularly, BEAST algorithm generated change model using the GNDVI time series performed better overall. Both NDVI and GNDVI predicted large-scale clear-cut deforestation events accurately. However, GNDVI was more sensitive to detecting the abrupt changes due to droughts, fire, and small-scale disturbances. The analysis of the NDVI time series sometimes failed to detect abrupt changes in areas that did not undergo complete land cover class changes. The sensitivity of NDVI to background variations in the canopy and herbaceous layers could explain why the use of NDVI failed to detect disturbances and drought impacts in these areas (Huete et al., 2002). For stable or recovered forests, BFAST and BEAST algorithms performed similarly in detecting gradual changes using NDVI and GNDVI time series. The similarity in the performance of the two indices can be attributed to the fact that the study area is covered in trees and less of herbaceous layer (see supplementary: D1 and D2 for field photo and LC8 time series images). The gradual increase in forest cover of the stable forest can be a result of limited disturbance from fire, wildlife, and logging. This suggests that the dryland forest can quickly recover from drought in areas where multiple disturbances have not been experienced.

4.5.1.2 Phenology

In this research study area, the dryland forests have a very pronounced seasonality controlled mainly by humidity, with a rapid response to the onset of the rainy season, reflected in the abrupt changes in NDVI and GNDVI responses. The interannual variation in precipitation caused the change detection algorithms to flag breakpoints related to dryland forest phenology (Grogan et al., 2016, Zhao et al., 2019). BEAST algorithm detected phenological changes resulting from drought years followed a large increase in precipitation and clear-cut deforestation in NDVI and GNDVI time series (Table 4.2). BFAST also failed to detect any seasonal change using both NDVI and GNDVI time series. The ability of BFAST algorithm to capture seasonal changes triggered by interannual variations or disturbances in the dryland biomes is limited. Studies that tested BFAST algorithm on different forest types also reported poor performance in detecting seasonal changes. This included limitations in identifying changes in the amplitude of the seasonal curve, or changes in the number of seasons in which tropical dryland forests were characterised by high inter-annual seasonal variability (Gao et al., 2021, Grogan et al., 2016).

The difference in the performance of the algorithms tested here can be attributed to the fact that BEAST incorporates non-linear change models (Burkett et al., 2005). BEAST not only detects the changepoints, but also quantifies their probability of being true, providing a confidence measure to interpret the changes in both trend and seasonality. A shortcoming of BFAST algorithm is that by relying on linear segments to describe underlying fluctuating trends, the model assumes vegetation trends are quasi-linear processes (i.e., regular, or stable seasonality) (Grogan et al., 2016). Deterministic models used within BFAST algorithm often do not therefore capture nonlinear behaviour as thresholds and complex interactions among ecosystem processes are unaccounted for (Burkett et al., 2005). For example, Jamali et al. (2014) accounted for non-linear vegetation changes in the Sahel using a polynomials fitting-based scheme to an annual NDVI time series and found it to describe general non-linear change trajectories. It has been widely observed that vegetation dynamics and land cover change can often occur in a non-linear pattern (Lambin et al., 1997). Additionally, climatic variations and change in moisture regimes, such as short- or long-term changes in rainfall patterns or temperature, may also drive nonlinear progressions in vegetation cover (Foley et al., 2003).

These results demonstrate that accounting for variations at the seasonal scale while simultaneously uncovering complex nonlinear trends in forest dynamics is important, particularly for dryland forests where seasonality may vary significantly in amplitude from year to year. Projected rapid climate change is of major concern in these regions, especially when viewed with other population stresses such as habitat conversion, the impacts of fire, and herbivores disturbances. In KAZA, it is reported that competition between wild species occurs when habitats become degraded, especially by elephants (FAO, 2009). These synergistic stresses are likely to prove to be the greatest challenge to wildlife conservation in the 21st century, hence tracking the occurrence of disturbance events and phenological shift events as they occur is an essential task in PAs conservation efforts.

4.5.2 Spectral index sensitivity in dryland forests

The study found that BFAST and BEAST change models using the GNDVI time series performed better than the more commonly used NDVI. Comparing results from NDVI and GNDVI and related these to the precipitation anomaly shows that the maximum differences in vegetation index performance occurred over the dryland forest relative to the grassland, and then shrubs. There is a general agreement between indices in areas undergoing browning and greening in the non-forested area (see: Fig. 4.4). GNDVI had the best performance in distinguishing browning and greening of forest from herbaceous layers affected by droughts. For example, analysis of the NDVI was able to detect a strong greening in forest areas in the severe droughts of 2015-2016 and 2019. These results are similar to a study by Loranty et al., (2018) that found positive decadal trends in NDVI in Siberian forests that ranged from sparse to dense canopy cover, which correspond to increases in understory productivity rather than an increase in forest cover. This study results also concur with the study by Otsu et al. (2019) that found that GNDVI performed best in distinguishing broad leaf from needle leaf forests as compared to NDVI. Another study by Yoder et al. (1994) used the green channel in a vegetation index and found that it had a better correlation with the photosynthetic activity of the tree canopy in miniature Douglas-fir trees as compared to the red channel. The main reason for the difference in the performance of NDVI and GNDVI is likely because the former is more sensitive to low chlorophyll concentrations, while GNDVI is more sensitive to high chlorophyll concentrations and so is more accurate for assessing chlorophyll content at the tree crown level (Gitelson et al., 1996). A study by Grogan et al., (2016) tested BFAST on Land Surface Water Index (LSWI) and used NDVI on dry-deciduous and evergreen forests and found that the LSWI time series outperformed the more commonly used NDVI and EVI indices.

In conjunction with observations from the field, these results indicate that understory vegetation likely exerts a strong influence on NDVI. It has been shown in other research that different plant functional types, including canopy background variations and herbaceous vegetation, also have a pronounced seasonal effect on the NDVI signal, while also not being directly correlated with woody cover (Grogan et al., 2016, Prince, 1991). This is apparent in my observations and suggests that the NDVI pattern of a higher-than-average anomaly during the growing season of 2015 and 2019 may correspond primarily to increases in understory productivity rather than an increase in forest cover. For this study, a possible explanation for this is that tropical vegetation greenness can recover rapidly soon after forest clearing as the low herbaceous cover such as grassland and saplings grow vigorously due to increased light levels, resulting in reduced sensitivities to detect disturbances in greenness-based indices such as NDVI. The use of VIs for biophysical parameter retrievals is therefore a challenging task and there remains much work in understanding VI sensitivity across and within dryland biomes (Huete et al., 2002). Ground field validation test sites are essential in this regard and help provide valuable insight in interpreting spatial and temporal variability in VI that arises from vegetation-related properties, including LAI, canopy structure, and understory vegetation. Hence, both soil characteristics and the reflectance of lower plant communities may lead to misinterpretations of the open dry forest dynamics and an under or overestimation of ecosystem productivity in similar semiarid environments.

4.5.3 Land cover classification and spatial pattern of forest changes using breakpoints and magnitude

This study applied remote sensing techniques to classify satellite imagery of the Zambezi region of Namibia in 2004 and 2019. Despite the good classification obtained in this study, there were some general issues which may have reduced the accuracy of the overall classification. For example, the spectral signature of forests was mixing with the signature of open forests/shrubs, resulting in low producer’s accuracies for both classified map due to their noisy Landsat spectral signatures and difficulty in interpreting them. A similar problem was also encountered by Lu et al. (2003) and Zhao et al. (2016). To overcome this mixed pixel problem, higher spatial resolution multispectral images such as SPOT images reduced the mixed pixel problem, resulting in improved forest classification accuracy (Lu et al., 2008). However, using higher spatial resolution with pixel-based tree species classification approaches also increased spectral variations, especially in savannas with open forests, because of their complex forest stand structure and canopy shadows, resulting in poor classification accuracies (Lu and Weng, 2005; Myeong e al., 2001; Pu et al., 2018; McElhinny et al., 2005). Incorporation of these relatively medium spatial resolution images such as Landsat with 30-meter spatial resolution with other data sources such as digital elevation models (along with their derivatives such as slope and aspect), spatial texture, and SAR can improve classification accuracy (Myeong e al., 2001).

In this study, the LULC change trajectories included the conversions to-and-from land cover classes. Unchanged areas, particularly forest land and open forest/shrub land, are of exceptional importance for biodiversity management, providing forest habitat and increases connectivity between forest patches for wildlife population dynamics, and migratory species (Stoldt et al., 2020; Wegmann et al., 2015; Wintle et al., 2019). In addition, unchanged areas provide timber and non-timber product supply, and carbon storage in the study area (David et al., 2022a). The large areas of unchanged forest land may provide an indication of the effectiveness of intensified efforts for forest protection and biodiversity management such as forest fire protection programs and awareness creation on the sustainable use of forests implemented by the Government (Russell-Smith et al., 2017). Conversely, the large area of forest conversion to open forests/shrubs and agricultural/Barren land could also indicate the degradation of forests from continuous drought events and logging of forests for timbers from the Chinese companies in the Zambezi region (Asanzi et al., 2014; Chikoore and Jury, 2021; Weng et al., 2015). The most valuable timber tree species in Namibia include Pterocarpus angolensis, Baikiaea plurijuga, and Guibourtia coleosperma. However, the harvest of these trees has increased because of the high demand for timber from dense tropical hardwood species from Chinese (Asanzi et al., 2014).

Making full use of the opportunities that the Landsat and MODIS archive provides, this study provides an assessment of land cover change and forest disturbances in the KAZA region, from 2002/2004 to 2019, explored with change detection algorithms. The main aim was to quantify and identify the Land cover change, locations, types, and trends of the land cover during the 19-year period in communal and protected areas of Namibia. Methodologically, this study showed that dryland forest disturbances associated with deforestation and degradation can be mapped reliably with both BFAST and BEAST change detection algorithms. In terms of the performance of indices utilised, this study suggests that the GNDVI was found to have the best performance in monitoring degradation and detecting disturbances from droughts and fires as compared to NDVI. This study found the NDVI is less sensitive to changes in dryland forests as compared to GNDVI, and this result is consistent with studies that found that metrics based on the short-wave infrared (SWIR) outperform NDVI in temperate and savanna ecosystems in the USA (Jin and Sader, 2005, Kennedy et al., 2010, Zhu, Woodcock and Olofsson, 2012).

Thematically, this study yielded three main insights. First, the study found diverse spatial patterns of forest disturbances are more prevalent in the communal areas and state forests such as the Zambezi ST, particularly when compared to protected areas such as Mudumu NP. These changes are driven by different disturbance agents, including both natural processes (e.g., drought) and anthropogenic impacts (e.g., timber logging, fire). This suggests disturbance attribution is central for understanding the drivers and impacts of forest degradation. According to land cover change analysis in Fig. 4.13, agricultural/barren land has increased dramatically during 2004 to 2019. Agricultural/ barren land may be caused by (1) cut trees for households and wood processing businesses, or (2) slash-and-burn agricultural activities (Kamwi et al., 2017) and (3) timber trade (Asanzi et al. 2014). That unsuitable farming practice is mainly taken by local ethnic groups living in the province, while the tree logging is due to a strong presence of logging companies primarily from China (Nott et al, 2019). This is in agreement with previous studies on land cover and land use analysis such as Kamwi et al. (2017) that found agricultural expansion to be the most predominant driver in the same study area.

Second, the study found large areas of the dryland forest in the Zambezi ST have experienced major disturbances from 2016 to 2019 from clear-cut of forests coupled with fire, and extreme drought events, suggesting deforestation and degradation is a widespread phenomenon in KAZA. Similar to the research presented by Kamwi et al. (2015), the land cover analysis from this study (see: Fig. 4.13 and Fig.4.14) found that small-holder agriculture and shifting cultivation was largely responsible for breakpoints of large magnitudes in the communal areas of the Zambezi region detected by BFAST change detection (see: Fig 4. 12). The BFAST change detection also detected vegetation disturbances/degradation, stable vegetation, and vegetation regrowth, and these level of disturbances, trend and direction of change were not detected by the bi-temporal classification. Third, a clear association between forest disturbance and precipitation was found. Forest disturbance was particularly widespread during severe drought years such as 2015-2016 and 2019. This study results also showed positive magnitude breakpoints, which represented forest recovery and vegetation regrowth, which could be attributed to increased precipitation and lack of disturbance in protected areas such as Mudumu NP, as compared to community conservancies and the Zambezi SF. This study disturbance maps, land cover change and field observations suggest that drought, forest logging, agricultural expansion, large herbivore disturbance, and increased fire may explain some of the observed pattern by the

BFAST and BEAST change detection algorithms (Kamwi et al., 2017); Nott et al, 2019), (also see: Fig. B2, B3, B4 and B5). Similar patterns of increases in forest disturbance during drought seasons were found both in the Amazon and the Gran Chaco of Argentina (Bullock et al., 2020, De Marzo et al., 2021).

Previous land cover mapping research in the KAZA region has shown contrasting results. Kamwi et al. (2015) reported forest and woodlands are expanding in communal land in the Zambezi region, while Meyer et al. (2021) reported that woodland cover reduced by 2.1% within the same study area and time period of 1990 to 2010. The land cover mapping from this study shows that forests reduced by 9% in the same region between 2004 and 2019. The deforestation and widespread degradation identified in this study are consistent with findings by McNicol et al. (2018) that found Southern African woodland is highly dynamic with widespread degradation and deforestation, but also extensive vegetation regrowth. The further step on assessing the magnitude of change reported in this study demonstrates first that forest change occurs in an incremental manner, and second, by making use of the magnitude parameter, that conventional bi-temporal classification studies could further be improved and complimented by extent and severity of forest disturbances derive here (DeVries et al., 2015). The ability to describe these change processes with high temporal detail highlights the advantage of a time series change detection approach used here and the additional information they provide to conventional bi-temporal classification maps of forest versus non-forest maps conducted in KAZA region (Kamwi et al., 2017, Meyer et al., 2021, Fox et al., 2017).

4.6 Conclusion

This study evaluated the applicability of BFAST and BEAST algorithms to detect a range of abrupt, gradual, and seasonal changes using MODIS vegetation index (VI) time series data in tropical dryland forests in Southern Africa from 2002–2019. The change detection algorithms complemented the bi-temporal Land cover change detection in Zambezi region from 2004 and 2019. The study has shown that analysis of monthly MODIS VI time series, climate data, and field validation can effectively describe and help to interpret longer-term changes of vegetation dynamics. Changes occurring in the trend component identified indicate both gradual and abrupt changes, while giving insights into the influence of drought and phenological variation on the forest. Four main conclusions can be drawn from this study:

First, dryland forests are highly dynamic and water sensitive with high rates of deforestation and widespread degradation, but also continuous vegetation recovery and regrowth are identified in protected areas compared to unprotected areas.

Second, BEAST algorithm was found to give the best performance overall, correctly identifying abrupt changes of vegetation response to fire and drought impacts. BFAST did not perform well in identifying abrupt changes resulting from fire and low magnitude drought events. Based on the results, the best decomposition of trend and seasonal breakpoints were given by BEAST using the GNDVI.

Third, BEAST algorithm outperformed BFAST algorithm in detecting seasonal changes driven by climatic and clear-cutting events. BEAST algorithm detected the abnormality of deforestation and climate-driven changes in seasonality, which helped identify the potential drivers of these phenological shifts. However, BFAST failed to detect any seasonal changes within the entire study period (2002-2019) using either the NDVI or GNDVI.

Fourth, conventional NDVI was highly influenced by canopy background variations and herbaceous layers, as compared to the GNDVI. NDVI performed best in the robust detection of areas with complete land cover class changes, while GNDVI performed well in detecting changes within areas of partial (low magnitude change) and complete land cover class changes. The analysis suggests that GNDVI is more sensitive to chlorophyll concentration in vegetation when the leaf area index is moderately high as is the case in tropical dryland forests, while NDVI is more sensitive to forest types with low chlorophyll concentrations.

Finally, the study shows that the droughts that took place in 2015 and 2019 were longer and more extreme than the droughts in 2002-2003, 2005, 2007 and 2011-2013. Overall, the results also show that a large part of the growing season and phenology is highly influenced by seasonal and inter-annual variations in climatic conditions, particularly in the case of severe drought in the KAZA region.

These results highlight the importance of complementing the conventional bi-temporal classification studies on Land cover change with improved time series change detection algorithms to detect the magnitude, extent, and severity of forest disturbances with high temporal detail. The study also showed the importance of considering the sensitivities of VIs used in forest monitoring when trying to identify non-linear dynamics of dryland forests. Two extreme record droughts in less than two years (2015-2016 and 2018-2019) are evidence of the negative impacts of extremes of climate variability and climate change in the region. Therefore, an in-depth assessment of the intensity, spatial coverage, and geography of impacts of future droughts are of fundamental importance to the region. The approach described above is transferable to other tropical forest areas with high inter-annual variability that is influenced by seasonal climatic variations and disturbance. These methods are subject to further tests with other datasets of higher spatial resolution such as Landsat, Sentinel, or simulated datasets, to ensure their efficacy.

4.7 Acknowledgments

This work was supported by Commonwealth Scholarship Commission PhD grant number: NACS-2017-409 from the 2017–2021, Geography doctoral program at Durham University. The authors acknowledge financial support from the Royal Geographical Society (grant number: MC 08/19) and WWF Namibia Mike Knight for travel support grant number: T225. I thank WWF KAZA TFCA Secretariat Nyambe Nyambe, Chobe National Park Authority Michael Flyman, and University of Namibia (Katima Branch) Dr. Ekkehard Klingelhoeffer for the support during the fieldwork. I also thank Morgan Kamwi who helped with transportation and data collection in the field.

4.8 Supplementary Information 2

MODIS Data Processing and Filtering

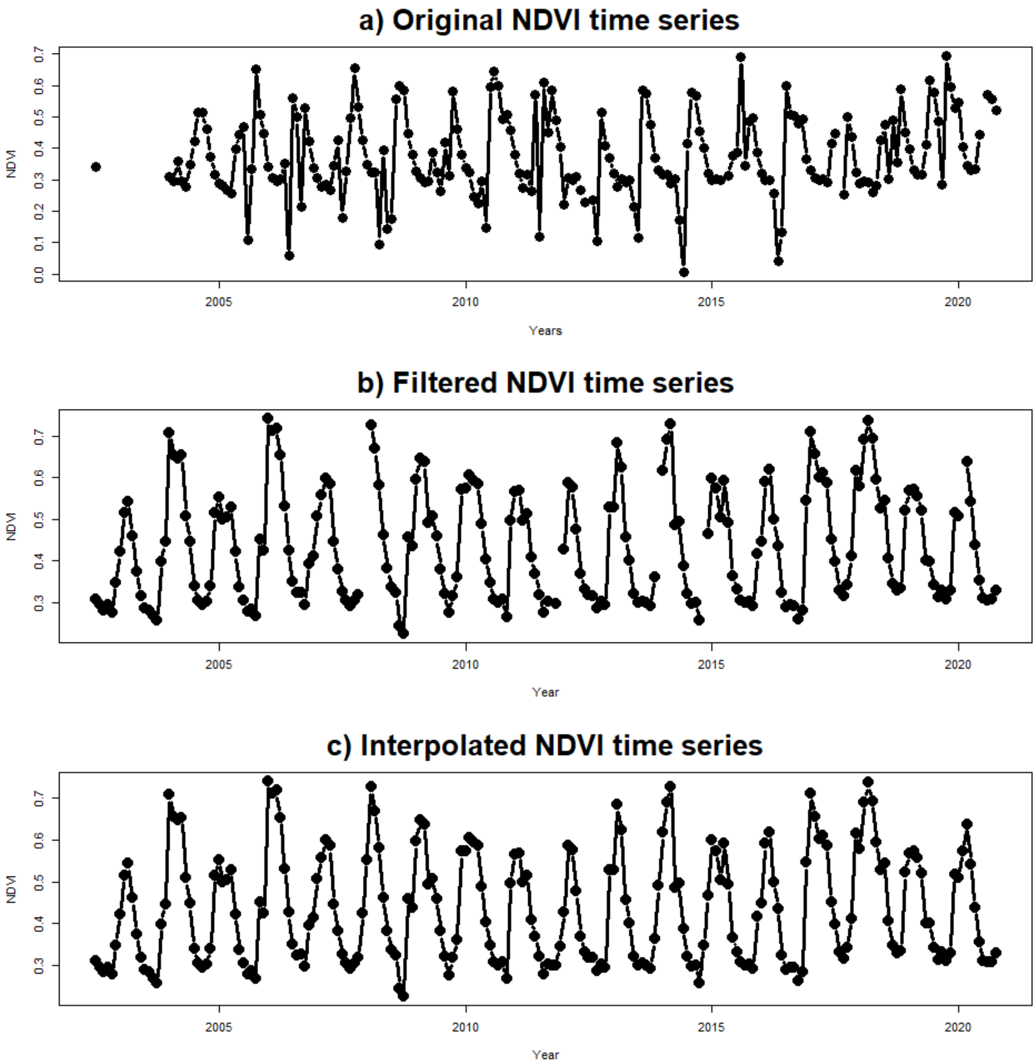

Fig. B 1. Temporal profiles of raw and cleaned MODIS NDVI data for a forest plot: (a) original time series after MCV method; (b) time series retained after filtering, and (c) time series with linear interpolation on filtered points over a 17-year period.

Clear-cut and burnt forest

Fig. B 2. A and B shows field photo evidence of a deforestation event in a dryland forest dominated by Baikiaea plurijuga species, the area was burned in 2017 and clear-cut for timbers in around 2018-2019. The photo location coordinate is 17.49°S, 24.21°E taken from ground survey in Namibia in 2019.

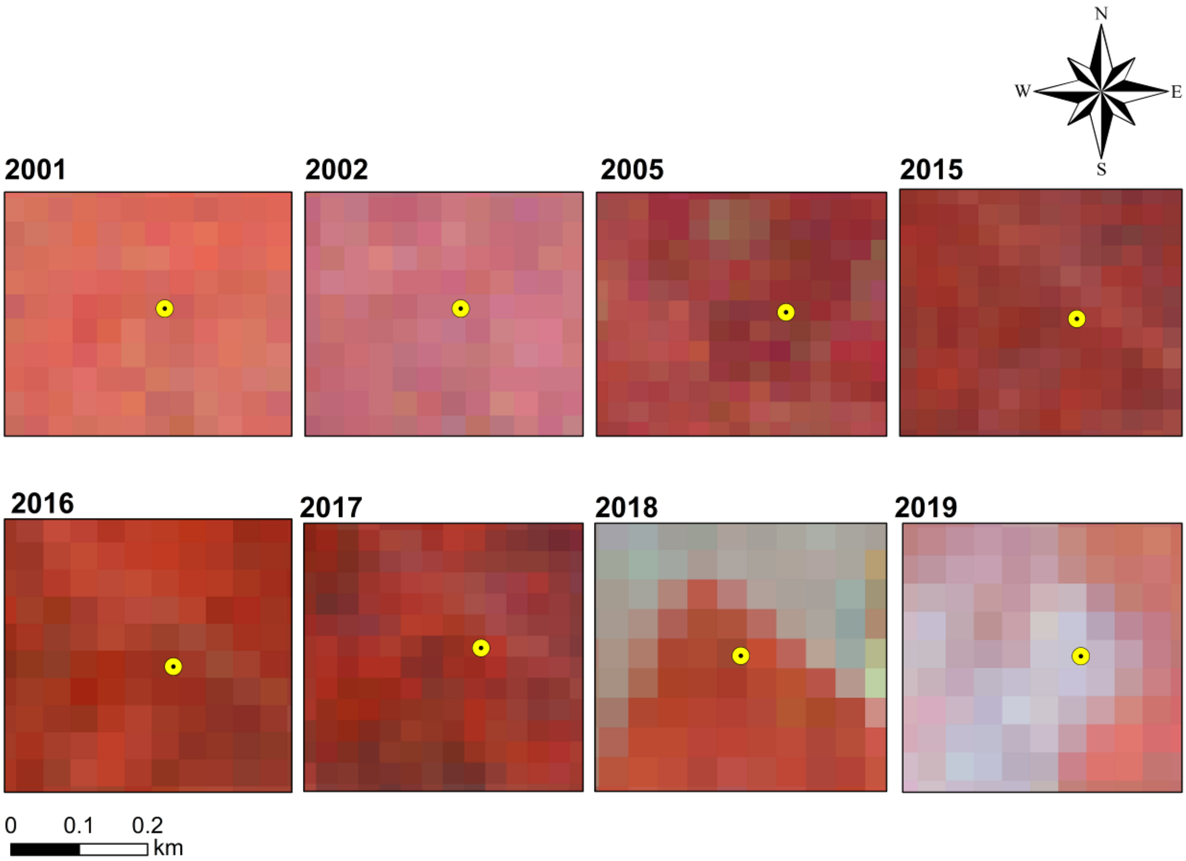

Fig. B 3. Shows the corresponding time series of Landsat images with no cloud cover in the pixels documenting changes in the forest (forest to shrubs) from 2015 to 2019, respectively. The yellow dot represents the location ID (coordinate: 17.49°S, 24.21°E). The year 2002 and 2005 was included because it is a drought year and 2001 was used as a baseline year.

Drought impacts and degraded forest

Fig. B 4. shows field photo evidence of a degrading forest dominated by baobabs and riparian woodlands species near Chobe River frontage. The photo location coordinate is 17.80°S, 24.95°E taken from ground survey in Botswana in 2019.

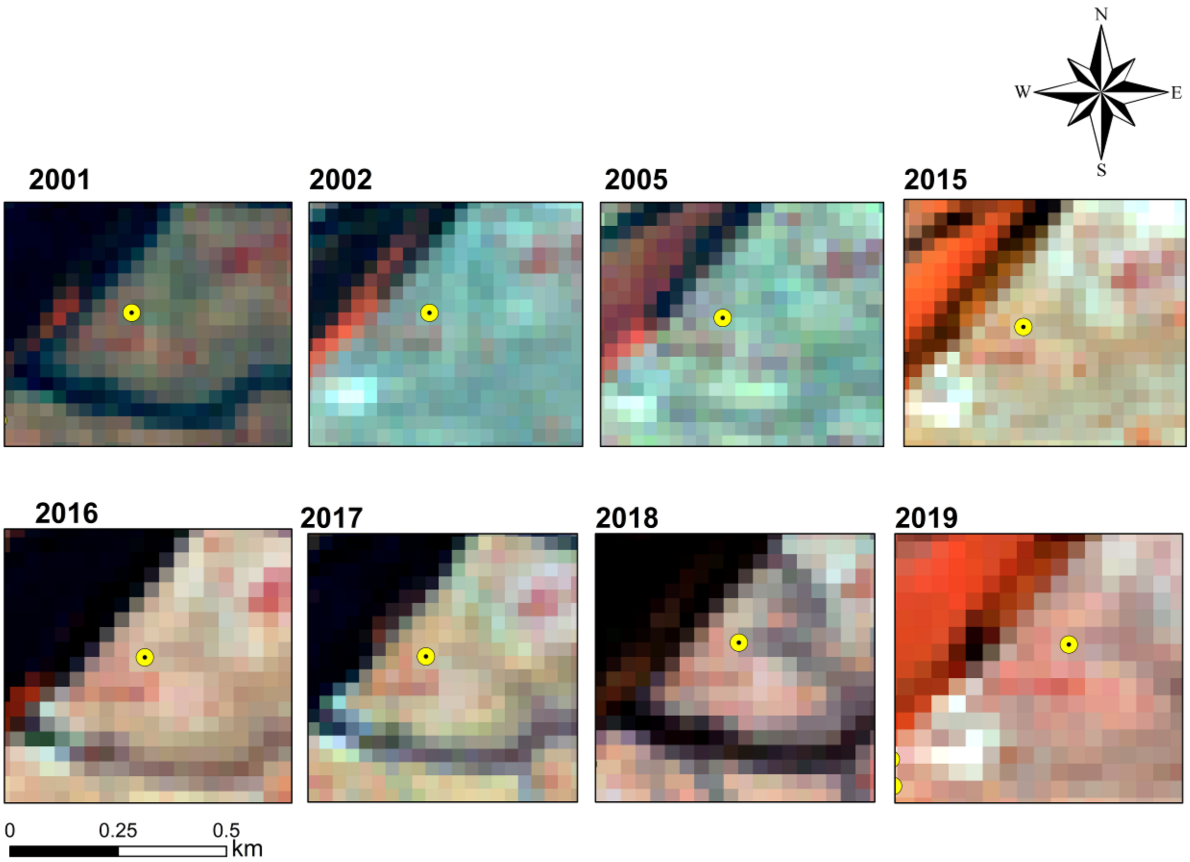

Fig. B 5. shows the corresponding time series of Landsat images with no cloud cover in the pixels documenting changes in the plot from 2015 to 2019, respectively. The yellow dot represents the location ID (coordinate: 17.80°S, 24.95°E). The year 2002 and 2005 was included because it is a drought year and 2001 was used as a baseline year.

A stable and recovering forest

Fig. B 6. Shows field photo evidence of a forest that has not experienced any disturbance for the period of the study. The photo location coordinate is 17.57°S, 24.28°E taken from ground survey in Botswana in 2019.

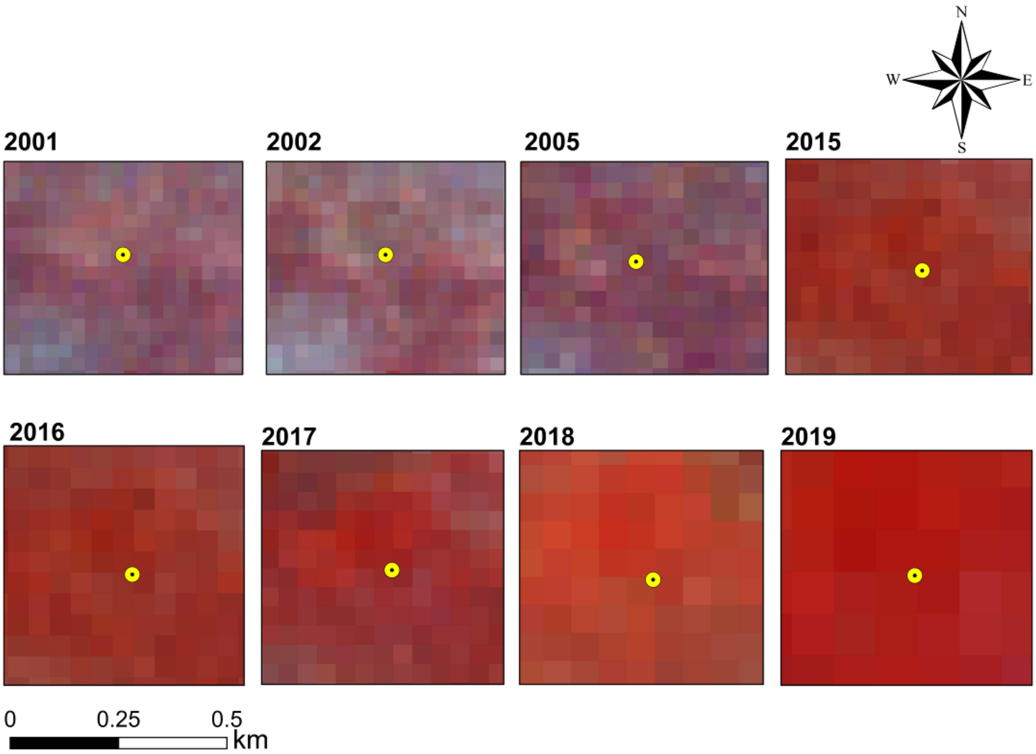

Fig. B 7. shows a time series of LC8 images from 2015 to 2019 is shown below. The yellow dot represents the location ID (coordinate: 17.57°S, 24.28°E). The year 2002 and 2005 was included because they are drought years and 2001 was used as a baseline year

Table B. 1. Land cover areas in the study area per year (2004 and 2019) in km^2 and hectares.

Class name	**2004 Area (km^2)**	**2004 Area (ha)**	**2004 Area (%)**	**2018 Area (km^2)**	**2018 Area (ha)**	**2019 Area (%)**
Water	5	508	0	6	600	0
Forest	2,351	2351,411	46	1,893	189,335	34
Open forests/Shrub	2,564	256,410	51	2,735	273,512	54
Urban	3	262	0	3	318	0
Agriculture	143	14,378	3	429	42,934	8

Table B. 2. Area changes of BFAST (2002-2019) using sample-based estimates and the observed disturbance change rates in hectares.

Change identified by BFAST	**Area (ha)**	**Standard Error (ha)**	**2.5 % (ha)**	**97.5 % (ha)**
Non-disturbance (No change) *(Stable Forest)*	106,390	9,817	87,148	125,631
Low negative changes (no change) *(Degradation)*	90,929	10,636	70,083	111,776
Large negative changes (No change) *(Non-forest)*	38,873	7,162	24,836	52,910
Non-disturbance -Low negative changes *(Stable forest to Degradation)*	33,132	6,859	19,688	46,576
Non-disturbance -Large negative	99,911	9,753	80,795	119,027

changes *(Stable Forest to Deforestation)*				
Low negative changes -Large negative changes *(Degradation to Deforestation)*	59,515	8,154	43,533	75,497
Low negative changes -Non-disturbance *(Degradation to Stable Forest)*	23,409	556,8	12,497	34,322
Large negative changes -Low negative changes *(Deforestation to Degradation)*	48,537	8,353	32,167	64,908
Large negative changes -Non-disturbance *(Deforestation to Stable Forest)*	5,980	2,966	167	11,792
Total	506,676			

Table B. 3. Area changes for the Random Forest classification in the Zambezi region in hectares.

Change identified by two-interval classification	**Area (ha)**
Forest-Forest	147,876
Non-forest-Non-forest (no change)	201,157
Forest - Non- Forest	87,251

Non-forest - Forest	41,447
Non-forest - Non-Forest (change)	28,944
Total	506,676

Table B. 4. Area-based transition among land cover categories for the Random Forest classification for the period 2004–2019 in the Zambezi region in hectares.

Land cover class Change	**Re-organisation**	**Area Change (ha)**	**Area Change (%)**
Agriculture-Agriculture	Non-forest-Non-forest (no change)	8,501	2
Agriculture-Forest	Non-forest - Forest	1,109	0
Agriculture-Open forest/Shrub	Non-forest -Non-Forest (change)	4,707	1
Agriculture-Urban	Non-forest -Non-forest (change)	58	0
Agriculture-Water	Non-forest -Non-forest (change)	4	0
Forest-Agriculture	Forest to Non-forest	10,634	2
Forest-Forest	Forest-Forest	14,7876	29
Forest- Open forest/Shrub	Forest to Non-forest	76,346	15
Forest-Urban	Forest to Non-forest	16	0
Forest-Water	Forest to Non-forest	256	0
Open forest/Shrub -Agriculture	Non-forest -Non-forest (change)	23,677	5
Open forest/Shrub -Forest	Non-forest - Forest	40,173	8
Open forest/Shrub - Open Forest/Shrub	Non-forest-Non-forest (no change)	192,313	38
Open forest/Shrub -Urban	Non-forest -Non-forest (change)	205	0
Open forest/Shrub -Water	Non-forest -Non-forest (change)	34	0
Urban-Agriculture	Non-forest -Non-forest (change)	115	0
Urban-Forest	Non-forest - Forest	5	0
Urban- Open forest/Shrub	Non-forest -Non-forest (change)	101	0
Urban-Urban	Non-forest-Non-forest (no change)	39	0
Urban-Water	Non-forest -Non-forest (change)	1	0
Water-Agriculture	Non-forest -Non-forest (change)	7	0
Water-Forest	Non-forest - Forest	161	0

Water- Open forest/Shrub	Non-forest -Non-forest (change)	36	0
Water-Urban	Non-forest -Non-forest (change)	0	0
Water-Water	Non-forest-Non-forest (no change)	305	0
Total		506,676	100

4535

5 A SPATIO-TEMPORAL DROUGHT AND FIRE ANALYSIS FOR SEMI-ARID DRYLAND ECOSYSTEMS IN SOUTHERN AFRICA USING MODERATE RESOLUTION SATELLITE IMAGERY.

Chapter 5 Manuscript in progress: Intended for submission to *Remote Sensing in Ecology and Conservation.*

Title: A spatio-temporal drought and fire analysis for semi-arid dryland ecosystems in southern Africa using moderate resolution satellite imagery.

Author contributions

David Ruusa- Design the research, perform the data analysis, interpret the results, wrote the manuscript, and revised the manuscript. Nick Rosser- Contributed to the research design, manuscript editing and supervision. Daniel Donoghue-Contributed to the research design, conducting fieldwork, manuscript editing and supervision.

Abstract

The dryland ecosystem of Southern Africa is fire-prone and has a long history of recurrent droughts that in turn, affect its ecology, structure, function and distribution. This chapter presents a spatiotemporal analysis of drought, water stress, fire impacts on dryland vegetation between 2002 and 2019 for the largest conservation area: Kavango-Zambezi Transfrontier Conservation Area (KAZA). To disentangle the relative contribution of climatic and fire regimes to dryland vegetation, Normalised Difference Vegetation Index (NDVI), precipitation data, temperature data, evapotranspiration, Root Soil Moisture (RSM) and Active Fire and Burned Area data products were used. For drought condition, this study shows most severe drought was in 2002/2003, 2005, 2015/2016 and 2018/2019. The worst drought with the longest duration and highest magnitude was recorded in 2019. In the KAZA region, about 149,410 km^2 of land is burned on an annual basis over the period 2002–2019, however significant differences were observed in the fire patterns among the five countries of KAZA. Fire incidence was higher in Angola and Zambia where burning is not strictly controlled; midrange fire incidences were observed in Namibia where fire control policy and awareness programs were introduced in 2006; and fire incidence was lower in Botswana and Zimbabwe, where there are effective and strict fire management policies. These results reveal that the areas with high dryland forests (or high tree cover), high rainfall, and long dry season length coincide with areas of high fire frequency resulting in relatively large burned areas. The combination of drought, water stress and high fire frequency observed in this study has led to an increase in land area classified as arid and semi-arid at the expense of dry sub-humid and humid land classes, which were reduced by 10% in the period 2002 to 2019. These findings have important implications on wildlife habitat management and climate change in Southern Africa's dryland forest ecosystems.

Keywords: Dryland vegetation, climate change, soil moisture, drought, forest fire, Southern Africa, remote sensing

5.1 Introduction

5.1.1 Drought stress on dryland vegetating

Drought is a regular and recurrent feature of Southern African climate, and climate change scenarios predict large-scale biogeographical shifts in vegetation in response to the severe drought and intense moisture surplus which will be exacerbated by higher temperatures (Diffenbaugh et al., 2017). Growing evidence suggests that the effects of drought on vegetation under warmer conditions can be severe, as highlighted by recent observations of regional-scale woody-plant die-off across Southern Africa (Naidoo et al., 2013), the Sahel (Anyamba et al., 2005), and more widely around the globe (De Jong et al., 2013). In Southern Africa's arid and semiarid areas, droughts are a frequent occurrence and can have severe ecological and economic consequences (Mason et al., 2000). While these events may be short duration followed by recovery during subsequent years of higher rainfall, in some cases droughts can trigger substantial and irreversible ecological and socioeconomic changes (Ellis et al., 1988).

The effects of drought on vegetation can vary considerably across ecosystems, depending on plant adaptations and interactions with other ecological processes (Engelbrecht et al., 2007). The responses of vegetation to variations in climate are expected to be most sensitive and extreme in tropical open woodlands and forests in arid and semi-arid ecosystems (Watson et al., 1996). Tropical open woodlands (hereafter called "dryland forest or woodland") are forests comprising mixtures of trees, shrubs, and grasses in which the tree canopies do not form a continuous closed cover (Grainger, 1999). There is evidence that anomalies in tropical vegetation greenness are linked to global inter-annual variations in sea surface temperature (SST), land surface temperature and precipitation, as evidenced in the dryland forests (Huang et al., 2017). The xeric areas of the dryland biome often have unreliable rainfall and are often subject to a substantial multi-year rainfall deficit. Furthermore, the impacts of drought tend to be aggravated by deforestation, land degradation, growing water demand and extremes of temperature, as a result of climate variability, anthropogenic activities and global warming (Dale et al., 2001). For example, Chagnon et al. (2004) found a large shift in local rainfall and seasonality with increases in deforested areas in the Amazon, associated with local atmospheric circulation that were changed by gradients in vegetation. Monitoring drought stress in vegetation is a critical component of proactive drought planning designed to mitigate the impact of this natural hazard. Although it is not possible to avoid drought, its impacts can be managed through preparedness planning. The success of drought preparedness and management depends, among others, on how well the droughts are defined and drought characteristics (e.g., intensity and duration) are quantified temporally and spatially.

A drought is a naturally recurring hazard and can alternatively be defined as a temporary, recurring reduction in the precipitation in an area. Droughts have a slow initiation and they are usually only recognised when the drought is already well established. The deficiency in precipitation is the main causes of all drought types, including: meteorological, agricultural, hydrological, and socioeconomic. Meteorological drought relates to precipitation deficiencies in absolute totals for a given period and is one of the primary causes of wider drought. On the other hand, agricultural drought is characterised by a soil moisture deficit and changed plant behaviours during the plant-growing period. The longer and the more spatially extensive this deficiency, the more likely the occurrence of other types of droughts, such as hydrological that is a reduction of streamflow, lake or reservoir storage, and a lowering of ground-water levels. Socioeconomic drought occurs when the demand for an economic good exceeds supply as a result of a weather-related shortfall in water supply (Maliva et al., 2012). Drought indices derived from meteorological data can be used to monitor not only meteorological droughts but also agricultural and hydrological droughts, and to categorise the seriousness of the drought, which is important for a wide range of management and planning decisions. Drought indices commonly applied around the world are summarised by Svoboda et al. (2016). Consequent impacts of warm droughts could include a reduction in habitat for wildlife, enhanced opportunities for invasion by exotic species, formation of novel communal areas, imbalances in the hydrologic cycle, and temporal disruptions to ecosystem goods and services (Rands et al., 2010).

5.1.2 Fire impacts on dryland vegetation

In addition to drought, within the forest-dryland mosaics other natural disturbances that affect forests include large pulses of forest disturbances from agents such large mammalian herbivore damage, insect outbreaks, strong winds and wildfires (Geist et al., 2004). Fire is considered a major determinant of the ecology and distribution of Africa's dryland forests and the frequency and severity of large wildfires has increased during some extremely dry years in past decades (Archibald et al., 2018). The burning of natural vegetation is common and widespread throughout the tropics and is considered to be a significant source of aerosol, trace gas and particles to the global atmosphere (Frost, 1999). Within the tropical landscape, 42% of CO2 emissions are estimated to come from Africa, 29% from Asia, 23% from South America, and 6% from Oceania (Andreae et al., 1998). In Africa, fire is generally viewed as key to ecosystem structure and function. For example fire is used to maintain grasslands by suppressing bush encroachment (Chidumayo, 1997). In Southern Africa, fire is started either by people or by lightning, and is intensified by a prolonged annual dry season combined with relatively rapid rates of fuel accumulation. Often, fires originate outside of protected areas but later burn uncontrolled into protected areas. Uncontrolled wildland fires can destroy extensive landscapes, posing a major threat to the survival of dryland tree species, human life and property, encouraging society and policy makers to take measures that mitigate its effects (Turner et al., 1999).

The fire regime of an area is defined by several variables, including the patterns of frequency, season, type, severity and extent. All of these characteristics are intricately linked to ecosystem structure and function, and are highly dependent on weather and climate oscillations (Archibald et al., 2009; Gill, 1975). Reliable observed data on fire frequency (or, alternately, the reciprocal of the fire return time) for calculating biomass burned at regional scales are fundamentally important (Frost, 1999). This is partly because biome characteristics, mainly biomass loads and moisture levels, determine fire behaviour, but also fire alters vegetation structure, composition and development (Bond et al., 2005; Hantson et al., 2016). On the other hand, climate affects fire occurrence through temperature and precipitation cycles, but climate is also affected by fire through by gaseous emissions (Bojinski et al., 2014). These mutual influences between vegetation, climate and fire highlight the importance of having long-term burned area (BA) and climate information that serves as an input for a holistic vegetation analysis. Therefore, better fire observations and improved estimates of fire impacts will reduce uncertainty and improve prediction for future ecosystem feedbacks on atmosphere interactions.

Recent research has also pointed out a decline of forest resilience to wildfires because of an intensification of the interactions between extreme droughts and fire (Brando et al., 2019). Fire and grazing regimes, in conjunction with changes in climate characteristics affecting soil moisture status, relative humidity, or drought stress, will have the greatest influence on grassland-woody species boundaries (Barros et al., 2018). A drying climate, in combination with non-adapted and unsustainable land-use therefore increases the risk of desertification (Geist et al., 2004). Intensifying disturbance regimes are thus expected to be among the most severe impacts of climate change on forest ecosystems and can bring forests to a threshold for massive die-off (Turner, 2010). The killing of plants causes substantial vegetation change and limits productivity, thereby causing shifts in plant communities resulting in species loss (Williams et al., 2013). Such forest disturbances significantly affect the global carbon cycle by, for example, vegetation loss or changing forest phenology. This is raising concerns that disturbances to dryland natural resources in these areas might increasingly interfere with sustainable provision of ecosystem services and wildlife habitat management in the tropics (Scholes et al., 2004).

A drying climate, in combination with unsustainable land use practises, in already water-scarce regions, increases the risk of drying conditions (Reynolds et al., 2007). Desertification is a complex phenomenon, driven by socio-economic and climate-related processes, such as increasing aridity and more frequent and/or severe droughts (Reynolds et al., 2007) (Fig. 5.1). Desertification is not confined to drylands, however, they are some of the most vulnerable regions to land degradation processes due to the delicate balance between natural resources (e.g., limited rainfall, low soil moisture, high temperature, low vegetation productivity) (Vogt et al., 2011) (Fig. 5.1). Consequently, an important contribution in the fight against desertification is to quantify whether the extent of drylands has changed and, if this process has taken place, where and to what degree it has occurred (UNCCD, 1994). In addition, this knowledge would allow natural resource managers to implement best management practices under drought conditions and other decision makers to better target assistance and response activities (e.g., early detection of hot spots for wildfires) in a timely manner.

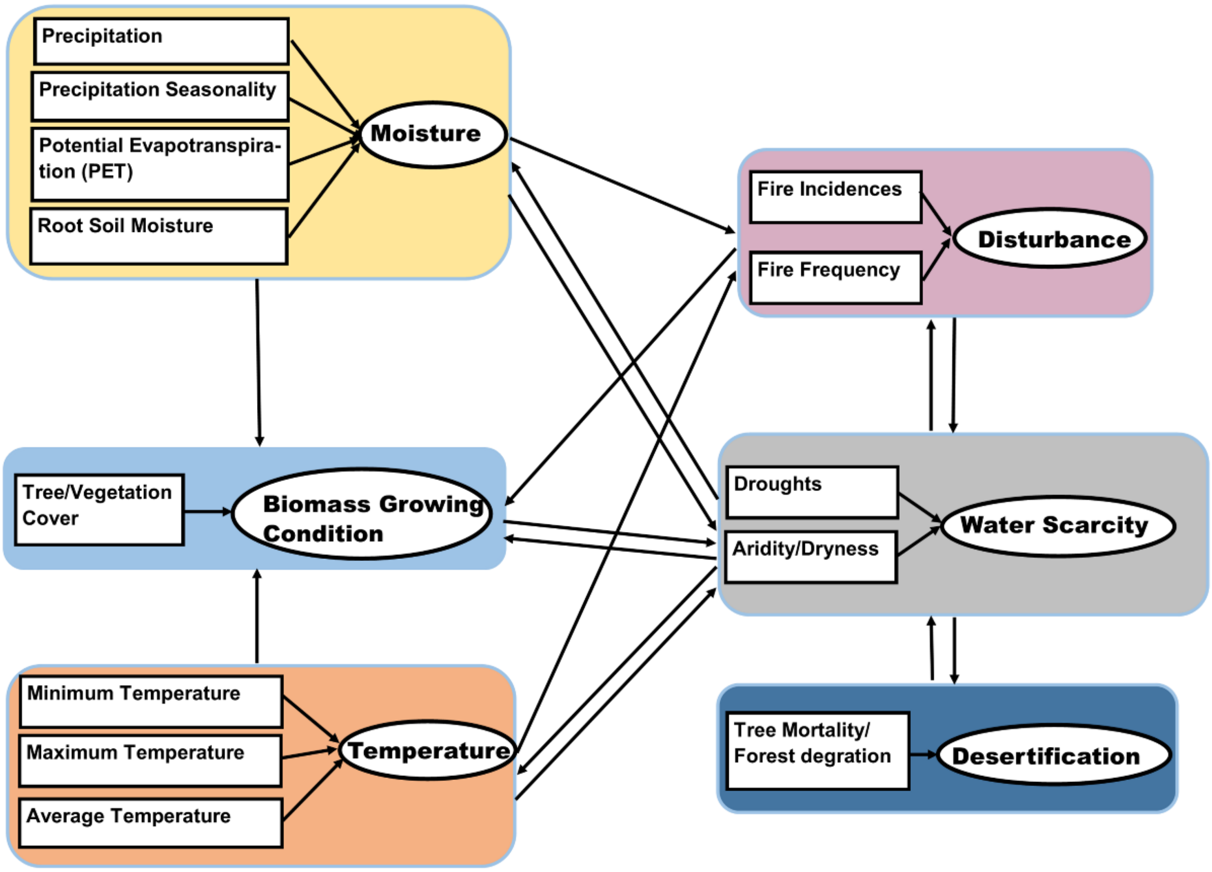

Fig. 5. 1. Conceptual model depicting theoretical relationships among moisture availability, temperature, plant growing conditions, and disturbance (fire frequency), water scarcity (droughts) and their effects on dryland vegetation cover directly or indirectly as it characterises desertification.

The interrelations between dryland fire regimes and vegetation dynamics are indeed complex; they are conditioned by various climatic, biotic and anthropogenic factors involving different feedbacks. Although many studies have been undertaken in southern Africa (see (Chidumayo, 1997; Korontzi et al., 2003), very few of these have investigated the combined effects of all these on dryland vegetation cover. The majority of research on the potential impacts on fire regimes and climate change on drylands has focused on the Amazon and West Africa (e.g., Sahel) (Aragão et al., 2007; Herrmann et al., 2005; Samanta et al., 2011). By contrast, the regional studies that analyse the impacts of climate and fire on dryland forests and vegetation in many parts of Southern Africa have been more sparse (Blackie et al., 2014). There is, to my knowledge, no study that has investigated drought and fire impacts on dryland vegetation cover across the KAZA region over a long-term basis. A study published by Pricope et al. (2012), did consider fire frequency from 2000 to 2010 in KAZA region, but only focused on the central part, while Mpakairi et al. (2019) only focused on Zimbabwean component of KAZA. Neither study considered the whole region and were solely based on fire analysis without incorporating vegetation information.

This chapter analyses trends of fire regimes of all the five of the national constituents of KAZA, noting that each country manages fire differently. Some aim to prevent fires, others legislate for seasonal prescribed burns, and others witness more uncontrolled fires in protected and unprotected areas. To investigate the drivers underlying the observed long-term vegetation cover change in the KAZA region, a conceptual model was constructed (see: Fig. 5.1) based on the knowledge that there are direct and indirect effects of climate, soil moisture, and fire on woody vegetation cover. Fire disturbance and soil moisture were included in the climate-vegetation analyses because they are considered an Essential Climate Variable (ECV) by the Global Climate Observing System (GCOS) program, which encourages the generation of long-term time series of ECVs to better understand climate trends (Bojinski et al., 2014; Mason et al., 2009). The present study was designed to investigate the relationship between moisture availability as a function of effective rainfall, rainfall seasonality, evapotranspiration, and root soil moisture, temperature, fire incidence and frequency, drought and vegetation index. This was used to characterise spatiotemporal changes in aridity in the KAZA region using long-term time series from both ground and satellite observations from 2002 to 2019.

5.2 Aims and Objectives

Aims

The aims of this study are to investigate the relationship between fire and different climate effects on vegetation spectral characteristics at the regional scale of KAZA.

Objectives

- To characterise drought conditions using climatic data (SPEI, root-soil moisture, temperature, and precipitation) and explore the variability of drought using monitoring indicators (i.e., the drought duration, severity and magnitude)
- To characterise the frequency, seasonality, and extent of fires through time on different land use management in KAZA region
- To investigate the spatiotemporal changes in aridity in KAZA region from 2002 to 2010 and 2011 to 2019

5.3 Materials and methods

5.3.1 Study Area

The Kavango Zambezi Transfrontier Conservation Area (KAZA TFCA) (18.00°S 23.00°E) in Southern Africa, is a large multi-nationally managed network of national parks (NP), wildlife and game management areas, forests reserves and communal. The KAZA TFCA is the largest transfrontier conservation area in the world, and encompasses an area of approximately almost 520 000 km^2 shared by Botswana, Namibia, Zambia, Zimbabwe, and Angola (KAZA, 2014). The KAZA was established to improve the cooperative management of shared resources, to improve links between wildlife habitats, to create economic development to the local communities adjacent to protected areas through tourism. KAZA was also intended as a means to contribute to peace and friendly relationships between participating countries through cooperation in nature protection and development (Stoldt et al., 2020). The region hosts the largest elephant population (*Loxodonta africana*) in the world and it is characterised by large-scale migrations of megafauna such as buffalo (*Syncerus caffer*), leopard (*Panthera pardus*), zebra (Equus quaaga). The region is home to numerous red-listed tree species, and contains the world-heritage listed Okavango Delta (Matswiri, 2017; Naidoo et al., 2012). The largest portion of KAZA is generally water- and nutrient-poor due to its location in the Kalahari Basin, and has a climate that is characterised by a single rainy season and a long dry season (see: Fig. 5.4), with an annual rainfall average of 300–950 mm from 1983 to 2019 (see: Fig. 5.3). During the dry season, as most natural pans dry up, water is mostly available at a large number of artificial waterholes across parts of the landscape and most animals migrate between seasons to other parts of KAZA converging to rivers such as Zambezi and Chobe Rivers in northern Botswana, and Gwaii river in Zimbabwe (Cumming, 1981; Tshipa et al., 2017). This rainfall seasonality provides a fire-prone climate such that the drylands of Africa are thought to experience the most extensive biomass burning in the world (Lehmann et al., 2014).

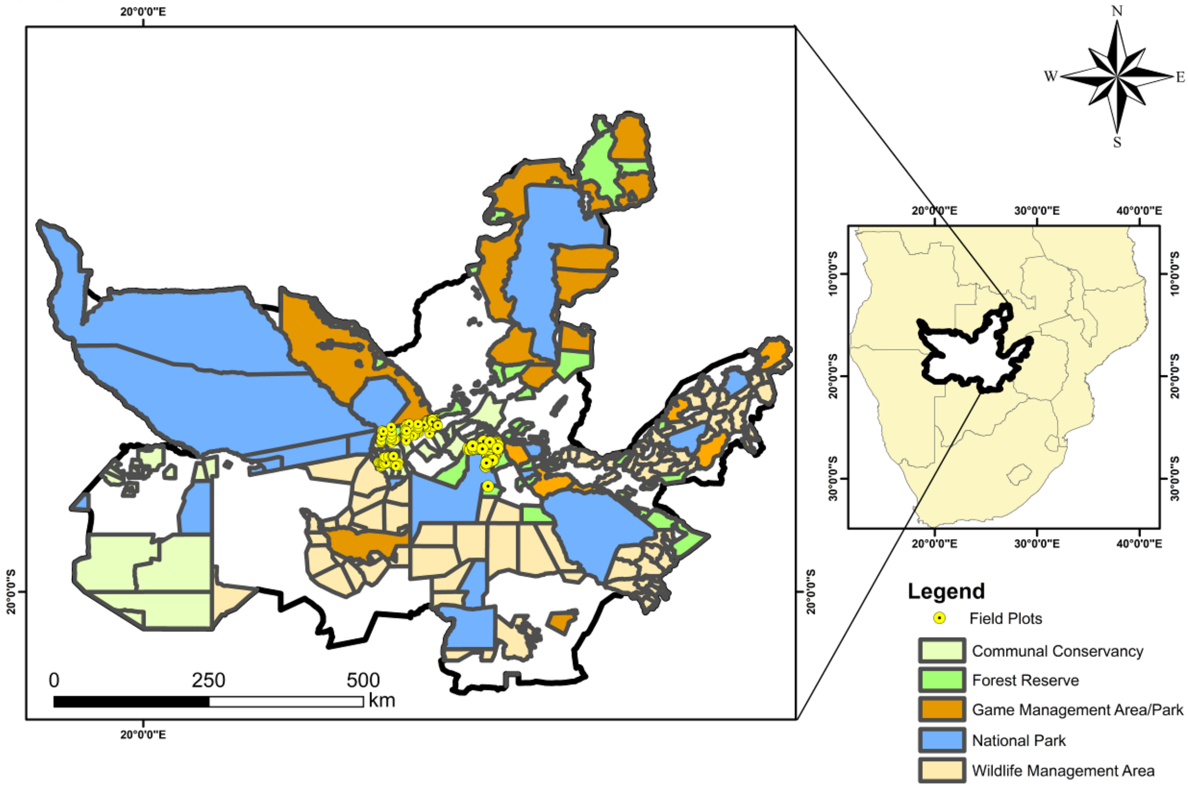

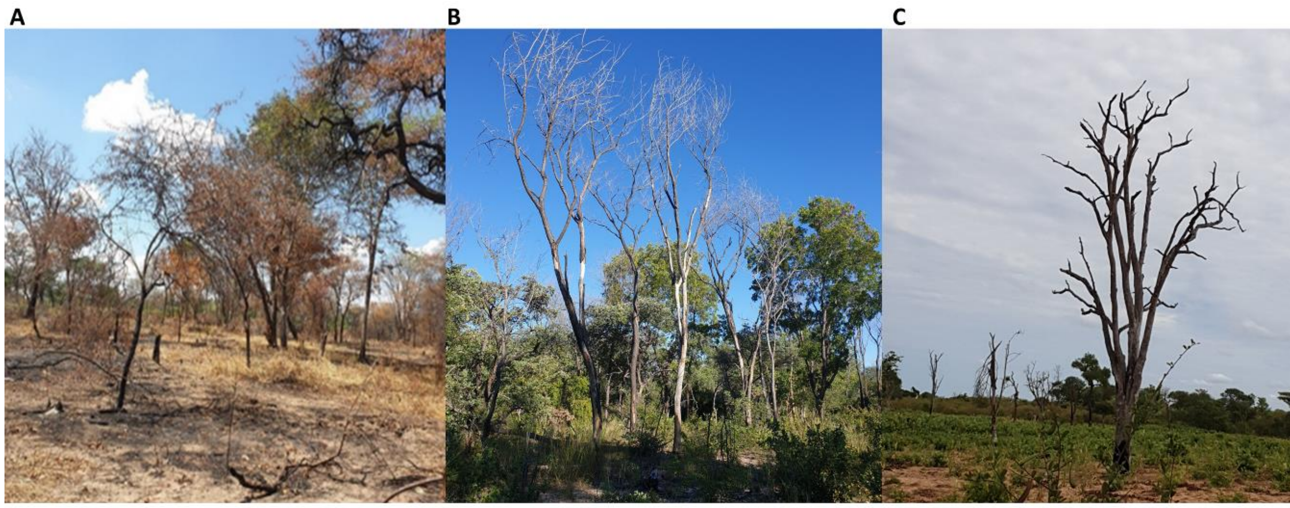

Fig. 5. 2. Location of the study area in KAZA Conservation Area Southern Africa, showing the yellow circles representing the sampling sites, protected areas and land management classes as designated by the World Database on Protected Areas (WDPA). Examples of sample plots representing degradation from fire captured during a field campaign in 2019 are shown, A) Burned Forest for cultivation near the protected area of Mudumu NP, Namibia, B) Forest scorched by wildfire with dead trees that could not recover in the Zambezi state forests (ST) C) forest or woodland burned down to create a field.

5.3.2 Fieldwork and Sampling Design

Field work was undertaken to measure forest stand characteristics from three locations with different land cover characteristics to provide ground validation in the KAZA region. The 2019 was one of the most severe droughts this century, which caused major impacts on vegetation and generated an economic shock felt throughout the region. Measurements were made in forests and woodlands, shrubland areas, and grassland agricultural land. One was located in Botswana, which is within the Chobe NP (18.7°S, 24.5°E). The other two site were located in Namibia, Mudumu NP and Zambezi ST (17.8° S, 23.9° E) (Fig. 5.2). These sites were chosen because dryland forests within and around the protected area have been particularly susceptible to disturbance and drought during the 21st century, with severe events in 2015 and 2019, warranting particular attention. For this reason, survey fieldwork was undertaken to record forest tree stand characteristics, and to observe the different land cover types present in the study area during the growing season (1st February - 30th May 2019). The 2019 was one of the most severe droughts this century, which caused major impacts on vegetation and generated an economic shock felt throughout the region. At each sample plot, and before the biophysical measurements, plot information such as land use, land cover, vegetation type, soil, and disturbance history (e.g., evidence of fire) was recorded (Fig 5.2). Also, information about regeneration, deadwood, and stumps was collected. Field sites were chosen to cover a range of landscapes given the constraints of road accessibility, wildlife danger, and public access restrictions allowed. Measurements were collected from a total of 250 individual sample plots. Field surveys of woody plants were conducted on sites where damage was specifically observed to identify sites where drought had an obvious impact. These sites can be used for further long-term monitoring.

5.3.3 Ground-based Climate Data

5.3.3.1 Rainfall Data

The climate in the region is considered subtropical with an annual rainfall of about 600-700 mm, dry winters, and hot, wet summers (Fig. 5.3 and 4). The daily and monthly rainfall data values recorded at Kasane and Kavimba have been used in this study (Table 5.1). The data set spans a period of 60 years from 1960 to 2019/20 from Kasane meteorological gauging station, and a period of 46 years from 1971 to 2017 for Kavimba meteorological police gauging station. The Kasane meteorological station data have a consistent and longer record and so was used in this study. All the rainfall observation data were from the Botswana Department of Meteorological Service (BDMS) Data Network.

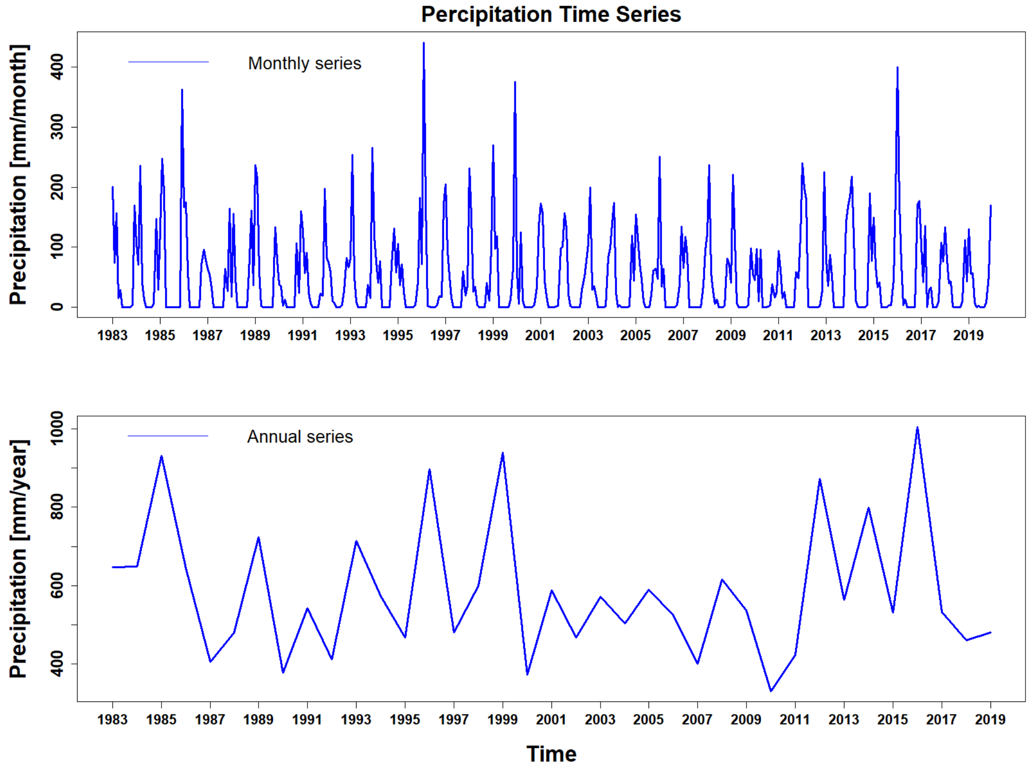

Fig. 5. 3. Monthly (top) and annual (bottom) precipitation (mm) for the period 1983 to 2019 using data obtained from Kasane meteorological station in Botswana.

5.3.3.2 Temperature Data

Monthly meteorological data (minimum and maximum temperature) were acquired from BDMS. A long record of temperature data was obtained from Kasane and Pandamatenga meteorological stations. The temperature data from the Kasane meteorological station is used in this study because it has a longer timespan covering 38 years from 1982/3 to 2019/20, compared to Pandamatenga meteorological station which is continuous only since 1989 (Table 5.1).

The climograph in Fig. 5.4 shows that rains in the region are expected in November, peaking in January and February and ending around March. These are warm summer months, with temperatures and humidity high. January averages the highest amount of precipitation and October observes the highest temperature.

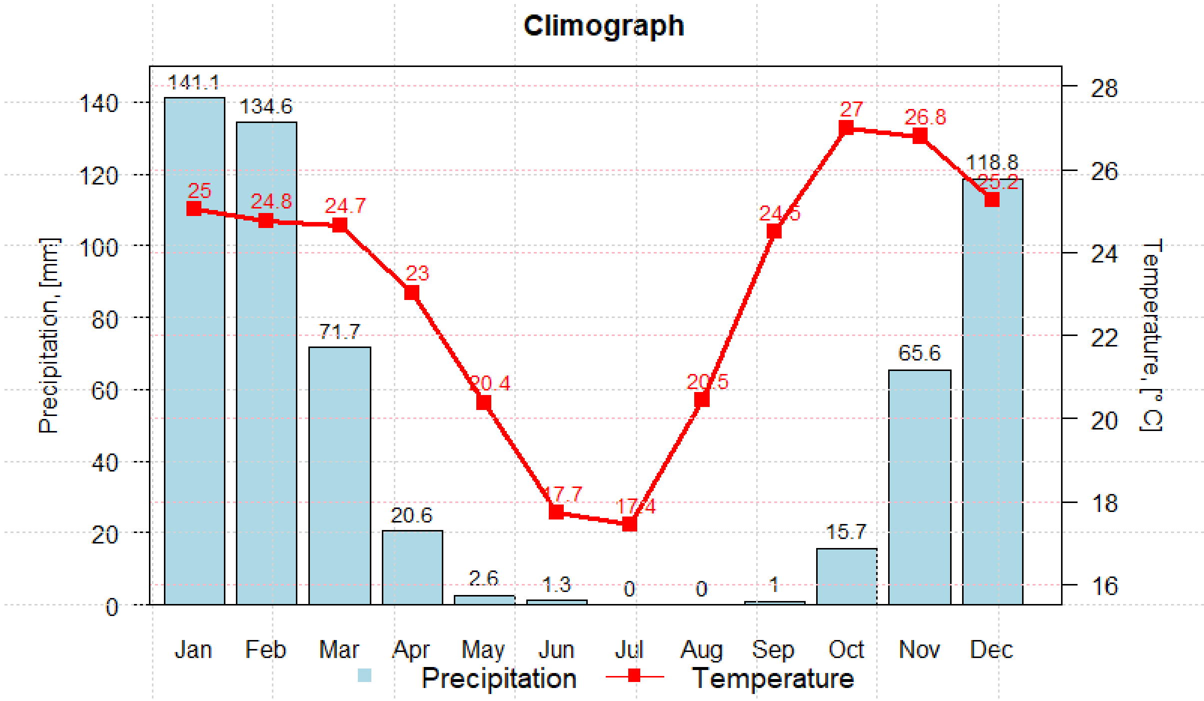

Fig. 5. 4. Climograph of average monthly precipitation and temperature from 1983 to 2019 using data obtained from Kasane meteorological station in Botswana.

Table 5. 1. Weather stations in the study area.

Station Name	**Data Type**	**Data Span**	**Data length**
Kasane	Precipitation	1960 to 2019/20	60
Kavimba	Precipitation	1971 to 2017	46
Kasane	Max and Min Temperature	1982/3-2019/20	38
Pandamatenga	Max and Min Temperature	1989-2020	31

5.3.4 Remote sensing based rainfall - Climate Hazards Group Infrared Precipitation with Station Data (CHIRPS)

The characteristics of the main satellite-based data used in this study is shown in Table 5.2. Drought monitoring has been historically carried out using ground-based observations (Chen et al., 2002). However, many regions do not have adequate gauge instruments, particularly in Africa (e.g., remote regions or agricultural areas) to obtain detailed precipitation, temperature, relative humidity and wind speed data, necessary for accurate assessment of drought (Washington-Allen et al., 2006). Furthermore, gauge (point) data do not capture the spatial variability of drought events. Satellite measurements overcome the limitations of gauge-based meteorological observation through continuous spatial observation that allows drought conditions to be determined where gauge sampling is otherwise unavailable. Often satellite-only rainfall estimates are merged with gauge-based observations for calibration and validation. This results in merged data sets, which exploit the strengths of each of the data source, and so improve the overall quality of key environmental variables (Xie et al., 1995).

Climate Hazards Group Infrared Precipitation (CHIRP) with Station Data (CHIRPS) is a recently-developed, high-resolution, daily, pentadal, decadal, and monthly precipitation dataset, from 1981 to near present. It was created by the US Geological Survey (USGS) Earth Resources Observation and Science (EROS) Centre, with collaborators at the University of California, Santa Barbara, Climate Hazards Group (Funk et al., 2015a). It was developed for drought early warning and environmental monitoring to support the Famine Early Warning Systems Network (FEWS-NET). It was produced by blending a set of satellite-only precipitation estimates with monthly and pentadal station observations. The CHIRP is based on infrared cold cloud duration (CCD) estimates calibrated with the Tropical Rainfall Measuring Mission Multi-Satellite Precipitation Analysis v.7 (TMPA 3B42 v.7) and the Climate Hazards Group Precipitation Climatology (CHPclim). The estimates are available at a resolution of 0.05° × 0.05° resolution, or at a coarser resolution of 0.25° × 0.25° (Funk et al., 2015). The fine resolution 0.05° × 0.05° dataset was used in this study.

5.3.5 Root Soil Moisture (GLEAM)

GLEAM stands for Global Land Evaporation Amsterdam Model, and is designed to estimate land surface evaporation and root-zone soil moisture from satellite observations and re-analysis data (Miralles et al., 2011). The potential evaporation is computed from surface net radiation and near-surface air temperature data using a Priestley & Taylor equation. The root-zone soil moisture (SMroot) is calculated using a multi-layer running water balance model, which combines observed precipitation and soil moisture observations (Martens et al., 2017). GLEAM v3.3b provides global monthly potential and actual evaporation, evaporative stress conditions and root zone soil moisture spanning the approximately 18-year period between 2003–2020 at a spatial resolution of 0.25°. The vegetation fractional cover in v3.5b comes from MOD44B and uses the latest version of CERES radiation (v4.1), AIRS temperature (v7.0), MSWEP precipitation (v2.8), and ESA-CCI soil moisture (v5.3) (Martens et al., 2017). GLEAM datasets have already been comprehensively evaluated and used for multiple drought analysis and monitoring applications (Peng et al., 2019; Vicente-Serrano et al., 2018). For this study, the GLEAM root zone soil moisture was used. GLEAM datasets are openly available globally at daily temporal resolution and 0.25° spatial resolution for 1980–2019 (https://www.gleam.eu/#downloads/(accessed 10 July 2020).

5.3.6 Vegetation Indices from Remote Sensing Imagery

Vegetation indices uses vegetation reflectance in the near and shortwave infrared regions for reducing the effects of irradiance and exposure, and enhancing the contrast between vegetation and the ground (Xue et al., 2017). NDVI has been widely used in many studies to monitor drought impacts on vegetation and forests, predict agricultural production, assist in hazardous fire zone prediction, and to map desert encroachment which defines the vegetation growth status (Anyamba et al., 2005; Myneni et al., 1997; Xulu et al., 2018). The NDVI was used in this study because it is a biophysical parameter that correlates with the photosynthetic activity of vegetation and is an indicator of the greenness of the biomes (Robinson et al., 2017; Tucker, 1979). NDVI is also able to offer valuable information to monitor vegetation health, drought effects, changes in plant growth, land degradation, deforestation, change detection/monitoring, and in relating large-scale inter-annual variations in vegetation to climate (Smith et al., 2019). As shown in Eq. 5.1, vegetation reflectance is at a minimum in the visible (red) part of the electromagnetic spectrum due to absorption of radiation by chlorophyll pigments, whereas maximum reflection is in the Near Infra-Red (NIR) spectral region owing to refraction of radiation by leaf cellular structure. The NDVI index outputs values range between -1.0 and 1.0, and has been shown to correlate well with leaf area index (LAI), and fraction of photosynthetically active radiation absorbed by vegetation (fAPAR) (Fensholt et al., 2004; Tucker, 1979). Negative values are mostly due to clouds, snow, water, and values near zero are generally generated from rock and bare soil. Lower NDVI values often correspond to stressed or sparse vegetation. Shrubs and grasslands have moderate values (0.2 to 0.5) and high values (0.5 to 0.8) are typical of healthy vegetation with different densities. I analysed the NDVI patterns during the growing season (January – March) using 2002 to 2019 time series data from the MODIS (MYD09A1.006) 8-day product, with a 500 m spatial resolution.

$$\mathrm{NDVI} = \frac{NIR - Red}{NIR + Red} \qquad \text{(Eq. 5. 1)}$$

where NIR is the near infrared range of the electromagnetic spectrum (841–876 nm) and RED is the red spectrum of the electromagnetic spectrum (620–670 nm), respectively, as measured by the MODIS sensor.

5.3.7 Product of burnt area MODIS MCD64A1

Satellite-based strategies for large-area burn assessment may rely on two types of remote sensing data including postfire reflectance images and active fires and can be used in combination or separately (Fraser et al. 2000). So, this study used Burned Area Products of 500 m spatial resolution for analysing spatial dynamics of burned areas and FIRMS Active Fire Products was used for seasonal temporal variations. This is because Active Fire Products are unable to estimate burned areas with an acceptable degree of accuracy due to coarse resolution of 1 km spatial resolution, and untrivial spatial and temporal sampling issues as stated by Giglio et al. (2006b). The burnt area data were obtained from the MODIS burnt area sensor monthly product MCD64A1 v.6, and was accessed via Google Earth Engine (GEE). MCD64 (Giglio et al., 2009) is the latest product from the MODIS Burnt Area product, and was updated as reported in Giglio et al., (2018). This is a global grid-level 3 product at 500 m spatial resolution containing per-pixel burnt-area and quality information. It is based on an automated hybrid approach that employs 500 m surface reflectance imagery coupled with 1 km MODIS active fire observations. The algorithm applies dynamic thresholds to composite images generated from a burn sensitive vegetation index, which in turn are derived from MODIS shortwave infrared surface reflectance band 5 and 7, and a measure of temporal texture (Giglio et al., 2016). Data layers include a recording of burn date, data uncertainty, quality assurance and the first and last day of reliable change in the year. The date on which the burn occurred with values assigned to unburnt land pixels is encoded in a single data layer as the ordinal day of the calendar year. The data layer also contains additional values reserved for missing data and water grid cells. Overall, the MCD64A1 has improved the detection of burnt areas, provides better detection of small fires and has proven adaptability to different regional conditions in multiple ecosystems.

5.3.8 MODIS MCD14ML Active Fire Product

Fire point location were obtained from the Aqua & Terra MODIS wildland fire data, with a spatial resolution of 1 km, Collection 6, from January 2002 to December 2019, available from the NASA Fire Information for Resource Management System (FIRMS) at https://firms.modaps.eosdis.nasa.gov/download/ (accessed 21 March 2020). The data have a 1-day temporal resolution, and the location of the fire nominally corresponds to the centre of a 1x1 km pixel, signalled by the algorithm as containing one or more fires within that pixel. A full description of the algorithms used to acquire the data can be found in Davies et al. (2008). FIRMS was developed to provide a simpler and faster means to obtain MODIS active fire locations and expand the distribution of MODIS fire data to a broader range of fire and forest monitoring organisations around the world. In this study, active fire products were used to determine fire seasons by determining the months when fire activity is very high. The fire seasons were determined from the cumulative ratio of active fires on a regional scale detected during each month across the seventeen years of observation (2002-2019) and the proportion of this number to the overall number of fires. FIRMS is an extension to the MODIS Rapid Response (MRR) system for near-real-time active fire information in a format that is easy to use, and for users that could not handle image files (Ilavajhala et al., 2014).

Table 5. 2. Characteristics of the main datasets used in this study.

Dataset	*Timespan*	*Resolution*	*Source*
Climate Data			
Climate Hazards Group InfraRed Precipitation with Station Data (CHIRPS)	*2002-2019*	*0.05 degrees*	*GEE*
High resolution Standardised Precipitation Evapotranspiration Index (SPEI) dataset for Africa	*2002-2016*	*5 km*	*CHIRPS and GLEAM*
The Global Land Evaporation Amsterdam Model (GLEAM v3.3b)	*2003-2019*	*0.25° x 0.25°*	*GLEAM*
Rainfall Data	*1975-2020*	-	*Botswana department of Meteorological Service (BDMS)*
Minimum and Maximum Temperature Data	*1983-2020*	-	*Botswana department of Meteorological Service (BDMS)*
Vegetation Data			
MODIS 8-day time series (MOD13Q1)	*2002-2020*	*250m*	*GEE (MODIS09, 2020).*
MODIS Terra Surface Reflectance 8-Day Global 500m (MOD09A1.006) and (MYD09A1.006)	*2002-2019*	*500m*	*GEE (MODIS09, 2020).*
Fire Data			

MODIS burnt area (MCD64A1)	*2002-2019*	*500m*	*GEE (MODIS09, 2020).*
MODIS wildland fire point data	*2002-2019*	*500m*	*FIRMS*

5.4 Methods

5.4.1 Calculating the standardised precipitation evapotranspiration index (SPEI) from ground observation

Satellite-based drought indices are capable of characterising spatial and temporal variability of drought based on the magnitude, duration, and intensity, and so they represent promising tools for monitoring drought at regional scales, which is important for developing a drought watch system for an area. A variety of drought indices have been developed to quantify whether or not a region is experiencing a drought, and to categorise the seriousness of that drought. Dryness severity was quantified using the multiscalar Standardised Precipitation Evapotranspiration Index (SPEI), calculated from ground meteorological data (rainfall and precipitation) from the Kasane meteorological station. Drought severity is predominantly caused by either precipitation decreases or increases in temperature induced evapotranspiration. Hence, precipitation does not represent the only control on ecologically and socially relevant water resources, such as stream flow, reservoir storage, and soil moisture (Cook et al. 2004). SPEI is used to measure environmental water stress by combining information from both evaporation and precipitation. The SPEI is a drought indicator that determines deviations from a location's average water balance (the ratio of temperature and precipitation) over a specified timeframe which is then fitted to a statistical distribution (Vicente-Serrano et al. 2012). The SPEI was quantified based on the Hargreaves equation (Hargreaves, 1994) using the 'SPEI' package (Bergueria et al., 2014) in the R software package. Due to the complex computation of Potential Evapotranspiration (PET), which involves several variables, including surface temperature, air humidity, soil, incoming radiation, water vapour pressure, and ground–atmosphere latent and sensible heat fluxes, this study made use of Hagreaves' and Samani's temperature-based method for PET estimation. The Hargreaves approach has the advantage of only requiring data on monthly mean minimum and maximum temperatures.

The SPEI was chosen over the commonly used Standardised Precipitation Index (SPI) because it includes PET as well as precipitation (Stagge et al. 2014). PET is the amount of evapotranspiration that could occur if enough water were available (Oudin et al. 2005). For example, Dutrieux et al., (2015) used SPI and they found it to perform poorly in tropical dry forest and concluded SPI was not the ideal way to include moisture conditions in the dryland environment. Limitations of SPI, which considers rainfall anomalies alone without including evaporative demand have also been discussed by Trenberth et al. (2014). The SPEI is calculated based on the accumulated difference between precipitation (P) and temperature used to compute potential evapotranspiration (PET). The SPEI can comprehensively reflect the change in surface water balance, hence automatically capturing the well-known temporal lag of vegetation response to rainfall (Stagge et al. 2014; Potop et al., 2014). Since SPEI is a standardised variable it can be used to compare droughts over different spatial and temporal scales. SPEI produces a graph with values ranging from 2 to -2 (Table 5.3).

This study places emphasis on moderate to extreme droughts and the SPEI index scale is given as: extreme drought (≤-2); severe drought (−2 to −1.5); and, moderate drought (−1.5 to −1). A continuously negative SPEI generally implies an abnormally drier climate/drought period based on intensity, severity, magnitude, and duration, while positive values correspond to abnormally wet periods. It should be noted that drought ends when the SPI/SPEI approaches zero and progresses to a positive value. For this study, the duration of the drought is considered as the number of months for which the drought has occurred, whilst the magnitude of the indices indicates the severity of the drought. Vegetation has been found predominantly responsive to short-term drought time scales, hence 1, 3 and 12 months were determined as an appropriate time scales for contextualizing meteorological, vegetation/crop and hydrological drought on vegetation (Vicente-Serrano et al. 2012). Two data periods were used in the SPEI analysis. The 1983–2019 period was used as the baseline period based on availability of the high-quality observed data for temperature and rainfall. The 2002-2019 time period was used in SPEI analysis to investigate sensitivity of the vegetation to drought events.

Table 5. 3. Categories of dry and wet conditions indicated by SPEI values.

SPEI	Category
2 and above	Extremely wet
1.5 to 1.99	Very wet
1.0 to 1.49	Moderately wet
−0.99 to 0.99	Near Normal
−1.0 to −1.49	Moderately dry
−1.5 to −1.99	Severely dry
−2 and less	Extremely dry

5.4.2 Calculation of the satellite-based aridity index (AI)

The degree of dryness is not determined by precipitation alone. If the temperature is high/low, evaporation is either large or small. Therefore, the degree of dryness is normally expressed as the ratio of PET and precipitation, giving the aridity index, which is an important indicator of regional climate. The study adopted the aridity index (AI) recommended by the United Nations Educational, Scientific and Cultural Organisation (UNESCO), the Global Environment Monitoring System (GEMS), the Global Resource Information Database (GRID), and the Desert Cure and Prevention Activity Centre (DC/PAS), to reflect the aridity changes of the KAZA region. The AI was calculated using the following form (Eq. 5.2).

$$AI = \frac{PRE}{PET} \qquad \text{(Eq. 5. 2)}$$

where PET is the Potential Evapotranspiration (in mm) and PRE is the precipitation (in mm). The aridity index (AI) has been widely used to divide climate zones and to assess changes in aridity trends. Under this quantitative indicator, drylands are defined as regions with AI < 0.65 and are further divided into subtypes of: hyper-arid (AI < 0.03); arid (0.03 ≤ AI < 0.2); semiarid (0.2 ≤ AI < 0.5); dry subhumid (0.5 ≤ AI < 0.65); and, humid (AI > 0.65) regions, as shown in Table 5.4 (Middleton et al., 1997).

AI was calculated using the MODIS data products MOD16A2 v.6 Evapotranspiration/Latent Heat Flux product, which is an 8-day composite product produced at 500 m resolution. The algorithm used for the MOD16A2 product is based on the logic of the Penman-Monteith equation, which includes inputs of daily meteorological reanalysis data along with MODIS data on vegetation property dynamics, albedo, and land cover. The pixel values for the PET layer are the sum of all values in the 8 days within the composite period.

Table 5. 4. UNESCO (1979) aridity classification and bioclimatic index thresholds

Threshold	$0.03 \leq AI < 0.2$	$0.2 \leq AI < 0.5$	$0.5 \leq AI < 0.65$	$AI > 0.65$	$AI > 0.75$
Arid conditions	*Arid*	*Semi-arid*	*Dry sub-humid*	*Humid*	
Desertification risk	*Risk*				*No risk*

5.4.3 Evaluation Criteria

Most of the currently employed indexes in climate and drought regionalisation reflect meteorological variables, without taking the diversity of landscape (such as soil condition) into consideration. Therefore, a single index is insufficient for a nationwide drought regionalisation program. In this respect, the regionalisation indexes presented above that can be used to reflect climate wetness and assess agricultural and plant droughts were developed. The SPEI at fine spatial resolution based on CHIRPS and GLEAM v3 (root zone soil moisture) is compared temporally and spatially to the CHIRPS precipitation dataset. In addition, the NDVI can also serve as an indicator for drought and vegetation health and was used to assess the performance of drought indices (Vicente-Serrano et al., 2013; Aadhar and Mishra, 2017). Furthermore, root zone soil moisture is an ideal hydrological variable for plant (soil moisture) drought monitoring.

A critical issue for identifying and quantifying droughts is the local historic climatic distribution (i.e., what is ‘‘normal’’?). The sample size must be large enough to guarantee that sample statistics are reasonable approximations of the corresponding population parameter (Maliva et al., 2012). For a region to receive its long-term average annual precipitation in a year should be a rare event; most years will be either wetter or drier than the mean or median. To facilitate direct comparison between SPEI, precipitation, NDVI and RSM, both precipitation, NDVI and RSM are standardised by subtracting their corresponding (2002–2019) mean and are expressed as the resulting anomalies in terms of numbers of standard deviations (Eq. 5.3). The monthly and seasonal standardised anomalies (*std. anomaly*) for vegetation and climate parameters were computed using Eq. 5.3, below

$$\text{std.anomaly} = \frac{x_i - \bar{\bar{x}}}{\delta} \qquad \text{(Eq. 5. 3)}$$

where x_i is the value of NDVI/climate at a particular time (month/season), $\bar{\bar{x}}$ and δ are the average (monthly/seasonal) and standard deviation (monthly/seasonal), respectively, over the study time period, 2002-2019. This standardisation has been applied by many studies to evaluate drought indices (e.g., Anderson et al., 2011; Mu et al., 2013; Zhao et al., 2017).

5.5 Results

5.5.1 Temporal analyses drought and water stress

5.5.1.1 Drought index at different scales

To demonstrate the temporal variation of drought at different time scales (1, 3 and 12 months) for the study period (1982–2019) in the KAZA region, the SPEIs were generated and presented in Fig. 5.5. All three timescales had SPEI values close to the extreme drought level of -2 for the entire hydrological year of 2019. In general, the index data show the same pattern of variability for each timescale, with different durations and magnitudes of drought. Also, the frequency of occurrence of droughts was higher for the shorter, compared to the longer timescales; hence, the meteorological droughts (1-month) show the highest frequency of occurrence, followed by agricultural droughts (3-months), and lastly the hydrological droughts (12-months). The number of drought events observed at the 3- and 12-month time scales were 77, compared to 80 in the 1-month time scale (Supplementary, Table C 1). It takes a shorter time (at most 1-month) of prevailing water deficiency for a meteorological drought to develop, hence the high variability of droughts. However, at the longer timescales the drought lasts longer and the SPEI magnitude increases. The variability shows that at the 12-month timescale, SPEI was found to be of greater severity and magnitude compared to the 1- and 3-month timescales. The SPEI event with the greatest magnitude at the 12-month scale was found in 2019 with the SPEI value >2.5 (Fig. 5.5).

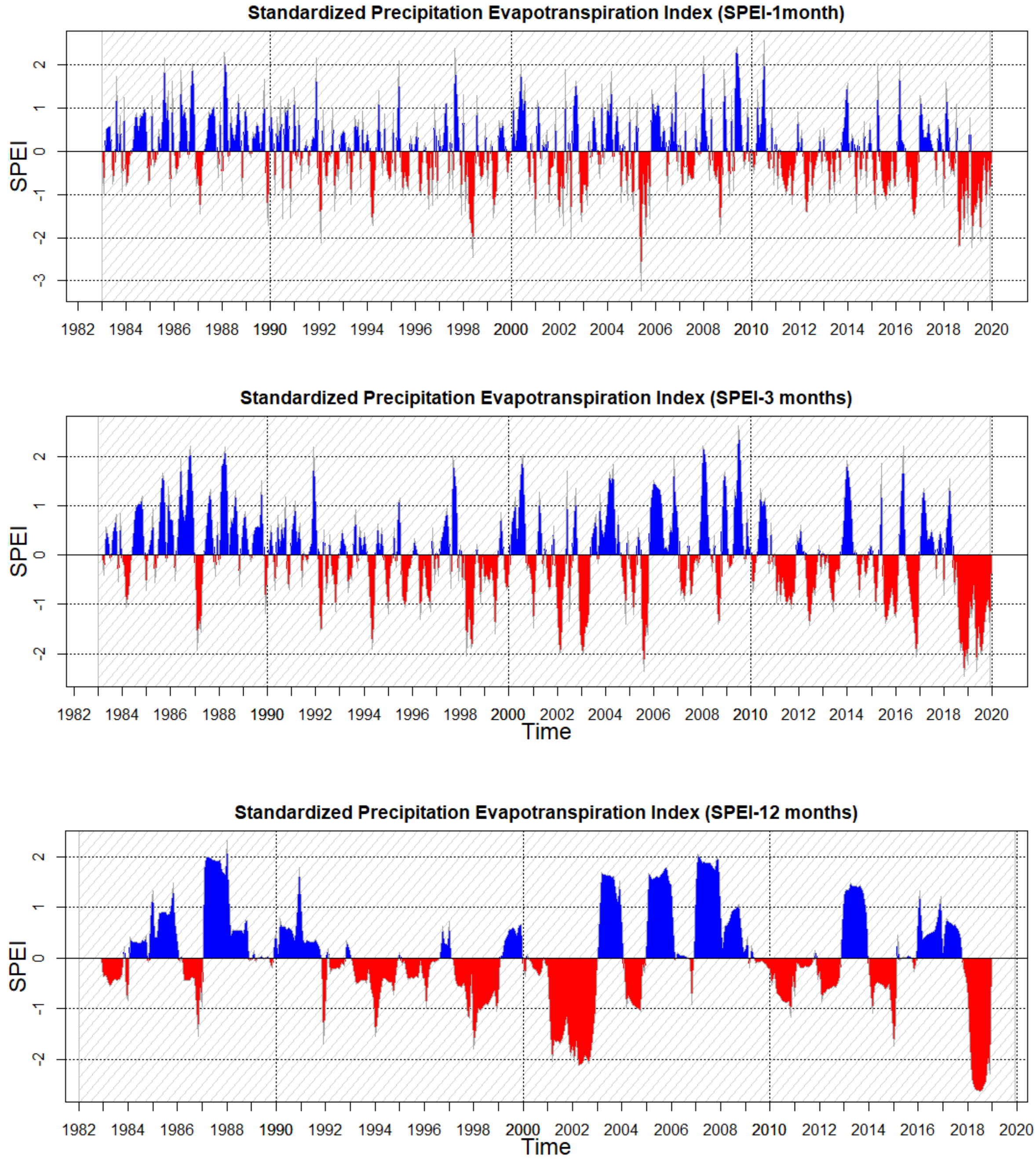

Fig. 5. 5. SPEI for 37 years calculated from ground precipitation and temperature at different timescales. SPEI index scale is given as, extreme drought (≤-2), severe drought (−2 to −1.5) and moderate drought (−1.5 to −1).

Given that it takes up to 3 months for most vegetation to be fully developed, a water deficiency accumulation of at least 3 months during the growing season will adversely impact vegetation and crop yields, thus quickly developing into an agricultural drought. On the other hand, a longer period of water deficit accumulation or depletion of water storage in rivers and reservoirs is required for a hydrological drought to occur. Fig. 5.6 shows the number of droughts per year at a time scale of 3 months, including the drought categories. For the period under observation (1983–2019), drought was more extreme in 1998/1999, 2002/2003, 2005, 2015/2016 and 2018/2019. Severe drought was also observed in 1987, 1992, 1994, and 1999. The SPEIs calculated for 2019 show the worst drought and accompanying effects on crops and vegetation ever recorded over the Southern African region.

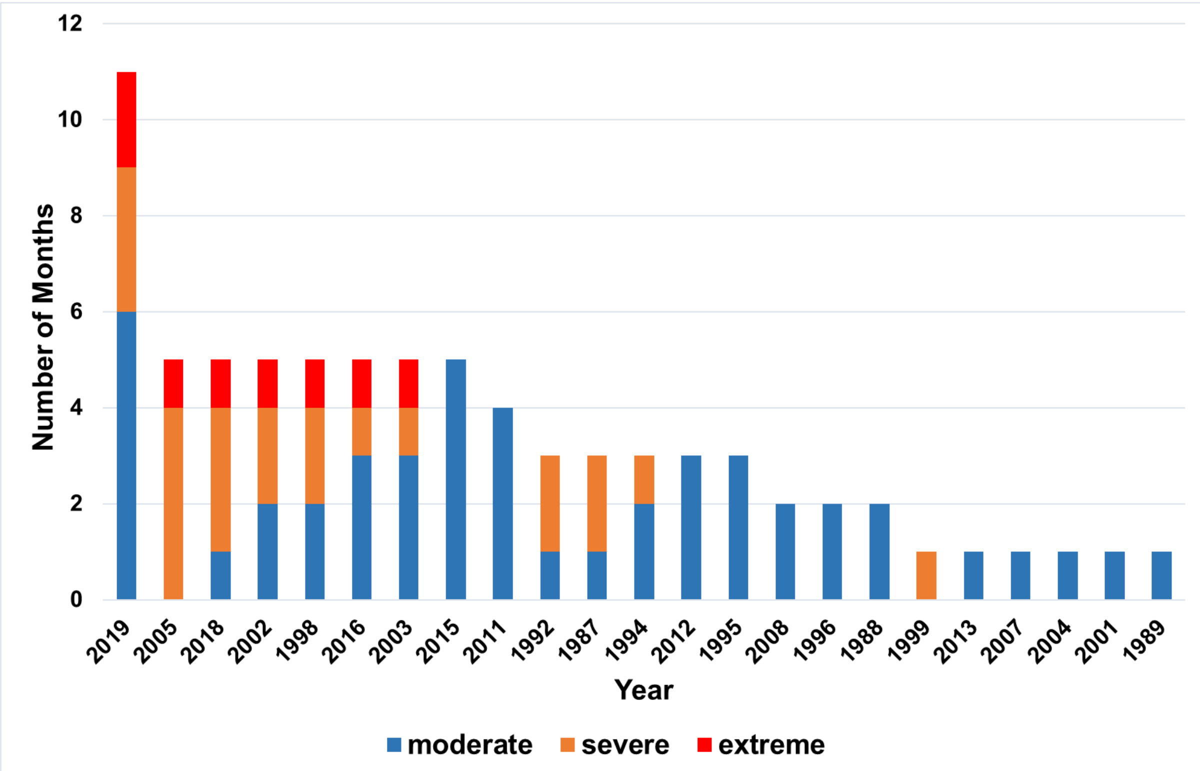

Fig. 5. 6. Number of drought events for the years that experienced droughts in the period of 1983 to 2019 using a 3-month time scale, ranked by number of drought months.

5.5.1.2 Drought index, precipitation and vegetation relationship

To contextualise the drought impacts on vegetation, the 3-month SPEI, precipitation from the ground station, and monthly NDVI values of a forested area between 2002 and 2019 were plotted to determine the interplay between vegetation and climate variability. Monthly NDVI varied closely as a function of rainfall distribution, as shown in Fig. 5.7. Low NDVI values appear to coincide with large drops in SPEI and these correspond to abnormally dry years as shown in the graph of precipitation. The lowest NDVI range was recorded in 2002-2003, 2005, 2010/2012, 2015/2016, and 2019, corresponding to the low rainfall values and drought years, visible in the SPEI data. Similarly, the highest NDVI was observed in 2004, 2006, 2008 /2009, and 2017, which are associated with good rainfall in the growing season. The SPEI values show that 2019 experienced extreme drought with a negative anomaly from the mean conditions reaching the level of -2, and this corresponds with reduced NDVI and rainfall levels.

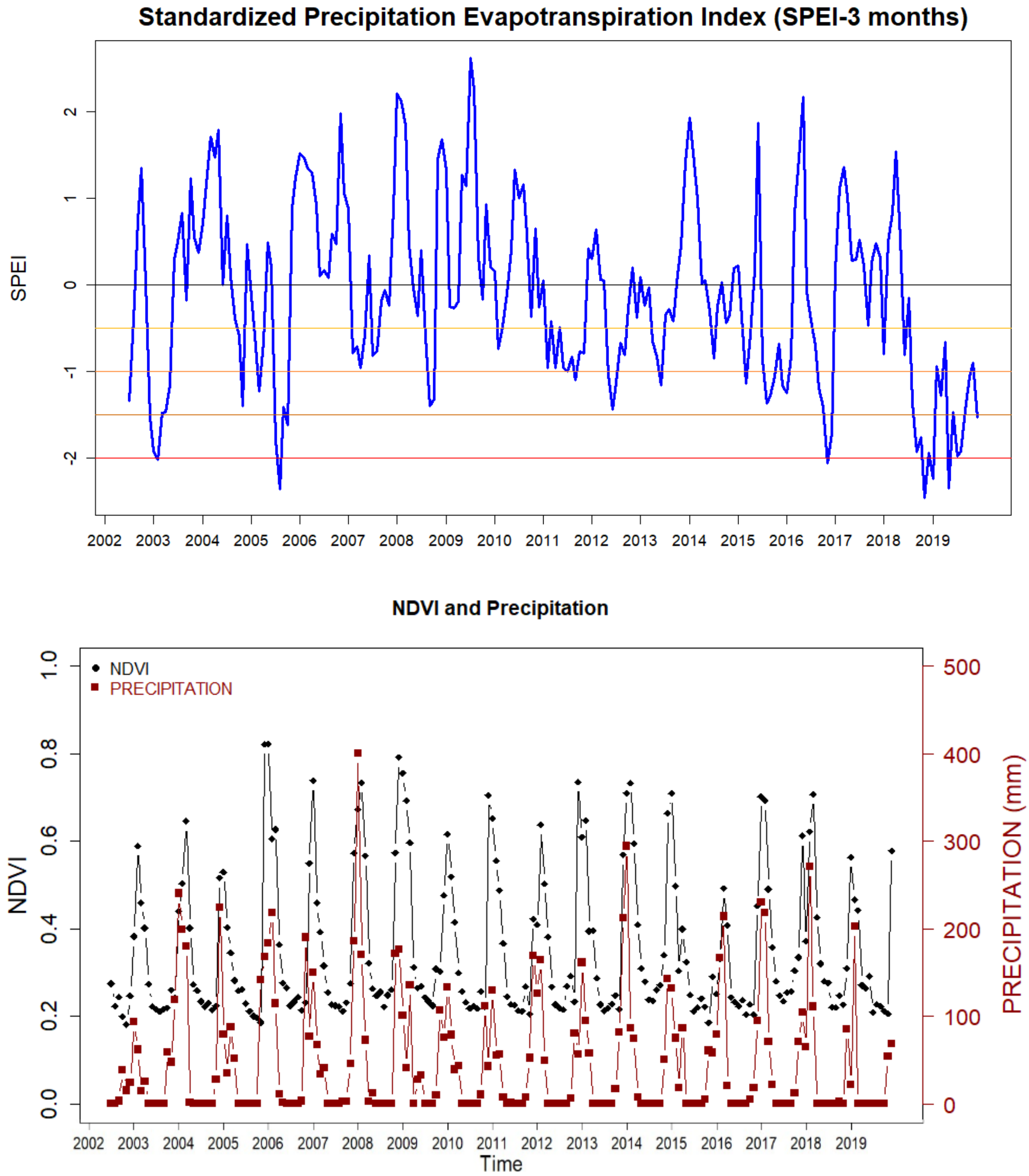

Fig. 5. 7. Top: SPEI from 2002 through 2019 calculated from ground precipitation and temperature at 3 months timescales. SPEI index scale is given as, extreme drought (≤-2),

severe drought (−2 to −1.5), and moderate drought (−1.5 to −1). The different vertical line colours represent the drought scale (yellow colour shows mild drought and red colour shows extreme drought). Bottom: Temporal variation of the NDVI (black circles) and inverted monthly precipitation from ground station data (red squares) from 2002 through 2019.

5.5.2 Spatial analyses of drought and water stress on vegetation

The precipitation, SPEI and RSM dataset are compared with NDVI to gain more insight into their significance, and to assess which climatic variables explain spatial patterns of forest and vegetation in this region. Fig. 5.8 shows the results of the spatial and temporal comparison from 2010 to 2019 for NDVI, precipitation, and RSM. Noter that SPEI maps end in 2016 due to lack of data availability. In general, these four variables reflect a progressive dry-out during the events from 2010-2019. The period between 2010 to 2019 was chosen because it is the period with more years experiencing severe drought events. For example, a severe drought is revealed by the SPEI in 2012, with values < −1, mostly in the west of the KAZA region, coinciding with a decline in NDVI in this area. The drought of 2012 in western KAZA could be exacerbated by low rainfall values in 2011 which lead to a considerable decrease in RSM and SPEI values. However, in 2012, the eastern part of KAZA experienced an increase in vegetation cover, despite receiving less than average rainfall. The high NDVI in eastern KAZA corresponds to high RSM with values >1.5 in the same area, which can be attributed to high rainfall, wet conditions, as reflected in the in SPEI and high RSM values from 2011 in the eastern KAZA. In 2013, extremely low rainfall was recorded which is reflected by a severe drought in SPEI with values <-1.5 over almost the whole of the KAZA region. This drought resulted in a decreased vegetation productivity, although not as severely as the RSM which was still high for most parts of KAZA. In 2015, the entire KAZA region experienced extremely low precipitation, with a value <-1. This resulted in a strong and extreme drought, as shown by the SPEI and RSM, with extremely low values <-1.5 across >80% of KAZA. The 2015 drought event impacted vegetation in the region severely, with an NDVI value <-1 in >50% of KAZA. Precipitation returned to normal in 2016, which corresponds to the SPEI data, as there was no drought or dry condition experienced in 2016. However, the NDVI progressively declined through 2016, which is explained by RSM values <-1 across the whole of KAZA, despite precipitation and SPEI showing a different pattern.

The slight increase in NDVI values in northern KAZA corresponds to the very few areas with average RSM in 2016. The RSM reflected the main drought conditions that are shown also by negative values in NDVI, rather than rainfall or SPEI. The extreme drought of 2015-2016 is followed by a high level of precipitation in 2017 over almost the entirety of KAZA region, showing wet condition values of >1.5. This corresponds to an increase in NDVI and RSM over most of the region, although most dryland forest in northern and central KAZA remained negative. In 2019, the whole of the region received extremely low precipitation with values <1.5. This resulted in a distressing drought with extremely low RSM values coinciding with a decline in NDVI. The location of the maximum precipitation and RSM deficit is concentrated in the north and east of KAZA in both 2015 and 2019. While the wetter conditions were mostly concentrated in south of KAZA, where it is more arid with less dryland forest such as in 2014 and 2017. RSM was useful in explaining the spatial-temporal patterns of vegetation lag effects and revealing the cumulative effect of climate anomalies on vegetation conditions, that were not explained by precipitation or SPEI.

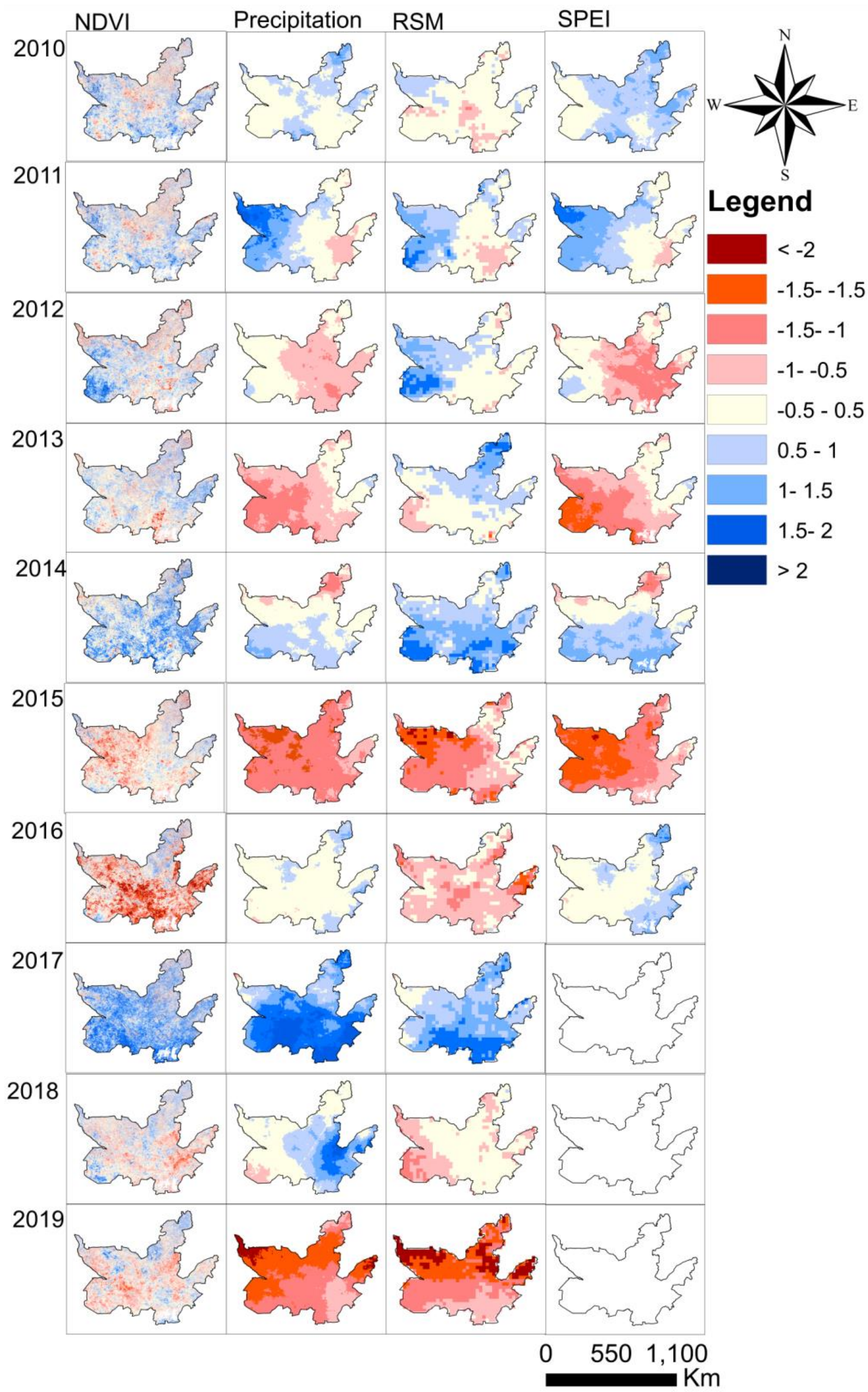

Fig. 5. 8. Spatial distribution of PRECIPITATION, NDVI, SPEI and RSM anomalies expressed as numbers of standard deviations sampled from the monthly data in the growing season from 2010 to 2019. Extreme droughts (≤-2), severe drought (−2 to −1.5) and moderate drought (−1.5 to −1), mild droughts (-1 to -0.5) and no drought (-0.5 to 0.5). The map shows the whole of KAZA region as represented by the study area in Fig. 5.2.

Comparisons of climate variables against the NDVI values show that reduced NDVI uniformly coincide with extremely high temperatures and with low precipitation. Similarly, low SPEI values (< -0.5) moisture coincides with low NDVI values (Fig. 5.9). SPEI values indicate that the drought event of 2019 was the worst with SPEI values falling below −1, followed by the drought event of 2015. The root soil moisture shows that the dry forest vegetation corresponds strongly to the drought events of 2019 and 2015, with both years experiencing the lowest root-soil moisture resulting in low NDVI values. In contrast, high NDVI values are captured for the year 2017 strongly responding to the high moisture availability as illustrated by the high value of precipitation, root soil moisture, and SPEI. The max and average temperature also show a sharp contrast of the drought years (2015 and 2019) and the wet years (2017 and 2014). The drought year (2019 and 2015) has the highest average and maximum temperatures, with low NDVI values coinciding with extremely high temperatures. On the other hand, the high NDVI values of wet years (2017 and 2014) correspond with the lowest average and maximum temperature. There is a lag observed in dryland vegetation productivity in some years following drought events such as 2016 and 2013, in which the NDVI remain very low despite an increase in precipitation and positive values in SPEI. The min temperature does not uniformly coincide with the NDVI deviation, with low NDVI values weakly responding to both low and high min temperatures (Fig. 5.9).

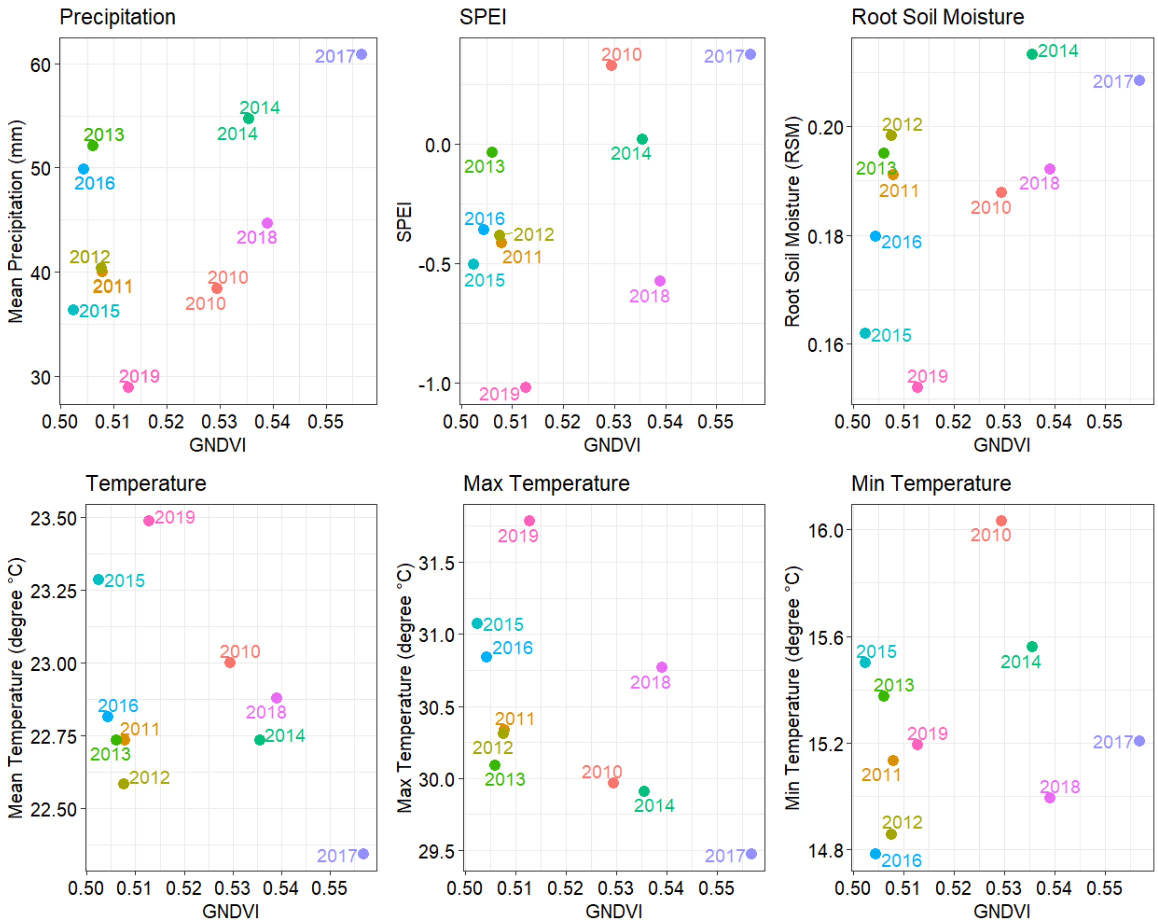

Fig. 5. 9. Association between climate variables and NDVI from the Kavango Zambezi region. The average daily mean, maximum temperatures, precipitation, SPEI and Root Soil Moisture were calculated from the monthly data in the growing season from 2010 to 2019.

The correlations of NDVI, precipitation, SPEI, root soil moisture, minimum temperature and maximum temperature are presented in Fig. 5.10. The NDVI shows a strong correlation with the root soil moisture (r = 0.66), highlighting the constraints imposed by root soil moisture deficit on dryland vegetation. The results also indicate a higher correlation between NDVI and SPEI (r = 0.58), as well as the NDVI and precipitation (r = 0.50), reaffirming the consistent mechanism of influence of drier conditions. The NDVI - maximum temperature correlation (r = -0.45) was also notable. The SPEI index showed a strong negative correlation with maximum temperature (r = -0.71), and a positive correlation with precipitation (r = 0.63).

Fig. 5. 10. Pearson's correlation of the NDVI, precipitation, SPEI, root soil moisture, minimum temperature and maximum temperature.

5.5.3 Temporal analyses of fire

5.5.3.1 Fire seasonality and extent

Fig. 5.11 shows the area burnt for each country in the KAZA region. Every year, between 110,173 km^2 (21%) and 203,849 km^2 (39%) of the land area in the KAZA region were burnt on an annual basis in the period 2002 to 2019. The year 2011 experienced the highest degree of burning with 203,849 km^2 (39%), followed by 2010 and 2012 with 177,493 km^2 (34%) and 184,186 km^2 (36%), respectively. The year 2019 experienced the lowest burning with only 110,173 km^2 (21%). In KAZA region, a mean 149,410 km^2 of land is burnt on an annual basis in the period 2002–2019. Most of this burnt area is situated in Angola and Zambia, with an average of 47,492 km^2 (32%; Angola) to 50,935 km^2 (35%; Zambia), respectively, of the land area burnt on an annual basis between 2002 and 2019 respectively. The average area burnt annually in Namibia, Botswana, and Zimbabwe was lower, varying between 23,806 km^2 (16%; Namibia), 19,554 km^2 (13%; Botswana) and 7,623 km^2 (5%; Zimbabwe), respectively (see supplementary: Fig. C. 1 and Table C 1).

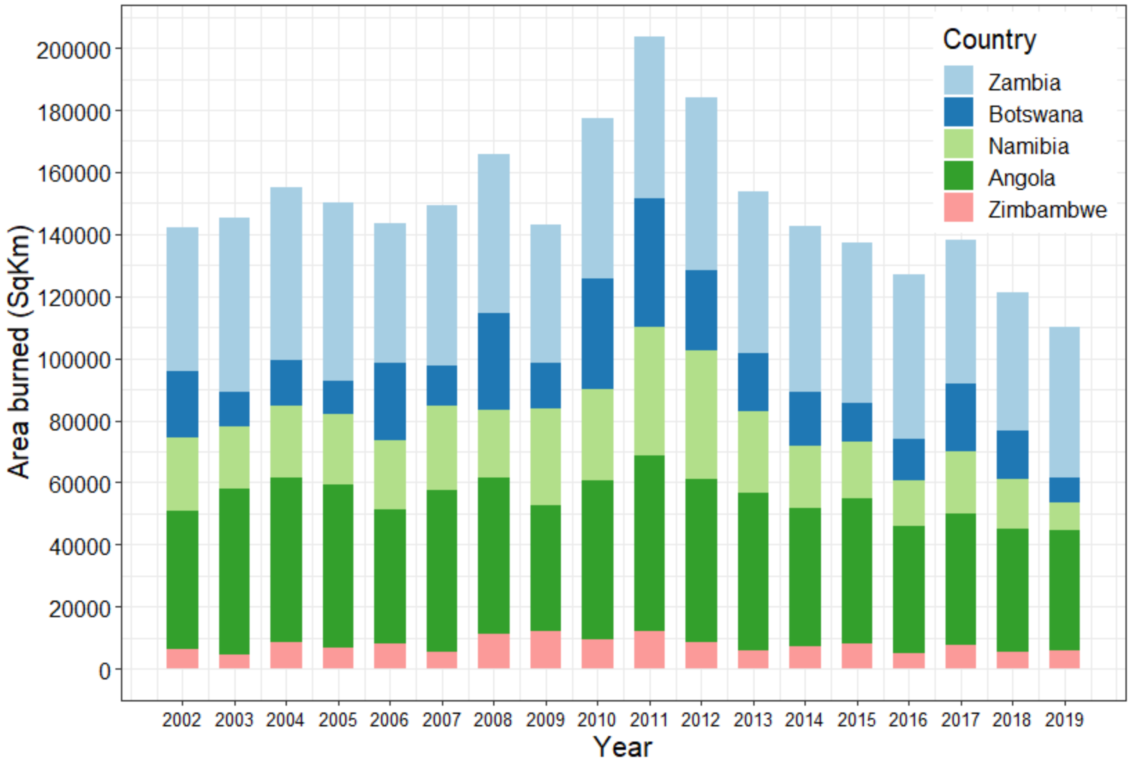

Fig. 5. 11. Total area burnt annually for each country of KAZA from 2002 to 2019 in km^2 based on the MODIS Burnt Area product data.

Fig. 5.12 shows the cumulative monthly seasonal distribution of fires in KAZA between 2002 to 2019, as determined from an analysis of the 1 km FIRMS fire activity data. The FIRMS data are reported to have considerable amount of uncertainty on individual fire number/size distribution. Therefore, FIRMS point data were used as complementary to MODIS burned data (Mouillot et al., 2014). Vegetation burning in the KAZA region occurs mainly in the dryland forests during the dry season between May to October each year. The highest degree of burning is experienced during the late dry season, with the months of August and September representing the peak months for fire incidences. More than 96% of the incidences are due to dry season fires from May to October. There is a relatively low level of fire incidences in the months of November, December, January, February, March and April (Fig. 5.12). Looking at burning incidences per individual country, Namibia, Botswana and Zimbabwe have the highest levels in September, while Zambia and Angola have the highest levels in August (see supplementary, Fig. C . 2). On a regional scale, August shows the highest burning rate followed by September because Zambia and Angola experience the highest burning incidences on an individual basis in comparison to the other three countries (Botswana, Namibia and Zimbabwe) combined, as shown below (Fig. 5.12).

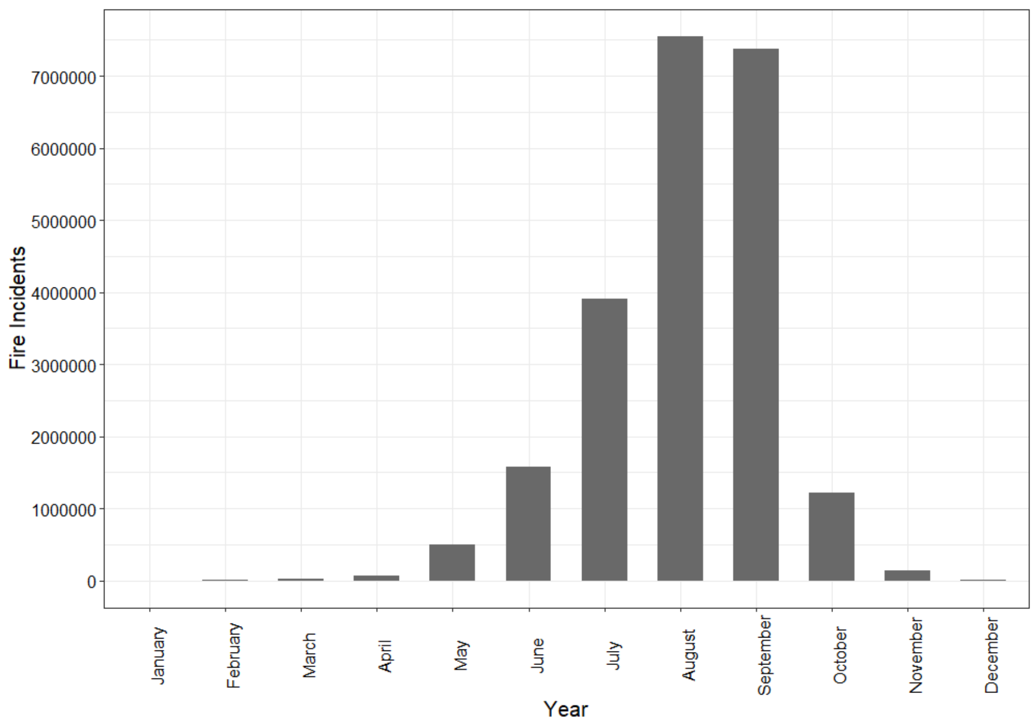

Fig. 5. 12. Cumulative monthly fire incidences for the whole of KAZA from 2002 to 2019 using FIRMS fire activity data.

5.5.4 Spatial analyses of fire seasonality and extent

Fig. 5.13 shows comparison between the fires burnt in September in drought and wet years. Data from the month of September are used because it represents the peak month for fire incidences in most of the KAZA countries. Spatial analysis indicates that the years with extreme drought, including 2002, 2005, 2015 and 2019, experience the lowest extent of area burnt as compared to normal and wet and less drought affected years. The burnt area was greatest in the wet years of 2004, 2006, 2008-2010 and 2017, and in the very low drought years (2011 to

2013) for all the five countries in the study area, and most of the burnt area is situated within National Parks. As shown in Fig. 5.13, the Chobe NP has no fire incidences during the drought years, but fire intensified in the normal/wet years. It can be noted that the northeastern section of Chobe NP (near Kasane Forest Reserve) is more prone to fire than the north and southern part of the park. The national parks including Chobe NP, Mudumu NP, Sioma Ngwesi NP and Luengue-Luiana NP and Kafue NP are more vulnerable to fires in wet years as compared to drought years. The Nxai Pan NP and Makgaikgadi Pans NP of Botswana and Hangwe NP of Zimbabwe has little to no fire incidence in most years. The National Parks in Angola, Zambia, and Namibia including Sioma Ngwesi NP and Luengue-Luiana NP, Kafue NP and Mudumu NP experience severe burning in both dry and wet years, even though the national parks are more vulnerable to fire in wet years as compared to drought years.

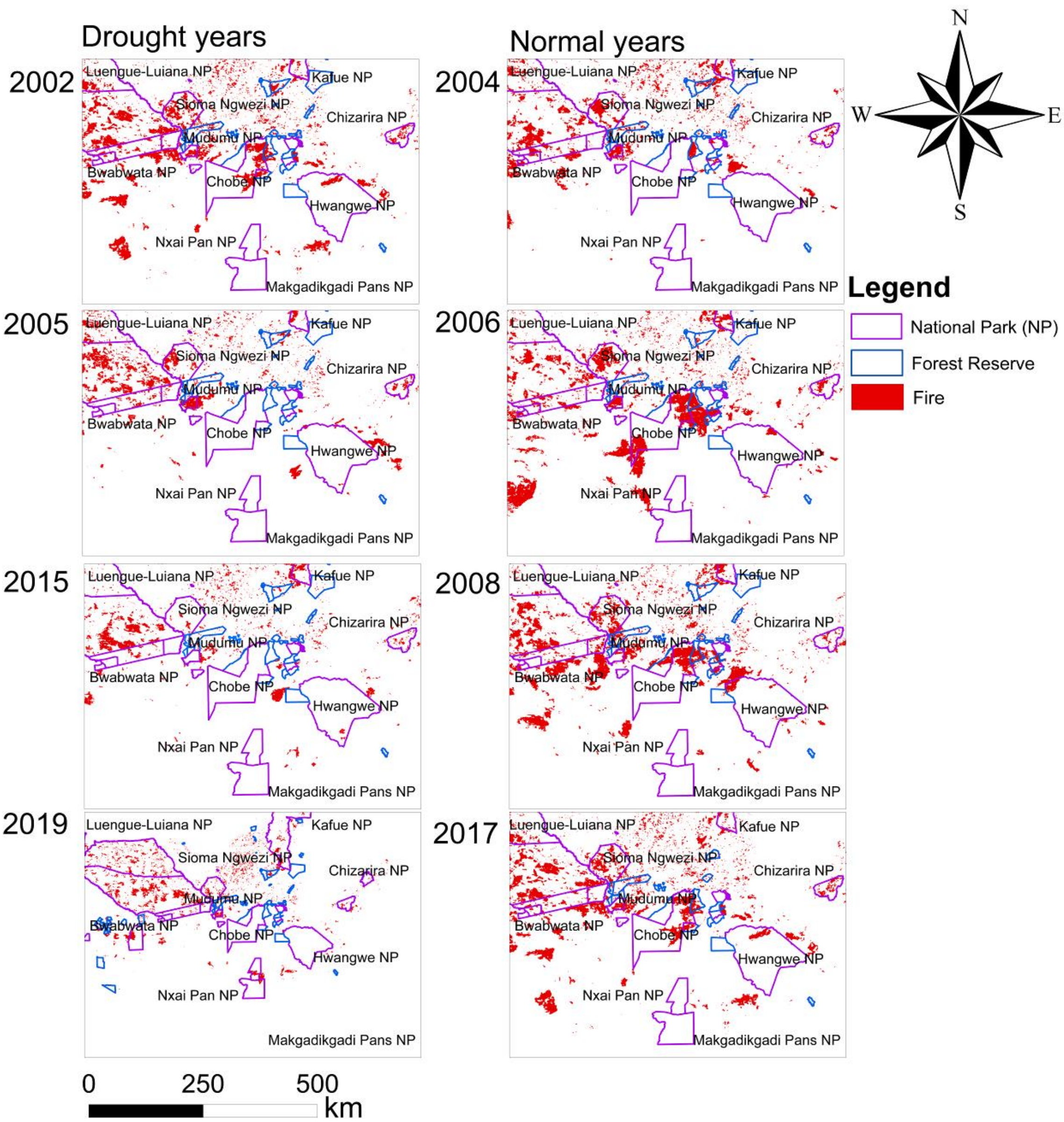

Fig. 5. 13. Burnt area derived from the September month of MODIS MCD64A1 product for selected drought years (2002, 2005, 2015 and 2019) and wet years (2004, 2006, 2008 and 2017) based on SPEI data.

5.5.5 Fire frequency index

Fire-affected pixels were considered as those area that burnt at least once in the 17-year monitoring period. As shown in Fig. 5.14, between 2002 and 2019, about 390,678 km^2 (75%) of the land area is classified as fire-affected at least once, and 127,989 km^2 (25%) of the area is not affected by fire (Fig. 5.14). Of the 390,678 km^2 (75%) of fire-affected area, 90,895 km^2 (18%) of the area burnt only once or twice during the 17 years, indicating a low overall fire frequency overall. The majority of the area, 114,222 km^2 (22%), burnt 2-6 times, while 87,955 km^2 (17%) burnt 6-10 times over the same period. About 28,177 km^2 (13%) burnt frequently, >10-14 times, and 28,177 km^2 (5%) burnt every in >14 of the 17 years indicating a high frequency overall (Table C 2). The national parks are affected by higher levels of fire occurrence than other protected areas such as forest reserves. The fire frequency map shows that Zambia including Sioma Ngwesi NP and Luengue-Luiana NP, Kafue NP experienced high rates of fire return with many of the same areas burning every year, during the monitoring period, with very large areas burnt in >14 out of 17 years. In Namibia, Mudumu, Bwabwata and Khaudum NPs also experienced very high rates of fire return for the majority of their total area ranging returning in 10 to 17 years. In Botswana and Zimbabwe, fire return is generally <6 years, with the exception of the Northeasten Chobe NP, Chizarirae NP and Matusadona NP, which had a fire return of between 6 to 14 years. Hwange NP in Zimbabwe experienced a fire return >6 years for a very small proportion of the northeast area adjacent but outside Hwange NP, and the two parks at the southernmost tip of Botswana (Makgadimkadi Pan NP, and Nzai Pan NP) have the lowest fire reoccurrence of <6 times out of the 17 monitored years. A large portion of the 25% of unburnt pixels were recorded south of Zambezi River in Botswana and Zimbabwe. By comparison, the fire return and incidence of burning are higher in Botswana than in Zimbabwe.

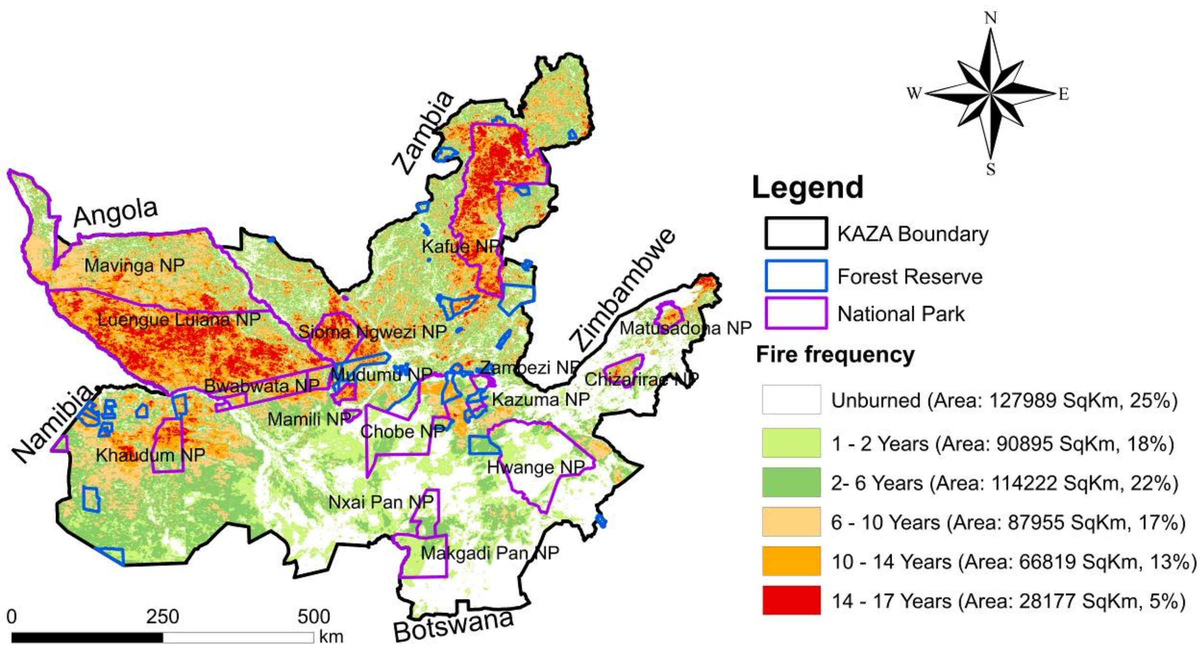

Fig. 5. 14. The area affected by fire determined from monthly using MODIS Burnt Area data from 2002 to 2019 for different land categories in the region. Colours indicate the number of times pixels were classified as burnt. White areas represent pixels that were classified as unburnt over the time period.

Fig. 5.15 shows climate, fire and vegetation indices data from 2002 to 2019. Very high and extremely low burnt areas coincide with a certain combination of climatic factors. A comparison of the distribution of these climatic data and burnt areas, with the spatial distribution of NDVI values, an index of 'greenness' of the vegetation also derived from the MODIS sensor, shows that burning is closely related to areas with proportions of high dryland forests. The areas with high dryland forests (or high tree cover), high rainfall, and dry season length correspond to areas with high fire frequency and large burnt areas (Fig. 5.15). For example, areas with high dryland tree cover and vegetation with NDVI >0.4 receiving mean annual precipitation >150 mm were burnt in approximately 6 to 17 out of the 17 monitored years, here it was common that the same areas burned frequently and recurrently. The areas with low tree cover and vegetation with NDVI <0.4 receiving mean annual precipitation <150 mm were burnt 1 to 6 times out of 17 years. The very dry areas, such as the succulent deserts, burnt once and, in most cases, remained unburnt in the 17 years. The precipitation variations corresponded with the highest degree of spatial similarity to the root soil moisture, and with consistent high rainfall in northern part of KAZA, and the extremely low rainfall (<150 mm) in the southern part of the region.

In contrast, the potential evapotranspiration has the lowest variation in the northern part of the study area (>550 mm) and highest variations in the south (<5500 mm). This is consistent with the root soil moisture, which have high variations (>0.25) in the northern part of the region in comparison to the northern side with very low soil moisture (<0.25). The northern part of the region is situated in the countries with the largest dryland forest cover, Angola and Zambia, which is consistent with high NDVI (light and dark green colours in Fig. 5.15). However, these areas also have a very high rate of burning in consecutive years, with a fire return of between 14 to 17 years within 17 years, as shown by the fire frequency index. The high fire return rate is also prevalent in other areas with dryland forests, such as the forest reserves and national parks in Namibia and

Botswana (e.g., Mudumu, Chobe NP, Zambezi ST and Kasane forest reserves), which display a fire return of between 6 to 14 in 17 years, with proportions of their areas experiencing fire recurrences in more than 14 years. The south of Zambezi River shows a very low fire frequency and a large portion of the 25% of unburnt pixels from 2002 to 2019 are recorded here (see supplementary: Table C 2).

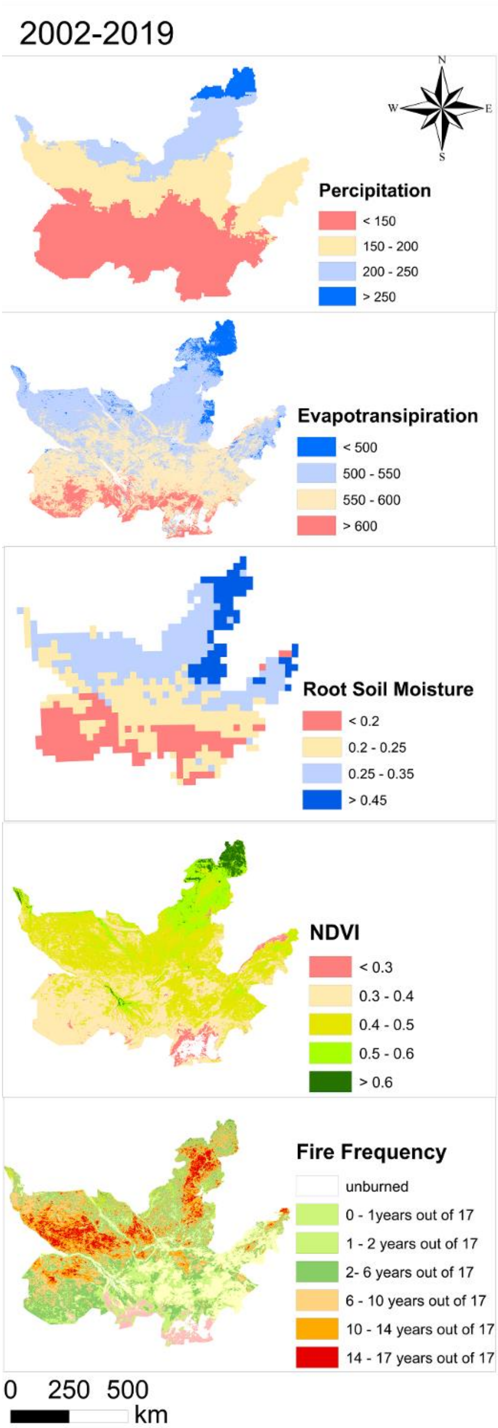

Fig. 5. 15. Areas where the fire frequency is under varying degrees of climatic condition (precipitation, potential evapotranspiration, root soil moisture), and NDVI sampled from the averaged monthly-mean of the growing season of 2002 to 2019.

5.5.6 Spatiotemporal changes in the Aridity Index

Fig. 5.16 presents the spatiotemporal aridity changes in the whole of the KAZA region to explore whether frequent drought and fire dynamics in recent years have led to increased dryness, and subsequent vegetation change. A subset of the AI data over the last 9 years of the period (2011–2019) is compared with the first 9 years (2002 - 2010) to highlight these temporal changes. The temporal changes of AI showed a significant increasing dryness since 2002. Observed areal changes (Fig. 5.16) are apparent, with the change to drier subtypes being dominant and mainly located in southern side of the region as compared to the northern side in the period of 2002-2010, as compared to 2011-2019. An increase in the drying variations and changes in the aridity index were observed in transition zones between arid, semi-arid, and sub-humid regions between 2011 and 2019. The arid and semi-arid regions have increased at the expense of neighbouring dry sub-humid areas, and represented 5.56% and 4.84%, respectively. The sub-humid areas experienced a significant decrease of approximately 10% of the KAZA land area. The largest expansion of drylands occurs in semiarid regions, which account for nearly half of the total dryland expansion and cover >70% of the region (Table C 3). The AI indicator detected areas with increasing aridity to be mainly in southern KAZA, and these areas are shifting towards more arid and hotter classes, while northern the KAZA areas with semi humid regions are shifting into semi-arid regions and, therefore, increasing climatological drying risk.

5487 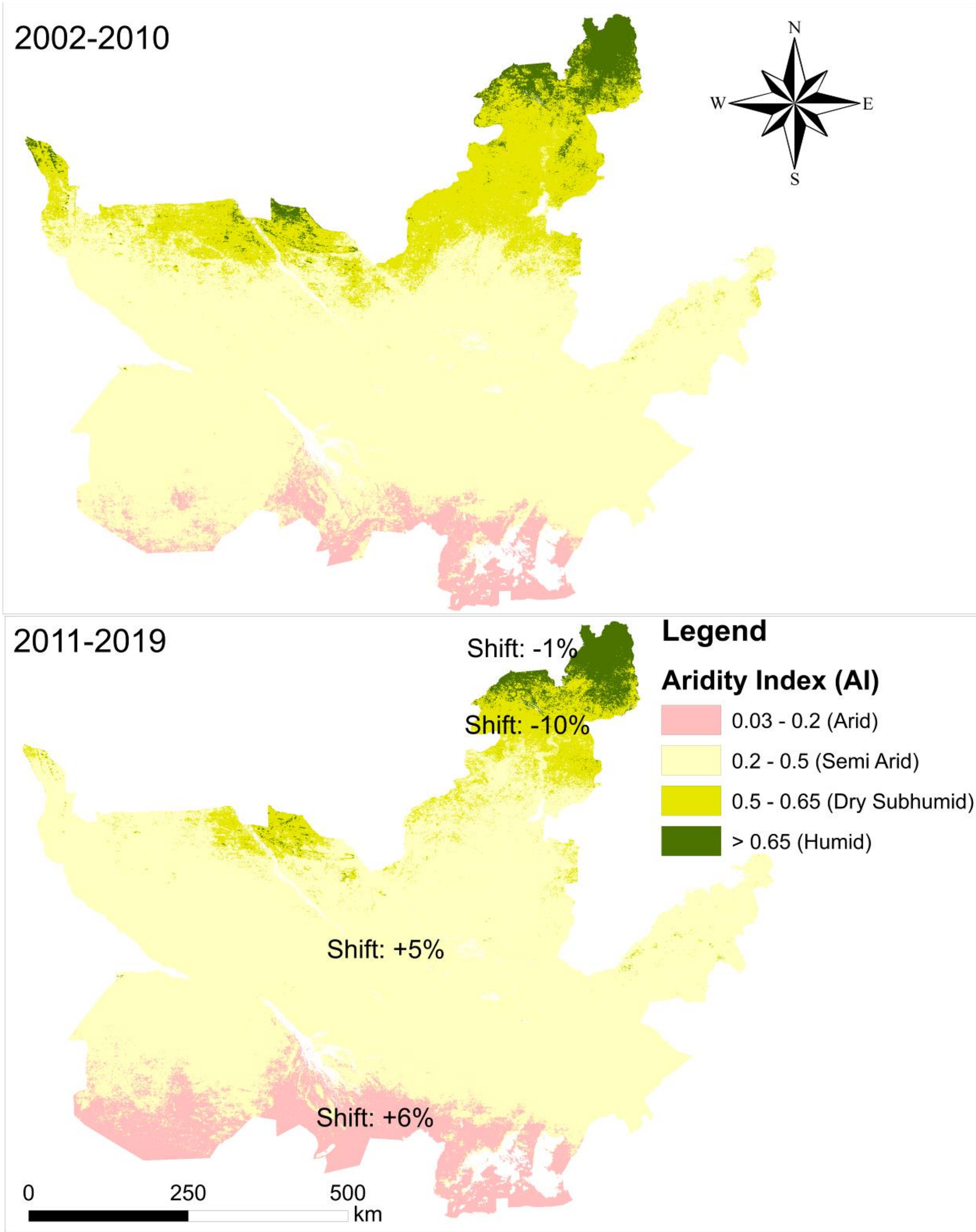

5488 Fig. 5. 16. Spatial distribution of averaged aridity over KAZA region for 2002-2010 and
5489 2011-2019.

5490

5.6 Discussion

5.6.1 Drought impacts on vegetation

Temporal analysis of the SPEI index, precipitation and soil moisture anomalies all reveal that the 2019 drought event surpasses the severity of events in 2002, 2005, 2010, and 2015, which were all considered severe drought events. The results show that the dryland vegetation in the region has a strong correlation with precipitation and closely responds to variability in precipitation and drought (see: Fig. 5.7). A study by Caylor et al. (2005) showed that vegetation in the Kalahari region depends on the stochastic distribution of rainfall events and interannual variation in rainfall that can induce shifts in vegetation structure with prolonged periods of wet (or dry) regime. Comparing the satellite-based rainfall anomalies (CHIRPS) with ground-based rainfall observations also indicates that the results are not sensitive to the precipitation data used in this analysis. The multi-year spatial patterns of change in climate, soil moisture and vegetation were categorised from 2002 through 2019 (see: Fig 5.8). Fig 5.8 shows the results of 2010 to 2019 as this period was more affected by drought impacts as compared to the period 2002-2009. As shown in Fig. 5.8, the severity and extensiveness of the 2015 and 2019 drought resulted in considerable precipitation and soil water deficit, which caused a significant change in dryland forest vegetation. A similar pattern was seen by Liu et al. (2013) who found climate variability to be extreme in dryland trees and grassland in the KAZA region. The browning hotspots are concentrated in unprotected woodland and grassland, although significant browning patterns were also observed in protected national parks (e.g., Chobe NP and Kafue NP). On the one hand, some large-scale browning patterns are not corresponding to the low precipitation values and drought years, which implies that they could not be directly associated with climate change (see: Fig. 5.8). Agricultural expansion, deforestation, and frequent fire burning could be associated with these changes, particularly in Namibia and Zambia.

The lag in greening rate in dryland biomes can be seen in some years following drought (e.g., 2016), with most dryland trees suffering drastically reduced growth rates despite an increase in rainfall and a subsequent lack of a dry spell, as shown in the SPEI of 2016 (see: Fig. 5.8 and 5.9). The root soil moisture data explained the consistent decrease in vegetation productivity in 2016, despite precipitation and the SPEI showing a positive trend, indicating that RSM root soil moisture is one of the major controlling factors that helps to explain changes in vegetation cover across the KAZA region, as indicated by Caylor et al. (2005). Sporadic, erratic and extremely poor rainfall accompanied by high temperatures in preceding years, seems to have resulted in an absence of soil water storage with root soil moisture levels becoming very low, resulting in potential carry-over effects on plants. Although SPEI considers the effects of both temperature and precipitation, and has been very useful in detecting vegetation drought in many studies (Marumbwa et al., 2020; Vicente-Serrano et al., 2015), the RSM showed a better performance in explaining the climatic relationship with vegetation vulnerability to prolonged drought resulting in lack of moisture in plant roots (see: Fig. 5.8 and 9). This finding is similar to Anderegg et al. (2013) and Case et al. (2019) who also observed lag-effect patterns between drought stress and extended multiyear tree disturbances in 2015-2016 in temperate forests in North America and dryland woodland in Kruger NP. These results confirm that MODIS-derived VIs time series coupled with climatic variables, soil moisture and ground measurements of forest stands can provide insights into the influence of water stress on dryland biomes.

5.6.2 Fire

Changes in fire regime were analysed in conjunction with climate data as the climate variability and change also modify the risks of fires, pest and pathogen outbreaks, which each negatively affect vegetation (IPCC, 2014). The data show that every year, between 110173 km^2 (21%) and 203849 km^2 (39%) of the land area in the KAZA region were burned in the period 2002 to 2019. The year 2011 experienced the highest amount of burning with 203849 km^2 (39%), and 2019 experienced the lowest burning with only 110173 km^2 (21%). The results show an increase in annual precipitation in the study region has led to a potential increase in fire incidence, and the reoccurrence of drought events have exacerbated fire incidences in the wet years. During wet years (2004, 2006, 2008-2009 and 2017) and less drought prone years (2011 to 2013), fire incidence in the KAZA was greatest across protected areas. By comparison, dry years of 2002-2003, 2005, 2015-2016 and 2018-2019 show unusually low fire incidence and notably, 2019 which experienced extreme drought conditions also experienced the lowest number of fire incidences (see: Fig. 5.11 and 13). The findings of this study are in agreement with Fox et al. (2017) who analysed fire incidences in Chobe NP from 2001 to 2013, and found more active fires recorded in years with higher rainfall. In addition, during wet seasons or low drought years, fire is also used to remove biomass from land being cleared for agriculture, shifting cultivation, weed and disease control, or, afterwards, for removal of the previous-year's agricultural waste (Eriksen, 2007; Frost, 1999). However, inverse results were found in the Amazon, where many studies demonstrate that fire incidence and extent increases in drought years (Aragão et al., 2007; Nobre et al., 2009)..

One explanation for the high incidence of fire in wet years is that in the KAZA region, more than 90% of fire incidences are due to dry season fires in June to October, the highest number of burning incidences occur in the late dry season between August and September (see Fig. 5.12), and the end of dry season affects the amount of fuel available in wet years (see: Fig 5.4). During the dry season, the herbaceous vegetation is either dry/dead (annual grasslands), and deciduous trees have shed their leaves, thereby contributing to the build-up on the surface of ignition sources after only a few weeks of dry weather (Higgins et al., 2000; Lehmann et al., 2014). This evidence suggests that most fires in the region are set by people, because there are few thunderstorms in the late dry season months that might naturally trigger fires. The late dry seasons are normally hot, windy with extremely dry conditions, which means the fires can spread easily and are difficult to control, and subsequently burn large areas (Archibald et al., 2010). On the other hand, severe drought conditions with very low rainfall does not permit the accumulation of sufficient fuel to become a source of ignition and then to sustain extensive fires (Stott, 2000). The fieldwork of 2019 revealed that a frequent late dry season fire transforms woodland into open, tall grass savanna with only isolated fire-tolerant canopy trees. This suppresses the regrowth of woody plants resulting in scattered understorey trees and shrubs. Similarly, in the Amazon, huge and successive fires have substantially increased forest disturbances and favoured the occurrence of short-life-cycle pioneer species (Nobre et al., 2016).

Between 2002 and 2019, about 390678 km^2 (75%) of the land area was classified as fire-affected at least once, and 127989 km^2 (25%) of the area was not affected by fire (see: Fig. 5.14). Even though all of the KAZA member countries have fire suppression policies that largely date back to colonial days, the striking difference in fire incidence and extent of area burnt is due to the different types of fire laws, and the enforcement of these laws. The national parks are more affected by high fire occurrence as compared to other protected areas, such as forest reserves, game reserves and wildlife management areas. The fire frequency map shows that a large portion of the 75% burned pixels were located in the Zambian and Angolan areas of KAZA. The two countries experienced high rates of fire return, with many of the same areas burning every year, in the last two decades, with very large areas burned in 14 to 17 years out of 17 years. Within Angola, anthropogenic fire is thought to be a significant cause of deforestation and the fire incidence rate is significantly higher during the dry season, which has a negative impact on forest resources and biodiversity in Kuando-Kubango Province (the Angolan component in KAZA), as recorded by United States Forest Service report (Zweede et al., 2006). Although there is legislation and regulation on fire control in Angola, these are rarely enforced, and so uncontrolled dry-season burning for clearing land and to flush animals for hunting are common practices (USAID, 2013). In Zambia, fire is perceived as an important land management tool in agricultural and caterpillar breeding. The Zambian State Forestry Department and local NGOs encourage burning earlier in the dry season to enable fire suppression in the late dry season across most national parks and other protected areas. Even though there is existing state law on fire regimes in Zambia, these laws are not strictly followed, again due to the difficulty of enforcement, and potentially a lack of understanding of the laws in many remote rural areas (Eriksen, 2007). A separate study by Archibald et al. (2010) also reported similar results, whereby Angola and Zambia have the highest burnt areas amongst Southern African countries, with much of their area burned >4 in the 8-year period monitored.

In Namibia, fire return periods for most of areas are midrange compared to other areas of KAZA (e.g., Mudumu, Bwabwata and Khaudum NP experienced high rates of fire return for most of its total area ranging from 10 to 17 years out of the 17 years). In Namibia, a fire management project that includes the establishment of a community fire break, and the implementation of awareness programs on fire, to manage and reduce wildfires was established in 1996 through the Namibia–

Finland Forestry Programme (NFFP) (Verlinden et al., 2006). In addition, an innovative integrated fire management program (Integrated Rural Development and Nature Conservation Caprivi Program) was implemented between 2006 and 2010 to support national parks and forestry agencies via decentralization of fire management decision-making to include community members in decision-making (Russell-Smith et al., 2017). Tire management in the Namibian section of the Wildlife Dispersal Area (WDA) has progressed significantly through collaborative efforts between the Directorate of Forestry, NGOs and local communities (KAZA, 2014). According to Verlinden et al. (2006), the implementation of fire management into schools and community meetings, through awareness raising interventions in Namibian were very effective and the results appear to show a significant decrease in burned area in comparison to the prior era.

A large portion of the 25% of unburned pixels from 2002 to 2019 are recorded in Zimbabwe and south of Zambezi River around the Makgadikgadi Pans National Park and Nxai Pan National Park in Botswana. This is due to the generally drier environment with low precipitation and low tree cover as both Makgadikgadi Pans National Park and Nxai Pan National Park are physically and ecologically part of the "Kalahari Desert,", and possibly due to better controlled fire regimes in these areas (Chinamatira et al., 2016; EMA, 2007). The incidence of burning is lower in Botswana than in Zimbabwe, despite the higher human population density in the latter. In the two countries, the fire return is generally low with <6 years experiencing burning from 17, with the exception of northeast of Chobe NP, the northeast of Hwange NP, Chizarirae NP and Matusadona NP, which have a fire return of between 6 and 14 years. This is in line with the findings by Mpakairi et al. (2019) who reported fire hotspots in Chizarira, Matusadona NP and northeast of Hwange NP. Botswana has a fire suppression management strategy through the use of fire breaks and firefighting crews including the military, police and volunteer members of the general public, mobilised through the District Commissioner (Dube, 2013). The Zimbabwean component have strict laws on fire management and control in place, dating back to colonial days bolstered by recent laws passed in 1998 (Zweede et al., 2006). The Zimbabwean Environmental Management Authority passed regulations on fire suppression in 2007, such that anyone caught setting a wildfire outside a residential or commercial premises during the dry summer period from 31 July to 31 October of each year are arrested, face expulsion from the area, or can be fined by decree (Chinamatira et al., 2016; EMA, 2007).

5.6.3 Changes in aridity

Understanding the long-term areal change in the aridity is essential for taking early action to prevent the aggravation of drying conditions. The results shown in Fig. 5.16 confirm that the KAZA region is becoming drier in the 20th century, and there is an increased risk of arid conditions as result of enhanced warming, wildfires and the rapidly growing human population in the drylands of KAZA region. Such an expansion of arid areas detected in this study is in agreement with the projection by IPCC (2007) that by 2020, most African countries are projected to be exposed to increased water stress due to climate change and this would lead to reduced carbon sequestration and enhanced regional warming, resulting in increased warming trends over the drylands. In the scientific literature, there are many publications dealing with aridity changes, but as there is no study of aridity change at a regional scale across KAZA, it is difficult to make detailed comparisons. At regional scale, climate shifts can be notably different to those observed at global scale. The most relevant precursor to this study aridity maps can be the global maps produced by Huang et al. (2017). Huang et al. (2017) compared aridity data over 10 years, from 1996 to 2005, to a 10 year period between 1948 to 1957. Their study found that most vegetation change from dry sub-humid to semi-arid occurred in the area of the KAZA region in Southern Africa. In comparison to this study, an increase in the drying variations and changes in the aridity index were observed in the arid and semi-arid regions represented by 5.56% and 4.84% between 2002 to 2019 (this study), as compared to 1.16% and 2.32% in the arid and semi-arid regions between 1948 to 1957 observed in Huang et al. (2017).

Another global study by Spinoni et al. (2015) compared AI from 1951 to 2010 using FAO AI and the KG climate classification. Their study found that the extent of arid lands increased in Africa by 1.95%, followed by Asia (0.55%) and decreased in the North and South Americas by -0.47 and -70%, respectively. Their study found that that the arid lands in Southern Africa are larger by the end of the period 1981 to 2010, as compared to the period 1951-1980, and the largest increase in arid regions of Southern Africa were located in the KAZA region (Southern Zambia, Zambezi region of Namibia and western Zimbabwe) as compared to any other part of Southern Africa. These findings more or less agree with the results presented here, with one exception: the shifts identified in this study were found to be larger in dry-sub-humid and humid area, with 10.40% of the regional land area becoming arid compared to the previously published 1.95% at a continental scale. The difference could be attributed to the difference in data, as this study used high-resolution precipitation and PET data at a much smaller scale, while the global studies used a more coarser resolution Global Precipitation Climatology Centre (GPCC) and the Climatic Research Unit (CRU) for precipitation and PET. This difference could also be due to the fact that the thesis considered data up to 2019, and the 21st century recorded the worst drought periods, notably in 2012-2013, 2015-2016 and 2018-2019.

As a result of the multiple effects of consecutive droughts, many countries such as Namibia and Angola, declared a state of emergency in response to drought 3 times in a period of 6 years, with the drought of 2019 declared as the worst in the last 90 years (Shikangalah, 2020). In addition, projected aridification-prone areas overlap with regions at risk of severe drought, marked soil moisture depletion, and shifts in potential vegetation distributions. This suggests that, compared with globally averaged aridity changes, the KAZA region show a much drier climate than most regions in Africa, and globally. The results sows that if future precipitation extremes become more severe, this region is likely to have vegetation that is more unstable or may even to experience extreme vegetation shifts that will be hard to adapt to, as predicted by (IPCC, 2014). Therefore, being able to understand areas at risk of risk of drying conditions through drought indices should give land managers information that may allow the implementation of mitigation or adaptation measures, which can be fundamental in terms of dryland vegetation sustainability.

5.7 Conclusion

This study detected spatial and temporal patterns of climate, burnt areas and dryland vegetation across KAZA, using a combination of ground-data and remote sensing imagery to understand the ecological effects of climate and fire. The long-term climate, fire, and vegetation data analysis led to the following conclusions:

First, the extreme droughts of 2015 and 2019 resulted in considerable precipitation and soil water deficits. Dryland forest vegetation is to be more susceptible to changes in soil moisture trends, as opposed to changes in rainfall and drought index.

Second, at decadal time scales, interannual variability in fire frequency and burnt area is likely to be driven largely by variation in rainfall, vegetation distribution and dry season length. The areas with high tree cover, high rainfall, and less severe drought season coincide with areas of high fire frequency and large burned areas, while low tree cover (e.g., succulent deserts), low rainfall and extended severe drought conditions correspond to areas with low fire frequency.

Finally, the detected aridification-prone areas overlap with regions at risk of severe drought, marked soil moisture depletion, and shifts in potential vegetation distribution. The KAZA region has become drier due to aridification in the period between 2002 to 2019 as a consequence of both drought and wildfire, which critically affect agriculture, water quality, vegetation productivity, and biodiversity.

The identification of the areas with significant trends of change is extremely important in tropical dryland areas where low levels of field data are available and limited financial resources can be invested in monitoring and assessment, as is the case in much of the KAZA region. The detailed relationship between remotely sensed drought/fire indicators and vegetation stress at the regional scale shown here allow us to make several suggestions to move towards a more impact-oriented drought and fire monitoring approach, with the potential to provide early warnings in to devise more practical measures to control aridity in vulnerable areas.

5.8 Supplementary Information 3

Temporal analyses: burned area

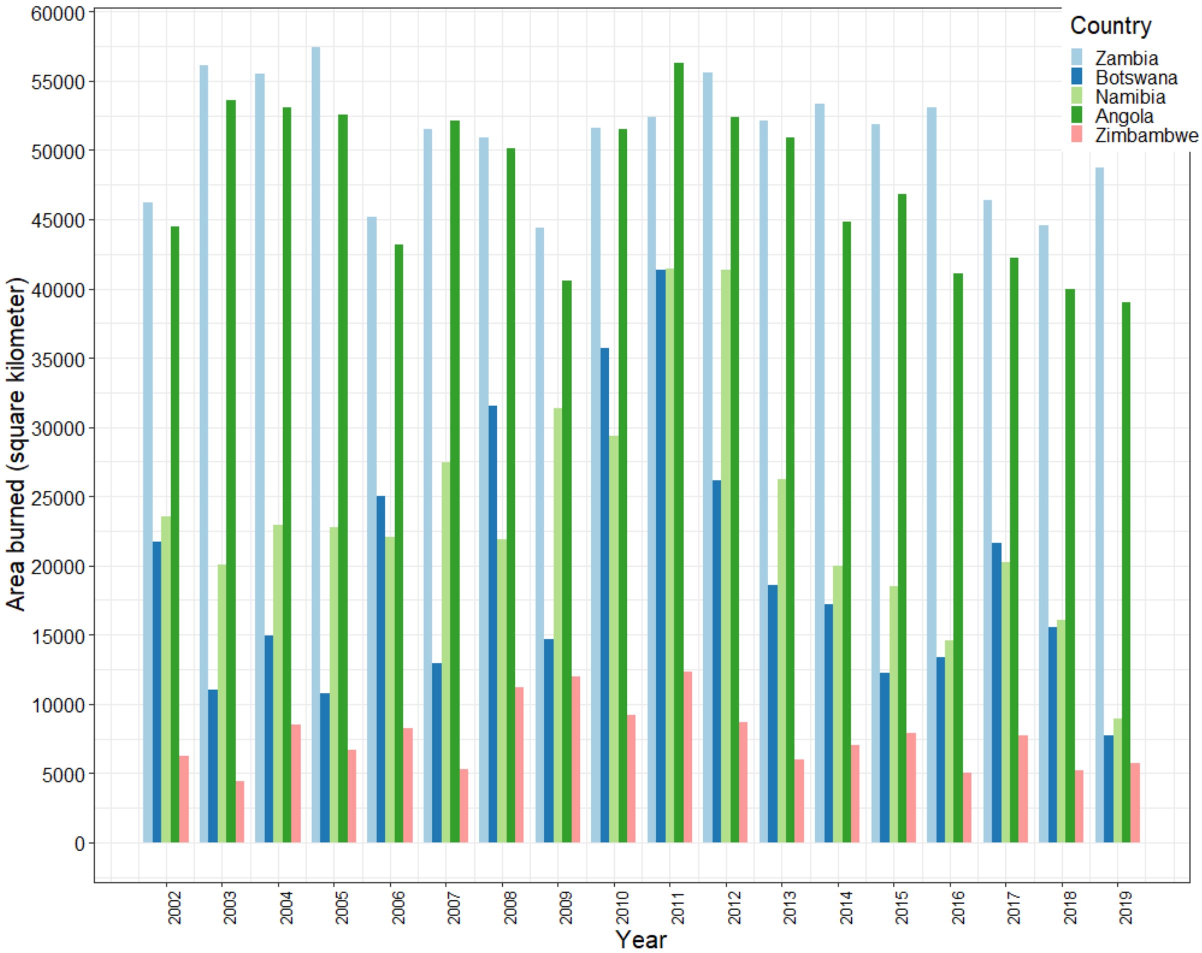

Fig C 1. Total area burned annually for each country of KAZA from 2002 to 2019 in km² based on the MODIS Burned Area product data.

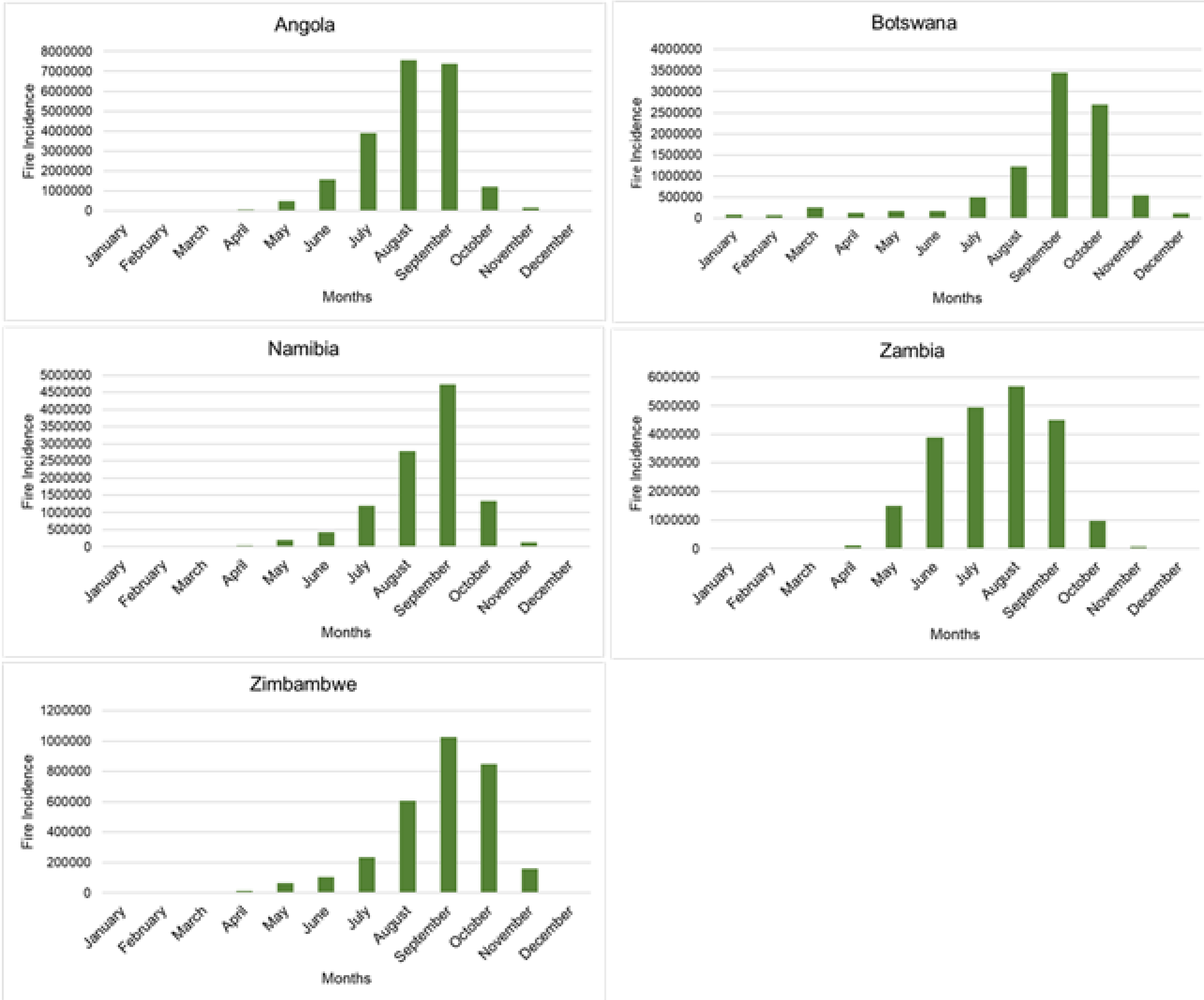

Fig C 2. Cumulative monthly fire frequency for all the countries from 2009 to 2019 using MODIS Active Fire product.

Spatial analyses: burned area

Table C 1. Estimates of the total area of burnt and unburnt areas in km² and their % from 2002 to 2017 in KAZA region

Year	Burnt area(km^2)	Burnt (%)	Unburnt (km^2)	Unburnt (%)
2002	142235	27	376463	73
2003	145168	28	373530	72
2004	154911	30	363783	70
2005	1501678	29	368530	71

2006	143703	28	374995	72
2007	149365	29	369333	71
2008	165706	32	352991	68
2009	142975	28	375723	72
2010	177493	34	341205	66
2011	203849	39	314849	61
2012	184186	36	334511	64
2013	153835	30	364863	70
2014	142463	27	376234	73
2015	137259	26	381439	74
2016	127181	25	391516	75
2017	138072	27	380626	73
2018	121363	23	397335	77
2019	110173	21	408525	79

Table C 2. Recorded areal fire frequencies of burnt and unburnt areas in km^2 and their % from 2002 to 2017 in KAZA region

Year	**Area (km^2)**	**Area (%)**
Unburnt	127989	25
1-2	90895	18
2-6	114222	22
6-10	87955	17

10-14	66819	13
14-17	28177	5

Table C 3. KAZA shifts of AI per class from 2001-2010 to 2011-2020

Class (SbAI)	**2001-2010 (km^2)**	**2001-2010 (%)**	**2011-2020 (km^2)**	**2011-2010 (%)**	**Shift %**
Arid	33957	6.75	61897	12.31	5.56%
Semi-Arid	368016	73.13	392072	77.97	4.84%
Dry Sub-humid	82464	16.39	35369	7.03	-9.36%
Humid	18769	3.73	13503	2.7	-1.04%

Drought

Table C 4. Drought years and drought categories of SPEI at different time scales

	SPEI1				**SPEI3**				**spei12**			
Year	**moderate**	**severe**	**extreme**	**Σ**	**moderate**	**severe**	**extreme**	**Σ**	**moderate**	**severe**	**extreme**	**Σ**
1983	2	-	-	2	-	-	-	-	-	-	-	-
1984	-	-	-	-	1	-	-	1	1	-	-	1
1985	1	-	-	1	-	-	-	-	-	-	-	-
1986	-	-	-	-	-	-	-	-	-	-	-	-
1987	1	-	-	1	1	2	-	3	3	1	-	4
1988	-	-	-	-	2	-	-	2	-	-	-	-
1989	-	1	-	1	1	-	-	1	1	-	-	1
1990	2	2	-	4	-	-	-	-	-	-	-	-
1991	-	-	-	-	-	-	-	-	-	-	-	-
1992	2	-	1	3	1	2	-	3	2	1	-	3
1993	1	-	-	1	-	-	-	-	-	-	-	-
1994	1	1	-	2	2	1		3	2	1	-	3
1995	2		-	2	3	-	-	3	1	-	-	1
1996	5	-	-	5	2	-	-	2	3	-	-	3

1997	2	-	-	2	-	-	-	-	-	-	-	-
1998	1	2	1	4	2	2	1	5	5	-	1	6
1999	1	1		2	-	1	-	1	2	-	-	2
2000	1	-	-	1	-	-	-	-	-	-	-	-
2001	2	1		3	1	-	-	1	1		-	1
2002	2	4	1	7	2	2	1	5	4	2	1	7
2003	1	-	-	1	3	1	1	5	4	3	1	8
2004	2	-	-	2	1	-	-	1	1			1
2005	2	2	1	5	-	4	1	5	-	3	1	4
2006	1	-	-	1	-	-	-	-	-	-	-	-
2007	-	-	-	-	1	-	-	1	1		-	1
2008	1	-	-	1	2	-	-	2	-	-	-	-
2009	2	-	-	2		-	-	-	-	-	-	-
2010	-	-	-	-	-	-	-	-	-	-	-	-
2011	2	-	-	2	4		-	4	3	-	-	3
2012	3	-	-	3	3		-	3	2	-	-	2
2013	2	-	-	2	1		-	1	1	-	-	1
2014	1	-	-	1	-	-	-	-	-	-	-	-
2015	5	-	-	5	5		-	5	4	-	-	4
2016	2		1	3	3	1	1	4	3	1	1	5
2017		-	-	-	-	-	-	-	-	-	-	-
2018	1	1	2	4	1	3	1	5	2		2	4
2019	4	1	2	7	6	3	2	11	4	6	2	12
Σ	55	16	9	80	47	22	8	77	50	18	9	77

5766

6 DISCUSSION

6.1 Introduction

Changes in climate, land-cover, and land-use intensification have contributed to land degradation and desertification in tropical forest ecosystems (Allen et al., 2010; Brink et al., 2014; Brown et al., 2002). Extreme climate events and human-induced environmental changes such as deforestation can act synergistically (Le Houérou, 1996). In tropical dryland ecosystems, deforested and degraded areas can affect regional climate, and the regional climate, in turn, can amplify deforestation and forest degradation (Chagnon et al., 2004; Huang et al., 2017). Climate change and anthropogenic processes appear to amplify fire occurrence and spreading, and land degradation in dryland tropical forest ecosystems (Fox et al., 2017).

As a consequence forests, plant species, and biomass have experienced changes in their species range, abundances, and shifts in their seasonality, resulting in an impacts on biodiversity and forest ecosystem services (Desanker et al., 2001). Severe dry forest biome shifts and land degradation as a result of climate change are predicted to be most severe in Southern Africa (IPCC, 2014; King, 2014). Already deforestation in Southern African countries is high, with about 1.4 million ha net forest loss annually (Darkoh, 2009; Lesolle, 2012). In Southern Africa, a range of policy options have been advocated to reduce the continuing loss and degradation of dryland forests, including expansion of protected area networks, improving governance and better management of dryland forests (Cumming, 2008; Hanks, 2003; KAZA, 2014). However, high-quality, long-term, and reliable information on dryland forests and ecosystems over large areas are needed to estimate and manage the impacts of forest changes on biodiversity, biomass carbon stocks and dryland ecosystem functions accurately.

There are significant advantages to forest analysis, such as remote sensing to better improve estimates of forest changes and biomass, characterise forest structures, and to understand the dynamics of tropical dryland forests in the context of climate changes (Andela et al., 2013; Donoghue, 2002; Lu, 2006).

However, such approaches that integrate forest studies and remote sensing need to be replicated and tested across different regions, geographic scales, and over relevant time periods to change (decades) (Lehmann et al., 2015; Mitchard et al., 2013). Existing literature shows limitations in terms of methodological inconsistency and generalisation, and constraints on the spatial and temporal scales of investigation which limits the actual effectiveness of integrating remote sensing into the tropical dryland forest assessment (Foody et al., 2001; Woodcock et al., 2001).

Given these challenges, this thesis set out to overcome such limitations to contribute to the ability to characterise above ground biomass, forest structural parameters, land cover change, and disturbances in the context of climate change in the dryland forests of the Kavango Zambezi Transfrontier Conservation Area (KAZA TFCA) of Southern Africa. KAZA is a conservation area with over thirty-six protected areas including national parks, game reserves, community conservancies and game management areas. It established to merge fragmented wildlife habitats into an interconnected mosaic of protected areas and transboundary wildlife corridors, to enhance the free movement of animals across international boundaries and to create economic development in the region (Cumming, 2008; Stoldt et al., 2020). However, the region is experiencing large-scale shifts in vegetation cover, biomass degradation and increased vulnerability to climate change, manifesting through altered disturbance regimes which hold significant implications for forest biodiversity and ecosystem function of this region. By addressing the above limitations, the thesis explored the use of novel application of improved satellite remote sensing approaches and datasets including optical and SAR, and their combination, that can in principle improve estimates of forest biomass and structural parameters, disturbances, and climatic impacts at a regional scale.

The research presented here was structured around three research priorities identified in a systematic review (chapter 2, David et al., 2022a). Specifically, the review identified a need to address (i) the feasibility of combining SAR, optical remote sensing data and ground measurements to estimate the forest stand parameters, (ii) vegetation dynamics, and spatially detailed patterns of change using different remote sensing proxies, (iii) characterisation of spatiotemporal changes in climate and fire using different climatic and vegetation time series data at regional scale. By combining improvements across each of the three research priorities, this thesis aims to combine ground measurements and multiple remote sensing including climate, fire, and vegetation data to enable estimates of forest biomass, and changes in dryland forests, across different spatial and temporal scales.

6.2 Suitability of remote sensing data

6.2.1 Combining sensors

Remote sensing techniques can be applied to detect changes, estimate forest structural parameters including biomass, and to monitor the extent in tropical dryland forest cover at different spatial scales, from individual trees, large blocks of the unbroken canopy, to regional and pantropical or even global extents (Baccini et al., 2004). However, there are large discrepancies in the methodologies used to quantify forest structural changes in tropical dryland forests, including attempts to relate forest cover and biomass to optical remote sensing measurements (Mitchell et al., 2017; Sexton et al., 2016). In the research presented in this thesis, the use of the medium to coarse resolution optical data, such as NASA's MODIS sensor, demonstrate an approach to monitoring forest cover change and degradation due to clear-cutting, fire, and drought (chapter 4 & 5), but also showed that certain types of change remain difficult to detect. The quantitative assessment of the ability of sensors with different spatial resolutions, and the integration of multiple datasets from optical and SAR sensors, to improve estimates of forest biomass and structures in the dryland ecosystems are limited and have not been carried out in Southern Africa (Chapter 2, David et al., 2022a). Consequently, there is an opportunity to exploit the benefits of different remote sensing in this context, alongside a need to consider the trade-offs between spectral and spatial resolution, and geographic coverage, when estimating biomass and forest structural parameters in dryland forests ecosystems (chapter 2, David et al., 2022a).

This thesis combined freely available Sentinel 1 (S1) SAR, Sentinel 2 (S2) and Landsat 8 (LC8) multispectral imagery to estimate biomass at regional level and the relatively fine resolution of S2 (10 m pixels) which reduced the mixed pixel problem observed in medium spatial resolution data (30 m pixels; e.g. LC8), and led to an increase in the precision of biomass estimation compared to using single sensors alone (Chapter 3, David et al., 2022b). In this research, AGB is more accurately estimated when adding Sentinel 1 SAR and Sentinel 2 to a Random Forest algorithm (instead of using multispectral or SAR on its own). For example, this research found that SAR data was better at detecting aggregations of individual trees in the dryland landscape than optical data. But this research also found that SAR data alone overestimated AGB in the dryland area (Fig 3.7, Chapter 3, David et al., 2022b). A similar problem of SAR overestimating AGB was noted by other studies such as Zhang et al. (2019), and this problem was overcome by fusing SAR and multispectral data in this thesis (Fig 3.7, Chapter 3, David et al., 2022b). The comparison of recently published pan-tropical AGB datasets (Avitabile et al., 2016; Baccini et al., 2017; Bouvet et al., 2018) with the regional scale maps produced in this thesis, using a combination of optical and SAR datasets with DBH and tree height measurement of more than 4300 tree ground-validation, resolves realistic spatial patterns in estimated biomass for the study area (Fig. 3.5, chapter 3, David et al., 2022b). Here, S1 SAR and S2 data were combined to show in fine detail AGB ranges, including a mix of very low biomass (due to different degrees of degradation) to intermediate biomass for certain areas with very large but scattered trees, through to higher biomass areas in high-density forests (Fig.3.7, chapter 3, David et al., 2022b).

Partly, this study has improved biomass estimation by investigating the capabilities and correlation of AGB with diverse spectral bands from Sentinel 2, Landsat 8, and radar backscatter polarisation from Sentinel 1 SAR data. For optical data, although NDVI and EVI remain two of the most widely used vegetation indices, they were outperformed by the red edge index (NDRE1) and the green channel index (GNDVI) in estimating AGB for dryland forests (Table 3.3, Chapter 3, David et al., 2022b). NDVI is utilised in biomass mapping by different studies such as (Cunliffe et al., 2020; Gizachew et al., 2020), however this study detected saturation in NDVI when the spectral values remain insensitive to increases in forest AGB value beyond 80 Mg/ha (Fig. 3.7, Chapter 3, David et al., 2022b). Gitelson et al., 1996 found the green channel index to be much more sensitive to the Chlorophyl concentration and enabled precise estimation of pigment concentration than the original "red" NDVI. The red edge-based indices were found to have a better correlation with the photosynthetic activity of the tree canopy and leaf cell structure reflection (Cho et al., 2008; Mutanga and Skidmore, 2004).

There has been concern that structural variation and understory herbaceous cover reduce measurement precision when mapping from remotely sensed estimates in semi-arid savanna and dryland forests (Baccini et al., 2004; Santos et al., 2002). Combining information from optical sensors that describe photosynthetic activity (e.g., through various vegetation indices) with SAR-derived information on forest structure and biomass in winter months, brings the benefits of higher spectral resolution, and compensates for the shortcomings of using single data products alone that are commonly subject to saturation, temporal gaps, and clouds cover (chapter 3, David et al., 2022b). Comparing the performance of ML and RF regression algorithm and considering the collinearity between predictor variables also improved biomass mapping and reduced uncertainty in the models. ML regression overestimated low values, and underestimated high biomass values, which is also common in previous studies using ML (Fuchs et al., 2009; Zheng et al., 2007). RF had a positive impact on the biomass estimation accuracy, and performed better than ML regression, reducing the RMSE for the estimation models by almost 50%. Therefore, it is important to assess the ability of combining improved methods and freely available optical and SAR data with sample plot survey data/forest inventory to characterise large-area biomass distributions to provide regional estimates of forest carbon stocks. Although this study has improved AGB estimation in dryland forests, there is room for improvement, for example RF regression model estimated medium and high-density forests with good accuracy but showed variation in low-density forests that include understoreys and low herbaceous cover such as grassland often with relatively low canopy density. This study did not consider multitemporal seasonal time series data and texture information from images in AGB modelling which provides additional information on seasonal variations and reduce the impacts of heterogeneity as suggested by studies in temperate and evergreen broad leaf forests (Sarker and Nichol, 2011; Zhu and Liu, 2015). Incorporation seasonal time series and textural information in AGB modelling in dryland forests could improve biomass modelling and is a topic for future research. Despite these limitations, this study aimed to improve the performance of the regional forest biomass model and can provide a reference and support for future plans of relevant forestry departments.

6.2.2 Spatial scale

In sensor integration, issues of scale are critical for biomass and habitat mapping, where the adequacy of spatial resolution to the problem in hand is key. Pan-tropical and global maps derived from satellite imagery can show large uncertainty in the extent and distribution of tropical dryland forest recorded, and typically underestimate the extent of forest cover and biomass in dryland areas (Bastin et al., 2017). This is illustrated by the substantial spatial disagreements between recent satellite-based global (Giri et al., 2005) and pantropical forest maps (Mitchard et al. (2013), and is further hindered by the relative scarcity of large-scale studies assessing forest cover in dryland biomes (Chapter 2; David et al., 2022a). The distribution of AGB and precision varied between this study and pantropical maps (Fig. 3.9, Chapter 3 David et al., 2022b). The observed discrepancies may have arisen due to satellite data characteristics (such as spatial resolution), unavailability of cloud-free images, availability of ground-truth information, and forest definitions (such as tree cover thresholds) used in the analyses (De Sy et al., 2012). In the research presented in this thesis, comparing three recent pan-tropical forest maps to estimate above ground biomass (AGB) revealed important differences: 0-30 Mg/ha using the pan-tropical AGB map (1 km resolution), 0-50 Mg/ha using Landsat (30 m), 0-70 Mg/ha using ALOS PALSAR (25 m); and 0-145 Mg/ha from this study using combined optical and SAR (10 m) (Fig. 3.8, Chapter 3, David et al., 2022b). This research has a high mean estimate of biomass of 51 mg/ha in comparison to Bouvet et al. (2018) using radar data, that estimated mean biomass of 26.7 Mg/ha which is 50 % less compared to this study mean biomass (Fig. 3.9, Chapter 3, David et al., 2022b). Avitabile et al. (2016) only estimated the mean biomass of 5.92 Mg/ha for the study area and predicted AGB values in the 0 to 30 Mg/ha range.

In this research, biomass mapping at a regional scale using SAR backscatter in conjunction with the strategically positioned optical bands (red edge wavebands) improved estimation at high AGB values and allowing the identification of small-scale degradation patterns of biomass such as roads compared to either sensor alone (Fig. 3.11, chapter 3, David et al., 2022b). In addition, the AGB model from this study showed that biomass for dryland forests exceeds estimates derived from pan-tropical products which underestimate biomass and forests in dryland ecosystems of less-studied areas such as the KAZA region, which are often neglected in this type of analysis (Chapter2; David et al., 2022).

However, the advent of free Landsat data combined with improving computational and data storage capabilities mean that large area Landsat land cover products are increasingly being generated. In this study, a large volume of Landsat data using high quality training data derived from the field survey was demonstrated using Google Earth Engine and Random Forest classifier (Fig. 4.13-4.14, Chapter 4). A 30 m Landsat land cover map was generated and was able to detect large scale deforestation and changes with an acceptable classification accuracy >80% (Chapter 4). This study used medium spatial resolution Landsat data because land cover maps based on coarse spatial resolution imagery (nominally at 500 or 250 m) limits the ability for detecting changes and provide a highly generalised representation of land cover and ultimately land cover change, over large areas (Hamunyela et al., 2020; Zhu and Woodcock, 2014). Using a two point in time classification is useful to detect changes in land cover, however such bi-temporal change detection approach can have some limitation of potentially masking considerable within-year vegetation dynamic and variations (Chapter 2; David et al., 2022a). For example, this type of change estimates risks interpreting natural phenological change as actual changes in the land cover (DeVries et al., 2015). Therefore, this study has moved from a relatively static, bi-temporal view of change toward a more continuous mapping of vegetation dynamics to improve the detection of disturbance's spatiotemporal patterns using change detection algorithms of BFAST and BEAST (Chapter 4). These change detections algorithms were useful in assessing small scale deforestation, degradation, and regrowth by capturing vegetation changes during the year and over longer time-periods at the regional scales (Chapter 3, David et al., 2022b). Such large area analyses on change detection conducted in this research can be used to adjust and update global land cover and biomass estimates. The pan-tropical and global maps are limited in their spatial resolution and temporal coverage, and most of them provide inadequate information for policymaker regarding restoration intervention efforts that are needed for regional- or local-scale restoration projects (Abbas et al., 2020). At regional-to-national scales, the adoption and application of satellite technology is highly variable across countries in the tropics. For example, many countries across Southern African are faced with scarcities of technology, finances, and computer time limitations, preventing the use of conventional downloaded high-resolution satellite data (chapter 2, David et al., 2022a). To overcome these limitations, the thesis utilised the recent developments in cloud computing platforms, such as Google Earth Engine (GEE), which have greatly increased access to pre-processed optical, SAR, and climatic datasets, enabling a comprehensive analysis of multiple threats including deforestation, and degradation from fire and climatic impacts on vegetation at regional scale (chapter 3, 4 & 5).

6.2.3 Temporal scale

To characterise vegetation and climate interactions, changes in forest cover must be quantified over different temporal scales, to capture both short term and gradual changes experienced by dryland ecosystems (chapter 2, David et al., 2022a). The study has shown that the impact of degradation varies from fine-scale structural changes in canopy, to broad-scale rapid loss of biomass (chapter 3 David et al., 2022b). Several methods and techniques are proposed in the literature to address land cover characterisation and forest cover change. Mapping changes through comparing images at two different times, based on discrete classification, are one of the most common forms of remote sensing change detection utilised (Jensen, 1996). This is despite change detection between two dates (pre-and post-disturbance imagery) is generally limited to the detection of broad-scale changes (chapter 2, David et al., 2022a).

Change detection is more powerful, however, when the signal is analysed over a long time period (decadal, or longer) in a continuous and consistent manner, providing an improved signal-to-noise ratio, detection of subtle/transient changes in forest cover or phenology and condition (Huang et al., 2009; Verbesselt et al., 2012). Here, the ability to make precise estimates of change in dryland forest distribution was improved by combining a long high frequency time-series of MODIS data with pixel-based break detection (chapter 4). The abrupt changes (e.g., deforestation), gradual change (e.g., forest degradation), and other slow processes (e.g., seasonal changes) in response to wildfire, disease, and climate variability were each detected effectively (chapter 4). In the research presented in this thesis, the fire estimates in the KAZA region reveal that between 2002 and 2019, about 390,678 km^2 (75%) of the landmass is classified as fire-affected for at least one time in the monitored period, leaving 127,989 km^2 (25%) of the area not affected by fire. This showed that national parks are more affected by high fire occurrence than other protected areas (chapter 5). As shown in this thesis, the failure of vegetation to recover and browning intensification following drought years reaffirm the consistent multiple threats from severe drought, soil moisture deficit, and high fire reoccurrence on dryland vegetation responses (chapter 4 & 5). Consequently, this combined approach to change assessment using long term monitoring (> decadal), as used here, allows spatiotemporal aridity information to be extracted, thereby enabling quantification of vegetation shifts and increased risks of land degradation and drying risk that cumulatively occur over many years in the dryland forest ecosystems (chapter 4 & 5). In addition to visual detection validation of historic change using high resolution data proposed by Cohen et al. (2010), this study demonstrated that the change estimates and precision from BFAST can be validated and improve using a stratum-based estimate of variance that will be more precise than using simple random sampling (Stehman and Czaplewski, 1998; Stehman, 2009; Potapov *et al.*, 2014). As shown in this study (Chapter 4), the large-scale changes such as clear felling of woodland for agriculture are comparable while more subtle changes such as land degradation were detected by BFAST better than interval-based per-pixel classification. Since this study used a rather small sample size (341 points), the change estimates need to be tested with training data of a larger sample size to be conclusive. In addition, the research conducted here can be improved with recently developed new algorithm such as Continuous Change Detection and Classification (CCDC) that make better use of the temporal domain of Landsat data to improve both continuous change detection and land cover classification at medium spatial resolution and high temporal frequency (Zhu and Woodcock, 2014) . CCDC use all available Landsat clear observation data to classify land cover from multiple time period. In addition to land cover classification from any time period in history, it can monitor large scale deforestation and small-scale changes such as degradation in near real time as the algorithms updates the time series model every time new observations are available (Arévalo et al., 2020).

6.2.4 Ecological relevance of mapping changes

There are two parts to the problem that this research has addressed; one was to show changes within the forest ecosystems (deforestation and degradation) and the other was to characterise forest structural parameters and to estimate biomass distribution in the forest. In both situations, methodologically consistent approaches were identified as one of the important needs to improve upon current monitoring of dryland forests (Mitchell et al., 2017); (chapter 2, David et al., 2022a). At the regional scale, monitoring poses a number of methodological challenges including the lack of quantitative, spatially explicit, and statistically representative methods, which have previously resulted in simplistic representations (Coppin et al., 2004). Therefore, as shown in this thesis, testing different models and their suitability to characterise trends and phenological patterns can reveal suitable algorithms for estimating dryland forest covers (chapter 4). Furthermore, Foody et al. (2003) and Woodcock et al. (2001) have pointed out concerns of generalising or transferring methods derived from remotely sensed imagery over both space and time, based on lessons learned in far better-studied ecosystems. Generalisation also limits the interpretation of change patterns and the impacts that these changes will have on the biodiversity of forests, conservation of wildlife habitats conservation, and dryland ecological function (chapter 2, David et al., 2022a).

Whilst models based on remote sensing data can show promising results in different ecosystems (e.g., rain forests), it can fail to detect non-linear vegetation patterns (e.g., degraded areas) in largely climate and fire-driven ecosystems, such as drylands, as shown here (chapter 4). This observation justifies the importance of testing and utilising a range of sensors and vegetation indices for forest structure parameter and change detection estimation. The results in this thesis, reveals that spectral indices based on the red edge spectral region and green normalised vegetation index (GNDVI) have a stronger relationship skill in describing dryland forests than conventional NDVI (chapter 3 & 4). Consequently, there is good reason to believe that NDVI is not an ideal indicator of stress response in dryland forests despite the widespread use of this index in studies of forest health decline. In the research presented in this thesis, indices based on fire, such as the fire frequency index, and several climatological indices, such as SPEI and the aridity index, were tested in dryland forest cover to assess vegetation response to environmental change over large areas (chapter 5). This was undertaken because testing different algorithm and sensor combinations can help detect specific strengths and limitations for a dryland ecosystem, particularly where climate change and variability negatively affecting dryland vegetation and biomass (chapter 3, 4 & 5).

Oliveira et al. (2021), working in Brazil, modelled biomass in tropical dryland forests using linear regression, and recommended testing the ability of non-parametric machine learning algorithms over linear regression analysis in dryland forests. Some image classification algorithms and traditional statistical approaches make unrealistic assumptions about the distributional properties of forests, and are unable to describe underlying fluctuating trends as these models assume vegetation trends to be quasi-linear (i.e., regular, or stable seasonality) (Grogan et al., 2016). In this research, multivariate machine learning models, integrated with stepwise-regression methods, enabled better adjustment and fit to ground measurement, which was tested against more than 4300 individual trees (Chapter 3, David et al., 2022b). This approach enabled both the interpretation and validation of remotely sensed forest structure and biomass estimates, providing a very high R^2 of 0.95 and a low RMSE error of 0.25 Mg/ha (Chapter 3, David et al., 2022b).

Despite prior concerns raised over the need to use ground truth verification for estimating biomass and changes in forest mapping (Grainger, 2008), there are few vegetation-related studies that link vegetation estimates to field measurements and forest inventory data (Chapter 2, David et al., 2022a). As shown in this thesis, obtaining field data for validation of remote sensing data in dryland ecosystems of protected areas, such as National parks, can be challenging because many areas are very remote and often dangerous to visit due to hazardous, and if present and in some cases unexploded landmines (chapter 3, David et al., 2022b). Consequently, most detected changes in the spectral signature that occur due to an increase in woody biomass, deforestation and forest degradation in the dryland ecosystems of

Southern Africa have not been validated (chapter 2, David et al., 2022a). The optical sensors at 250 m-1 km resolution (e.g., MODIS) used here make consistent and frequent measurements over large areas building a long time series, which helps identify locations of active forest change ('hotspots') with good precision and that was validated against ground-truth data (chapter 4). However, where possible, important areas of change and in particular for key forest structural parameters, such as AGB that are needed for baseline carbon stock maps, there are benefits to further ground measurement for validation and finer spatial resolution data. Maps of AGB, if sufficiently detailed, can assist conservation managers, practitioners, and policymakers to formulate specific interventions (e.g., corridor planning, tree thinning, fire control, biodiversity surveys) that are appropriate to support the conservation of forest habitats and their management.

6.3 Recommendation for policy and practice

Dryland forests in protected areas such as KAZA face an increasing number of threats ranging from those originating from climate change and competing economic pressures, especially when they span international borders. Learning from this research and past experience on dryland forests in KAZA (Cumming, 2008; WWF, 2016), there are often conflicting views related to the amount of biomass and changes in forest cover in dryland ecosystems. These differences are however not confined to science only, but also between the understanding of dryland monitoring programmes and policies (Appendix A: N8 AgriFood policy brief). These challenges present also an opportunity for a mutual benefit; with more freely accessible data, such as that explored in this thesis, scientists and policy makers may now refine their focus to share knowledge on the management of forestry, and the interface with land uses, including wildlife management and ecosystem function (Sexton et al., 2016). Based on the findings of this research, along with the challenges and lessons learnt throughout, there are three recommendations that can be made for policy and practice, which can subsequently be used in decision making of the KAZA region, and beyond, in Southern Africa more widely.

First, a large part of the knowledge base for dryland forest landscapes in Southern Africa is derived from research generated outside of Africa (chapter 2, David et al., 2022a), and so there is an opportunity to change academic narratives by working in partnership with local organisations to foreground local research and knowledge. Given the growing technical capacity for monitoring, reporting and verification, there is a need to shift the focus to producing and sharing transparent research maps with resource managers. Technology platforms such as the cloud-based image-analysis pipeline using freely available remote sensing imagery, as used here, is an opportunity to overcome the limitations previously enforced by data scarcity, volumes and costs, and can enhance substantially the collective knowledge of dryland forest environments (chapter 3, 4 &5). Sharing of research outputs and often captivating satellite imagery with the news media to inform citizens and to create awareness about the extent and location of deforestation hotspots is a potentially important component of the KAZA monitoring programme. If such information can influence local practitioners and public opinion, it can exert pressure on policymakers in democratic societies to strengthen enforcement and to tighten regulations around forest management and protection. Improved monitoring of forest cover itself is unlikely to produce any change in behaviour unless it is linked to research, forest management and practice, and all key stakeholders in these regions (Olsson et al., 2019).

Second, the process of monitoring dryland forests could be enhanced through the greater involvement of stakeholders in the modelling process itself. Building on the existing regional networks in the KAZA region, workshops could be facilitated between academic scientists, decision makers and practitioners to identify current gaps in knowledge, data requirements and training needs. Most studies in KAZA region on drought, fire and vegetation analyses are done at local level (e.g., within a single community) and others cover only a part of the KAZA region (Mpakairi et al., 2019; Pricope et al., 2012), making it impossible to compare to a regional perspective. Similar research studies on tropical dryland forest change analyses at large(r) scales (chapter 3, 4 & 5) are needed, ideally retaining fine spatial resolutions and a longer temporal duration. A significant proportion of studies in Southern Africa have been undertaken in Kruger National Park, leaving many other national parks and protected areas in KAZA relatively understudied. Furthermore, future efforts to estimate changes in important variables such as forest cover and biomass, need not be restricted by country boundaries but can extend across the less well studied private and international protected areas (chapter 2, David et al., 2022a). Such workshops would allow stakeholders and other users to have an opportunity to present their work, examine the research outputs in their area of interest with reference to existing or predicted scenarios of future change. Consequently, such structures can harness a wealth of existing research and expertise and help to provide a support network to stimulate high quality published outputs from scientists, and to facilitate input from local experts and practitioners (Appendix A: N8 AgriFood policy brief).

Lastly, the KAZA region concept recognises that borders are political rather than ecological and aims to ensure that key ecological processes continue to function where borders have previously divided ecosystems and/or wildlife migration corridors. Based on my own engagement with stakeholders such as WWF Namibia and the KAZA secretariat, Botswana, there is a willingness to work together and support research, across KAZA region to ensure such information will continue to support future conservation efforts and economic development in countries such as Angola, Botswana, Namibia, Zambia, and Zimbabwe. Such interdisciplinary knowledge and evidence-based policy, generated through partnership and data sharing, is urgently needed. In this region, climate change will cause large-scale shifts in vegetation cover and biomass degradation resulting in increases in the vulnerability of ecosystems across large areas of dryland forest in Southern Africa, which represents risks faced by all stakeholders.

6.4 Future work

The work presented in this thesis offers a platform to improve the understanding of biomass, disturbance patterns, and climate change relationships in dryland forest ecosystems. The thesis considered the factors that cause changes in forest, biodiversity, and ecological function. Numerous spectral indices have been developed to assess vegetation cover and growth dynamics, which provide useful insights for applications in forestry, biodiversity conservation, agriculture, and other related fields. However, most of these indices are derived from a limited selection of species and are typically developed in often quite different regions and ecosystems. The research presented in this thesis tested optimum spectral indices from multispectral data in dryland forests that improve the ability to effectively estimate forest stand characteristics (chapter 3, David et al., 2022b), identify shifts in vegetation dynamics and the timing of key phenological events (chapter 4), and helps us to assess forest health and vulnerability to different stressors, including fire and climate change (chapter 5).

One potential future avenue for research is different sensors. For example, airborne imaging spectroscopy can provide up to 2000 contiguous narrow-band spectral information across the solar spectrum, often at fine spatial resolution (Morley et al., 2020). Asner et al. (2016) used airborne imaging spectroscopy and satellite data trained on spectroscopy data to estimate water lost from California's forest ecosystems over the drought years between 2011 and 2015. To detect a decline in forest cover and shifts in the timing of phenological events requires spectral indices that are sufficiently sensitive to chlorophyll content, and in particular to capture the response of trees to a stress event. Therefore, further research could explore the potential to relate dryland forest cover to hyperspectral data, to identify more sensitive spectral bands corresponding to different vegetation species, and to identify the most important wavelength regions for predicting drought and fire-sensitive species.

Optical sensors have recently been presented as a viable alternative for estimating biomass and carbon stock in tropical forests, due to their global coverage, frequency of capture, and cost-effectiveness (Kumar et al., 2015). Furthering the research presented in this thesis, the primary challenge of MODIS data, despite its high temporal resolution, is the large spatial resolution of between 250 m and 500 m. The temporal resolution of Landsat (16-days, and now 8 days with the recent launch of Landsat 9), which is often occluded by cloud cover can be a major obstacle, despite the relatively fine spatial resolution of 30 m. The integration of MODIS with Landsat to combine fine spatial and temporal resolutions could therefore be used in future to improve the mapping of forests patterns of changes and disturbances.

On the other hand, there is a need to incorporate satellite imagery with a fine spatial resolution information for estimating biomass and carbon stock. For example, the thesis has shown that Sentinel-2 data show a better ability to improve the estimation of above ground biomass and forest structure in tropical dryland forests as compared to Landsat-8 (Chapter 3, David et al., 2022b). Despite improvements in the spatial precision of optical data, such as Sentinel-2, improved characterisation of forest structure may not be possible using multispectral imagery alone due to the spectral similarities between structural classes. Furthering the research presented in this thesis by improving the characterisation of forest structure using a fusion of data such as that from airborne light detection and ranging (LiDAR), collected from airborne platforms, SAR, and/or other forms of optical data, could further advance the understanding of the detailed structural information and accurate vertical distribution of canopy in tropical dryland forests. Li et al. (2017) highlighted that metrics derived from a LiDAR point cloud led to improved biomass estimates at nearly all resolutions in comparison to raster-derived metrics in the drylands of the US. Despite these benefits, LiDAR data are not widely available in many dryland ecosystems, particularly in developing countries, and the acquisition of new data sets can be prohibitively expensive. However, new satellites such as the Global Ecosystems Dynamics Investigation (GEDI) LiDAR and the Multi-footprint Observation Lidar and Imager (MOLI) promise space-borne imaging with laser altimetry, which can contribute to the development biomass, forest distribution, and its relationship with climate in tropical dryland forests (Coyle et al., 2015; Kimura et al., 2017). MOLI includes LIDAR to measure canopy height, vegetation phenology, vegetation indices, and an optical imager to measure the position of the canopy for improving biomass estimation (Sakaizawa et al., 2018). GEDI estimates mean aboveground biomass density at 1 km grid and provides metrics of tree height and canopy cover at a footprint of 25 m (Dubayah et al., 2020), and can be used in fusion with other existing radar data such as Sentinel-1, ALOS PALSAR, along with other optical data sets such as from Landsat and Sentinel-2. The successful unification of forested vegetation monitoring data with detailed information on three-dimensional (3-D) structure would represent a significant improvement in the capacity of ecologists and decision makers to estimate the impacts of forest cover change on biodiversity, wildlife habitat, and forest management approaches more widely, and should be a core focus of future research.

6.5 Conclusion

In this thesis, the close integration of field data, Sentinel-1 SAR, Landsat-8 and Sentinel-2, regional climate and MODIS time-series data, has enabled a more precise estimation of biomass and forest stand structural parameters, which has enabled the quantification of changes in vegetation patterns. The long-term changes and trends identified enabled the characterisation of various influences, from climate, fire and animals to be assessed in terms of their impact on forest biodiversity and dryland ecosystem function. The KAZA region has the highest population of elephants in Africa, which have a destructive influence on forest diversity and density, forest structure, and the wider landscape. The increasing human population, occurrence of wildfires, and changing climate variability, set in a wider context of limited levels of development, are aggravating forest and vegetation decline. Such declines risk the loss of dryland tree species, wildlife, and pose a significant threat to dryland biodiversity. Ongoing monitoring of changes within dryland forest ecosystems integrating open-access Earth observation data alongside improved methods of analysis is vital in the context of future climate change, and the expected impacts of this on dryland forest areas. The key findings of the research are therefore summarised as follow: The thesis has demonstrated that using a combination of radar backscatter in conjunction with strategically selected multispectral optical imagery at fine resolution (10 m pixels) significantly improved above ground biomass and forest stand structural parameter estimations, and reduced saturation effects in areas of high biomass, across large areas with mixed forest stands compared to using single sensors alone. This part of the thesis highlighted the importance of considering spatial scale when mapping forest characteristics that are relevant to management of biodiversity and wildlife in dryland forests, which can help improve the wider understanding of these habitats.The study demonstrated that long-term monthly time-series analysis in combination with change detection models (Breaks for Additive Seasonal and

Trend (BFAST) and the Bayesian analysis (BEAST)) can identify abrupt and gradual changes associated with fire, drought and seasonality driven by climate changes and clear-cutting. Critically, the results emphasised the importance of considering the sensitivity of the chosen vegetation indices, and the need to adopt advanced change detection methods, such as BEAST algorithm, that can fully characterise the complex non-linear dynamics of dryland forest ecosystems. This research has demonstrated that an analysis of long-continuous time series data describing drought, water stress and fire impacts across large spatial scales can reveal regional trends in vegetation change, drying patterns, and the expansion of drylands (arid and semi-arid). These findings highlighted the importance of a precise and timely assessment of the intensity and geography of impacts of droughts within and across conservation areas, both at present and into the future. This approach therefore creates a valuable evidence base for understanding the multiple and interacting impacts on forest biodiversity, wildlife and ecosystem function at a regional-scale, which has hitherto not been possible, and which is essential for more effective management of these critical ecosystems.

References

Abbas, S., Wong, M.S., Wu, J., Shahzad, N. and Muhammad Irteza, S., 2020. Approaches of Satellite Remote Sensing for the Assessment of Above-Ground Biomass across Tropical Forests: Pan-tropical to National Scales. *Remote Sensing*, *12*(20), p.3351.

Adam, E., Mutanga, O., Abdel-Rahman, E.M. and Ismail, R., 2014. Estimating standing biomass in papyrus (Cyperus papyrus L.) swamp: exploratory of in situ hyperspectral indices and random forest regression. International Journal of Remote Sensing, 35(2), 693-714.

Adelabu, S., Mutanga, O., Adam, E.E. and Cho, M.A., 2013. Exploiting machine learning algorithms for tree species classification in a semiarid woodland using RapidEye image. *Journal of Applied Remote Sensing*, *7*(1), p.073480.

Adjorlolo, C. and Mutanga, O., 2013. Integrating remote sensing and geostatistics to estimate woody vegetation in an African savanna. *Journal of Spatial Science*, *58*(2), pp.305-322.

Agbaje, G.I., 2010. Nigeria in space–an impetus for rapid mapping of the country for sustainable development planning. A report prepared for FIG Congress 2010 Facing the Challenges Building the Capacity Sydney, Australia. https://www.fig.net/resources/proceedings/fig_proceedings/fig2010/papers/ts03h/ts03h_agbaje_4621.pdf/(accessed 20 January 2021).

Aggarwal, S., 2004. Principles of remote sensing. Satellite remote sensing and GIS applications in agricultural meteorology, 23(2), pp.23-28.

Aguilar, M.A., Saldaña, M.M. and Aguilar, F.J., 2013. GeoEye-1 and WorldView-2 pan-sharpened imagery for object-based classification in urban environments. *International Journal of Remote Sensing*, *34*(7), pp.2583-2606.

Ahlström, A., Raupach, M. R., Schurgers, G., Smith, B., Arneth, A., Jung, M., Reichstein, M., Canadell, J.G., P. Friedlingstein, P., Jain, A.K., Kato, E., Poulter, B., Sitch, S., Stocker, B.D., Viovy, Y.P., Wang, A., Wiltshire, A., Zaehle, S., Zeng, N., 2015. The dominant role of semi-arid ecosystems in the trend and variability of the land CO2 sink. *Science*, 348(6237), 895-899.

Aide, T.M., Clark, M.L., Grau, H.R., López-Carr, D., Levy, M.A., Redo, D., Bonilla-Moheno, M., Riner, G., Andrade-Núñez, M.J. and Muñiz, M. (2013). Deforestation and Reforestation of L atin A merica and the C aribbean (2001–2010). *Biotropica, 45(2)*, pp.262-271.

Akinyemi, F.O. and Kgomo, M.O., 2019. Vegetation dynamics in African drylands: an assessment based on the Vegetation Degradation Index in an agro-pastoral region of Botswana. *Regional Environmental Change*, *19*(7), pp.2027-2039.

Alcañiz, I. and Gutierrez, R.A. (2020). Between the global commodity boom and subnational state capacities: payment for environmental services to fight deforestation in Argentina. *Global Environmental Politics, 20(1)*, pp.38-59.

Aleman, J.C., Jarzyna, M.A. and Staver, A.C. (2018). Forest extent and deforestation in tropical Africa since 1900. *Nature ecology & evolution, 2(1),* pp.26-33.

Ali, I., Greifeneder, F., Stamenkovic, J., Neumann, M. and Notarnicola, C. (2015). Review of machine learning approaches for biomass and soil moisture retrievals from remote sensing data. *Remote Sensing, 7(12),* pp.16398-16421.

Alleaume, S., Hely, C., Le Roux, J., Korontzi, S., Swap, R.J., Shugart, H.H. and Justice, C.O., 2005. Using MODIS to evaluate heterogeneity of biomass burning in southern African savannahs: a case study in Etosha. *International Journal of Remote Sensing*, *26*(19), pp.4219-4237.

Allen, C.D., Macalady, A.K., Chenchouni, H., Bachelet, D., McDowell, N., Vennetier, M., Kitzberger, T., Rigling, A., Breshears, D.D., Hogg, E.T. and Gonzalez, P., 2010. A global overview of drought and heat-induced tree mortality reveals emerging climate change risks for forests. *Forest ecology and management*, *259*(4), pp.660-684.

Alvarez-Añorve, M.Y., Quesada, M., Sánchez-Azofeifa, G.A., Avila-Cabadilla, L.D. and Gamon, J.A. (2012). Functional regeneration and spectral reflectance of trees during succession in a highly diverse tropical dry forest ecosystem. *American journal of botany, 99(5),* pp.816-826.

Andela, N., Liu, Y.Y., Van Dijk, A.I.J.M., De Jeu, R.A.M. and McVicar, T.R., 2013. Global changes in dryland vegetation dynamics (1988–2008) assessed by satellite remote sensing: comparing a new passive microwave vegetation density record with reflective greenness data. *Biogeosciences*, *10*(10), pp.6657-6676.

Anderegg, W.R., Plavcová, L., Anderegg, L.D., Hacke, U.G., Berry, J.A. and Field, C.B., 2013. Drought's legacy: multiyear hydraulic deterioration underlies widespread aspen forest die-off and portends increased future risk. *Global change biology*, *19*(4), pp.1188-1196.

Andreae, M., Andreae, T.W., Annegarn, H., Beer, J., Cachier, H., Le Canut, P., Elbert, W., Maenhaut, W., Salma, I., Wienhold, F.G. and Zenker, T., 1998. Airborne studies of aerosol emissions from savanna fires in southern Africa: 2. Aerosol chemical composition. *Journal of Geophysical Research: Atmospheres*, *103*(D24), pp.32119-32128.

Anyamba, A. and Tucker, C.J., 2005. Analysis of Sahelian vegetation dynamics using NOAA-AVHRR NDVI data from 1981–2003. *Journal of arid environments*, *63*(3), pp.596-614.

Anyamba, A., Tucker, C.J. and Mahoney, R., 2002. From El Niño to La Niña: Vegetation response patterns over east and southern Africa during the 1997–2000 period. *Journal of climate*, *15*(21), pp.3096-3103.

Aragão, L.E.O., Malhi, Y., Roman-Cuesta, R.M., Saatchi, S., Anderson, L.O. and Shimabukuro, Y.E., 2007. Spatial patterns and fire response of recent Amazonian droughts. *Geophysical Research Letters*, *34*(7).

Archibald, S. and Scholes, R.J., 2007. Leaf green-up in a semi-arid African savanna-separating tree and grass responses to environmental cues. *Journal of Vegetation Science*, *18*(4), pp.583-594.

Archibald, S., Lehmann, C.E., Belcher, C.M., Bond, W.J., Bradstock, R.A., Daniau, A.L., Dexter, K.G., Forrestel, E.J., Greve, M., He, T. and Higgins, S.I., 2018. Biological and geophysical feedbacks with fire in the Earth system. *Environmental Research Letters*, *13*(3), p.033003.

Archibald, S., Roy, D.P., van Wilgen, B.W. and Scholes, R.J., 2009. What limits fire? An examination of drivers of burnt area in Southern Africa. *Global Change Biology*, *15*(3), pp.613-630.

Archibald, S., Scholes, R.J., Roy, D.P., Roberts, G. and Boschetti, L., 2010. Southern African fire regimes as revealed by remote sensing. *International Journal of Wildland Fire*, *19*(7), pp.861-878.

Arévalo, P., Olofsson, P. and Woodcock, C.E., 2020. Continuous monitoring of land change activities and post-disturbance dynamics from Landsat time series: A test methodology for REDD+ reporting. *Remote Sensing of Environment*, *238*, p.111051.

Arino, O., Leroy, M., Ranera, F., Gross, D., Bicheron, P., Nino, F., Brockman, C., Defourny, P., Vancutsem, C., Achard, F. and Durieux, L., 2007, April. Globcover-a global land cover service with MERIS. In *Proceedings of the ENVISAT Symposium* (pp. 23-27).

Armston, J.D., Denham, R.J., Danaher, T.J., Scarth, P.F. and Moffiet, T.N., 2009. Prediction and validation of foliage projective cover from Landsat-5 TM and Landsat-7 ETM+ imagery. *Journal of Applied Remote Sensing*, *3*(1), p.033540.

Asanzi, P., Putzel, L., Gumbo, D. and Mupeta, M., 2014. Rural livelihoods and the Chinese timber trade in Zambia's Western Province. *International Forestry Review*, *16*(4), pp.447-458.

Asner, G. P., Hughes, R. F., Varga, T. A., Knapp, D. E., Kennedy-Bowdoin, T., 2009. Environmental and biotic controls over aboveground biomass throughout a tropical rain forest. Ecosystems, 12(2), 261-278.

Asner, G.P., Brodrick, P.G., Anderson, C.B., Vaughn, N., Knapp, D.E. and Martin, R.E., 2016. Progressive forest canopy water loss during the 2012–2015 California drought. *Proceedings of the National Academy of Sciences*, *113*(2), pp.E249-E255.

Asner, G.P., Hughes, R.F., Varga, T.A., Knapp, D.E. and Kennedy-Bowdoin, T., 2009. Environmental and biotic controls over aboveground biomass throughout a tropical rain forest. *Ecosystems*, *12*(2), pp.261-278.

Assessment & Ecosystems Protection) Regulations, 2007. http://www.fao.org/faolex/results/details/en/c/LEX-FAOC181644/ (accessed 21 July 2019).

Avitabile, V., Herold, M., Heuvelink, G.B.M., Lewis, S.L., Phillips, O.L., Asner, G.P., Armston, J., Ashton, P.S., Banin, L., Bayol, N., Berry, N.J., Boeckx, P., de Jong, B.H.J., DeVries, B., Girardin, C.A.J., Kearsley, E., Lindsell, J.A., Lopez-Gonzalez, G., Lucas, R., Malhi, Y., Morel, A., Mitchard, E.T.A., Nagy, L., Qie, L., Quinones, M.J., Ryan, C.M., Ferry, S.J.W., Sunderland, T., Laurin, G.V., Gatti, R.C., Valentini, R., Verbeeck, H., Wijaya, A., Willcock, S., 2016. An integrated pan-tropical biomass map using multiple reference datasets. *Global Change Biology*, 22(4), 1406-1420.

Avitabile, V., Baccini, A., Friedl, M.A. and Schmullius, C., 2012. Capabilities and limitations of Landsat and land cover data for aboveground woody biomass estimation of Uganda. *Remote Sensing of Environment*, *117*, pp.366-380.

Baccini, A., Friedl, M. A., Woodcock, C. E., Warbington, R., 2004. Forest biomass estimation over regional scales using multisource data. *Geophysical Research Letters*, 31(10).

Baccini, A., Goetz, S. J., Walker, W. S., Laporte, N. T., Sun, M., Sulla-Menashe, D., Hackler, J., Beck, P. S. A., Dubayah, R., Friedl, M. A., Samanta, S., Houghton, R. A., 2012. Estimated carbon dioxide emissions from tropical deforestation improved by carbon-density maps. *Nature Climate Change*, 2(3), 182-185.

Baccini, A., Walker, W., Carvalho, L., Farina, M., Sulla-Menashe, D. and Houghton, R.A., 2017. Tropical forests are a net carbon source based on aboveground measurements of gain and loss. *Science*, *358*(6360), pp.230-234.

Baker, T. R., Phillips, O. L., Malhi, Y., Almeida, S., Arroyo, L., Di Fiore, A., Erwin, T., Higuchi, N., Killeen, T.J., Laurance, S. G., Laurance, W.F., Lewis, S.L., Monteagudo, A., Neill, D.A., Nunez Vargas, P., Pitman, N.C.A., Silva, J.N.M., Vasquez Martinez, R., 2004. Increasing biomass in Amazonian forest plots. Philosophical Transactions of the Royal Society of London. Series B: *Biological Sciences*, 359(1443), 353-365.

Balint, P.J. and Mashinya, J., 2006. The decline of a model community-based conservation project: Governance, capacity, and devolution in Mahenye, Zimbabwe. *Geoforum, 37(5)*, pp.805-815.

Balzter, H., 2001. Forest mapping and monitoring with interferometric synthetic aperture radar (InSAR). *Progress in physical geography*, *25*(2), pp.159-177.

Barbosa, J.M., Broadbent, E.N. and Bitencourt, M.D., 2014. Remote sensing of aboveground biomass in tropical secondary forests: A review. *International Journal of Forestry Research*, *2014*.

Barros, C., Thuiller, W. and Münkemüller, T., 2018. Drought effects on the stability of forest-grassland ecotones under gradual climate change. *PloS one*, *13*(10), p.e0206138.

Bartholome, E. and Belward, A.S., 2005. GLC2000: a new approach to global land cover mapping from Earth observation data. International Journal of Remote Sensing, 26(9), 1959-1977.

Bastin, J.F., Mollicone, D., Grainger, A., Sparrow, B., Picard, N., Lowe, A. and Castro, R., 2017. Response to Comment on "The extent of forest in dryland biomes". *Science*, *358*(6362).

Bastin, J.F., Rutishauser, E., Kellner, J.R., Saatchi, S., Pélissier, R., Herault, B., Slik, F., Bogaert, J., De Cannière, C., Marshall, A.R. and Poulsen, J., 2018. Pan-tropical prediction of forest structure from the largest trees. *Global Ecology and Biogeography*, *27*(11), pp.1366-1383

Basuki, T.M., Skidmore, A.K., Hussin, Y.A. and Van Duren, I., 2013. Estimating tropical forest biomass more accurately by integrating ALOS PALSAR and Landsat-7 ETM+ data. *International journal of remote sensing*, *34*(13), pp.4871-4888.

Becker, F. and Choudhury, B.J. (1988). Relative sensitivity of normalized difference vegetation index (NDVI) and microwave polarization difference index (MPDI) for vegetation and desertification monitoring. *Remote sensing of environment, 24(2)*, pp.297-311.

Belgiu, M. and Drăguţ, L., 2016. Random forest in remote sensing: A review of applications and future directions. ISPRS journal of photogrammetry and remote sensing, 114, 24-31.

Ben-Shahar, R, 1996. Do elephants over-utilize mopane woodlands in northern Botswana? *Journal of Tropical Ecology*, 12(4), 505-515.

Berger, C., Werner, S., Wigley-Coetsee, C., Smit, I. and Schmullius, C., 2019, July. Multi-temporal sentinel-1 data for wall-to-wall herbaceous biomass mapping in Kruger National Park, South Africa—first results. In *IGARSS 2019-2019 IEEE International Geoscience and Remote Sensing Symposium* (pp. 7358-7360). IEEE.

Berninger, A., Lohberger, S., Zhang, D., & Siegert, F., 2019. Canopy height and above-ground biomass retrieval in tropical forests using multi-pass X-and C-band Pol-InSAR data. Remote Sensing, 11(18), 2105.

Biggs, R., Simons, H., Bakkenes, M., Scholes, R.J., Eickhout, B., van Vuuren, D. and Alkemade, R., 2008. Scenarios of biodiversity loss in southern Africa in the 21st century. *Global Environmental Change*, *18*(2), pp.296-309.

Blackburn, G.A., 2007. Hyperspectral remote sensing of plant pigments. *Journal of experimental botany*, *58*(4), pp.855-867.

Blackie, R., Baldauf, C., Gautier, D., Gumbo, D., Kassa, H., Parthasarathy, N., Paumgarten, F., Sola, P., Pulla, S., Waeber, P. and Sunderland, T., 2014. *Tropical dry forests: The state of global knowledge and recommendations for future research* (Vol. 2). Cifor.

Bollig, M. and Vehrs, H.P., 2021. The making of a conservation landscape: the emergence of a conservationist environmental infrastructure along the Kwando River in Namibia's Zambezi region. Africa, 91(2), pp.270-295.

Bodart, C., Brink, A.B., Donnay, F., Lupi, A., Mayaux, P. and Achard, F., 2013. Continental estimates of forest cover and forest cover changes in the dry ecosystems of Africa between 1990 and 2000. *Journal of biogeography*, *40*(6), pp.1036-1047.

Boggs, G.S., 2010. Assessment of SPOT 5 and QuickBird remotely sensed imagery for mapping tree cover in savannas. *International journal of applied earth observation and geoinformation*, *12*(4), pp.217-224.

Boisvenue, C. and White, J.C., 2019. Information needs of next-generation forest carbon models: opportunities for remote sensing science. Remote Sensing, 11(4), 463.

Bojinski, S., Verstraete, M., Peterson, T. C., Richter, C., Simmons, A., Zemp, M., 2014. The concept of essential climate variables in support of climate research, applications, and policy. *Bulletin of the American Meteorological Society,* 95(9), 1431-1443.

Bollig, M. and Vehrs, H.P., 2021. The making of a conservation landscape: the emergence of a conservationist environmental infrastructure along the Kwando River in Namibia's Zambezi region. *Africa*, *91*(2), pp.270-295.

Bond, W.J. and Keeley, J.E., 2005. Fire as a global 'herbivore': the ecology and evolution of flammable ecosystems. *Trends in ecology & evolution*, *20*(7), pp.387-394.

Bouvet, A., Mermoz, S., Le Toan, T., Villard, L., Mathieu, R., Naidoo, L. and Asner, G.P., 2018. An above-ground biomass map of African savannahs and woodlands at 25 m resolution derived from ALOS PALSAR. *Remote sensing of environment*, *206*, pp.156-173.

Boyd, D.S. and Danson, F.M., 2005. Satellite remote sensing of forest resources: three decades of research development. *Progress in Physical Geography*, *29*(1), pp.1-26.

Bozdogan, H, 1987. Model selection and Akaike's information criterion (AIC): The general theory and its analytical extensions. *Psychometrik*a, 52(3), 345-370.

Božić, M., Čavlović, J., Lukić, N., Teslak, K., Kos, D., 2005. Efficiency of ultrasonic Vertex III hypsometer compared to the most commonly used hypsometers in Croatian forestry. Croatian Journal of Forest Engineering: *Journal for Theory and Application of Forestry Engineering*, 26(2), 91-99.

Brando, P.M., Paolucci, L., Ummenhofer, C.C., Ordway, E.M., Hartmann, H., Cattau, M.E., Rattis, L., Medjibe, V., Coe, M.T. and Balch, J., 2019. Droughts, wildfires, and forest carbon cycling: A pantropical synthesis. *Annual Review of Earth and Planetary Sciences*, *47*, pp.555-581.

Brandt, M., Hiernaux, P., Rasmussen, K., Mbow, C., Kergoat, L., Tagesson, T., Ibrahim, Y.Z., Wélé, A., Tucker, C.J. and Fensholt, R. (2016). Assessing woody vegetation trends in Sahelian drylands using MODIS based seasonal metrics. *Remote Sensing of Environment, 183*, pp.215-225.

Brandt, M., Rasmussen, K., Hiernaux, P., Herrmann, S., Tucker, C.J., Tong, X., Tian, F., Mertz, O., Kergoat, L., Mbow, C. and David, J.L. (2018a). Reduction of tree cover in West African woodlands and promotion in semi-arid farmlands. *Nature Geoscience, 11(5)*, pp.328-333

Brandt, M., Wigneron, J.P., Chave, J., Tagesson, T., Penuelas, J., Ciais, P., Rasmussen, K., Tian, F., Mbow, C., Al-Yaari, A. and Rodriguez-Fernandez, N., 2018b. Satellite passive microwaves reveal recent climate-induced carbon losses in African drylands. Nature ecology & evolution, 2(5), pp.827-835.

Breiman, L. (2001), Random forests. *Machine Learning*, 45(1), 5-32.

Brink, A.B. and Eva, H.D., 2009. Monitoring 25 years of land cover change dynamics in Africa: A sample based remote sensing approach. *Applied geography*, *29*(4), pp.501-512.

Brink, A.B., Bodart, C., Brodsky, L., Defourney, P., Ernst, C., Donney, F., Lupi, A. and Tuckova, K., 2014. Anthropogenic pressure in East Africa—Monitoring 20 years of land cover changes by means of medium resolution satellite data. *International Journal of Applied Earth Observation and Geoinformation*, *28*, pp.60-69.

Broge, N.H. and Leblanc, E., 2001. Comparing prediction power and stability of broadband and hyperspectral vegetation indices for estimation of green leaf area index and canopy chlorophyll density. *Remote sensing of environment*, 76(2), pp.156-172.

Brown, S., Lugo, A. E., 1982. The storage and production of organic matter in tropical forests and their role in the global carbon cycle. Biotropica, 161-187.

Brown, S., Lugo, A. E., 1982. The storage and production of organic matter in tropical forests and their role in the global carbon cycle. *Biotropica*, 161-187.

Brown, S., Swingland, I.R., Hanbury-Tenison, R., Prance, G.T. and Myers, N., 2002. Changes in the use and management of forests for abating carbon emissions: issues and challenges under the Kyoto Protocol. *Philosophical Transactions of the Royal Society of London. Series A: Mathematical, Physical and Engineering Sciences*, *360*(1797), pp.1593-1605.

Bucini, G., Hanan, N.P., Boone, R.B., Smit, I.P., Saatchi, S.S., Lefsky, M.A. and Asner, G.P., 2010. Woody fractional cover in Kruger National Park, South Africa: remote sensing-based maps and ecological insights. In Ecosystem function in savannas: measurement and modeling at landscape to global scales (pp. 219-237). *CRC Press*.

Bucini, G., Saatchi, S., Hanan, N., Boone, R.B. and Smit, I., 2009, July. Woody cover and heterogeneity in the savannas of the Kruger National Park, South Africa. In *2009 IEEE International Geoscience and Remote Sensing Symposium* (Vol. 4, pp. IV-334). IEEE.

Buhne, H. S. T., Pettorelli, N., 2018. Better together: Integrating and fusing multispectral and radar satellite imagery to inform biodiversity monitoring, ecological research and conservation science. *Methods in Ecology and Evolution*, 9(4), pp. 849-865.

Bullock, E.L., Woodcock, C.E., Souza Jr, C. and Olofsson, P., 2020. Satellite-based estimates reveal widespread forest degradation in the Amazon. *Global Change Biology*, 26(5), pp.2956-2969.

Bullock, S.H., Mooney, H.A. and Medina, E. eds., 1995. *Seasonally dry tropical forests*. Cambridge University Press.

Bunting, E.L., Southworth, J., Herrero, H., Ryan, S.J. and Waylen, P., 2018. Understanding Long-Term Savanna Vegetation Persistence across Three Drainage Basins in Southern Africa. *Remote Sensing*, *10*(7), p.1013.

Bunyavejchewin, S., Baker, P.J. and Davies, S.J., 2011. Seasonally dry tropical forests in continental Southeast Asia: structure, compositon and dynamics. In *The ecology and conservation of seasonally dry forests in Asia* (pp. 9-35). Smithsonian Institution Scholarly Press.

Burkett, V.R., Wilcox, D.A., Stottlemyer, R., Barrow, W., Fagre, D., Baron, J., Price, J., Nielsen, J.L., Allen, C.D., Peterson, D.L. and Ruggerone, G., 2005. Nonlinear dynamics in ecosystem response to climatic change: case studies and policy implications. *Ecological complexity*, 2(4), pp.357-394

Cabral, A.I.R., Vasconcelos, M.J., Oom, D. and Sardinha, R. (2011). Spatial dynamics and quantification of deforestation in the central-plateau woodlands of Angola (1990–2009). *Applied Geography, 31(3)*, pp.1185-1193.

Cáceres, A., Melo, M., Barlow, J., Cardoso, P., Maiato, F. and Mills, M.S., 2015. Threatened birds of the Angolan Central Escarpment: distribution and response to habitat change at Kumbira Forest. *Oryx*, *49*(4), pp.727-734.

Campo-Bescós, M.A., Muñoz-Carpena, R., Southworth, J., Zhu, L., Waylen, P.R. and Bunting, E., 2013. Combined spatial and temporal effects of environmental controls on long-term monthly NDVI in the southern Africa Savanna. *Remote Sensing*, *5*(12), pp.6513-6538.

Cánovas-García, F., Alonso-Sarría, F., Gomariz-Castillo, F. and Oñate-Valdivieso, F., 2017. Modification of the random forest algorithm to avoid statistical dependence problems when classifying remote sensing imagery. *Computers & Geosciences*, *103*, pp.1-11.

Carlotto, M.J., 2009. Effect of errors in ground truth on classification accuracy. *International Journal of Remote Sensing*, *30*(18), pp.4831-4849.

Carreiras, J., Melo, J.B. and Vasconcelos, M.J., 2013. Estimating the above-ground biomass in miombo savanna woodlands (Mozambique, East Africa) using L-band synthetic aperture radar data. *Remote Sensing*, *5*(4), pp.1524-1548.

Carter, G.A., 1993. Responses of leaf spectral reflectance to plant stress. *American journal of botany*, 80(3), pp.239-243.

Case, M.F., Wigley-Coetsee, C., Nzima, N., Scogings, P.F. and Staver, A.C., 2019. Severe drought limits trees in a semi-arid savanna. *Ecology*, *100*(11), p.e02842.

Castillo, A., Magaña, A., Pujadas, A., Martínez, L. and Godínez, C. (2005). Understanding the interaction of rural people with ecosystems: a case study in a tropical dry forest of Mexico. *Ecosystems, 8(6)*, pp.630-643.

Castro, K.L., Sanchez-Azofeifa, G.A. and Rivard, B., 2003. Monitoring secondary tropical forests using space-borne data: implications for Central America. *International Journal of Remote Sensing*, *24*(9), pp.1853-1894.

Castro, S.M., Sanchez-Azofeifa, G.A. and Sato, H. 2018. Effect of drought on productivity in a Costa Rican tropical dry forest. *Environmental Research Letters, 13(4),* p.045001.

Catarino, S., Romeiras, M.M., Figueira, R., Aubard, V., Silva, J. and Pereira, J., 2020. Spatial and temporal trends of burnt area in Angola: implications for natural vegetation and protected area management. *Diversity*, *12*(8), p.307.

Caylor, K.K., Shugart, H.H. and Rodriguez-Iturbe, I., 2005. Tree canopy effects on simulated water stress in southern African savannas. *Ecosystems*, *8*(1), pp.17-32.

Chadwick, R., Good, P., Martin, G. and Rowell, D.P., 2016. Large rainfall changes consistently projected over substantial areas of tropical land. *Nature Climate Change*, *6*(2), pp.177-181.

Chagnon, F.J.F., Bras, R.L. and Wang, J., 2004. Climatic shift in patterns of shallow clouds over the Amazon. *Geophysical Research Letters*, *31*(24).

Chagumaira, C., Rurinda, J., Nezomba, H., Mtambanengwe, F. and Mapfumo, P., 2016. Use patterns of natural resources supporting livelihoods of smallholder communities and implications for climate change adaptation in Zimbabwe. Environment, development and sustainability, 18(1), pp.237-255.

Chambers, J.Q., Asner, G.P., Morton, D.C., Anderson, L.O., Saatchi, S.S., Espírito-Santo, F.D., Palace, M. and Souza Jr, C., 2007. Regional ecosystem structure and function: ecological insights from remote sensing of tropical forests. *Trends in Ecology & Evolution*, *22*(8), pp.414-423.

Chapungu, L., Nhamo, L., Gatti, R.C. and Chitakira, M., 2020. Quantifying changes in plant species diversity in a savanna ecosystem through observed and remotely sensed data. *Sustainability*, *12*(6), p.2345.

Charles-Dominique, T., Staver, A.C., Midgley, G.F. and Bond, W.J., 2015. Functional differentiation of biomes in an African savanna/forest mosaic. *South African Journal of Botany*, *101*, pp.82-90.

Chave, J., Andalo, C., Brown, S., Cairns, M.A., Chambers, J.Q., Eamus, D., Fölster, H., Fromard, F., Higuchi, N., Kira, T. and Lescure, J.P., 2005. Tree allometry and improved estimation of carbon stocks and balance in tropical forests. *Oecologia*, *145*(1), pp.87-99.

Chazdon, R.L., Brancalion, P.H., Laestadius, L., Bennett-Curry, A., Buckingham, K., Kumar, C., Moll-Rocek, J., Vieira, I.C.G. and Wilson, S.J., 2016. When is a forest a forest? Forest concepts and definitions in the era of forest and landscape restoration. Ambio, 45(5), pp.538-550.

Chazdon, R.L., Broadbent, E.N., Rozendaal, D.M., Bongers, F., Zambrano, A.M.A., Aide, T.M., Balvanera, P., Becknell, J.M., Boukili, V., Brancalion, P.H. and Craven, D. (2016). Carbon sequestration potential of second-growth forest regeneration in the Latin American tropics. *Science Advances, 2(5)*, p.e1501639.

Chen, M., Xie, P., Janowiak, J.E. and Arkin, P.A., 2002. Global land precipitation: A 50-yr monthly analysis based on gauge observations. *Journal of Hydrometeorology*, *3*(3), pp.249-266.

Chidumayo, E.N. 2013. Forest degradation and recovery in a miombo woodland landscape in Zambia: 22 years of observations on permanent sample plots. *Forest Ecology and Management, 291*, pp.154-161.

Chidumayo, E.N. and Gumbo, D.J. eds., 2010. *The dry forests and woodlands of Africa: managing for products and services*. Earthscan.

Chidumayo, E.N., 1997. Annual and spatial variation in herbaceous biomass production in a Zambian dry miombo woodland. *South African Journal of Botany*, *63*(2), pp.74-81.

Chidumayo, E.N., 2001. Climate and phenology of savanna vegetation in southern Africa. *Journal of Vegetation Science*, pp.347-354.

Chidumayo, E.N., 2013. Forest degradation and recovery in a miombo woodland landscape in Zambia: 22 years of observations on permanent sample plots. *Forest Ecology and Management*, *291*, pp.154-161.

Chikoore, H. and Jury, M.R., 2021. South African drought, deconstructed. Weather and Climate Extremes, 33, 100334.

Child, B.A., Musengezi, J., Parent, G.D. and Child, G.F. (2012). The economics and institutional economics of wildlife on private land in Africa. *Pastoralism: Research, Policy and Practice, 2(1),* pp.1-32.

Chinamatira, L., Mtetwa, S. and Nyamadzawo, G., 2016. Causes of wildland fires, associated socio-economic impacts and challenges with policing, in chakari resettlement area, kadoma, zimbabwe. *Fire Science Reviews*, *5*(1), pp.1-11.

Chiteculo, V., Abdollahnejad, A., Panagiotidis, D., Surový, P. and Sharma, R.P., 2019. Defining deforestation patterns using satellite images from 2000 and 2017: Assessment of forest management in miombo forests—A case study of Huambo Province in Angola. *Sustainability*, *11*(1), p.98.

Cho, M.A., Debba, P., Mutanga, O., Dudeni-Tlhone, N., Magadla, T. and Khuluse, S.A., 2012. Potential utility of the spectral red-edge region of SumbandilaSat imagery for assessing indigenous forest structure and health. *International journal of applied earth observation and Geoinformation*, *16*, pp.85-93.

Cho, M.A., Malahlela, O. and Ramoelo, A., 2015. Assessing the utility WorldView-2 imagery for tree species mapping in South African subtropical humid forest and the conservation implications: Dukuduku forest patch as case study. *International Journal of Applied Earth Observation and Geoinformation*, *38*, pp.349-357.

Cho, M.A., Ramoelo, A., Debba, P., Mutanga, O., Mathieu, R., Van Deventer, H. and Ndlovu, N., 2013. Assessing the effects of subtropical forest fragmentation on leaf nitrogen distribution using remote sensing data. *Landscape ecology*, *28*(8), pp.1479-1491.

Cho, M.A., Skidmore, A., Corsi, F., Van Wieren, S.E. and Sobhan, I., 2007. Estimation of green grass/herb biomass from airborne hyperspectral imagery using spectral indices and partial least squares regression. International journal of applied Earth observation and geoinformation, 9(4), pp.414-424.

Cho, M.A., Skidmore, A.K. and Atzberger, C., 2008. Towards red-edge positions less sensitive to canopy biophysical parameters for leaf chlorophyll estimation using properties optique spectrales des feuilles (PROSPECT) and scattering by arbitrarily inclined leaves (SAILH) simulated data. *International Journal of Remote Sensing*, *29*(8), pp.2241-2255.

Chongo, D., Nagasawa, R., Ahmed, A.O.C. and Perveen, M.F., 2007. Fire monitoring in savanna ecosystems using MODIS data: a case study of Kruger National Park, South Africa. *Landscape and Ecological Engineering*, *3*(1), pp.79-88.

Clark, S., Bolt, K. and Campbell, A., 2008. Protected areas: an effective tool to reduce emissions from deforestation and forest degradation in developing countries. *UNEP-WCMC*, Cambridge, UK.

Claverie, M., Vermote, E.F., Franch, B. and Masek, J.G., 2015. Evaluation of the Landsat-5 TM and Landsat-7 ETM+ surface reflectance products. Remote Sensing of Environment, 169, pp.390-403.

Coetzer-Hanack, K.L., Witkowski, E.T.F. and Erasmus, B.F., 2016. Thresholds of change in a multi-use conservation landscape of South Africa: historical land-cover, future transformation and consequences for environmental decision-making. *Environmental Conservation*, *43*(3), pp.253-262.

Cohen, W.B., Yang, Z. and Kennedy, R., 2010. Detecting trends in forest disturbance and recovery using yearly Landsat time series: 2. TimeSync—Tools for calibration and validation. *Remote Sensing of Environment*, 114(12), pp.2911-2924.

Collaboration for Environmental Evidence. (2013). Guidelines for systematic review and evidence synthesis in environmental management. *Environmental Evidence*.

Congalton, R.G. (1988). A comparison of sampling schemes used in generating error matrices for assessing the accuracy of maps generated from remotely sensed data. Photogrammetric engineering and remote sensing.

Congalton, R.G. and Green, K., 2019. Assessing the accuracy of remotely sensed data: principles and practices. *CRC press*.

Congalton, R.G., 2018. Landsat's enduring legacy: pioneering global land observations from space. *Photogrammetric Engineering & Remote Sensing*, *84*(1), pp.9-10

Congalton, R.G., Oderwald, R.G. and Mead, R.A., 1983. Assessing Landsat classification accuracy using discrete multivariate analysis statistical techniques. *Photogrammetric engineering and remote sensing*, *49*(12), pp.1671-1678.

Cook, C., Reason, C.J. and Hewitson, B.C., 2004. Wet and dry spells within particularly wet and dry summers in the South African summer rainfall region. *Climate Research*, *26*(1), pp.17-31.

Coppin, P., Jonckheere, I., Nackaerts, K., Muys, B. and Lambin, E., 2004. Review ArticleDigital change detection methods in ecosystem monitoring: a review. *International journal of remote sensing*, *25*(9), pp.1565-1596.

Coyle, D.B., Stysley, P.R., Poulios, D., Clarke, G.B. and Kay, R.B., 2015, September. Laser transmitter development for NASA's Global Ecosystem Dynamics Investigation (GEDI) lidar. In *Lidar Remote Sensing for Environmental Monitoring XV* (Vol. 9612, p. 961208). International Society for Optics and Photonics.

Cui, Q., Shi, J., Du, J., Zhao, T. and Xiong, C. (2015). An approach for monitoring global vegetation based on multiangular observations from SMOS*. IEEE Journal of Selected Topics in Applied Earth Observations and Remote Sensing, 8(2),* pp.604-616.

Cumming, D. H. M., 2008. Large scale conservation planning and priorities for the Kavango-Zambezi transfrontier conservation area. A report prepared for Conservation International. http://www.wcs-ahead.org/kaza/kaza_tfca_large_scale_planning_final_7nov08_logo.pdf/ (accessed 24 May 2021).

Cumming, D.H.M., 1981. The management of elephant and other large mammals in Zimbabwe. In "Problems in Management of Locally Abundant Wild Mammals"(P. Jewel1 and S. Holt, Eds.) pp. 91-118.

Cunliffe, A.M., Assmann, J.J., Daskalova, G.N., Kerby, J.T. and Myers-Smith, I.H., 2020. Aboveground biomass corresponds strongly with drone-derived canopy height but weakly with greenness (NDVI) in a shrub tundra landscape. *Environmental Research Letters*, *15*(12), p.125004.

Curran, P., 1980. Multispectral remote sensing of vegetation amount. *Progress in physical geography*, *4*(3), pp.315-341.

Curry, T.R. (2020). Mexico's Tropical Dry Forests. In Shobert, A.L. and Maguire, R.O. Reference Module in Earth Systems and Environmental Science.

Cutler, M.E.J., Boyd, D.S., Foody, G.M. and Vetrivel, A., 2012. Estimating tropical forest biomass with a combination of SAR image texture and Landsat TM data: An assessment of predictions between regions. *ISPRS Journal of Photogrammetry and Remote Sensing*, *70*, pp.66-77.

Dai, A., 2013. Increasing drought under global warming in observations and models. *Nature climate change*, *3*(1), pp.52-58.

Dale, V.H., Joyce, L.A., McNulty, S., Neilson, R.P., Ayres, M.P., Flannigan, M.D., Hanson, P.J., Irland, L.C., Lugo, A.E., Peterson, C.J. and Simberloff, D., 2001. Climate change and forest disturbances: climate change can affect forests by altering the frequency, intensity, duration, and timing of fire, drought, introduced species, insect and pathogen outbreaks, hurricanes, windstorms, ice storms, or landslides. *BioScience*, *51*(9), pp.723-734.

Darkoh, M.B.K., 2009. An overview of environmental issues in Southern Africa. *African Journal of Ecology*, *47*, pp.93-98.

Daskin, J.H., Stalmans, M. and Pringle, R.M., 2016. Ecological legacies of civil war: 35-year increase in savanna tree cover following wholesale large-mammal declines. *Journal of Ecology*, *104*(1), pp.79-89.

David, R.M., Rosser, N.J. and Donoghue, D.N., 2022b. Improving above ground biomass estimates of Southern Africa dryland forests by combining Sentinel-1 SAR and Sentinel-2 multispectral imagery. *Remote Sensing of Environment*, *282*, p.113232.

David, R.M., Rosser, N.J. and Donoghue, D.N., 2022a. Remote sensing for monitoring tropical dryland forests: a review of current research, knowledge gaps and future directions for Southern Africa. Environmental Research Communications, 4(4), 042001.

Davies, D.K., Ilavajhala, S., Wong, M.M. and Justice, C.O., 2008. Fire information for resource management system: archiving and distributing MODIS active fire data. *IEEE Transactions on Geoscience and Remote Sensing*, *47*(1), pp.72-79.

Davis, C.L., Hoffman, M.T. and Roberts, W., 2017. Long-term trends in vegetation phenology and productivity over Namaqualand using the GIMMS AVHRR NDVI3g data from 1982 to 2011. *South African Journal of Botany*, *111*, pp.76-85.

Dawson, T.P., Cutler, M.E.J. and Brown, C., 2016. The role of remote sensing in the development of SMART indicators for ecosystem services assessment. *Biodiversity*, *17*(4), pp.136-148.

Day, M., Baldauf, C., Rutishauser, E., Sunderland, T. C., 2014. Relationships between tree species diversity and above-ground biomass in Central African rainforests: implications for REDD. *Environmental Conservation*, 41(1), 64-72.

de Araujo Barbosa, C.C., Atkinson, P.M. and Dearing, J.A., 2015. Remote sensing of ecosystem services: A systematic review. *Ecological Indicators*, *52*, pp.430-443.

De Jong, R., Verbesselt, J., Zeileis, A. and Schaepman, M.E., 2013. Shifts in global vegetation activity trends. *Remote Sensing*, *5*(3), pp.1117-1133.

De Marzo, T., Pflugmacher, D., Baumann, M., Lambin, E.F., Gasparri, I. and Kuemmerle, T., 2021. Characterizing forest disturbances across the Argentine Dry Chaco based on Landsat time series. *International Journal of Applied Earth Observation and Geoinformation*, 98, p.102310.

de Oliveira, W.N., Miziara, F. and Ferreira, N.C., 2019. Mapeamento do Uso e Cobertura do Solo de Moçambique Utilizando a Plataforma Google Earth Engine. *Anuário do Instituto de Geociências*, *42*(1), pp.336-345.

De Sy, V., Herold, M., Achard, F., Asner, G.P., Held, A., Kellndorfer, J. and Verbesselt, J., 2012. Synergies of multiple remote sensing data sources for REDD+ monitoring. *Current Opinion in Environmental Sustainability*, *4*(6), pp.696-706.

Desanker, P.V. and Justice, C.O., 2001. Africa and global climate change: critical issues and suggestions for further research and integrated assessment modeling. *Climate Research*, *17*(2), pp.93-103.

DeVries, B., Decuyper, M., Verbesselt, J., Zeileis, A., Herold, M. and Joseph, S., 2015. Tracking disturbance-regrowth dynamics in tropical forests using structural change detection and Landsat time series. *Remote Sensing of Environment*, 169, pp.320-334.

DeVries, B., Verbesselt, J., Kooistra, L. and Herold, M., 2015. Robust monitoring of small-scale forest disturbances in a tropical montane forest using Landsat time series. *Remote Sensing of Environment*, *161*, pp.107-121.

Dewees, P.A. (1994). Social and economic aspects of miombo woodland management in southern Africa: options and opportunities for research. *CIFOR Occasional paper, (2).*

Dexter, K.G., Smart, B., Baldauf, C., Baker, T.R., Balinga, M.P., Brienen, R.J.W., Fauset, S., Feldpausch, T.R., Silva, L., Muledi, J.I. and Lewis, S.L., 2015. Floristics and biogeography of vegetation in seasonally dry tropical regions. *International Forestry Review*, *17*(2), pp.10-32.

Diffenbaugh, N.S., Singh, D., Mankin, J.S., Horton, D.E., Swain, D.L., Touma, D., Charland, A., Liu, Y., Haugen, M., Tsiang, M. and Rajaratnam, B., 2017. Quantifying the influence of global warming on unprecedented extreme climate events. *Proceedings of the National Academy of Sciences*, *114*(19), pp.4881-4886.

Djoudi, H., Vergles, E., Blackie, R.R., Koame, C.K. and Gautier, D., 2015. Dry forests, livelihoods and poverty alleviation: understanding current trends. *International Forestry Review*, *17*(2), pp.54-69.

Dlamini, W.M., 2017. Mapping forest and woodland loss in Swaziland: 1990–2015. *Remote Sensing Applications: Society and Environment*, *5*, pp.45-53.

do Espírito-Santo, M.M., Rocha, A.M., Leite, M.E., Silva, J.O., da Silva, L.P. and Sanchez-Azofeifa, G.A. (2020). Biophysical and socioeconomic factors associated to deforestation and forest recovery in Brazilian tropical dry forests. *Frontiers in Forests and Global Change, 3*, p.141.

Dogru, A.O., Goksel, C., David, R.M., Tolunay, D., Sözen, S. and Orhon, D., 2020. Detrimental environmental impact of large scale land use through deforestation and deterioration of carbon balance in Istanbul Northern Forest Area. *Environmental Earth Sciences*, *79*, pp.1-13.

Dong, J., Kaufmann, R.K., Myneni, R.B., Tucker, C.J., Kauppi, P.E., Liski, J., Buermann, W., Alexeyev, V. and Hughes, M.K., 2003. Remote sensing estimates of boreal and temperate forest woody biomass: carbon pools, sources, and sinks. *Remote sensing of Environment*, *84*(3), pp.393-410.

Donoghue, D. N., 2002. Remote sensing: environmental change. *Progress in Physical Geography*, 26(1), pp.144-151.

Donoghue, D.N., 2000. Remote sensing: sensors and applications. *Progress in Physical Geography*, *24*(3), pp.407-414.

Dubayah, R., Blair, J.B., Goetz, S., Fatoyinbo, L., Hansen, M., Healey, S., Hofton, M., Hurtt, G., Kellner, J., Luthcke, S. and Armston, J., 2020. The Global Ecosystem Dynamics Investigation: High-resolution laser ranging of the Earth's forests and topography. *Science of remote sensing*, *1*, p.100002.

Dube, O. P, 2013. Challenges of wildland fire management in Botswana: Towards a community inclusive fire management approach. *Weather and Climate Extremes*, 1, 26-41.

Dube, T., Gara, T.W., Mutanga, O., Sibanda, M., Shoko, C., Murwira, A., Masocha, M., Ndaimani, H. and Hatendi, C.M., 2018. Estimating forest standing biomass in savanna woodlands as an indicator of forest productivity using the new generation WorldView-2 sensor. *Geocarto International*, *33*(2), pp.178-188.

Dube, T., Mutanga, O., Adam, E. and Ismail, R., 2014. Intra-and-inter species biomass prediction in a plantation forest: testing the utility of high spatial resolution spaceborne multispectral rapideye sensor and advanced machine learning algorithms. *Sensors*, *14*(8), pp.15348-15370.

Ducheyne, E., Mweempwa, C., De Pus, C., Vernieuwe, H., De Deken, R., Hendrickx, G. and Van den Bossche, P., 2009. The impact of habitat fragmentation on tsetse abundance on the plateau of eastern Zambia. *Preventive veterinary medicine*, *91*(1), pp.11-18.

Dupuis, C., Lejeune, P., Michez, A. and Fayolle, A., 2020. How can remote sensing help monitor tropical moist forest degradation?—a systematic review. *Remote Sensing*, *12*(7), p.1087.

Durant, S.M., Pettorelli, N., Bashir, S., Woodroffe, R., Wacher, T., De Ornellas, P., Ransom, C., Abáigar, T., Abdelgadir, M., El Alqamy, H. and Beddiaf, M., 2012. Forgotten biodiversity in desert ecosystems. *Science*, *336*(6087), pp.1379-1380.

Durden, S.L., Van Zyl, J.J. and Zebker, H.A., 1989. Modeling and observation of the radar polarization signature of forested areas. *IEEE Transactions on Geoscience and Remote Sensing*, *27*(3), pp.290-301.

Dutrieux, L.P., Verbesselt, J., Kooistra, L. and Herold, M., 2015. Monitoring forest cover loss using multiple data streams, a case study of a tropical dry forest in Bolivia. *ISPRS Journal of Photogrammetry and Remote Sensing*, 107, pp.112-125.

Eitel, J.U., Vierling, L.A., Litvak, M.E., Long, D.S., Schulthess, U., Ager, A.A., Krofcheck, D.J. and Stoscheck, L., 2011. Broadband, red-edge information from satellites improves early stress detection in a New Mexico conifer woodland. Remote Sensing of Environment, 115(12), 3640-3646.

Ellis, J.E. and Swift, D.M., 1988. Stability of African pastoral ecosystems: alternate paradigms and implications for development. *Rangeland Ecology & Management/Journal of Range Management Archives*, *41*(6), pp.450-459.

EMA., 2007. Chapter 20:27 Environment Management Act (Environmental Impact

Engelbrecht, B.M., Comita, L.S., Condit, R., Kursar, T.A., Tyree, M.T., Turner, B.L. and Hubbell, S.P., 2007. Drought sensitivity shapes species distribution patterns in tropical forests. *Nature*, *447*(7140), pp.80-82.

Eriksen, C., 2007. Why do they burn the 'bush'? Fire, rural livelihoods, and conservation in Zambia. *Geographical Journal*, *173*(3), pp.242-256.

Erkkilä, A. and Löfman, S., 1999. Forest cover change in the Ohangwena region, northern Namibia: A case study based on multitemporal Landsat images and aerial photography. *Southern African Forestry Journal*, *184*(1), pp.25-32.

ESA, 2014. Global land cover map for the epoch 2005. Available at: http://www.esa-landcover-cci.org/ (accessed 9 July 2015)

ESA, 2020. Level-1. https://earth.esa.int/web/sentinel/user-guides/sentinel-1-sar/product-types-processing-levels/level-1/ (accessed 19 November 2020).

ESA. 2013. SENTINEL-2 User Handbook. https://sentinel.esa.int/documents/247904/685211/Sentinel-2_User_Handbook/ (accessed 19 March 2021).

Estes, L., Elsen, P.R., Treuer, T., Ahmed, L., Caylor, K., Chang, J., Choi, J.J. and Ellis, E.C., 2018. The spatial and temporal domains of modern ecology. *Nature ecology & evolution*, *2*(5), pp.819-826.

Eva, H.D., Brink, A. and Simonetti, D., 2006. Monitoring land cover dynamics in sub-Saharan Africa. *Institute for Environmental and Sustainability, Tech. Rep. EUR*, *22498*.

Fajardo, L., Gonzalez, V., Nassar, J.M., Lacabana, P., Portillo Q, C.A., Carrasquel, F. and Rodriguez, J.P. (2005). Tropical Dry Forests of Venezuela: Characterization and Current Conservation Status 1. *Biotropica: The Journal of Biology and Conservation, 37(4),* pp.531-546.

Falkowski, M.J., Smith, A.M., Gessler, P.E., Hudak, A.T., Vierling, L.A. and Evans, J.S., 2008. The influence of conifer forest canopy cover on the accuracy of two individual tree measurement algorithms using lidar data. *Canadian Journal of Remote Sensing*, *34*(sup2), pp. S338-S350

FAO, 2011 FAO Global Forest Resources Assessment 2010. Rome, Italy (2011)

FAO. (1999). Tropical forest management techniques: a review of the sustainability of forest management practices in tropical countries, from https://www.fao.org/documents/card/en/c/10c5f896-03f8-536d-b253-aebb36dd2cef/ , accessed 24 March 2021)

AO. 2000. FRA 2000: On Definitions of Forest and Forest Change. Forest Resources Assessment.

FAO., 2001. FRA 2000: Global Ecological Zoning for the Global Forest Resources Assessment 2000, Final Report, Food and Agriculture Organization of the United Nations. Forestry Department, Rome. http://www.fao.org/3/ad652e/ad652e00.htm/ (accessed 19 March 2021).

FAO., 2009. Human-wildlife conflict in Africa: causes, consequences and management strategies: Food and Agriculture Organization of the United Nations (FAO).

FAO., 2010. Assessing forest degradation-towards the development of globally applicable guidelines. Forest Resources Assessment Working Paper, 177.

Fassnacht, F.E., Hartig, F., Latifi, H., Berger, C., Hernández, J., Corvalán, P. and Koch, B., 2014. Importance of sample size, data type and prediction method for remote sensing-based estimations of aboveground forest biomass. Remote Sensing of Environment, 154, 102-114.

Feng, S. and Fu, Q., 2013. Expansion of global drylands under a warming climate. Atmospheric Chemistry and Physics, 13(19), pp.10081-10094.

Fensham, R.J. and Fairfax, R.J. 2002. Aerial photography for assessing vegetation change: a review of applications and the relevance of findings for Australian vegetation history. *Australian Journal of Botany, 50(4)*, pp.415-429.

Fensholt, R., Sandholt, I. and Rasmussen, M.S., 2004. Evaluation of MODIS LAI, fAPAR and the relation between fAPAR and NDVI in a semi-arid environment using in situ measurements. *Remote sensing of Environment*, *91*(3-4), pp.490-507.

Fidzani, N, 2014. The Management of Forest Reserves in Botswana, in Rietbergen-McCracken, J., Abaza, H. (Eds.), Economic Instruments for Environmental Management: A Worldwide Compendium of Case Studies. *Routledge*, pp. 39-46.

Field, C.B., Randerson, J.T. and Malmström, C.M., 1995. Global net primary production: combining ecology and remote sensing. Remote sensing of Environment, 51(1), pp.74-88.

Foley, J.A., Coe, M.T., Scheffer, M. and Wang, G., 2003. Regime shifts in the Sahara and Sahel: interactions between ecological and climatic systems in Northern Africa. *Ecosystems*, 6(6), pp.524-532.

Foody, G.M., 2003. Remote sensing of tropical forest environments: towards the monitoring of environmental resources for sustainable development. *International journal of remote sensing*, *24*(20), pp.4035-4046.

Foody, G.M., Boyd, D.S. and Cutler, M.E., 2003. Predictive relations of tropical forest biomass from Landsat TM data and their transferability between regions. *Remote sensing of environment*, *85*(4), pp.463-474.

Foody, G.M., Cutler, M.E., McMorrow, J., Pelz, D., Tangki, H., Boyd, D.S. and Douglas, I.A.N., 2001. Mapping the biomass of Bornean tropical rain forest from remotely sensed data. *Global Ecology and Biogeography*, *10*(4), pp.379-387.

Forkuor, G., Dimobe, K., Serme, I. and Tondoh, J.E., 2018. Landsat-8 vs. Sentinel-2: examining the added value of sentinel-2's red-edge bands to land-use and land-cover mapping in Burkina Faso. GIScience & remote sensing, 55(3), 331-354.

Forkuor, G., Zoungrana, J.-B. B., Dimobe, K., Ouattara, B., Vadrevu, K. P., Tondoh, J. E., 2020. Above-ground biomass mapping in West African dryland forest using Sentinel-1 and 2 datasets-A case study. *Remote Sensing of Environment*, 236, 111496.

Fox, J., 2015. Applied regression analysis and generalized linear models. Sage Publications.

Fox, J.T., Vandewalle, M.E. and Alexander, K.A., 2017. Land cover change in northern botswana: the influence of climate, fire, and elephants on semi-arid dryland woodlands. *Land*, 6(4), p.73.

Frankie, G.W., Mata, A. and Vinson, S.B. eds. (2004). Biodiversity conservation in Costa Rica: Learning the lessons in a seasonal dry forest. *Univ of California Press.*

Frost17, P.G., 1999. Fire in southern African woodlands: origins, impacts, effects and control. *Carbon*, *8*(7,000), p.181.

Fuchs, H., Magdon, P., Kleinn, C. and Flessa, H., 2009. Estimating aboveground carbon in a catchment of the Siberian forest tundra: Combining satellite imagery and field inventory. *Remote Sensing of Environment*, *113*(3), pp.518-531.

Fullman, T. J, 2009. Spatial dynamics of elephant impacts on trees in Chobe National Park, Botswana. MS Thesis. University of Florida, Gainesville (USA).

Fullman, T. J., Child, B., 2013. Water distribution at local and landscape scales affects tree utilization by elephants in C hobe N ational P ark, B otswana. African Journal of Ecology, 51(2), 235-243.

Fullman, T.J. and Bunting, E.L., 2014. Analyzing vegetation change in an elephant-impacted landscape using the moving standard deviation index. *Land*, *3*(1), pp.74-104.

Fung, T. and LeDrew, E., 1988. For change detection using various accuracy. *Photogrammetric engineering and remote sensing*, *54*(10), pp.1449-1454.

Funk, C., Peterson, P., Landsfeld, M., Pedreros, D., Verdin, J., Shukla, S., Husak, G., Rowland, J., Harrison, L., Hoell, A. and Michaelsen, J., 2015. The climate hazards infrared precipitation with stations—a new environmental record for monitoring extremes. *Scientific data*, 2(1), pp.1-21.

Gallego, F.J., 2000. Double sampling for area estimation and map accuracy assessment. Quantifying Spatial Uncertainty in Natural Resources: Theory and Applications from GIS and Remote Sensing, pp.65-77.

Galiatsatos, N., Donoghue, D.N., Watt, P., Bholanath, P., Pickering, J., Hansen, M.C. and Mahmood, A.R., 2020. An assessment of global forest change datasets for national forest monitoring and reporting. *Remote Sensing*, 12(11), p.1790.

Gao, Y., Solórzano, J.V., Quevedo, A. and Loya-Carrillo, J.O., 2021. How BFAST Trend and Seasonal Model Components Affect Disturbance Detection in Tropical Dry Forest and Temperate Forest. *Remote Sensing*, 13(11), p.2033.

Gara, T.W., Murwira, A. and Ndaimani, H., 2016. Predicting forest carbon stocks from high resolution satellite data in dry forests of Zimbabwe: exploring the effect of the red-edge band in forest carbon stocks estimation. *Geocarto international*, *31*(2), pp.176-192.

Gara, T.W., Murwira, A., Dube, T., Sibanda, M., Rwasoka, D.T., Ndaimani, H., Chivhenge, E. and Hatendi, C.M., 2017. Estimating forest carbon stocks in tropical dry forests of Zimbabwe: exploring the performance of high and medium spatial-resolution multispectral sensors. *Southern Forests: a Journal of Forest Science*, *79*(1), pp.31-40.

Gasparri, N.I. and Grau, H.R., 2009. Deforestation and fragmentation of Chaco dry forest in NW Argentina (1972–2007). *Forest ecology and Management, 258(6),* pp.913-921.

Gasparri, N.I., Parmuchi, M.G., Bono, J., Karszenbaum, H. and Montenegro, C.L., 2010. Assessing multi-temporal Landsat 7 ETM+ images for estimating above-ground biomass in subtropical dry forests of Argentina. *Journal of Arid Environments*, *74*(10), pp.1262-1270.

Geiß, C., Pelizari, P.A., Schrade, H., Brenning, A. and Taubenböck, H., 2017. On the effect of spatially non-disjoint training and test samples on estimated model generalization capabilities in supervised classification with spatial features. *IEEE Geoscience and Remote Sensing Letters*, *14*(11), pp.2008-2012.

Geist, H.J. and Lambin, E.F., 2004. Dynamic causal patterns of desertification. *Bioscience*, *54*(9), pp.817-829.

Geist, H.J., 2002. Causes and Pathways of Land Change in Southern Africa during the Past 300 Years: Moving from Simplifications to Generality and Complexity (Ursachen-und Verlaufsanalyse von terrestrischem Wandel im südlichen Afrika (1700–1990). Generalisierung und Komplexität statt Vereinfachung). *Erdkunde*, pp.144-156.

Gessner, U., Machwitz, M., Conrad, C. and Dech, S., 2013. Estimating the fractional cover of growth forms and bare surface in savannas. A multi-resolution approach based on regression tree ensembles. *Remote Sensing of Environment*, *129*, pp.90-102.

GFOI, 2016. Integration of remote-sensing and ground-based observations for estimation of emissions and removals of greenhouse gases in forests: Methods and Guidance from the Global Forest Observations Initiative (GFOI), Edition 2.0. UN Food and Agriculture Organization.

Gibbs, H.K., Brown, S., Niles, J.O. and Foley, J.A., 2007. Monitoring and estimating tropical forest carbon stocks: making REDD a reality. *Environmental research letters*, *2*(4), p.045023.

Gibson, L.A., Jarmain, C., Su, Z. and Eckardt, F.E., 2013. Estimating evapotranspiration using remote sensing and the Surface Energy Balance System–A South African perspective. *Water Sa*, *39*(4), pp.477-484.

Giglio, L., Boschetti, L., Roy, D., Hoffmann, A.A., Humber, M. and Hall, J.V., 2016. Collection 6 modis burned area product user's guide version 1.0. *NASA EOSDIS Land Processes DAAC: Sioux Falls, SD, USA*.

Giglio, L., Boschetti, L., Roy, D.P., Humber, M.L. and Justice, C.O., 2018. The Collection 6 MODIS burned area mapping algorithm and product. *Remote sensing of environment*, *217*, pp.72-85.

Giglio, L., Loboda, T., Roy, D.P., Quayle, B. and Justice, C.O., 2009. An active-fire based burned area mapping algorithm for the MODIS sensor. *Remote sensing of environment*, *113*(2), pp.408-420.

Gill, A.M., 1975. Fire and the Australian flora: a review. *Australian forestry*, *38*(1), pp.4-25.

Gillespie, T.W., Grijalva, A. and Farris, C.N., 2000. Diversity, composition, and structure of tropical dry forests in Central America. *Plant ecology, 147(1),* pp.37-47.

Giri, C., Zhu, Z. and Reed, B., 2005. A comparative analysis of the Global Land Cover 2000 and MODIS land cover data sets. *Remote sensing of environment*, *94*(1), pp.123-132.

Gitelson, A.A., Kaufman, Y.J. and Merzlyak, M.N., 1996. Use of a green channel in remote sensing of global vegetation from EOS-MODIS. *Remote sensing of Environment*, *58*(3), pp.289-298.

Gizachew, B., Astrup, R., Vedeld, P., Zahabu, E.M. and Duguma, L.A., 2017, May. REDD+ in A frica: c ontexts and challenges. In *Natural Resources Forum* (Vol. 41, No. 2, pp. 92-104). Oxford, UK: Blackwell Publishing Ltd.

Gizachew, B., Solberg, S., Næsset, E., Gobakken, T., Bollandsås, O.M., Breidenbach, J., Zahabu, E. and Mauya, E.W., 2016. Mapping and estimating the total living biomass and carbon in low-biomass woodlands using Landsat 8 CDR data. *Carbon balance and management*, *11*(1), pp.1-14.

Glick, H.B., Bettigole, C., Maynard, D.S., Covey, K.R., Smith, J.R. and Crowther, T.W., 2016. Spatially-explicit models of global tree density. Scientific data, 3(1), pp.1-11.

Gnauck, A., 2004. Interpolation and approximation of water quality time series and process identification. *Analytical and bioanalytical chemistry*, 380(3), pp.484-492.

GOFC-GOLD., 2014. A sourcebook of methods and procedures for monitoring and reporting anthropogenic greenhouse gas emissions and removals associated with deforestation, gains and losses of carbon stocks in forests remaining forests, and forestation (No. COP20-1). GOFC-GOLD. Land Cover Project Office, Wageningen University, The Netherlands).

Göksel, Ç., David, R.M. and Dogru, A.O., 2018. Environmental monitoring of spatio-temporal changes in northern Istanbul using remote sensing and GIS. *International Journal of Environment and Geoinformatics*, *5*(1), pp.94-103.

González-M, R., Posada, J.M., Carmona, C.P., Garzón, F., Salinas, V., Idárraga-Piedrahita, Á., Pizano, C., Avella, A., López-Camacho, R., Norden, N. and Nieto, J. (2021). Diverging functional strategies but high sensitivity to an extreme drought in tropical dry forests*. Ecology Letters, 24(3),* pp.451-463.

Google. 2020, Google Earth Engine. https://developers.google.com/earth-engine/sentinel1/ (accessed 26 November 2020).

Gorelick, N., Hancher, M., Dixon, M., Ilyushchenko, S., Thau, D. and Moore, R., 2017. Google Earth Engine: Planetary-scale geospatial analysis for everyone. *Remote sensing of Environment*, 202, pp.18-27.

Grainger, A., 1999. Constraints on modelling the deforestation and degradation of tropical open woodlands. *Global Ecology and Biogeography*, 8(3-4), pp.179-190.

Grainger, A., 2008. Difficulties in tracking the long-term global trend in tropical forest area. *Proceedings of the National Academy of Sciences*, *105*(2), pp.818-823.

Grogan, K., Pflugmacher, D., Hostert, P., Verbesselt, J. and Fensholt, R., 2016. Mapping clearances in tropical dry forests using breakpoints, trend, and seasonal components from MODIS time series: does forest type matter?. *Remote Sensing*, *8*(8), p.657.

Guirado, E., Alcaraz-Segura, D., Cabello, J., Puertas-Ruíz, S., Herrera, F. and Tabik, S., 2020. Tree cover estimation in global drylands from space using deep learning. *Remote Sensing*, *12*(3), p.343.

Guyon, I. and Elisseeff, A., 2003. An introduction to variable and feature selection. Journal of machine learning research, 3(Mar), 1157-1182.

Halperin, J., LeMay, V., Chidumayo, E., Verchot, L. and Marshall, P., 2016. Model-based estimation of above-ground biomass in the miombo ecoregion of Zambia. *Forest Ecosystems*, *3*(1), pp.1-17.

Hamunyela, E., Brandt, P., Shirima, D., Do, H.T.T., Herold, M. and Roman-Cuesta, R.M., 2020. Space-time detection of deforestation, forest degradation and regeneration in montane forests of Eastern Tanzania. *International Journal of Applied Earth Observation and Geoinformation*, *88*, p.102063.

Hamunyela, E., Verbesselt, J. and Herold, M., 2016. Using spatial context to improve early detection of deforestation from Landsat time series. *Remote Sensing of Environment*, *172*, pp.126-138.

Hanks, J., 2003. Transfrontier Conservation Areas (TFCAs) in Southern Africa: their role in conserving biodiversity, socioeconomic development and promoting a culture of peace. *Journal of Sustainable Forestry*, 17(1-2), pp.127-148.

Hansen, M.C. and Loveland, T.R., 2012. A review of large area monitoring of land cover change using Landsat data. *Remote sensing of Environment*, *122*, pp.66-74.

Hansen, M.C., Potapov, P.V., Moore, R., Hancher, M., Turubanova, S.A., Tyukavina, A., Thau, D., Stehman, S.V., Goetz, S.J., Loveland, T.R. and Kommareddy, A., 2013. High-resolution global maps of 21st-century forest cover change. *science*, *342*(6160), pp.850-853.

Hantson, S., Pueyo, S. and Chuvieco, E., 2016. Global fire size distribution: from power law to log-normal. *International journal of wildland fire*, *25*(4), pp.403-412.

Harris, A., Carr, A.S. and Dash, J., 2014. Remote sensing of vegetation cover dynamics and resilience across southern Africa. *International Journal of Applied Earth Observation and Geoinformation*, *28*, pp.131-139.

Harris, N.L., Brown, S., Hagen, S.C., Saatchi, S.S., Petrova, S., Salas, W., Hansen, M.C., Potapov, P.V. and Lotsch, A., 2012. Baseline map of carbon emissions from deforestation in tropical regions. Science, 336(6088), 1573-1576.

Hastie, T., Tibshirani, R., Friedman, J., 2009. The elements of statistical learning: data mining, inference, and prediction, *Springer*, New York.

Hawryło, P., Bednarz, B., Wężyk, P., Szostak, M., 2018. Estimating defoliation of Scots pine stands using machine learning methods and vegetation indices of Sentinel-2. *European Journal of Remote Sensing*, 51(1), 194-204.

Hayward, R.M., Banin, L.F., Burslem, D.F., Chapman, D.S., Philipson, C.D., Cutler, M.E., Reynolds, G., Nilus, R. and Dent, D.H., 2021. Three decades of post-logging tree community recovery in naturally regenerating and actively restored dipterocarp forest in Borneo. *Forest Ecology and Management*, *488*, p.119036.

Heckel, K., Urban, M., Schratz, P., Mahecha, M.D. and Schmullius, C., 2020. Predicting forest cover in distinct ecosystems: The potential of multi-source Sentinel-1 and-2 data fusion. *Remote Sensing*, *12*(2), p.302.

Herold, M., Mayaux, P., Woodcock, C.E., Baccini, A. and Schmullius, C., 2008. Some challenges in global land cover mapping: An assessment of agreement and accuracy in existing 1 km datasets. *Remote Sensing of Environment*, *112*(5), pp.2538-2556.

Herrero, H., Southworth, J., Muir, C., Khatami, R., Bunting, E. and Child, B., 2020. An Evaluation of Vegetation Health in and around Southern African National Parks during the 21st Century (2000–2016). *Applied Sciences*, *10*(7), p.2366.

Herrmann, S.M., Anyamba, A. and Tucker, C.J., 2005. Recent trends in vegetation dynamics in the African Sahel and their relationship to climate. *Global Environmental Change*, *15*(4), pp.394-404.

Higginbottom, T.P., Symeonakis, E., Meyer, H. and van der Linden, S., 2018. Mapping fractional woody cover in semi-arid savannahs using multi-seasonal composites from Landsat data. *ISPRS Journal of Photogrammetry and Remote Sensing*, *139*, pp.88-102.

Higgins, S.I., Bond, W.J. and Trollope, W.S., 2000. Fire, resprouting and variability: a recipe for grass–tree coexistence in savanna. *Journal of Ecology*, *88*(2), pp.213-229.

Higgins, S.I., Delgado-Cartay, M.D., February, E.C. and Combrink, H.J., 2011. Is there a temporal niche separation in the leaf phenology of savanna trees and grasses?. *Journal of Biogeography*, *38*(11), pp.2165-2175.

Hoffman, M.T. and Todd, S., 2000. A national review of land degradation in South Africa: the influence of biophysical and socio-economic factors. *Journal of Southern African Studies*, *26*(4), pp.743-758.

Holben, B.N., 1986. Characteristics of maximum-value composite images from temporal AVHRR data. *International journal of remote sensing*, 7(11), pp.1417-1434.

Holloway, J. and Mengersen, K., 2018. Statistical machine learning methods and remote sensing for sustainable development goals: a review. *Remote Sensing*, *10*(9), p.1365.

Horion, S., Fensholt, R., Tagesson, T. and Ehammer, A. (2014). Using earth observation-based dry season NDVI trends for assessment of changes in tree cover in the Sahel. *International Journal of Remote Sensing, 35(7)*, pp.2493-2515.

Houghton, R.A., Hall, F. and Goetz, S.J., 2009. Importance of biomass in the global carbon cycle. Journal of Geophysical Research: Biogeosciences, 114(G2).

Housman, I.W., Chastain, R.A. and Finco, M.V., 2018. An evaluation of forest health insect and disease survey data and satellite-based remote sensing forest change detection methods: Case studies in the United States. *Remote Sensing*, *10*(8), p.1184.

Huang, C., Goward, S.N., Schleeweis, K., Thomas, N., Masek, J.G. and Zhu, Z., 2009. Dynamics of national forests assessed using the Landsat record: Case studies in eastern United States. *Remote sensing of Environment*, *113*(7), pp.1430-1442.

Huang, J., Li, Y., Fu, C., Chen, F., Fu, Q., Dai, A., Shinoda, M., Ma, Z., Guo, W., Li, Z. and Zhang, L., 2017. Dryland climate change: Recent progress and challenges. *Reviews of Geophysics*, *55*(3), pp.719-778.

Huang, J., Yu, H., Guan, X., Wang, G. and Guo, R., 2016. Accelerated dryland expansion under climate change. *Nature Climate Change*, *6*(2), pp.166-171.

Huang, W., Sun, G., Ni, W., Zhang, Z. and Dubayah, R., 2015. Sensitivity of multi-source SAR backscatter to changes in forest aboveground biomass. *Remote Sensing*, *7*(8), pp.9587-9609.

Huemmrich, K.F., Privette, J.L., Mukelabai, M., Myneni, R.B. and Knyazikhin, Y., 2005. Time-series validation of MODIS land biophysical products in a Kalahari woodland, Africa. *International Journal of Remote Sensing*, *26*(19), pp.4381-4398.

Huete, A., Didan, K., Miura, T., Rodriguez, E.P., Gao, X. and Ferreira, L.G., 2002. Overview of the radiometric and biophysical performance of the MODIS vegetation indices. *Remote sensing of environment*, *83*(1-2), pp.195-213.

Huete, A., Justice, C. and Van Leeuwen, W., 1999. MODIS vegetation index (MOD13). *Algorithm theoretical basis document*, *3*(213), pp.295-309.

Hunt, E.R., Hively, W.D., Daughtry, C.S., McCarty, G.W., Fujikawa, S.J., Ng, T.L., Tranchitella, M., Linden, D.S. and Yoel, D.W., 2008, November. Remote sensing of crop leaf area index using unmanned airborne vehicles. In Proceedings of the Pecora (Vol. 17, pp. 18-20).

Hüttich, C., Gessner, U., Herold, M., Strohbach, B.J., Schmidt, M., Keil, M. and Dech, S., 2009. On the suitability of MODIS time series metrics to map vegetation types in dry savanna ecosystems: A case study in the Kalahari of NE Namibia. *Remote sensing*, *1*(4), pp.620-643.

Hüttich, C., Herold, M., Strohbach, B.J. and Dech, S., 2011. Integrating in-situ, Landsat, and MODIS data for mapping in Southern African savannas: experiences of LCCS-based land-cover mapping in the Kalahari in Namibia. *Environmental monitoring and assessment*, *176*(1), pp.531-547.

Hyde, P., Dubayah, R., Walker, W., Blair, J.B., Hofton, M. and Hunsaker, C., 2006. Mapping forest structure for wildlife habitat analysis using multi-sensor (LiDAR, SAR/InSAR, ETM+, Quickbird) synergy. *Remote Sensing of Environment*, *102*(1-2), pp.63-73.

Ibrahim, S.A., Balzter, H., Tansey, K., Tsutsumida, N. and Mathieu, R., 2018. Estimating fractional cover of plant functional types in African savannah from harmonic analysis of MODIS time-series data. *International Journal of Remote Sensing*, *39*(9), pp.2718-2745.

Ilavajhala, S., Davies, D., Schmaltz, J.E. and Murphy, K.J., 2014, December. Early warning of active fire hotspots through NASA FIRMS fire information system. In *2014 AGU Fall Meeting*. AGU.

Immitzer, M., Böck, S., Einzmann, K., Vuolo, F., Pinnel, N., Wallner, A. and Atzberger, C., 2018. Fractional cover mapping of spruce and pine at 1 ha resolution combining very high and medium spatial resolution satellite imagery. *Remote sensing of environment*, *204*, pp.690-703.

IPCC, 2014. Climate change 2014–Impacts, adaptation and vulnerability: Regional aspects. Cambridge: Cambridge University Press.

IPCC. (2007). Climate Change 2007 : An Assessment of the Intergovernmental Panel on Climate Change'. *Cambridge: Cambridge University Press*.

IPCC. (2014). Climate change 2014–Impacts, adaptation and vulnerability: Regional aspects. Niang, I., O.C. Ruppel, M.A. Abdrabo, A. Essel, C. Lennard, J. Padgham, and P. Urquhart, 2014: Africa. In: Climate Change 2014: Impacts, Adaptation, and Vulnerability. Part B: Regional Aspects. Contribution of Working Group II to the Fifth Assessment Report of the Intergovernmental Panel on Climate Change [Barros, V.R., C.B. Field, D.J. Dokken, M.D. Mastrandrea, K.J. Mach, T.E. Bilir, M. Chatterjee, K.L. Ebi, Y.O. Estrada, R.C. Genova, B. Girma, E.S. Kissel, A.N. Levy, S. MacCracken, P.R. Mastrandrea, and L.L. White (eds.)]. Cambridge University Press, Cambridge, United Kingdom and New York, NY, USA, pp. 1199-1265

IPCC. 2003. Definitions and Methodological Options to Inventory Emissions from Direct Human induced Degradation of Forests and Devegetation of Other Vegetation Types. Penman, J., Gytarsky, M., Krug, T., Kruger, D., Pipatti, R., Buendia, L., Miwa, K., Ngara, T., Tanabe, K. and Wagner, F. (eds.), IPCC-IGES, Kanagawa. IPCC National Greenhouse Gas Inventories Programme, Japan. http://www.ipcc-nggip.iges.or.jp/public/gpglulucf/degradation_contents.htm

IPCC., 2007. Climate Change 2007 : An Assessment of the Intergovernmental Panel on Climate Change'*. Cambridge: Cambridge University Press*.

IPCC., 2014. Climate change 2014–Impacts, adaptation and vulnerability: Regional aspects. *Cambridge: Cambridge University Press.*

ITTO. 2002. Guidelines for the restoration, management and rehabilitation of degraded and secondary tropical forests (No. 13). International Tropical Timber Organization (ITTO).

IUCN. (2020). The IUCN Red List of Threatened Species. www.iucnredlist.org/species/. (accessed 21 February 2020).

Jamali, S., Jönsson, P., Eklundh, L., Ardö, J. and Seaquist, J., 2015. Detecting changes in vegetation trends using time series segmentation. *Remote Sensing of Environment*, 156, pp.182-195.

Jamali, S., Seaquist, J., Eklundh, L. and Ardö, J., 2014. Automated mapping of vegetation trends with polynomials using NDVI imagery over the Sahel. *Remote Sensing of Environment*, 141, pp.79-89.

James, G., Witten, D., Hastie, T. and Tibshirani, R., 2013. An introduction to statistical learning (Vol. 112, 101). New York: springer.

Janssen, L.L. and Vanderwel, F.J., 1994. Accuracy assessment of satellite derived land-cover data: a review. *Photogrammetric engineering and remote sensing;(United States)*, *60*(4).

Janzen, D. H., 1988. Tropical dry forests. *Biodiversity*, 130-137.

Jensen, J.R., 2005. Digital image processing: a remote sensing perspective. *Upper Saddle River, NJ: sPrentice Hall*.

Jin, S. and Sader, S.A., 2005. Comparison of time series tasseled cap wetness and the normalized difference moisture index in detecting forest disturbances. *Remote sensing of Environment*, 94(3), pp.364-372.

Jolly, W.M. and Running, S.W., 2004. Effects of precipitation and soil water potential on drought deciduous phenology in the Kalahari. *Global Change Biology*, *10*(3), pp.303-308.

Jones, M.O., Jones, L.A., Kimball, J.S. and McDonald, K.C. (2011). Satellite passive microwave remote sensing for monitoring global land surface phenology. *Remote Sensing of Environment, 115(4)*, pp.1102-1114.

Joshi, N., Baumann, M., Ehammer, A., Fensholt, R., Grogan, K., Hostert, P., Jepsen, M.R., Kuemmerle, T., Meyfroidt, P., Mitchard, E.T. and Reiche, J., 2016. A review of the application of optical and radar remote sensing data fusion to land use mapping and monitoring. *Remote Sensing*, *8*(1), p.70.

Junker, J., 2009. An analysis of numerical trends in African elephant populations (Doctoral dissertation, *University of Pretoria*).

Kajisa, T., Murakami, T., Mizoue, N., Top, N. and Yoshida, S., 2009. Object-based forest biomass estimation using Landsat ETM+ in Kampong Thom Province, Cambodia. *Journal of Forest Research*, *14*(4), pp.203-211.

Kamwi, J.M. and Mbidzo, M., 2020. Impact of land use and land cover changes on landscape structure in the dry lands of Southern Africa: a case of the Zambezi Region, Namibia. *GeoJournal*, pp.1-12.

Kamwi, J.M., Chirwa, P.W., Manda, S.O., Graz, P.F. and Kätsch, C., 2015. Livelihoods, land use and land cover change in the Zambezi Region, Namibia. *Population and Environment*, *37*(2), pp.207-230.

Kamwi, J.M., Kaetsch, C., Graz, F.P., Chirwa, P. and Manda, S., 2017. Trends in land use and land cover change in the protected and communal areas of the Zambezi Region, Namibia. Environmental monitoring and assessment, 189(5), p.242.

Karidozo, M., La Grange, M. and Osborn, F.V., 2016. Assessment of the human wildlife conflict mitigation measures being implemented by the Kavango-Zambezi Transfrontier Conservation Area (KAZA TFCA) partner countries. Report to the KAZA TFCA Secretariat. *Report to the KAZA TFCA Secretariat (BMZ No.: 2009 66 788 and BMZ No.: 2006 65 646).*

Kasischke, E.S., Melack, J.M. and Dobson, M.C., 1997. The use of imaging radars for ecological applications—A review. *Remote sensing of environment*, *59*(2), pp.141-156.

Kattenborn, T., Leitloff, J., Schiefer, F. and Hinz, S. (2021). Review on Convolutional Neural Networks (CNN) in vegetation remote sensing. *ISPRS Journal of Photogrammetry and Remote Sensing, 173*, pp.24-49.

KAZA., 2014., Kavango-Zambezi Transfrontier Conservation Area, Master Integrated Development Plan 2015-2020.

Kellndorfer, J.M., Walker, W.S., LaPoint, E., Kirsch, K., Bishop, J. and Fiske, G., 2010. Statistical fusion of Lidar, InSAR, and optical remote sensing data for forest stand height characterization: A regional-scale method based on LVIS, SRTM, Landsat ETM+, and ancillary data sets. Journal of Geophysical Research: Biogeosciences, 115(G2).

Kennedy, R.E., Andréfouët, S., Cohen, W.B., Gómez, C., Griffiths, P., Hais, M., Healey, S.P., Helmer, E.H., Hostert, P., Lyons, M.B. and Meigs, G.W., 2014. Bringing an ecological view of change to Landsat-based remote sensing. *Frontiers in Ecology and the Environment*, *12*(6), pp.339-346.

Kennedy, R.E., Yang, Z. and Cohen, W.B., 2010. Detecting trends in forest disturbance and recovery using yearly Landsat time series: 1. LandTrendr—Temporal segmentation algorithms. *Remote Sensing of Environment*, 114(12), pp.2897-2910.

Kimura, T., Imai, T., Sakaizawa, D., Murooka, J. and Mitsuhashi, R., 2017, July. The overview and status of vegetation Lidar mission, MOLI. In *2017 IEEE International Geoscience and Remote Sensing Symposium (IGARSS)* (pp. 4228-4230). IEEE.

King, E. (2014). Southern Africa's Dryland Forests and Climate Change Adaptation. A policy briefing prepared for Governance of Africa’s Resources Programme. https://media.africaportal.org/documents/saia_spb__91_king_20140702.pdf/ (accessed 23 August 2020).

Klogo, G.S., Gasonoo, A. and Ampomah, I.K., 2013. On the Performance of Filters for Reduction of Speckle Noise in SAR Images off the Coast of the Gulf of Guinea. *arXiv preprint arXiv:1312.2383*.

Koch, B, 2010. Status and future of laser scanning, synthetic aperture radar and hyperspectral remote sensing data for forest biomass assessment. ISPRS Journal of Photogrammetry and Remote Sensing, 65(6), 581-590.

Korontzi, S., Justice, C.O. and Scholes, R.J., 2003. Influence of timing and spatial extent of savanna fires in southern Africa on atmospheric emissions. *Journal of Arid Environments*, *54*(2), pp.395-404.

Kuenzer, C., Bluemel, A., Gebhardt, S., Quoc, T.V. and Dech, S., 2011. Remote sensing of mangrove ecosystems: A review. *Remote Sensing*, *3*(5), pp.878-928.

Kuplich, T.M., Moreira, A. and Fontana, D.C., 2013. Série temporal de índice de vegetação sobre diferentes tipologias vegetais no Rio Grande do Sul. *Revista Brasileira de Engenharia Agrícola e Ambiental*, *17*, pp.1116-1123.

Kussul, N., Lavreniuk, M., Skakun, S. and Shelestov, A. (2017). Deep learning classification of land cover and crop types using remote sensing data. *IEEE Geoscience and Remote Sensing Letters, 14(5)*, pp.778-782.

Lambin, E.F. and Ehrlich, D., 1997. Land-cover changes in sub-Saharan Africa (1982–1991): Application of a change index based on remotely sensed surface temperature and vegetation indices at a continental scale. *Remote sensing of environment*, 61(2), pp.181-200.

Lambin, E.F. and Meyfroidt, P., 2010. Land use transitions: Socio-ecological feedback versus socio-economic change. *Land use policy*, *27*(2), pp.108-118.

Lambin, E.F., Geist, H.J. and Lepers, E., 2003. Dynamics of land-use and land-cover change in tropical regions. *Annual review of environment and resources*, 28(1), pp.205-241.

Latifi, H., Nothdurft, A. and Koch, B., 2010. Non-parametric prediction and mapping of standing timber volume and biomass in a temperate forest: application of multiple optical/LiDAR-derived predictors. *Forestry*, *83*(4), pp.395-407.

Laurin, G.V., Puletti, N., Hawthorne, W., Liesenberg, V., Corona, P., Papale, D., Chen, Q. and Valentini, R., 2016. Discrimination of tropical forest types, dominant species, and mapping of functional guilds by hyperspectral and simulated multispectral Sentinel-2 data. Remote Sensing of Environment, 176, 163-176.

Lawal, S., Lennard, C., Jack, C., Wolski, P., Hewitson, B. and Abiodun, B., 2019. The observed and model-simulated response of southern African vegetation to drought. *Agricultural and Forest Meteorology*, *279*, p.107698.

Lawley, V., Lewis, M., Clarke, K. and Ostendorf, B. (2016). Site-based and remote sensing methods for monitoring indicators of vegetation condition: An Australian review. *Ecological Indicators, 60*, pp.1273-1283.

Le Canut, P., Andreae, M.O., Harris, G.W., Wienhold, F.G. and Zenker, T., 1996. Airborne studies of emissions from savanna fires in southern Africa: 1. Aerosol emissions measured with a laser optical particle counter. *Journal of Geophysical Research: Atmospheres*, *101*(D19), pp.23615-23630.

Le Houérou, H.N., 1996. Climate change, drought and desertification. *Journal of arid Environments*, *34*(2), pp.133-185.

Lehmann, C.E., Anderson, T.M., Sankaran, M., Higgins, S.I., Archibald, S., Hoffmann, W.A., Hanan, N.P., Williams, R.J., Fensham, R.J., Felfili, J. and Hutley, L.B., 2014. Savanna vegetation-fire-climate relationships differ among continents. *Science*, *343*(6170), pp.548-552.

Lehmann, E.A., Caccetta, P., Lowell, K., Mitchell, A., Zhou, Z.S., Held, A., Milne, T. and Tapley, I., 2015. SAR and optical remote sensing: Assessment of complementarity and interoperability in the context of a large-scale operational forest monitoring system. *Remote Sensing of Environment*, *156*, pp.335-348.

Leite, A., Cáceres, A., Melo, M., Mills, M.S. and Monteiro, A.T., 2018. Reducing emissions from Deforestation and forest Degradation in Angola: Insights from the scarp forest conservation 'hotspot'. *Land Degradation & Development*, *29*(12), pp.4291-4300.

Lesolle, D., 2012. SADC Policy Paper on Climate Change: Assessing the Policy Options for SADC Member States; SADC Secretariat, Policy, Planning. *Resource Mobilisation Directorate: Gaborone, Botswana*.

Lewis, S.L., Sonké, B., Sunderland, T., Begne, S.K., Lopez-Gonzalez, G., Van Der Heijden, G.M., Phillips, O.L., Affum-Baffoe, K., Baker, T.R., Banin, L. and Bastin, J.F., 2013., Above-ground biomass and structure of 260 African tropical forests. *Philosophical Transactions of the Royal Society B: Biological Sciences*, 368(1625), p.20120295.

Li, A., Dhakal, S., Glenn, N.F., Spaete, L.P., Shinneman, D.J., Pilliod, D.S., Arkle, R.S. and McIlroy, S.K., 2017. Lidar aboveground vegetation biomass estimates in shrublands: Prediction, uncertainties and application to coarser scales. *Remote Sensing*, *9*(9), p.903.

Li, C., Gong, P., Wang, J., Zhu, Z., Biging, G.S., Yuan, C., Hu, T., Zhang, H., Wang, Q., Li, X. and Liu, X., 2017. The first all-season sample set for mapping global land cover with Landsat-8 data. *Science Bulletin*, *62*(7), pp.508-515.

Li, C., Zhou, L. and Xu, W., 2021. Estimating aboveground biomass using Sentinel-2 MSI data and ensemble algorithms for grassland in the Shengjin Lake Wetland, China. Remote Sensing, 13(8), 1595

Liao, W., Van Coillie, F., Gao, L., Li, L., Zhang, B. and Chanussot, J. (2018). Deep learning for fusion of APEX hyperspectral and full-waveform LiDAR remote sensing data for tree species mapping. *IEEE Access, 6*, pp.68716-68729.

Liaw, A., Wiener, M., 2002. Classification and regression by randomForest. *R news*, 2(3), 18-22.

Liaw, A., Wiener, M., 2002. Classification and regression by randomForest. R news, 2(3), 18-22.

Linares-Palomino, R., Oliveira-Filho, A.T. and Pennington, R.T., 2011. Neotropical seasonally dry forests: diversity, endemism, and biogeography of woody plants. In Seasonally dry tropical forests (pp. 3-21). *Island Press,* Washington, DC.

Liu, G., Liu, H. and Yin, Y., 2013. Global patterns of NDVI-indicated vegetation extremes and their sensitivity to climate extremes. *Environmental Research Letters*, *8*(2), p.025009.

Liu, X. and Zhou, J., 2021. Assessment of the Continuous Extreme Drought Events in Namibia during the last decade. Water, 13(20), 2942.

Liu, X., Wigneron, J.P., Fan, L., Frappart, F., Ciais, P., Baghdadi, N., Zribi, M., Jagdhuber, T., Li, X., Wang, M. and Bai, X. (2021). ASCAT IB: A radar-based vegetation optical depth retrieved from the ASCAT scatterometer satellite*. Remote Sensing of Environment, 264*, p.112587.

Liu, Y. A., Gong, W. S., Xing, Y. Q., Hu, X. Y., ong, J. Y., 2019. Estimation of the forest stand mean height and aboveground biomass in Northeast China using SAR Sentinel-1B, multispectral Sentinel-2A, and DEM imagery. *ISPRS Journal of Photogrammetry and Remote Sensing*, 151, 277-289.

Liu, Y.Y., De Jeu, R.A., McCabe, M.F., Evans, J.P. and Van Dijk, A.I. (2011). Global long-term passive microwave satellite-based retrievals of vegetation optical depth. *Geophysical Research Letters, 38(18).*

Liu, Y.Y., Van Dijk, A.I., De Jeu, R.A., Canadell, J.G., McCabe, M.F., Evans, J.P. and Wang, G. (2015). Recent reversal in loss of global terrestrial biomass. *Nature Climate Change, 5(5),* pp.470-474.

Liu, Z., Wimberly, M.C. and Dwomoh, F.K., 2017. Vegetation dynamics in the upper guinean forest region of West Africa from 2001 to 2015. *Remote Sensing*, 9(1), p.5.

Lu, D. and Weng, Q., 2005. Urban classification using full spectral information of Landsat ETM+ imagery in Marion County, Indiana. *Photogrammetric Engineering & Remote Sensing*, *71*(11), pp.1275-1284.

Lu, D., 2006. The potential and challenge of remote sensing-based biomass estimation. *International journal of remote sensing*, *27*(7), pp.1297-1328.

Lu, D., Batistella, M., Moran, E. and de Miranda, E.E., 2008. A comparative study of Landsat TM and SPOT HRG images for vegetation classification in the Brazilian Amazon. *Photogrammetric Engineering & Remote Sensing*, *74*(3), pp.311-321.

Lu, D., Chen, Q., Wang, G., Liu, L., Li, G., Moran, E., 2016. A survey of remote sensing-based aboveground biomass estimation methods in forest ecosystems. *International Journal of Digital Earth*, 9(1), 63-105.

Lu, D., Chen, Q., Wang, G., Moran, E., Batistella, M., Zhang, M., Vaglio Laurin, G. and Saah, D., 2012. Aboveground forest biomass estimation with Landsat and LiDAR data and uncertainty analysis of the estimates. *International Journal of Forestry Research*, *2012.*

Lu, D., Mausel, P., Brondızio, E., Moran, E., 2004. Relationships between forest stand parameters and Landsat TM spectral responses in the Brazilian Amazon Basin. *Forest Ecology and Management*, 198(1-3), 149-167.

Lu, D., Moran, E. and Batistella, M., 2003. Linear mixture model applied to Amazonian vegetation classification. *Remote sensing of environment*, *87*(4), pp.456-469.

Lucas, R., Accad, A., Randall, L., Bunting, P., Armston, J., 2008. Assessing Human Impacts on Australian Forests through Integration of Remote Sensing Data, in Lafortezza, R., Chen, J., Sanesi, G., Crow, Th.R. (Eds.), Patterns and Processes in Forest Landscapes, *Springer, Dordrecht*, pp. 213-239.

Lucas, R.M., Cronin, N., Lee, A., Moghaddam, M., Witte, C. and Tickle, P., 2006. Empirical relationships between AIRSAR backscatter and LiDAR-derived forest biomass, Queensland, Australia. Remote Sensing of Environment, 100(3), 407-425.

Lucas, R.M., Mitchell, A.L. and Armston, J., 2015. Measurement of forest above-ground biomass using active and passive remote sensing at large (subnational to global) scales. *Current Forestry Reports*, *1*(3), pp.162-177.

Lück, W. and Van Niekerk, A., 2016. Evaluation of a rule-based compositing technique for Landsat-5 TM and Landsat-7 ETM+ images. *International Journal of Applied Earth Observation and Geoinformation*, *47*, pp.1-14

Lund, H.G., 2009. What is a degraded forest. Gainesville, VA. USA: Forest Information Services.

Lyon, B. and Mason, S.J., 2007. The 1997–98 summer rainfall season in southern Africa. Part I: Observations. *Journal of Climate*, 20(20), pp.5134-5148.

Madonsela, S., Cho, M.A., Ramoelo, A., Mutanga, O. and Naidoo, L., 2018. Estimating tree species diversity in the savannah using NDVI and woody canopy cover. *International journal of applied earth observation and geoinformation*, *66*, pp.106-115.

Maglione, P., 2016. Very high resolution optical satellites: An overview of the most commonly used. *American Journal of Applied Sciences*, *13*(1), p.91.

Maliva, R. and Missimer, T., 2012. Aridity and drought. In *Arid lands water evaluation and management* (pp. 21-39). *Springer, Berlin, Heidelberg*.

Manatsha, B. T., Malebang, G. G., 2016. The Botswana-Japan Diplomatic Relations, 1966-2016. *Botswana Notes and Records*, 48, 97-108.

Mapfumo, R.B., Murwira, A., Masocha, M. and Andriani, R., 2016. The relationship between satellite-derived indices and species diversity across African savanna ecosystems. *International journal of applied earth observation and geoinformation*, *52*, pp.306-317.

Mareya, H.T., Tagwireyi, P., Ndaimani, H., Gara, T.W. and Gwenzi, D., 2018. Estimating tree crown area and aboveground biomass in miombo woodlands from high-resolution RGB-only imagery. *IEEE Journal of selected topics in applied earth observations and remote sensing*, *11*(3), pp.868-875.

Marín-Spiotta, E., Cusack, D.F., Ostertag, R. and Silver, W.L. (2008). Trends in above and belowground carbon with forest regrowth after agricultural abandonment in the neotropics. In Post-agricultural succession in the neotropics (pp. 22-72). Springer, New York, NY.

Marston, C.G., Wilkinson, D.M., Sponheimer, M., Codron, D., Codron, J. and O'Regan, H.J., 2020. 'Remote'behavioural ecology: do megaherbivores consume vegetation in proportion to its presence in the landscape?. *PeerJ*, *8*, p.e8622.

Marta, S., 2018. Planet Imagery Product Specifications. *Planet Labs: San Francisco, CA, USA*, p.91.

Martens, B., Miralles, D.G., Lievens, H., Van Der Schalie, R., De Jeu, R.A., Fernández-Prieto, D., Beck, H.E., Dorigo, W.A. and Verhoest, N.E., 2017. GLEAM v3: Satellite-based land evaporation and root-zone soil moisture. *Geoscientific Model Development*, *10*(5), pp.1903-1925.

Marumbwa, F.M., Cho, M.A. and Chirwa, P.W., 2020. An assessment of remote sensing-based drought index over different land cover types in southern Africa. *International Journal of Remote Sensing*, *41*(19), pp.7368-7382.

Marumbwa, F.M., Cho, M.A. and Chirwa, P.W., 2021. Geospatial analysis of meteorological drought impact on Southern Africa biomes. *International Journal of Remote Sensing*, *42*(6), pp.2155-2173.

Masiello, G., Cersosimo, A., Mastro, P., Serio, C., Venafra, S. and Pasquariello, P., 2020, September. Emissivity-based vegetation indices to monitor deforestation and forest degradation in the Congo basin rainforest. In Remote Sensing for Agriculture, Ecosystems, and Hydrology XXII (Vol. 11528, p. 115280L). *International Society for Optics and Photonics*.

Mason, P.J., Zillman, J.W., Simmons, A., Lindstrom, E.J., Harrison, D.E., Dolman, H., Bojinski, S., Fischer, A., Latham, J., Rasmussen, J. and Arkin, P., 2009, December. Implementation plan for the global observing system for climate in support of the UNFCCC (2010 Update). In *Proceedings of the Conference of the Parties (COP), Copenhagen, Denmark* (pp. 7-18).

Mason, S.J. and Tyson, P., 2000. The occurrence and predictability of droughts over southern Africa, *Routledge*. https://doi.org/10.4324 9781315830896/ (accessed 04 August 2021).

Matavire, M. M., Sibanda, M., & Dube, T. (2015). Assessing the aftermath of the fast track land reform programme in Zimbabwe on land-use and land-cover changes. *Transactions of the Royal Society of South Africa*, 70(2), pp.181-186.

Mathieu, R., Main, R., Roy, D.P., Naidoo, L. and Yang, H., 2019. The Effect of Surface Fire in Savannah Systems in the Kruger National Park (KNP), South Africa, on the Backscatter of C-Band Sentinel-1 Images. *Fire*, *2*(3), p.37.

Mathieu, R., Naidoo, L., Cho, M.A., Leblon, B., Main, R., Wessels, K., Asner, G.P., Buckley, J., Van Aardt, J., Erasmus, B.F. and Smit, I.P., 2013. Toward structural assessment of semi-arid

African savannahs and woodlands: The potential of multitemporal polarimetric RADARSAT-2 fine beam images. *Remote Sensing of Environment*, *138*, pp.215-231.

Matswiri, G.M., 2017. Two in one: explaining the management of the Okavango Delta World Heritage Site, Botswana (*Master's thesis, University of Cape Town*).

Mayes, M., Mustard, J., Melillo, J., Neill, C. and Nyadzi, G., 2017. Going beyond the green: senesced vegetation material predicts basal area and biomass in remote sensing of tree cover conditions in an African tropical dry forest (miombo woodland) landscape. *Environmental Research Letters*, *12*(8), p.085004.

Mayr, M.J., Vanselow, K.A. and Samimi, C., 2018. Fire regimes at the arid fringe: A 16-year remote sensing perspective (2000–2016) on the controls of fire activity in Namibia from spatial predictive models. *Ecological Indicators*, *91*, pp.324-337.

Mbow, C., Brandt, M., Ouedraogo, I., De Leeuw, J. and Marshall, M., 2015. What four decades of earth observation tell us about land degradation in the Sahel?. *Remote Sensing*, *7*(4), pp.4048-4067.

McCarthy, J., Gumbricht, T. and McCarthy, T.S., 2005. Ecoregion classification in the Okavango Delta, Botswana from multitemporal remote sensing. *International Journal of Remote Sensing*, *26*(19), pp.4339-4357.

McClean, C.J., Lovett, J.C., Küper, W., Hannah, L., Sommer, J.H., Barthlott, W., Termansen, M., Smith, G.F., Tokumine, S. and Taplin, J.R., 2005. African plant diversity and climate change. *Annals of the Missouri Botanical Garden*, pp.139-152.

McElhinny, C., Gibbons, P., Brack, C. and Bauhus, J., 2005. Forest and woodland stand structural complexity: its definition and measurement. *Forest Ecology and Management*, *218*(1-3), pp.1-24.

McGann, J, 2004. The current status of unfccc article 6 work program implementation in Namibia. *In African Workshop on Article*, vol. 6, pp. 28-30.

McIntyre, C, 2010. Botswana: Okavango Delta-Chobe-Northern Kalahari: *Bradt Travel Guides*, pp. 197-214.

McKenzie, J.E., Brennan, S.E., Ryan, R.E., Thomson, H.J., Johnston, R.V. and Thomas, J., 2019. Defining the criteria for including studies and how they will be grouped for the synthesis. *Cochrane handbook for systematic reviews of interventions*, pp.33-65.

McNicol, I.M., Ryan, C.M. and Mitchard, E.T., 2018. Carbon losses from deforestation and widespread degradation offset by extensive growth in African woodlands. *Nature communications*, 9(1), pp.1-11.

Meadows, M.E., 2006. Global change and southern Africa. *Geographical Research*, *44*(2), pp.135-145.

Melton, D.A., 1985. The status of elephants in northern Botswana. Biological Conservation, 31(4), 317-333.

Méndez, V.E., Gliessman, S.R. and Gilbert, G.S. (2007). Tree biodiversity in farmer cooperatives of a shade coffee landscape in western El Salvador. Agriculture, *Ecosystems & Environment, 119(1-2),* pp.145-159.

Mendivelso, H.A., Camarero, J.J., Gutiérrez, E. and Zuidema, P.A. (2014). Time-dependent effects of climate and drought on tree growth in a Neotropical dry forest: Short-term tolerance vs. long-term sensitivity. *Agricultural and Forest Meteorology, 188*, pp.13-23

Menzel, A. and Fabian, P., 1999. Growing season extended in Europe. *Nature*, 397(6721), pp.659-659.

Metternicht, G., Zinck, J.A., Blanco, P.D. and del Valle, H.F. (2010). Remote sensing of land degradation: Experiences from Latin America and the Caribbean. *Journal of environmental quality, 39(1),* pp.42-61.

Meyer, M., Klingelhoeffer, E., Naidoo, R., Wingate, V. and Börner, J., 2021. Tourism opportunities drive woodland and wildlife conservation outcomes of community-based conservation in Namibia's Zambezi region. *Ecological Economics*, 180, p.106863.

Meyer, T., D'Odorico, P., Okin, G.S., Shugart, H.H., Caylor, K.K., O'Donnell, F.C., Bhattachan, A. and Dintwe, K., 2014. An analysis of structure: biomass structure relationships for characteristic species of the western K alahari, B otswana. *African journal of ecology*, *52*(1), pp.20-29.

Michelakis, D., Stuart, N., Lopez, G., Linares, V. and Woodhouse, I.H., 2014. Local-scale mapping of biomass in tropical lowland pine savannas using ALOS PALSAR. *Forests*, *5*(9), pp.2377-2399.

Middleton, N. and Thomas, D., 1997. World atlas of desertification*.. ed. 2*. *Edward Arnold, London*. (pp. 66).

Midgley, G.F. and Thuiller, W., 2011. Potential responses of terrestrial biodiversity in Southern Africa to anthropogenic climate change. *Regional Environmental Change*, *11*(1), pp.127-135.

Miles, L., Newton, A. C., DeFries, R. S., Ravilious, C., May, I., Blyth, S., Kapos, V., Gordon, J. E., 2006. A global overview of the conservation status of tropical dry forests. *Journal of Biogeography*, 33(3), 491-505.

Mitchard, E. T., Saatchi, S. S., Baccini, A., Asner, G. P., Goetz, S. J., Harris, N. L., Brown, S., 2013. Uncertainty in the spatial distribution of tropical forest biomass: a comparison of pan-tropical maps. *Carbon Balance and Management*, 8(1), 1-13.

Mitchard, E.T. and Flintrop, C.M. (2013). Woody encroachment and forest degradation in sub-Saharan Africa's woodlands and savannas 1982–2006. Philosophical Transactions of the Royal Society B: *Biological Sciences, 368(1625)*, p.20120406.

Mitchard, E.T., Saatchi, S.S., Lewis, S.L., Feldpausch, T.R., Woodhouse, I.H., Sonké, B., Rowland, C. and Meir, P., 2011. Measuring biomass changes due to woody encroachment and deforestation/degradation in a forest–savanna boundary region of central Africa using multi-temporal L-band radar backscatter. Remote Sensing of Environment, 115(11), 2861-2873.

Mitchard, E.T., Saatchi, S.S., Woodhouse, I.H., Nangendo, G., Ribeiro, N.S., Williams, M., Ryan, C.M., Lewis, S.L., Feldpausch, T.R. and Meir, P., 2009. Using satellite radar backscatter to predict above-ground woody biomass: A consistent relationship across four different African landscapes. *Geophysical Research Letters*, *36*(23).

Mitchell, A.L., Rosenqvist, A. and Mora, B., 2017. Current remote sensing approaches to monitoring forest degradation in support of countries measurement, reporting and verification (MRV) systems for REDD+. *Carbon balance and management*, *12*(1), pp.1-22.

Moher, D., Liberati, A., Tetzlaff, J., Altman, D.G. and Prisma Group, 2009. Preferred reporting items for systematic reviews and meta-analyses: the PRISMA statement. *PLoS medicine*, *6*(7), p.e1000097.

Mooney, H. A., Bullock, S. H., and Medina, E., 1995. Introduction. In: Bullock SH, Mooney HA, Medina E (eds) Seasonally dry tropical forests. *Cambridge: Cambridge University Press.*

Moore, C.E., Brown, T., Keenan, T.F., Duursma, R.A., Van Dijk, A.I., Beringer, J., Culvenor, D., Evans, B., Huete, A., Hutley, L.B. and Maier, S. (2016). Reviews and syntheses: Australian vegetation phenology: new insights from satellite remote sensing and digital repeat photography. *Biogeosciences, 13(17)*, pp.5085-5102.

Morley, P.J., Donoghue, D.N., Chen, J.C. and Jump, A.S., 2019. Quantifying structural diversity to better estimate change at mountain forest margins. *Remote Sensing of Environment*, *223*, pp.291-306.

Morley, P.J., Jump, A.S., West, M.D. and Donoghue, D.N., 2020. Spectral response of chlorophyll content during leaf senescence in European beech trees. *Environmental Research Communications*, *2*(7), p.071002.

Mosugelo, D. K., Moe, S. R., Ringrose, S., Nellemann, C., 2002. Vegetation changes during a 36-year period in northern Chobe National Park, Botswana. *African Journal of Ecology*, 40(3), 232-240.

Mouillot, F., Schultz, M.G., Yue, C., Cadule, P., Tansey, K., Ciais, P. and Chuvieco, E., 2014. Ten years of global burned area products from spaceborne remote sensing—A review: Analysis of user needs and recommendations for future developments. *International Journal of Applied Earth Observation and Geoinformation*, *26*, pp.64-79.

Mpakairi, K.S., Tagwireyi, P., Ndaimani, H. and Madiri, H.T., 2019. Distribution of wildland fires and possible hotspots for the Zimbabwean component of Kavango-Zambezi Transfrontier Conservation Area. *South African Geographical Journal= Suid-Afrikaanse Geografiese Tydskrif*, *101*(1), pp.110-120.

Muraoka, H. and Koizumi, H., 2009. Satellite Ecology (SATECO)—linking ecology, remote sensing and micrometeorology, from plot to regional scale, for the study of ecosystem structure and function. *Journal of plant research*, *122*(1), pp.3-20.

Murphy, C.A., 2008. Living in a Global Commons–the case of residents of a national park in the Kavango-Zambezi Transfrontier Conservation Area (KaZa TFCA), southern Africa.

Murphy, P.G. and Lugo, A.E., 1986. Ecology of tropical dry forest. *Annual review of ecology and systematics*, *17*(1), pp.67-88.

Mutanga, O. and Rugege, D., 2006. Integrating remote sensing and spatial statistics to model herbaceous biomass distribution in a tropical savanna. *International Journal of Remote Sensing*, *27*(16), pp.3499-3514.

Mutanga, O. and Skidmore, A.K., 2004. Narrow band vegetation indices overcome the saturation problem in biomass estimation. *International journal of remote sensing*, *25*(19), pp.3999-4014.

Mutanga, O., Adam, E. and Cho, M.A., 2012. High density biomass estimation for wetland vegetation using WorldView-2 imagery and random forest regression algorithm. International Journal of Applied Earth Observation and Geoinformation, 18, 399-406.

Mutanga, O., Dube, T. and Ahmed, F., 2016. Progress in remote sensing: vegetation monitoring in South Africa. *South African Geographical Journal*, *98*(3), pp.461-471.

Mutanga, O., Van Aardt, J. and Kumar, L., 2009. Imaging spectroscopy (hyperspectral remote sensing) in southern Africa: an overview. *South African Journal of Science*, *105*(5), pp.193-198.

Myeong, S., Nowak, D.J., Hopkins, P.F. and Brock, R.H., 2001. Urban cover mapping using digital, high-spatial resolution aerial imagery. *Urban ecosystems*, *5*(4), pp.243-256.

Myneni, R.B., Keeling, C.D., Tucker, C.J., Asrar, G. and Nemani, R.R., 1997. Increased plant growth in the northern high latitudes from 1981 to 1991. *Nature*, *386*(6626), pp.698-702.

NACSO. (2014). The state of community conservation in namibia. A review of communal conservancies,community forests and other CBNRM initiatives. *Windhoek, NASCO*.

Næsset, E., McRoberts, R.E., Pekkarinen, A., Saatchi, S., Santoro, M., Trier, Ø.D., Zahabu, E. and Gobakken, T., 2020. Use of local and global maps of forest canopy height and aboveground biomass to enhance local estimates of biomass in miombo woodlands in Tanzania. International Journal of Applied Earth Observation and Geoinformation, 93, 102138.

Naidoo, L., Mathieu, R., Main, R., Wessels, K. and Asner, G.P., 2016. L-band Synthetic Aperture Radar imagery performs better than optical datasets at retrieving woody fractional cover in deciduous, dry savannahs. *International journal of applied earth observation and geoinformation*, *52*, pp.54-64.

Naidoo, R., Chase, M.J., Beytell, P., Du Preez, P., Landen, K., Stuart-Hill, G. and Taylor, R., 2016. A newly discovered wildlife migration in Namibia and Botswana is the longest in Africa. *Oryx*, *50*(1), pp.138-146.

Naidoo, R., Du Preez, P., Stuart-Hill, G., Jago, M. and Wegmann, M., 2012. Home on the range: factors explaining partial migration of African buffalo in a tropical environment. *PLoS one*, *7*(5), p.e36527.

Naidoo, S., Davis, C. and Van Garderen, E.A., 2013. Forests, rangelands and climate change in southern Africa. *Forests and climate change working paper*, *12*.

Naik, M., 2015. Modeling the potential impacts of vegetation change on the future climate of Southern Africa (*Master's thesis, University of Cape Town*).

Nandy, S., Singh, R., Ghosh, S., Watham, T., Kushwaha, S.P.S., Kumar, A.S. and Dadhwal, V.K., 2017. Neural network-based modelling for forest biomass assessment. Carbon Management, 8(4), 305-317.

Nanni, A.S., Sloan, S., Aide, T.M., Graesser, J., Edwards, D. and Grau, H.R. (2019). The neotropical reforestation hotspots: A biophysical and socioeconomic typology of contemporary forest expansion. *Global environmental change, 54*, pp.148-159.

Narine, L.L., Popescu, S.C. and Malambo, L. (2019). Synergy of ICESat-2 and Landsat for mapping forest aboveground biomass with deep learning. *Remote Sensing, 11(12),* p.1503.

Nemani, R.R., Keeling, C.D., Hashimoto, H., Jolly, W.M., Piper, S.C., Tucker, C.J., Myneni, R.B. and Running, S.W., 2003. Climate-driven increases in global terrestrial net primary production from 1982 to 1999. science, 300(5625), pp.1560-1563.

Niang, I., Ruppel, O. C., Abdrabo, M. A., Essel, A., Lennard, C., Padgham, J., and Urquhart, P., 2014. Climate Change 2014: Impacts, Adaptation and Vulnerability - Contributions of the

Working Group II to the Fifth Assessment Report of the Intergovernmental Panel on Climate Change*., (*pp. 1199–1265*).*

Nichols, C., Vandewalle, M., Alexander, K., 2017. Emerging threats to dryland forest resources: elephants and fire are only part of the story. Forestry: *An International Journal of Forest Research*, 90(4), 473-484.

Nicholson, S.E., 2011. Dryland climatology.

Nizalapur, V., Jha, C.S. and Madugundu, R., 2010. Estimation of above ground biomass in Indian tropical forested area using multi-frequency DLR-ESAR data. International Journal of Geomatics and Geosciences, 1(2), 167.

Nobre, C.A. and Borma, L.D.S., 2009. 'Tipping points' for the Amazon forest. *Current Opinion in Environmental Sustainability*, *1*(1), pp.28-36.

Nobre, C.A., Sampaio, G., Borma, L.S., Castilla-Rubio, J.C., Silva, J.S. and Cardoso, M., 2016. Land-use and climate change risks in the Amazon and the need of a novel sustainable development paradigm. *Proceedings of the National Academy of Sciences*, *113*(39), pp.10759-10768.

Nott, K., Nott, A. and Newton, D., 2020. NAMIBIAN INDIGENOUS FOREST/TIMBER INDUSTRY.

O'brien, R.M., 2007. A caution regarding rules of thumb for variance inflation factors. Quality & quantity, 41(5),673-690.

O'Connell-Rodwell, C.E., Rodwell, T., Rice, M. and Hart, L.A., 2000. Living with the modern conservation paradigm: can agricultural communities co-exist with elephants? A five-year case study in East Caprivi, Namibia. *Biological conservation*, *93*(3), pp.381-391.

Olander, L.P., Gibbs, H.K., Steininger, M., Swenson, J.J. and Murray, B.C., 2008. Reference scenarios for deforestation and forest degradation in support of REDD: a review of data and methods. *Environmental Research Letters*, *3*(2), p.025011.

Oliveira, C.P.D., Ferreira, R.L.C., da Silva, J.A.A., Lima, R.B.D., Silva, E.A., Silva, A.F.D., Lucena, J.D.S.D., dos Santos, N.A.T., Lopes, I.J.C., Pessoa, M.M.D.L. and Melo, C.L.S.M.S.D., 2021. Modeling and Spatialization of Biomass and Carbon Stock Using LiDAR Metrics in Tropical Dry Forest, Brazil. *Forests*, *12*(4), p.473.

Olson, D. M., Dinerstein, E., 2002. The Global 200: Priority ecoregions for global conservation. *Annals of the Missouri Botanical Garden*, 199-224.

Olson, D.M., Dinerstein, E., Wikramanayake, E.D., Burgess, N.D., Powell, G.V., Underwood, E.C., D'amico, J.A., Itoua, I., Strand, H.E., Morrison, J.C. and Loucks, C.J. (2001). Terrestrial Ecoregions of the World: A New Map of Life on EarthA new global map of terrestrial ecoregions provides an innovative tool for conserving biodiversity. *BioScience, 51(11),* pp.933-938.

Olsson, L., Barbosa, H., Bhadwal, S., Cowie, A., Delusca, K., Flores-Renteria, D., Hermans, K., Jobbagy, E., Kurz, W., Li, D. and Sonwa, D.J., 2019. Land degradation: IPCC special report on climate change, desertification, land 5 degradation, sustainable land management, food security, and 6 greenhouse gas fluxes in terrestrial ecosystems. In *IPCC Special Report on Climate Change, Desertification, Land 5 Degradation, Sustainable Land Management, Food Security, and 6 Greenhouse gas fluxes in Terrestrial Ecosystems* (p. 1). Intergovernmental Panel on Climate Change (IPCC).

Olsson, L., Eklundh, L. and Ardö, J. (2005). A recent greening of the Sahel—trends, patterns and potential causes. *Journal of Arid Environments, 63(3),* pp.556-566.

Omar, H., Misman, M. A., Kassim, A., 2017. Synergetic of PALSAR-2 and Sentinel-1A SAR Polarimetry for Retrieving Aboveground Biomass in Dipterocarp Forest of Malaysia. *Applied Sciences*, 7(7), 675.

Omphile, U.J. and Powell, J., 2002. Large ungulate habitat preference in Chobe National Park, Botswana. *Rangeland Ecology & Management/Journal of Range Management Archives*, 55(4), pp.341-349.

Otsu, K., Pla, M., Duane, A., Cardil, A. and Brotons, L., 2019. Estimating the threshold of detection on tree crown defoliation using vegetation indices from UAS multispectral imagery. *Drones*, 3(4), p.80.

Ouaadi, N., Jarlan, L., Ezzahar, J., Zribi, M., Khabba, S., Bouras, E., Bousbih, S. and Frison, P.L., 2020. Monitoring of wheat crops using the backscattering coefficient and the interferometric coherence derived from Sentinel-1 in semi-arid areas. Remote Sensing of Environment, 251, 112050.

Owe, M., Van de Griend, A.A. and Chang, A.T.C. (1992). Surface moisture and satellite microwave observations in semiarid southern Africa. *Water Resources Research, 28(3*), pp.829-839.

Paradzayi, C. and Annegarn, H.J., 2012. Estimating potential woody biomass in communal savanna woodlands from synthetic aperture radar (SAR). *International Journal of Applied Geospatial Research (IJAGR)*, *3*(1), pp.53-62.

Paruelo, J.M., Texeira, M., Staiano, L., Mastrángelo, M., Amdan, L. and Gallego, F. (2016). An integrative index of Ecosystem Services provision based on remotely sensed data. *Ecological Indicators, 71*, pp.145-154.

Pause, M., Schweitzer, C., Rosenthal, M., Keuck, V., Bumberger, J., Dietrich, P., Heurich, M., Jung, A. and Lausch, A., 2016. In situ/remote sensing integration to assess forest health—A review. *Remote Sensing*, *8*(6), p.471.

Pearse, G.D., Watt, M.S., Dash, J.P., Stone, C. and Caccamo, G., 2019. Comparison of models describing forest inventory attributes using standard and voxel-based lidar predictors across a range of pulse densities. International Journal of Applied Earth Observation and Geoinformation, 78, 341-351.

Peng, J., Dadson, S., Leng, G., Duan, Z., Jagdhuber, T., Guo, W. and Ludwig, R., 2019. The impact of the Madden-Julian Oscillation on hydrological extremes. *Journal of Hydrology*, *571*, pp.142-149.

Pennington, R.T., Lehmann, C.E. and Rowland, L.M., 2018. Tropical savannas and dry forests. *Current Biology*, *28*(9), pp.R541-R545.

Pereira Júnior, A.C., Oliveira, S.L., Pereira, J.M. and Turkman, M.A.A. (2014). Modelling fire frequency in a Cerrado savanna protected area. *PloS one, 9(7),* p.e102380.

Petheram, L., Campbell, B.M., Marunda, C.T., Tiveau, D. and Shackleton, S., 2006. The wealth of the dry forests: can sound forest management contribute to the millennium development goals in Sub-Saharan Africa?

Pettorelli, N., Vik, J.O., Mysterud, A., Gaillard, J.M., Tucker, C.J. and Stenseth, N.C., 2005. Using the satellite-derived NDVI to assess ecological responses to environmental change. *Trends in ecology & evolution*, *20*(9), pp.503-510.

Pham, M.H., Do, T.H., Pham, V.M. and Bui, Q.T., 2020. Mangrove forest classification and aboveground biomass estimation using an atom search algorithm and adaptive neuro-fuzzy inference system. Plos one, 15(5), e0233110.

Pirotti, F., 2011. Analysis of full-waveform LiDAR data for forestry applications: a review of investigations and methods. iForest-Biogeosciences and Forestry, 4(3), p.100.

Popescu, S.C., 2007. Estimating biomass of individual pine trees using airborne lidar. Biomass and Bioenergy, 31(9), 646-655.

Portillo, C. 2010. Assessing the Conservation status of Neotropical Dry forests using Geographic Information Systems and Optical Remote Sensing.

Portillo-Quintero, C.A., Sanchez, A.M., Valbuena, C.A., Gonzalez, Y.Y. and Larreal, J.T. (2012). Forest cover and deforestation patterns in the Northern Andes (Lake Maracaibo Basin): a synoptic assessment using MODIS and Landsat imagery. *Applied Geography, 35(1-2),* pp.152-163.

Potapov, P.V., Dempewolf, J., Talero, Y., Hansen, M.C., Stehman, S.V., Vargas, C., Rojas, E.J., Castillo, D., Mendoza, E., Calderón, A. and Giudice, R., 2014. National satellite-based humid tropical forest change assessment in Peru in support of REDD+ implementation. Environmental Research Letters, 9(12), p.124012.

Poulter, B., Frank, D., Ciais, P., Myneni, R.B., Andela, N., Bi, J., Broquet, G., Canadell, J.G., Chevallier, F., Liu, Y.Y., Running, S.W., 2014. Contribution of semi-arid ecosystems to interannual variability of the global carbon cycle. *Nature*, 509(7502), 600-603.

Powell, S.L., Cohen, W.B., Healey, S.P., Kennedy, R.E., Moisen, G.G., Pierce, K.B. and Ohmann, J.L., 2010. Quantification of live aboveground forest biomass dynamics with Landsat time-series and field inventory data: A comparison of empirical modeling approaches. *Remote Sensing of Environment*, *114*(5), pp.1053-1068.

Prado, D., Pennington, R. and Pendry, C. (2000). Neotropical seasonally dry forests and Quaternary vegetation changes. *Journal of Biogeography, 27*, pp.261-273.

Pricope, N.G. and Binford, M.W., 2012. A spatio-temporal analysis of fire recurrence and extent for semi-arid savanna ecosystems in southern Africa using moderate-resolution satellite imagery. *Journal of environmental management*, *100*, pp.72-85.

Pricope, N.G., Gaughan, A.E., All, J.D., Binford, M.W. and Rutina, L.P., 2015. Spatio-temporal analysis of vegetation dynamics in relation to shifting inundation and fire regimes: disentangling environmental variability from land management decisions in a Southern African Transboundary Watershed. *Land*, *4*(3), pp.627-655.

Prince, S. D., 2012. Mapping desertification in southern Africa. In Land Change Science (pp. 163-184): *Springer.*

Prince, S.D., 1991. Satellite remote sensing of primary production: comparison of results for Sahelian grasslands 1981-1988. International Journal of remote sensing, 12(6), pp.1301-1311.

Privette, J.L. and Roy, D.P., 2005. Southern Africa as a remote sensing test bed: The SAFARI 2000 Special Issue overview. *International journal of remote sensing*, *26*(19), pp.4141-4158.

Propastin, P., 2012. Modifying geographically weighted regression for estimating aboveground biomass in tropical rainforests by multispectral remote sensing data. International Journal of Applied Earth Observation and Geoinformation, 18, 82-90.

Pu, R., Landry, S. and Yu, Q., 2018. Assessing the potential of multi-seasonal high resolution Pléiades satellite imagery for mapping urban tree species. *International Journal of Applied Earth Observation and Geoinformation*, *71*, pp.144-158.

Puhr, C.B. and Donoghue, D.N.M., 2000. Remote sensing of upland conifer plantations using Landsat TM data: a case study from Galloway, south-west Scotland. *International Journal of Remote Sensing*, *21*(4), pp.633-646.

Putz, F.E. and Redford, K.H., 2010. The importance of defining 'forest': Tropical forest degradation, deforestation, long-term phase shifts, and further transitions. *Biotropica*, *42*(1), pp.10-20.

Quijas, S., Romero-Duque, L.P., Trilleras, J.M., Conti, G., Kolb, M., Brignone, E. and Dellafiore, C. (2019). Linking biodiversity, ecosystem services, and beneficiaries of tropical dry forests of Latin America: Review and new perspectives. *Ecosystem services, 36*, p.100909.

R CORE TEAM, 2013. R: A language and environment for statistical computing. https://www.R-project.org/

Visscher, D., 2006. GPS measurement error and resource selection functions in a fragmented landscape. *Ecography*, *29*(3), pp.458-464.

Rahmoune, R., Ferrazzoli, P., Kerr, Y.H. and Richaume, P. (2013). SMOS level 2 retrieval algorithm over forests: Description and generation of global maps. *IEEE Journal of Selected Topics in Applied Earth Observations and Remote Sensing, 6(3)*, pp.1430-1439.

Ramoelo, A., Cho, M.A., Mathieu, R., Madonsela, S., Van De Kerchove, R., Kaszta, Z. and Wolff, E., 2015. Monitoring grass nutrients and biomass as indicators of rangeland quality and quantity using random forest modelling and WorldView-2 data. International journal of applied earth observation and geoinformation, 43, 43-54.

Rampheri, M., Dube, T. and Dhau, I., 2020. Use of remotely sensed data to estimate tree species diversity as an indicator of biodiversity in Blouberg Nature Reserve, South Africa. *Geocarto International*, pp.1-17.

Rands, M.R., Adams, W.M., Bennun, L., Butchart, S.H., Clements, A., Coomes, D., Entwistle, A., Hodge, I., Kapos, V., Scharlemann, J.P. and Sutherland, W.J., 2010. Biodiversity conservation: challenges beyond 2010. *science*, *329*(5997), pp.1298-1303.

Ranjan, R., Chopra, U.K., Sahoo, R.N., Singh, A.K. and Pradhan, S., 2012. Assessment of plant nitrogen stress in wheat (Triticum aestivum L.) through hyperspectral indices. International Journal of Remote Sensing, 33(20), pp.6342-6360.

Reiche, J., Lucas, R., Mitchell, A.L., Verbesselt, J., Hoekman, D.H., Haarpaintner, J., Kellndorfer, J.M., Rosenqvist, A., Lehmann, E.A., Woodcock, C.E. and Seifert, F.M., 2016. Combining satellite data for better tropical forest monitoring. *Nature Climate Change*, *6*(2), pp.120-122.

Reynolds, J., Wesson, K., Desbiez, A.L., Ochoa-Quintero, J.M. and Leimgruber, P. (2016). Using remote sensing and random forest to assess the conservation status of critical Cerrado habitats in Mato Grosso do Sul, Brazil. *Land, 5(2)*, p.12.

Reynolds, J.F., Smith, D.M.S., Lambin, E.F., Turner, B.L., Mortimore, M., Batterbury, S.P., Downing, T.E., Dowlatabadi, H., Fernández, R.J., Herrick, J.E. and Huber-Sannwald, E., 2007. Global desertification: building a science for dryland development. *science*, *316*(5826), pp.847-851.

Ringrose, S., Chipanshi, A.C., Matheson, W., Chanda, R., Motoma, L., Magole, I. and Jellema, A., 2002. Climate-and human-induced woody vegetation changes in Botswana and their implications for human adaptation. *Environmental management*, *30*(1), pp.98-109.

Ringrose, S., Matheson, W., Matlala, C.J.S.S., O'Neill, T. and Werner, P.A., 1994. Vegetation spectral reflectance along a north-south vegetation gradient in northern Australia. *Journal of Biogeography*, pp.33-47.

Rodríguez, J.P., Nassar, J.M., Rodríguez-Clark, K.M., Zager, I., Portillo-Quintero, C.A., Carrasquel, F. and Zambrano, S. (2008). Tropical dry forests in Venezuela: assessing status, threats and future prospects. Environmental Conservation, 35(4), pp.311-318.

Rouse, J.W., 1974. Monitoring the vernal advancement of retrogradation of natural vegetation. NASA/GSFC, type III, *final report, greenbelt*, MD, 371.

Rumiano, F., Wielgus, E., Miguel, E., Chamaillé-Jammes, S., Valls-Fox, H., Cornélis, D., Garine-Wichatitsky, M.D., Fritz, H., Caron, A. and Tran, A., 2020. Remote sensing of environmental drivers influencing the movement ecology of sympatric wild and domestic ungulates in semi-arid savannas, a review. *Remote Sensing*, *12*(19), p.3218.

Russell-Smith, J., Monagle, C., Jacobsohn, M., Beatty, R.L., Bilbao, B., Millán, A., Vessuri, H. and Sánchez-Rose, I., 2017. Can savanna burning projects deliver measurable greenhouse emissions reductions and sustainable livelihood opportunities in fire-prone settings?. *Climatic Change*, *140*(1), pp.47-61.

Rwanga, S.S. and Ndambuki, J.M., 2017. Accuracy assessment of land use/land cover classification using remote sensing and GIS. *International Journal of Geosciences*, *8*(04), p.611.

Saatchi, S.S., Harris, N.L., Brown, S., Lefsky, M., Mitchard, E.T., Salas, W., Zutta, B.R., Buermann, W., Lewis, S.L., Hagen, S., Petrova, S., 2011. Benchmark map of forest carbon stocks in tropical regions across three continents. *Proceedings of the National Academy of Sciences*, 108(24), 9899-9904.

Sader, S.A., Waide, R.B., Lawrence, W.T. and Joyce, A.T., 1989. Tropical forest biomass and successional age class relationships to a vegetation index derived from Landsat TM data. *Remote Sensing of Environment*, *28*, pp.143-198.

Safriel, U., Adeel, Z., Niemeijer, D., Puigdefabregas, J., White, R., Lal, R., Winslow, M., Ziedler, J., Prince, S., Archer, E. and King, C., 2005. Dryland systems. In *Ecosystems and Human Well-being: Current State and Trends.: Findings of the Condition and Trends Working Group* (pp. 623-662). Island Press.

Sakaizawa, D., MITSUHAHI, R., MUROOKA, J., Tadashi, I.M.A.I., Kimura, T. and Kazuhiro, A.S.A.I., 2018, July. Current status of the ISS-vegetation lidar Mission-MOLI. In *IGARSS 2018-2018 IEEE International Geoscience and Remote Sensing Symposium* (pp. 1861-1864). IEEE.

Salajanu, D. and Olson, C.E., 2001. The significance of spatial resolution: Identifying forest cover from satellite data. Journal of forestry, 99(6), pp.32-38.

Salis, S. M., Assis, M. A., Mattos, P. P., & Pião, A. C., 2006. Estimating the aboveground biomass and wood volume of savanna woodlands in Brazil's Pantanal wetlands based on allometric correlations. Forest Ecology and Management, 228(1-3), 61-68.

Samanta, A., Ganguly, S. and Myneni, R.B., 2011. MODIS enhanced vegetation index data do not show greening of Amazon forests during the 2005 drought. *The New Phytologist*, *189*(1), pp.11-15.

Sanchez-Azofeifa, A., Portillo-Quintero, C., Wilson-Fernandes, G., Stoner, K. and Shimizu, T. (2013). The policy process for land use/cover change and forest degradation in the semi-arid Latin American/Caribbean region: perspectives and opportunities. A literature review prepared for the Inter-American Development Bank. A literature review prepared for the Inter-American Development Bank.

Sánchez-Azofeifa, G.A., Castro, K.L., Rivard, B., Kalascka, M.R. and Harriss, R.C. (2003). Remote sensing research priorities in tropical dry forest environments. Biotropica, 35(2), pp.134-142.

Sánchez-Azofeifa, G.A., Quesada, M., Rodríguez, J.P., Nassar, J.M., Stoner, K.E., Castillo, A., Garvin, T., Zent, E.L., Calvo-Alvarado, J.C., Kalacska, M.E. and Fajardo, L., 2005. Research priorities for Neotropical dry forests 1. *Biotropica: The Journal of Biology and Conservation*, *37*(4), pp.477-485

Santoro, M., Beer, C., Cartus, O., Schmullius, C., Shvidenko, A., McCallum, I., Wegmüller, U. and Wiesmann, A., 2011. Retrieval of growing stock volume in boreal forest using hyper-temporal series of Envisat ASAR ScanSAR backscatter measurements. Remote Sensing of Environment, 115(2), pp.490-507.

Santos, J.R., Lacruz, M.P., Araujo, L.S. and Keil, M., 2002. Savanna and tropical rainforest biomass estimation and spatialization using JERS-1 data. *International Journal of Remote Sensing*, *23*(7), pp.1217-1229

Sarker, L.R. and Nichol, J.E., 2011. Improved forest biomass estimates using ALOS AVNIR-2 texture indices. *Remote Sensing of Environment*, *115*(4), pp.968-977.

Schimel, D., Pavlick, R., Fisher, J.B., Asner, G.P., Saatchi, S., Townsend, P., Miller, C., Frankenberg, C., Hibbard, K. and Cox, P., 2015. Observing terrestrial ecosystems and the carbon cycle from space. Global Change Biology, 21(5), 1762-1776.

Scholes, R.J. and Biggs, R.A., 2004. *Ecosystem services in Southern Africa a regional assessment* (No. 33355 Caja (533)). CSIR.

Scholes, R.J., Frost, P.G. and Tian, Y., 2004. Canopy structure in savannas along a moisture gradient on Kalahari sands. *Global Change Biology*, *10*(3), pp.292-302.

Scholes, R.J., Montanarella, L., Brainich, E., Barger, N., Ten Brink, B., Cantele, M., Erasmus, B., Fisher, J., Gardner, T., Holland, T.G. and Kohler, F., 2018. IPBES (2018): Summary for policymakers of the assessment report on land degradation and restoration of the Intergovernmental Science-Policy Platform on Biodiversity and Ecosystem Services.

Schröder, J.M., Rodriguez, L.P.A. and Günter, S., 2021. Research trends: Tropical dry forests: The neglected research agenda?. *Forest Policy and Economics*, *122*, p.102333.

Schulte to Bühne, H. and Pettorelli, N., 2018. Better together: Integrating and fusing multispectral and radar satellite imagery to inform biodiversity monitoring, ecological research and conservation science. *Methods in Ecology and Evolution*, *9*(4), pp.849-865.

Schultz, M., Shapiro, A., Clevers, J.G., Beech, C. and Herold, M., 2018. Forest cover and vegetation degradation detection in the Kavango Zambezi Transfrontier Conservation area using BFAST monitor. *Remote Sensing*, *10*(11), p.1850.

Senf, C., Pflugmacher, D., Hostert, P. and Seidl, R., 2017. Using Landsat time series for characterizing forest disturbance dynamics in the coupled human and natural systems of Central Europe. *ISPRS Journal of Photogrammetry and Remote Sensing*, *130*, pp.453-463.

Sexton, J.O., Noojipady, P., Song, X.P., Feng, M., Song, D.X., Kim, D.H., Anand, A., Huang, C., Channan, S., Pimm, S.L. and Townshend, J.R., 2016. Conservation policy and the measurement of forests. *Nature Climate Change*, *6*(2), pp.192-196.

Sexton, J.O., Song, X.P., Feng, M., Noojipady, P., Anand, A., Huang, C., Kim, D.H., Collins, K.M., Channan, S., DiMiceli, C. and Townshend, J.R., 2013. Global, 30-m resolution continuous fields of tree cover: Landsat-based rescaling of MODIS vegetation continuous fields with lidar-based estimates of error. International Journal of Digital Earth, 6(5), pp.427-448.

Shackleton, C., Shackleton, S.E., Gambiza, J., Nel, E., Rowntree, K., Urquhart, P., Fabricius, C. and Ainslie, A., 2010. *Livelihoods and vulnerability in the arid and semi-arid lands of southern Africa: exploring the links between ecosystem services and poverty alleviation*. Nova Publishers.

Shannon, G., Thaker, M., Vanak, A. T., Page, B. R., Grant, R., Slotow, R., 2011. Relative impacts of elephant and fire on large trees in a savanna ecosystem. Ecosystems, 14(8), 1372-1381.

Shao, Z., Zhang, L. and Wang, L. (2017). Stacked sparse autoencoder modeling using the synergy of airborne LiDAR and satellite optical and SAR data to map forest above-ground biomass*.* *IEEE Journal of Selected Topics in Applied Earth Observations and Remote Sensing, 10(12)*, pp.5569-5582.

Sheffield, J. and Wood, E.F., 2008. Projected changes in drought occurrence under future global warming from multi-model, multi-scenario, IPCC AR4 simulations. *Climate dynamics*, 31(1), pp.79-105.

Shelestov, A., Lavreniuk, M., Kussul, N., Novikov, A. and Skakun, S., 2017. Exploring Google Earth Engine platform for big data processing: Classification of multi-temporal satellite imagery for crop mapping. *frontiers in Earth Science*, *5*, p.17.

Shi, J., Jackson, T., Tao, J., Du, J., Bindlish, R., Lu, L. and Chen, K.S. (2008). Microwave vegetation indices for short vegetation covers from satellite passive microwave sensor AMSR-E. *Remote sensing of environment, 112(12)*, pp.4285-4300.

Shikangalah, R.N., 2020. The 2019 drought in Namibia: an overview. *J. Namibian Stud*, *27*, pp.37-58.

Shimada, M., 2018. *Imaging from spaceborne and airborne SARs, calibration, and applications*. CRC Press.

Sibanda, M., Mutanga, O. and Rouget, M., 2016. Discriminating rangeland management practices using simulated hyspIRI, landsat 8 OLI, sentinel 2 MSI, and VENμs spectral data. IEEE Journal of Selected Topics in Applied Earth Observations and Remote Sensing, 9(9), 3957-3969.

Silva, J.M., Pereira, J.M., Cabral, A.I., Sá, A.C., Vasconcelos, M.J., Mota, B. and Grégoire, J.M., 2003. An estimate of the area burned in southern Africa during the 2000 dry season using SPOT-VEGETATION satellite data. *Journal of Geophysical Research: Atmospheres*, *108*(D13).

Silvy, N.J. ed., 2020. *The Wildlife Techniques Manual: Volume 1: Research. Volume 2: Management*. JHU Press.

Simard, M., Pinto, N., Fisher, J.B. and Baccini, A., 2011. Mapping forest canopy height globally with spaceborne lidar. Journal of Geophysical Research: Biogeosciences, 116(G4).

Simula, M., 2009. Towards defining forest degradation: comparative analysis of existing definitions. Forest Resources Assessment Working Paper, 154, p.59.

Smith, W.K., Dannenberg, M.P., Yan, D., Herrmann, S., Barnes, M.L., Barron-Gafford, G.A., Biederman, J.A., Ferrenberg, S., Fox, A.M., Hudson, A. and Knowles, J.F., 2019. Remote sensing of dryland ecosystem structure and function: Progress, challenges, and opportunities. *Remote Sensing of Environment*, *233*, p.111401.

Spinoni, J., Vogt, J., Naumann, G., Carrao, H. and Barbosa, P., 2015. Towards identifying areas at climatological risk of desertification using the Köppen–Geiger classification and FAO aridity index. *International Journal of Climatology*, *35*(9), pp.2210-2222.

Stan, K. and Sanchez-Azofeifa, A. (2019). Tropical dry forest diversity, climatic response, and resilience in a changing climate. *Forests, 10(5),* p.443.

Staver, A.C., Archibald, S. and Levin, S.A. (2011). The global extent and determinants of savanna and forest as alternative biome states. *science, 334(6053),* pp.230-232.

Steininger, M.K., 2000. Satellite estimation of tropical secondary forest above-ground biomass: data from Brazil and Bolivia. International journal of remote sensing, 21(6-7), 1139-1157.

Stehman, S.V. and Czaplewski, R.L., 1998. Design and analysis for thematic map accuracy assessment: fundamental principles. Remote sensing of environment, 64(3), pp.331-344.

Stehman, S.V., 2009. Sampling designs for accuracy assessment of land cover. International Journal of Remote Sensing, 30(20), pp.5243-5272.

Stehman, S.V., 2009. Sampling designs for accuracy assessment of land cover. International Journal of Remote Sensing, 30(20), pp.5243-5272.

Stoldt, M., Göttert, T., Mann, C. and Zeller, U., 2020. Transfrontier conservation areas and human-wildlife conflict: the case of the Namibian component of the Kavango-Zambezi (KAZA) TFCA. *Scientific reports*, *10*(1), pp.1-16.

Stoner, K.E., Timm, R.M., Frankie, G.W., Mata, A. and Vinson, S.B. (2004). Tropical dry-forest mammals of Palo Verde. Biodiversity conservation in Costa Rica. Learning the lessons in a seasonal dry forest. *University of California Press. Berkeley, Los Angeles*, pp.48-66.

Story, M. and Congalton, R.G., 1986. Accuracy assessment: a user's perspective. *Photogrammetric Engineering and remote sensing*, *52*(3), pp.397-399.

Stott, P., 2000. Combustion in tropical biomass fires: a critical review. *Progress in Physical Geography*, *24*(3), pp.355-377.

Stratoulias, D., Balzter, H., Sykioti, O., Zlinszky, A. and Tóth, V.R., 2015. Evaluating sentinel-2 for lakeshore habitat mapping based on airborne hyperspectral data. Sensors, 15(9), pp.22956-22969.

Sunderland, T., Apgaua, D., Baldauf, C., Blackie, R., Colfer, C., Cunningham, A.B., Dexter, K., Djoudi, H., Gautier, D., Gumbo, D. and Ickowitz, A., 2015. Global dry forests: a prologue. *International Forestry Review*, *17*(2), pp.1-9.

Suresh, H.S., Dattaraja, H.S., Mondal, N. and Sukumar, R., 2011. Seasonally dry tropical forests in Southern India. An analysis of floristic composition, structure, and dynamics in Mudumalai Wildlife Sanctuary. *The ecology and conservation of seasonally dry forests in Asia*, pp.37-58.

Svoboda, M. and Fuchs, B.A., 2016. Handbook of drought indicators and indices. Integrated drought management programme (IDMP), integrated drought management tools and guidelines series 2. *World meteorological organization and global water partnership, Geneva, Switzerland*, *52*.

Symeonakis, E., Higginbottom, T.P., Petroulaki, K. and Rabe, A., 2018. Optimisation of savannah land cover characterisation with optical and SAR data. *Remote Sensing*, *10*(4), p.499.

Symeonakis, E., Korkofigkas, A., Vamvoukakis, G., Stamou, G. and Arnau-Rosalen, E. (2020). Deep Learning Monitoring of Woody Vegetation Density in a South African Savannah Region. *International Archives of the Photogrammetry, Remote Sensing and Spatial Information Sciences-ISPRS Archives, 43*, pp.1645-1649.

Thompson, I.D., Guariguata, M.R., Okabe, K., Bahamondez, C., Nasi, R., Heymell, V. and Sabogal, C., 2013. An operational framework for defining and monitoring forest degradation. *Ecology and Society*, *18*(2).

Tian, F., Brandt, M., Liu, Y.Y., Rasmussen, K. and Fensholt, R. (2017). Mapping gains and losses in woody vegetation across global tropical drylands. *Global change biology, 23(4),* pp.1748-1760.

Timothy, D., Onisimo, M. and Riyad, I., 2016. Quantifying aboveground biomass in African environments: A review of the trade-offs between sensor estimation accuracy and costs. *Tropical Ecology*, *57*(3), pp.393-405.

Toth, C. and Jóźków, G. (2016). Remote sensing platforms and sensors: A survey. *ISPRS Journal of Photogrammetry and Remote Sensing, 115*, pp.22-36.

Townsend, P. A, 2002. Estimating forest structure in wetlands using multitemporal SAR. *Remote Sensing of Environment*, 79(2-3), 288-304.

Trejo, I. and Dirzo, R. (2000). Deforestation of seasonally dry tropical forest: a national and local analysis in Mexico. *Biological conservation, 94(2),* pp.133-142.

Treuhaft, R. N., Law, B. E., Asner, G. P., 2004. Forest attributes from radar interferometric structure and its fusion with optical remote sensing. *BioScience*, 54(6), 561-571.

Trier, Ø.D., Salberg, A.B., Kermit, M., Rudjord, Ø., Gobakken, T., Næsset, E. and Aarsten, D. (2018). Tree species classification in Norway from airborne hyperspectral and airborne laser scanning data. *European Journal of Remote Sensing, 51(1),* pp.336-351

Trollope, W.S.W., 1984. Fire in savanna. In *Ecological effects of fire in South African ecosystems* (pp. 149-175). Springer, Berlin, Heidelberg.

Tsalyuk, M., Kelly, M. and Getz, W.M., 2017. Improving the prediction of African savanna vegetation variables using time series of MODIS products. *ISPRS Journal of Photogrammetry and Remote Sensing*, *131*, pp.77-91.

Tshipa, A., Valls-Fox, H., Fritz, H., Collins, K., Sebele, L., Mundy, P. and Chamaillé-Jammes, S., 2017. Partial migration links local surface-water management to large-scale elephant conservation in the world's largest transfrontier conservation area. *Biological Conservation*, *215*, pp.46-50.

Tu, M.C., Smith, P. and Filippi, A.M., 2018. Hybrid forward-selection method-based water-quality estimation via combining Landsat TM, ETM+, and OLI/TIRS images and ancillary environmental data. Plos one, 13(7), e0201255.

Tucker, C.J., 1979. Red and photographic infrared linear combinations for monitoring vegetation. *Remote sensing of Environment*, *8*(2), pp.127-150.

Turner, D.P., Cohen, W.B., Kennedy, R.E., Fassnacht, K.S. and Briggs, J.M., 1999. Relationships between leaf area index and Landsat TM spectral vegetation indices across three temperate zone sites. *Remote sensing of environment*, *70*(1), pp.52-68.

Turner, M.G., 2010. Disturbance and landscape dynamics in a changing world. *Ecology*, *91*(10), pp.2833-2849.

UN., 2011. Global drylands: a UN system-wide response. Environment Management Group of the United Nations Geneva. http://www.unccd.int/Lists/SiteDocumentLibrary/Publications/Global_Drylands_Full_Report.pdf/ (accessed 19 July 2021).

UN., 2015. Transforming our world: the 2030 Agenda for Sustainable Development. *United Nations: New York, NY, USA*.

UNCCD., 1994. United Nations: Convention to combat desertification in those countries experiencing serious drought and/or desertification, particularly in Africa. *Int. Legal Mater*, *33*, pp.1328-1382.

UNCCD., 2009. United Nations Convention to Combat Desertification: Climate Change in the African Drylands. Options and Opportunities for Adaptation and Mitigation. In: UNDP and UNEP Nairobi.

UNCCD., 2015. United Nations Convention to Combat Desertification (UNCCD),UNCCD's support for the New Partnership for Africa's Development (NEPAD). http://www.un.org/en/africa/osaa/pdf/unsystemfolder/2016/unccd2016.pdf/ (accessed 01 July 2021).

UNFCCC., 2009. Methodological guidance for activities relating to reducing emissions from deforestation and forest degradation and the role of conservation, sustainable management of forests and enhancement of forest carbon stocks in developing countries. In. Decision 4/CP.15. *United Nations Framework Convention on Climate Change,: Bonn*.

Unger, D.R., Hung, I.K., Brooks, R. and Williams, H., 2014. Estimating number of trees, tree height and crown width using Lidar data. *GIScience & remote sensing*, *51*(3), pp.227-238.

Urban, M., Berger, C., Mudau, T.E., Heckel, K., Truckenbrodt, J., Onyango Odipo, V., Smit, I.P. and Schmullius, C., 2018. Surface moisture and vegetation cover analysis for drought monitoring in the Southern Kruger National Park using sentinel-1, sentinel-2, and landsat-8. *Remote Sensing*, *10*(9), p.1482.

USAID., 2010. USAID/NAMIBIA Environmental Threats and opportunities assessment with an emphasis on tropical forestry and biodiversity conservation. Prepared by the International Resource Group (IRG) for the United States Agency for International Development (USAID). *Washington, DC, USA.*

USAID., 2013. ANGOLA BIODIVERSITY AND TROPICAL FORESTS: 118/119 ASSESSMENT. https://usaidgems.org/Documents/FAA&Regs/FAA118119/Angola2013.pdf/ (accessed 14 March 2021).

Valentini, R., Arneth, A., Bombelli, A., Castaldi, S., Cazzolla Gatti, R., Chevallier, F., Ciais, P., Grieco, E., Hartmann, J., Henry, M. and Houghton, R.A., 2014. A full greenhouse gases budget of Africa: synthesis, uncertainties, and vulnerabilities. *Biogeosciences*, *11*(2), pp.381-407.

van Bommel, F.P., Heitkönig, I.M., Epema, G.F., Ringrose, S., Bonyongo, C. and Veenendaal, E.M., 2006. Remotely sensed habitat indicators for predicting distribution of impala (Aepyceros melampus) in the Okavango Delta, Botswana. *Journal of tropical ecology*, *22*(1), pp.101-110.

van der Sande, M.T., Peña-Claros, M., Ascarrunz, N., Arets, E.J., Licona, J.C., Toledo, M. and Poorter, L., 2017. Abiotic and biotic drivers of biomass change in a Neotropical forest. *Journal of Ecology*, *105*(5), pp.1223-1234.

van der Werf, G.R., Randerson, J.T., Giglio, L., Collatz, G.J., Kasibhatla, P.S. and Arellano Jr, A.F., 2006. Interannual variability in global biomass burning emissions from 1997 to 2004. *Atmospheric Chemistry and Physics*, *6*(11), pp.3423-3441.

Van Marle, M.J.E., Van Der Werf, G.R., De Jeu, R.A.M. and Liu, Y.Y. (2016). Annual South American forest loss estimates based on passive microwave remote sensing (1990–2010). *Biogeosciences, 13(2),* pp.609-624.

Van Wilgen, B.W., Govender, N. and Biggs, H.C., 2007. The contribution of fire research to fire management: a critical review of a long-term experiment in the Kruger National Park, South Africa. *International Journal of Wildland Fire*, *16*(5), pp.519-530.

Veldkamp, A. and Lambin, E. F., 2001. Predicting land-use change. *Agriculture, Ecosystems & Environment*, 85(1-3), pp. 1-6.

Venter, Z.S., Scott, S.L., Desmet, P.G. and Hoffman, M.T., 2020. Application of Landsat-derived vegetation trends over South Africa: Potential for monitoring land degradation and restoration. *Ecological Indicators*, *113*, p.106206.

Verbesselt, J., Hyndman, R., Newnham, G. and Culvenor, D., 2010a. Detecting trend and seasonal changes in satellite image time series. *Remote sensing of Environment*, 114(1), pp.106-115.

Verbesselt, J., Hyndman, R., Zeileis, A. and Culvenor, D., 2010b. Phenological change detection while accounting for abrupt and gradual trends in satellite image time series. *Remote Sensing of Environmen*t, 114(12), pp.2970-2980.

Verbesselt, J., Somers, B., Lhermitte, S., Jonckheere, I., van Aardt, J., and Coppin, P., 2007. Monitoring herbaceous fuel moisture content with SPOT VEGETATION time-series for fire risk prediction in savanna ecosystems. *Remote Sensing of Environment*, 108(4), pp.357-368.

Verbesselt, J., Somers, B., van Aardt, J., Jonckheere, I., and Coppin, P., 2006. Monitoning herbaceous biomass and water content with SPOT VEGETATION time-series to improve fire risk assessment in savanna ecosystems. *Remote Sensing of Environment*, 101(3), pp.399-414.

Verbesselt, J., Zeileis, A. and Herold, M., 2012. Near real-time disturbance detection using satellite image time series. *Remote Sensing of Environment*, 123, pp.98-108.

Verlinden, A. and Laamanen, R., 2006a. Long term fire scar monitoring with remote sensing in northern Namibia: Relations between fire frequency, rainfall, land cover, fire management and trees. *Environmental Monitoring and Assessment*, 112(1-3), pp.231-253.

Verlinden, A. and Laamanen, R., 2006b. Modeling woody vegetation resources using Landsat TM imagery in northern Namibia. *Southern African Forestry Journal*, 207(1), pp.27-39.

Vermote, E.F., El Saleous, N.Z. and Justice, C.O., 2002. Atmospheric correction of MODIS data in the visible to middle infrared: first results. *Remote Sensing of Environment*, 83(1-2), pp.97-111.

Vicente-Serrano, S.M., Cabello, D., Tomás-Burguera, M., Martín-Hernández, N., Beguería, S., Azorin-Molina, C. and Kenawy, A.E., 2015. Drought variability and land degradation in semiarid regions: Assessment using remote sensing data and drought indices (1982–2011). *Remote Sensing*, *7*(4), pp.4391-4423.

Vicente-Serrano, S.M., Miralles, D.G., Domínguez-Castro, F., Azorin-Molina, C., El Kenawy, A., McVicar, T.R., Tomás-Burguera, M., Beguería, S., Maneta, M. and Peña-Gallardo, M., 2018. Global assessment of the Standardized Evapotranspiration Deficit Index (SEDI) for drought analysis and monitoring. *Journal of Climate*, *31*(14), pp.5371-5393.

Viovy, N., Arino, O. and Belward, A.S., 1992. The Best Index Slope Extraction (BISE): A method for reducing noise in NDVI time-series. *International Journal of remote sensing*, 13(8), pp.1585-1590.

Vogt, J.V., Safriel, U., Von Maltitz, G., Sokona, Y., Zougmore, R., Bastin, G. and Hill, J., 2011. Monitoring and assessment of land degradation and desertification: towards new conceptual and integrated approaches. *Land Degradation & Development*, *22*(2), pp.150-165.

Wagenseil, H. and Samimi, C., 2006. Assessing spatio-temporal variations in plant phenology using Fourier analysis on NDVI time series: results from a dry savannah environment in Namibia. *International Journal of Remote Sensing*, *27*(16), pp.3455-3471.

Walter, H. and Burnett, J.H., 1971. *Ecology of tropical and subtropical vegetation* (Vol. 539). Edinburgh: Oliver and Boyd.

Wang, F. M., Huang, J. F., Tang, Y. L., Wang, X. Z., 2007. New vegetation index and its application in estimating leaf area index of rice. Rice Science, 14(3), 195-203.

Wang, L., Jia, M., Yin, D., and Tian, J., 2019. A review of remote sensing for mangrove forests: 1956–2018. *Remote Sensing of Environment*, 231, 111223.

Wang, Y., Day, J. L., and Davis, F. W., 1998. Sensitivity of modeled C- and L-band radar backscatter to ground surface parameters in loblolly pine forest. *Remote Sensing of Environment*, 66(3),pp. 331-342.

Warren, M.S., Brumby, S.P., Skillman, S.W., Kelton, T., Wohlberg, B., Mathis, M., Chartrand, R., Keisler, R. and Johnson, M., 2015, October. Seeing the Earth in the Cloud: Processing one petabyte of satellite imagery in one day. In *2015 IEEE Applied Imagery Pattern Recognition Workshop (AIPR)* (pp. 1-12). IEEE.

Washington-Allen, R.A., Ramsey, R.D., West, N.E. and Norton, B.E., 2008. Quantification of the ecological resilience of drylands using digital remote sensing. *Ecology and Society*, *13*(1).

Washington-Allen, R.A., West, N.E., Ramsey, R.D. and Efroymson, R.A., 2006. A protocol for retrospective remote sensing–based ecological monitoring of rangelands. *Rangeland Ecology & Management*, *59*(1), pp.19-29.

Watson, R.T., Zinyowera, M.C. and Moss, R.H., 1996. Climate change 1995. Impacts, adaptations and mitigation of climate change: scientific-technical analyses. *Cambridge: Cambridge University Press.*[*http://www.repositorio.cenpatconicet.gob.ar/bitstream/handle/123456789/577/climateChange1995ImpactsAdpatationsMitigation.pdf?sequence=1*](http://www.repositorio.cenpatconicet.gob.ar/bitstream/handle/123456789/577/climateChange1995ImpactsAdpatationsMitigation.pdf?sequence=1) (accessed 25 August 2021).

Watt, P., Bholanath, P., Dewnath, N., Smartt, T., Chan, C. and Donoghue, D., 2020. INTEROPERABILITY OF VARIOUS DATA STREAMS WITHIN GUYANA's MRV SYSTEM. International Archives of the Photogrammetry, Remote Sensing and Spatial Information Sciences, 42(3/W11).

Watts, L.M. and Laffan, S.W., 2014. Effectiveness of the BFAST algorithm for detecting vegetation response patterns in a semi-arid region. *Remote Sensing of Environment*, 154, pp.234-245.

Wegmann, M., Santini, L., Leutner, B., Safi, K., Rocchini, D., Bevanda, M., Latifi, H., Dech, S. and Rondinini, C., 2014. Role of African protected areas in maintaining connectivity for large mammals. *Philosophical Transactions of the Royal Society B: Biological Sciences*, *369*(1643), p.20130193

Weng, X., Dong, Z., Wu, Q. and Qin, Y., 2015. China's path to a green economy. *Decoding China's green economy concepts and policies. Country report. IEED, London*.

Wessels, K.J., Prince, S.D., Zambatis, N., MacFadyen, S., Frost, P.E. and Van Zyl, D., 2006. Relationship between herbaceous biomass and 1-km^2 Advanced Very High Resolution Radiometer (AVHRR) NDVI in Kruger National Park, South Africa. *International Journal of Remote Sensing*, *27*(05), pp.951-973.

Westinga, E., Beltran, A.P.R., De Bie, C.A. and van Gils, H.A., 2020. A novel approach to optimize hierarchical vegetation mapping from hyper-temporal NDVI imagery, demonstrated at national level for Namibia. *International Journal of Applied Earth Observation and Geoinformation*, *91*, p.102152

White, B.L.A. (2019). Satellite detection of wildland fires in South America. *Floresta, 49(4),* pp.851-858.

Whitecross, M.A., Witkowski, E.T. and Archibald, S., 2017. Assessing the frequency and drivers of early-greening in broad-leaved woodlands along a latitudinal gradient in southern Africa. *Austral ecology*, *42*(3), pp.341-353.

Wiens, J., Sutter, R., Anderson, M., Blanchard, J., Barnett, A., Aguilar-Amuchastegui, N., Avery, C. and Laine, S., 2009. Selecting and conserving lands for biodiversity: The role of remote sensing. *Remote sensing of Environment*, 113(7), pp.1370-1381.

Wijaya, A., Liesenberg, V., Susanti, A., Karyanto, O. and Verchot, L.V., 2015. Estimation of Biomass Carbon Stocks over Peat Swamp Forests using Multi-Temporal and Multi-Polratizations SAR Data. Int. Arch. Photogramm. Remote Sens. Spat. Inf. Sci, 551-556

Wilcox, B.P., Sorice, M.G. and Young, M.H., 2011. Dryland ecohydrology in the anthropocene: Taking stock of human–ecological interactions. *Geography Compass*, *5*(3), pp.112-127.

Williams, A.P., Allen, C.D., Macalady, A.K., Griffin, D., Woodhouse, C.A., Meko, D.M., Swetnam, T.W., Rauscher, S.A., Seager, R., Grissino-Mayer, H.D. and Dean, J.S., 2013. Temperature as a potent driver of regional forest drought stress and tree mortality. *Nature climate change*, *3*(3), pp.292-297.

Williams, M. R. C. M., Ryan, C. M., Rees, R. M., Sambane, E., Fernando, J., & Grace, J., 2008. Carbon sequestration and biodiversity of re-growing miombo woodlands in Mozambique. Forest Ecology and management, 254(2), 145-155.

Williams, M., Hill, T.C. and Ryan, C.M., 2013. Using biomass distributions to determine probability and intensity of tropical forest disturbance. *Plant Ecology & Diversity*, *6*(1), pp.87-99.

Wingate, V.R., Phinn, S.R., Kuhn, N. and Scarth, P., 2018. Estimating aboveground woody biomass change in Kalahari woodland: combining field, radar, and optical data sets. *International Journal of Remote Sensing*, *39*(2), pp.577-606.

Wintle, B.A., Kujala, H., Whitehead, A., Cameron, A., Veloz, S., Kukkala, A., Moilanen, A., Gordon, A., Lentini, P.E., Cadenhead, N.C. and Bekessy, S.A., 2019. Global synthesis of conservation studies reveals the importance of small habitat patches for biodiversity. *Proceedings of the National Academy of Sciences*, *116*(3), pp.909-914.

Wood, E.M., Pidgeon, A.M., Radeloff, V.C. and Keuler, N.S., 2012. Image texture as a remotely sensed measure of vegetation structure. *Remote Sensing of Environment*, *121*, pp.516-526.

Woodcock, C.E., Macomber, S.A., Pax-Lenney, M. and Cohen, W.B., 2001. Monitoring large areas for forest change using Landsat: Generalization across space, time and Landsat sensors. *Remote sensing of environment*, *78*(1-2), pp.194-203.

Worldagroforestry, 2019. Worldwide open access tree functional attributes and ecological database. http://db.worldagroforestry.org//species/properties/Baikiaea_plurijuga/ (accessed 12 December 2019).

Wu, C., Shen, H., Shen, A., Deng, J., Gan, M., Zhu, J., Xu, H. and Wang, K., 2016. Comparison of machine-learning methods for above-ground biomass estimation based on Landsat imagery. Journal of Applied Remote Sensing, 10(3), 035010.

Wu, L., Li, Z., Liu, X., Zhu, L., Tang, Y., Zhang, B., Xu, B., Liu, M., Meng, Y. and Liu, B., 2020. Multi-type forest change detection using BFAST and monthly landsat time series for monitoring spatiotemporal dynamics of forests in subtropical wetland. *Remote Sensing*, 12(2), p.341

Wulder, M.A., Hall, R.J., Coops, N.C. and Franklin, S.E., 2004. High spatial resolution remotely sensed data for ecosystem characterization. BioScience, 54(6), pp.511-521.

Wulder, M.A., White, J.C., Nelson, R.F., Næsset, E., Ørka, H.O., Coops, N.C., Hilker, T., Bater, C.W. Gobakken, T., 2012. Lidar sampling for large-area forest characterization: A review. *Remote Sensing of Environment*, 121, 196-209.

WWF., 2016. Five countries work toward a common goal in southern Africa, *Magazine Articles, WWF*. World Wildlife Fund. https://www.worldwildlife.org/magazine/issues/spring-2016/articles/five-countries-work-toward-a-common-goal-in-southern-africa/ (accessed 01 July 2021).

Xie, H., Zhang, Y., Wu, Z. and Lv, T., 2020. A bibliometric analysis on land degradation: Current status, development, and future directions. *Land*, *9*(1), p.28.

Xie, P. and Arkin, P.A., 1995. An intercomparison of gauge observations and satellite estimates of monthly precipitation. *Journal of Applied Meteorology and Climatology*, *34*(5), pp.1143-1160.

Xu, K., Zhang, Z., Yu, W., Zhao, P., Yue, J., Deng, Y. and Geng, J., 2021. How spatial resolution affects forest phenology and tree-species classification based on satellite and up-scaled time-series images. Remote Sensing, 13(14), p.2716.

Xue, J. and Su, B., 2017. Significant remote sensing vegetation indices: A review of developments and applications. *Journal of sensors*, *2017*.

Xulu, S., Peerbhay, K., Gebreslasie, M. and Ismail, R., 2018. Drought influence on forest plantations in Zululand, South Africa, using MODIS time series and climate data. *Forests*, *9*(9), p.528.

Yang, J. and Prince, S.D., 2000. Remote sensing of savanna vegetation changes in Eastern Zambia 1972-1989. *International Journal of Remote Sensing*, *21*(2), pp.301-322.

Yang, J., Weisberg, P.J. and Bristow, N.A., 2012. Landsat remote sensing approaches for monitoring long-term tree cover dynamics in semi-arid woodlands: Comparison of vegetation indices and spectral mixture analysis. Remote sensing of environment, 119, 62-71.

Yengoh, G.T., Dent, D., Olsson, L., Tengberg, A.E. and Tucker III, C.J., 2015. Use of the Normalized Difference Vegetation Index (NDVI) to assess Land degradation at multiple scales: current status, future trends, and practical considerations. *Springer*.

Yoder, B.J. and Waring, R.H., 1994. The normalized difference vegetation index of small Douglas-fir canopies with varying chlorophyll concentrations. *Remote Sensing of Environment*, 49(1), pp.81-91.

Zeileis, A., Leisch, F., Kleiber, C. and Hornik, K., 2005. Monitoring structural change in dynamic econometric models. *Journal of Applied Econometrics*, 20(1), pp.99-121.

Zhang, W., Brandt, M., Wang, Q., Prishchepov, A.V., Tucker, C.J., Li, Y., Lyu, H., Fensholt, R., 2019.. From woody cover to woody canopies: How Sentinel-1 and Sentinel-2 data advance the mapping of woody plants in savannas. *Remote Sensing of Environment*, 234, 111465.

Zhang, X., Kondragunta, S. and Quayle, B., 2011. Estimation of biomass burned areas using multiple-satellite-observed active fires. *IEEE Transactions on Geoscience and Remote Sensing*, *49*(11), pp.4469-4482.

Zhao, K., Wulder, M.A., Hu, T., Bright, R., Wu, Q., Qin, H., Li, Y., Toman, E., Mallick, B., Zhang, X. and Brown, M., 2019. Detecting change-point, trend, and seasonality in satellite time series data to track abrupt changes and nonlinear dynamics: A Bayesian ensemble algorithm. *Remote sensing of Environment*, 232, p.111181.

Zhao, P., Lu, D., Wang, G., Wu, C., Huang, Y., Yu, S., 2016. Examining spectral reflectance saturation in Landsat imagery and corresponding solutions to improve forest aboveground biomass estimation. *Remote Sensing*, 8(6), 469.

Zhao, Z., Li, W., Ciais, P., Santoro, M., Cartus, O., Peng, S., Yin, Y., Yue, C., Yang, H., Yu, L. and Zhu, L., 2021. Fire enhances forest degradation within forest edge zones in Africa. *Nature Geoscience*, *14*(7), pp.479-483.

Zheng, G., Chen, J.M., Tian, Q.J., Ju, W.M. and Xia, X.Q., 2007. Combining remote sensing imagery and forest age inventory for biomass mapping. *Journal of Environmental Management*, *85*(3), pp.616-623.

Zhou, B., Okin, G.S. and Zhang, J., 2020. Leveraging Google Earth Engine (GEE) and machine learning algorithms to incorporate in situ measurement from different times for rangelands monitoring. *Remote Sensing of Environment*, *236*, p.111521

Zhu, X. and Liu, D., 2015. Improving forest aboveground biomass estimation using seasonal Landsat NDVI time-series. *ISPRS Journal of Photogrammetry and Remote Sensing*, *102*, pp.222-231.

Zhu, X.X., Tuia, D., Mou, L., Xia, G.S., Zhang, L., Xu, F. and Fraundorfer, F. (2017). Deep learning in remote sensing: A comprehensive review and list of resources. *IEEE Geoscience and Remote Sensing Magazine, 5(4),* pp.8-36.

Zhu, Z. and Woodcock, C.E., 2012. Object-based cloud and cloud shadow detection in Landsat imagery. *Remote sensing of environment*, *118*, pp.83-94.

Zhu, Z. and Woodcock, C.E., 2014. Continuous change detection and classification of land cover using all available Landsat data. *Remote sensing of Environment*, *144*, pp.152-171.

Zhu, Z., 2017. Change detection using landsat time series: A review of frequencies, preprocessing, algorithms, and applications. *ISPRS Journal of Photogrammetry and Remote Sensing*, *130*, pp.370-384.

Zhu, Z., Woodcock, C.E. and Olofsson, P., 2012. Continuous monitoring of forest disturbance using all available Landsat imagery. *Remote sensing of environment*, 122, pp.75-91.

Zweede, M., Safford, H. and Juergens, G., 2006. USDA Forest Service Forest Resource Assessment Trip Kuando Kubango Province, Angola. support of the USAID Southern Africa's Okavango Integrated River Basin and the Angolan Ministry of Agriculture and Rural Development's National Institute for Forestry Development and Management Project, May 16 – June 1, 2006. *US-AID, Washington D.C., USA*.

Appendix A

A policy brief published with N8 AgriFood at https://policyhub.n8agrifood.ac.uk/

N8 AgriFood
Food Systems
Policy Hub

Durham University

Remote sensing could enable more evidence-based policy to monitor and manage tropical dryland forests

Key Messages

- Remote sensing and Earth Observation technologies help to assess and monitor forest ecosystems and provide spatially explicit, operational, and long-term data to assist the sustainable use of tropical environment landscapes.
- However, few studies assess carbon storage or biomass, and there is little research on EO methods for assessing REDD+ initiatives in dryland forests in most Southern African countries.
- Africa has the potential to emulate other continents, such as Latin America, that have made notable progress in employing freely available remote sensing data to monitor tropical dryland forest area change and biomass on a large scale.
- Greater use of a wider range of EO products could enable more evidence-based policy to prioritise sustainable use of forests, enabling the policy community to learn what works to reduce deforestation and forest degradation, to improve livelihoods in a changing climate.

The Research

Researchers have assessed the evidence base for a number of tropical dryland forests-remote sensing options, asking how remote sensing technology was used to monitor and estimate changes in dryland forests in southern Africa. The researchers considering evidence from over 130 peer-reviewed papers including research on land-use/land-cover, forest cover/types, biomass, forest structure, biodiversity/habitats, phenology, plant traits, and disturbances from drought and fire. It considered publication trends over time, study location, remote sensing sensor/platform used, spatial and temporal coverage, remote sensing product (e.g., biophysical indices) used, and application areas of the study (e.g., land cover, forest biomass).

Key findings and evidence

Publication trends	Although the volume of scientific literature has demonstrated a sharp increase, the use of remote sensing is still limited, and up until 2013, the number of publications on tropical dryland forests was relatively small.
Time scales	Time series analysis on dryland forests, which enables tracking changes is scarce, only 22 (16%) out of 137 studies feature time series lengths that exceed 15 years and only 11 (8%) studies that cover more than 20 years. Longer time series of remote sensing data afford the ability to assess the dynamics of forest structures, biodiversity, degradation, disturbance from climatic extremes, and change in phenology, in which a gap still exists.

Spatial scales	Despite new sensor and EO data availability, it is clear that a systematic and consistent regional monitoring of dryland forests is not yet fully exploited and is still in its infancy in Southern Africa. In fact, the majority of publications 88 (64%) concentrated their research efforts on local scale investigations. To fully assess regional and long-term implications for tropical dryland forest change studies, analyses on large(r) scales are needed, ideally with higher spatial resolutions and longer temporal duration.
Geographical focus	The Republic of South Africa is, by far the most studied nation across all categories in Southern Africa and the dryland forests of Angola, Mozambique, Lesotho, Swaziland, and Zambia are noticeably very poorly studied. In terms of National Parks, a large proportion of studies were undertaken in the Kruger National Park, leaving many other private and international protected areas relatively understudied. Future efforts to estimate important variables such as forest cover and biomass need not be restricted by country boundaries.
Research categories	Most studies focused on forest cover/types 41 (26%) and land cover/land use 36 (23%) categories while there is limited research on forest biomass and structures, disturbances from drought, phenology, plant traits, and biodiversity/habitats.
Vegetation indices	More than half of the studies, 84 (54%) of papers utilised the normalized difference vegetation index (NDVI, and few studies used other vegetation indices. Testing other vegetation indices beyond NDVI such as the Sentinel-2 red-edge related indices is needed in tropical dryland forests.
Remote sensing sensors	Imagery from optical sensors is most commonly used, out of all sensor types. More than 90% of papers investigated used optical sensors, 6% used SAR data and only 4% used a combination of SAR and Optical sensors. Further improvements should focus on extensive combination and fusion of SAR and optical data.
Validation and accuracy assessments	Our results show there is limited information on sources of error and uncertainty levels of the estimates provided by most studies, with only 54 (39%) of the studies appearing to have performed some form of accuracy assessment. Evidence indicates a need for more frequent use of field observation and inventory data, a greater use of validation/accuracy assessments.
Use of innovative remote sensing platforms	Only nine papers (6%) out of 137 used cloud-based geospatial analysis platforms such as Google Earth Engine (GEE) to access or analyse remote sensing data. The web-based platforms that reduce the need for costly local infrastructure (e.g., GEE), is an opportunity to overcome the limitations previously enforced by data scarcity, large volumes of data, and the scale of analysis.

Limitations

- There is limited information on sources of error and uncertainty levels of the estimates provided by most studies assessed. As a result, for some interventions, there is not sufficient evidence to determine whether the number of studies done equates to research quality, which remains difficult to articulate from a review of this nature.
- One major problem encountered is that commonly used vegetation indices and classification schemes are generalised from better-studied ecosystems, such as temperate and rain forests and this has led to poor accuracy results when extrapolated to, for example, tropical dryland forests, making it difficult to create robust syntheses for decision-makers in policy and practice.

Find out more

For more information, please contact:
Ruusa-Magano David
Email: ruusa-magano.david@durham.ac.uk
Department of Geography, University of Durham

Policy Brief: doi.org/10.5281/zenodo.5566493

N8 AgriFood Food Systems Policy Hub
Email: policy@n8agrifood.ac.uk
Website: https://policyhub.n8agrifood.ac.uk

This brief is one of a collection produced by participants on the Rapid Evidence Synthesis Training (REST) programme. REST was delivered through a collaboration between the University of Leeds, Newcastle University and the N8 AgriFood Programme, supported by Research England QR-SPF funds from the University of Leeds and the University of York.

Appendix B

The analytical codes used in this thesis have been written in R and Google Earth Engine developed by Ruusa David. The substantial code will be uploaded in GitHub.

CHAPTER 2

2A. R CODE FOR ANALYSING AND PLOTTING DATA

This part of the R code is for analysing data for the systematic review

Number of papers integrating remote sensing and dryland forests in Southern Africa.

 # Install needed packages through the pkgTest which is a helper function to load packages and install packages only when they are not installed yet.

```
pkgTest <- function(x)
{
  if (x %in% rownames(installed.packages()) == FALSE) {
    install.packages(x, dependencies= TRUE)
  }
  library(x, character.only = TRUE)
}
neededPackages <- c("sp","zoo", "ggplot2", "dplyr")
for (package in neededPackages){pkgTest(package)}
```

#Load the library

```
library(ggplot2)
library(dplyr)
library(tidyverse)
library(sf)
```

```
library(scales)

library(ggrepel)
```

#path to data

```
path=("C:/ ")
```

#Read the data

```
No_study_SA <-read.csv(paste(path,"File.csv",sep="",collapse=""))
```

#Create the chart

```
No_study_SA_plot1<- ggplot(No_study_SA, aes(y = NoPublication, x = Year,
width=.60)) + geom_col(fill = "aquamarine4", colour = "grey38", width=.85)

No_study_SA_plot2<- No_study_SA _plot1 + labs(x = "Year", y = "Number of
publications")+scale_x_continuous(breaks=seq(1997,2020,2))+scale_y_continuous
(breaks = breaks_width(2))+theme_bw()+geom_smooth(method = "lm",
colour="red", linetype="dashed", size=1.5,se=FALSE)


No_study_SA_plot2<- No_study_R_topic_country_plot2 +
theme(text=element_text(family="Tahoma",colour="black", size = 15),

        axis.text.x=element_text(colour="black", size =12),

        axis.text.y=element_text(colour="black", size = 12))
```

#run lm to get the intercept and slope

```
lm(formula = NoPublication ~Year, data = No_study_SA_plot2)
```

#plot a trend line on the line graph

```
No_study_SA_plot2<- No_study_SA _plot2 + geom_abline(intercept = -1100.7132 ,
slope =  0.5509    , colour="red", linetype="dashed", size=1.5)
```

#Plot the Chart

```
No_study_SA_plot2
```

Number of papers by research institutions.

#Read the data

```
No_study_Inst <-read.csv(paste(path," File.csv ",sep="",collapse=""))
```

#Create the Chart

```
No_study_Inst_plot1<- ggplot(No_study_Inst (x = NoPublication, y =Institution.Category, fill = Institution.Type)) +  geom_col()

No_study_Inst_plot2<- No_study_R_topic_country_plot1 + labs(x = "Published papers", y = "1st author Country")+ scale_fill_brewer(palette = "Dark2") +theme_bw()

No_study_Inst_plot2<- No_study_R_topic_country_plot2 + theme(text=element_text(family="Tahoma",colour="black", size = 15),

          axis.text.x=element_text(colour="black", size = 12),

          axis.text.y=element_text(colour="black", size = 12))

No_study_Inst_plot2<- No_study_Inst_plot2 + guides(fill=guide_legend(title="Institution category"))
```

#Plot the Chart

```
No_study_Inst_plot2
```

Spatial extent of studies.

#Read the data

```
No_study_S_extent <-read.csv(paste(path," File.csv ",sep="",collapse=""))
```

#Create the chart

```
No_study_S_extent_plot1<- ggplot(No_study_S_extent, aes(x =Scale, y =NumberofPublication, fill = fct_inorder(Scale))) +

  geom_col(colour = "grey50",width=0.9)

No_study_S_extent_plot2<- No_study_R_topic_country_plot1 + labs(x = "Spatial extent", y = "Number of publications")+  scale_colour_brewer() +scale_y_continuous(breaks = breaks_width(4))+ theme_bw()


No_study_S_extent_plot2<- No_study_S_extent_plot2 + theme(text=element_text(family="Tahoma",colour="black", size = 15),

          axis.text.x=element_text(colour="black", size =12),

          axis.text.y=element_text(colour="black", size = 12))
```

```
No_study_S_extent_plot2<- No_study_S_extent_plot2 +
guides(fill=guide_legend(title="Spatial scale"))
```

#Plot the Chart

```
No_study_S_extent_plot2
```

Temporal duration of studies.

#Read the data

```
No_study_T_extent <-read.csv(paste(path," File.csv ",sep="",collapse=""))
```

#Create the chart

```
No_study_T_extent_plot1<- ggplot(No_study_T_extent, aes(x = Year, y
=NoPublication, fill = TemporalResolution, width=.85)) +
geom_col(colour="grey39", size=0.60)

No_study_T_extent_plot2<- No_study_T_extent_plot1 + labs(x = "Temporal extent
(years)", y = "Number of publications")+  scale_fill_brewer(palette = "Set1")
+scale_x_continuous(labels = 1:34, breaks = 1:34)+scale_y_continuous(breaks =
breaks_width(4))+ theme_bw()

No_study_T_extent_plot2<- No_study_T_extent_plot2 +
theme(text=element_text(family="Tahoma",colour="black", size = 15),
        axis.text.x=element_text(colour="black", size =10),
        axis.text.y=element_text(colour="black", size = 12))

No_study_T_extent_plot2<- No_study_T_extent_plot2
+guides(fill=guide_legend(title="Temporal resolution"))
```

#Plot the Data

```
No_study_T_extent_plot2
```

Research topic categories

#Read the data

```
No_study_R_topic <-read.csv(paste(path," File.csv.csv",sep="",collapse=""))
```

 # Add label position   #Note, calculate this before adding % sign to the number of publication

```
No_study_R_topic <- No_study_R_topic %>%
```

```
  arrange(desc(Research.focus)) %>% mutate(midpoint =
cumsum(Number.of.Publication) - 0.5*Number.of.Publication)


mycols <- c("#0073C2FF", "#EFC000FF", "#868686FF",
"#CD984CFF","#007672FF", "#EFC000CC", "#896686FF", "#CD529CFF")


ggplot(No_study_R_topic, aes(x = "", y =Number.of.Publication, fill =
Research.focus)) +
  geom_bar(width = 1, stat = "identity", colour = "white") + coord_polar("y", start =
0)+
  geom_text(aes(y = midpoint, label = Number.of.Publication), colour = "white")+
  scale_fill_manual(values = mycols) +  theme_void()
```

#add columns for percentage

```
No_study_R_topic <- No_study_R_topic %>%
  mutate(Research.focus = factor(Research.focus,
                  levels = Research.focus[length(Research.focus):1]),
         cumulative = cumsum(Number.of.Publication),
         midpoint = cumulative - Number.of.Publication / 2,
         labels = paste0(round((Number.of.Publication/ sum(Number.of.Publication))
* 100, 0), "%" , " (", Number.of.Publication, ") "))
```

 # Get the Pie Chart positions

```
No_study_R_topic <- No_study_R_topic%>%   mutate(csum =
rev(cumsum(rev(Number.of.Publication))),
         pos = Number.of.Publication/2 + lead(csum, 1),
         pos = if_else(is.na(pos), Number.of.Publication/2, pos))
```

#Plot the chart

```
ggplot(No_study_R_topic, aes(x = "" , y =Number.of.Publication, fill =
fct_inorder(Research.focus))) +
  geom_col(width = 1, colour = 1) +
  coord_polar(theta = "y") +
  scale_fill_brewer(palette = "Set3") +
```

```
geom_label_repel(data = No_study_R_topic,
         aes(y = pos, label =labels),
         size = 4.5, nudge_x = 0.14, show.legend = FALSE) +
guides(fill = guide_legend(title = "Resesarch topic")) +
theme_void()
```

Number of studies based upon platform and sensor type.

#Read the data

```
No_study_R_sensor <-read.csv(paste(path," File.csv ",sep="",collapse=""))
```

#Create the chart

```
No_study_R_sensor_plot1<- ggplot(No_study_R_sensor, aes(x =InstrumentName, y =NumberofPublication, fill = Sensor.Type,width=.60)) +
 geom_col()

No_study_R_sensor_plot2<- No_study_R_sensor_plot1 + labs(x = "Platform", y = "Number of publications")+  scale_colour_brewer(palette = "Greens") +scale_y_continuous(breaks = breaks_width(10))+ theme_bw()+theme(axis.text.x = element_text(angle = 90))

No_study_R_sensor_plot2<- No_study_R_sensor_plot2 + theme(text=element_text(family="Tahoma",colour="black", size = 15),
          axis.text.x=element_text(colour="black", size =12),
          axis.text.y=element_text(colour="black", size = 12))

No_study_R_sensor_plot2<- No_study_R_sensor_plot2 + guides(fill=guide_legend(title="Sensor Type"))
```

#Plot the Chart

```
No_study_R_sensor_plot2
```

Research topic by country

#Read the data

```
No_study_R_topic_country<-read.csv(paste(path,"Article Assessment_reseracharea_bycountry_2.csv",sep="",collapse=""))
```

#Create the chart

```
No_study_R_topic_country_plot1<- ggplot(No_study_R_topic_country, aes(x = Country, y =Publications, fill = Research.Topic,width=.60)) + geom_col()

No_study_R_topic_country_plot2<- No_study_R_topic_country_plot1 + labs(x = "Country", y = "Number of publications")+ scale_fill_brewer(palette =
```

```
"Set2")+theme_bw()+scale_y_continuous(breaks =
breaks_width(5))+theme(axis.text.x = element_text(angle = 90))

No_study_R_topic_country_plot2<- No_study_R_topic_country_plot2 +
theme(text=element_text(family="Tahoma",colour="black", size = 15),
                axis.text.x=element_text(colour="black", size =12),
                axis.text.y=element_text(colour="black", size = 12))
```

#Plot the Chart

```
No_study_R_topic_country_plot2
```

CHAPTER 3

3A. GOOGLE EARTH ENGINE CODE FOR DOWNLOADING IMAGES, CLASSIFICATION AND CHANGE DETECTION

Google Earth Engine Code for downloading Landsat, Sentinel 1 and 2 images, satellite image classification and change detection

Image classification for Landsat 2004

https://code.earthengine.google.com/5f543641fb703ab0bbf23ea869e3d4a8?noload=1

Image classification for 2018 code

https://code.earthengine.google.com/57348f290a26907372d530f21762c718?noload=1

Perform a Change detection

https://code.earthengine.google.com/d7618eedeaf46fcf53a7de56df0af330?noload=1

Landsat image code

https://code.earthengine.google.com/421117de52df03e0fabf48edac554aae?noload=1

Sentinel image code

https://code.earthengine.google.com/33b7477b23ad3a8bf1f220486c283da1?noload=1

3B. R CODE FOR ESTIMATING FOREST STAND PARAMETERS

This part of the R code is for estimating forest stand parameters

Estimates for forest stand parameters using Chave et al., 2005 allometric Equation

ESTIMATES FOREST STAND PARAMETERS

 # Install needed packages through the pkgTest

```
pkgTest <- function(x)
{
 if (x %in% rownames(installed.packages()) == FALSE) {
  install.packages(x, dependencies= TRUE)
 }
 library(x, character.only = TRUE)
}
neededPackages <- c("rgeos "," raster ", "ggplot2", "dplyr")
for (package in neededPackages){pkgTest(package)}
```

#Load the library

```
library(rgdal)
library(raster)
library(rgeos)
library(ggplot2)
library(rcompanion)  #for transforming
library(Hmisc)  # compute significance levels for pearson
library(dplyr)  # to use select
library(ggpubr) #for ggscatterForest
library(ggpmisc)
library(corrplot)   #Forest correlation
library(MASS)  #for BOXCOX Transformation
library(devtools)
library(ithir)  #To check regression prediction
library(MASS)
library(car)#for vif to test multicollinearity
```

```
library(performance)  #To test model performance
library(randomForest)
library(DAAG) #for k fold validation in linear regression
to test multicollinearity
library(performance)
```

#Apply the allometric equation from Chave et al., 2005 for dry forest

```
ForestPlots <-  plotdata %>%

  mutate(BasalArea_m2 = 0.0001*pi*(DBH/2)^2,

        standBasalArea_m2=0.0001*pi*(DBH/2)^2/0.05*20,

        WoodDensity = 0.79,
```

#Estimate DBH

```
AGB_kg_Chave_DBH = WoodDensity*exp(-
0.667+(1.784*log(DBH))+(0.207*(log(DBH))^2)-(0.0281*(log(DBH))^3)))
```

#Estimate with DBH and total tree height (H)

```
 AGB_kg_Chave_H_DBH = exp(-2.187+(0.916*log(WoodDensity*DBH^2*Height))),
```

CALCULATE/ ESTIMATES OF STAND LEVEL PARAMETERS

(including DBH, Basal Area, Height, AGB, Carbon etc)

```
StandPhysicalParams <- Plotmeta %>%

  group_by(ForestID) %>%

  mutate(PlotArea_m2 = pi * PlotSize^2,

        scalingFactor = 10000/PlotArea_m2)   #convert to hectare


StandForestParams <- ForestPlots %>%

  group_by(ForestID) %>%

  summarise(DBH_mean = mean(DBH, na.rm = T),

          DBH_sd = sd(DBH, na.rm = T),

          DBH_median= median(DBH, na.rm = T),

          BA_mean = mean(BasalArea_m2, na.rm = T),

          BA_sum = sum(BasalArea_m2, na.rm = T),

          BA_sd = sd(BasalArea_m2, na.rm = T),
```

```
            standBA_sum=sum(standBasalArea_m2, na.rm = T),
            standBA_mean=mean(standBasalArea_m2, na.rm = T),
            Height_mean = mean(Height, na.rm = T),
            Height_median = median(Height, na.rm = T),
            Height_sd = sd(Height, na.rm = T),
            Tree_Density = n(),
            AGB_kg_sum_Chav_Height_DBH = sum(AGB_kg_Chave_H_DBH, na.rm = T),
            AGB_kg_sum_Chav_DBH =sum(AGB_kg_Chave_DBH, na.rm = T))
standParams <- left_join(StandPhysicalParams,StandForestParams, by =
"ForestID") %>%
  mutate(Tree_DensityHa = Tree_Density*scalingFactor,
         BA_m2Ha = BA_sum*scalingFactor,
         AGB_kgHa_Chav_H =  AGB_kg_sum_Chav_Height_DBH*scalingFactor,
         AGB_tHa_Chav_H = AGB_kgHa_Chav_H/1000,
         AGB_tCHa_Chav_H = AGB_tHa_Chav_H*0.5,


         AGB_kgHa_Chav_DBH =  AGB_kg_sum_Chav_DBH*scalingFactor,
         AGB_tHa_Chav_DBH = AGB_kgHa_Chav_DBH/1000,
         AGB_tCHa_Chav_DBH = AGB_tHa_Chav_DBH*0.5)
```

<u># Plots of forest stand parameters</u>

```
library (cowplot)
library(ggpubr)
```

#Stand forest DBH

```
Stand_DBH <-
  ggplot(aes(ForestID, DBH_mean),
         data = standParams[1:78,]) +
  geom_col(aes()) +
  theme_bw() +
  theme(panel.grid.major.x = element_blank(),
        text = element_text(size=12),
        axis.text.x = element_text(angle = 55, hjust = 1)) +
```

```
  labs(x = "Plot ID", y = "Mean DBH (cm)") +
  geom_errorbar(aes(ymin=DBH_mean-DBH_sd, ymax=DBH_mean+DBH_sd),
                width=.5)

# Stand forest Basal Area
Stand_BA <-
  ggplot(aes(ForestID, BA_mean),
         data = standParams[1:78,]) +
  geom_col(aes()) +
  theme_bw() +
  theme(panel.grid.major.x = element_blank(),
        text = element_text(size=12),
        axis.text.x = element_text(angle = 55, hjust = 1)) +
  labs(x = "Plot ID", y = "Mean Basal Area (m2)") +
  geom_errorbar(aes(ymin=BA_mean-BA_sd, ymax=BA_mean+BA_sd),
                width=.5)

# Stand forest  Height
Stand_Height <-
  ggplot(aes(ForestID, Height_mean),
         data = standParams[1:78,]) +
  geom_col(aes()) +
  theme_bw() +
  theme(panel.grid.major.x = element_blank(),
        text = element_text(size=12),
        axis.text.x = element_text(angle = 55, hjust = 1)) +
  labs(x = "Plot ID", y = "Mean Tree Height (m)") +
  geom_errorbar(aes(ymin=Height_mean-Height_sd, ymax=Height_mean+Height_sd),
                width=.5)

# Stand forest Tree Density
Stand_Density <-
```

```
  ggplot(aes(ForestID, Tree_DensityHa),
         data = standParams[1:78,]) +
  geom_col(aes()) +
  theme_bw() +
  theme(panel.grid.major.x = element_blank(),
        text = element_text(size=12),
        axis.text.x = element_text(angle = 55, hjust = 1)) +
  labs(x = "Plot ID", y = "Tree Density (Trees ha-1)")
```

 # Above Ground Biomass using DBH for CHAVE

```
Stand_AGB_tha_DBH_Chav <-
  ggplot(aes(ForestID, AGB_tHa_Chav_DBH),
         data = standParams[1:78,]) +
  geom_col(aes()) +
  theme_bw() +
  theme(panel.grid.major.x = element_blank(),
        text = element_text(size=12),
        axis.text.x = element_text(angle = 55, hjust = 1)) +
  labs(x = "Plot ID", y = "AGB with DBH; (t ha-1)")

Stand_AGB_tCha_DBH_Chav <-
  ggplot(aes(ForestID, AGB_tCHa_Chav_DBH),
         data = standParams[1:78,]) +
  geom_col(aes()) +
  theme_bw() +
  theme(panel.grid.major.x = element_blank(),
        text = element_text(size=12),
        axis.text.x = element_text(angle = 55, hjust = 1)) +
  labs(x = "Plot ID", y = "Total Carbon with DBH; (t C ha-1)")
```

 # Stand forest AGB with Height

```
Stand_AGB_tha_H_Chav <-
  ggplot(aes(ForestID, AGB_tHa_Chav_H),
         data = standParams[1:78,]) +
  geom_col(aes()) +
  theme_bw() +
  theme(panel.grid.major.x = element_blank(),
        text = element_text(size=16),
        axis.text.x = element_text(angle = 55, hjust = 1)) +
  labs(x = "Plot ID", y = "AGB (Mg/ha)")

Stand_AGB_tCha_H_Chav <-
  ggplot(aes(ForestID, AGB_tCHa_Chav_H),
         data = standParams[1:78,]) +
  geom_col(aes()) +
  theme_bw() +
  theme(panel.grid.major.x = element_blank(),
        text = element_text(size=16),
        axis.text.x = element_text(angle = 55, hjust = 1)) +
  labs(x = "Plot ID", y = "Total Carbon (Mg/ha)")
```

<u>#Plot the forest stand parameters Individually</u>

```
plot_grid(Stand_DBH)
plot_grid(Stand_BA)
plot_grid(Stand_Height)
plot_grid(Stand_Density)
plot_grid(Stand_AGB_tha_H_Chav)
plot_grid(Stand_AGB_tCha_H_Chav,labels = "auto",
          label_size = 18,
          align = "v")
plot_grid(Stand_AGB_tha_DBH_Chav)
plot_grid(Stand_AGB_tCha_DBH_Chav)
```

#Plot the forest stand parameters in one Figure

```
StandFigure <- hist(Stand_AGB_tha_H_Chav,Stand_AGB_tCha_H_Chav,
  ncol = 1, nrow = 2, align = "v", axis = "r",labels="auto", label_size = 18)
StandFigure
```

PLOT THE DENSITY AND HISTOGRAM PLOTS FOR AGB AND CARBON

3.1 Create density and histogram plots for Aboveground biomass (AGB)of each field plot with woodland trees.

```
AGB<-ggplot(standParams[1:78,], aes(x=AGB_tHa_Chav_H)) +
  geom_histogram(aes(y =..density..),
                 breaks=seq(2, 170, by = 10),
                 col="Black",
                 fill="#FF6666", alpha = .1 ) +  theme_bw()+
  geom_density(alpha=.2, fill="black") +
 # labs(title="AGB (Mg/ha)") +
  labs(x="AGB (Mg/ha)", y="Count")  +
  theme(axis.line = element_line(size=1, colour = "black"),
        panel.grid.major = element_blank(),
        panel.grid.minor = element_blank(),
        panel.border = element_blank(),
        panel.background = element_blank(),
        plot.title=element_text(size = 20,face="bold"),
        text=element_text(size = 16),
        axis.text.x=element_text(colour="black", size = 14,face="bold"),
        axis.text.y=element_text(colour="black", size = 14,face="bold"),
        axis.title.x = element_text(colour="black", size=16, face="bold"),
        axis.title.y = element_text(colour="black", size=16, face="bold"),
        axis.text=element_text(colour="black", size=14))
```

3.2 CARBON: Create density and histogram plots Carbon stock (Mg/ha) of each field plot with woodland trees.

```
carbon<-ggplot(standParams[1:78,], aes(x=AGB_tCHa_Chav_H)) +
  geom_histogram(aes(y =..density..),
                 breaks=seq(1.03, 84, by = 10),
                 col="black",
                 fill="#FF6666", alpha = .1
  ) +  theme_bw()+
  geom_density(alpha=.2, fill="black") +
  # labs(title="AGB (Mg/ha)") +
  labs(x="Total Carbon (Mg/ha)", y="")  +
  theme(axis.line = element_line(size=1, colour = "black"),
        panel.grid.major = element_blank(),
        panel.grid.minor = element_blank(),
        panel.border = element_blank(),
        panel.background = element_blank(),
        plot.title=element_text(size = 20,face="bold"),
        text=element_text(size = 16),
        axis.text.x=element_text(colour="black", size = 14,face="bold"),
        axis.text.y=element_text(colour="black", size = 14,face="bold"),
        axis.title.x = element_text(colour="black", size=16, face="bold"),
        axis.title.y = element_text(colour="black", size=16, face="bold"),
        axis.text=element_text(colour="black", size=14))
```

 # Plot the density and histogram plot for carbon

```
carbon
```

#Combine all the plots

```
ggarrange(AGB, carbon,
          labels = c("A", "B"),common.legend=TRUE,legend = "top",# specify the legend position and specify whether they should share the common legend or not.
          ncol = 2, nrow = 2) # column and row numbers
```

2. Estimates the AGB using Linear Model (Raster data)

#Read the csv data

S2chobezam_wo.num<-read.csv(paste(path,"File.csv",sep="",collapse=""))

#Transform the data for normality

S2chobezam_wo.num$AGBL<-log(S2chobezam_wo.num$AGB_tHa_Chav_H)

#display histogram for transformed AGB

hist(S2chobezam_wo.num$AGBL)

#choose variables to work (Sentinel 1, Sentinel 2 and Landsat 8 bands and indices)

S2chobezam_wo.num=dplyr::select(S2chobezam_wo.num,AGBL,B2,B3,B4,B5,B6,B7,B8,B8A,B11,B12,S1_VH,S1_VV,ndvi,grvi,evi,savi,msav,nbr,nbr2,gndvi,nR1,nR2,nR3,nR4,ndi45,ireci,srtm)

#read in Raster data-sentinel

 # NB: Load Sentinel 1, Sentinel 2, and Landsat 8 tif files, Below is an example of Sentinel 2 data loaded in r

S2_chobe<-list.files ("Path/", pattern = ".tif$", full.names = TRUE)

#stack all bands

#covariates are of the same scale in terms of resolution and extent.

S2_03_chobe<- stack(S2_chobe[])

 # Linear Model prediction

hv.MLR.rh <-lm(AGBL~B3+B5+S1_VH+S1_VV, data =S2chobezam_wo.num)

vif(hv.MLR.rh)

summary(hv.MLR.rh)

#Estimate AGB using Linear Model

#predict from raster data

map.MLR1<- exp(predict(S2_03_chobe,hv.MLR.rh,format = "GTiff", datatype = "FLT4S", overwrite = TRUE)) ***# backtransform the log data to original***

plot(map.MLR1, main = "S2 Biomass prediction with linear model")

 # including all bands and indices, and choose the right variables

tempD <- data.frame(cellNos = seq(1:ncell(S2_03_chobe)))

vals <- as.data.frame(getValues(S2_03_chobe))

tempD <- cbind(tempD, vals)

tempD <- tempD[complete.cases(tempD),]

cellNos <- c(tempD$cellNos)

gXY <- data.frame(xyFromCell(S2_03_chobe, cellNos, spatial = FALSE))

tempD <- cbind(gXY, tempD)

str(tempD)

 # backtransform the log data to original scale with exp

map.MLR <- exp(predict(hv.MLR.rh, newdata = tempD))

map.MLR <- cbind(data.frame(tempD[, c("x", "y")]), map.MLR) ***#include x and y coordinates***

#rasterise the predictions for mapping

map.MLR.r <- rasterFromXYZ(as.data.frame(map.MLR[, 1:3])) ***#include the cell numbers***

plot(map.MLR.r, main = "S2 Biomass prediction with glm forest")

Validate the AGB using Linear Model

 # validate the Linear model

#split the data 70 and 30% for validation

set.seed(123)

training <- sample(nrow(S2chobezam_wo.num), 0.7 * nrow(S2chobezam_wo.num))

#display the calibration data

training

#fit the model

hv.MLR.rh <-lm(AGBL~B3+B5+S1_VH+S1_VV+gndvi+ndi45, data =S2chobezam_wo.num,y=TRUE, x=TRUE)

AGB.pred.F <- predict(hv.MLR.rh, S2chobezam_wo.num)

#Evaluate the model with goof:

goof(observed = S2chobezam_wo.num$AGBL, predicted= AGB.pred.F,plot.it = TRUE)

#Check model performance

model_performance(hv.MLR.rh)

#Evaluate the calibration model

AGB.pred.C <- predict(hv.MLR.rh, S2chobezam_wo.num[training,])

goof(observed = S2chobezam_wo.num$AGBL[training], predicted

= AGB.pred.C,plot.it = TRUE)

#Evaluate the validation model

AGB.pred.V <- predict(hv.MLR.rh, S2chobezam_wo.num[-training,])

goof(observed = S2chobezam_wo.num$AGBL[-training], predicted

= AGB.pred.V,plot.it = TRUE)

 # set the CRS to +zone=35 +south +datum=WGS84

crs(map.MLR.r) <- "+proj=utm +zone=35 +south +datum=WGS84 +units=m +no_defs +ellps=WGS84 +towgs84=0,0,0"

#Export the map

writeRaster(map.MLR.r, filename="Path", datatype = "FLT4S", overwrite = TRUE)

Estimated AGB vs Field-based AGB for Linear Models (Calibration Data: 70%)

#Plot the predicted vs the observed for Linear Model

#fit the model

chobe.MLR<-lm(AGBL~B3+B5+S1_VV, data =S2chobezam_wo.num)

summary(chobe.MLR)

predicted_AGB <- predict(chobe.MLR, S2chobezam_wo.num)

goof(observed = S2chobezam_wo.num$AGBL, predicted= predicted_AGB)

#plot the model

gg0 <- ggplot(S2chobezam_wo.num,aes(AGBL,predicted_AGB))+geom_point(aes()) #colour by forest types

gg0<-gg0+geom_point(size=4)

gg1 <- gg0 + geom_smooth(method="lm",se=FALSE, colour="black")#+geom_abline(linetype="dashed",col="red")

gg1

glm1<- gg1+stat_regline_equation (aes(label = paste(..adj.rr.label.., sep = "~~~~")), label.x.npc = "left", label.y.npc = 0.95,hjust=0,size=5.5,face="bold") #include Y

 # Calculate RMSE

chobe.MLR1 <-lm(AGBL~predicted_AGB, data =S2chobezam_wo.num)

rmse <- round(sqrt(mean(resid(chobe.MLR1)^2)), 2)

#plot the rmse

gg<-glm1 + geom_text(aes(x=0.5, y=4.8,size=30, label= paste("RMSE= ", rmse, "Mg/ha"), hjust=0))

gg<-gg+theme_bw()

gg<-gg + labs(y="Predicted AGB (Mg/ha)", x = "Observed AGB (Mg/ha)", title = "(a) MLR AGB Model")

rmse_xy<-gg + theme(

plot.title = element_text(colour="black", size=20, face="bold.italic"),

axis.title.x = element_text(colour="black", size=20, face="bold"),

axis.title.y = element_text(colour="black", size=20, face="bold"),

axis.text=element_text(colour="black", size=20, face="bold")

)

rmse_xy

#Calculate the residuals

```
chobe.MLR <-lm(AGBL~B3+B5+S1_VV, data =S2chobezam_wo.num)

predicted_AGB <- predict(chobe.MLR, S2chobezam_wo.num)

err<-predicted_AGB- S2chobezam_wo.num$AGBL

df<-data.frame(residuals=err, fitted.values=predicted_AGB )

df2<-df[order(df$fitted.values),]

plot(residuals~fitted.values, data=df2, ylab="Residuals", xlab="AGB (Mg/ha)",
  main="(a MLR AGB residuals ", cex.lab=2.0, cex.main=2.0,
cex.axis=2.0,pch=19,cex=1.4, font = 2, font.lab=2,font.main=4) +abline(0,0,
col="black")
```

*Estimated AGB vs Field-based AGB for Linear Models (Validation Data: 30%)*

#Plot the predicted vs the observed for Linear Model

#fit the model

```
chobe.MLR<-lm(AGBL~B3+B5+S1_VV, data =S2chobezam_wo.num)

summary(chobe.MLR)

predicted_AGB <- predict(chobe.MLR, S2chobezam_wo.num)

goof(observed = S2chobezam_wo.num$AGBL, predicted= predicted_AGB)
```

#plot the model

```
gg0 <- ggplot(S2chobezam_wo.num,aes(
AGBL,predicted_AGB))+geom_point(aes()) #colour by forest types

gg1 <- gg0 + geom_smooth(method="lm",se=FALSE,
colour="black")#+geom_abline(linetype="dashed",col="red")

gg1

glm1<-  gg1+stat_regline_equation (aes(label =  paste(..adj.rr.label.., sep =
"~~~~")), label.x.npc = "left", label.y.npc = 0.95,hjust=0,face="bold")    #include Y
```

 # Calculate RMSE

chobe.MLR1 <-lm(AGBL~predicted_AGB, data =S2chobezam_wo.num)

rmse <- round(sqrt(mean(resid(chobe.MLR1)^2)), 2)

#plot the rmse

gg<-glm1 + geom_text(aes(x=0.5, y=4.8, label= paste("RMSE= ", rmse, "Mg/ha"), hjust=0))

gg<-gg+theme_bw()

gg<-gg + labs(y="Predicted AGB (Mg/ha)", x = "Observed AGB (Mg/ha)", title = "AGB Model (a) Linear regression")

gg

rmse_xy<-gg + theme(

plot.title = element_text(colour="black", size=20, face="bold.italic"),

axis.title.x = element_text(colour="black", size=16, face="bold"),

axis.title.y = element_text(colour="black", size=16, face="bold"),

axis.text=element_text(colour="black", size=14)

)

rmse_xy

#Calculate the residuals

chobe.MLR <-lm(AGBL~B3+B5+S1_VV, data =S2chobezam_wo.num)

predicted_AGB <- predict(chobe.MLR, S2chobezam_wo.num)

err<-predicted_AGB- S2chobezam_wo.num$AGBL

df<-data.frame(residuals=err, fitted.values=predicted_AGB)

df2<-df[order(df$fitted.values),]

#Plot the residuals

plot(residuals~fitted.values, data=df2, ylab="Residuals", xlab="AGB (Mg/ha)",

main="AGB residuals (a) Linear regression ", cex.lab=1.5, cex.main=1.5, cex.axis=1.5) +

abline(0,0, col="black")

Validate Estimated AGB vs Field-based AGB for Linear Models

#split the data 70 and 30% for validation

training <- sample(nrow(S2chobezam_wo.num), 0.7 * nrow(S2chobezam_wo.num))

#fit the model

chobe.MLR <-lm(AGBL~B3+B5+S1_VV, data =S2chobezam_wo.num[-training,])

summary(chobe.MLR)

predicted_AGB <- predict(chobe.MLR, S2chobezam_wo.num[-training,])

goof(observed = S2chobezam_wo.num[-training,]$AGBL, predicted= predicted_AGB)

RF.pred.C <- predict(chobe.MLR, newdata =S2chobezam_wo.num[training,])

#calibration

goof(observed = S2chobezam_wo.num$AGBL[training], predicted = RF.pred.C, plot.it=TRUE)

#Validation

MLR.pred.V <- predict(chobe.MLR, newdata = S2chobezam_wo.num[-training,])

goof(observed = S2chobezam_wo.num$AGBL[-training], predicted =MLR.pred.V,plot.it = TRUE)

Estimates the AGB using Random Forest Model (Raster data)

#Split the data into calibration and validation dataset

set.seed(123)

training <- sample(nrow(S2chobezam_wo.num), 0.7 * nrow(S2chobezam_wo.num))

#fit the RF model

chobe.rf.mod <-randomForest(AGBL~B3+B5+S1_VV, data =S2chobezam_wo.num,mtry=3,importance=TRUE,ntree=1000)

print(chobe.rf.mod)

#Plot variable importance

varImpPlot(chobe.rf.mod)

#check the model residuals

S2chobezam_wo.num$residual <- S2chobezam_wo.num$AGBL-predict(chobe.rf.mod,

newdata = S2chobezam_wo.num, plot.it=True)

hist(S2chobezam_wo.num$residual)

mean(S2chobezam_wo.num$residual)

 # backtransform the log data to original

map.RF.r1 <- exp(predict(S2_03_chobe, chobe.rf.mod, "Chobe Biomass_RF.tif",

format = "GTiff", datatype = "FLT4S", overwrite = TRUE))

#Plot the data

plot(map.RF.r1 , main = "Random Forest model predicted Biomass")

Estimated AGB vs Field-based AGB for Random Forest Model (Calibration Data: 70%)

#Plot the predicted vs the observed

#fit the model

chobe.rf.mod <-randomForest(AGBL~B3+B5+S1_VV, data =S2chobezam_wo.num,mtry=3,importance=TRUE,ntree=1000, trace=true)

print(chobe.rf.mod)

predicted_AGB <- predict(chobe.rf.mod, S2chobezam_wo.num)

goof(observed = S2chobezam_wo.num$AGBL, predicted= predicted_AGB)

#plot the model

gg0 <- ggplot(S2chobezam_wo.num,aes(AGBL,predicted_AGB))+geom_point(aes()) #colour by forest types

gg0<-gg0+geom_point(size=4)

gg1 <- gg0 + geom_smooth(method="randomForest", colour="black")+geom_abline(linetype="dashed",col="red")

gg1<-gg1+geom_abline(intercept = 0,slope=1,col="black")

glm1<- gg1+stat_regline_equation (aes(label = paste(..adj.rr.label.., sep = "~~~~")), label.x.npc = "left", label.y.npc = 0.9,hjust=0,size=5.5,face="bold") #include Y

 # Calculate RMSE

chobe.rf.mod1 <-randomForest(AGBL~predicted_AGB, data =S2chobezam_wo.num,importance=TRUE,ntree=1000)

rmse_function<-function(pred,actual){

  sqrt(sum(pred-actual)^2)

}

rmse<-round(rmse_function(predicted_AGB,S2chobezam_wo.num$AGB),2)

rmse

#plot the rmse

gg<-glm1 + geom_text(aes(x=0.5, y=4.3,size=30,face="bold", label= paste("RMSE= ", rmse, "Mg/ha"), hjust=0))

gg<-gg+theme_bw()

gg<-gg + labs(y="Predicted AGB (Mg/ha)", x = "Observed AGB (Mg/ha)", title = "(b) RFR AGB Model")

gg

rmse_xy<-gg + theme(

  plot.title = element_text(colour="black", size=20, face="bold.italic"),

  axis.title.x = element_text(colour="black", size=20, face="bold"),

  axis.title.y = element_text(colour="black", size=20, face="bold"),

  axis.text=element_text(colour="black", size=20, face="bold")

)

rmse_xy

#Calculate the residuals

chobe.rf.mod <-randomForest(AGBL~B3+B5+S1_VV, data =S2chobezam_wo.num,mtry=3, importance=TRUE,ntree=1000) print(chobe.rf.mod)

predicted_AGB <- predict(chobe.rf.mod, S2chobezam_wo.num)

err<-predicted_AGB- S2chobezam_wo.num$AGBL

df<-data.frame(residuals=err, fitted.values=predicted_AGB)

df2<-df[order(df$fitted.values),]

#Plot the residuals

plot(residuals~fitted.values, data=df2, ylab="Residuals", xlab="AGB (Mg/ha)",

main="(b) RFR AGB residuals ", cex.lab=2.0, cex.main=2.0, cex.axis=2.0,pch=19,cex=1.4, font = 2, font.lab=2,font.main=4) +

abline(0,0, col="black",lwd=2.5)

Validate Estimated AGB vs Field-based AGB for Random Forest Model

#split the data 70 and 30% for validation

training <- sample(nrow(S2chobezam_wo.num), 0.7 * nrow(S2chobezam_wo.num))

#fit the model

chobe.rf.mod <-randomForest(AGBL~B3+B5+S1_VV, data =S2chobezam_wo.num,mtry=3,importance=TRUE,ntree=1000)

print(chobe.rf.mod)

predicted_AGB <- predict(chobe.rf.mod, S2chobezam_wo.num)

goof(observed = S2chobezam_wo.num$AGBL, predicted= predicted_AGB)

Internal validation

RF.pred.C <- predict(chobe.rf.mod, newdata =S2chobezam_wo.num[training,])

goof(observed = S2chobezam_wo.num$AGBL[training], predicted = RF.pred.C, plot.it=TRUE)

#External validation

RF.pred.V <- predict(chobe.rf.mod, newdata = S2chobezam_wo.num[-training,]) goof(observed = S2chobezam_wo.num$AGBL[-training], predicted = RF.pred.V,plot.it = TRUE)

Computing variables correlation

(i) PEARSON CORRELATION WITH S2 BANDS

#Read the csv data

S2chobezam_wo.num<-read.csv(paste(path," File.csv ",sep="",collapse=""))

#Choose the variable (Sentinel 1, Sentinel 2 and Landsat 8 bands and indices)

S2chobezam_wo.num2=dplyr::select(S2chobezam_wo.num,AGBL, B2,B3,B4,B5,B6,B7,B8,B8A,B11,B12,S1_VH,S1_VV,ndvi,grvi,evi,savi,msav,nbr,nbr2, gndvi,nR1,nR2,nR3,nR4,ndi45,ireci,srtm, HeightL, DenHAL)

compute the correlation matrix

cor2<-rcorr((as.matrix(S2chobezam_wo.num2)))

 # compute variable p-values

cor2$P

(ii) CREATE A SCATTER PLOTS FOR CORRELATION

#SAR sentinel 1 scatterplot

#Plot S1_VV and AGB

```
S1_VV <- ggplot(data = S2chobezam_wo.num, aes(x =S1_VV, y = AGBL))+
geom_point(aes())
S1_VV<-S1_VV+geom_point( size=4)
S1_VV<-S1_VV+geom_smooth(method = "lm", se=FALSE, colour="black", formula =
y ~ x) #to exclude the line in the middle set (se=FALSE),
```

 # Get equation and r-squared as string
#make a function to plot the equation

```
lm_eqn <- function(S2chobezam_wo.num){
  m <- lm(AGBL~S1_VV, S2chobezam_wo.num);
  eq <- substitute(italic(y) == a + b %.% italic(x)*","~~italic(r)^2~"="~r2,
          list(a = format(unname(coef(m)[1]), digits = 2),
             b = format(unname(coef(m)[2]), digits = 2),
             r2 = format(summary(m)$r.squared, digits = 2)))
  as.character(as.expression(eq));}
S1_VV_eq <- S1_VV + geom_text(x = -15.0, y = 4.8, size=5.5,label =
lm_eqn(S2chobezam_wo.num), parse = TRUE)
S1_VV_eq
```

 # Calculate RMSE

```
S1_VV_model<-lm(AGBL~S1_VV, data=S2chobezam_wo.num)
rmse <- round(sqrt(mean(resid(S1_VV_model)^2)), 2)
```

 # Plot_RMSE

```
S1_VV_rmse<-S1_VV_eq + geom_text(aes(x=-16.0, y=4.5, size=35,label=
paste("RMSE= ", rmse, "Mg/ha"), hjust=0))+theme_bw()
S1_VV_rmse_xy <- S1_VV_rmse + labs(y="AGB (Mg/ha)", x="S1 VV
Polarisation",title="(a) Sentinel-1 Backscatter Value on VV")
S1_VV_rmse_xy<-S1_VV_rmse_xy + theme(text = element_text(size = 14))
S1_VH_rmse_xy
```

#Sentinel 2 scatterplot

#Plot Sentinel 2 variable ands AGB

```
B2 <- ggplot(data = S2chobezam_wo.num, aes(x =B2, y = AGBL))+
geom_point(aes())

B2<-B2+geom_smooth(method = "lm",  colour="black", formula = y ~ x) #to
exclude the line in the middle set (se=FALSE),
```

#Get equation and r-squared as string

#make a function to plot the equation

```
lm_eqn <- function(S2chobezam_wo.num){
  m <- lm(AGBL~B2, S2chobezam_wo.num);
  eq <- substitute(italic(y) == a + b %.% italic(x)*","~~italic(r)^2~"="~r2,
            list(a = format(unname(coef(m)[1]), digits = 2),
                 b = format(unname(coef(m)[2]), digits = 2),
                 r2 = format(summary(m)$r.squared, digits = 2)))
  as.character(as.expression(eq));
}

B2_eq <- B2 + geom_text(x = 0.06, y = 2, label = lm_eqn(S2chobezam_wo.num),
parse = TRUE)
```

 # Calculate RMSE

```
B2_model<-lm(AGBL~B2, data=S2chobezam_wo.num)
rmse <- round(sqrt(mean(resid(B2_model)^2)), 2)
```

 # Plot_RMSE

```
B2_rmse<-B2_eq + geom_text(aes(x=0.05, y=1.5, label= paste("RMSE= ", rmse,
"mg/ha"), hjust=0))+theme_bw()
B2_rmse
B2_rmse_xy <- B2_rmse + labs(y="AGB (Mg/ha)", x="Reflectance in
B2",title="Sentinel 2")
B2_rmse_xy<-B2_rmse_xy + theme(text = element_text(size = 14))
```

Simple and Multivariate regression models

CREATE THE SIMPLE MODEL FOR AGB USING SAR S1, S2 SPECTRAL BANDS, S2 INDICES. *NB: Only showed certain models, the rest of the models can be provided upon request*

#B3

B2_lm <-lm(AGBL~B2, data =S2chobezam_wo.num)

summary(B2_lm)

r2(B2_lm)

model_performance(B2_lm)

#B3

B3_lm <-lm(AGBL~B3, data =S2chobezam_wo.num)

summary(B3_lm)

r2(B3_lm)

model_performance(B3_lm)

#B5

B5_lm <-lm(AGBL~B5, data =S2chobezam_wo.num)

summary(B5_lm)

r2(B5_lm)

model_performance(B5_lm)

#NDVI

ndvi_m <-lm(AGBL~ndvi, data =S2chobezam_wo.num)

summary(ndvi_lm)

r2(ndvi_m)

model_performance(ndvi_m)

#GRVI

grvi_m <-lm(AGBL~grvi, data =S2chobezam_wo.num)

summary(grvi_lm)

r2(grvi_m)

model_performance(grvi_m)

#S1_VV

S1_VV_lm <-lm(AGBL~S1_VV, data =S2chobezam_wo.num)

summary(S1_VV_lm)

r2(S1_VV_lm)

model_performance(S1_VV_lm)

#S1_VH

S1_VH_lm <-lm(AGBL~S1_VH, data =S2chobezam_wo.num)

summary(S1_VH_lm)

r2(S1_VH_lm)

model_performance(S1_VH_lm)

#CREATE THE MULTIVARIATE MODEL AND PREDICTION FOR ABOVE GROUND BIOMASS USING SAR S1, S2 SPECTRAL BANDS, S2 INDICES COMBINATIONS. *NB: Only showed certain models, the rest of the models can be provided upon request*

 # a)model SAR S1

sar.model<-lm(AGBL~S1_VH+S1_VV, data=S2chobezam_wo.num)

summary(sar.model)

r2(sar.model)

model_performance(sar.model)

vif(sar.model)

 # b)Sentinel 2 bands

sentinel2.model<-lm(AGBL~B3+B5+B4+B5+B6+B7+B8+B8A+B11+B12, data=S2chobezam_wo.num) summary(sentinel2.model)

r2(sentinel2.model)

model_performance(sentinel2.model)

vif(sentinel2.model)

<u># c)Sentinel 2 and Sentinel 1 bands</u>

sentinel2SAR.model<-
lm(AGBL~B3+B5+B4+B5+B6+B7+B8+B8A+B11+B12+S1_VV+S1_VH,
data=S2chobezam_wo.num)

summary(sentinel2SAR.model)

r2(sentinel2SAR.model)

model_performance(sentinel2SAR.model)

vif(sentinel2SAR.model)

<u># d) S2 indices only</u>

S2ind.model<-
lm(AGBL~ndvi+grvi+evi+savi+msav+nbr+nbr2+gndvi+nR1+nR2+nR3+nR4+ndi4
5+ireci, data=S2chobezam_wo.num)

summary(S2ind.model)

r2(S2ind.model)

model_performance(S2ind.model)

vif(S2ind.model)

CHAPTER 4

GOOGLE EARTH ENGINE CODE FOR THE VEGETATION INDICES

Google Earth Engine Code for the vegetation Indices time series time series

https://code.earthengine.google.com/fe5b816a2cde4a03c63183cb3f1b2cfb?noload=1 /*//

Code generated for calculating different vegetation Indices using 8 day MODIS at 500m, developed by-Ruusa David August 2020

*//

//add the shapefile to the map

```
Map.addLayer(Chobe, ndviVis,'NDVI 8 days')

Map.addLayer(Chobe, ndviVis,'NDVI 8 days')
```

// mask out cloud and bad pixels

```
var maskclouds = function(image) {

    return image.updateMask(image.select("SummaryQA").eq(0));

  };


var maskcloudsQC = function(image) {

 var QA = image.select('StateQA')

 var bitMask = 1 << 10;

 return image.updateMask(QA.bitwiseAnd(bitMask).eq(0))

}
```

// Load MODIS image collection

```
var MODIS = ee.ImageCollection("MODIS/006/MOD09A1")

.filterDate('2019-12-01', '2019-12-31')

 .map(maskcloudsQC).max().clip(Chobe);
```

//create a function to calculate NDVI

```
var addNDVI = function(image){
  var newImg = image.normalisedDifference(['sur_refl_b02',
'sur_refl_b01']).double()
  .rename('ndvi');
  return newImg.
    set({
      'system:index' : image.get('system:index'),
      'system:time_start' : image.get('system:time_start')
    });
};
var ndvi =addNDVI(MODIS);
```

//Define visualisation parameters

```
var ndviVis = {
        min: 0.0,
        max: 1.0,
        palette: [
          'FFFFFF', 'CE7E45', 'DF923D', 'F1B555', 'FCD163', '99B718', '74A901',
          '66A000', '529400', '3E8601', '207401', '056201', '004C00', '023B01',
          '001E01', '011D01', '011301'
        ], };
Map.addLayer(ndvi, ndviVis,'NDVI 8 days')
```

//create EVI function

```
var addEVI = function(image) {
  return image.expression(
      '(NIR-RED) / (NIR + 6*RED - 7.5*BLUE + 1)',
    {
      'NIR': image.select('sur_refl_b02'),
```

```
      'RED': image.select('sur_refl_b01'),
      'BLUE': image.select('sur_refl_b03')
    }
  ).rename('evi') }
var evi = addEVI(MODIS)
Map.addLayer(evi,ndviVis,'EVI 16 days')
```

//create a function to calculate GNDVI

```
var addGNDVI = function(image){
  var newImg = image.normalisedDifference(['sur_refl_b02',
'sur_refl_b04']).double()
  .rename('gndvi');
  return newImg.
    set({
      'system:index' : image.get('system:index'),
      'system:time_start' : image.get('system:time_start')
    }); };
var gndvi =addGNDVI(MODIS);
Map.addLayer(gndvi, ndviVis,'GNDVI 16 days')
```

//Export the NDVI data

```
Export.image.toDrive({
  image:ndvi ,
  folder: 'ChobeMODIS_1',
  fileNamePrefix: 'ND_12_2020',
  description:"Modis_ndvi_8_days_02_500m",
  region: Chobe,
   crs:"EPSG:32735 ",
  scale: 500,
  maxPixels:1e13
});
```

__//Export the EVI data__

```
Export.image.toDrive({
  image: evi,
  folder: 'ChobeMODIS_1',
  fileNamePrefix: 'EV_12_2020',
  description:"Modis_evi_8_days_02_500m",
  region: Chobe,
   crs:"EPSG:32735 ",
  scale: 500,
  maxPixels:1e13
});
```

__//Export the GNDVI data__

```
Export.image.toDrive({
  image: gndvi,
  folder: 'ChobeMODIS_1',
  fileNamePrefix: 'GN_12_2020',
  description:"Modis_gndvi_8_days_02_500m",
  region: Chobe,
   crs:"EPSG:32735 ",
  scale: 500,
  maxPixels:1e13
});
```

R CODE FOR ANALYSING TIME SERIES OF DIFFERENT VEGETATION INDICES, AND CLIMATE DATA

This part of the R code is for analysing time series of different vegetation indices, climate data with change detection algorithms

__Script for gap filling Vegetation Index e.g. NDVI values derived from MODIS composites.__

 # Script for gap filling site level NDVI values derived from MODIS composites.

 # Install needed packages through the pkgTest

```
pkgTest <- function(x)
{
  if (x %in% rownames(installed.packages()) == FALSE) {
    install.packages(x, dependencies= TRUE)
  }
  library(x, character.only = TRUE)
}
neededPackages <- c("r imputeTS "," (lubridate )
for (package in neededPackages){pkgTest(package)}
```

 # load Libraries

```
library(tidyverse)
library(imputeTS)
library(lubridate)
```

#Read the data

```
MODIS<-read.csv(paste("File.csv",sep="",collapse=""))
```

 # Convert date to Date format

```
MODIS$Date <- as.Date(MODIS$Date, "%d.%m.%Y")
```

 # Plot all the land cover types (forest, grassland, water etc) to analyse the data

```
ggplot(MODIS %>% filter(NDVI > -1)) +
  geom_point(aes(Date, NDVI, col = PlotType)) +
  facet_wrap(~PlotType, ncol = 1)
```

 # Plot one land cover types (forest, grassland, water etc) for all the 12 months to see data distribution

```
ggplot(MODIS %>% filter(NDVI > -1) %>% filter(PlotType == "grass")) +
  geom_point(aes(Date, NDVI, col = PlotType)) +
```

```
  facet_wrap(~month)
```

<u># In this section, remove the lowest 1% of values in each month</u>

<u># this method assumes low values are contamination and not real change so use with caution</u>

<u>#   1% could be changed to 5% by swapping 'probs=0:100/100' for 'probs=0:20/20' or by selecting</u>

```
MODISa <- MODIS %>%
  filter(NDVI > -1) %>%
  group_by(PlotType,month) %>%
  mutate(quantile = as.integer(cut(NDVI, quantile(NDVI, probs=0:100/100),
include.lowest=TRUE)),
       NDVI=replace(NDVI, quantile==1, NA)) %>%
  drop_na(NDVI) %>%
  ungroup() %>%
  select(!c(Year,month))
```

<u># Reformat data in preparation for gap filling</u>

<u>## Expand data frame to include all date values for every site id</u>

```
MODISb <- MODISa %>%
  complete(Date = seq(floor_date(min(MODISa$Date),unit = "month"),
                floor_date(max(MODISa$Date), unit = "month"), by = "month"),
         nesting(ForestID,PlotType))
ggplot(MODISb) +
  geom_point(aes(Date, NDVI, col = PlotType)) +
  facet_wrap(~PlotType, ncol = 1)
```

<u># Reformat data and fill missing metadata values</u>

```
MODISb <- MODISb %>%
  mutate(DATE = as.Date(Date,"%Y-%m-%d"),
       DOY  = lubridate::yday(DATE)) %>%
  separate(Date, into = c("YEAR","MONTH","DAY"), sep = "([-])")
```

```
MODISb <- MODISb %>%
  group_by(ForestID) %>%
  fill(PlotType, .direction = "updown")
```

 # check how many na values are there in the NDVI series?

```
sum(is.na(MODISb$NDVI))
```

 # Gap fill missing NDVI data

 # This first stage will only be carried out where there is 1 missing value. if there are 2 or more

 # consecutive missing values then this first step will not fill the gap

```
MODISb <- MODISb %>%
  arrange(DATE) %>%
  group_by(ForestID) %>%
  mutate(GapFill1 = na_interpolation(NDVI, option = "stine", maxgap = 1))
```

#check how many na values are there in the NDVI series?

```
sum(is.na(MODISb$GapFill1)) # in this dataset we have no filled all of the missing data
```

 # If there are still missing values then we can fill gaps based on the next nearest matching month from a different year

 # using the linear interpolation between the values in

```
MODISb <- MODISb %>%
  arrange(DATE) %>%
  group_by(ForestID, MONTH) %>%
  mutate(GapFill2 = na_interpolation(GapFill1, option = "linear"))
```

 # check how many na values are there in the NDVI series?

```
sum(is.na(MODISb$GapFill2))
```

 # Plot restulant data

```
ggplot(MODISb) +
  geom_point(aes(DATE, GapFill2, col = PlotType)) +
  facet_wrap(~PlotType, ncol = 1)
```

 # investigate difference in Gapfill 1(filled from the month immediately adjacent to missing value)

 # and 2(filled from nearest matching month)

```
ggplot(MODISb %>% filter(ForestID == "STATE128")) +
  geom_point(aes(DATE, GapFill2), col = "red") +
  geom_point(aes(DATE, GapFill1), col = "blue") +
  geom_point(aes(DATE, NDVI), col = "black") +
  ylab("NDVI")
```

 # Write csv for future use

```
write_csv(MODISb,"modis_ndvi_2000_2020_Gapfilled.csv" )
```

Script for BFAST and BEAST algorithm on time series data

 # load Libraries

```
library(tidyverse)
library(imputeTS)
library(lubridate)
library(zoo)
library(bfast)
library(strucchange)
library(ggplot2)
library(tidyverse)
library(Rbeast)
library(sp)
library(stringr)
```

library(raster)

library(devtools)

library(bfastSpatial)

library(rgdal)

 # Read MODIS and climate monthly data

modisall<-read.csv(paste("File.csv",sep="",collapse=""))

str(modisall)

#cconvert the date from factor to DATE format

modisall$DATE=as.Date(modisall$DATE, "%d/%m/%Y")

#convert the csv to a dataframe

modisall.df<-as.data.frame(modisall)

 # aggregate the data and calculate average based on plottype and location(e.g., Namibia and Botswana)

mean<-aggregate(modisall.df[,13:18], list(PlotType=modisall.df$PlotType,Location=modisall.df$Location, Date=modisall.df$DATE), mean)

#Plot Different types of land cover/ forest types

 # create the time series for mediumforest

NDVI_QA_zammedium.ts <- ts(

data = meanmedium.zam$NDVI_QA,

start = c(2002, as.numeric(format(meanmedium.zam$NDVI_QA[1], 07))),

end = c(2020,as.numeric(format(meanmedium.zam$NDVI_QA[1], 10))),

frequency = 12 ***#number of observations per year***)

plot(NDVI_QA_zammedium.ts ,type='b', ylab="NDVI",xlab="Year", main =" Average of mediumforest plots (n=48)",cex=2.0,lwd = 3.5, pch=16,cex.main = 2.0,cex.lab=3.5)

 # create the time series for closedforest

```r
NDVI_QA_zamclosed.ts <- ts(
  data = meanclosed.zam$NDVI_QA,
  start = c(2002, as.numeric(format(meanclosed.zam$NDVI_QA[1], 07))),
  end = c(2020,as.numeric(format(meanclosed.zam$NDVI_QA[1], 10))),
  frequency = 12 # number of observations per year
plot(NDVI_QA_zamclosed.ts ,type='b',ylab="NDVI",xlab="Year", main =" Average of closedforest plots (n=16), Zambezi Namibia",cex=2.0,lwd = 3.5, pch=16,cex.main = 2.0,cex.lab=3.5)

#create the time series for agriculture
NDVI_QA_zamagri.ts <- ts(
  data = meanagri.zam$NDVI_QA,
  start = c(2002, as.numeric(format(meanagri.zam$NDVI_QA[1], 07))),
  end = c(2020,as.numeric(format(meanagri.zam$NDVI_QA[1], 10))),
  frequency = 12 # number of observations per year)
plot(NDVI_QA_zamagri.ts ,type='b', ylab="NDVI",xlab="Date", main =" Average of agricultural plots (n=7)",cex=2.0,lwd = 3.5, pch=16,cex.main = 2.0,cex.lab=3.5)

#Alternatively choose a single plot type
mean_Chobe001<-mean%>%  dplyr::filter(
     ForestID=="STATE035")

#create the NDVI time series for the chosen plot
NDVI_Chobe001.ts <- ts(
  data = mean_Chobe001$NDVI,
  start = c(2002, 7),
  end = c(2019,12),
  frequency = 12 # number of observations per year)
plot(MSAVI_Chobe001.ts ,type='b', ylab="MSAVI",xlab="Year", main =" Disturbed forest plot",cex=2.0,lwd = 3.5, pch=16,cex.main = 2.0,cex.lab=3.5)
#axis(side=1, at=c(2002:2020))
axis(side=1, at=seq(2002, 2019, by=1))
#box()
```

#create the GNDVI time series for the chosen plot

GNDVI_Chobe001.ts <- ts(

data = mean_Chobe001$GNDVI,

start = c(2002,7),

end = c(2019,12),

frequency = 12 ***#number of observations per year)***

plot(MSAVI_Chobe001.ts ,type='b', ylab="MSAVI",xlab="Year", main =" Disturbed forest plot",cex=2.0,lwd = 3.5, pch=16,cex.main = 2.0,cex.lab=3.5)

#axis(side=1, at=c(2002:2020))

axis(side=1, at=seq(2002, 2019, by=1))

#box()

#create the EVI time series for the chosen plot

EVI_Chobe001.ts <- ts(

data = mean_Chobe001$EVI,

start = c(2002, 7),

end = c(2020,6),

frequency = 12 ***# number of observations per year***)

plot(EVI_Chobe001.ts ,type='b', ylab="EVI",xlab="Year", main =" Disturbed forest plot",cex=2.0,lwd = 3.5, pch=16,cex.main = 2.0,cex.lab=3.5)

#Run BFAST algorithm on NDVI

 # define the ratio of distance between breaks (time steps) and length of the time series

rdist <- 15/length(NDVI_Chobe001.ts)

fit <- bfast(NDVI_Chobe001.ts, h=rdist,

season="harmonic", max.iter=1)

plot(fit, xlab="DATE", main="NDVI",axes=F)

#Run BEAST algorithm on NDVI

fit <- beast(NDVI_Chobe001.ts,12)

```
plot(fit,xlab="", main="NDVI",axes=FALSE,labels=F)
```

#Run BFAST algorithm on GNDVI

```
rdist <-15/length(GNDVI_Chobe001.ts)  #I tried 25 , but 15 work best
fit <- bfast(GNDVI_Chobe001.ts, h=rdist,
        season="harmonic", max.iter=1)
plot(fit, main="GNDVI")
```

#Run BEAST algorithm on GNDVI

```
fit <- beast(GNDVI_Chobe001.ts,12)
plot(fit,main="GNDVI")
```

Script for SPATIAL ANALYSIS OF BFAST ALGORITHM (RASTER ANALYSES)

PREPROCESS and ANALYSE THE RASTER DATA WITH BFAST

 # Define path to files

```
VIpathGNDVI <- "Path/"
```

 # Load list of raster file names

```
MODIS8GNDVI.fileList <- list.files(VIpathGNDVI , pattern = "*.tif")
```

 # load individual files into a raster brick

```
MODIS8dayGNDVI <-
do.call("brick",lapply(paste0(VIpathGNDVI,"/",MODIS8GNDVI.fileList[1:216]),
                FUN = function(x){
                  r <- raster(x)
                }))
```

#project the raster

crs(MODIS8dayGNDVI)

#rename the files

names(MODIS8dayGNDVI) <- MODIS8GNDVI.fileList

 # create object for original names

MODISnamesGNDVI <- names(MODIS8dayGNDVI)

Create object for each part of the required name

band <- str_sub(MODISnamesGNDVI, 1,2)

month <- str_sub(MODISnamesGNDVI, 4,5)

year <- str_sub(MODISnamesGNDVI, 7,10)

 # create a new object with the new layernames

MODISnamesGNDVI.new <- paste(band,month,year,sep = ".")

 # relabel modis data with new names

names(MODIS8dayGNDVI) <- MODISnamesGNDVI.new

 # reorder the raster brick according to new names

MODIS8dayGNDVI.reordered <- subset(MODIS8dayGNDVI, order(MODISnamesGNDVI.new))

names(MODIS8dayGNDVI.reordered)

 # Save the stacked image data in a single file, .grd with ENVI header file preserves the layer names

MODISStackGNDVI <- writeRaster(MODIS8dayGNDVI.reordered,paste0(VIpathGNDVI,"/MODIS_NDVIstack.grd"), format="raster",overwrite=TRUE)

s<-hdr(MODISStack, format = "ENVI")

par(mar=c(1,2,2,1))

#assign dates from 2002 to 2019

dtGNDVI<-c('2002-01-01','2003-01-01','2004-01-01','2005-01-01','2006-01-01', '2007-01-01','2008-01-01','2009-01-01','2010-01-01','2011-01-01','2012-01-01',

'2013-01-01','2014-01-01','2015-01-01','2016-01-01','2017-01-01','2018-01-01',

'2019-01-01','2002-02-01','2003-02-01','2004-02-01',

'2005-02-01','2006-02-01','2007-02-01','2008-02-01','2009-02-01','2010-02-01',

'2011-02-01','2012-02-01','2013-02-01','2014-02-01','2015-02-01','2016-02-01',

'2017-02-01','2018-02-01','2019-02-01',

'2002-03-01','2003-03-01','2004-03-01','2005-03-01','2006-03-01','2007-03-01',

'2008-03-01','2009-03-01','2010-03-01','2011-03-01','2012-03-01','2013-03-01',

'2014-03-01','2015-03-01','2016-03-01','2017-03-01','2018-03-01','2019-03-01',

'2002-04-01','2003-04-01','2004-04-01',

'2005-04-01', '2006-04-01','2007-04-01', '2008-04-01','2009-04-01','2010-04-01',

'2011-04-01','2012-04-01','2013-04-01','2014-04-01','2015-04-01','2016-04-01',

'2017-04-01','2018-04-01', '2019-04-01',

'2002-05-01', '2003-05-01', '2004-05-01', '2005-05-01','2006-05-01','2007-05-01',

'2008-05-01', '2009-05-01','2010-05-01','2011-05-01','2012-05-01','2013-05-01',

'2014-05-01','2015-05-01', '2016-05-01','2017-05-01','2018-05-01', '2019-05-01',

'2002-06-01','2003-06-01','2004-06-01',

'2005-06-01','2006-06-01', '2007-06-01','2008-06-01','2009-06-01','2010-06-01',

'2011-06-01','2012-06-01','2013-06-01','2014-06-01','2015-06-01','2016-06-01',

'2017-06-01','2018-06-01','2019-06-01',

'2002-07-01','2003-07-01','2004-07-01','2005-07-01','2006-07-01', '2007-07-01', '2008-07-01','2009-07-01', '2010-07-01','2011-07-01','2012-07-01', '2013-07-01',

'2014-07-01','2015-07-01','2016-07-01','2017-07-01','2018-07-01', '2019-07-01',

'2002-08-01','2003-08-01','2004-08-01',

'2005-08-01','2006-08-01','2007-08-01','2008-08-01','2009-08-01','2010-08-01',

'2011-08-01','2012-08-01','2013-08-01','2014-08-01','2015-08-01','2016-08-01',

'2017-08-01','2018-08-01','2019-08-01',

'2002-09-01', '2003-09-01','2004-09-01','2005-09-01','2006-09-01','2007-09-01',

'2008-09-01', '2009-09-01','2010-09-01','2011-09-01','2012-09-01','2013-09-01',

'2014-09-01', '2015-09-01','2016-09-01','2017-09-01','2018-09-01','2019-09-01',

'2002-10-01','2003-10-01','2004-10-01',

'2005-10-01','2006-10-01','2007-10-01','2008-10-01','2009-10-01','2010-10-01',

'2011-10-01','2012-10-01', '2013-10-01','2014-10-01' ,'2015-10-01','2016-10-01',

'2017-10-01','2018-10-01', '2019-10-01',

'2002-11-01','2003-11-01','2004-11-01','2005-11-01','2006-11-01','2007-11-01',

'2008-11-01','2009-11-01','2010-11-01', '2011-11-01','2012-11-01','2013-11-01',

'2014-11-01','2015-11-01', '2016-11-01','2017-11-01','2018-11-01','2019-11-01',

'2002-12-01','2003-12-01','2004-12-01','2005-12-01',

'2006-12-01','2007-12-01','2008-12-01','2009-12-01','2010-12-01','2011-12-01',

'2012-12-01','2013-12-01','2014-12-01', '2015-12-01', '2016-12-01','2017-12-01',

'2018-12-01','2019-12-01')# corresponding dates to all rasters

my_datesGNDVI <- as.Date(dtGNDVI, format ="%Y-%m-%d")

 # define the function that will be applied across the brick using the calc function

bfmRaster = function(pixels)

{

  tspx <- timeser(pixels, my_datesGNDVI) # create a timeseries of all pixels

  bfm <- bfastmonitor(tspx, response ~ trend + harmon, order = 3, start = c(2014,1)) # run bfast on all pixels

  return(c(bfm$breakpoint, bfm$magnitude))

}

 # calc function

bfmRGNDVI <- calc(MODIS8dayGNDVI.reordered, bfmRaster)

names(bfmRGNDVI) <- c('time of break', 'magnitude of change')

plot(bfmRGNDVI) ***# resulting time and magnitude of change***

 # Ensure the raster images have correct number of rows and collumnsrGNDVI<- raster(ncol= 210, nrow=166)

sGNDVI <- stack(lapply(1:216, function(x) setValues(rGNDVI, runif(ncell(rGNDVI)))))

MODIS8dayGNDVI.reordereds <- setZ(MODIS8dayGNDVI.reordered, my_datesGNDVI)

MODIS8dayGNDVI.reordereds

getZ(MODIS8dayGNDVI.reordereds)

plot(MODIS8dayGNDVI.reordereds[[1]])

 # Define path to files to export

VIpathGNDVI_out <- "path/"

#Define output path

outsGNDVI <- file.path(VIpathGNDVI_out , "bfmSpatial_start2010,1_gndvi_until2019.tif")

#Run the bfmSpatial on raster data starting 2010

bfmSpatial(MODIS8dayGNDVI.reordereds, start = c(2010, 1),formula = response~harmon,order = 1, filename = outsGNDVI)

PREPARE THE RASTER DATA AND EXTRACT THE MAGNITUDE

#Read in the data

gndvistate2010_ha1 <- brick("File.tif")

plot(gndvistate2010_ha1,1, main="Monitoring period 2013-2020, gndvi ")

 # extract change raster

changegndvistate2010_ha1 <- raster(gndvistate2010_ha1, 1)

extract magn raster

magngndvistate2010_ha1 <- raster(gndvistate2010_ha1, 2)

make a version showing only breakpoing pixels

magn_bkpgndvistate2010_ha1 <- magngndvistate2010_ha1

magn_bkpgndvistate2010_ha1[is.na(changegndvistate2010_ha1)] <- NA

op <- par(mfrow=c(1, 3))

plot(magn_bkpgndvistate2010_ha1, main="Magnitude: breakpoints")

plot(magngndvistate2010_ha1, main="Magnitude: all pixels")

 # extract and rescale magnitude and apply a threshold

magn09threshgndvistate2010_ha1 <- magngndvistate2010_ha1

magn09threshgndvistate2010_ha1 [magngndvistate2010_ha1 > 0.00] <- NA

 # compare all magn rasters

op <- par(mfrow=c(2, 2))

plot(magn09threshgndvistate2010_ha1, main="magnitude")

plot(magn09_sievegndvistate2010_ha1, main="pixel sieve")

plot(magn09_areasievegndvistate2010_ha1, main="0.5ha sieve")

plot(magn09_as_rookgndvistate2010_ha1, main="0.5ha sieve, rook's case")

changeSize_queengndvistate2010_ha1 <- clumpSize(magn09_areasievegndvistate2010_ha1)

changeSize_rookgndvistate2010_ha1 <-
clumpSize(magn09_areasievegndvistate2010_ha1, directions=4)

#Calculate the change size

op <- par(mfrow=c(1, 2))

plot(changeSize_queengndvistate2010_ha1, col=bpy.colours(50), main="Clump size: Queen's case")

plot(changeSize_rookgndvistate2010_ha1, col=bpy.colours(50), main="Clump size: Rook's case")

changeSize <- clumpSize(magn09_areasievegndvistate2010_ha1, f=250000/10000)

plot(changeSize, col=bpy.colours(50), main="Pixel size gndvi (hectares)")

#export path

writeFormats()

GNDVI_VIpath <-"path/"

#***Write the year of change and magnitude of change raster and export it out for further analysis in ArcGIS***

MODISStack <- writeRaster(changegndvistate2010_ha1,paste0(File.tif"), format = "GTiff",overwrite=TRUE)

MODISStack <- writeRaster(magngndvistate2010_ha1,paste0(File.tif"), format = "GTiff",overwrite=TRUE)

CHAPTER 5

GOOGLE EARTH ENGINE CODE FOR FIRE

Google Earth Engine Code for the fire time series

https://code.earthengine.google.com/7a868676bc7ac534247a19d7cdc6b150?noload=1

/*///

Code geerated for MODIS Burned Area Monthly at 500m, developed by-Ruusa David August 2020

*//

//This is a code to get the monthly Burned pixels

// Get list of images

var MODISBurn_Image = ee.ImageCollection(MonthlyBurnedArea)

  .filterDate('2019-09-01', '2019-09-30') ***//define the month, change this to the month of your*** choice

  .filterBounds(kaza).mean().clip(kaza); ***//get the mean and clip the data***

//Get the burn date

var MODISBurn_Image = MODISBurn_Image.select('BurnDate');

var firesVis = {

  min: 325.0,

  max: 400.0,

  palette: ['red', 'orange', 'yellow'],};

//Display on the map

Map.addLayer(MODISBurn_Image, firesVis, 'Fires');

print(MODISBurn_Image)

print('ImageList')

//export the burned data out

Export.image.toDrive({

image: MODISBurn_Image,

  folder: 'MCD64A1_fireUncertainty_2019',

  description:"MCD64A1_fire_2019_12_500m",

  region: kaza.geometry().bounds(),

   crs:"EPSG:32735 ",

  scale: 500,

maxPixels:210984237950});

//This is a code to get the uncertainity of the Burned pixels

// Get list of images to test

```
var MODISUncertainty_Image = ee.ImageCollection(MonthlyBurnedArea)
  .filterDate('2019-12-01', '2019-12-30')
  .filterBounds(kaza).mean().clip(kaza);
```

//Get the uncertainity burn date

```
var MODISUncertainty_Image =  MODISUncertainty_Image.select('Uncertainty');
var firesVis = {
  min: 325.0,
  max: 400.0,
  palette: ['red', 'orange', 'yellow'],};
```

//Display on the map

```
Map.addLayer(MODISUncertainty_Image, firesVis, 'Fires');
print(MODISUncertainty_Image)
print('ImageList')

//export the uncertainity out
Export.image.toDrive({
image: MODISUncertainty_Image,
  folder: 'MCD64A1_fireUncertainty_2019',
  description:"MCD64A1_fireUncertainty_2019_12_500m",
  region: kaza.geometry().bounds(),
   crs:"EPSG:32735 ",
  scale: 500,
maxPixels:210984237950});
```

GOOGLE EARTH ENGINE CODE FOR THE CLIMATE DATA

Google Earth Engine Code for the climate time series https://code.earthengine.google.com/93b50f3bd714cb527ce6573fbd1f23dc?noload=1

```
/*/////////////////////////////////////////////////////////////
Code generated for comparing Ground precipitation and satellite based precipitation, developed by-Ruusa David June 2019
*/////////////////////////////////////////////////////////////
//Add the ground preciptation on the map
Map.addLayer(gpcc1981)
Map.addLayer(gpcc2016)

//extract all the climate data
var collections = [ {
  name: 'CHIRPS', scale: 5000,
  collection: ee.ImageCollection('UCSB-CHG/CHIRPS/PENTAD')
 },
  {
  name: 'gpcc', scale: 3000,
  collection: ee.ImageCollection('users/ruusadavid2/gpccCollection_1891')
 },
 {
  name: 'cru', scale: 3000,
  collection: ee.ImageCollection('users/ruusadavid2/cruCollection')
 },
 {
  name: 'CFSV2', scale: 5000,
  collection: ee.ImageCollection('NOAA/CFSV2/FOR6H')
   .select('Precipitation_rate_surface_6_Hour_Average')
   .map(function(i) {
     return i.multiply(60 * 60 * 6) // convert to mm by 6 since it is in mm/second and is a 6 hour basis
       .copyProperties(i, ['system:time_start'])
   })} ];
```

//create a function to define the the range of date to be mapped through

```
function getDates(start, stop, step) {
  return ee.List.sequence(start, stop).map(function(year) {
    return ee.List.sequence(1, 12, step).map(function(month) {
      return ee.Date.fromYMD(year, month, 1)
    })
  }).flatten()
}
```

//create a function to compute the sum and mean through all precipitation bands in all images

```
function compute(start, stop, step) {
  var dates = getDates(start, stop, step)
  var features = collections.map(function(c) {
    return dates.map(function(d) {
      var p = c.collection
        .filterDate(d, ee.Date(d).advance(step, 'month'))
        .sum()
        .reduceRegion(ee.Reducer.mean(), southAfrica,  c.scale).values().get(0)
            return ee.Feature(null)
        .set('system:time_start', ee.Date(d).millis())
        .set(c.name, p)
    })
  })
    return ee.FeatureCollection(ee.List(features).flatten())
}
```

//define the the time period to be computed on

```
var monthly = compute(1981, 2016, 1)
var annual = compute(1981, 2016, 12)
```

//set a function to define the chart titles, x and y axis titles

```
function chart(features, title) {
 var chart = ui.Chart.feature.byFeature(features, 'system:time_start')
 chart.setOptions({
  vAxis: { title: 'Precipitation [mm]' },
  title: title
 })
 print(chart)
}
```

//create the charts

```
chart(monthly, 'Monthly precipitation in Southern Africa Subcontinent (2001-2015)')
chart(annual, 'Raingauge and satellite-based annual precipitation in Central Angola, coordnates[18.71,-11.00)(1981-2016)')
```

R CODE FOR ANALYSING TIME SERIES OF VEGETATION DATA AND CLIMATE DATA

This part of the R code is for analysing time series of Vegetation Data and Climate Data

ANALYSE AND PLOT THE GROUND RAINFALL AND TEMPERATURE

#Load the Library

```
library(corrr)
library(dplyr)
library(tidyverse)
library(igraph)
library(ggraph)
```

```
library(Hmisc )
library(corrplot)
library(sp)
library(zoo)
library(xts)
library(hydroTSM)
library(ggplot2)
library(dplyr)
```

#Import the data

```
precip8<-read.csv(paste("File.csv",sep="",collapse=""))
```

#prepare the data

#convert to data frame

```
x<-as.data.frame(precip8)
```

 # Convert date to Date format

```
x$Dates=as.Date(x$Date, "%d.%m.%Y")
#anyDuplicated(x$Dates)
#duplicated(x$Dates) | duplicated(x$Dates, fromLast = TRUE)
```

#create a zoo object for time series

```
x<- zoo(x$Rainfall,x$Dates)
```

#plot rainfall

```
plot(x, main="rainfall", ylab="precipitation (mm)", xlab="Time")
```

#find the number of years

```
( nyears <- yip(from=start(x), to=end(x), out.type="nmbr" ) )
```

#plot the prepared data with hydroplot

```
hydroplot(x, var.type="Precipitation", main="at Chobe National Park",
```

```
         pfreq = "dm", from="1975-01-01")
dwi(x)
```

#Analyse the rainfall time series data

#Monthly analysis

```
monthlyfunction(x, FUN=median, na.rm=TRUE)
cmonth <- format(time(x), "%b")
months <- factor(cmonth, levels=unique(cmonth), ordered=TRUE)
```

#Boxplot of the monthly values

```
boxplot( coredata(x) ~ months, col="lightblue", main="Monthly Precipitation",
        ylab="Precipitation, [mm]", xlab="Month")
```

#Average seasonal values of precipitation

```
seasonalfunction(x, FUN=sum, na.rm=TRUE) / nyears
```

#Extracting the seasonal values for each year

```
m<-monthlyfunction(x, FUN=sum, na.rm=TRUE)
( DJF <- dm2seasonal(x, season="DJF", FUN=sum) )
(MAM <- dm2seasonal(x, season="MAM", FUN=sum) )
(JJA  <- dm2seasonal(x, season="JJA", FUN=sum))
(SON  <- dm2seasonal(x, season="SON", FUN=sum) )
```

#Extract the seasonal values for each year

```
hydroplot(x, pfreq="seasonal", FUN=sum, stype="default",ylab="Precipitation
(mm)",lwd=2)
```

 # Mean winter (DJF) values of streamflow for each year of 'x'

```
 dm2seasonal(x, FUN=sum, season="DJF")
  dm2seasonal(x, FUN=sum, season="MAM")
 dm2seasonal(x, FUN=sum, season="JJA")
```

dm2seasonal(x, FUN=sum, season="SON")

 # Selecting only a three-year time slice for the analysis

x <- window(x, start=as.Date("1975-01-01"))

#Plotting the selected time series

hydroplot(x, FUN=sum, ptype="ts", pfreq="ma", var.unit="mm",ylab="Precipitation",lwd=1.8)

Create the Climograph from the rainfall and temperature data

#Read the Preciptation and Temperature data

preciptemp<-read.csv(paste("File.csv",sep="",collapse=""))

#convert to data frame

y<-as.data.frame(preciptemp)

 # Convert date to Date format

Dates=as.Date(y$Date, "%d.%m.%Y")

#create a zoo for time series

z <- zoo(y[, 2:4], as.Date(as.character(y[, 1]), format="%d.%m.%Y"))

colnames(z) <- c("Precipitation", "Max Temperature", "Min Temperature")

 # extracting individual ts of precipitation, maximum and minimum temperature

pcp <-z[,1]

tmx <- z[,2]

tmn <-z[, 3]

 # Plotting the climograph

m <- climograph(pcp=pcp, tmx=tmx, tmn=tmn, na.rm=TRUE, main="Monthly Precipitation, Min and Max Temperature")

plot(z, main = "Monthly Rainfall, Maximum and Minimum Temperature",xlab="Years", lwd=2, col=c("blue", "red","black"),cex.axis =1.5,cex.main = 2)

CALCULATING SPEI FROM GROUND RAINFALL AND TEMPERATURE

#Calculating SPEI using Ground rainfall and temperature from Kasane Chobe Botswana

#Read the data

raintemp<-read.csv(paste("File.csv",sep="",collapse="")) #with all data and outliers removed

#convert points into dataframe

raintemp<-data.frame(raintemp)

str(raintemp)

#calculate potentioal evapotranspiration

raintemp$PET<-hargreaves(Tmin=raintemp$Tempmin, Tmax=raintemp$Tempmax, lat =-17.82947)

raintemp$PET

#calculate climatic water balance

raintemp$ClWaBAL<-raintemp$Precip-raintemp$PET

raintemp$ClWaBAL

ClWaBAL<-raintemp$Precip-raintemp$PET

#calculate standardised precipitation evapotranspiration index, and define the scale by 1 moth or two months or 12 etc

SPEI1<-spei(raintemp$ClWaBAL,1)   #for 1 month

raintemp$SPEI1.dataframe=as.data.frame(fitted(SPEI1))   #convert to dataframe

par(mar=c(5, 4, 4, 6) + 0.1)

#calculate SPEI for 1 month

plot.spei(spei(ts(raintemp$ClWaBAL, freq=12,start=c(1983,1)),1,ref.start=c(1983,1),ref.end=c(2020,10)),main ="Standardised Precipitation Evapotranspiration Index (SPEI-1 months)",textSize = 8) mtext(side=1, line=2, "Time", font=2,cex=1.2)

#calculate SPEI for 2 month

plot.spei(spei(ts(raintemp$ClWaBAL, freq=12,start=c(1983,1)),2,ref.start=c(1983,1),ref.end=c(2020,10)),main ="Standardised Precipitation Evapotranspiration Index (SPEI-2 months)",textSize = 8)

mtext(side=1, line=2, "Time", font=2,cex=1.2)

#calculate SPEI for 12 month

plot.spei(spei(ts(raintemp$ClWaBAL, freq=12,start=c(1983,1)),12,ref.start=c(1983,1),ref.end=c(2020,10)),main ="Standardised Precipitation Evapotranspiration Index (SPEI-12 months)",textSize = 8)

mtext(side=1, line=2, "Time", font=2,cex=1.2)

#Plot all three SPEI timescale (1,3,12 months) in one plot

par(mar=c(5, 4, 5, 6) + 0.1)

par(mfrow=c(1,1))

#Plot first plot for 1 month

plot.spei(spei(ts(raintemp$ClWaBAL, freq=12,start=c(2002,7)),1,ref.start=c(2002,7),ref.end=c(2019,12)),main ="Standardised Precipitation Evapotranspiration Index (SPEI-1month)",textSize =12, xlab="", ylab="", axes=FALSE,)

#mtext(side=1, line=2, "Time", cex=1.5)

mtext(side=2, line=2, "SPEI", cex=1.5)

axis(side=1, at=seq(2002, 2019, by=1),cex.axis = 1.0, cex.lab = 1)

box()

#Plot second plot for 2 months

plot.spei(spei(ts(raintemp$ClWaBAL, freq=12,start=c(1983,1)),3,ref.start=c(1983,1),ref.end=c(2019,12)),main ="Standardised Precipitation Evapotranspiration Index (SPEI-3 months)",textSize =12, xlab="", ylab="", axes=FALSE,)

```
mtext(side=1, line=2, "Time", cex=1.5)

mtext(side=2, line=2, "SPEI", cex=1.5)

axis(side=1, at=seq(1982, 2019, by=1),cex.axis = 1.0, cex.lab = 1)

box()
```

#Plot second plot for 22 months

```
plot.spei(spei(ts(raintemp$ClWaBAL, freq=12,start=c(1982,1)),12,ref.start=c(1982,1),ref.end=c(2019,12)),main ="Standardised Precipitation Evapotranspiration Index (SPEI-12 months)",textSize =12, xlab="", ylab="", axes=FALSE, )

mtext(side=1, line=2, "Time", cex=1.5)

mtext(side=2, line=2, "SPEI", cex=1.5)

axis(side=1, at=seq(1982, 2019, by=1),cex.axis = 1.0, cex.lab = 1)

box()
```

ANALYSE THE CLIMATE DATA AND VEGETATION DATA (NDVI)

#Plotting climate and NDVI

#Read the data

```
preciptemp<-read.csv(paste("File.csv",sep="",collapse=""))

head( preciptemp)
```

#Covert the data to a dataframe

```
y<-as.data.frame( preciptemp)
```

#Covertto the Date understood by r

```
y$Dates=as.Date(y$Date, "%d.%m.%Y")

tail( preciptemp)
```

 # Plot first set of data (NDVI in this case) and draw its axis

```
plot(y$Dates, y$NDVI, pch=16, axes=TRUE, ylim=c(0,1), xlab="", ylab="",
    cex.axis = 1.3, cex.lab = 2, type="b",col="black", main="NDVI and Precipitation")

#axis(2, ylim=c(0,1),col="black",las=1)  # las=1 makes horizontal labels
```

mtext("NDVI",side=2,line=2.5, cex=1.5)

box()

 # Allow a second plot on the same graph

par(new=TRUE)

 # Plot the second plot (precipitation) and put axis scale on right

plot(y$Dates, y$Precip, pch=15, xlab="", ylab="", ylim=c(0,500), axes=FALSE, type="b", col="dark red",)

 # add lables

mtext("PRECIPITATION",side=4,col="dark red",line=4, cex=1.5)

axis(4, ylim=c(500), col="dark red",col.axis="dark red",las=1,cex.axis = 1.3, cex.lab = 2)

 # Draw the time axis

mtext("Time",side=1,col="black",line=2.5, cex= 1.8)

 # Add Legend

legend("topleft",legend=c("NDVI","PRECIPITATION"),bty = "n",

text.col=c("black","dark red"),pch=c(16,15), col=c("black","dark red"))

ANALYSE THE RELATIONSHIP BETWEEN CLIMATE DATA (SOIL MOISTURE, SPEI, RSM, PRECIPITATION, TEMPERATURE) ANDVEGETATION DATA

#Read the data

modis8<-read.csv(paste("XFile.csv",sep="",collapse=""))

#Create a function to plot

```
flattenCorrMatrix <- function(cormat, pmat) {
  ut <- upper.tri(cormat)
  data.frame(
    row = rownames(cormat)[row(cormat)[ut]],
    column = rownames(cormat)[col(cormat)[ut]],
```

```
    cor  =(cormat)[ut],
    p = pmat[ut]
  )
}
s2corAll3<-rcorr(as.matrix(modis8.num[]))
flattenCorrMatrix(s2corAll3$r,s2corAll3$P)
```

<u># Mark the insignificant coefficients according to the specified p-value significance level</u>

```
cor_5 <- rcorr(as.matrix(modis8.num))
M <- cor_5$r
p_mat <- cor_5$P
col <- colourRampPalette(c("#BB4444", "#EE9988", "#FFFFFF", "#77AADD",
"#4477AA"))
corrplot(M, method = "colour", col = col(200),
        type = "upper", order = "hclust",
        addCoef.col = "black", # Add coefficient of correlation
        # Combine with significance level
        p.mat = p_mat, sig.level = 0.01,
        # hide correlation coefficient on the principal diagonal
        diag = FALSE )
```